# CELL-CELL INTERACTIONS CONTROLLING CEREBRAL MICROVASCULATURE UNDER PHYSIOLOGICAL AND PATHOPHYSIOLOGICAL CONDITIONS

EDITED BY: Xinchun Jin, Dmitriy N. Atochin, Junlei Chang, Wenlan Liu and Xiaoxing Xiong

PUBLISHED IN: Frontiers in Cellular Neuroscience

frontiers Research Topics

# frontiers



ISSN 1664-8714
ISBN 978-2-88976-451-8
DOI 10.3389/978-2-88976-451-8

## About Frontiers

Frontiers is more than just an open-access publisher of scholarly articles: it is a pioneering approach to the world of academia, radically improving the way scholarly research is managed. The grand vision of Frontiers is a world where all people have an equal opportunity to seek, share and generate knowledge. Frontiers provides immediate and permanent online open access to all its publications, but this alone is not enough to realize our grand goals.

## Frontiers Journal Series

The Frontiers Journal Series is a multi-tier and interdisciplinary set of open-access, online journals, promising a paradigm shift from the current review, selection and dissemination processes in academic publishing. All Frontiers journals are driven by researchers for researchers; therefore, they constitute a service to the scholarly community. At the same time, the Frontiers Journal Series operates on a revolutionary invention, the tiered publishing system, initially addressing specific communities of scholars, and gradually climbing up to broader public understanding, thus serving the interests of the lay society, too.

## Dedication to Quality

Each Frontiers article is a landmark of the highest quality, thanks to genuinely collaborative interactions between authors and review editors, who include some of the world's best academicians. Research must be certified by peers before entering a stream of knowledge that may eventually reach the public - and shape society; therefore, Frontiers only applies the most rigorous and unbiased reviews.
Frontiers revolutionizes research publishing by freely delivering the most outstanding research, evaluated with no bias from both the academic and social point of view. By applying the most advanced information technologies, Frontiers is catapulting scholarly publishing into a new generation.

## What are Frontiers Research Topics?

Frontiers Research Topics are very popular trademarks of the Frontiers Journals Series: they are collections of at least ten articles, all centered on a particular subject. With their unique mix of varied contributions from Original Research to Review Articles, Frontiers Research Topics unify the most influential researchers, the latest key findings and historical advances in a hot research area! Find out more on how to host your own Frontiers Research Topic or contribute to one as an author by contacting the Frontiers Editorial Office: frontiersin.org/about/contact

# CELL-CELL INTERACTIONS CONTROLLING CEREBRAL MICROVASCULATURE UNDER PHYSIOLOGICAL AND PATHOPHYSIOLOGICAL CONDITIONS

Topic Editors:
**Xinchun Jin,** Capital Medical University, China
**Dmitriy N. Atochin,** Harvard Medical School, United States
**Junlei Chang,** Shenzhen Institutes of Advanced Technology, Chinese Academy of Sciences (CAS), China
**Wenlan Liu,** Shenzhen University, China
**Xiaoxing Xiong,** Renmin Hospital of Wuhan University, China

**Citation:** Jin, X., Atochin, D. N., Chang, J., Liu, W., Xiong, X., eds. (2022). Cell-Cell Interactions Controlling Cerebral Microvasculature Under Physiological and Pathophysiological Conditions. Lausanne: Frontiers Media SA.
doi: 10.3389/978-2-88976-451-8

# Table of Contents

frontiers in Cellular Neuroscience

ORIGINAL RESEARCH
published: 17 March 2021
doi: 10.3389/fncel.2021.644663

# Effects of CRMP2 DNA Methylation in the Hippocampus on Depressive-Like Behaviors and Cytoskeletal Proteins in Rats

*Dan Xiang*[1], *Siqi Sun*[1], *Gaohua Wang*[1,2]* *and Zhongchun Liu*[1,2]*

[1]*Department of Psychiatry, Renmin Hospital of Wuhan University, Wuhan, China,* [2]*Institute of Neuropsychiatry, Renmin Hospital, Wuhan University, Wuhan, China*

Chronic stress appears to alter DNA methylation and DNA methyltransferases (DNMTs) in brain regions related to emotion. Collapsin response mediator protein-2 (CRMP2) mediates the development of depression by regulating microtubule dynamics. In this study, rats were subjected to chronic unpredictable mild stress (CUMS). At the end of the CUMS procedure, normal saline or fluoxetine was administered to the rats. Moreover, normal saline or the 5-aza-2'-deoxycytidine (5-aza) was administered to the hippocampal CA1 region of the rats. Behavioral tests were performed to evaluate the depressive-like phenotypes. The CRMP2 DNA methylation levels and cytoskeletal microtubular system-related biomarkers were detected by several molecular biology techniques. The results showed that the rat model of depression was successfully established by exposure to CUMS, and fluoxetine treatment exerted an antidepressant-like effect. We observed the upregulation of DNMT1 and DNMT3a in the hippocampus of stressed rats. CUMS induced a decrease in CRMP2 expression and an increase in phosphorylated CRMP2 (pCRMP2) expression in the hippocampus of rats. The rate of DNA methylation in the CpG island of the CRMP2 promoter region in the hippocampus of stressed rats was significantly higher than that in control rats. Moreover, CUMS significantly decreased the interaction between CRMP2 and α-tubulin and decreased the microtubule dynamics. Chronic fluoxetine treatment reversed these changes. Also, hypomethylation induced by 5-aza injection into the hippocampal CA1 region caused antidepressant-like effects and increased CRMP2 expression and microtubule dynamics. These results suggested that CRMP2 DNA methylation may be involved in regulating the cytoskeletal microtubular system and mediating depressive-like behaviors.

**Keywords: depression, CRMP2, DNA methylation, CUMS, microtubule dynamics**

OPEN ACCESS

***Edited by:***
*Junlei Chang,*
*Chinese Academy of Sciences (CAS), China*

***Reviewed by:***
*Ci MA,*
*University of California, San Diego, United States*
*Shaohua Hu,*
*Zhejiang University, China*

***Correspondence:**
*Gaohua Wang*
*wgh6402@163.com*
*Zhongchun Liu*
*zcliu6@whu.edu.cn*

***Specialty section:***
*This article was submitted to Cellular Neuropathology, a section of the journal Frontiers in Cellular Neuroscience*

***Received:*** *21 December 2020*
***Accepted:*** *26 February 2021*
***Published:*** *17 March 2021*

***Citation:***
*Xiang D, Sun S, Wang G and Liu Z (2021) Effects of CRMP2 DNA Methylation in the Hippocampus on Depressive-Like Behaviors and Cytoskeletal Proteins in Rats. Front. Cell. Neurosci. 15:644663. doi: 10.3389/fncel.2021.644663*

## INTRODUCTION

As a severe psychiatric disorder, depression is characterized by a depressed mood or a marked loss of interest or pleasure for most of the day. Depression is a common illness worldwide, and more than 300 million people are currently depressed. Depression has substantial adverse effects on personal health, with high recurrence and mortality. Depression is linked to cerebrovascular disease, and depressed patients are at higher risk of stroke, with an enormous

burden for patients, families, and society as a whole (Kolovos et al., 2017; Winter et al., 2018). Although various treatments are effective against depression, some patients are resistant to the currently available treatments. The underlying mechanisms that cause depression are still unclear. Therefore, it is necessary to identify the mechanisms underlying depression.

Collapsin response mediator protein-2 (CRMP2), which has also been identified as dihydropyrimidinase-like 2 (DPYSL2), belongs to the CRMP family that includes 5 homologs (CRMP1-5). CRMP2 is enriched in brain areas that retain plasticity and neurogenesis, such as the hippocampus, olfactory bulb, and cerebellum (Inagaki et al., 2001). CRMP2 binds to tubulin and is phosphorylated by various kinases, which regulates its activity (Yamashita and Goshima, 2012). Microtubules are crucial cytoskeletal constituents in growing neurites and axons. Several studies have suggested that CRMP2 assists microtubule assembly together with the tubulin heterodimer (Fukata et al., 2002; Niwa et al., 2017). CRMP2 binds to the tubulin heterodimer, and upon phosphorylated CRMP2 (pCRMP2) by various kinases, the binding affinity of CRMP2 to tubulin weakens. CRMP2 is a microtubule-associated protein that regulates the dynamic process of microtubule assembly (Gu and Ihara, 2000). Microtubule dynamics can be identified by analyzing the stable form, acetylated α-tubulin (Acet-tubulin), and the dynamic form, tyrosinated α-tubulin (Tyr-tubulin), which are associated with neuronal plasticity (Bianchi et al., 2006). Consistent with the role of CRMP2 in neuronal functions, CRMP2 has shown to be implicated in several neuropsychiatric disorders, including cerebral ischemia, schizophrenia, and depression (Quach et al., 2015). CRMP2 levels are decreased in the brains of patients with depression (Johnston-Wilson et al., 2000). Additionally, the proteomic analysis showed that chronic treatment with the antidepressive agents venlafaxine or fluoxetine increased CRMP2 levels in the rat hippocampus (Khawaja et al., 2004). In the previous research of our group, Wu et al. have confirmed the effect of CRMP2-mediated neuronal plasticity in depression induced by chronic stress (Wu et al., 2018). However, the molecular mechanisms by which CRMP2 contributes to the pathogenesis of depression remain to be elucidated.

Exposure to adverse environmental events is one of the strongest risk factors for depression. Mechanisms of epigenetic modification include DNA methylation, chromatin conformational changes, long noncoding RNAs, and histone modifications, and these mechanisms can modulate gene expression in response to the environment (Mahgoub and Monteggia, 2013). DNA methylation is the most stable form of epigenetic modification, and several lines of evidence suggest a critical role for this modification in depression (Chen et al., 2017; Lisoway et al., 2018). DNA methylation is accomplished by DNA methyltransferases (DNMTs), which catalyze the addition of a methyl group to the cytosine in the 5' position of cytosine-phosphate-guanine sites. The DNMTs family mainly includes DNMT1, DNMT3a, and DNMT3b (Kader et al., 2018). DNMT1 is predominantly associated with the maintenance of DNA methylation, and DNMT3a and DNMT3b are more strongly associated with de novo methylation (Okano et al., 1999). Candidate genes that undergo DNA methylation, such as brain-derived neurotrophic factor (BDNF), NR3C1 (encoding the glucocorticoid receptor), SLC6A4 (encoding the serotonin transporter), have been regarded as potential biomarkers of depression. Previous studies demonstrated that increased DNA methylation in the promoter region of BDNF was associated with the pathophysiology of depression (Januar et al., 2015). A study has shown that animals subjected to early life stress were associated with a specific increase in DNA methylation levels of the exon 1F NR3C1 gene (Weaver et al., 2004). Additionally, several studies have demonstrated an increase in DNA methylation of SLC6A4 in depression (Philibert et al., 2008; Zhao et al., 2013). CRMP2 has been proposed to be a candidate gene for the treatment of depression. In our previous study, the results showed a reduction in CRMP2 expression in the hippocampus of stressed rats, which may correlate with a significant increase in the DNA methylation levels of the CRMP2 promoter region (Xiang et al., 2020). Moreover, several studies suggested the important role of DNMTs in regulating depressive-like behaviors (Ignácio et al., 2017; Shen et al., 2019). Systemic or intrahippocampal administration of DNMTs inhibitors induces antidepressant-like effects in animals subjected to the forced swimming test (FST) and open field test (OFT; Sales et al., 2011). As described above, these studies support the hypothesis that DNA methylation is an important epigenetic modification involved in the pathogenesis of depression.

Despite these pieces of evidence, little is known about the role of CRMP2 DNA methylation in the etiology of depression. In this study, chronic unpredictable mild stress (CUMS) was used to establish a model of depression. The sucrose preference test (SPT), FST, and OFT were used to evaluate depressive-like behaviors. We investigated how CUMS and fluoxetine treatment affect DNMTs expression and CRMP2 DNA methylation in the hippocampus of rats. We also detected CRMP2, pCRMP2, and α-tubulin isoform expression in the hippocampus of rats to elucidate the underlying mechanisms by which CRMP2 is involved in the pathological processes of depression. Hippocampus is the most commonly studied brain region in depression research, and it is part of the limbic structures, which are associated with emotional responses. In this study, we focused on the role of the hippocampal region, as neural plasticity in this brain region has been related to depressive-like behavior.

We investigated the effect caused by injecting the DNMTs inhibitor 5-aza-2'-deoxycytidine (5-aza) into the hippocampal CA1 regions of rats. The effect of 5-aza on the levels of CRMP2, pCRMP2, and α-tubulin isoforms in the hippocampal CA1 region was also assessed to further explore the mechanism by which CRMP2 is involved in the pathogenesis of depression.

# MATERIALS AND METHODS

## Animals

Adult male Sprague–Dawley rats weighing 180–200 g were purchased from the Company of Experimental Animals of Hunan Slack King (Hunan, China). Before the experiment,

the rats were housed under laboratory conditions for seven days to adapt to the new environment. The rats were housed at 22 ± 2°C with a 12-h light/12-h dark schedule with free access to food and water. All the procedures and animal experiments of this study were performed in agreement with the guidelines outlined in the legislation of the P.R. China regarding the ethical use of laboratory animals and approved by the Institutional Animals Care Committee of Renmin Hospital of Wuhan University.

## Experimental Design

The experimental design is shown in **Figure 1**. Experiment one: The rats were randomly divided into three groups: the control group ($n$ = 20), the CUMS group ($n$ = 20), and the fluoxetine group ($n$ = 20). In both the CUMS and fluoxetine groups, the rats were subjected to CUMS daily for four weeks. At the end of the CUMS procedure, the rats in the CUMS group were given an intraperitoneal injection of saline vehicle, and the rats in the fluoxetine group were given an intraperitoneal injection of fluoxetine (10 mg/kg) for 4 weeks. The rats in the control group did not receive any stimuli throughout the entire procedure. Behavioral tests were used to evaluate the effects of stress and fluoxetine on anhedonia and activity. We investigated the effects of CUMS and fluoxetine treatment on DNA methylation in the CRMP2 promoter and DNMTs expression. Additionally, we analyzed the protein expression of CRMP2 and pCRMP2 and the expression of α-tubulin isoforms, which are thought to reflect microtubule dynamics. We also explored the effect of chronic stress and antidepressant treatment on the interaction between CRMP2 and α-tubulin.

Experiment two: a total of 20 rats were subjected to the CUMS procedure and were further divided into two groups ($n$ = 10/group): the CUMS + normal saline group (CUMS + Nacl group) and the CUMS + 5-aza group. Intrahippocampal injections of the saline vehicle were administered to rats in the CUMS + Nacl group. 5-aza was diluted in normal saline and administered into the hippocampus of the rats in the CUMS + 5-aza group. Behavioral tests were used to evaluate the effects of 5-aza on depressive-like behaviors. We examined the global DNA methylation levels in the hippocampal CA1 region of the rats treated with 5-aza. Moreover, the expression of CRMP2, pCRMP2, and α-tubulin isoforms in the hippocampal CA1 region was analyzed, and the interaction between CRMP2 and α-tubulin was examined in the rats treated with 5-aza.

## CUMS Procedure

The CUMS procedure was performed as previously described (Xiang et al., 2019). The CUMS procedure consisted of a series of seven different stressors: food deprivation for 24 h; water deprivation for 24 h; cage tilted at 45° for 24 h; swimming in 4° ice water for 5 min; tails clamped for 3 min; exposure to damp sawdust for 24 h and inversion of the light/dark cycle for 24 h. The same stressor was not applied on any two consecutive days.

## Stereotaxic Surgery and Hippocampal CA1 Region Administration

The rats subjected to stereotaxic surgery were anesthetized with sodium pentobarbital (25 mg/kg) and fixed in a stereotaxic frame. The rats were bilaterally implanted with stainless steel guide cannulae aimed at the hippocampal CA1 region (coordinates:

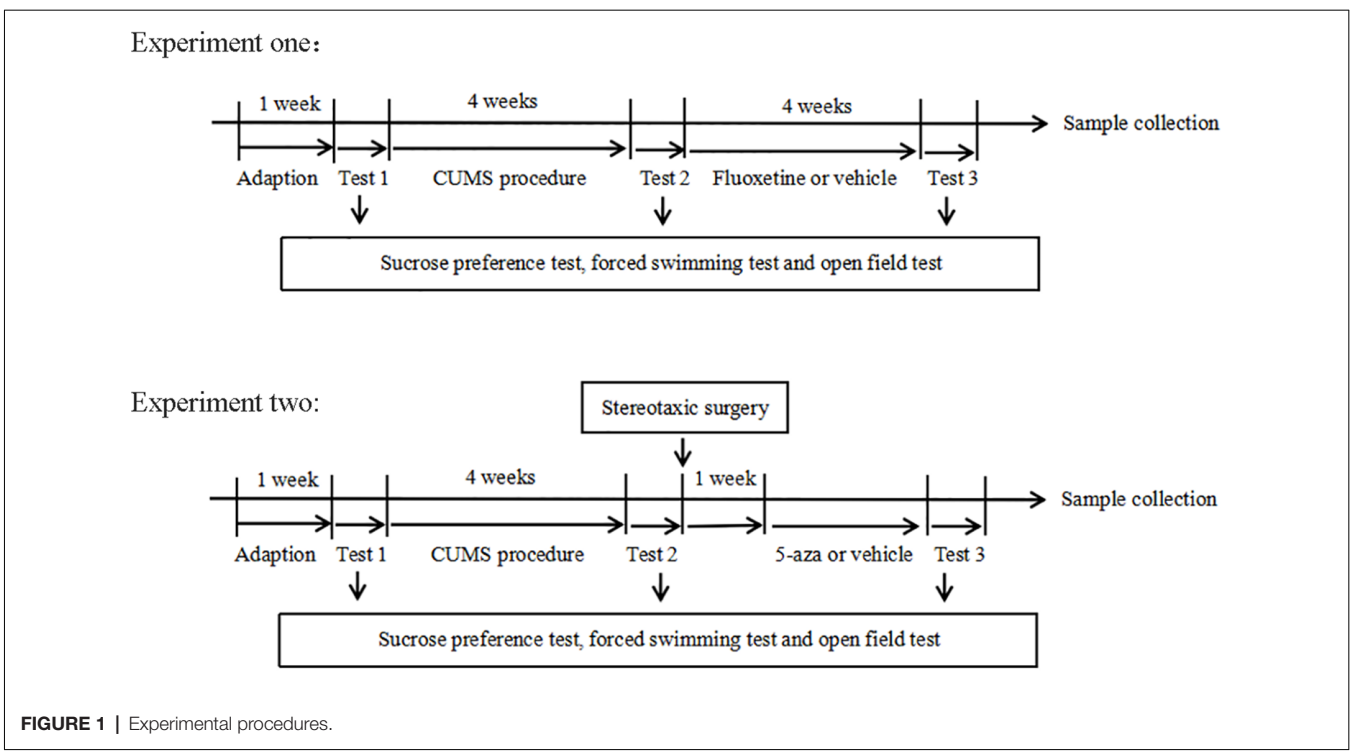


**FIGURE 1** | Experimental procedures.

3.5 mm posterior to the bregma, ±2.3 mm lateral, 2.6 mm from the cortical surface). Matched stylets were inserted into the guide cannulae to prevent obstruction. After the surgery, the rats were injected with penicillin for 3 days to prevent infection.

Seven days after the surgery, hippocampal CA1 administration was performed with a microsyringe. 5-aza (Sigma–Aldrich, A3656; 100 nmol/0.5 μl) was dissolved in normal saline and injected into the hippocampal CA1 region (0.5 μl per side). 5-aza was slowly infused over 1 min, and the microsyringe was maintained in the guide cannula for 2 min to prevent backflow. Rats received three injections of 5-aza or saline vehicle, and the third injection was given 1 h before the behavioral tests.

## Behavioral Tests

The SPT, OFT, and FST were performed in this study. The SPT was performed as previously described. Before the test, the rats were trained to consume 1% sucrose solution. After the training, the rats were deprived of water for 24 h and then offered a bottle of 1% sucrose solution and a bottle of water for the next 24-h period. Sucrose consumption was measured by comparing the weights of the bottles before and after the test. The locomotor activity of the rats was assessed using the OFT. In the test, one rat was placed in a square arena (100 × 100 × 35 cm) and observed using a video tracking system (Ethovision XT 11.5) for 5 min. The total distance traveled, the average velocity, and the rearing frequency were recorded. The apparatus was cleaned with a 75% alcohol solution after each test. In the FST, a rat was placed in a glass cylinder (30 cm diameter × 40 cm height) that was filled with water to a height of 28 cm and maintained at 25°C. The rat was forced to swim for 6 min, and the immobility time was recorded during the final 4 min. The immobility time in the FST was regarded as the time the rats spent floating in the water without struggling or exhibiting only slight movement to keep their heads above the water.

## Bisulfite Sequencing PCR (BSP)

Genomic DNA was extracted from hippocampal tissue using a genomic DNA extraction kit (Tiangen, DP304), and bisulfite conversion was performed using an EpiTect Bisulfite Kit (Qiagen, 59104) according to the manufacturer's protocol. The bisulfite-modified DNA samples were amplified by bisulfite sequencing PCR with primers specific to the CRMP2 gene promoter. The promoter of the CRMP2 gene is generally considered to be a 2,000-bp sequence upstream of the transcription start site. The primers were designed by MethPrimer software. The BSP primers were as follows: F: 5'-TTTGTATTGTAGATGAAGTA TTTGGG-3'; R: 5'-AACAATAAAAACCTTAATTCCAATC-3'. The PCR conditions were as follows: 95°C for 30 s, 40 cycles of 95°C for 5 s, 50°C for 30 s, and 72°C for 30 s. The PCR products were separated by 2% agarose gel electrophoresis, purified with a gel extraction kit (Cwbio, CW2302M), and then cloned into the pEASY-T1 cloning vector (TransGen, CT101–01). The recombinant plasmids were transformed into *E. coli* DH5α. At least ten clones of each sample were randomly chosen and sequenced by the Wuhan Tianyi Huiyuan Company.

## 5-mC DNA ELISA

Genomic DNA was extracted from the hippocampal CA1 region using the TIANamp Genomic DNA kit (TIANGEN Biotech, DP304) following the manufacturer's protocol. The DNA samples were quantified by a Nanodrop, and the global DNA methylation levels were determined by measuring the levels of 5-mC using a 5-mC DNA ELISA Kit (Zymo Research, D5325) following the manufacturer's protocol. One hundred nanograms of genomic DNA was measured per well, and independent samples were run in triplicate. The absorbance was analyzed at 420 nm using a microplate reader. The mean percentages of 5-mC were calculated using the second-order regression equation of the standard curve as described in the manufacturer's protocol.

## Western Blot

The proteins from the hippocampus were separated using a 10-12% SDS-PAGE gel and transferred to PVDF membranes. The membranes were blocked with 5% fat-free milk for 1 h at room temperature and incubated with primary antibodies overnight at 4°C; the primary antibodies included anti-CRMP2 (1:20,000; Abcam, ab129082); anti-pCRMP2 (Thr514 site) (7 μl: 5 ml; Abcam, ab85934); anti-DNMT1 (1:5,000); anti-DNMT3a (1:5,000); anti-DNMT3b (1:5,000); anti-α-tubulin (1:5,000; Abcam, ab7291); anti-Tyr-Tubulin (1:2,500; Sigma, T9028); anti-Acet-Tubulin (1:200; Santa Cruz Biochemistry, sc-23950); and anti-GAPDH (1:5,000; Beyotime, AF1186). After washing three times, the membranes were incubated with the appropriate horseradish peroxidase (HRP)-conjugated secondary antibodies (Beyotime, 1:5,000) at room temperature for 1 h. Then, the membranes were visualized by an ECL chemiluminescent detection kit (Beyotime, P0018S), and the intensities of the protein bands were calculated by ImageJ software. The relative expression of the proteins was normalized to that of GAPDH.

## Co-immunoprecipitation Analysis

Total protein (500 μg) was incubated with anti-CRMP2 (1:50; Abcam, ab129082) or anti-α-tubulin (1:50) (Abcam, ab7291) overnight at 4°C. An equal amount of protein was incubated with mouse IgG (Beyotime, A7028) or rabbit IgG (Beyotime, A7016) as negative controls. The protein samples were loaded as the input control. Protein A + G agarose (Beyotime, P2012) was washed with PBS three times and mixed with the samples. The mixtures were incubated at 4°C for 2 h. The beads were then washed with PBS three times. The immunoprecipitates were subsequently subjected to 12% SDS-PAGE and analyzed *via* western blot using anti-α-tubulin (1:5,000) or anti-CRMP2 (1:20,000) antibodies. The protein bands were visualized using an ECL chemiluminescent detection kit (Beyotime, P0018S).

## Statistical Analysis

Statistical analysis was performed using SPSS 20.0 software, and the data are expressed as the mean ± standard error of the mean (SEM). The normality of the data distribution was analyzed. For differences between the two groups, Student's *t*-test was used to determine statistical significance. For multiple

comparisons, ANOVA followed by an LSD *post hoc* test was used. Differences were considered to be statistically significant at $P < 0.05$.

# RESULTS

## Effect of CUMS and Fluoxetine Treatment on Depressive-Like Behaviors

CUMS-induced behavioral changes were measured using the SPT, OFT, and FST. There were significant differences in the sucrose preference, distance traveled, rearing frequency and velocity in the OFT among the three groups (sucrose preference: $F = 39.24$, $P < 0.05$, **Figure 2A**; distance traveled: $F = 20.34$, $P < 0.05$, **Figure 2C**; rearing frequency: $F = 13.99$, $P < 0.05$, **Figure 2D**; velocity: $F = 16.13$, $P < 0.05$, **Figure 2E**). Compared with the rats in the control group, the rats in the CUMS group displayed significantly decreased sucrose preference ($P < 0.05$), distance traveled ($P < 0.05$), rearing frequency ($P < 0.05$), and velocity ($P < 0.05$). Treatment with fluoxetine for 4 weeks significantly alleviated depressive behaviors in the rats. Fluoxetine administration significantly reversed the decrease in sucrose preference ($P < 0.05$), distance traveled ($P < 0.05$), rearing frequency ($P < 0.05$), and velocity ($P < 0.05$) in the stressed rats. Moreover, there were significant differences in immobility time in the FST among the three groups ($F = 16.70$, $P < 0.05$, **Figure 2B**). Compared with the rats in the control group, after exposure to CUMS for 4 weeks, the rats in the CUMS group exhibited significantly increased immobility times in the FST ($P < 0.05$), and the rats treated with fluoxetine exhibited significantly decreased immobility times compared to the rats exposed to CUMS alone ($P < 0.05$).

## Effect of CUMS and Fluoxetine Treatment on DNA Methylation in the CRMP2 Promoter

Using MethPrimer online software, 1 CpG island region located from −694 to −105 with 29 CpG sites was identified based on the CRMP2 promoter sequence (**Figure 3A**). The CpG island sequence in the CRMP2 promoter is shown in **Figure 3B**, and the CG dinucleotides are highlighted. CpG islands are regions of genomic DNA enriched for CG dinucleotides. Treatment of genomic DNA with bisulfite resulted in the conversion of unmethylated cytosine to uracil, however, the methylated cytosine remains unchanged. The DNA methylation rate was calculated as the "CG" sites divided by the sum of the "CG" + "TG" sites. In the CpG island region, the BSP results showed that the DNA methylation of CRMP2 in the hippocampus of rats exposed to CUMS was increased compared with that in the hippocampus of control rats, and fluoxetine treatment significantly decreased the DNA methylation in the CRMP2 promoter (DNA methylation rate: control group: 6.0 ± 0.9%; CUMS group: 11.6 ± 1.9%; fluoxetine group: 7.3 ± 1.2%; $F = 4.27$, $P < 0.05$, **Figures 3C,D**).

## Effect of CUMS and Fluoxetine Treatment on DNMT Expression

Western blotting was conducted to evaluate the effect of CUMS and fluoxetine treatment on the expression of DNMTs. Compared with that in the control group, the

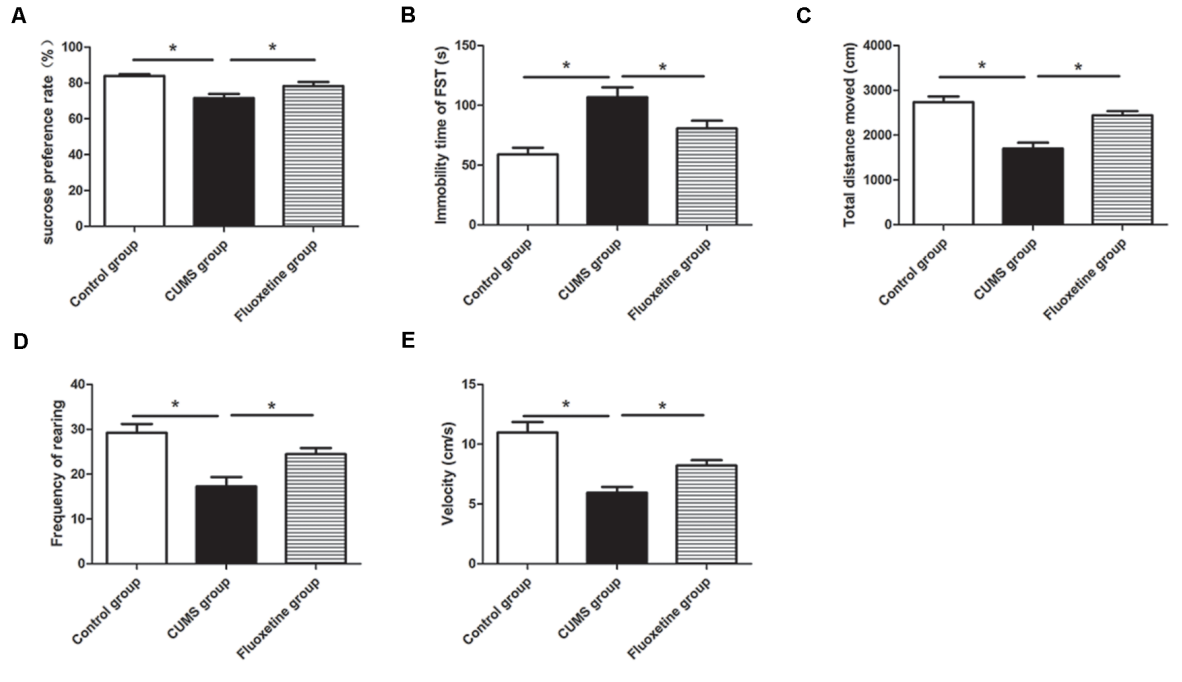


**FIGURE 2 |** Effect of chronic unpredictable mild stress (CUMS) and fluoxetine treatment on depressive-like behaviors: sucrose preference rate in the sucrose preference test (SPT; **A**), immobility time in the FST **(B)**, total distance traveled **(C)**, rearing frequency **(D)**, and velocity **(E)** in the open field test (OFT). *$P < 0.05$.

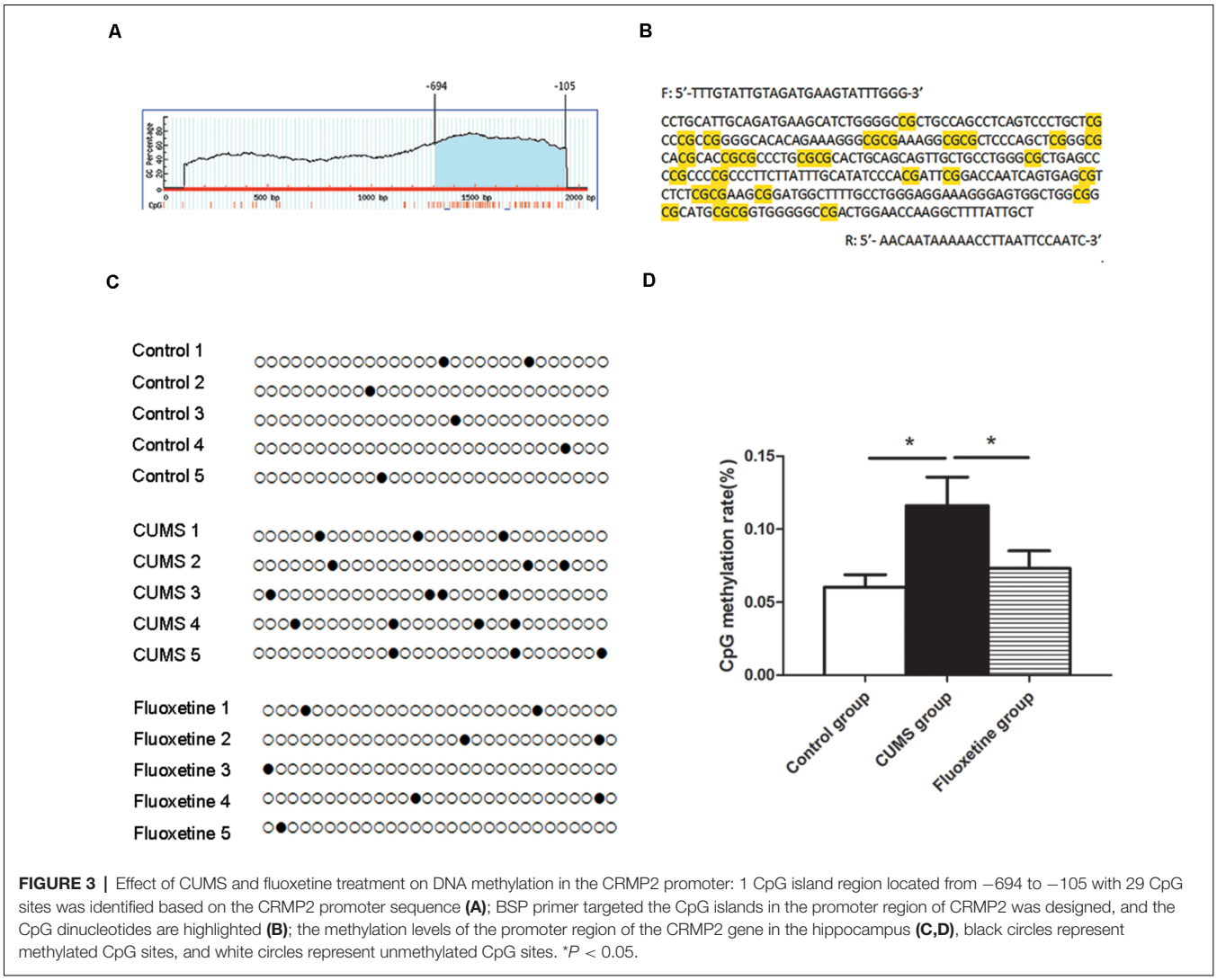


**FIGURE 3 |** Effect of CUMS and fluoxetine treatment on DNA methylation in the CRMP2 promoter: 1 CpG island region located from −694 to −105 with 29 CpG sites was identified based on the CRMP2 promoter sequence **(A)**; BSP primer targeted the CpG islands in the promoter region of CRMP2 was designed, and the CpG dinucleotides are highlighted **(B)**; the methylation levels of the promoter region of the CRMP2 gene in the hippocampus **(C,D)**, black circles represent methylated CpG sites, and white circles represent unmethylated CpG sites. *$P < 0.05$.

protein expression of DNMT1 and DNMT3a was significantly increased in the hippocampus of the CUMS group, and fluoxetine administration significantly downregulated the protein expression of DNMT1 and DNMT3a (DNMT1 $F = 7.39$, $P < 0.05$, **Figure 4C**; DNMT3a $F = 6.74$, $P < 0.05$, **Figure 4D**; DNMT3b $F = 0.46$, $P > 0.05$, **Figure 4E**).

## Effect of CUMS and Fluoxetine Treatment on CRMP2, pCRMP2, and α-Tubulin Isoform Expression

Compared with that in the control group, CRMP2 protein expression was decreased in the hippocampus of the CUMS group, and fluoxetine treatment increased CRMP2 protein expression ($F = 7.11$, $P < 0.05$, **Figure 4A**). The pCRMP2 protein expression in the hippocampus of rats exposed to CUMS was significantly higher than that observed in the control rats and rats treated with fluoxetine ($F = 9.07$, $P < 0.05$, **Figure 4B**). We further explored the α-tubulin, Tyr-Tubulin, and Acet-Tubulin protein expression in the three groups. The results showed that the α-tubulin protein expression in the hippocampus of the rats in each group was not significantly different ($F = 0.68$, $P > 0.05$, **Figure 4F**). Compared with those in the control group, Tyr-tubulin protein expression was downregulated and Acet-tubulin protein expression was upregulated in the hippocampus of the CUMS group, and fluoxetine treatment reversed these changes (Tyr-tubulin: $F = 7.47$, $P < 0.05$, **Figure 4G**; Acet-tubulin: $F = 6.41$, $P < 0.05$, **Figure 4H**).

## Effect of CUMS and Fluoxetine Treatment on the Interaction Between CRMP2 and α-Tubulin

To investigate the interaction between CRMP2 and α-tubulin, Co-immunoprecipitation was performed using an anti-CRMP2 antibody to precipitate α-tubulin and an anti-α-tubulin antibody to precipitate CRMP2. Both types of experiments confirmed the interaction between CRMP2 and α-tubulin in the hippocampus of rats. First, anti-CRMP2 was used for immunoprecipitation, and anti-α-tubulin was used for western blotting. Compared

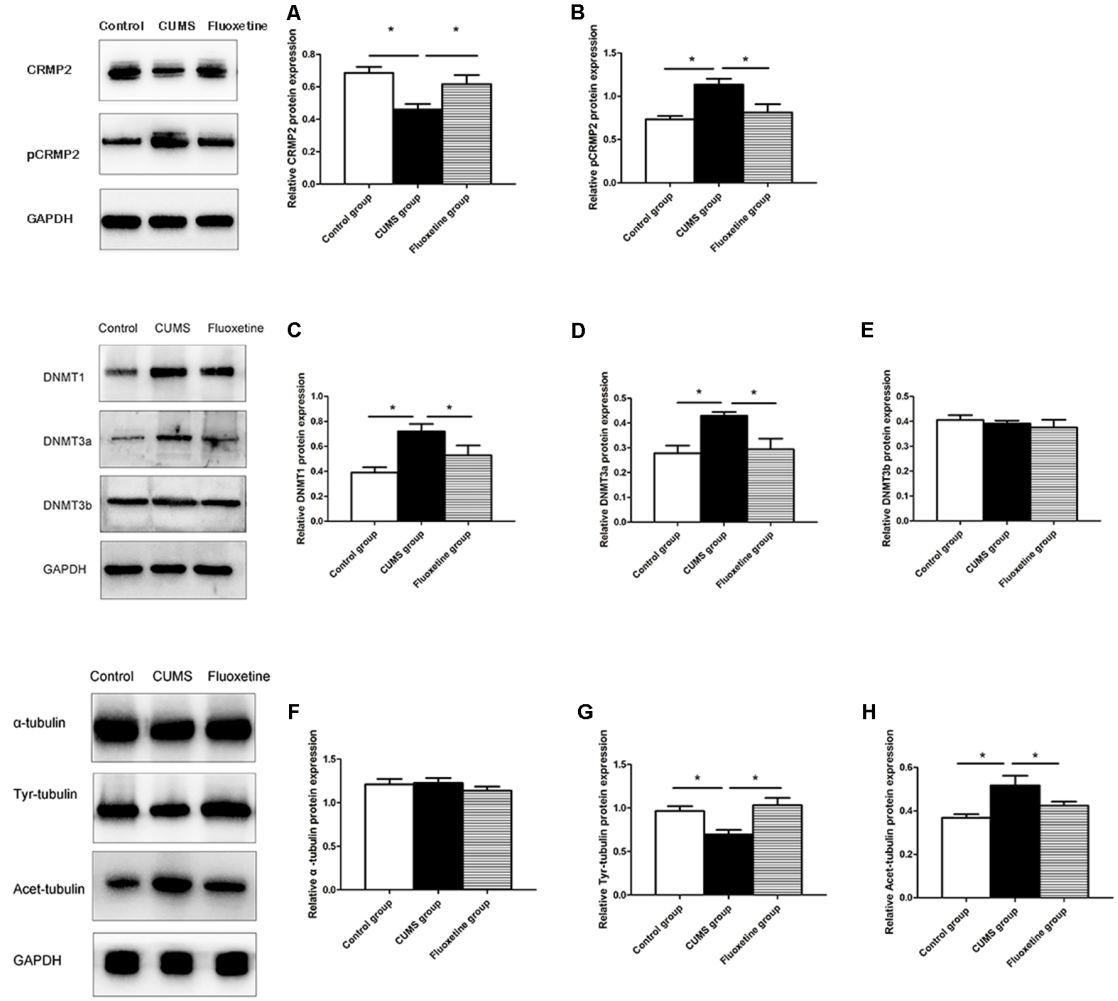


**FIGURE 4 |** Effect of CUMS and fluoxetine treatment on CRMP2 **(A)**, pCRMP2 **(B)**, DNMTs (DNMT1: **C**; DNMT3a: **D**; DNMT3b: **E**), and α-tubulin isoform (α-tubulin: **F**; Tyr-tubulin: **G**; Acet-tubulin: **H**) expression in the hippocampus of rats. *$P < 0.05$.

with that in the control group, the CRMP2-α-tubulin interaction was decreased in the hippocampus of the CUMS group, and it was increased after fluoxetine treatment ($F = 4.92$, $P < 0.05$, **Figure 5A**). Similarly, anti-α-tubulin was used for immunoprecipitation, and anti-CRMP2 was used for western blot. The α-tubulin-CRMP2 interaction was comparatively weaker in the CUMS group ($F = 5.03$, $P < 0.05$, **Figure 5B**).

## Effect of Microinjecting 5-aza Into the Hippocampal CA1 Region on Depressive-Like Behaviors

The SPT, OFT, and FST were used to evaluate the effects of microinjecting 5-aza into the CA1 region of the hippocampus on depressive-like behaviors. The results showed that compared with those of the rats in the CUMS + Nacl group, the distance traveled, rearing frequency, and velocity of the rats in the CUMS + 5-aza group were remarkably increased (distance traveled: $t = -3.75$, $P < 0.05$, **Figure 6C**; rearing frequency: $t = -2.31$, $P < 0.05$, **Figure 6D**; velocity: $t = -3.19$, $P < 0.05$, **Figure 6E**), and the immobility time in the FST of the rats of the CUMS + 5-aza group was significantly decreased ($t = 2.30$, $P < 0.05$, **Figure 6B**). However, no significant difference was observed in the sucrose preference of the rats in the CUMS + 5-aza group, although it tended to increase ($t = -0.55$, $P > 0.05$, **Figure 6A**).

## Effect of 5-aza Administration on Global DNA Methylation in the CA1 Region of the Hippocampus

The percentages of 5-mC of total DNA were measured as an indication of global DNA methylation levels. The 5-mC ELISA test was used to evaluate the effect of 5-aza treatment on global DNA methylation levels in the hippocampal CA1 region of rats. The results showed that microinjecting 5-aza into the CA1 region of the hippocampus significantly reduced the percent levels of global DNA methylation ($t = 2.39$, $P < 0.05$, **Figure 7**).

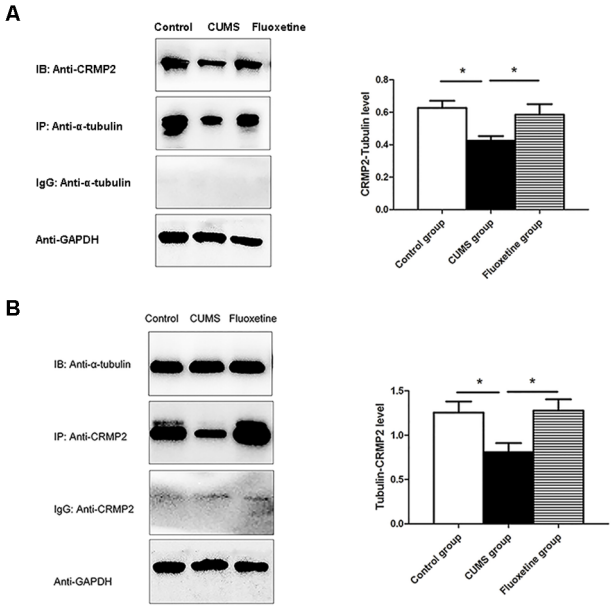


**FIGURE 5 |** Effect of CUMS and fluoxetine treatment on the interaction between CRMP2 and α-tubulin **(A,B)**. *$P < 0.05$.

## Effect of 5-aza Treatment on CRMP2, pCRMP2, and α-Tubulin Isoform Expression

Compared with those in the rats in the CUMS + Nacl group, CRMP2 protein expression was increased and pCRMP2 protein expression was decreased in the hippocampal CA1 region of the rats in the CUMS + 5-aza group (CRMP2: $t = -2.44$, $P < 0.05$, **Figure 8A**; pCRMP2: $t = 3.62$, $P < 0.05$, **Figure 8B**). Additionally, 5-aza treatment increased Tyr-Tubulin protein expression and decreased Acet-tubulin protein expression in the hippocampal CA1 region of the rats (α-tubulin $t = 1.543$, $P > 0.05$, **Figure 8C**; Tyr-Tubulin: $t = -2.59$, $P < 0.05$, **Figure 8D**; Acet-tubulin: $t = 2.65$, $P < 0.05$, **Figure 8E**).

## Effect of 5-aza Treatment on the Interaction Between CRMP2 and α-Tubulin

Co-immunoprecipitation was performed to assess the interaction between CRMP2 and α-tubulin in the hippocampal CA1 region of the 5-aza-treated rats. The CRMP2-α-tubulin interaction was also observed in the hippocampal CA1 region of the rats. The results showed that the α-tubulin band was detected in the immunoprecipitate of the anti-CRMP2 antibody. Compared with that in rats in the CUMS + Nacl group, the CRMP2-α-tubulin interaction was increased in the hippocampal CA1 region of the rats in the CUMS + 5-aza group ($t = -4.00$, $P < 0.05$, **Figure 9A**). Similarly, a CRMP2 band was detected in the immunoprecipitate of the anti-α-tubulin antibody. The α-tubulin-CRMP2 interaction also increased after 5-aza administration in the hippocampal CA1 region of rats ($t = -3.97$, $P < 0.05$, **Figure 9B**).

# DISCUSSION

The CUMS rat model has been widely used to study mechanisms of depressive-like behaviors and actions of antidepressants.

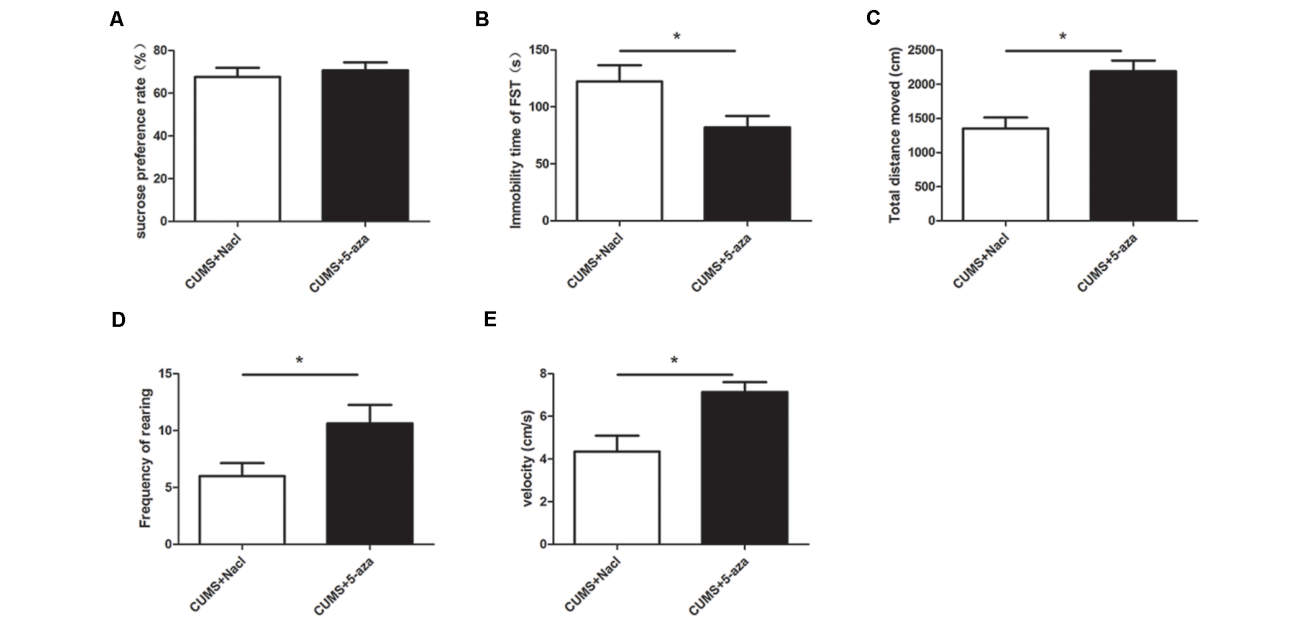


**FIGURE 6 |** Effect of microinjecting 5-aza into the hippocampal CA1 region on depressive-like behaviors: sucrose preference rate in the SPT **(A)**, immobility time in the FST **(B)**, total distance traveled **(C)**, rearing frequency **(D)**, and velocity **(E)** in the OFT. *$P < 0.05$.

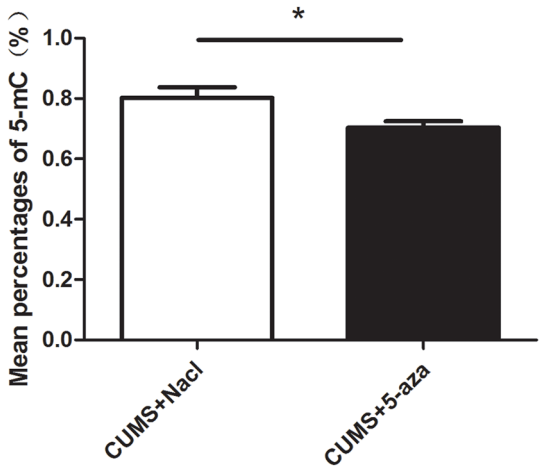


**FIGURE 7 |** Effect of 5-aza administration on global DNA methylation in the CA1 region of the hippocampus. *$P < 0.05$.

The SPT was used to assess anhedonia, which is one of the core symptoms of depression (Anisman and Matheson, 2005). The OFT was performed to assess general locomotor activity. Immobility time in the FST was used to evaluate the symptom of helplessness in a rat model of depression (Paré, 1992). In this study, the rat model of depression was successfully established by exposure to CUMS for 4 weeks. The rats exposed to CUMS showed reduced sucrose intake in the SPT, reduced distance traveled, rearing frequency and velocity in the OFT, and longer immobility time in the FST, which were similar to results from previous studies (Ayuob, 2017; Liu et al., 2018). Chronic fluoxetine treatment reversed the reduction in sucrose preference in the SPT, distance traveled, rearing frequency and velocity in the OFT, and increased immobility time in the FST, which indicated that fluoxetine has antidepressant-like effects.

In the present study, we investigated the effect of CUMS and fluoxetine treatment on the expression of DNMTs in the hippocampus of rats. DNA methylation in mammals is catalyzed by three main DNMTs: DNMT1, DNMT3a, and DNMT3b. We observed an upregulation of DNMT1 and DNMT3a in the hippocampus of stressed rats, and fluoxetine treatment significantly downregulated the expression of DNMT1 and DNMT3a. We further explored the CRMP2 expression and DNA methylation levels in the hippocampus of rats. Our data showed a downregulation of the CRMP2 protein levels in the hippocampus of stressed rats, and fluoxetine treatment upregulated the CRMP2 protein levels. This finding proves the results of previous publications, which showed a decrease in CRMP2 in the hippocampus of an animal model of depression (Carboni et al., 2006). Furthermore, we initially analyzed the CpG island DNA methylation levels in the CRMP2 promoter region, and the results showed that the rate of DNA methylation in the CpG island of the CRMP2 promoter region in the hippocampus of stressed rats was significantly higher than that in the hippocampus of control rats. Fluoxetine treatment significantly decreased the CpG island DNA methylation levels

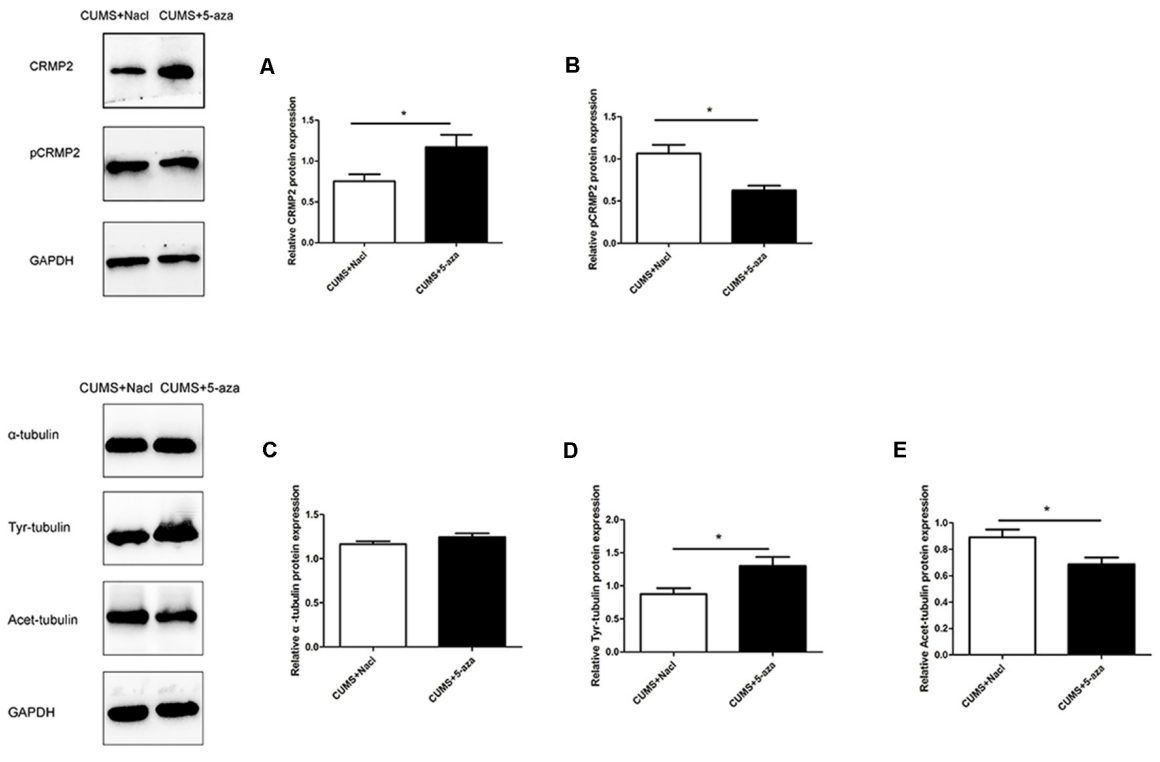


**FIGURE 8 |** Effect of 5-aza treatment on CRMP2 **(A)**, pCRMP2 **(B)**, and α-tubulin (α-tubulin: **C**; Tyr-tubulin: **D**; Acet-tubulin: **E**) isoform expression. *$P < 0.05$.

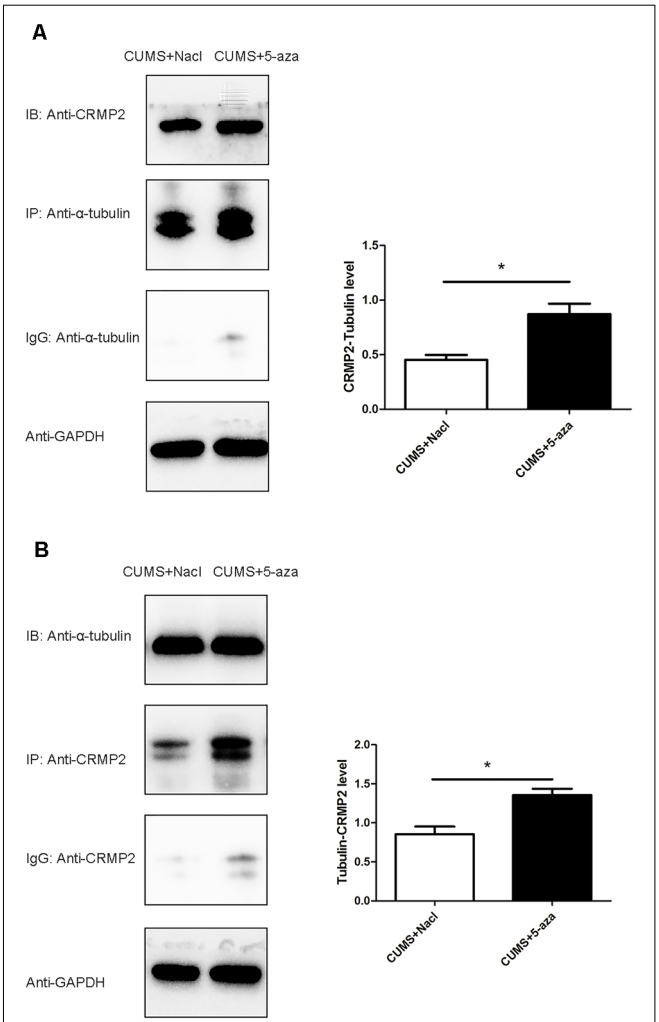


**FIGURE 9 |** Effect of 5-aza treatment on the interaction between CRMP2 and α-tubulin **(A,B)**. *$P < 0.05$.

in the CRMP2 promoter region. Previous studies have suggested that the silencing or low expression of genes is due to CpG island DNA methylation, which is associated with high DNMTs expression (Tammen et al., 2013). Therefore, our results demonstrated that DNMT1 and DNMT3a regulate the level of DNA methylation in the CRMP2 gene promoter region, thus affecting the expression of CRMP2 in the hippocampus of rats and participating in the pathogenesis of depression.

Current evidence supports the idea that CRMP2 contributes to the etiology of depression. However, the regulatory mechanisms underlying the role of CRMP2 remain unclear. CRMP2 is involved in neuronal migration, axonal growth, dendritic development, and synaptic plasticity (Ip et al., 2014). The cytoskeletal microtubular system is essential for the remodeling and extension of axons and dendrites (Bianchi et al., 2005a). CRMP2 acts as a signaling phosphoprotein that modulates cytoskeletal organization and participates in neurite formation and axonal outgrowth. The phosphorylation of CRMP2 might change its binding partners and functions (Zhu et al., 2010). The dynamics of the cytoskeletal microtubular system are strictly correlated with neuronal plasticity (Bianchi et al., 2005b). Therefore, in the present study, we analyzed the functions of CRMP2 in the cytoskeletal microtubular system. The results showed that exposure to CUMS for 4 weeks induced a decrease in CRMP2 expression and an increase in pCRMP2 expression in the hippocampus of rats, and chronic fluoxetine treatment reversed these effects on the expression of CRMP2 and pCRMP2. Additionally, the co-immunoprecipitation results showed that CRMP2 formed a complex with α-tubulin. Compared with that in the control group and fluoxetine group, the CRMP2-α-tubulin interaction in the CUMS group was comparatively weaker. We further examined microtubule dynamics by analyzing Acet-tubulin and Tyr-tubulin. Together with previous findings (Bianchi et al., 2003), our data showed that exposure to CUMS for 4 weeks decreased the expression of Tyr-tubulin, which is associated with the dynamic form of microtubules; these results indicated decreased microtubule dynamics. Chronic fluoxetine treatment decreased the stable form of microtubule Acet-tubulin, suggesting that fluoxetine could be effective in rescuing microtubule stabilization in the hippocampus of stressed rats. These data suggest that CRMP2 is involved in the pathogenesis of depression by regulating the cytoskeletal microtubule system.

Environmental stress was shown to upregulate the expression of specific DNMTs in the hippocampus and to change the expression of depression-related candidate proteins (Menke and Binder, 2014). In the present study, stressed rats that exhibit depressive behaviors showed an upregulation of the DNMT1 and DNMT3a proteins in the hippocampus. Considering the susceptibility of the hippocampal CA1 region to stress, we investigated the involvement of DNA methylation in the regulation of CUMS-induced depressive-like behaviors and the underlying mechanisms by injecting 5-aza into the hippocampal CA1 regions of rats. In our study, microinjecting 5-aza into the hippocampal CA1 region effectively reduced global DNA methylation, suggesting that 5-aza treatment effectively altered the DNA methylation status and might be used in subsequent studies. Additionally, injection of 5-aza into the hippocampal CA1 region of rats induced antidepressant-like effects, including increased distance traveled, rearing frequency and velocity in the OFT, and decreased immobility time in the FST. Our findings supported the possibility that DNA methylation in the hippocampal CA1 region is crucial for the development of depressive-like behaviors.

Previous data indicate that an increase in DNA methylation at specific genomic sites may reduce gene expression (Boyes and Bird, 1992). These genes may play an important role under stress conditions and, therefore, predispose to the development of stress-induced depressive-like behaviors. In the present study, 5-aza treatment not only exerted antidepressant-like effects and reduced DNA methylation but also significantly increased CRMP2 protein expression in the hippocampal CA1 region, further supporting the notion

that DNA methylation-dependent CRMP2 gene expression is involved in the pathogenesis of depression. Additionally, 5-aza treatment increased Tyr-Tubulin protein expression and decreased Acet-tubulin protein expression in the hippocampal CA1 regions of rats, indicating that 5-aza could increase microtubule dynamics. The α-tubulin-CRMP2 interaction also increased after 5-aza injection into the hippocampal CA1 regions of rats. These results further suggest that the DNA methylation-mediated regulation of CRMP2 is indicative of its role in the cytoskeletal microtubule system in depression.

In recent years, there has been increasing interest in the correlation between depression and cerebrovascular disease. Cerebral infarction increases the incidence of post-stroke depression, with increased morbidity and mortality, which has become a common and acute disease. Several studies have reported the changes in CRMP2 expression during the process of ischemia (Chen et al., 2007; Yang et al., 2016). Proteomic technology has revealed elevation of CRMP2 protein expression in the ischemic brain of rats (Koh, 2011). In a rodent study, the result found higher BDNF promoter IV methylation levels in the hippocampus of post-stroke depression (Jin et al., 2017). Based on these findings, it would be worth exploring the underlying mechanisms of CRMP2 DNA methylation in the pathological processes of post-stroke depression.

Taken together, our results identified a crucial role of CRMP2 in the pathogenesis of depression. These observations implicate DNA methylation in the molecular mechanisms that control stress-induced depressive-like behaviors and could ultimately lead to the development of improved treatment for depression. However, some questions remain in this study. As a broad-spectrum inhibitor of DNA methylation, 5-aza lacks gene-specific effects. Further studies using inhibitors of gene-specific DNA methylation are necessary to explore the role of CRMP2 in depression. Additionally, we did not verify our findings *in vitro* in this study, and an *in vitro* cell model should be established in future studies.

## DATA AVAILABILITY STATEMENT

The original contributions presented in the study are included in the article, further inquiries can be directed to the corresponding authors.

## ETHICS STATEMENT

The animal study was reviewed and approved and all the procedures and animal experiments of this study were performed in agreement with the guidelines outlined in the legislation of the P.R. China regarding the ethical use of laboratory animals and approved by the Institutional Animals Care Committee of Renmin Hospital of Wuhan University.

## AUTHOR CONTRIBUTIONS

ZL was responsible for funding acquisition. GW and ZL designed and supervised the study. DX and SS carried out the experimental procedures and analyzed the date. ZL and DX interpreted results of experiments and drafted the manuscript. GW and ZL revised the manuscript. All authors provided feedback on manuscript. All authors contributed to the article and approved the submitted version.

## FUNDING

This study was supported by grants from the National Key R&D Program of China (2018YFC1314600) and the National Natural Science Foundation of China (81771472 and 81271496).

## REFERENCES

Anisman, H., and Matheson, K. (2005). Stress, depression and anhedonia: caveats concerning animal models. *Neurosci. Biobehav. Rev.* 29, 525–546. doi: 10.1016/j.neubiorev.2005.03.007

Ayuob, N. N. (2017). Evaluation of the antidepressant-like effect of musk in an animal model of depression: How it works. *Anat. Sci. Int.* 92, 539–553. doi: 10.1007/s12565-016-0357-7

Bianchi, M., Fone, K. F., Azmi, N., Heidbreder, C. A., Hagan, J. J., and Marsden, C. A. (2006). Isolation rearing induces recognition memory deficits accompanied by cytoskeletal alterations in rat hippocampus. *Eur. J. Neurosci.* 24, 2894–2902. doi: 10.1111/j.1460-9568.2006.05170.x

Bianchi, M., Hagan, J. J., and Heidbreder, C. A. (2005). Neuronal plasticity, stress and depression: involvement of the cytoskeletal microtubular system? *Curr. Drug Targets CNS Neurol. Disord.* 4, 597–611. doi: 10.2174/156800705774322012

Bianchi, M., Heidbreder, C., and Crespi, F. (2003). Cytoskeletal changes in the hippocampus following restraint stress: role of serotonin and microtubules. *Synapse* 49, 188–194. doi: 10.1002/syn.10230

Boyes, J., and Bird, A. (1992). Repression of genes by DNA methylation depends on CpG density and promoter strength: evidence for involvement of a methyl-CpG binding protein. *EMBO J.* 11, 327–333.

Carboni, L., Vighini, M., Piubelli, C., Castelletti, L., Milli, A., and Domenici, E. (2006). Proteomic analysis of rat hippocampus and frontal cortex after chronic treatment with fluoxetine or putative novel antidepressants: CRF1 and NK1 receptor antagonists. *Eur. Neuropsychopharmacol.* 16, 521–537. doi: 10.1016/j.euroneuro.2006.01.007

Chen, A., Liao, W. P., Lu, Q., Wong, W. S., and Wong, P. T.-H. (2007). Upregulation of dihydropyrimidinase-related protein 2, spectrin alpha II chain, heat shock cognate protein 70 pseudogene 1 and tropomodulin 2 after focal cerebral ischemia in rats—a proteomics approach. *Neurochem. Int.* 50, 1078–1086. doi: 10.1016/j.neuint.2006.11.008

Chen, D., Meng, L., Pei, F., Zheng, Y., and Leng, J. (2017). A review of DNA methylation in depression. *J. Clin. Neurosci.* 43, 39–46. doi: 10.1016/j.jocn.2017.05.022

Fukata, Y., Itoh, T. J., Kimura, T., Ménager, C., Nishimura, T., Shiromizu, T., et al. (2002). CRMP-2 binds to tubulin heterodimers to promote microtubule assembly. *Nat. Cell Biol.* 4, 583–591. doi: 10.1038/ncb825

Gu, Y., and Ihara, Y. (2000). Evidence that collapsin response mediator protein-2 is involved in the dynamics of microtubules. *J. Biol. Chem.* 275, 17917–17920. doi: 10.1074/jbc.C000179200

Ignácio, Z. M., Réus, G. Z., Abelaira, H. M., Maciel, A. L., de Moura, A. B., Matos, D., et al. (2017). Quetiapine treatment reverses depressive-like behavior and reduces DNA methyltransferase activity induced by maternal deprivation. *Behav. Brain Res.* 320, 225–232. doi: 10.1016/j.bbr.2016.11.044

Inagaki, N., Chihara, K., Arimura, N., Ménager, C., Kawano, Y., Matsuo, N., et al. (2001). CRMP-2 induces axons in cultured hippocampal neurons. *Nat. Neurosci.* 4, 781–782. doi: 10.1038/90476

Ip, J. P. K., Fu, A. K., and Ip, N. Y. (2014). CRMP2: functional roles in neural development and therapeutic potential in neurological diseases. *Neuroscientist* 20, 589–598. doi: 10.1177/1073858413514278

Januar, V., Ancelin, M. L., Ritchie, K., Saffery, R., and Ryan, J. (2015). BDNF promoter methylation and genetic variation in late-life depression. *Transl. Psychiatry* 5:e619. doi: 10.1038/tp.2015.114

Jin, H. J., Pei, L., Li, Y. N., Zheng, H., Yang, S., Wan, Y., et al. (2017). Alleviative effects of fluoxetine on depressive-like behaviors by epigenetic regulation of BDNF gene transcription in mouse model of post-stroke depression. *Sci. Rep.* 7:14926. doi: 10.1038/s41598-017-13929-5

Johnston-Wilson, N. L., Sims, C. D., Hofmann, J. P., Anderson, L., Shore, A. D., Torrey, E. F., et al. (2000). Disease-specific alterations in frontal cortex brain proteins in schizophrenia, bipolar disorder and major depressive disorder. The stanley neuropathology consortium. *Mol. Psychiatry* 5, 142–149. doi: 10.1038/sj.mp.4000696

Kader, F., Ghai, M., and Maharaj, L. (2018). The effects of DNA methylation on human psychology. *Behav. Brain Res.* 346, 47–65. doi: 10.1016/j.bbr.2017.12.004

Khawaja, X., Xu, J., Liang, J. J., and Barrett, J. E. (2004). Proteomic analysis of protein changes developing in rat hippocampus after chronic antidepressant treatment: implications for depressive disorders and future therapies. *J. Neurosci. Res.* 75, 451–460. doi: 10.1002/jnr.10869

Koh, P. O. (2011). Identification of proteins differentially expressed in cerebral cortexes of Ginkgo biloba extract (EGb761)-treated rats in a middle cerebral artery occlusion model—a proteomics approach. *Am. J. Chin. Med.* 39, 315–324. doi: 10.1142/S0192415X11008841

Kolovos, S., Bosmans, J. E., Riper, H., Chevreul, K., Coupé, V., and van Tulder, M. W. (2017). Model-based economic evaluation of treatments for depression: a systematic literature review. *PharmacoEconomics Open* 1, 149–165. doi: 10.1007/s41669-017-0014-7

Lisoway, A. J., Zai, C. C., Tiwari, A. K., and Kennedy, J. L. (2018). DNA methylation and clinical response to antidepressant medication in major depressive disorder: a review and recommendations. *Neurosci. Lett.* 669, 14–23. doi: 10.1016/j.neulet.2016.12.071

Liu, W., Xue, X., Xia, J., Liu, J., and Qi, Z. (2018). Swimming exercise reverses CUMS-induced changes in depression-like behaviors and hippocampal plasticity-related proteins. *J. Affect. Disord.* 227, 126–135. doi: 10.1016/j.jad.2017.10.019

Mahgoub, M., and Monteggia, L. M. (2013). Epigenetics and psychiatry. *Neurotherapeutics* 10, 734–741. doi: 10.1007/s13311-013-0213-6

Menke, A., and Binder, E. B. (2014). Epigenetic alterations in depression and antidepressant treatment. *Dialogues Clin. Neurosci.* 16, 395–404. doi: 10.31887/DCNS.2014.16.3/amenke

Niwa, S., Nakamura, F., Tomabechi, Y., Aoki, M., Shigematsu, H., Matsumoto, T., et al. (2017). Structural basis for CRMP2-induced axonal microtubule formation. *Sci. Rep.* 7:10681. doi: 10.1038/s41598-017-11031-4

Okano, M., Bell, D. W., Haber, D. A., and Li, E. (1999). DNA methyltransferases Dnmt3a and Dnmt3b are essential for de novo methylation and mammalian development. *Cell* 99, 247–257. doi: 10.1016/s0092-8674(00)81656-6

Paré, W. P. (1992). Learning behavior, escape behavior and depression in an ulcer susceptible rat strain. *Integr. Physiol. Behav. Sci.* 27, 130–141. doi: 10.1007/BF02698502

Philibert, R. A., Sandhu, H., Hollenbeck, N., Gunter, T., Adams, W., and Madan, A. (2008). The relationship of 5HTT (SLC6A4) methylation and genotype on mRNA expression and liability to major depression and alcohol dependence in subjects from the iowa adoption studies. *Am. J. Med. Genet. B Neuropsychiatr. Genet.* 147B, 543–549. doi: 10.1002/ajmg.b.30657

Quach, T. T., Honnorat, J., Kolattukudy, P. E., Khanna, R., and Duchemin, A. M. (2015). CRMPs: critical molecules for neurite morphogenesis and neuropsychiatric diseases. *Mol. Psychiatry* 20, 1037–1045. doi: 10.1038/mp.2015.77

Sales, A. J., Biojone, C., Terceti, M. S., Guimaraes, F. S., Gomes, M. V. M., and Joca, S. R. L. (2011). Antidepressant-like effect induced by systemic and intra-hippocampal administration of DNA methylation inhibitors. *Br. J. Pharmacol.* 164, 1711–1721. doi: 10.1111/j.1476-5381.2011.01489.x

Shen, X.-F., Yuan, H.-B., Wang, G.-Q., Xue, H., Liu, Y.-F., and Zhang, C.-X. (2019). Role of DNA hypomethylation in lateral habenular nucleus in the development of depressive-like behavior in rats. *J. Affect. Disord.* 252, 373–381. doi: 10.1016/j.jad.2019.03.062

Tammen, S. A., Friso, S., and Choi, S.-W. (2013). Epigenetics: the link between nature and nurture. *Mol. Aspects Med.* 34, 753–764. doi: 10.1016/j.mam.2012.07.018

Weaver, I. C., Cervoni, N., Champagne, F. A., D'Alessio, A. C., Sharma, S., Seckl, J. R., et al. (2004). Epigenetic programming by maternal behavior. *Nat. Neurosci.* 7, 847–854. doi: 10.1038/nn1276

Winter, G., Hart, R. A., Charlesworth, R., and Sharpley, C. F. (2018). Gut microbiome and depression: what we know and what we need to know. *Rev. Neurosci.* 29, 629–643. doi: 10.1515/revneuro-2017-0072

Wu, Z., Wang, G., Wei, Y., Xiao, L., and Wang, H. (2018). PI3K/AKT/GSK3beta/CRMP-2-mediated neuroplasticity in depression induced by stress. *Neuroreport* 29, 1256–1263. doi: 10.1097/WNR.0000000000001096

Xiang, D., Xiao, J., Fu, L., Yao, L., Wan, Q., Xiao, L., et al. (2019). DNA methylation of the Tacr2 gene in a CUMS model of depression. *Behav. Brain Res.* 365, 103–109. doi: 10.1016/j.bbr.2019.01.059

Xiang, D., Xiao, J., Sun, S., Fu, L., Yao, L., Wang, G., et al. (2020). Differential regulation of DNA methylation at the CRMP2 promoter region between the hippocampus and prefrontal cortex in a CUMS depression model. *Front. Psychiatry* 11:141. doi: 10.3389/fpsyt.2020.00141

Yamashita, N., and Goshima, Y. (2012). Collapsin response mediator proteins regulate neuronal development and plasticity by switching their phosphorylation status. *Mol. Neurobiol.* 45, 234–246. doi: 10.1007/s12035-012-8242-4

Yang, X., Zhang, X., Li, Y., Han, S., Howells, D. W., Li, S., et al. (2016). Conventional protein kinase Cbeta-mediated phosphorylation inhibits collapsin response-mediated protein 2 proteolysis and alleviates ischemic injury in cultured cortical neurons and ischemic stroke-induced mice. *J. Neurochem.* 137, 446–459. doi: 10.1111/jnc.13538

Zhao, J., Goldberg, J., Bremner, J. D., and Vaccarino, V. (2013). Association between promoter methylation of serotonin transporter gene and depressive symptoms: a monozygotic twin study. *Psychosom. Med.* 75, 523–529. doi: 10.1097/PSY.0b013e3182924cf4

Zhu, L.-Q., Zheng, H.-Y., Peng, C.-X., Liu, D., Li, H.-L., Wang, Q., et al. (2010). Protein phosphatase 2A facilitates axonogenesis by dephosphorylating CRMP2. *J. Neurosci.* 30, 3839–3848. doi: 10.1523/JNEUROSCI.5174-09.2010

**Conflict of Interest**: The authors declare that the research was conducted in the absence of any commercial or financial relationships that could be construed as a potential conflict of interest.

frontiers in Cellular Neuroscience

REVIEW
published: 21 April 2021
doi: 10.3389/fncel.2021.652647

# Inflammation-Mediated Angiogenesis in Ischemic Stroke

*Hua Zhu*[1,2†], *Yonggang Zhang*[1,2†], *Yi Zhong*[1], *Yingze Ye*[1], *Xinyao Hu*[3], *Lijuan Gu*[2,4*] and *Xiaoxing Xiong*[1,2*]

[1] Department of Neurosurgery, Renmin Hospital of Wuhan University, Wuhan, China, [2] Central Laboratory, Renmin Hospital of Wuhan University, Wuhan, China, [3] Department of Oncology, Renmin Hospital of Wuhan University, Wuhan, China, [4] Department of Anesthesiology, Renmin Hospital of Wuhan University, Wuhan, China

Stroke is the leading cause of disability and mortality in the world, but the pathogenesis of ischemic stroke (IS) is not completely clear and treatments are limited. Mounting evidence indicate that neovascularization is a critical defensive reaction to hypoxia that modulates the process of long-term neurologic recovery after IS. Angiogenesis is a complex process in which the original endothelial cells in blood vessels are differentiated, proliferated, migrated, and finally remolded into new blood vessels. Many immune cells and cytokines, as well as growth factors, are directly or indirectly involved in the regulation of angiogenesis. Inflammatory cells can affect endothelial cell proliferation, migration, and activation by secreting a variety of cytokines via various inflammation-relative signaling pathways and thus participate in the process of angiogenesis. However, the mechanism of inflammation-mediated angiogenesis has not been fully elucidated. Hence, this review aimed to discuss the mechanism of inflammation-mediated angiogenesis in IS and to provide new ideas for clinical treatment of IS.

**Keywords: angiogenesis, stroke, immune cells, inflammation, inflammatory cytokine**

OPEN ACCESS

***Edited by:***
*Ertugrul Kilic,*
*Istanbul Medipol University, Turkey*

***Reviewed by:***
*Ahmet Burak Caglayan,*
*Istanbul Medipol University, Turkey*
*Hulya Karatas,*
*Hacettepe University, Turkey*

***Correspondence:**
*Lijuan Gu*
*gulijuan@whu.edu.cn*
*Xiaoxing Xiong*
*xiaoxingxiong@whu.edu.cn*

[†]*These authors have contributed equally to this work*

***Specialty section:***
*This article was submitted to Cellular Neuropathology, a section of the journal Frontiers in Cellular Neuroscience*

***Received:*** *12 January 2021*
***Accepted:*** *16 February 2021*
***Published:*** *21 April 2021*

***Citation:***
*Zhu H, Zhang Y, Zhong Y, Ye Y, Hu X, Gu L and Xiong X (2021) Inflammation-Mediated Angiogenesis in Ischemic Stroke. Front. Cell. Neurosci. 15:652647. doi: 10.3389/fncel.2021.652647*

## INTRODUCTION

Ischemic stroke (IS) is one of the diseases with the highest incidence and disability rate in the world. Currently, the effective treatment measure for IS is thrombolytic therapy with tissue plasminogen activator to recirculate cerebral blood flow. However, due to the limitation of the treatment time window, only a small number of patients are suited to this treatment (Zhou et al., 2019). Thus, clarifying the pathogenesis and exploring new therapies are urgently needed to improve outcomes. Normal collateral circulation can effectively improve the blood flow supply of brain tissue. The extension of neovascularization from normal brain tissue to the ischemic penumbra and central necrotic area can improve the blood perfusion of the surrounding ischemic area, reduce the volume of cerebral infarction, remold the nerve structure, and restore the central nervous system (CNS) function. Therefore, more and more studies have been conducted to promote the formation of neovascularization in the ischemic and surrounding areas after IS. Immune cells, such as mononuclear macrophages, T cells, and microglia, are involved in angiogenesis after stroke through different mechanisms. Here, we focus on the role of immune cells and related cytokines in neurovascular remodeling after IS and discuss the potential therapies for stroke that target neurovascular remodeling.

## OVERVIEW OF ANGIOGENESIS

Angiogenesis, known as the formation of neovascularization that is induced by the sprouting of endothelial cells (ECs) from preexisting vessels, occurs under a variety of physiological (e.g., reproduction) and pathological (e.g., IS) conditions (Potente et al., 2011). During the sprouting process, ECs degrade the basement membrane, migrate into adjacent tissues, proliferate, and aggregate into tubes to form new blood vessels and establish blood flow. Basement membrane starts to form under the joint action of pericytes, ECs, and the microenvironment and further promotes the maturation and stability of new tubes, then finally completes the vascular remodeling (Marti et al., 2000). The proliferation and migration of ECs, increased vascular permeability, and the degradation of the surrounding stroma, as well as the stabilization and cessation of angiogenesis, are essential steps of angiogenesis (Hayashi et al., 2003). Under physiological state, angiogenesis is in the dynamic balance of the angiogenesis-promoting factor and the inhibiting factor. Once the balance is broken, insufficient angiogenesis will lead to slow wound healing, such as stroke. Angiogenesis can salvage cerebral blood flow and supply nutrients/oxygen to the ischemic brain tissue, finally rescuing grievous neurons and impaired tissues (Krupinski et al., 1994). An elevated vascular density in the brain ischemic penumbra region was observed 3 days after IS in animal and human brain specimens (Hayashi et al., 2003). Excessive angiogenesis is commonly seen in the occurrence, development, and metastasis of tumors.

## THE ROLE OF ANGIOGENESIS IN IS

Stroke is usually the result of focal cerebral ischemia caused by cerebral stenosis or occlusion. The blood flow of the brain tissue in the cerebrovascular region drops sharply, leading to a sharp decrease in the supply of oxygen and nutrients and eventually leading to tissue cell damage and even death. The potential mechanism of compensatory increased oxygen supply to ischemic brain tissue is the induction of new vessels. Neovascularization in the ischemic infarction area regulates the cerebral blood flow, neuron repair and regeneration, and the degree of functional recovery of patients as well as the functional reconstruction or rebuilding of synaptic connections between nerve cells (Pan et al., 2010). The collateral circulation in the initial phase of IS relies on the opening of a preexisting vascular network, while in the later period, it mainly depends on the formation of new blood vessels. New blood vessels begin to be observed at 3 days after IS and increase continuously for 21 days or more (del Zoppo and Mabuchi, 2003). Angiogenesis after stroke has therapeutic potential. Postmortem examination of the cerebral tissue of stroke patients with different survival times showed that the density of microvessels on the infarcted side was notably higher than that of the normal hemisphere on the opposite side. The number of new blood vessels around the infarct is positively correlated with the survival rate, survival time, and neurological function recovery of stroke patients (Krupinski et al., 1994). Other studies have found that patients with dementia show severe decreased cerebral blood flow in non-infarcted areas, indicating that angiogenesis can improve patients' daily activities by increasing cerebral blood flow (Schmidt et al., 2000). In a mouse model of middle cerebral artery occlusion (MCAO), proliferating ECs were found in the ischemic penumbra and were associated with increased vascular density (Kim et al., 2020). The ischemic penumbra, a structurally intact but functionally impaired region around the ischemic core area after cerebral infarction, is the main target of therapeutic intervention. Further exploration of the mechanism of angiogenesis after IS is conducive to research on more treatment options.

## INFLAMMATORY-MEDIATED ANGIOGENESIS AFTER IS

Previous studies have identified that various immune cell subgroups regulate angiogenesis, such as natural killer (NK) cells, T helper 17 (Th17) cells, regulatory T lymphocytes (Tregs), and a functional subset of macrophages (M2 macrophages) (la Sala et al., 2012). Numerous angiogenic growth factors, commonly associated with inflammatory response, including vascular endothelial growth factor (VEGF), tumor necrosis factor-α (TNF-α), monocyte chemotactic protein-1 (MCP-1/CCL2), transforming growth factor-β (TGF-β), fibroblast growth factor (FGF), granulocyte-macrophage colony-stimulating factor (GM-CSF)/granulocyte colony-stimulating factor (G-CSF), hepatocyte growth factor (HGF), platelet-derived growth factor (PDGF), and interleukins (ILs), play crucial roles in inflammatory-mediated angiogenesis after IS (Schierling et al., 2009). The molecular mechanisms of inflammation-mediated angiogenesis involved in IS are discussed below.

## THE ROLE OF IMMUNE CELL SUBSETS AND INFLAMMATORY CELLS IN ANGIOGENESIS AFTER IS

### NK Cells

NK cells, an important subgroup of immune cells, infiltrate into local ischemic brain tissue and act as a bridge between the immune system and the CNS in IS patients. NK cells are closely associated with immunosuppression, inflammation, and infection after IS (Chen et al., 2019). Studies have confirmed that in pathological and physiological conditions, NK cells produce cytokines that promote angiogenesis and independently regulate angiogenesis (Ribatti et al., 2019). IS leads to other complications, such as cerebral small vessel disease. In the cerebral microvasculature of spontaneously hypertensive (a model for early-onset cerebral small vessel disease) rats after IS, NK cells infiltrated markedly in the cerebral microvessels, leading to inflammatory reactions and hypertension-associated cognitive dysfunction (Kaiser et al., 2014). The activated NK cells are involved in endothelial and vascular function deficits by promoting the expression of interferon gamma (IFN-γ) (Kossmann et al., 2013). Angiogenesis is an important compensation method for arterial obstruction. In addition, NK

cells play crucial roles in cerebrovascular formation in hindlimb ischemia mice (van Weel et al., 2007).

## $CD4^+$ T Cells

$CD4^+$ T cells (consisting of Th1, Th2, Th17, and Tregs), which are responsible for inflammatory response, boost arteriogenesis in a murine model of hindlimb ischemia (Nossent et al., 2017). Moreover, $CD4^+$ T cells play essential roles in activating and polarizing macrophages, which have been demonstrated to have the ability to promote angiogenesis (Zhang et al., 2020). Th17 promotes angiogenesis and increases cerebral blood flow in the ischemic penumbra, partly owing to its potent effect in promoting the migration and sprouting of ECs (Kwee et al., 2018). The study has shown that hyperforin could promote subependymal ventricular zone angiogenesis, neurogenesis, and functional recovery through suppressing Th1 cell differentiation while facilitating Th2/Treg cell differentiation in the ischemic area, which is mediated by astrocyte IL-6 (Yao et al., 2019). Hence, it indicates that the infiltration of Th2 cells into the ischemic hemisphere increased Th2-derived cytokine IL-4, increased Treg-derived IL-10 and TGF-β, as well as decreased Th1 and Th1-derived cytokine IFN-γ, which are all key events that promote angiogenesis during stroke recovery.

## Microglia/Macrophage Cells

Resident microglia and infiltrated macrophages activate the immune defense in the CNS to regulate the inflammatory condition dynamically in the injured brain (Zhu et al., 2019). Microglia/macrophages can polarize into the M1 and M2 phenotypes to participate in IS damage or repair (Liu et al., 2018). M1 is known to be classically activated and to exert pro-inflammatory effects, whereas M2 is alternatively activated and plays an anti-inflammatory role in IS. M2 macrophages, a more heterogeneous phenotype, can be further divided into M2a and M2c according to their function. The M2a subset activated by IL-4 is regarded as the wound healing macrophages that also belong to the alternatively activated macrophages; the M2c subgroup activated by numerous stimulants, including glucocorticoids, immune complexes, and IL-10, as well as prostaglandins, is known as the regulatory macrophages.

Microglial/macrophage cells are also crucial to angiogenesis after IS. Evidence shows that increased microvessel density after IS was detected only in the regions also containing macrophages, suggesting that angiogenesis is related to the increased number of macrophages (Manoonkitiwongsa et al., 2001). Moreover, the brain may synthesize microvessels and open capillaries needed for macrophage infiltration for the destruction and removal of necrotic brain tissue via the angiogenic signaling cascade. Microglial activation and the related neuroinflammation in the ischemic penumbra region were alleviated by polarizing the microglia toward the M2 phenotype (Shang et al., 2020). Previous studies have indicated that M2 microglia/macrophages have a higher potential to promote angiogenesis than other subgroups. Moreover, FGF signaling for M2a- and placenta growth factor (PlGF) signaling for M2c-induced angiogenesis may be the possible working mechanisms (Jetten et al., 2014). Hence, further researches are needed to illustrate the exact mechanism of angiogenesis induced by M2.

## Brain Pericytes

Brain pericytes are perivascular cells that play a critical role in the regulation of capillary function and the development of cerebral microcirculation, and their location puts them in a crucial position to regulate the neuroinflammation at the neurovascular unit (NVU), which consists of neuronal cells, pericytes, ECs, astrocytes, microglia, and the extracellular matrix (Bell et al., 2010; Muoio et al., 2014). Brain pericytes are involved in a variety of brain functions, such as the generation and stabilization of the blood–brain barrier (BBB), brain inflammation, and tissue regeneration, as well as the propagation of CNS and peripheral inflammation (Umehara et al., 2018). Moreover, pericytes recently have been verified to exert many functions of immunomodulatory cells, including producing and responding to inflammatory cytokines, presenting antigen, and exhibiting phagocytosis. Hence, brain pericytes are increasingly considered to be mediators of neuroinflammation (Rustenhoven et al., 2017), thereby participating in inflammatory reaction during IS.

Previous studies have shown that the continuous constriction and necrocytosis of pericytes in the hyperacute phase leads to the no-reflow phenomenon, and the inflammatory responses and the separation of pericytes in the acute phase may exacerbate the BBB injury (Uemura et al., 2020). However, pericytes also exert a neuroprotective role via releasing neurotrophins, EC protection, and BBB stabilization (Franco et al., 2011; Winkler et al., 2011; Ishitsuka et al., 2012). Pericytes play a powerful role in neural restoration after IS via promoting angiogenesis and neurogenesis. The bidirectional ECs–pericytes signaling is essential during angiogenesis (Stapor et al., 2014). Firstly, after being stimulated by pro-angiogenic factors, pericytes produce numerous matrix metalloproteinases (MMPs) (MMP-2, MMP-3, and MMP-9) to degrade the components of the basement membrane, resulting in the separation of pericytes and the succeeding release of ECs (Virgintino et al., 2007; Candelario-Jalil et al., 2009; Potente et al., 2011). Furthermore, increased vascular permeability promotes plasma protein extravasation and provides a temporary scaffold for vascular germination (Carmeliet and Collen, 2000). In addition, pericytes generate VEGF-A, which activates ECs to protrude filopodia, leading to the formation of tip cells (Jakobsson et al., 2010; Franco et al., 2011). Then, stalk cells multiply to support the extension of sprouts and construct a vascular vessel (Eilken and Adams, 2010). Meanwhile, pericytes adhere to ECs, regulate the sediment of the extracellular matrix and the modeling of the inter-endothelial tight junctions, and stabilize neovascularization. Lastly, tip cells anastomose with adjacent sprouts to form microvascular rings (Jain, 2003). Then, pericytes are transformed to suppress EC multiplication and reestablish the quiescence state of ECs to stop angiogenesis (Yang et al., 2017). The primary pericyte-associated pathways propelling neovascularization after IS include the PDGF-BB/PDGFRβ pathway (Gaengel et al., 2009), VEGF-A/VEGFR2 pathway (Greenberg and Jin, 2005), TGF-β/TGFRβ2 pathway (Walshe et al., 2009; Li et al., 2011), Notch pathway (Kume, 2012), and the Ang/Tie2 pathway (Armulik et al., 2011).

Here, we have roughly concluded the mechanism of pericytes involved in angiogenesis after IS; further studies are needed to elucidate the mechanism of angiogenesis after IS and to explore feasible pro-angiogenic therapies.

## THE ROLE OF INFLAMMATORY CYTOKINES IN ANGIOGENESIS AFTER IS

### VEGF

VEGF, diffusely distributed in brain tissue, has essential effects in brain inflammation through promoting inflammatory cell recruitment and adjusting angiopoietin II (Ang II) secretion (Yin et al., 2020). VEGFs and their receptors (VEGFRs) are also pivotal regulators of blood vessel formation. VEGF is mainly divided into matrix-bound and soluble subtypes. Matrix-bound subtypes stimulate more vessel branching, while soluble VEGF facilitates vascular dilation (Carmeliet, 2003). The VEGF family consists of seven subsets of ligands: VEGF-A, VEGF-B, VEGF-C, VEGF-D, VEGF-E, VEGF-F, and PlGF. PlGF, VEGF-A, and VEGF-B are required for angiogenesis (Takahashi and Shibuya, 2005). VEGF-A (also known as VEGF) is the major member of the VEGF family and promotes angiogenesis via binding to VEGF receptor-2 (VEGFR-2) (Zhong et al., 2020). VEGF-B, functionally and structurally related to VEGF-A and PlGF, regulates the bioavailability of VEGF-A (Olofsson et al., 1996). The binding of VEGFs to their receptors on the cytomembrane of ECs activates the mitogen-activated protein kinase (MAPK)/extracellular signal-regulated kinase (ERK) 1/2 and phosphatidylinositol-3 kinase (PI3K)/protein kinase B (AKT) pathways, leading to EC survival, proliferation, differentiation, migration, and tube formation (Assareh et al., 2019). Deficiency of VEGF and/or VEGFR-2 leads to vascular formation defects. In addition, the biological effects of VEGFR-2 may vary greatly due to its subcellular localization. For example, VEGFR-2 must signal from the endocellular compartments when VEGF induces arterial morphogenesis (Lanahan et al., 2010). In addition, autocrine VEGF, secreted by ECs, maintains vascular stabilization (Lee et al., 2007), whereas paracrine VEGF, produced by myeloid, tumor, or stromal cells, renders tumor vessels abnormal and increase vessel branching (Stockmann et al., 2008). Endostatin inhibited VEGF-induced endothelial tube formation by stabilizing the newly formed endothelial tubes (Ergün et al., 2001). Hence, endostatin may be a new anti-angiogenic agent in tumor therapy.

As a potent angiogenic factor, VEGF also has neuroprotective activity. A previous study has illustrated that VEGF promotes neurovascular remodeling in the ischemic hemisphere, contralesional corticobulbar plasticity, and neurological recovery. This brain remodeling by VEGF may be achieved by the deactivation of MMP9, activation of c-Jun, and the suppression of caspase-3-dependent apoptotic cell death as well as the downregulation of growth inhibitory proteoglycans and guidance molecules (Reitmeir et al., 2012). In addition, VEGF has been reported to attenuate the $CD45^+$ leukocyte infiltrates at 14 days after ischemia and to diminish the activation of the microglia. Intracerebroventricularly delivered VEGF promotes contralesional corticorubral plasticity through its anti-inflammatory action via the downregulation of a broad set of inflammatory cytokines and chemokines in both brain hemispheres (Herz et al., 2012). Although the overexpression of VEGF exerts neuroprotection after IS, VEGF facilitates a hemodynamic steal phenomena with reduced blood flow in ischemic areas and increased flow values only outside the MCA territory. The overexpression of VEGF can significantly alleviate neurological deficits and infarct volume and reduce the disseminated neuronal injury and caspase-3 activity, confirming that VEGF has neuroprotective properties. However, a mild blood–brain barrier leakage has been reported to be induced by VEGF (Wang et al., 2005). Hence, the overexpression of VEGF may worsen rather than improve cerebral hemodynamics after IS. The survival-enhancing effect of VEGF is purchased at the expense of increased BBB permeability, which may be regulated by the PI3K/AKT pathway (Kilic et al., 2006). Taken together, the neuroprotective functions of VEGF cannot be easily exploited without accepting the adverse consequences of increased vascular permeability.

### MCP-1

MCP-1, also known as CCL2, a key chemokine that regulates the activation and recruitment of monocytes and microglias as well as T cells, has been implicated in inflammatory and angioproliferative CNS disease (Zhang and Luo, 2019). Both MCP-1 and its receptor C–C chemokine receptor type 2 (CCR2) expressed in the brain are crucial regulators of CNS inflammation and activation of the microglia, involved in various neuroinflammatory diseases (Hinojosa et al., 2011). During inflammatory response, MCP-1 attracts peripheral monocytes to the brain and regulates Th cell development by stimulating Th2 polarization (Saoud et al., 2019). Coincidentally, we have discussed above that the infiltration of Th2 cells to the ischemic hemisphere and the increased Th2-derived cytokine IL-4 can promote angiogenesis during stroke recovery. MCP-1 is also acknowledged as an angiogenic chemokine. However, the mechanism of angiogenesis mediated by MCP-1 has not been fully elucidated. Previous studies indicate that MCP-1-mediated angiogenesis mainly consists of two successive steps: the expression of VEGF-A gene induced by MCP-1 and the subsequent neovascularization induced by VEGF-A. MCP-1 upregulates the expression of the hypoxia-inducible factor 1 alpha (HIF-1α) gene in human aortic ECs, which induces VEGF-A expression in the human aortic wall and ECs via activating MAPK (Hong et al., 2005). A previous study has illustrated that VEGF also induces the expression of MCP-1, mainly through activating NF-kB and the activator protein 1 (AP-1) in retinal ECs (Marumo et al., 1999). MCP-1-mediated angiogenesis is also induced by MCP-1-induced protein (MCPIP), at least partly via the transcriptional activation of cadherin (cdh) 12 and cdh19. Additionally, MCP-1 is involved in neurological recovery after IS and delivers varieties of cells into the brain through MCP-1/CCR2 interplay. Moreover, after intravenous transplantation of human umbilical cord-derived mesenchymal stem cells (hUC-MSCs) with overexpression of MCP-1 in MCAO rats, angiogenesis was promoted in the ischemic penumbra region

(Lee et al., 2020). This indicates that MCP-1-overexpressing hUC-MSCs distinctly repaired functional deficits in rats with MCAO by accelerating persistent increases in MCP-1 levels in brain tissue, promoting neurogenesis and angiogenesis and inhibiting neuroinflammation. These results demonstrate that MCP-1-overexpressing MSCs might be an alternative therapeutic method for cell therapy of IS.

## TNF-α

TNF-α, a cytokine with diverse pro-inflammatory actions, plays crucial roles in both pathological and physiological conditions (Saha and Smith, 2018). TNF-α is induced in the ischemic cerebral tissue within 1 h, peaks at 6–10 h, and subsides 1–2 days post-IS (Liu et al., 1994). Increased TNF-α exerts both neuroprotective and neurotoxic effects after IS (Wilde et al., 2000). TNF-α acts via interacting with two kinds of receptors, TNF receptor 1 (TNFR1) and TNFR2, which can mediate hindlimb ischemia-induced angiogenesis (Luo et al., 2006). Researches in neuroprotection have shown that TNFR1 targeting the erythropoietin receptor (EPOR) and VEGF can alleviate cortical neuronal injury after IS (Taoufik et al., 2008). Moreover, the interplay between TNF-α and TNFR1 primes brain ECs for erythropoietin (EPO)-enhanced angiogenesis by the upregulation of EPOR that amplifies the effect of EPO on the activation of VEGF/VEGFR2 and the angiopoietin 1 (Ang1)/angiopoietin receptor (Tie2) signaling pathway (Wang et al., 2011). In addition, TNF/TNFR1 can act directly on ECs to regulate angiogenesis via activating VEGF signaling (Sugano et al., 2004). TNF also activates various pathways, such as NF-κB and AKT. The NF-κB activated by TNF may trigger the activation of AKT signaling, whereas both NF-κB and PI3K/AKT pathways are essential for the TNF/TNFR1-upregulated expression of EPOR (Wang et al., 2011). These evidences certify the network between TNF/TNFR1 and EPOR to coordinate the occurrence of neovascularization in brain ECs. Additionally, other studies illuminated that IS-induced angiogenesis relies on the TNFR1-mediated upregulation of α5β1 and αVβ3 integrins (Huang et al., 2016).

## TGF-β

The TGF-βs consist of three mammalian subtypes (TGF-β1, TGF-β2, and TGF-β3). The component of TGF-β signaling transduction, including the serine kinase-type receptor on the cytomembrane, exists in the CNS. TGF-βs are pluripotent cytokines whose potential neuroprotective actions are gradually acknowledged. Actually, the expression of TGF-β can be activated following various brain injuries. The neuroprotective action of TGF-β is mostly induced by IS (Dobolyi et al., 2012). Injury in animal models of local and global cerebral ischemia was observed to be suppressed by TGF-βs. A previous study has shown that TGF-βs inhibit microglias, thereby exerting an anti-inflammatory effect (Lund et al., 2018). Since the microglia is the main source of TGF-β1 in the CNS, they may have an autoinhibitory effect on the microglia (Lenzlinger et al., 2001). The potential neuroprotective mechanisms of TGF-βs include anti-inflammatory, anti-excitotoxic, and anti-apoptotic abilities and the facilitation of angiogenesis, neurogenesis, and scar formation.

The secretion of TGF-β1 was proven following IS damage. The expression of TGF-β1 in the ischemic penumbra region was significantly elevated after MCAO in baboons and rats (Ali et al., 2001; Vincze et al., 2010). Moreover, increased levels of TGF-β1 were also found in human brain following IS (Krupinski et al., 1996). Activated microglia/macrophages have been demonstrated to be the primary sources of TGF-β1 messenger RNA (mRNA) after focal ischemic attack (Lehrmann et al., 1998; Doyle et al., 2010). In addition, astrocytes and neuronal cells may also contribute to the upregulated TGF-β1 expression after IS (Zhu et al., 2001; Malik et al., 2020).

TGF-β is known to facilitate angiogenesis. After subcutaneous injection of TGF-β in neonatal mice, collagen production by fibroblasts and increased angiogenesis were observed at the injection site (Roberts et al., 1986). A previous study has demonstrated that TGF-β1 can enhance the actions of other growth factors. In fact, TGF-β1 amplified the therapeutic action of VEGF-induced angiogenesis in patients with peritoneal dialysis (Kariya et al., 2018). Using a two-dimensional Petri dish and three-dimensional hydrated collagen gel cultures, a low concentration of TGF-β1 amplified the stimulating effect of basic fibroblast growth factor. TGF-β1 also promoted the proliferation of ECs in the disc angiogenesis system (Gajdusek et al., 1993). To explore the effect of endogenic TGF-β on spontaneous vascular growth of wound healing, the application of an anti-TGF-β antibody suppressed the spontaneous angiogenesis lower than the control group (Fajardo et al., 1996). Therefore, endogenous TGF-β exerts the effect of promoting spontaneous angiogenesis. Additionally, deficiency of the different components of TGF-β signaling has verified that TGF-β is essential for angiogenesis, and TGF-β receptor mutations are associated with a vascular disease called hereditary hemorrhagic telangiectasia (Bertolino et al., 2005). What is more, in ischemic rat brain following MCAO, leucine-rich α2-glycoprotein 1 (LRG1) may protect the rat brain tissue from ischemic attack through accelerating angiogenesis via upregulating the TGF-β1 pathway (Meng et al., 2016). It has been suggested that there is a complex interaction between VEGF and TGF-β1, both of which promote angiogenesis but have opposite effects on ECs. VEGF protects ECs against apoptosis, whereas TGF-β1 induces apoptosis. Moreover, the suppression of VEGF inhibited both the angiogenesis and apoptosis induced by TGF-β1, suggesting a refined regulation of angiogenesis through the interaction of these growth factors (Ferrari et al., 2009). In the injured brain, the application of TGF-β distinctly facilitated the re-elongation of axons in the injured site in a concentration-dependent manner, suggesting that TGF-β1 can also facilitate axonal regeneration of injured brain neuronal cells (Abe et al., 1996).

## GM-CSF/G-CSF

GM-CSF is known to stimulate the growth and polarization of granulocytes and macrophages, exerting a crucial effect in the regulation of innate and adaptive immunity (Seledtsov et al., 2019). As a potent survival factor for monocytes/macrophages, GM-CSF may promote arterial formation in patients with

cerebral ischemia to enhance their collateral capacity, thereby reducing the brain infarction risk (Lee et al., 2005; Maurer et al., 2008). A previous clinical trial has shown that GM-CSF has a positive effect on the therapeutic enhancement of angiogenesis in a group of patients with coronary artery disease (Werner, 2002). Previous research results of GM-CSF subcutaneous injection in hypoperfused rat brain showed that: (1) GM-CSF induced an enlargement of posterior cerebral artery caliber on three-vessel occlusion (3-VO, a non-lethal brain hypoperfusion model); (2) morphological and functional changes could be caused by subcutaneous GM-CSF treatment; (3) GM-CSF improved the cerebral hemodynamic parameters on 3-VO, such as $CO_2$ reactivity; and (4) GM-CSF enhanced the infiltration of monocytes/macrophages in the area of vascular collateral formation (Buschmann et al., 2003). These facts indicate that GM-CSF treatment can induce arteriogenesis in hypoperfused rat brain.

G-CSF activates the survival, multiplication, and maturation of cells in the neutrophil lineage (Malashchenko et al., 2018). It is also a neuroprotective cytokine and has a positive effect on angiogenesis and neurogenesis after IS. G-CSF plays a role in regulating the PI3K/AKT signaling pathway, affecting cell proliferation and apoptosis and inducing VEGF expression (Liang et al., 2018). G-CSF increases EC multiplication, the vasal branch points, the vascular surface area, and the length of blood vessels in the ischemic penumbra region (Lee et al., 2005). In addition, the neuroprotective action of G-CSF may be confirmed from all the decreases of the infarct size, the inflammatory infiltration, the BBB disruption, and the hemispheric atrophy after G-CSF treatment (Menzie-Suderam et al., 2020; Modi et al., 2020). Two possible molecular mechanisms deserve to be considered in angiogenesis induced by G-CSF: (1) the direct activation of cerebral ECs (Liang et al., 2018) and (2) the transference of bone marrow endothelial progenitor cells (EPCs) to the ischemic penumbra area. G-CSF was confirmed to stimulate ECs in order to initiate an activation/differentiation procedure, including multiplication and migration, associated with angiogenesis (Bussolino et al., 1991). Moreover, evidences demonstrate that G-CSF increases the expression of angiopoietin-2 (Ang2) and endothelial nitric oxide synthase (eNOS) in the ischemic penumbra of the cerebral cortex (Lee et al., 2005). eNOS is known to be essential to increasing both angiogenesis and the number of circulating EPCs (Endres et al., 2004), while Ang2 has been shown to promote a rapid proliferation of capillary diameter, the basal lamina reestablishment, and the development of new vessels (Ramsauer and D'Amore, 2002).

## FGF

Presently, the FGF family is known to contain more than 20 factors. FGFs are secreted by ECs and are presented in the ectocytic matrix. FGFs are affected by different factors in different tissues. The members of the FGF family exert critical roles in angiogenesis for new blood vessel formation, which dramatically affects the proliferation, mobilization, metastasis, and mobilization of vascular ECs (Chen M. et al., 2020). In particular, FGF-1 (acidic FGF) and FGF-2 (basic FGF) have been verified to affect the modeling of new vessels in some tissues *in vivo* by regulating ECs (Zhou et al., 2009; Oladipupo et al., 2014). Moreover, FGF-1 and FGF-2 may restrain endothelial-dependent monocyte recruitment and thus have an anti-inflammatory function during angiogenesis in chronic inflammation (Zhang and Issekutz, 2002). Previous researches have illustrated that FGF-1 can initiate angiogenesis and neurogenesis in rats following IS (Cheng et al., 2011) and protect hippocampal neuronal cells against apoptosis induced by IS (Cuevas et al., 1998). Additionally, in mice after IS and human brain microvascular ECs after oxygen–glucose deprivation (OGD), non-mitogenic FGF-1 enhanced angiogenesis through regulating sphingosine-1-phosphate 1 (S1P1) signaling mediated by the activation of FGF receptor 1 (FGFR1) (Zou et al., 2020). FGF-2 also plays crucial roles in neurogenesis, angiogenesis, and neuronal survival as well as BBB protection. The expression of FGF-2 in the ischemic penumbra zone of all patients was distinctly increased compared with the infarcted tissue and normal contralateral hemisphere (Issa et al., 2005). Upregulated FGF-2 expression was observed to enhance endogenous neovascularization and hemodynamic changes in the infarct region and to upregulate the number of neuroblast cells migrating toward the ischemic striatum (Oyamada et al., 2008). Moreover, the function of promoting angiogenesis and BBB protection effect as well as the neuroprotective function of FGF-2 are partially via relieving the OGD/R-induced reduction of S1P1 receptor 1 (S1PR1) (Lin et al., 2018), binding of FGFR1 and activating the ERK signaling pathway (Chen P. et al., 2020), and regulating via the PI3K–AKT–Rac1 pathway (Wang et al., 2016).

## HGF

HGF is a multifunctional growth factor that plays critical roles in mitogenesis, morphogenesis, motogenesis, anti-apoptosis, and angiogenesis. In the brain, HGF functions as an angiogenic factor and a neurotrophic factor. In addition, HGF exhibits neuroprotective actions on ischemia-induced damage through promoting angiogenesis, neurogenesis, and synaptogenesis and inhibiting fibrotic change (Shang et al., 2011). The application of dental pulp stem cells overexpressing HGF in the acute stage of stroke enhanced their neuroprotective actions through regulating inflammation and BBB permeability, thereby mitigating cerebral ischemia–reperfusion injury (CIRI) (Sowa et al., 2018). HGF may also be involved in the prognosis of acute IS at 3 months (Zhu et al., 2018).

## PDGF

The PDGF family is composed of four elements: PDGF-A, PDGF-B, PDGF-C, and PDGF-D. PDGF is known to be angiogenic and neuroprotective in IS where PDGFR-α activation in circumvascular astrocyte cells is involved in the acute opening of the BBB. Evidence shows that PDGF-B and its receptor on microvessel ECs may be involved in angiogenesis following IS (Krupinski et al., 1997). Deficiency of either PDGF-B or PDGFR-β is closely related to characteristics of vascular rupture, including vascular dysfunction, pericyte defects, and the formation of microaneurysms (Gaengel et al., 2009). PDGFR-β expression is low in adult normal matured brain. However, its expression

gradually increases mainly in pericytes and fibroblast-like cells in the ischemic penumbra zone after IS. PDGFR-β mediates a variety of functions, including the modulation of the BBB and the rescue of infarcted tissues after IS (Nakamura et al., 2016). Moreover, a current study has shown critical actions of PDGF-C and PDGF-D in neovascularization, fibrosis, atherosclerosis, and restenosis (Folestad et al., 2018).

## Interleukins

### IL-1

IL-1 is known to be a primary mediator of central and peripheral inflammation after IS, primarily via the action of both of its subtypes, IL-1α and IL-1β, at cerebral ECs. Previous preclinical studies have demonstrated the deleterious actions of IL-1 following IS, while blocking its actions is salutary in preclinical and clinical settings. However, the pro-inflammatory cytokine IL-1α was found to increase the brain EC activation, migration, and the proliferation of ECs and to induce chemokine (C–X–C motif) ligand 1 (CXCL-1) and IL-6 (recognized to have angiogenic effects in cerebral ECs) expression as well as promote the construction of capillary tube-like structures in cerebral ECs *in vitro* (Salmeron et al., 2016). Hence, these findings demonstrate that IL-1α has angiogenic effects in post-stroke angiogenesis. After ischemia injury, oligodendrocytes respond to inflammatory IL-1β signaling and produce MMP-9 to enhance angiogenesis (Pham et al., 2012).

### IL-4

As an important anti-inflammatory cytokine, IL-4 induces mononuclear/macrophages to differentiate into M2 macrophages through its receptor IL-4R and then secretes more anti-inflammatory factors such as IL-10 and TGF-β, while inhibiting the formation of M1 macrophages and the release of TNF-α and IL-1 (Bhattacharjee et al., 2013). M2 macrophages are known to promote angiogenesis after IS, partially through regulating the HIF1-α/VEGF/NO signaling pathway. Evidence shows that the blockade of IL-4 abrogates the promoting role of hyperforin in post-stroke angiogenesis, neuronal regeneration, and functional rehabilitation (Yao et al., 2019).

### IL-6

Four weeks after MCAO, IL-6 knockout mice displayed a distinctly elevated chronic lesion size and showed a damaged angiogenic response to cerebral ischemia with the reduction of neonatal EC numbers, perfused microvessel density, absolute focal cerebral blood flow, and vessel responsivity in ischemic striatum. These findings suggest that IL-6 plays an important role in angiogenesis after IS. Moreover, resident cerebral cells are the main sources of elevated levels of IL-6 in the early-phase post-stroke. IL-6 stimulates the phosphorylation of signal transducer and activator of transcription 3 (STAT3) and the early transcriptional activation of angiogenesis relative genes, thereby leading to the enhanced angiogenesis and increased brain blood flow in the delayed phase after IS (Gertz et al., 2012). IL-6R simultaneously activates the PI3K/AKT and Janus kinase (JAK)/STAT signaling pathways (Xu et al., 2005), which play vital roles in angiogenesis after stroke.

# THE ROLE OF INFLAMMATION-RELATIVE SIGNALING PATHWAYS IN POST-STROKE ANGIOGENESIS

## JAK2/STAT3 Pathway

STAT3 is known to be a key regulator of various inflammatory signals. STAT3 is phosphorylated by phospho-JAK2 (p-JAK2) and is subsequently transferred into the nucleus to regulate the expression of particular genes. Numerous evidences have shown that JAK2/STAT3 signaling activation plays a protective effect against CIRI (Hoffmann et al., 2015; Li et al., 2017). As a direct transcriptional activator of VEGF under hypoxia conditions, STAT3 has recently been confirmed to regulate post-stroke angiogenesis, axon growth, and extracellular matrix remodeling (Hoffmann et al., 2015). Moreover, deficiency of STAT3 signaling is involved in the inhibition of pancreatic carcinoma and kidney cancer through suppressing cancerous angiogenesis (Li et al., 2013). The potential molecular mechanism of angiogenesis induced by the JAK2/STAT3 signaling pathway may be the induction of VEGF production and the regulation of Ang-1 and Ang-2 expression (Li et al., 2017) (**Figure 1**). As is known, Ang-1 promotes the maturity of new blood vessels and Ang-2 is a destabilizing signaling that reverts vessels to a more malleable state. Numerous cytokines and agents can promote STAT3 phosphorylation or directly activate the JAK2/STAT3 signaling pathway, including IL-6, secretoneurin (Shyu et al., 2008), salvianolic acids (Li et al., 2017), catalpol (Dong et al., 2016), ginkgolide K (Chen et al., 2018), etc., exerting an angiogenic action. What is more, the activation of the JAK2/STAT3 signaling pathway can shift the microglia toward M2 polarization (Qin et al., 2017), which promotes angiogenesis in IS. Additionally, the STAT3 signaling pathway is essential for HIF-1α expression regulated by VEGF and PI3K/AKT. The expressions of HIF-1α and VEGF disappeared after STAT3 was blocked by its inhibitor, such as CPA-7 or STAT3 small interfering RNA (siRNA) (Xu et al., 2005). However, the inhibition of STAT3-dependent autophagy can also promote angiogenesis after IS (Xia et al., 2020).

## PI3K/AKT Signaling Pathway

The PI3K/AKT pathway is known to exert a crucial effect in various physiological conditions such as inflammation, oxidative stress, and apoptosis. The activation of the PI3K/AKT pathway can decrease the expression of inflammatory genes and then maintain the vascular capacity. Furthermore, the PI3K/AKT signaling pathway promotes neuronal survival activation and enhances cell survival after IS (Zhang et al., 2016; Li et al., 2019). Activated AKT can promptly stimulate some molecular signals such as rapamycin (mTOR), which promotes protein synthesis and regulates cytotrophy and energy supply. A previous study has illustrated that the activated PI3K/AKT/mTOR pathway exerts essential actions on the effect of apoptosis and inflammation in the brain (Li et al., 2015).

What is noteworthy is that the PI3K/AKT/mTOR pathway has been proven to be essential for angiogenesis (**Figure 2**), including EC survival, migration, and new vessel formation. The activated PI3K/AKT/mTOR signaling activates its downstream factor

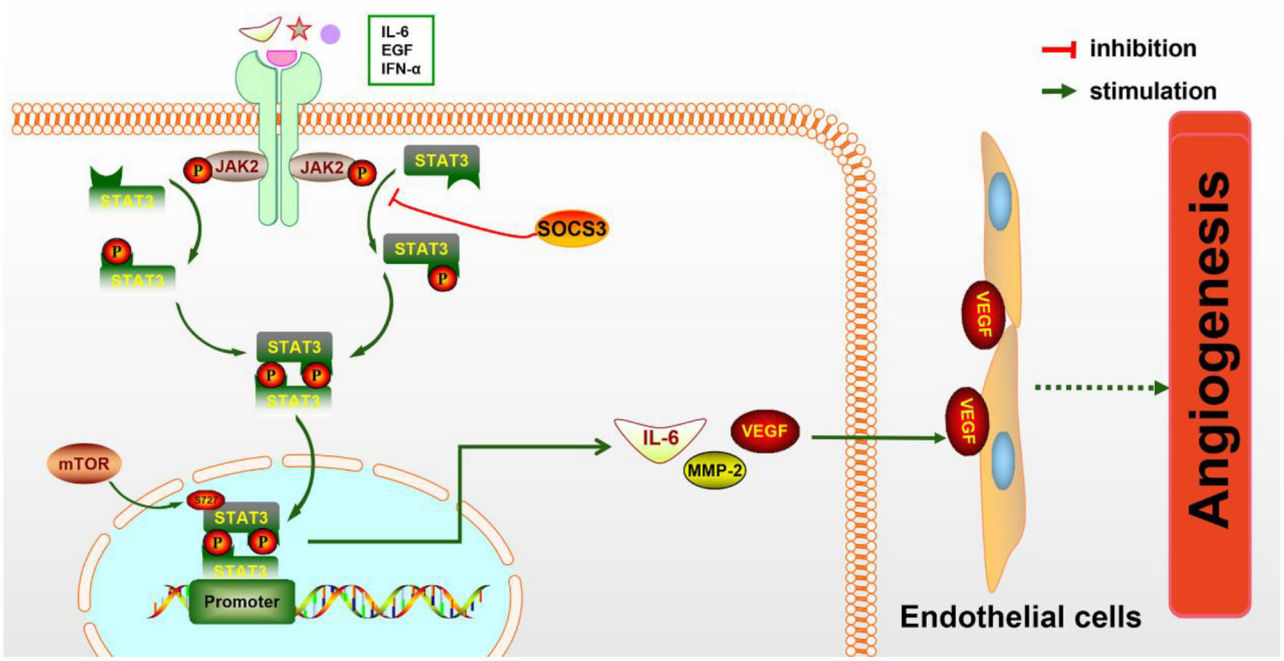


**FIGURE 1 |** The molecular mechanism of angiogenesis mediated by the JAK2/STAT3 pathway. JAK2 is activated and phosphorylated by inflammatory cytokines such as IL-6 and IFN-α, resulting in the phosphorylation of downstream STAT3 and the formation of the p-STAT3 dimer, which is subsequently transferred to the nucleus to promote the expression of particular genes. IL-6, MMP-2, VEGF, and other cytokines are increased, then secreted to the extracellular matrix and act on endothelial cells (ECs), eventually leading to increased angiogenesis.

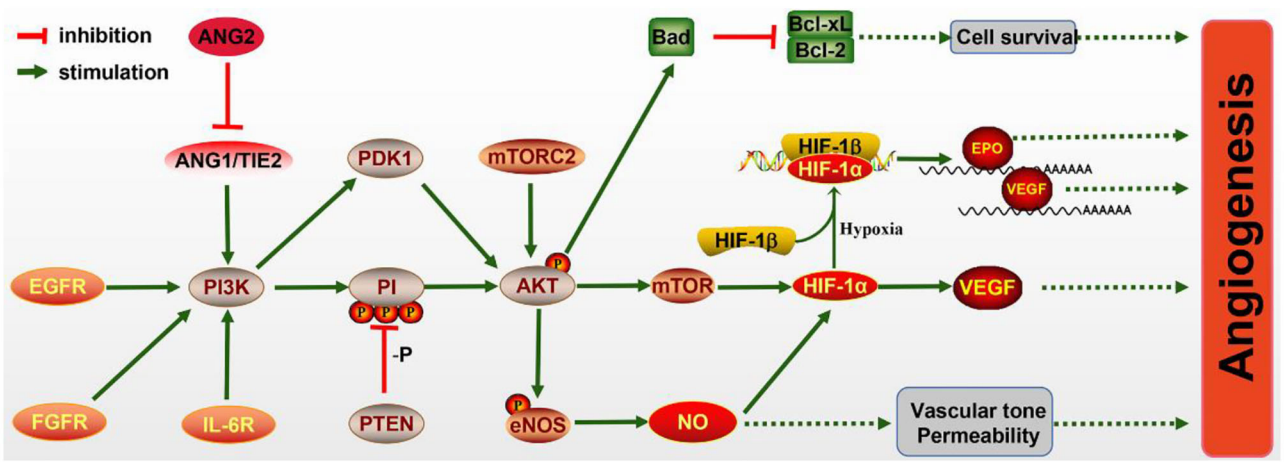


**FIGURE 2 |** The molecular mechanism of angiogenesis mediated by the PI3K/AKT pathway. PI3K signaling is activated by the endothelial growth factor receptor (EGFR), fibroblast growth factor receptor (FGFR), IL-6R, and Ang/Tie2 signaling molecules, leading to AKT activation. Activated AKT promotes the expression of Bad, which inhibits Bcl-CL/Bcl-2, thereby promoting the survival of pro-angiogenic cells. The mechanistic target of rapamycin (mTOR) is also activated by AKT and increases the level of HIF-1α, which can directly increase the expression of vascular endothelial growth factor (VEGF) or bind to HIF-1β in hypoxia conditions and transfer to the nucleus to promote the expressions of erythropoietin (EPO) and VEGF. Meanwhile, endothelial nitric oxide synthase (eNOS) activated by AKT promotes the production of NO, which protects vascular tone permeability. These potential mechanisms contribute to angiogenesis through the PI3K/AKT pathway.

HIF-1α, thereby regulating VEGF expression (Patra et al., 2019), which is known to enhance angiogenesis after IS. In addition, epidermal growth factor (EGF) exerts neuroprotective effects on cerebral ischemia via activating the EGF receptor (EGFR), which also contributes to the activation of the PI3K/AKT/mTOR pathway and elevated HIF-1α (Karar and Maity, 2011).

In ECs, the PI3K/AKT pathway participates in angiogenesis via regulating nitric oxide (NO) signaling, which is modulated

by the enzyme NO synthase (NOS). Evidence has illuminated that NO donors can promote the transcriptional activity and expression of HIF-1, thereby inducing the VEGF mRNA (Papapetropoulos et al., 1997). Furthermore, VEGF can initiate NO generation, which is suppressed by the PI3K inhibitor. Hypoxia can also accelerate the phosphorylation of eNOS via activating the PI3K/AKT pathway and HSP9O binding to eNOS. NO production may also be induced *via* the phosphorylation of eNOS by AKT (Kasuno et al., 2004).

The Ang1/Tie2 system, including the angiopoietins and their receptors, can also activate the PI3K/AKT pathway and promote EC survival. Ang1 and Ang2 bind to Tie2 receptor tyrosine kinase, which is mainly expressed in ECs (Davis et al., 1996; Karar and Maity, 2011). Ang1 is essential for endothelial development, while Ang2 resists the Ang1/Tie2 system and can disrupt vascularization. Research has shown that Ang2 can activate the PI3K/AKT pathway and serve as a stimulant of the Tie2 receptor in the deficiency of Ang1, although weaker than Ang1 (Yuan et al., 2009).

## MAPK Pathways

MAPK pathways amplify, transmit, and integrate signals from a various range of stimuli and induce appropriate physiological reactions including proliferation, differentiation, development, transformation, apoptosis, and inflammatory responses. To date, three MAPK families have been characterized: ERK, p38 MAPK, and c-Jun N-terminal kinase/stress-activated protein kinase (JNK/SAPK). The activation of p38 MAPK/HIF-1α/VEGF-A exerts anti-apoptotic and angiogenic effects against CIRI (Cheng et al., 2017). The application of MAPK/ERK pathway inhibitors disrupts VEGF-induced angiogenesis, thereby indicating that the MAPK/ERK signaling pathway mediates this process (Pulous et al., 2020). Moreover, hyperbaric oxygen-induced VEGF is activated by C-Jun/ AP-1 and through simultaneously activating the JNK and ERK signaling pathways (Lee et al., 2006). These findings indicate that ERK, p38 MAPK, and JNK are all involved in regulating angiogenesis in different ways.

## NF-κB Signaling Pathway

NF-κB, a typical pro-inflammatory signaling molecule, is a key transcriptional factor that plays an important role in the regulation of inflammation, angiogenesis, functional circuit formation, and neurite outgrowth (Cui et al., 2015). The expression of angiogenesis-stimulating factors is partially mediated through the transcriptional activation of NF-κB in response to the inflammatory cytokines IL-1 α/β and TNF-α in vascular ECs and monocytes/macrophages, as well as in cancer cells. Inflammatory angiogenesis and the enhanced production of VEGF, in response to IL-1 α/β and TNF-α, are partially due to the activation of the NF-κB pathway (Watari et al., 2012). Furthermore, it has been verified that VEGF application activates NF-κB in vascular ECs. The activation of the NF-κB signaling pathway is through the activation of the PLCγ-sphingosine kinase-PKC cascade, resulting in the upregulation of vascular cell adhesion molecule-1 (VCAM-1) and intercellular adhesion molecule-1 (ICAM-1) in monocytes/macrophages or vascular ECs stimulated by VEGF (Kim et al., 2001). In addition, NF-κB is also essential for the stem cell factor (SCF)+G-CSF-induced

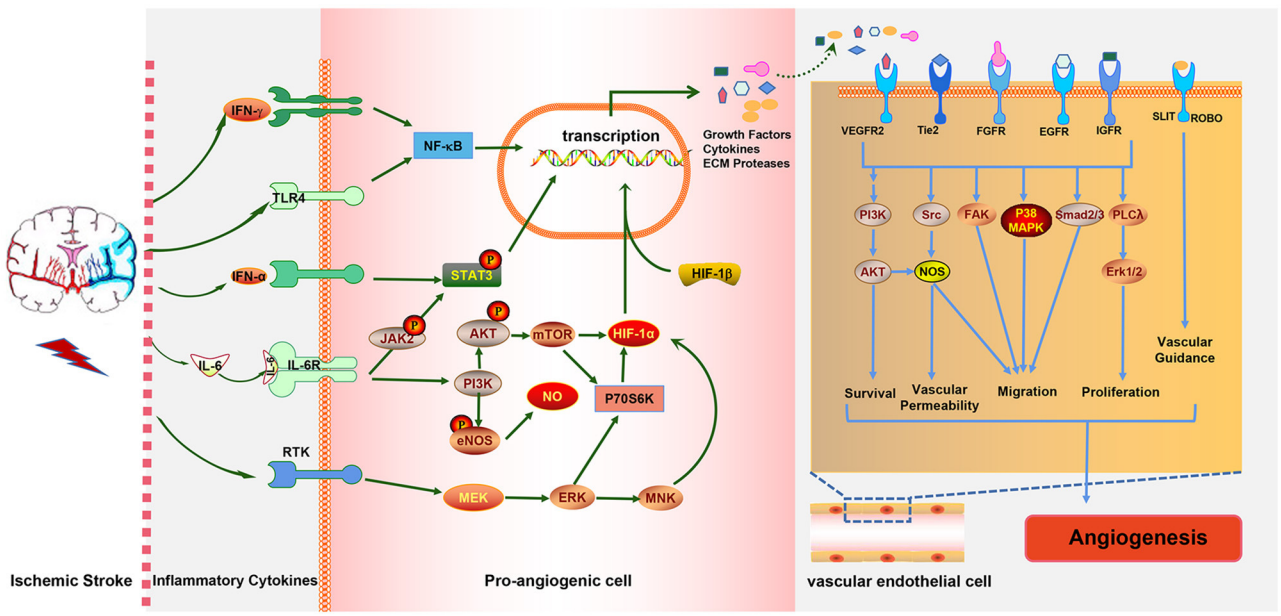


**FIGURE 3 |** The interaction between ischemic stroke, inflammatory cytokines, and inflammation-associated pathways. Ischemic stroke increases the expressions of the pro-inflammatory cytokines IFN-γ, IL-6 and IFN-α, which activate the NF-κB, JAK2/STAT3, PI3K/AKT, and MAPK pathways in pro-angiogenic cells, leading to the elevated expressions of growth factors, cytokines, and extracellular matrix (ECM) proteases. These cytokines act on endothelial cells (ECs) to promote EC survival, vascular permeability, and migration proliferation and, ultimately, to promote angiogenesis, which in turn alleviates stroke injury.

angiogenesis in the ipsilateral somato-sensorimotor cortex after stroke (Cui et al., 2015).

## CONCLUSIONS AND PERSPECTIVES

Numerous studies have repeatedly shown that inflammatory reactions play multiphasic and complex roles in the progression and pathogenesis of IS. As mentioned above, pro-inflammatory cytokines such as IL-1β and TNF-α can promote angiogenesis after IS, but too many pro-inflammatory cytokines have a detrimental effect on the progression of IS. Analogously, anti-inflammatory cytokines such as IL-10 exert a protective effect after stroke, but too many anti-inflammatory factors produce immunosuppression after stroke. Thus, a balance between pro-inflammatory and anti-inflammatory signals is urgently needed to improve IS outcomes.

Various inflammatory cells and inflammatory cytokines, as well as the immune cell subtypes mentioned above, play crucial roles in ischemia-induced angiogenesis. The occurrence of IS induces immune inflammatory responses in brain tissue which can promote angiogenesis. Ultimately, angiogenesis improves stroke prognosis, and eventually, the immune response is mitigated. It is obvious that the three are directly related to each other in a complex way. Moreover, there is also an interaction network between immune cells, inflammatory cytokines, and inflammation-relative signaling pathways involved in post-stroke angiogenesis. For example, IL-6R simultaneously activates the PI3K/AKT and JAK2/STAT3 signaling pathways; in turn, the activation of the JAK2/STAT3 pathway induces the generation of IL-6 (**Figure 3**). The STAT3 signaling pathway is also essential for the expression of HIF-1α mediated by VEGF and PI3K/AKT, whereas HIF-1α induced by the PI3K/AKT pathway promotes VEGF expression.

In conclusion, in this paper, we mainly discussed the inflammatory and immune cell subsets as well as the associated signaling pathways that contribute to angiogenesis in IS. The immune cell subsets and inflammatory cells involved in angiogenesis after IS mainly contain microglia/macrophage cells, NK cells, $CD4^+$ T cells, brain pericytes, ECs, etc. Meanwhile, inflammatory cytokines, such as VEGF, MCP-1/CCL2, TNF-α, TGF-β, GM-CSF/G-CSF, FGF, HGF, PDGF, IL, and HIF-1α, play a critical role in the inflammatory-mediated angiogenesis after IS. Targeting these inflammatory cytokines and immune cells may provide the theoretical basis for potential therapies for IS.

## AUTHOR CONTRIBUTIONS

All the listed authors directly, substantially, and intellectually contributed to the preparation of this manuscript and approved the publication.

## FUNDING

This work was supported by the National Natural Science Foundation of China (Grant no. 81870939 to XX, Grant nos. 81771283 and 82071339 to LG) and the Natural Science Foundation of Hubei Province, China (Grant no. 2019CFB498 to LG).

## REFERENCES

Abe, K., Chu, P. J., Ishihara, A., and Saito, H. (1996). Transforming growth factor-beta 1 promotes re-elongation of injured axons of cultured rat hippocampal neurons. *Brain Res.* 723, 206–209. doi: 10.1016/0006-8993(96)00253-3

Ali, C., Docagne, F., Nicole, O., Lesné, S., Toutain, J., Young, A., et al. (2001). Increased expression of transforming growth factor-beta after cerebral ischemia in the baboon: an endogenous marker of neuronal stress? *J. Cereb. Blood Flow Metab.* 21, 820–827. doi: 10.1097/00004647-200107000-00007

Armulik, A., Genové, G., and Betsholtz, C. (2011). Pericytes: developmental, physiological, and pathological perspectives, problems, and promises. *Dev. Cell* 21, 193–215. doi: 10.1016/j.devcel.2011.07.001

Assareh, E., Mehrnejad, F., Mansouri, K., Esmaeili Rastaghi, A. R., Naderi-Manesh, H., and Asghari, S. M. (2019). A cyclic peptide reproducing the α1 helix of VEGF-B binds to VEGFR-1 and VEGFR-2 and inhibits angiogenesis and tumor growth. *Biochem. J.* 476, 645–663. doi: 10.1042/BCJ20180823

Bell, R. D., Winkler, E. A., Sagare, A. P., Singh, I., LaRue, B., Deane, R., et al. (2010). Pericytes control key neurovascular functions and neuronal phenotype in the adult brain and during brain aging. *Neuron* 68, 409–427. doi: 10.1016/j.neuron.2010.09.043

Bertolino, P., Deckers, M., Lebrin, F., and ten Dijke, P. (2005). Transforming growth factor-beta signal transduction in angiogenesis and vascular disorders. *Chest* 128, 585–590. doi: 10.1378/chest.128.6_suppl.585S

Bhattacharjee, A., Shukla, M., Yakubenko, V. P., Mulya, A., Kundu, S., and Cathcart, M. K. (2013). IL-4 and IL-13 employ discrete signaling pathways for target gene expression in alternatively activated monocytes/macrophages. *Free Radic. Biol. Med.* 54, 1–16. doi: 10.1016/j.freeradbiomed.2012.10.553

Buschmann, I. R., Busch, H. J., Mies, G., and Hossmann, K. A. (2003). Therapeutic induction of arteriogenesis in hypoperfused rat brain via granulocyte-macrophage colony-stimulating factor. *Circulation* 108, 610–615. doi: 10.1161/01.CIR.0000074209.17561.99

Bussolino, F., Ziche, M., Wang, J. M., Alessi, D., Morbidelli, L., Cremona, O., et al. (1991). *In vitro* and *in vivo* activation of endothelial cells by colony-stimulating factors. *J. Clin. Invest.* 87, 986–995. doi: 10.1172/JCI115107

Candelario-Jalil, E., Yang, Y., and Rosenberg, G. A. (2009). Diverse roles of matrix metalloproteinases and tissue inhibitors of metalloproteinases in neuroinflammation and cerebral ischemia. *Neuroscience* 158, 983–994. doi: 10.1016/j.neuroscience.2008.06.025

Carmeliet, P. (2003). Angiogenesis in health and disease. *Nat. Med.* 9, 653–660. doi: 10.1038/nm0603-653

Carmeliet, P., and Collen, D. (2000). Molecular basis of angiogenesis. Role of VEGF and VE-cadherin. *Ann. N. Y. Acad. Sci.* 902, 249–262; discussion 262–244. doi: 10.1111/j.1749-6632.2000.tb06320.x

Chen, C., Ai, Q. D., Chu, S. F., Zhang, Z., and Chen, N. H. (2019). NK cells in cerebral ischemia. *Biomed. Pharmacother.* 109, 547–554. doi: 10.1016/j.biopha.2018.10.103

Chen, M., Bao, L., Zhao, M., Cao, J., and Zheng, H. (2020). Progress in research on the role of FGF in the formation and treatment of corneal neovascularization. *Front. Pharmacol.* 11:111. doi: 10.3389/fphar.2020.00111

Chen, M., Zou, W., Chen, M., Cao, L., Ding, J., Xiao, W., et al. (2018). Ginkgolide K promotes angiogenesis in a middle cerebral artery occlusion mouse model via activating JAK2/STAT3 pathway. *Eur. J. Pharmacol.* 833, 221–229. doi: 10.1016/j.ejphar.2018.06.012

Chen, P., Tang, H., Zhang, Q., Xu, L., Zhou, W., Hu, X., et al. (2020). Basic fibroblast growth factor (bFGF) protects the blood-brain barrier by binding of FGFR1 and activating the ERK signaling pathway after intra-abdominal hypertension and traumatic brain injury. *Med. Sci. Monit.* 26:e922009. doi: 10.12659/MSM.922009

Cheng, C. Y., Ho, T. Y., Hsiang, C. Y., Tang, N. Y., Hsieh, C. L., Kao, S. T., et al. (2017). Angelica sinensis exerts angiogenic and anti-apoptotic effects against cerebral ischemia-reperfusion injury by activating p38MAPK/HIF-1[Formula:

see text]/VEGF-A signaling in rats. *Am. J. Chin. Med.* 45, 1683–1708. doi: 10.1142/S0192415X17500914

Cheng, X., Wang, Z., Yang, J., Ma, M., Lu, T., Xu, G., et al. (2011). Acidic fibroblast growth factor delivered intranasally induces neurogenesis and angiogenesis in rats after ischemic stroke. *Neurol. Res.* 33, 675–680. doi: 10.1179/1743132810Y.0000000004

Cuevas, P., Carceller, F., Reimers, D., Saenz de Tejada, I., and Giménez-Gallego, G. (1998). Acidic fibroblast growth factor rescues gerbil hippocampal neurons from ischemic apoptotic death. *Neurol. Res.* 20, 271–274. doi: 10.1080/01616412.1998.11740518

Cui, L., Duchamp, N. S., Boston, D. J., Ren, X., Zhang, X., Hu, H., et al. (2015). NF-κB is involved in brain repair by stem cell factor and granulocyte-colony stimulating factor in chronic stroke. *Exp. Neurol.* 263, 17–27. doi: 10.1016/j.expneurol.2014.08.026

Davis, S., Aldrich, T. H., Jones, P. F., Acheson, A., Compton, D. L., Jain, V., et al. (1996). Isolation of angiopoietin-1, a ligand for the TIE2 receptor, by secretion-trap expression cloning. *Cell* 87, 1161–1169. doi: 10.1016/S0092-8674(00)81812-7

del Zoppo, G. J., and Mabuchi, T. (2003). Cerebral microvessel responses to focal ischemia. *J. Cereb. Blood Flow Metab.* 23, 879–894. doi: 10.1097/01.WCB.0000078322.96027.78

Dobolyi, A., Vincze, C., Pál, G., and Lovas, G. (2012). The neuroprotective functions of transforming growth factor beta proteins. *Int. J. Mol. Sci.* 13, 8219–8258. doi: 10.3390/ijms13078219

Dong, W., Xian, Y., Yuan, W., Huifeng, Z., Tao, W., Zhiqiang, L., et al. (2016). Catalpol stimulates VEGF production via the JAK2/STAT3 pathway to improve angiogenesis in rats' stroke model. *J. Ethnopharmacol.* 191, 169–179. doi: 10.1016/j.jep.2016.06.030

Doyle, K. P., Cekanaviciute, E., Mamer, L. E., and Buckwalter, M. S. (2010). TGFβ signaling in the brain increases with aging and signals to astrocytes and innate immune cells in the weeks after stroke. *J. Neuroinflammation* 7:62. doi: 10.1186/1742-2094-7-62

Eilken, H. M., and Adams, R. H. (2010). Dynamics of endothelial cell behavior in sprouting angiogenesis. *Curr. Opin. Cell Biol.* 22, 617–625. doi: 10.1016/j.ceb.2010.08.010

Endres, M., Laufs, U., Liao, J. K., and Moskowitz, M. A. (2004). Targeting eNOS for stroke protection. *Trends Neurosci.* 27, 283–289. doi: 10.1016/j.tins.2004.03.009

Ergün, S., Kilic, N., Wurmbach, J. H., Ebrahimnejad, A., Fernando, M., Sevinc, S., et al. (2001). Endostatin inhibits angiogenesis by stabilization of newly formed endothelial tubes. *Angiogenesis* 4, 193–206. doi: 10.1023/A:1014027218980

Fajardo, L. F., Prionas, S. D., Kwan, H. H., Kowalski, J., and Allison, A. C. (1996). Transforming growth factor beta1 induces angiogenesis *in vivo* with a threshold pattern. *Lab. Invest.* 74, 600–608.

Ferrari, G., Cook, B. D., Terushkin, V., Pintucci, G., and Mignatti, P. (2009). Transforming growth factor-beta 1 (TGF-beta1) induces angiogenesis through vascular endothelial growth factor (VEGF)-mediated apoptosis. *J. Cell. Physiol.* 219, 449–458. doi: 10.1002/jcp.21706

Folestad, E., Kunath, A., and Wågsäter, D. (2018). PDGF-C and PDGF-D signaling in vascular diseases and animal models. *Mol. Aspects Med.* 62, 1–11. doi: 10.1016/j.mam.2018.01.005

Franco, M., Roswall, P., Cortez, E., Hanahan, D., and Pietras, K. (2011). Pericytes promote endothelial cell survival through induction of autocrine VEGF-A signaling and Bcl-w expression. *Blood* 118, 2906–2917. doi: 10.1182/blood-2011-01-331694

Gaengel, K., Genové, G., Armulik, A., and Betsholtz, C. (2009). Endothelial-mural cell signaling in vascular development and angiogenesis. *Arterioscler. Thromb. Vasc. Biol.* 29, 630–638. doi: 10.1161/ATVBAHA.107.161521

Gajdusek, C. M., Luo, Z., and Mayberg, M. R. (1993). Basic fibroblast growth factor and transforming growth factor beta-1: synergistic mediators of angiogenesis *in vitro*. *J. Cell. Physiol.* 157, 133–144. doi: 10.1002/jcp.1041570118

Gertz, K., Kronenberg, G., Kälin, R. E., Baldinger, T., Werner, C., Balkaya, M., et al. (2012). Essential role of interleukin-6 in post-stroke angiogenesis. *Brain* 135, 1964–1980. doi: 10.1093/brain/aws075

Greenberg, D. A., and Jin, K. (2005). From angiogenesis to neuropathology. *Nature* 438, 954–959. doi: 10.1038/nature04481

Hayashi, T., Noshita, N., Sugawara, T., and Chan, P. H. (2003). Temporal profile of angiogenesis and expression of related genes in the brain after ischemia. *J. Cereb. Blood Flow Metab.* 23, 166–180. doi: 10.1097/01.WCB.0000041283.53351.CB

Herz, J., Reitmeir, R., Hagen, S. I., Reinboth, B. S., Guo, Z., Zechariah, A., et al. (2012). Intracerebroventricularly delivered VEGF promotes contralesional corticorubral plasticity after focal cerebral ischemia via mechanisms involving anti-inflammatory actions. *Neurobiol. Dis.* 45, 1077–1085. doi: 10.1016/j.nbd.2011.12.026

Hinojosa, A. E., Garcia-Bueno, B., Leza, J. C., and Madrigal, J. L. (2011). CCL2/MCP-1 modulation of microglial activation and proliferation. *J. Neuroinflammation* 8:77. doi: 10.1186/1742-2094-8-77

Hoffmann, C. J., Harms, U., Rex, A., Szulzewsky, F., Wolf, S. A., Grittner, U., et al. (2015). Vascular signal transducer and activator of transcription-3 promotes angiogenesis and neuroplasticity long-term after stroke. *Circulation* 131, 1772–1782. doi: 10.1161/CIRCULATIONAHA.114.013003

Hong, K. H., Ryu, J., and Han, K. H. (2005). Monocyte chemoattractant protein-1-induced angiogenesis is mediated by vascular endothelial growth factor-A. *Blood* 105, 1405–1407. doi: 10.1182/blood-2004-08-3178

Huang, H., Huang, Q., Wang, F., Milner, R., and Li, L. (2016). Cerebral ischemia-induced angiogenesis is dependent on tumor necrosis factor receptor 1-mediated upregulation of α5β1 and αVβ3 integrins. *J. Neuroinflammation* 13:227. doi: 10.1186/s12974-016-0697-1

Ishitsuka, K., Ago, T., Arimura, K., Nakamura, K., Tokami, H., Makihara, N., et al. (2012). Neurotrophin production in brain pericytes during hypoxia: a role of pericytes for neuroprotection. *Microvasc. Res.* 83, 352–359. doi: 10.1016/j.mvr.2012.02.009

Issa, R., AlQteishat, A., Mitsios, N., Saka, M., Krupinski, J., Tarkowski, E., et al. (2005). Expression of basic fibroblast growth factor mRNA and protein in the human brain following ischaemic stroke. *Angiogenesis* 8, 53–62. doi: 10.1007/s10456-005-5613-8

Jain, R. K. (2003). Molecular regulation of vessel maturation. *Nat. Med.* 9, 685–693. doi: 10.1038/nm0603-685

Jakobsson, L., Franco, C. A., Bentley, K., Collins, R. T., Ponsioen, B., Aspalter, I. M., et al. (2010). Endothelial cells dynamically compete for the tip cell position during angiogenic sprouting. *Nat. Cell Biol.* 12, 943–953. doi: 10.1038/ncb2103

Jetten, N., Verbruggen, S., Gijbels, M. J., Post, M. J., De Winther, M. P., and Donners, M. M. (2014). Anti-inflammatory M2, but not pro-inflammatory M1 macrophages promote angiogenesis *in vivo*. *Angiogenesis* 17, 109–118. doi: 10.1007/s10456-013-9381-6

Kaiser, D., Weise, G., Möller, K., Scheibe, J., Pösel, C., Baasch, S., et al. (2014). Spontaneous white matter damage, cognitive decline and neuroinflammation in middle-aged hypertensive rats: an animal model of early-stage cerebral small vessel disease. *Acta Neuropathol. Commun.* 2:169. doi: 10.1186/s40478-014-0169-8

Karar, J., and Maity, A. (2011). PI3K/AKT/mTOR pathway in angiogenesis. *Front. Mol. Neurosci.* 4:51. doi: 10.3389/fnmol.2011.00051

Kariya, T., Nishimura, H., Mizuno, M., Suzuki, Y., Matsukawa, Y., Sakata, F., et al. (2018). TGF-β1-VEGF-A pathway induces neoangiogenesis with peritoneal fibrosis in patients undergoing peritoneal dialysis. *Am. J. Physiol. Renal Physiol.* 314, 167–180. doi: 10.1152/ajprenal.00052.2017

Kasuno, K., Takabuchi, S., Fukuda, K., Kizaka-Kondoh, S., Yodoi, J., Adachi, T., et al. (2004). Nitric oxide induces hypoxia-inducible factor 1 activation that is dependent on MAPK and phosphatidylinositol 3-kinase signaling. *J. Biol. Chem.* 279, 2550–2558. doi: 10.1074/jbc.M308197200

Kilic, E., Kilic, U., Wang, Y., Bassetti, C. L., Marti, H. H., and Hermann, D. M. (2006). The phosphatidylinositol-3 kinase/Akt pathway mediates VEGF's neuroprotective activity and induces blood brain barrier permeability after focal cerebral ischemia. *FASEB J.* 20, 1185–1187. doi: 10.1096/fj.05-4829fje

Kim, I., Moon, S. O., Kim, S. H., Kim, H. J., Koh, Y. S., and Koh, G. Y. (2001). Vascular endothelial growth factor expression of intercellular adhesion molecule 1 (ICAM-1), vascular cell adhesion molecule 1 (VCAM-1), and E-selectin through nuclear factor-kappa B activation in endothelial cells. *J. Biol. Chem.* 276, 7614–7620. doi: 10.1074/jbc.M009705200

Kim, J. J., Kim, D. H., Lee, J. Y., Lee, B. C., Kang, I., Kook, M. G., et al. (2020). cAMP/EPAC signaling enables ETV2 to induce endothelial cells with high angiogenesis potential. *Mol. Ther.* 28, 466–478. doi: 10.1016/j.ymthe.2019.11.019

Kossmann, S., Schwenk, M., Hausding, M., Karbach, S. H., Schmidgen, M. I., Brandt, M., et al. (2013). Angiotensin II-induced vascular dysfunction depends on interferon-γ-driven immune cell recruitment and mutual activation of monocytes and NK-cells. *Arterioscler. Thromb. Vasc. Biol.* 33, 1313–1319. doi: 10.1161/ATVBAHA.113.301437

Krupinski, J., Issa, R., Bujny, T., Slevin, M., Kumar, P., Kumar, S., et al. (1997). A putative role for platelet-derived growth factor in angiogenesis and neuroprotection after ischemic stroke in humans. *Stroke* 28, 564–573. doi: 10.1161/01.STR.28.3.564

Krupinski, J., Kaluza, J., Kumar, P., Kumar, S., and Wang, J. M. (1994). Role of angiogenesis in patients with cerebral ischemic stroke. *Stroke* 25, 1794–1798. doi: 10.1161/01.STR.25.9.1794

Krupinski, J., Kumar, P., Kumar, S., and Kaluza, J. (1996). Increased expression of TGF-beta 1 in brain tissue after ischemic stroke in humans. *Stroke* 27, 852–857. doi: 10.1161/01.STR.27.5.852

Kume, T. (2012). Ligand-dependent Notch signaling in vascular formation. *Adv. Exp. Med. Biol.* 727, 210–222. doi: 10.1007/978-1-4614-0899-4_16

Kwee, B. J., Budina, E., Najibi, A. J., and Mooney, D. J. (2018). CD4 T-cells regulate angiogenesis and myogenesis. *Biomaterials* 178, 109–121. doi: 10.1016/j.biomaterials.2018.06.003

la Sala, A., Pontecorvo, L., Agresta, A., Rosano, G., and Stabile, E. (2012). Regulation of collateral blood vessel development by the innate and adaptive immune system. *Trends Mol. Med.* 18, 494–501. doi: 10.1016/j.molmed.2012.06.007

Lanahan, A. A., Hermans, K., Claes, F., Kerley-Hamilton, J. S., Zhuang, Z. W., Giordano, F. J., et al. (2010). VEGF receptor 2 endocytic trafficking regulates arterial morphogenesis. *Dev. Cell.* 18, 713–724. doi: 10.1016/j.devcel.2010.02.016

Lee, C. C., Chen, S. C., Tsai, S. C., Wang, B. W., Liu, Y. C., Lee, H. M., et al. (2006). Hyperbaric oxygen induces VEGF expression through ERK, JNK and c-Jun/AP-1 activation in human umbilical vein endothelial cells. *J. Biomed. Sci.* 13, 143–156. doi: 10.1007/s11373-005-9037-7

Lee, S., Chen, T. T., Barber, C. L., Jordan, M. C., Murdock, J., Desai, S., et al. (2007). Autocrine VEGF signaling is required for vascular homeostasis. *Cell* 130, 691–703. doi: 10.1016/j.cell.2007.06.054

Lee, S., Kim, O. J., Lee, K. O., Jung, H., Oh, S. H., and Kim, N. K. (2020). Enhancing the therapeutic potential of CCL2-overexpressing mesenchymal stem cells in acute stroke. *Int. J. Mol. Sci.* 21:7795. doi: 10.3390/ijms21207795

Lee, S. T., Chu, K., Jung, K. H., Ko, S. Y., Kim, E. H., Sinn, D. I., et al. (2005). Granulocyte colony-stimulating factor enhances angiogenesis after focal cerebral ischemia. *Brain Res.* 1058, 120–128. doi: 10.1016/j.brainres.2005.07.076

Lehrmann, E., Kiefer, R., Christensen, T., Toyka, K. V., Zimmer, J., Diemer, N. H., et al. (1998). Microglia and macrophages are major sources of locally produced transforming growth factor-beta1 after transient middle cerebral artery occlusion in rats. *Glia* 24, 437–448. doi: 10.1002/(SICI)1098-1136(199812)24:4<437::AID-GLIA9>3.0.CO;2-X

Lenzlinger, P. M., Morganti-Kossmann, M. C., Laurer, H. L., and McIntosh, T. K. (2001). The duality of the inflammatory response to traumatic brain injury. *Mol. Neurobiol.* 24, 169–181. doi: 10.1385/MN:24:1-3:169

Li, F., Lan, Y., Wang, Y., Wang, J., Yang, G., Meng, F., et al. (2011). Endothelial Smad4 maintains cerebrovascular integrity by activating N-cadherin through cooperation with Notch. *Dev. Cell* 20, 291–302. doi: 10.1016/j.devcel.2011.01.011

Li, S., Priceman, S. J., Xin, H., Zhang, W., Deng, J., Liu, Y., et al. (2013). Icaritin inhibits JAK/STAT3 signaling and growth of renal cell carcinoma. *PLoS ONE* 8:e81657. doi: 10.1371/journal.pone.0081657

Li, T. F., Ma, J., Han, X. W., Jia, Y. X., Yuan, H. F., Shui, S. F., et al. (2019). Chrysin ameliorates cerebral ischemia/reperfusion (I/R) injury in rats by regulating the PI3K/Akt/mTOR pathway. *Neurochem. Int.* 129:104496. doi: 10.1016/j.neuint.2019.104496

Li, W., Yang, Y., Hu, Z., Ling, S., and Fang, M. (2015). Neuroprotective effects of DAHP and Triptolide in focal cerebral ischemia via apoptosis inhibition and PI3K/Akt/mTOR pathway activation. *Front. Neuroanat.* 9:48. doi: 10.3389/fnana.2015.00048

Li, Y., Zhang, X., Cui, L., Chen, R., Zhang, Y., Zhang, C., et al. (2017). Salvianolic acids enhance cerebral angiogenesis and neurological recovery by activating JAK2/STAT3 signaling pathway after ischemic stroke in mice. *J. Neurochem.* 143, 87–99. doi: 10.1111/jnc.14140

Liang, S. D., Ma, L. Q., Gao, Z. Y., Zhuang, Y. Y., and Zhao, Y. Z. (2018). Granulocyte colony-stimulating factor improves neurological function and angiogenesis in intracerebral hemorrhage rats. *Eur. Rev. Med. Pharmacol. Sci.* 22, 2005–2014. doi: 10.26355/eurrev_201804_14729

Lin, L., Wang, Q., Qian, K., Cao, Z., Xiao, J., Wang, X., et al. (2018). bFGF protects against oxygen glucose deprivation/reoxygenation-induced endothelial monolayer permeability via S1PR1-dependent mechanisms. *Mol. Neurobiol.* 55, 3131–3142. doi: 10.1007/s12035-017-0544-0

Liu, T., Clark, R. K., McDonnell, P. C., Young, P. R., White, R. F., Barone, F. C., et al. (1994). Tumor necrosis factor-alpha expression in ischemic neurons. *Stroke* 25, 1481–1488. doi: 10.1161/01.STR.25.7.1481

Liu, X., Wen, S., Yan, F., Liu, K., Liu, L., Wang, L., et al. (2018). Salidroside provides neuroprotection by modulating microglial polarization after cerebral ischemia. *J. Neuroinflammation* 15:39. doi: 10.1186/s12974-018-1081-0

Lund, H., Pieber, M., Parsa, R., Grommisch, D., Ewing, E., Kular, L., et al. (2018). Fatal demyelinating disease is induced by monocyte-derived macrophages in the absence of TGF-β signaling. *Nat. Immunol.* 19, 1–7. doi: 10.1038/s41590-018-0091-5

Luo, D., Luo, Y., He, Y., Zhang, H., Zhang, R., Li, X., et al. (2006). Differential functions of tumor necrosis factor receptor 1 and 2 signaling in ischemia-mediated arteriogenesis and angiogenesis. *Am. J. Pathol.* 169, 1886–1898. doi: 10.2353/ajpath.2006.060603

Malashchenko, V. V., Meniailo, M. E., Shmarov, V. A., Gazatova, N. D., Melashchenko, O. B., Goncharov, A. G., et al. (2018). Direct anti-inflammatory effects of granulocyte colony-stimulating factor (G-CSF) on activation and functional properties of human T cell subpopulations *in vitro*. *Cell. Immunol.* 325, 23–32. doi: 10.1016/j.cellimm.2018.01.007

Malik, A. R., Lips, J., Gorniak-Walas, M., Broekaart, D. W. M., Asaro, A., Kuffner, M. T. C., et al. (2020). SorCS2 facilitates release of endostatin from astrocytes and controls post-stroke angiogenesis. *Glia* 68, 1304–1316. doi: 10.1002/glia.23778

Manoonkitiwongsa, P. S., Jackson-Friedman, C., McMillan, P. J., Schultz, R. L., and Lyden, P. D. (2001). Angiogenesis after stroke is correlated with increased numbers of macrophages: the clean-up hypothesis. *J. Cereb. Blood Flow Metab.* 21, 1223–1231. doi: 10.1097/00004647-200110000-00011

Marti, H. J., Bernaudin, M., Bellail, A., Schoch, H., Euler, M., Petit, E., et al. (2000). Hypoxia-induced vascular endothelial growth factor expression precedes neovascularization after cerebral ischemia. *Am. J. Pathol.* 156, 965–976. doi: 10.1016/S0002-9440(10)64964-4

Marumo, T., Schini-Kerth, V. B., and Busse, R. (1999). Vascular endothelial growth factor activates nuclear factor-kappaB and induces monocyte chemoattractant protein-1 in bovine retinal endothelial cells. *Diabetes* 48, 1131–1137. doi: 10.2337/diabetes.48.5.1131

Maurer, M. H., Schäbitz, W. R., and Schneider, A. (2008). Old friends in new constellations–the hematopoetic growth factors G-CSF, GM-CSF, and EPO for the treatment of neurological diseases. *Curr. Med. Chem.* 15, 1407–1411. doi: 10.2174/092986708784567671

Meng, H., Song, Y., Zhu, J., Liu, Q., Lu, P., Ye, N., et al. (2016). LRG1 promotes angiogenesis through upregulating the TGF-β1 pathway in ischemic rat brain. *Mol. Med. Rep.* 14, 5535–5543. doi: 10.3892/mmr.2016.5925

Menzie-Suderam, J. M., Modi, J., Xu, H., Bent, A., Trujillo, P., Medley, K., et al. (2020). Granulocyte-colony stimulating factor gene therapy as a novel therapeutics for stroke in a mouse model. *J. Biomed. Sci.* 27:99. doi: 10.1186/s12929-020-00692-5

Modi, J., Menzie-Suderam, J., Xu, H., Trujillo, P., Medley, K., Marshall, M. L., et al. (2020). Mode of action of granulocyte-colony stimulating factor (G-CSF) as a novel therapy for stroke in a mouse model. *J. Biomed. Sci.* 27:19. doi: 10.1186/s12929-019-0597-7

Muoio, V., Persson, P. B., and Sendeski, M. M. (2014). The neurovascular unit - concept review. *Acta Physiol.* 210, 790–798. doi: 10.1111/apha.12250

Nakamura, K., Arimura, K., Nishimura, A., Tachibana, M., Yoshikawa, Y., Makihara, N., et al. (2016). Possible involvement of basic FGF in the upregulation of PDGFRβ in pericytes after ischemic stroke. *Brain Res.* 1630, 98–108. doi: 10.1016/j.brainres.2015.11.003

Nossent, A. Y., Bastiaansen, A. J., Peters, E. A., de Vries, M. R., Aref, Z., Welten, S. M., et al. (2017). CCR7-CCL19/CCL21 axis is essential for effective arteriogenesis in a murine model of hindlimb ischemia. *J. Am. Heart Assoc.* 6:e005281. doi: 10.1161/JAHA.116.005281

Oladipupo, S. S., Smith, C., Santeford, A., Park, C., Sene, A., Wiley, L. A., et al. (2014). Endothelial cell FGF signaling is required for injury response but not for vascular homeostasis. *Proc. Natl. Acad. Sci. U. S. A.* 111, 13379–13384. doi: 10.1073/pnas.1324235111

Olofsson, B., Pajusola, K., von Euler, G., Chilov, D., Alitalo, K., and Eriksson, U. (1996). Genomic organization of the mouse and human genes for vascular endothelial growth factor B (VEGF-B) and characterization of a second splice isoform. *J. Biol. Chem.* 271, 19310–19317. doi: 10.1074/jbc.271.32.19310

Oyamada, N., Sone, M., Miyashita, K., Park, K., Taura, D., Inuzuka, M., et al. (2008). The role of mineralocorticoid receptor expression in brain remodeling after cerebral ischemia. *Endocrinology* 149, 3764–3777. doi: 10.1210/en.2007-1770

Pan, J. R., Li, Y., Pei, Z., Li, X. P., Peng, Y., and Wang, Y. D. (2010). Hypoxic tissues are associated with microvessel density following brain ischemia-reperfusion. *Neurol. Sci.* 31, 765–771. doi: 10.1007/s10072-010-0441-z

Papapetropoulos, A., García-Cardeña, G., Madri, J. A., and Sessa, W. C. (1997). Nitric oxide production contributes to the angiogenic properties of vascular endothelial growth factor in human endothelial cells. *J. Clin. Invest.* 100, 3131–3139. doi: 10.1172/JCI119868

Patra, K., Jana, S., Sarkar, A., Mandal, D. P., and Bhattacharjee, S. (2019). The inhibition of hypoxia-induced angiogenesis and metastasis by cinnamaldehyde is mediated by decreasing HIF-1α protein synthesis via PI3K/Akt pathway. *Biofactors* 45, 401–415. doi: 10.1002/biof.1499

Pham, L. D., Hayakawa, K., Seo, J. H., Nguyen, M. N., Som, A. T., Lee, B. J., et al. (2012). Crosstalk between oligodendrocytes and cerebral endothelium contributes to vascular remodeling after white matter injury. *Glia* 60, 875–881. doi: 10.1002/glia.22320

Potente, M., Gerhardt, H., and Carmeliet, P. (2011). Basic and therapeutic aspects of angiogenesis. *Cell* 146, 873–887. doi: 10.1016/j.cell.2011.08.039

Pulous, F. E., Carnevale, J. C., Al-Yafeai, Z., Pearson, B. H., Hamilton, J. A. G., Henry, C. J., et al. (2020). Talin-dependent integrin activation is required for endothelial proliferation and postnatal angiogenesis. *Angiogenesis* 24, 177–190. doi: 10.1007/s10456-020-09756-4

Qin, C., Fan, W. H., Liu, Q., Shang, K., Murugan, M., Wu, L. J., et al. (2017). Fingolimod protects against ischemic white matter damage by modulating microglia toward M2 polarization via STAT3 pathway. *Stroke* 48, 3336–3346. doi: 10.1161/STROKEAHA.117.018505

Ramsauer, M., and D'Amore, P. A. (2002). Getting Tie(2)d up in angiogenesis. *J. Clin. Invest.* 110, 1615–1617. doi: 10.1172/JCI0217326

Reitmeir, R., Kilic, E., Reinboth, B. S., Guo, Z., ElAli, A., Zechariah, A., et al. (2012). Vascular endothelial growth factor induces contralesional corticobulbar plasticity and functional neurological recovery in the ischemic brain. *Acta Neuropathol.* 123, 273–284. doi: 10.1007/s00401-011-0914-z

Ribatti, D., Tamma, R., and Crivellato, E. (2019). Cross talk between natural killer cells and mast cells in tumor angiogenesis. *Inflamm. Res.* 68, 19–23. doi: 10.1007/s00011-018-1181-4

Roberts, A. B., Sporn, M. B., Assoian, R. K., Smith, J. M., Roche, N. S., Wakefield, L. M., et al. (1986). Transforming growth factor type beta: rapid induction of fibrosis and angiogenesis *in vivo* and stimulation of collagen formation *in vitro*. *Proc. Natl. Acad. Sci. U. S. A.* 83, 4167–4171. doi: 10.1073/pnas.83.12.4167

Rustenhoven, J., Jansson, D., Smyth, L. C., and Dragunow, M. (2017). Brain pericytes as mediators of neuroinflammation. *Trends Pharmacol. Sci.* 38, 291–304. doi: 10.1016/j.tips.2016.12.001

Saha, P., and Smith, A. (2018). TNF-α (Tumor Necrosis Factor-α). *Arterioscler. Thromb. Vasc. Biol.* 38, 2542–2543. doi: 10.1161/ATVBAHA.118.311660

Salmeron, K., Aihara, T., Redondo-Castro, E., Pinteaux, E., and Bix, G. (2016). IL-1alpha induces angiogenesis in brain endothelial cells in vitro: implications for brain angiogenesis after acute injury. *J. Neurochem.* 136, 573–580. doi: 10.1111/jnc.13422

Saoud, H., Inoubli, O., Ben Fredj, S., Hassine, M., Ben Mohamed, B., Gaha, L., et al. (2019). Protective effect of the MCP-1 gene haplotype against schizophrenia. *Biomed. Res. Int.* 2019:4042615. doi: 10.1155/2019/4042615

Schierling, W., Troidl, K., Mueller, C., Troidl, C., Wustrack, H., Bachmann, G., et al. (2009). Increased intravascular flow rate triggers cerebral arteriogenesis. *J. Cereb. Blood Flow Metab.* 29, 726–737. doi: 10.1038/jcbfm.2008.165

Schmidt, R., Schmidt, H., and Fazekas, F. (2000). Vascular risk factors in dementia. *J. Neurol.* 247, 81–87. doi: 10.1007/s004150050021

Seledtsov, V. I., Malashchenko, V. V., Gazatova, N. D., Meniailo, M. E., Morozova, E. M., and Seledtsova, G. V. (2019). Directs effects of granulocyte-macrophage colony stimulating factor (GM-CSF) on adaptive immunogenesis. *Hum. Vaccin. Immunother.* 15, 2903–2909. doi: 10.1080/21645515.2019.1614396

Shang, J., Deguchi, K., Ohta, Y., Liu, N., Zhang, X., Tian, F., et al. (2011). Strong neurogenesis, angiogenesis, synaptogenesis, and antifibrosis of hepatocyte growth factor in rats brain after transient middle cerebral artery occlusion. *J. Neurosci. Res.* 89, 86–95. doi: 10.1002/jnr.22524

Shang, K., He, J., Zou, J., Qin, C., Lin, L., Zhou, L. Q., et al. (2020). Fingolimod promotes angiogenesis and attenuates ischemic brain damage via modulating microglial polarization. *Brain Res.* 1726:146509. doi: 10.1016/j.brainres.2019.146509

Shyu, W. C., Lin, S. Z., Chiang, M. F., Chen, D. C., Su, C. Y., Wang, H. J., et al. (2008). Secretoneurin promotes neuroprotection and neuronal plasticity via the Jak2/Stat3 pathway in murine models of stroke. *J. Clin. Invest.* 118, 133–148. doi: 10.1172/JCI32723

Sowa, K., Nito, C., Nakajima, M., Suda, S., Nishiyama, Y., Sakamoto, Y., et al. (2018). Impact of dental pulp stem cells overexpressing hepatocyte growth factor after cerebral ischemia/reperfusion in rats. *Mol. Ther. Methods Clin. Dev.* 10, 281–290. doi: 10.1016/j.omtm.2018.07.009

Stapor, P. C., Sweat, R. S., Dashti, D. C., Betancourt, A. M., and Murfee, W. L. (2014). Pericyte dynamics during angiogenesis: new insights from new identities. *J. Vasc. Res.* 51, 163–174. doi: 10.1159/000362276

Stockmann, C., Doedens, A., Weidemann, A., Zhang, N., Takeda, N., Greenberg, J. I., et al. (2008). Deletion of vascular endothelial growth factor in myeloid cells accelerates tumorigenesis. *Nature* 456, 814–818. doi: 10.1038/nature07445

Sugano, M., Tsuchida, K., and Makino, N. (2004). Intramuscular gene transfer of soluble tumor necrosis factor-alpha receptor 1 activates vascular endothelial growth factor receptor and accelerates angiogenesis in a rat model of hindlimb ischemia. *Circulation* 109, 797–802. doi: 10.1161/01.CIR.0000112579.61522.67

Takahashi, H., and Shibuya, M. (2005). The vascular endothelial growth factor (VEGF)/VEGF receptor system and its role under physiological and pathological conditions. *Clin. Sci.* 109, 227–241. doi: 10.1042/CS20040370

Taoufik, E., Petit, E., Divoux, D., Tseveleki, V., Mengozzi, M., Roberts, M. L., et al. (2008). TNF receptor I sensitizes neurons to erythropoietin- and VEGF-mediated neuroprotection after ischemic and excitotoxic injury. *Proc. Natl. Acad. Sci. U. S. A.* 105, 6185–6190. doi: 10.1073/pnas.0801447105

Uemura, M. T., Maki, T., Ihara, M., Lee, V. M. Y., and Trojanowski, J. Q. (2020). Brain microvascular pericytes in vascular cognitive impairment and dementia. *Front. Aging Neurosci.* 12:80. doi: 10.3389/fnagi.2020.00080

Umehara, K., Sun, Y., Hiura, S., Hamada, K., Itoh, M., Kitamura, K., et al. (2018). A new conditionally immortalized human fetal brain pericyte cell line: establishment and functional characterization as a promising tool for human brain pericyte studies. *Mol. Neurobiol.* 55, 5993–6006. doi: 10.1007/s12035-017-0815-9

van Weel, V., Toes, R. E., Seghers, L., Deckers, M. M., de Vries, M. R., Eilers, P. H., et al. (2007). Natural killer cells and CD4+ T-cells modulate collateral artery development. *Arterioscler. Thromb. Vasc. Biol.* 27, 2310–2318. doi: 10.1161/ATVBAHA.107.151407

Vincze, C., Pál, G., Wappler, E. A., Szabó, E. R., Nagy, Z. G., Lovas, G., et al. (2010). Distribution of mRNAs encoding transforming growth factors-beta1,−2, and−3 in the intact rat brain and after experimentally induced focal ischemia. *J. Comp. Neurol.* 518, 3752–3770. doi: 10.1002/cne.22422

Virgintino, D., Girolamo, F., Errede, M., Capobianco, C., Robertson, D., Stallcup, W. B., et al. (2007). An intimate interplay between precocious, migrating pericytes and endothelial cells governs human fetal brain angiogenesis. *Angiogenesis* 10, 35–45. doi: 10.1007/s10456-006-9061-x

Walshe, T. E., Saint-Geniez, M., Maharaj, A. S., Sekiyama, E., Maldonado, A. E., and D'Amore, P. A. (2009). TGF-beta is required for vascular barrier function, endothelial survival and homeostasis of the adult microvasculature. *PLoS ONE* 4:e5149. doi: 10.1371/journal.pone.0005149

Wang, L., Chopp, M., Teng, H., Bolz, M., Francisco, M. A., Aluigi, D. M., et al. (2011). Tumor necrosis factor α primes cerebral endothelial cells for erythropoietin-induced angiogenesis. *J. Cereb. Blood Flow Metab.* 31, 640–647. doi: 10.1038/jcbfm.2010.138

Wang, Y., Kilic, E., Kilic, U., Weber, B., Bassetti, C. L., Marti, H. H., et al. (2005). VEGF overexpression induces post-ischaemic neuroprotection, but facilitates haemodynamic steal phenomena. *Brain* 128, 52–63. doi: 10.1093/brain/awh325

Wang, Z. G., Cheng, Y., Yu, X. C., Ye, L. B., Xia, Q. H., Johnson, N. R., et al. (2016). bFGF protects against blood-brain barrier damage through junction protein regulation via PI3K-Akt-Rac1 pathway following traumatic brain injury. *Mol. Neurobiol.* 53, 7298–7311. doi: 10.1007/s12035-015-9583-6

Watari, K., Nakamura, M., Fukunaga, Y., Furuno, A., Shibata, T., Kawahara, A., et al. (2012). The antitumor effect of a novel angiogenesis inhibitor (an octahydronaphthalene derivative) targeting both VEGF receptor and NF-κB pathway. *Int. J. Cancer* 131, 310–321. doi: 10.1002/ijc.26356

Werner, G. S. (2002). Promotion of collateral growth by granulocyte-macrophage colony-stimulating factor in patients with coronary artery disease. *Circulation* 105:e175; author reply e175. doi: 10.1161/01.CIR.0000016154.35658.00

Wilde, G. J., Pringle, A. K., Sundstrom, L. E., Mann, D. A., and Iannotti, F. (2000). Attenuation and augmentation of ischaemia-related neuronal death by tumour necrosis factor-alpha *in vitro*. *Eur. J. Neurosci.* 12, 3863–3870. doi: 10.1046/j.1460-9568.2000.00273.x

Winkler, E. A., Bell, R. D., and Zlokovic, B. V. (2011). Central nervous system pericytes in health and disease. *Nat. Neurosci.* 14, 1398–1405. doi: 10.1038/nn.2946

Xia, Y., Ling, X., Hu, G., Zhu, Q., Zhang, J., Li, Q., et al. (2020). Small extracellular vesicles secreted by human iPSC-derived MSC enhance angiogenesis through inhibiting STAT3-dependent autophagy in ischemic stroke. *Stem Cell Res. Ther.* 11:313. doi: 10.1186/s13287-020-01834-0

Xu, Q., Briggs, J., Park, S., Niu, G., Kortylewski, M., Zhang, S., et al. (2005). Targeting Stat3 blocks both HIF-1 and VEGF expression induced by multiple oncogenic growth signaling pathways. *Oncogene* 24, 5552–5560. doi: 10.1038/sj.onc.1208719

Yang, S., Jin, H., Zhu, Y., Wan, Y., Opoku, E. N., Zhu, L., et al. (2017). Diverse functions and mechanisms of pericytes in ischemic stroke. *Curr. Neuropharmacol.* 15, 892–905. doi: 10.2174/1570159X15666170112170226

Yao, H., Zhang, Y., Shu, H., Xie, B., Tao, Y., Yuan, Y., et al. (2019). Hyperforin promotes post-stroke neuroangiogenesis via astrocytic il-6-mediated negative immune regulation in the ischemic brain. *Front. Cell. Neurosci.* 13:201. doi: 10.3389/fncel.2019.00201

Yin, X. X., Zheng, X. R., Peng, W., Wu, M. L., and Mao, X. Y. (2020). Vascular endothelial growth factor (VEGF) as a vital target for brain inflammation during the COVID-19 outbreak. *ACS Chem. Neurosci.* 11, 1704–1705. doi: 10.1021/acschemneuro.0c00294

Yuan, H. T., Khankin, E. V., Karumanchi, S. A., and Parikh, S. M. (2009). Angiopoietin 2 is a partial agonist/antagonist of Tie2 signaling in the endothelium. *Mol. Cell. Biol.* 29, 2011–2022. doi: 10.1128/MCB.01472-08

Zhang, H., and Issekutz, A. C. (2002). Down-modulation of monocyte transendothelial migration and endothelial adhesion molecule expression by fibroblast growth factor: reversal by the anti-angiogenic agent SU6668. *Am. J. Pathol.* 160, 2219–2230. doi: 10.1016/S0002-9440(10)61169-8

Zhang, H., Xiong, X., Liu, J., Gu, L., Li, F., Wan, Y., et al. (2016). Emulsified isoflurane protects against transient focal cerebral ischemia injury in rats via the PI3K/Akt signaling pathway. *Anesth. Analg.* 122, 1377–1384. doi: 10.1213/ANE.0000000000001172

Zhang, J., Cui, Q., Zhao, Y., Guo, R., Zhan, C., Jiang, P., et al. (2020). Mechanism of angiogenesis promotion with Shexiang Baoxin Pills by regulating function and signaling pathway of endothelial cells through macrophages. *Atherosclerosis* 292, 99–111. doi: 10.1016/j.atherosclerosis.2019.11.005

Zhang, K., and Luo, J. (2019). Role of MCP-1 and CCR2 in alcohol neurotoxicity. *Pharmacol. Res.* 139, 360–366. doi: 10.1016/j.phrs.2018.11.030

Zhong, M., Li, N., Qiu, X., Ye, Y., Chen, H., Hua, J., et al. (2020). TIPE regulates VEGFR2 expression and promotes angiogenesis in colorectal cancer. *Int. J. Biol. Sci.* 16, 272–283. doi: 10.7150/ijbs.37906

Zhou, W., Feng, X., Wu, Y., Benge, J., Zhang, Z., and Chen, Z. (2009). FGF-receptor substrate 2 functions as a molecular sensor integrating external regulatory signals into the FGF pathway. *Cell Res.* 19, 1165–1177. doi: 10.1038/cr.2009.95

Zhou, Y. F., Chen, A. Q., Wu, J. H., Mao, L., Xia, Y. P., Jin, H. J., et al. (2019). Sema3E/PlexinD1 signaling inhibits postischemic angiogenesis by regulating endothelial DLL4 and filopodia formation in a rat model of ischemic stroke. *FASEB J.* 33, 4947–4961. doi: 10.1096/fj.201801706RR

Zhu, J., Cao, D., Guo, C., Liu, M., Tao, Y., Zhou, J., et al. (2019). Berberine facilitates angiogenesis against ischemic stroke through modulating microglial polarization via AMPK signaling. *Cell. Mol. Neurobiol.* 39, 751–768. doi: 10.1007/s10571-019-00675-7

Zhu, Y., Culmsee, C., Roth-Eichhorn, S., and Krieglstein, J. (2001). Beta(2)-adrenoceptor stimulation enhances latent transforming growth factor-beta-binding protein-1 and transforming growth factor-beta1 expression in rat hippocampus after transient forebrain ischemia. *Neuroscience* 107, 593–602. doi: 10.1016/S0306-4522(01)00357-8

Zhu, Z., Xu, T., Guo, D., Huangfu, X., Zhong, C., Yang, J., et al. (2018). Serum hepatocyte growth factor is probably associated with 3-month prognosis of acute ischemic stroke. *Stroke* 49, 377–383. doi: 10.1161/STROKEAHA.117.019476

Zou, Y., Hu, J., Huang, W., Ye, S., Han, F., Du, J., et al. (2020). Non-mitogenic fibroblast growth factor 1 enhanced angiogenesis following ischemic stroke by regulating the sphingosine-1-phosphate 1 pathway. *Front. Pharmacol.* 11:59. doi: 10.3389/fphar.2020.00059

**Conflict of Interest:** The authors declare that the research was conducted in the absence of any commercial or financial relationships that could be construed as a potential conflict of interest.

frontiers in Cellular Neuroscience

ORIGINAL RESEARCH
published: 06 May 2021
doi: 10.3389/fncel.2021.656832

# Beta-Secretase 1 Underlies Reactive Astrocytes and Endothelial Disruption in Neurodegeneration

*María Victoria Chacón-Quintero[1,2†], Lina Gisela Pineda-López[1,2†], Carlos Andrés Villegas-Lanau[3], Rafael Posada-Duque[1,2] and Gloria Patricia Cardona-Gómez[1*]*

[1] Neuroscience Group of Antioquia, Faculty of Medicine, University of Antioquia, Cellular and Molecular Neurobiology Area, Medellin, Colombia, [2] Institute of Biology, Faculty of Exact and Natural Sciences, University of Antioquia, Medellin, Colombia, [3] Neurobank, Faculty of Medicine, SIU, University of Antioquia, Medellin, Colombia

OPEN ACCESS

**Edited by:**
Junlei Chang,
Chinese Academy of Sciences (CAS), China

**Reviewed by:**
Wolfgang Härtig,
Leipzig University, Germany
Yu Chen,
Chinese Academy of Sciences (CAS), China
Liang Gao,
Chinese Academy of Sciences, China

***Correspondence:**
Gloria Patricia Cardona-Gómez
patricia.cardonag@udea.edu.co

[†] These authors have contributed equally to this work

**Specialty section:**
This article was submitted to Cellular Neuropathology, a section of the journal Frontiers in Cellular Neuroscience

**Received:** 21 January 2021
**Accepted:** 12 April 2021
**Published:** 06 May 2021

**Citation:**
Chacón-Quintero MV, Pineda-López LG, Villegas-Lanau CA, Posada-Duque R and Cardona-Gómez GP (2021) Beta-Secretase 1 Underlies Reactive Astrocytes and Endothelial Disruption in Neurodegeneration. Front. Cell. Neurosci. 15:656832. doi: 10.3389/fncel.2021.656832

Dysfunction in the neurovascular unit (NVU) is a key component in the progressive deterioration of Alzheimer's disease (AD) and is critical in vascular dementia. Recent studies have shown that inflammation plays early and perhaps causal roles in the pathogenesis of AD related to NVU damage, possibly in part by overactivating the aspartic acid protease activity of β-site amyloid precursor protein-cleaving enzyme 1 (BACE1), which until now has almost solely been studied in the context of the β-amyloid cascade. In this study, we analyzed the relationship of BACE1 with astrocytes and blood vessels in human brains with sporadic and familial dementia [Autosomal dominant cerebral arteriopathy with subcortical infarcts and leukoencephalopathy (CADASIL), sporadic Alzheimer's disease (SAD), and familial Alzheimer's disease (FAD)] and how BACE1 inhibition affects astrocytes and endothelial cells under conditions of glutamate toxicity. Our results show increased BACE1, PHF (Paired helical filaments)-tau and GFAP (Glial Fibrillary Acid Protein) immunoreactivity (IR) in the CA1 hippocampal regions of FAD and SAD brains. Furthermore, BACE1 immunoprecipitated with GFAP in tissue samples from all study cases, but their immunofluorescence close to (10 $\mu m^3$) or overlapping blood vessels was only increased in FAD and SAD brains, and PHF-tau was present around the vessels mainly in FAD brains. Interestingly, the increased BACE1 levels were associated with reactive astrocytes, characterized by morphological changes and upregulation of GFAP under pathological and stressful conditions, and endothelial disruption by glutamate excitotoxicity, and these effects were reversed by BACE1 inhibition; further, BACE1-inhibited astrocytes protected endothelial cell integrity by preserving zonula occludens-1 (ZO-1) distribution and decreasing the expression of inflammatory markers. Taken together, these findings suggest that BACE1 dysregulation in astrocytes may have a role in the alterations in NVU integrity implicated in neurodegeneration.

**Keywords: BACE1, reactive astrocytes, endothelial disruption, neurodegeneration, neurovascular unit**

## INTRODUCTION

The blood brain-barrier (BBB) is a specialized structure which allow the exchange of molecules between peripheral circulatory system and the central nervous system (CNS) (Zenaro et al., 2016). The properties of the BBB are regulated by the function of the neurovascular unit (NVU), which is composed of endothelial cells (ECs) in contact with the basal lamina, pericytes, astrocytes, and neurons and is closely associated with the extracellular matrix (Posada-Duque et al., 2014; Villabona-Rueda et al., 2019). Its importance and definition emerged from "First stroke progress review group meeting of the National Institute of Neurological disorders and stroke of the NIH" in July 2001, as the coupling of the cerebral blood flow and the neural activity (Iadecola, 2017), allowing the bi-directional communication between neurons and microvessels, which was comprehensively analyzed in stroke research (del Zoppo, 2010). Astrocytes are closely related to the ECs that comprise the BBB and support its functions through the release of trophic factors and maintain the integrity of tight junctions such as Claudin-5 (CLDN5) and ZO-1 (Barrier et al., 1997; Gaillard et al., 2000; Sofroniew and Vinters, 2010; Alvarez et al., 2011). These astroglial cells maintain the homeostasis of the brain parenchyma by regulating energy and metabolism, blood flow and synapse function. NVU components are susceptible to damage from high glutamate concentrations; specifically, in ECs, glutamate triggers apoptosis mediated by oxidative stress (Parfenova et al., 2006; Jean et al., 2013) and, in astrocytes, astrogliosis (Pekny et al., 2018). Reactive astrocytes propagate pro-inflammatory signals in addition to activating catabolic processes and triggering apoptosis; however, they also facilitate the uptake and synthesis of neurotransmitters, induce angiogenesis and mediate antioxidation, thus contributing to neuroprotection. The roles of reactive astrocytes depend on the profile of genes that are differentially expressed and the postinjury time (Becerra-Calixto and Cardona-Gómez, 2017).

BACE1 is expressed in the ECs of the human BBB; it has also been shown to be predominantly localized to the membrane with an abluminal distribution of BACE1 in brain microvessels having a role in the vascular aspects of Alzheimer's disease, particularly in the development of amyloid cerebral angiopathy (Devraj et al., 2016). BACE1 is a protease found in lipid rafts localized in endosomes and to a lesser extent in the trans-Golgi network (Koelsch, 2017). It has been characterized by its participation in amyloidosis and vascular deterioration. Although its expression was initially described in neurons, it has since been reported to be expressed in astrocytes and ECs at higher levels during stressful events such as ischemic stroke, in which a pro-inflammatory microenvironment is generated (Hartlage-Rübsamen et al., 2003; Bettegazzi et al., 2011; Zhao et al., 2011; Bulbarelli et al., 2012; Devraj et al., 2016).

Cerebrovascular dysfunction has been documented in vascular-type dementia, a group of heterogeneous brain disorders in which cognitive decline is associated with pre-existing pathological conditions in the cerebral vasculature (Costantino Iadecola, 2013). Some recent studies suggest that NVU dysfunction is not only a key component in the progressive deterioration of Alzheimer's pathology and critical in vascular dementia but also an early mediating factor in the initiation of the neurodegenerative cascades observed in both diseases (Zenaro et al., 2016; Nation et al., 2019). Consequently, an understanding of the cellular mechanisms involved in NVU dysfunction would be an extraordinary tool to improve our knowledge of the pathobiology of dementias, which would lead to the development of new therapeutic approaches (ElAli, 2014). Therefore, it is necessary to advance the understanding of BACE1 dysregulation and its role in the alterations of components of the NVU in neurodegenerative processes. To pursue this aim, we analyzed the relationship of BACE1 with astrocytes and blood vessels in human brains from individuals with sporadic and familial dementia (CADASIL, SAD, and FAD) and how BACE1-inhibited astrocytes acting on endothelial cells in a glutamate toxic environment. We found an increased expression of BACE1 in reactive astrocytes associated with hyperphosphorylated tau and located close to or overlapping with blood vessels in the AD cases. In addition, BACE1-inhibited astrocytes reduced the induced damage by glutamate in ECs in an *in vitro* model. Therefore, we propose that an overload of BACE1 in reactive astrocytes close to vessels is a triggering factor for neurodegeneration in AD.

## MATERIALS AND METHODS

### Human Brain Tissue

Postmortem hippocampal brain tissue from 5 cases of FAD (PSEN1 E280A mutation), 5 cases of SAD, 5 cases of CADASIL and 5 healthy age-matched individuals (Control) obtained from the Neurobank of the University of Antioquia were included in this study. Informed consent was obtained for the research, and the study was approved by the bioethics committee for human studies at the University of Antioquia. The brain tissue was fixed in tissue blocks by immersion in a 4% paraformaldehyde solution in 0.1 M phosphate buffer (PB) (pH 7.4) at 4°C for 7 days. After 7 days, the tissues were subjected to a sucrose gradient of 7, 25, and 30% in PB. The hippocampal tissue was embedded in isopentane and subsequently stored at −80°C. Then, 50-μm sections were cut in a cryostat (Leica CM1850). The cases used to carry out this study are shown in **Table 1**.

### Immunohistochemistry

Floating human hippocampal tissue sections (50 μm thick) were exposed to epitopes in 98% formic acid (Sigma, 100264) for 5–6 min at 85°C, and 30% Triton $^{TM}$ X-100 (Sigma, 93443) in PB for 5 min. Endogenous peroxidase activity was blocked using 1:1 methanol with 1% hydrogen peroxide in PB for 20 min at room temperature. Non-specific antibody binding sites were blocked with 1% bovine serum albumin (BSA) (Sigma-Aldrich) and 0.3% Triton X-100 in PB for 1 h. The sections were incubated

**TABLE 1 |** Study cases used according to pathological condition.

| Nbiol code | Neuro Biobank code | Condition | Gender | Onset age | Age of death | CERAD | Braak | Thal |
|---|---|---|---|---|---|---|---|---|
| C2 | 240 | Control -Healthy | F | Does not apply | 67 | 0 | 1 | 0 |
| C3 | 243 | Control -Healthy | F | Does not apply | 75 | 0 | 0 | 0 |
| C4 | 262 | Control -Healthy | M | Does not apply | 69 | A | 1 | 2 |
| C5 | 319 | Control -Healthy | M | Does not apply | 61 | 0 | 0 | 0 |
| C7 | 342 | Control -Healthy | F | Does not apply | 44 | 0 | 0 | 0 |
| F2 | 127 | FAD (E280A) | F | 49 | 62 | B | 4 | 5 |
| F3 | 322 | FAD (E280A) | F | 44 | 50 | C | 6 | 5 |
| F5 | 328 | FAD (E280A) | F | 50 | 63 | C | 6 | 5 |
| F6 | 335 | FAD (E280A) | M | 49 | 59 | C | 6 | 5 |
| F7 | 339 | FAD (E280A) | F | 51 | 65 | B | 5 | 5 |
| SI | 99 | Late SAD | F | 82 | 92 | C | 5 | 4 |
| S2 | 112 | Late SAD | F | 62 | 74 | B | 5 | 4 |
| S3 | 117 | Early SAD | F | 55 | 76 | B | 4 | 5 |
| S6 | 332 | SAD | F | 81 | 94 | B | 4 | 5 |
| S10 | 338 | SAD | F | 92 | 98 | A | 3 | 3 |
| AI | 118 | CADASIL | F | 52 | 65 | B | 1 | 2 |
| A2 | 147 | CADASIL | F | 35 | 45 | 0 | 0 | 0 |
| A3 | 160 | CADASIL | F | 32 | 49 | 0 | 0 | 0 |
| A4 | 201 | CADASIL | M | 41 | 59 | 0 | 0 | 0 |
| A5 | 321 | CADASIL | F | 55 | 78 | 0 | 0 | 0 |

*We used postmortem brain samples from n = 5 CNT, n = 5 SAD, n = 5 FAD (PSEN1 E280A mutation), and n = 5 CADASIL (Notch 3 mutation) cases obtained from the University of Antioquia Neurobank. The cases were classified as healthy controls (C), familial Alzheimer's (F), sporadic Alzheimer's (S), or CADASIL (A). The table includes the age of onset, age of death, postmortem index as the time between the patient's death and sampling, Consortium to Establish a Registry for Alzheimer's Disease (CERAD) Braak stage to classify the degree of AD, and Thal phase to show the intersection of tau and amyloid β. NA, not available; NAP, not applicable; B, histological findings suggest the diagnosis of AD; C, histological findings indicate the diagnosis of AD.*

with rabbit anti-BACE1 (ab108394, Abcam, 1:100), mouse-anti-human phospho-tau recognizing phosphorylated serine 202 and threonine 205 from tau. (PHF-tau, MN1020, Thermo Fisher Scientific, 1:1000), mouse anti-glial fibrillary acid protein (GFAP, G3893, Sigma-Aldrich, 1:250), or rabbit anti-vimentin (ab137321, Abcam, 1:250) primary antibody in PB with 0.3% Triton X-100 and 0.3% BSA at 4°C for 3 nights. The slices were then incubated with anti-mouse (31800, Invitrogen, 1:250) or anti-rabbit (B2770, Invitrogen, 1:250) biotinylated secondary antibody for 1 h and then incubated with the avidin biotin complex (ABC Standard Peroxidase Staining Kit, Pierce #32020, 1:250 reagent A:B) for 1 h. Staining was performed using diaminobenzidine (DAB, 12623957, Thermo Fisher Scientific) in 1% hydrogen peroxide. The slices were mounted and dried on slides, dehydrated by an alcohol gradient, and covered with the Consul-Mount mounting solution (Thermo Fisher Scientific; 9990440).

## Microscopy, Image Processing, and Analysis

The tissue IR was analyzed at 10× (air objective, NA 0,25, Nikon) magnification by light microscopy (Nikon Epsilon E200) with a Nikon digital sight DS-L1 camera. For each slide, two consecutive images were taken allowing encompass all the extension of CA1 area for its analysis. The images were transformed to 8-bit and then analyzed using the binary threshold in the ImageJ software (NIH ImageJ). To calculate the total stained area, segmentation of all images was performed using intensity thresholding.

## Immunofluorescence

For immunofluorescence staining, a procedure similar to that described above for immunohistochemistry was performed. After antigen retrieval with formic acid, tissue and background autofluorescence were blocked with 0.1% Sudan Black B (Sigma, S0395) in 70% ethanol for 10 min. Preincubation was performed with 1% BSA and 0.3% Triton, and the sections were then incubated with primary antibody mixtures for triple immunofluorescent staining. The first antibody mixture contained rabbit anti-GFAP (PA516291, Invitrogen, 1:250), mouse-anti-phospho-PHF-tau (MN1020, Thermo Fisher Scientific, 1:250) and DyLight 649-labeled *Ulex Europaeus agglutinin* (UAE) lectin (Vector Labs; DL-1068; 1:750), and the second antibody mixture contained anti-BACE1 (ab108394, Abcam, 1:100), mouse anti-GFAP (G3893, Sigma-Aldrich, 1:250) and DyLight 649-labeled UAE lectin. Both antibody mixtures were prepared in 0.3% Triton X-100 and 0.3% BSA in PB, and the sections were incubated in each mixture at 4°C for 3 nights. The fluorescent anti-rabbit antibodies Alexa 488 (A11008, Invitrogen, 1:750), anti-mouse Alexa 594 (A11005, Invitrogen, 1:750), anti-rabbit Alexa 594 (A11012, Invitrogen, 1:750) and anti-mouse Alexa 488 (A11001, Invitrogen, 1:750) were incubated for 1 h. The tissue sections were washed three times for 5 min and then mounted on slide plates and

sealed on coverslips with FluorSave (Millipore; 345789). Sections incubated in parallel to the sections described above but without the primary antibodies were included as negative controls for the background binding of the secondary antibody and to discriminate autofluorescence. The omission of the primary antibodies did not produce staining.

## Confocal Microscopy

The triple-stained mounted tissue sections were analyzed by a confocal laser scanning microscope (FV1000 Olympus, Japan) using a 60X objective (immersion oil, NA 1.42) and the Olympus FluoView program. A total of two random fields in the CA1 area were imaged for each section. For each experimental case, 21 consecutive individual images were obtained at 0.5 μm intervals in all channels along the *Z* axis of the sample. The image acquisition parameters remained the same between the samples. 16-bit TIFF images of 1024 x 1024 pixels (105.47 x 105.47 μm) were obtained with an XY pixel size of 103 nm and 500 nm between Z-sections. The confocal images were deconvolved, processed, and segmented for quantifying the Z stack signal represented as volumetric information; also, maximum projection images were generated for each field for illustrative purposes. The images were deconvolved using the Huygens Professional 19.10 software (Scientific Volume Imaging B.V.). After, these were transformed to 8-bit and then processed and analyzed by the FIJI software (Image J NIH). Then, immunofluorescent signals were segmented using machine learning and intensity thresholding by Otsu algorithm, to standardize the signals in all the images. The total area of staining and the areas of colocalization were measured. Colocalizing signals were identified using the algorithm and from the image calculator tool. A distance map tool from the 3D suite plugin (Ollion et al., 2013) was used to isolate signals located between 0 and 10 μm from the vessel surface to characterize the association of astrocytic endfeet with the vessels and the association with PHF-tau and BACE1 in the CA1 area. Z projections of the deconvolved images were made using the max intensity option, while segmented images were projected using the standard deviation.

## Immunoprecipitation

To confirm the relationship between both $GFAP^+$ astrocytes and BACE1, we immunoprecipitated BACE1 and then the co-immunoprecipitated GFAP. Briefly, samples were lysed in 10 mM Tris (pH 7.4), 100 mM NaCl, 1 mM EDTA, 1 mM EGTA, 10% glycerol, 1% NP40, 1 nM orthovanadate, 5 mM NaF, 1 mM phenylmethylsulfonyl fluoride with a protease inhibitor cocktail (Sigma-Aldrich). The lysates were clarified by centrifugation at 14,000 rpm for 5 min. A Pierce Protein Quantification Assay was performed, and then 200 μg total protein was incubated overnight at 4°C in the presence of the anti-BACE1 antibody (ab108394, Abcam, 1:100). Protein G Sepharose beads were added, and the samples were incubated for an additional 2 h at room temperature. The immune complexes were washed three times using immunoprecipitation lysis buffer before SDS-PAGE and immunoblotting. The proteins were separated using 10% SDS-PAGE, transferred to nitrocellulose membranes (Amersham) and probed with mouse anti-GFAP antibody (G3893, Sigma-Aldrich, 1:250). Whole lysates were used as positive controls, and incubation with an IgG peptide (395040065, Thermo, 1:500) was used as a negative control for immunoprecipitation. The blots were visualized using the Odyssey Infrared Imaging System (LI-COR Biosciences). To minimize interassay variation, samples from all experimental groups were run in parallel.

## bEnd.3 Cell Line Cultures

The bEnd.3 (ATCC CRL-2299) murine cell line was used as an endothelial cell model as we described previously (Becerra-Calixto et al., 2018). The bEnd.3 cells were thawed in DMEM (Sigma-Aldrich) supplemented with 20% fetal bovine serum (FBS, Eurobio) and 1% penicillin–streptomycin (Gibco). After 24 h, the medium was replaced with the maintenance medium [DMEM supplemented with 10% fetal bovine serum and 1% penicillin–streptomycin (Gibco)]. The cells were incubated at 37°C in 5% CO2. To perform the subcultures, the cells were trypsinized using a 0.25% trypsin/EDTA mixture (Gibco) for 5 min and subcultured in 12-well plates at a density of $2.5 \times 10^5$ cells per well.

## Astrocyte Primary Cultures

Astrocytes were obtained from primary cultures of cortical astrocytes from Wistar rat brains extracted on postnatal day 1 or 2 as we described previously (Posada-Duque et al., 2015). The cortex was enzymatically dissociated with 0.25% trypsin/EDTA mixture (Gibco, 15400054) during 15 min, cultured in T75 flasks (surface area 75 $cm^2$) and maintained in DMEM (Sigma-Aldrich) supplemented with 10% FBS and 1% penicillin–streptomycin (Gibco). The cells were incubated at 37°C in 5% $CO_2$. The culture medium was changed every 2 days. From day *in vitro* (DIV) 8 to DIV 10, the flasks were shaken at 350 rpm for a sequence of 6, 18, and 24 h to minimize the amount of microglia and oligodendrocytes. Then, the cells were trypsinized using a 0.25% trypsin/EDTA mixture (Gibco) for 5 min and subcultured in 12-well plates at a density of $7.5 \times 10^4$ cells per well.

## bEnd.3 and Astrocyte Coculture

Astrocytes were subcultured on DIV 10 on coverslips in 12-well plates. The bEnd.3 cells were thawed and subcultured on gelatinized coverslips with four paraffin dots at the ends until DIV 15 when the coculture was performed. The co-culture assembly consisted in superimposing one coverslip on the other so that both cell types are close and share the culture medium, the paraffin dots allow that there is no direct contact between the cells and therefore, without mechanical damage between them. On DIV 21, the coculture was disassembled to inhibit BACE1 only in astrocytes, and 24 h later, the coculture was reassembled and treated with glutamate (Becerra-Calixto et al., 2018). On DIV 23, the culture medium was collected to measure cytotoxicity, and both cell types were fixed for immunofluorescence staining.

## Glutamate-Induced Toxicity Assay and Inhibitor Treatment

### bEnd.3

The bEnd.3 cell cultures were pretreated on DIV 8 with β-secretase inhibitor IV (CAS 797035-11-1, Merck) at 1 μM. Twenty-four hours later, the cells were treated with glutamate at 125 μM for 20 min and were subsequently treated with the inhibitor again. On DIV 10, the culture medium was collected to measure the cytotoxicity, and the cells were fixed for immunofluorescence staining.

### Primary Astrocytes

The astrocytes were pretreated on DIV 21 with β-secretase inhibitor IV at 1 μM. Twenty-four hours later, the cells were treated with glutamate at 125 μM for 24 h and were subsequently treated with the inhibitor again. On DIV 23, the culture medium was collected to measure the cytotoxicity, and the cells were fixed for immunofluorescence staining.

### Coculture

In the coculture, BACE1 was inhibited in the astrocytes at the previously described concentration; however, both cell types were exposed to glutamate treatment for 20 min. On DIV 23, the medium was collected to measure the cytotoxicity, and the coculture was disassembled to fix both cell types.

## LDH Cytotoxicity Assay

The cytotoxicity was measured by evaluating the percentage of LDH release with the Roche LDH Cytotoxicity Detection Kit. The assay was performed by mixing the media with a mixture of the two kit solutions, incubating the combined mixture for 30 min in the dark, and measuring the absorbances of the samples at 490 nm in a microplate reader. The percentage of LDH release was calculated using the following formula: %LDH release ((A − low control)/(high control − low control)) 100, where A was the absorbance indicating the LDH activity level, the low control was the LDH activity of basal release from untreated cells and the high control was the measure of maximum LDH release from the cells, which was obtained from cells treated with 1% Triton X-100.

## *In vitro* Immunofluorescence

The cell cultures were fixed with 4% paraformaldehyde in cytoskeleton buffer with sucrose (CBS) (Posada-Duque et al., 2017). Autofluorescence was eliminated using 50 mM ammonium chloride (NH4Cl) for 10 min. The cells were permeabilized with 0.2% Triton. X-100 prepared in CBS and then treated with a blocking solution (2.5% FBS in CBS). The cultures were incubated overnight at 4°C with mouse primary antibodies against mouse CLDN5 (Invitrogen, 1:750), mouse GFAP (Sigma-Aldrich, 1:750), rabbit BACE1 (Abcam, 1:500) and mouse IL-1β (Abcam, 1:500). Subsequently, the cultures were incubated for 1 hour with Alexa 594- or Alexa 488-tagged secondary antibodies (Molecular Probes, 1:500), and the nuclei and cytoskeleton were stained with Hoechst 33258 (Invitrogen, 1:5000) and phalloidin conjugated with Alexa 594 or Alexa 488 (1:500, Molecular Probes). Then, serial washes with PBS (phosphate-buffered saline) were performed, and the coverslips with the immunolabeled cells were fixed to slides with FluorSave. The cells were observed under an Olympus IX 81 epifluorescence microscope, and the images were captured with an oil immersion objective (60X, NA 1.42) and then processed.

## Morphological Analysis

### Condensed Nuclei

The average diameter of each nucleus was quantified by automatic measurements using the "Count and measure objects" tool of the Image-Pro Plus software. Nuclei with diameters between 3.0 and 6.0 μm were defined as condensed. The percentage of condensed nuclei was calculated using the following formula: Percentage of condensed nuclei= [(condensed nuclei/(condensed nuclei + normal nuclei)] × 100.

### Number and Area of Gaps

The gaps are visualized as spaces between ECs indicate damage in the cell monolayer. This term was defined as: disruption of endothelial cells involving extravasation (Hirata et al., 1995) and inflammation more than cell death (Israelov et al., 2020). To determine the number of these spaces, F-actin signals were segmented using machine learning and intensity thresholding by Otsu algorithm, to standardize the signals in all the images, a binary image of each analyzed field was generated using the "Magic Wand" tool of the Adobe Photoshop software (González-Molina et al., 2021). With the images obtained, the number and area of gaps were measured using the "Count and measure objects" tool of the Image-Pro Plus software.

### Fluorescence Intensity Quantification

Fluorescence intensity (FI) measurements for each protein were obtained from the color channels by calculating the intensity using the "Measure" tool, which was relativized with the cell area. These analyses were performed using ImageJ (NIH software).

### Fluorescence Profiles

To determine the CLDN5 distribution, a fluorescence profile was established by drawing a white line of 50 μm through the cells (tracing it through the membrane, the cytoplasm and the nucleus) using the "Line profile" tool of the Image-Pro Plus software. The fluorescence profiles capturing the changes per channel of 20 cells were made for each treatment and the most representative ones were chosen for the figures.

## Statistical Analysis

The statistical analysis of the human data was performed with the GraphPad Prism software (version 6.0). Data were plotted as the mean ± standard error of the mean (SEM) for the quantitative variables. A variance homogeneity test was performed, and multivariate analyses were performed for one-way ANOVA parametric data, post hoc Kruskal-Wallis tests and Student's t tests. Values of $p < 0.05$ were considered significant.

For the *in vitro* analyses, the parametric data were compared using one-way ANOVA followed by the Tukey-Kramer post hoc test to identify the means that were significantly different from

each other. The nonparametric data were compared using the Kruskal-Wallis test and Dunn's test with Bonferroni correction. The results were considered significant when $p < 0.05$ (* indicates $p < 0.05$, ** indicates $p < 0.01$, and *** indicates $p < 0.001$). The data analysis was performed using the R version 3.4.4 software (R Core Team, 2018).

## RESULTS

### BACE1 Expression Is Increased in the PHF-tau$^+$ CA1 Area and Subiculum of Sporadic and Familial Alzheimer's Disease Brains

We analyzed the IR of BACE1, PHF-tau, GFAP and CLDN5 in human hippocampal tissue samples from patients with FAD, SAD, and CADASIL and from healthy control samples (**Figures 1A–D**). In the CA1 area, we found a significant increase in BACE1 IR in the FAD and SAD groups compared to that in the control group, while no significant differences were found in the CADASIL group (**Figure 1A**). The PHF-tau IR was increased in the CA1 area in the FAD and SAD groups and was significantly greater in the CA1 area in the FAD group than in the control group. The PHF-tau IR in the CADASIL group did not differ from that in the control group (**Figure 1B**). On the other hand, the GFAP IR was significantly higher in the FAD group than in the control group, and nonsignificant differences were observed in the SAD and CADASIL groups (**Figure 1C**). Finally, the CLDN5 data suggest a clear tendency toward increased expression in the CA1 area in the SAD group compared to that in the control group (**Figure 1D**), whereas the other groups did not show any differences.

Furthermore, we analyzed the IR of subiculum and CA4 areas in the same slices of human hippocampal tissues from FAD, SAD, CADASIL, and healthy control cases (**Supplementary Figures 1A, 2A**, respectively). In subiculum we detected a significant increase of BACE1 in all dementia cases being significant in FAD and CADASIL respect to the control group (**Supplementary Figure 1B**). Additionally, the PHF-tau IR presented an augment in FAD and SAD compared respect to the control, without change in CADASIL (**Supplementary Figure 1C**). Moreover, the levels of GFAP IR has a clear tendency to increase in all dementias cases, it was significant higher in FAD (**Supplementary Figure 1D**). On this way, CLDN5 data suggest a slight augment in the SAD group respect to the control and the other groups (**Supplementary Figure 1E**).

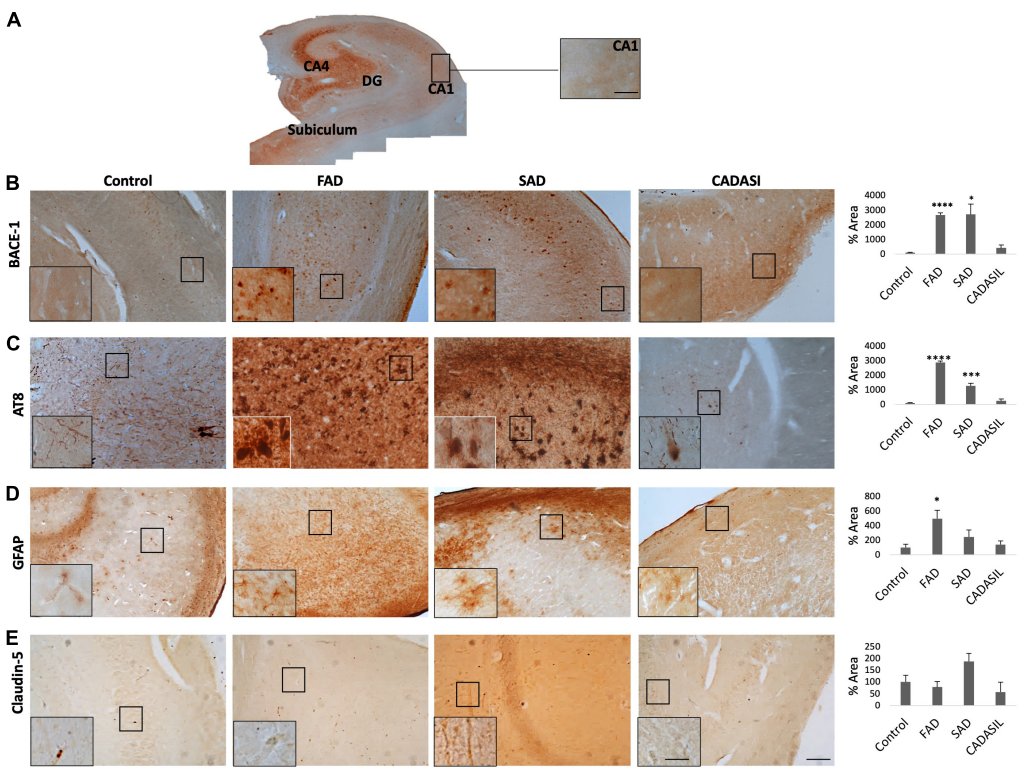


**FIGURE 1 |** BACE1, PHF-tau, GFAP, and CLDN5 immunoreactivities in the CA1 area of dementia brains. **(A)** Representative image of location in human Control hippocampus of area ca1. Magnification: 10×. Scale bar: 25 μm. **(B)** Representative images of the BACE1, **(C)** PHF-tau, **(D)** GFAP, and **(E)** CLDN5 immunoreactivities in the CA1 area of human hippocampal tissue. Magnification: 10×. Scale bar: 50 μm. Inset: 25 μm scale bar. The values in the bar graph are expressed as a densitometric percentage of the BACE1 IR in the CA1 area. FAD, familial-type Alzheimer's disease (presenilin 1 mutation E280A); SAD, sporadic Alzheimer's disease; CADASIL, autosomal dominant cerebral arteriopathy with subcortical infarcts and leukoencephalopathy. The data are expressed as the means ± SEM. $n = 4$. *$p < 0.05$; ***$p < 0.001$; ****$p < 0.0001$.

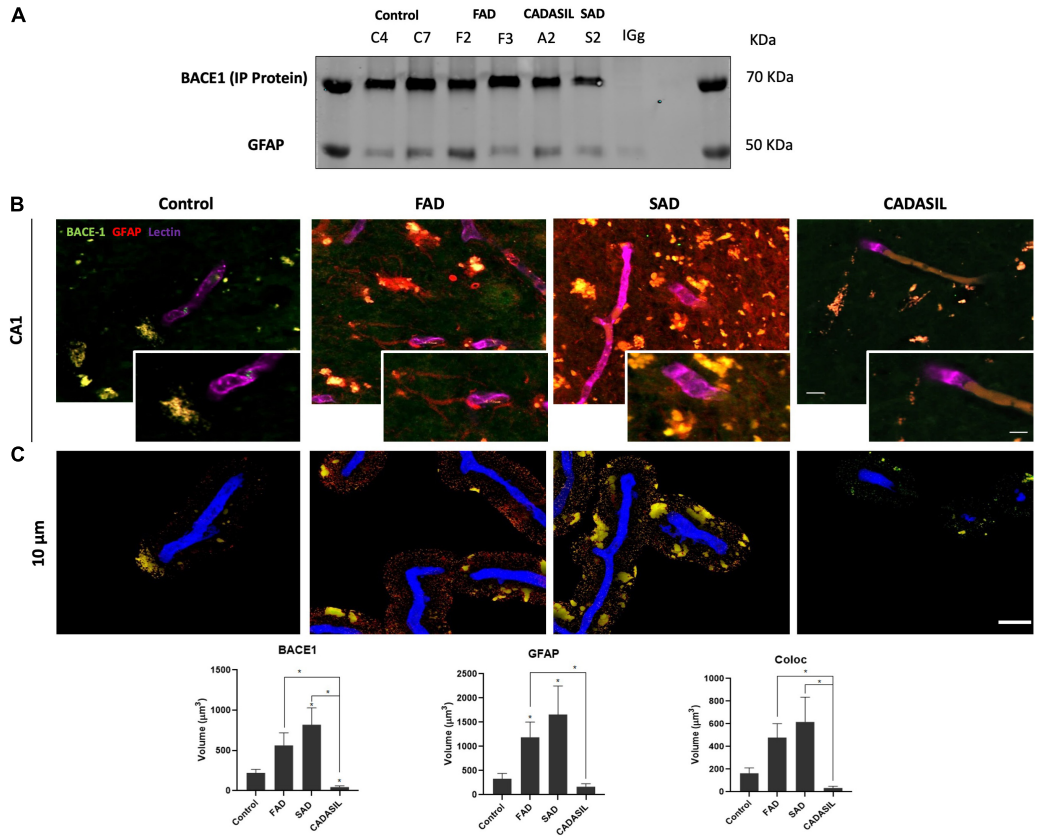


**FIGURE 2 |** BACE1 association with astrocytes and vessels in dementia brains. **(A)** Representative protein bands from the immunoprecipitation of BACE1 and co-inmunoprecipitation of GFAP are shown. IgG was used as a negative control for immunoprecipitation. **(B)** Z projection of Immunofluorescence of blood vessels triple-stained with DyLight 649- tagged UEA (color-coded in blue), anti-BACE1 antibody probed with Alexa Fluor 488 (green) and reactive astrocytes marked with Alexa Fluor 594 (red) in the hippocampal CA1 area. Magnification: 60x. Scale bar: 25 µm. Insets: 5 µm scale bar in B. **(C)** Z projection of the deconvolved images from the 3D reconstruction of the confocal images at 0 to 10 µm away from the vessel surface. Scale bar: 25 µm. The values represent the volumes in $\mu m^3$ for the levels of BACE1 and GFAP and the colocalization of BACE1 and GFAP. The data are expressed as the means ± SEM. $n = 4$. $^*p < 0.05$.

Inversely, in the CA4 area we found a significant decrease in BACE1 in SAD and CADASIL compared to the control group (**Supplementary Figure 2B**). Furthermore, PHF-tau IR was increased in FAD and SAD cases, and the increase was significant higher in FAD respect to SAD (**Supplementary Figure 2C**). However, GFAP and CLDN5 IRs did not present significant changes in CA4 area between the analyzed groups (**Supplementary Figures 2D,E**).

Finally, we selected the CA1 area for the subsequent analyses as a representative zone of neurodegeneration in the hippocampus.

## BACE1 Expression Is Increased in Reactive Astrocytes Around Blood Vessels, Which Are Associated With Hyperphosphorylated Tau in the Human AD Hippocampus

After the confirmation of BACE1 and GFAP expressions in the hippocampus, we assessed if both proteins presented association by co-immunoprecipitation, how it had been reported previously (Sil et al., 2020) and if presented differential association between dementias. However, we found the complex in all cases, which at least confirm the presence of BACE1 in GFAP+ astrocytes (Liang et al., 2020; **Figure 2A**). This finding was confirmed qualitatively by immunofluorescence in the SAD and FAD cases, which showed astrogliosis (increase of reactive astrocytes) (**Figure 2B**). After, we performed a deeper analysis of the association of BACE1 with GFAP around vessels in the CA1 area of the hippocampus in human brains with dementia. We confirmed a significant increase in the BACE1 and GFAP levels in the FAD and SAD groups compared with those in the control group and found that BACE1 and GFAP colocalized close to (10 $\mu m^3$) or overlapped with vessels mainly in the FAD and SAD groups, although the vessels were disrupted in the SAD group (**Figure 2C**). In addition, we found a significant increase in PHF-tau close to (10 $\mu m^3$) or overlapping with the vessels, and more of the PHF-tau$^+$ cells associated with GFAP+ cells in the FAD group than in the SAD group (**Figure 3**); both the FAD and SAD groups exhibited a higher association of PHF-tau+ cells with GFAP+ cells than the control and CADASIL groups. Additionally, vessel disruption mainly appeared in the SAD group samples.

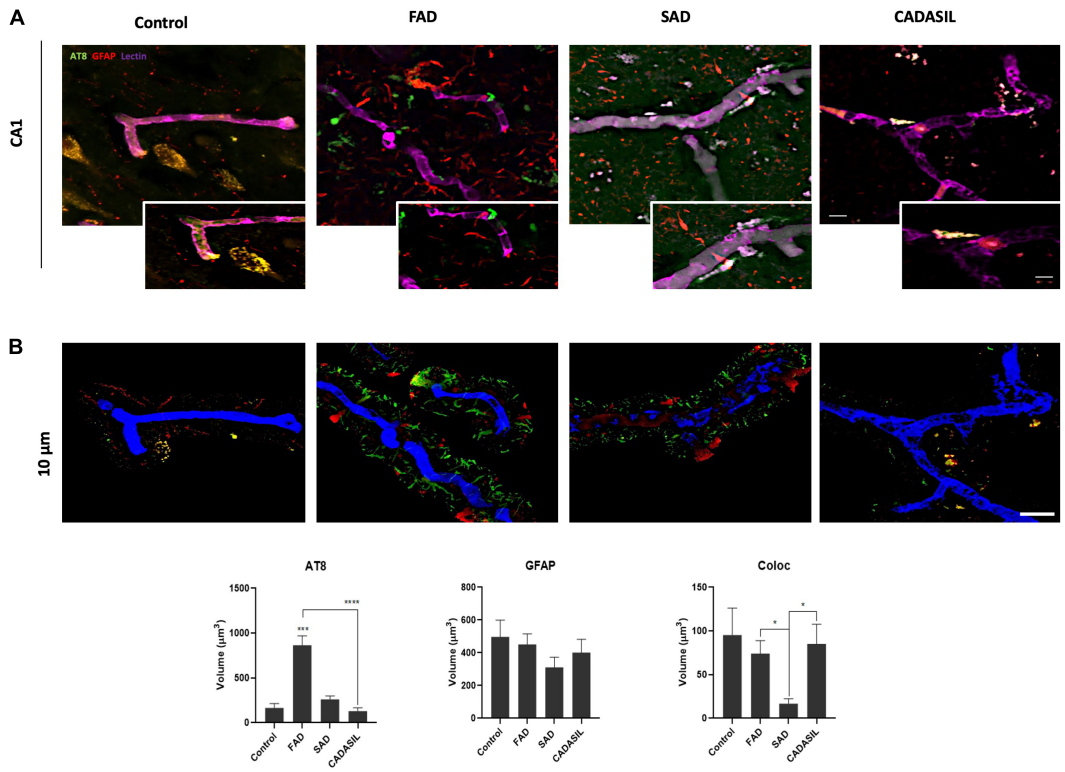


**FIGURE 3 |** PHF-tau association with astrocytes and vessels in dementia brains. **(A)** Z projection of Immunofluorescence of blood vessels triple-stained with DyLight 649 UEA (blue), PHF-tau antibody probed with Alexa Fluor 488 (green), and reactive astrocytes marked with Alexa Fluor 594 (red) in the hippocampal CA1 area. Magnification: 60x. Scale bar: 25 µm. Insets: 5 µm scale bar in A. **(B)** Z projection of the deconvolved images from the 3D reconstruction of the confocal images in A showing the triple staining present at 0 to 10 µm away from the vessel surface. Scale bar: 25 µm. The quantification of the volume in $\mu m^3$ for the levels of PHF-tau and GFAP and the colocalization between PHF-tau and GFAP. The data are expressed as the means ± SEM. $n = 4$. $^*p < 0.05$; $^{***}p < 0.001$; $^{****}p < 0.0001$.

## BACE1 Inhibition Protects Endothelial Cell Integrity Under Glutamate Toxicity by Reversing Structural and Inflammatory Damage

To confirm the potential relationship of BACE1 with ECs, ECs were treated with the BACE1 inhibitor at concentrations of 1, 5, 7.5, and 10 µM to measure the resulting cytotoxicity and determine the concentration to be used in subsequent experiments (**Supplementary Figure 3**). Treatment with 1 µM BACE1 inhibitor exhibited the least toxicity; therefore, this concentration was used for the cell treatments. To characterize the effects of glutamate and the BACE1 inhibitor on the bEnd.3 endothelial cell line, cytotoxicity was measured by determining the percentage of LDH release, and immunolabeling was performed to determine the cell state. In terms of the percentage of LDH released, there were no significant differences among the treatments, but a trend toward increased LDH release in response to glutamate treatment and an apparent reversal of this effect by the inhibitor were observed (**Figure 4A**). However, the glutamate treatment caused a significant increase in the percentage of condensed nuclei (**Figure 4B**) and in the number and area of gaps between cells (**Figures 4C,D**). These effects, except the number of gaps, were significantly reduced by the BACE1 inhibitor. Although the glutamate treatment caused depolymerization of the actin cytoskeleton that was not reversed by BACE1 inhibition (**Figure 4F**). The tight junction protein CLDN5 was partially recovered by BACE1 inhibition and was distributed to the membrane from the cytoplasm (**Figures 4E,G**). This finding was confirmed by the CLDN5 FI profile, in which BACE1 inhibition prevented the glutamate-induced increase in CLDN5 immunoreactivity in the cytoplasm, and CLDN5 was partially redistributed to the cell membrane (**Figure 4G**).

Complementarily, BACE1 inhibition decreased the BACE1 IR, which was increased by the glutamate treatment, and reversed the glutamate-induced inflammatory damage as shown by the reduction in the IL-1β IR (**Figures 5A,B**). BACE1 distribution in the controls appeared to be perinuclear, while IL-1β was localized throughout the entire cell in a largely diffuse pattern with a few brighter spots that looked like vesicles. The glutamate treatment expanded the distribution of BACE1 to the entire cell, although the highest concentration remains in the perinuclear zone where it apparently collocates with IL-1β. BACE1 inhibition upon stimulation with glutamate prevents IL-1β perinuclear concentration, but not in the case of BACE1 which is maintained mainly in such zone but with a diffuse pattern throughout the cells (**Figure 5C**). Together, these results suggest that BACE1 inhibition maintains the endothelial cell integrity

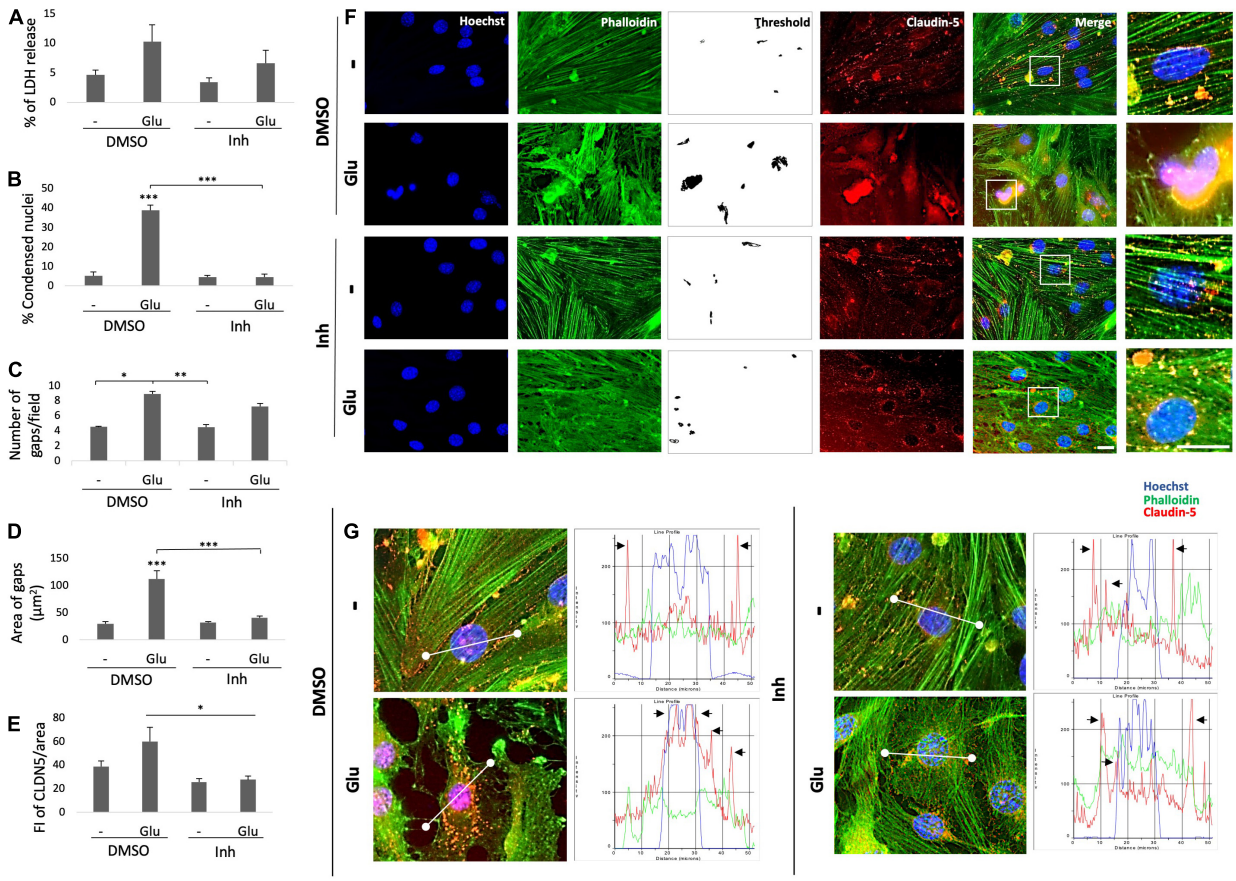


**FIGURE 4 |** BACE1 inhibition protects ECs from the damaging effects of glutamate. **(A)** Percentage of LDH release by ECs (bEnd.3) after 24 h of treatment. The data are presented as the mean ± SEM of *n* = 7. Kruskal-Wallis test. **(B)** Percentage of condensed nuclei for each treatment. These were quantified from 20 fields per treatment for each n (*n* = 4). The data are presented as the means ± SEM. **(C)** Number of gaps per field from threshold image (gaps = spaces between cells indicating disruption of the monolayer) presented as the mean ± SEM of *n* = 4. Kruskal-Wallis test followed by Dunn's test with the Bonferroni correction. **(D)** Area of gaps between cells expressed in $\mu m^2$; the area was quantified as the mean of the black area in threshold images from 20 fields per treatment for each n (*n* = 4). ANOVA followed by Tukey's test. **(E)** FI of CLDN5 per unit area was quantified from 20 cells per treatment for each n (*n* = 4 performed in duplicate) and divided by unit area. f) Morphological characterization of ECs showing the nuclei stained with Hoechst (blue), the F-actin cytoskeleton visualized with Alexa Fluor 488 phalloidin (green), and the tight junction protein CLDN5 visualized with Alexa Fluor 594 (red). Magnification: 60x. Scale bar: 20 µm. The zoomed insets show the condition of the nuclei, the state of the actin cytoskeleton and the distribution of CLDN5. **(G)** Fluorescence profiles (right column) showing the cellular distribution of CLDN5 (red line) in relation to the nucleus (blue line) and cytoskeleton (green line) based on the representative images (left column). The black arrows indicate the tight junction peaks to show the changes in CLDN5 distribution by the treatment. The white line drawn on each cell represents a distance of 50 µm. The data are presented as the means ± SEM, ANOVA followed by Tukey's test. DMSO = vehicle, Inh = β-secretase inhibitor IV, - or Glu refers to glutamate treatment. All experiments were performed in duplicate. *$P < 0.05$, **$P < 0.01$, ***$P < 0.001$.

preventing inflammation, cell junction disruption and cell stress by glutamate toxicity.

## BACE1 Inhibition Reverses Astrocytic Reactivity, Causing Cytoskeletal Remodeling and Cell Inflammation

Reactive astrocytes present morphological and functional changes after injury (Escartin et al., 2021). Therefore, we assessed the morphology astrocytes under stress by glutamate toxicity and BACE1 inhibition. GFAP immunolabeling was performed and the cytotoxicity was measured through determining the percentage of LDH release. The glutamate treatment increased the percentage of LDH released in the treated cells compared with that in the control cells, and BACE1 inhibition did not significantly reduce the percentage of LDH release, although there was a downward trend (**Figure 6A**). On the other hand, the GFAP FI increased with the glutamate treatment, and BACE1 inhibition reduced the GFAP FI to the baseline level observed in the controls (**Figure 6B**). The morphological characterization showed the above as well as changes in the microfilaments and intermediate filaments of the cytoskeleton (**Figure 6E**). BACE1 inhibition induced the production of actin processes which looks like filopodia and depolymerized GFAP, even detected at the extracellular space. These effects were found even when the astrocytes had been treated with glutamate. The IL-1β immunoreactivity showed a clear trend to decrease, although this trend was not significant, whereas the BACE1 protein levels

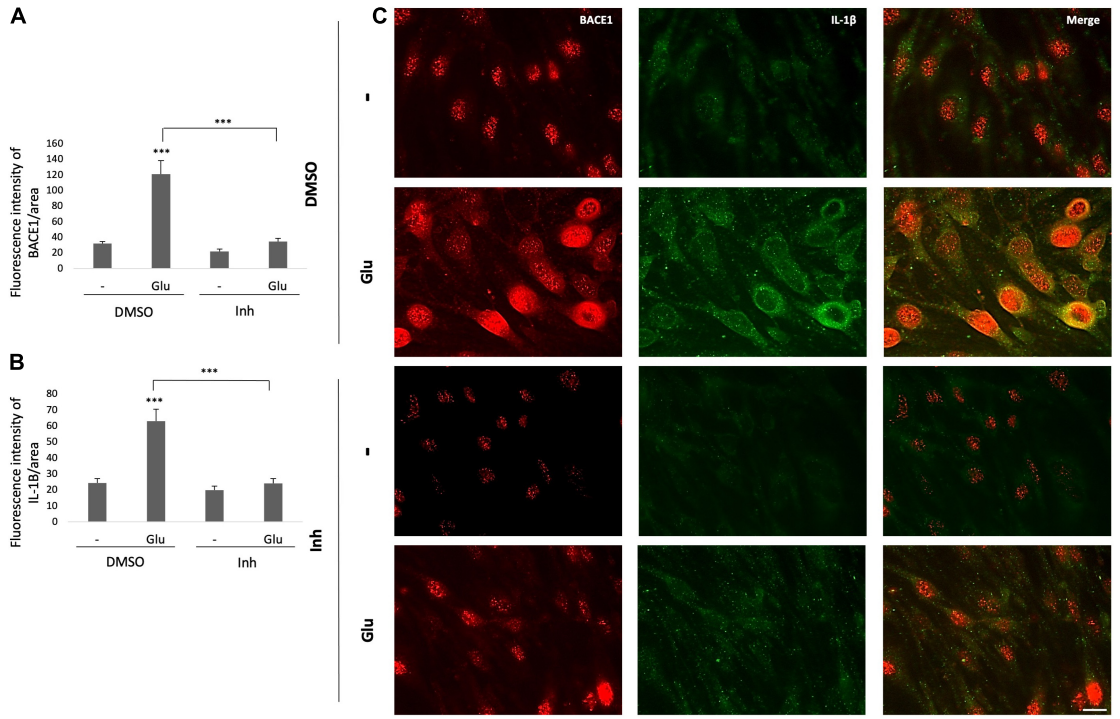


**FIGURE 5 |** BACE1 inhibitor reduces the glutamate-induced increases in BACE1 IR and the IL-1β inflammation marker in ECs. **(A,B)** Fluorescence intensities of BACE1 and IL-1β, respectively, per unit area, quantified from 20 cells per treatment for each n ($n$ = 4 performed in duplicate) and divided by unit area. **(C)** Representative images showing BACE1 (red, visualized with Alexa Fluor 594) and IL-1β (green, visualized with Alexa Fluor 488) expression in ECs (bEnd.3) under different treatments. Magnification: 60x. Scale bar: 20 μm. The data are presented as the means ± SEM, ANOVA followed by Tukey's test. ***$P < 0.001$. The bEnd.3 cell cultures were pretreated on DIV 8 with β-secretase inhibitor IV (CAS 797035-11-1, Merck) at 1 μM. Twenty-four hours later, the cells were treated with glutamate at 125 μM for 20 min and were subsequently treated with the inhibitor again. On DIV 10 the cells were fixed for immunofluorescence staining.

decreased significantly to the baseline levels observed in the controls (**Figures 6C,D**). The BACE1 immunolabeling was distributed throughout the entire cell, with a stronger bright spot at the perinucleus where it appeared to overlap with IL-1β, whose subcellular localization remains to be confirmed (**Figure 6F**). In summary, these findings suggest that BACE1 is involved in astrocyte activation and that its inhibition during toxic events could reverse reactive astrocyte and inflammation.

## BACE1-Inhibited Astrocytes Protect Endothelial Cell Integrity by Regulating ZO-1 Distribution and Decreasing Inflammation Caused by Glutamate

To validate the effect of BACE1-inhibited astrocytes on endothelial inflammation and apoptosis, astrocyte-endothelial cell coculture was performed under conditions of glutamate toxicity. The levels of ZO-1 and IL-1β and the percentage of LDH release were analyzed to determine the cellular effect. The glutamate treatment significantly increased the percentage of LDH release compared with that of the DMSO control, but this effect was not reversed by coculture with BACE1-inhibited astrocytes. However, the cytotoxicity values that were presented were low since the increase in the cells treated with glutamate was approximately 2.2% compared to that in the control cells (**Figure 7A**). Accordingly, the glutamate treatment increased the percentage of condensed nuclei by 3% compared to that of the DMSO control, and coculture with BACE1-inhibited astrocytes did not significantly reduce this percentage, although there was a downward trend (**Figure 7B**). The percentage of condensed nuclei caused by the glutamate treatment in the ECs not cocultured with astrocytes was 38% (**Figure 4D**), while in the coculture this value was 5% (**Figure 7B**), indicating that the BACE1-inhibited astrocytes had a protective effect on the endothelium under this stressful condition. In terms of structural damage, both the number and area of gaps between cells were increased by the glutamate treatment, and coculture with BACE1-inhibited astrocytes significantly reduced only the number of gaps (**Figure 7C**), although there was an evident trend toward decreased gap area (**Figure 7D**). Regarding inflammation, there was a significant increase in the IL-1β IR of the cells treated with glutamate compared with that of the cells treated with the inhibitor alone, but the IL-1β immunoreactivity of the glutamate-treated cells was not significantly different from that of the DMSO control cells. Coculturing with BACE1-inhibited astrocytes reduced this increase about 4%, which is a clear downward trend (**Figure 7E**). Furthermore, the basal levels of this cytokine were lower in the cells cocultured with astrocytes than in the cells not cocultured with astrocytes (**Figure 5C**).

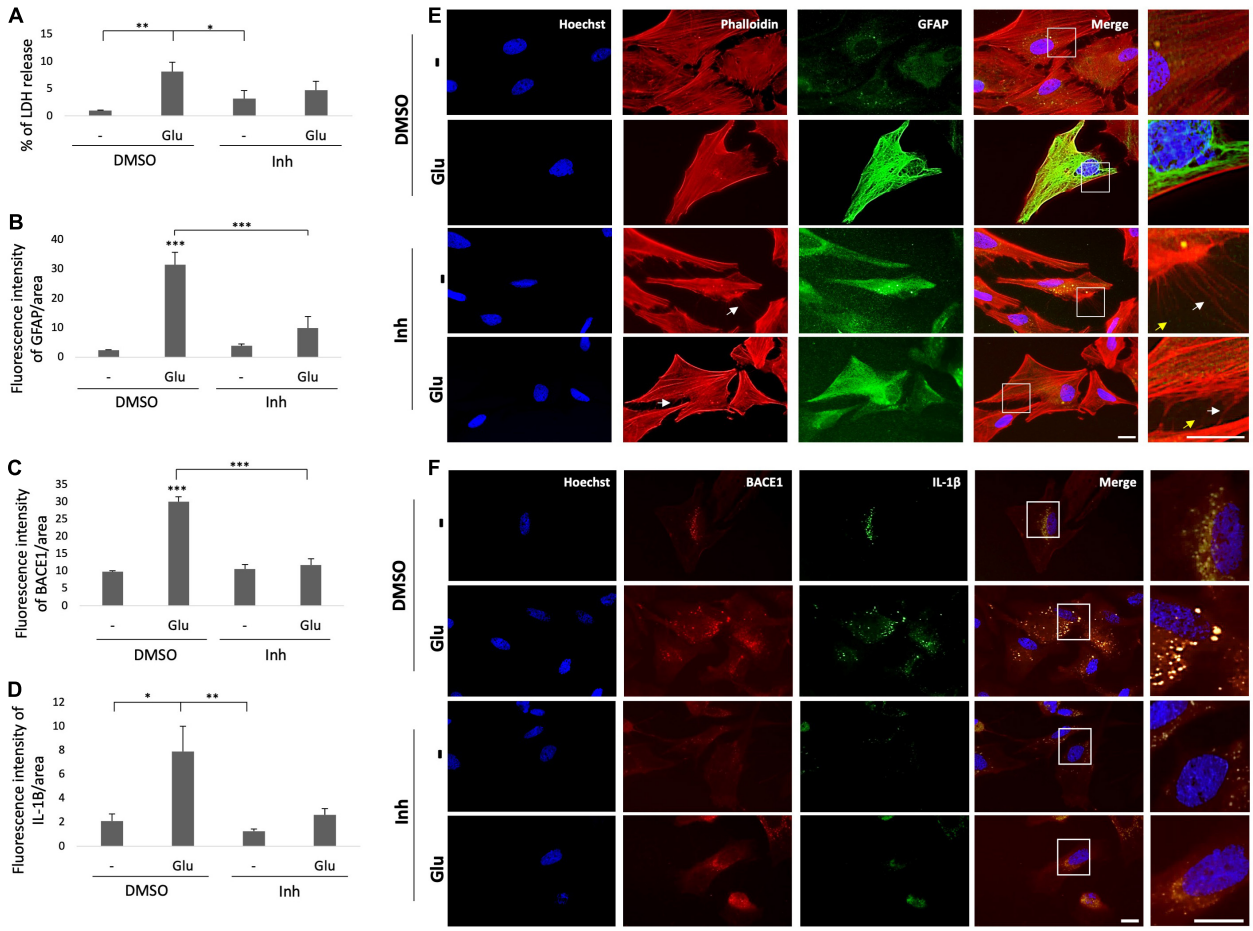


**FIGURE 6 |** BACE1 inhibition reduces astrocytic reactivity and induces filopodia-like processes. **(A)** Astrocytic cytotoxicity expressed as the percentage of LDH release after 24 h of treatment. The data are presented as the means ± SEM of $n = 8$. Kruskal-Wallis test followed by Dunn's test with Bonferroni correction. **(B)** FI of GFAP per unit area, quantified from 20 cells per treatment for each n ($n = 4$) and divided by unit area. The data are presented as the means ± SEM. ANOVA followed by Tukey's test. **(C)** FI of BACE1 per unit area, quantified from 20 cells per treatment for each n ($n = 4$) and divided by unit area. ANOVA followed by Tukey's test. **(D)** FI of IL-1β per unit area, quantified from 20 cells per treatment for each n ($n = 4$) and divided by unit area. **(E)** Morphological characterization of astrocytes showing the nuclei stained with Hoechst (blue), the F-actin cytoskeleton visualized with Alexa Fluor 594 phalloidin (red), and GFAP visualized with Alexa Fluor 488 (green). Magnification: 60x. Scale bar: 20 μm. In the zoomed insets, the white arrows indicate projections of the actin cytoskeleton, and the yellow arrows indicate extracellular GFAP IR puncta. **(F)** Representative images showing BACE1 (red, visualized with Alexa Fluor 594) and IL-1β (green, visualized with Alexa Fluor 488) expression in primary astrocytes under different treatments. The zoomed insets show the distributions of both proteins and an apparent perinuclear colocalization in vesicles (yellow). Magnification: 60x. Scale bar: 20 μm. DMSO = vehicle, Inh = β-secretase inhibitor IV, - or Glu refers to glutamate treatment. Kruskal-Wallis test followed by Dunn's test with Bonferroni correction. The data are presented as the means ± SEM, and the experiments were performed in duplicate. $^{*}P < 0.05$, $^{**}P < 0.01$, $^{***}P < 0.001$.

The observed changes in the cytoplasmic distribution and immunoreactivity of CLDN5 induced by the glutamate treatment also occurred with the tight junction protein ZO-1 (**Figure 7F**). BACE1-inhibited astrocytes reduced the increase in immunoreactivity caused by glutamate at the cytoplasm, and through fluorescence profiles, it was determined that they also cause the redistribution of ZO-1 to the cell membrane, although a portion remained in the cytoplasm, which follows the subcellular distribution described for this protein under nonpathological conditions (**Figures 8A,B**). Together, these results suggest that BACE1-inhibited astrocytes protect against tight junction damage and inflammation in ECS under glutamate toxicity.

## DISCUSSION

The results of this investigation suggest that BACE1 dysregulation could have a role in the changes observed in the NVU in Alzheimer's-type dementia. BACE1 augmentation was associated with reactive astrocytes and endothelial disruption in a neurodegenerative environment in the postmortem human brain and *in vitro*. This finding was supported by the increased expression of BACE1 observed in reactive astrocytes associated with PHF-tau and located close to or overlapping with blood vessels in the AD cases respect to the control group. Although, these characteristics were not so evident in the CADASIL cases, there was an increase of BACE1 in subiculum. Complementarily,

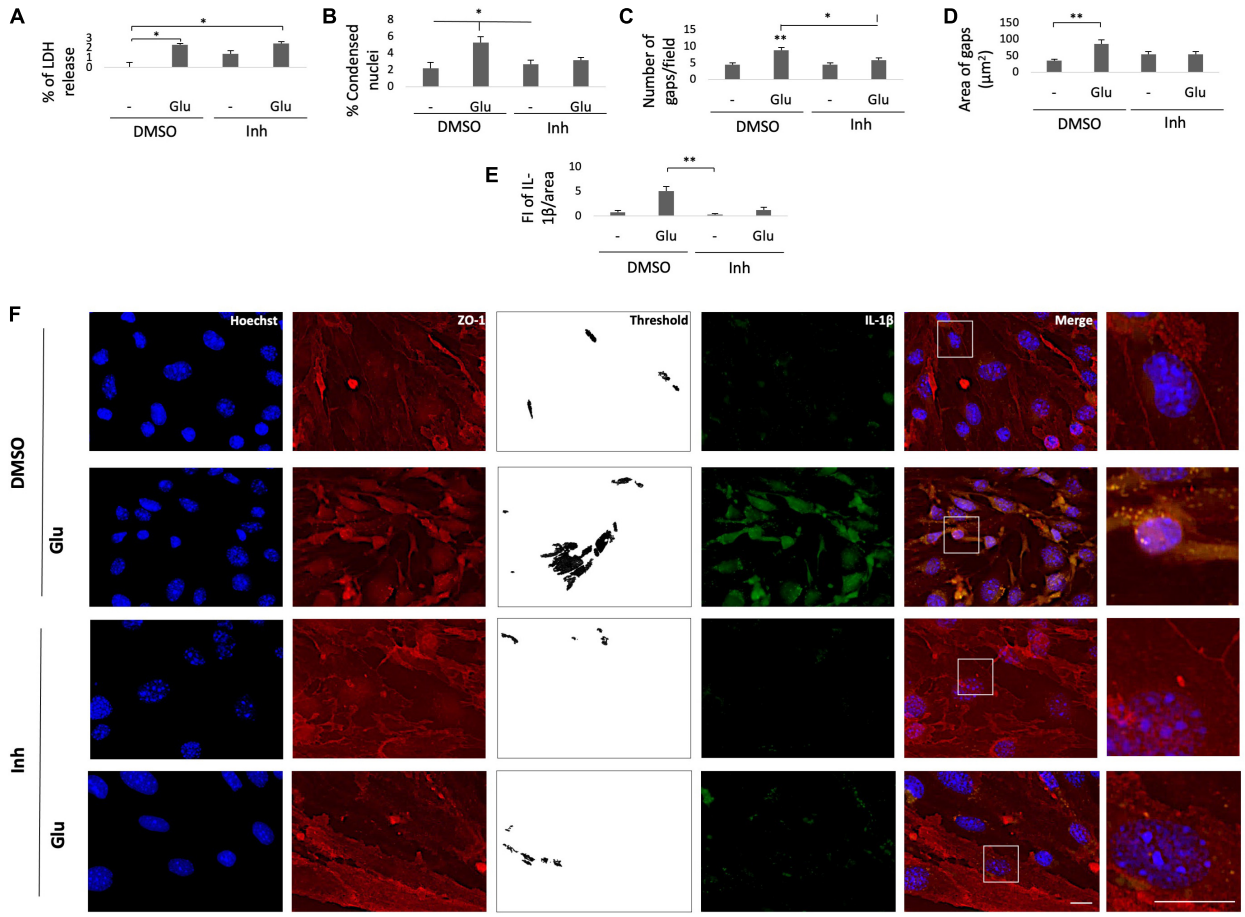


**FIGURE 7 |** BACE1-inhibited astrocytes protect the integrity of cocultured ECs from damage caused by glutamate. **(A)** Percentage of LDH release by the astrocyte-endothelium coculture after different treatments. **(B)** Percentage of condensed nuclei for each treatment, quantified from 20 fields per treatment for each n. **(C)** The number of gaps per field from threshold images. **(D)** The area of gaps between cells expressed in $\mu m^2$, quantified as the mean of the black area in threshold images from 20 fields per treatment for each n. **(E)** FI of IL-1β per unit area, quantified from 20 cells per treatment for each n and divided by unit area. All data just described are presented as the means ± SEM of $n = 4$. **(F)** Morphological characterization of endothelial cells that were cocultured with primary astrocytes showing nuclei stained with Hoechst (blue), IL-1β visualized with Alexa Fluor 488 (green) and the tight junction protein ZO-1 visualized with Alexa Fluor 594 (red). Magnification: 60x. Scale bar: 20 µm. The zoomed insets show the condition of the nuclei and the distributions of ZO-1 and IL-1β. DMSO = vehicle, Inh = β-secretase inhibitor IV, - or Glu refers to glutamate treatment. All experiments were performed in duplicate. **(A–D)** ANOVA followed by Tukey's test and **(E)** Kruskal-Wallis test followed by Dunn's test with Bonferroni correction. $^*P < 0.05$, $^{**}P < 0.01$.

*in vitro* studies showed that BACE1-inhibited astrocytes reduced the disruption of tight junction (ZO-$1^+$) and the increase of IL-1β IF glutamate-induced in cocultured ECs. Therefore, we propose that an overload of BACE1 in reactive astrocytes close to vessels is a triggering factor for neurodegeneration in AD.

It is known that the basal expression of BACE1 is located at CA4 area in human brain and is expressed in dentate gyrus in mice and rat brains (Laird et al., 2005; Xue et al., 2015). This protein is widely described in neurons, but also it has been found in astrocytes (Liang et al., 2020) and brain vessels (Devraj et al., 2016). However, the crucial role of BACE1 in NVU integrity and its implication on dementia has not detailed explored (Huang et al., 2020). In this research, our data support a generalized increase of BACE1 IR in the hippocampus of all dementia cases by immunohistochemistry. Specifically, we confirm that BACE1 was expressed in astrocytes, in concordance with previous studies (Liang et al., 2020). Although we did not observe changes between dementia cases by immunoprecipitation, it was clear by confocal microscopy that BACE1 was overregulated mainly in astrocytes on FAD and SAD groups, with a particular association with vessels in SAD. Additionally accumulated CLDN5 was found according to previous reports (Villar-Vesga et al., 2020; González-Molina et al., 2021). Such BACE$1^+$ reactive astrocytes associated to disrupted vessels were also closer but not overlapping with PHF-tau. A potential explanation why vessels are more affected in SAD, it is because SAD is associated to unhealthy lifestyle by metabolic disorders, inducing a slow and chronic impairment of NVU (Cardona-Gómez and Lopera, 2016), being longer this type of vessel affection than on FAD and CADASIL, where the genetic origin starts altering endosomes and endothelial smooth muscle, respectively, with faster and more aggressive progression.

Additional studies have shown BACE1 expression in reactive astrocytes close to β-amyloid peptide (Aβ) plaques in AD brains (Hartlage-Rübsamen et al., 2003). Thus far, it is understood

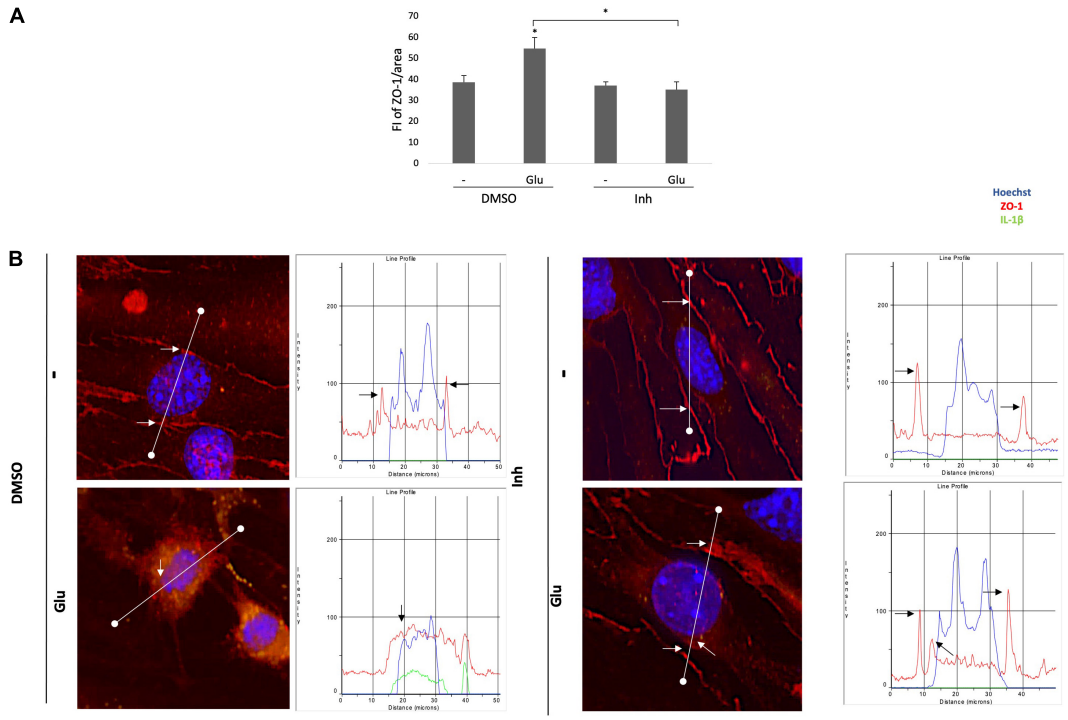


**FIGURE 8 |** BACE1-inhibited astrocytes reversed the increased IR and cytoplasmic distribution of the ZO-1 protein caused by glutamate in ECs. **(A)** FI of ZO-1 per unit area, quantified from 20 cells per treatment for each n ($n$ = 4 performed in duplicate) and divided by unit area. The data are presented as the means ± SEM. ANOVA followed by Tukey's test. *$P$ < 0.05. **(B)** Fluorescence profiles (right column) showing the cellular distributions of ZO-1 (red line) in relation to the nucleus (blue line) and IL-1β (green line) based on the representative images (left column). The black arrows indicate the tight junction peaks to show the changes in ZO-1 distribution by the treatment. The white line drawn on each cell represents a distance of 50 μm. DMSO = vehicle, Inh = β-secretase inhibitor IV, - or Glu refers to glutamate treatment.

that the astrocytic expression of BACE1 is only relevant to the development of AD if astrocytes also express APP as a substrate of BACE1. For example, primary astrocytes expressing APP generate significant amounts of Aβ peptides (Gray and Patel, 1993; Amara et al., 1999; Beck et al., 1999; Blasko et al., 2000; Docagne et al., 2004). Furthermore, APP is also expressed by reactive astrocytes in experimental models of chronic gliosis (Martins et al., 2001), and the expression of astrocytic APP results in increased generation of Aβ and A4-CT fragments derived from BACE1 activity (Bates et al., 2002; Lesné et al., 2003). However, may exist other explanations to our present results, because BACE1 in addition to neuronal targets; also has targets present in oligodendrocytes affecting myelin production (Pigoni et al., 2016; Fledrich et al., 2018; Zamparo et al., 2019); in astrocytes and ECs (Hemming et al., 2009) have the target LRP1 which is related with lipid and glucose metabolism (Liu et al., 2017; Mao et al., 2017), and the ST6Gal-l protein involved in monocytes trans-endothelial migration through BBB (Deng et al., 2017). Also the target Jagged/Notch in ECs is associated with angiogenesis in AD (Durrant et al., 2020) and astrocytic inflammation (Acaz-Fonseca et al., 2019). Which is in line with our findings about a potential role of BACE1 in astrocyte-endothelium interaction. Complementarily to these data, we have found differential patterns of astrocytes implication in dementia using additional markers such as AQP4, GS1, GLAST1, and for ECs such as Lectin UEA, vimentin, PECAM1 and CLDN5. However, SAD always showed more affection in relationship with disrupted vessels, less thickness, and more production of $CLDN5^{+}$ extracellular vesicles (EVs) [Henao-Restrepo J et al data non published (Villar-Vesga et al., 2020; González-Molina et al., 2021)]. Furthermore, the study from Gonzalez-Molina et al. suggested that EVs from astrocytes of 3xTgAD mice and AD human brain carried out messages that produced endothelial disruption and neuronal retraction (González-Molina et al., 2021).

On the other side, reactive astrocytes express neurofibrillary tangles (NFTs) and have been implicated in neurodegenerative processes (Arima et al., 1998; Botez et al., 1999; Beach et al., 2003; Schultz et al., 2004; Hishikawa et al., 2005; Jellinger and Attems, 2007; Munoz et al., 2007; Lace et al., 2012; Kovacs et al., 2013; López-González et al., 2013; Ferrer et al., 2014). Interestingly, tau hyperphosphorylation and the related cognitive impairment have been reversed by BACE1 targeting in hippocampus, involving Hsc70 and LAMP2 proteins associated to autophagy-related mediated by chaperones (CMA) and increased mTOR activation (Piedrahita et al., 2016), also reducing arachidonic acid, cPLA2 and COX2 proinflammatory signals *in vivo* (Cardona-Gómez and Lopera, 2016). These findings were supported by the reduction of neuronal proinflammatory environment *in vitro* depending on desaturases of fatty acids (Villamil-Ortiz et al., 2016). Furthermore, BACE1 silencing increased HADHA (hydroxyacyl-CoA dehydrogenase/3-ketoacyl-CoA thiolase/enoyl-CoA hydratase) downregulated by glutamate (data non published),

suggesting a role of BACE1 in the alteration of fatty acid oxidation. These findings are in concordance with (Sayre et al., 2017), who showed the improvement of fatty oxidation in astrocytes generate neuroprotection. In turn, it make sense if we considered that BACE1 reduction upregulates mTOR signaling and this pathway are involved in lipid metabolism sensing (Menon et al., 2017). The above is possible considering that mTOR does express in astrocytes (Latacz et al., 2015), and mTOR and HADHA potentially interact in proinflammatory environment (Zhang et al., 2017). Therefore, it is important consider a wider role of BACE1 in inflammatory processes even involving lipid metabolism.

Complementarily, *in vitro* results supported our data on human tissue findings. Because glutamate is critical involved in most neurological diseases and must be regulated by recycling in astrocytes (Abbink et al., 2019), where the overload of glutamate produces ATP failure and lipid peroxidation (Sabogal-Guáqueta et al., 2018). Also, a previous study showed that glutamate treatment affected the endothelial resistance in coculture with astrocytes, being more severe without astrocytes coculture, and this physiological measurement was correlated with LDH release and nuclear condensation (Becerra-Calixto et al., 2018). This context could help to explain why the BACE1 inhibitor [Inhibitor IV, specific for BACE1 well characterized previously (Stachel et al., 2004; Ben Halima et al., 2016)], produced astrocytes and ECs protection, since the inhibitor induced changes in the actin filaments with aspect of filopodia-like protrusions, which in astrocytes has been related to release of neurotrophic factors associated to neuroprotection (Posada-Duque et al., 2015). That is very interesting, considering that the overexpression of BACE1 in neurons has been related to decrease F-actin- rich levels through the regulation of B4, an auxiliary subunit of a voltage-gated sodium channel (Miyazaki et al., 2007). Moreover, BACE1 has also been related to the regulation of growth cone collapse (Bărao et al., 2015). However, additional studies are necessaries to describe the relation between BACE1 and cytoskeletal dynamic.

In addition, BACE1 inhibitor prevented the nuclear condensation and reduce the IL-1β proinflammatory marker not only in astrocytes as well as recovered co-cultured ECs, reducing GAPs that are more related with extravasation and inflammation than with cell death (Hirata et al., 1995; Israelov et al., 2020). In the case of the ECs, our data showed that the percentage of released LDH after glutamate treatment was very low contrasted with nuclear condensation levels, since chromatin condensation occurs in the early stages of excitotoxicity prior to the disruption of the plasma membrane and the release of LDH, that occurs later in an advanced cell detriment (Bezvenyuk et al., 2003; Elmore, 2007). Moreover, the relationship between excitotoxicity and inflammatory phenomena, specifically regarding IL-1β, has been extensively studied (Fogal and Hewett, 2008). Also, tumor necrosis factor-α (TNF-α) has been linked to the disruption of tight and adherent junctions between ECs by increasing BACE1 levels (Deng et al., 2017). And regarding ZO-1, it could be recovered by Sonic hedgehog (Shh) and glial-derived neurotrophic factor (GDNF) released by astrocytes, exerting a protective effect on ECs (Michinaga and Koyama, 2019). However, further experiments are required for a better understanding. Alternatively, the IL-1β increased in glial cells can cause the activation of the inflammatory mediator Cyclooxygenase 2 (COX-2) in neurons, which in turn upregulates BACE1 through Prostaglandin E2 (PGE2) and cAMP in a reciprocal interaction between the two cell types (Wang et al., 2014). Since astrocytes interact not just with neurons but also with ECs, and the molecules mentioned above are conserved in different cell types, it is probable that the increase in astrocyte IL-1β also promotes the activity of cyclooxygenases in ECs, which would result in not only would increase BACE1 but also the vasoconstriction (Wang et al., 2014; Mishra et al., 2016).

Finally, until now, the development of β-secretase inhibitors as therapeutic candidates has been slow because many did not reach the brain, were rapidly transported to the bloodstream, blocked BACE1 in all cells in the brain parenchyma or those are in initial phases (Gosh et al., 2012; Vassar, 2014) and is necessary improve the security and efficacy. There are other alternatives as BBB transporters (Joy Yu et al., 2011), or higher bioavailability of the BACE1 antibody in the parenchyma (Simpson et al., 2014). Other studies have suggested BACE1 in the BBB as a fundamental target for treating the vascular aspects of AD (Roßner et al., 2005). And how had been mentioned before: "Targeting drugs to BACE1-specific extracellular epitopes on the blood-facing luminal side of the endothelium could facilitate drug design, as the need for BBB penetration and resistance to active transport out of the brain can be avoided" (Devraj et al., 2016). In addition, our findings suggest that targeting BACE1 in the NVU in a cell-specific manner (i.e., in astrocytes or vessels) could be converted into new AD therapies that may lead to clinical outcomes. In summary, our work highlights the increased BACE1 expression of reactive astrocytes associated with endothelial disruption as a triggering factor of neurodegeneration in AD, therefore continue being crucial as therapeutical target.

## AUTHOR'S NOTE

BACE1 augment in reactive astrocytes around vessels were associated with Alzheimer's-type neurodegeneration in the human hippocampus. Increased BACE1 expression was associated with reactive astrocytes and endothelial disruption by glutamate toxicity *in vitro*. In this context, BACE1-inhibited astrocytes protect endothelial cell integrity by preserving ZO-1 distribution and decreasing inflammatory markers.

## DATA AVAILABILITY STATEMENT

The raw data supporting the conclusions of this article will be made available by the authors, without undue reservation.

## ETHICS STATEMENT

The studies involving human participants were reviewed and approved by Human Ethical Committee, University of Antioquia. The patients/participants provided their written informed consent to participate in this study. The animal study was reviewed and approved by Ethical Committee of Experimental Animal, University of Antioquia. Written informed consent

was obtained from the individual(s) for the publication of any potentially identifiable images or data included in this article.

## AUTHOR CONTRIBUTIONS

MC-Q, LP-L, GC-G, and RP-D designed experiments, analyzed data, and reviewed and edited the manuscript. MC-Q and GC-G realized human tissue experiments. LP-L performed *in vitro* experiments. CV-L contributed to sampling and diagnosis of human tissue. MC-Q, LP-L, and GC-G wrote the manuscript. All authors contributed to the article and approved the submitted version.

## FUNDING

This research was funded by grants from COLCIENCIAS 111577757084 (2017–2020), (LGP-L) Young 1624 Researchers Program of the University of Antioquia, 2018 No. 1625 (20260002/1263/2019), and (C-Q MV) Young talent program Colciencias # 752-2018.

## ACKNOWLEDGMENTS

We would like to thank Luis Gonzalez for his technical training and advice, and Tania Marquez for her support in the vivarium facility. We also thank to SCIAN Lab, from Chile by the advise and use of the Huygens software.

## SUPPLEMENTARY MATERIAL

The Supplementary Material for this article can be found online at: https://www.frontiersin.org/articles/10.3389/fncel.2021.656832/full#supplementary-material

**Supplementary Figure 1 |** BACE1, Phospho-tau, GFAP and CLDN5 immunoreactivities in subiculum area of dementia brains **(A)** Representative image of the subiculum from a human control case. Magnification: 10×. Scale bar: 25 $\mu$m. **(B)** Representative images of the BACE1, **(C)** Phospho-tau, **(D)** GFAP, and **(E)** CLDN5 immunoreactivities in subiculum area of human hippocampal tissue. Magnification: 10×. Scale bar: 50 $\mu$m. Inset: 25 $\mu$m scale bar. The values in the bar graph are expressed as a densitometric percentage of the BACE1 IR in the CA1 area. FAD: familial-type Alzheimer's disease (presenilin 1 mutation E280A); SAD: sporadic Alzheimer's disease; CADASIL: autosomal dominant cerebral arteriopathy with subcortical infarcts and leukoencephalopathy. The data are expressed as the means ± SEM. $n = 4$. $^{*}p < 0.05$; $^{**}p < 0.01$.

**Supplementary Figure 2 |** BACE1, Phospho-tau, GFAP and CLDN5 immunoreactivities in the CA4 area from demented cases **(A)** Representative image of area CA4 in the hippocampus from a control case. Magnification: 10×. Scale bar: 25 $\mu$m. **(B)** Representative images of the BACE1, **(C)** Phospho-tau, **(D)** GFAP, and **(E)** CLDN5 immunoreactivities in the CA4 area of human hippocampal tissue. Magnification: 10×. Scale bar: 50 $\mu$m. Inset: 25 $\mu$m scale bar. The values in the bar graph are expressed as a densitometric percentage of the BACE1 IR in the CA1 area. FAD: familial-type Alzheimer's disease (presenilin 1 mutation E280A); SAD: sporadic Alzheimer's disease; CADASIL: autosomal dominant cerebral arteriopathy with subcortical infarcts and leukoencephalopathy. The data are expressed as the means ± SEM. $n = 4$. $^{*}p < 0.05$; $^{****}p < 0.0001$.

**Supplementary Figure 3 |** Cytotoxicity of BACE1 inhibitor at different concentrations. Percentage of LDH released by ECs of the bEnd.3 cell line at BACE1 inhibitor concentrations of 1, 5, 7.5, and 10 $\mu$M. The data are presented as the mean of $n = 3$, and the experiment was performed in duplicate. Control = inhibitor vehicle (DMSO).

## REFERENCES

Abbink, M. R., van Deijk, A. L. F., Heine, V. M., Verheijen, M. H., and Korosi, A. (2019). The involvement of astrocytes in early-life adversity induced programming of the brain. *Glia* 67, 1637–1653. doi: 10.1002/glia.23625

Acaz-Fonseca, E., Ortiz-Rodriguez, A., Azcoitia, I., Garcia-Segura, L. M., and Arevalo, M. A. (2019). Notch signaling in astrocytes mediates their morphological response to an inflammatory challenge. *Cell Death Discov.* 5:85. doi: 10.1038/s41420-019-0166-6

Alvarez, J. I., Dodelet-Devillers, A., Kebir, H., Ifergan, I., Fabre, P. J., Terouz, S., et al. (2011). The hedgehog pathway promotes blood-brain barrier integrity and CNS immune quiescence. *Science* 334, 1727–1731. doi: 10.1126/science.1206936

Amara, F. M., Junaid, A., Clough, R. R., and Liang, B. (1999). TGF-β1, regulation of Alzheimer amyloid precursor protein mRNA expression in a normal human astrocyte cell line: mRNA stabilization. *Mol. Brain Res.* 71, 42–49. doi: 10.1016/S0169-328X(99)00158-8

Arima, K., Izumiyama, Y., Nakamura, M., Nakayama, H., Ando, S., Ikeda, K., et al. (1998). Argyrophilic tau-positive twisted and non-twisted tubules in astrocytic processes in brains of Alzheimer-type dementia: an electron microscopical study. *Acta Neuropathol.* 95, 28–39.

Bārao, S., Gärtner, A., Leyva-Díaz, E., Demyanenko, G., Munck, S., Vanhoutvin, T., et al. (2015). Antagonistic effects of BACE1 and APH1B- g – secretase control axonal guidance by regulating growth cone collapse. *Cell Rep.* 12, 1367–1376. doi: 10.1016/j.celrep.2015.07.059

Barrier, A. I., Gardner, T. W., Lieth, E., Bonsall, D., Lesher, T., and Rice, K. (1997). Astrocytes increase barrier properties and ZO-1 expression in retinal vascular endothelial cells. *Invest. Ophthalmol. Vis. Sci.* 38, 2423–2427.

Bates, K. A., Fonte, J., Robertson, T. A., Martins, R. N., and Harvey, A. R. (2002). Chronic gliosis triggers Alzheimer's disease-like processing of amyloid precursor protein. *Neuroscience* 113, 785–796. doi: 10.1016/S0306-4522(02)00230-0

Beach, T. G., Sue, L., Scott, S., Layne, K., Newell, A., Walker, D., et al. (2003). Hippocampal sclerosis dementia with tauopathy. *Brain Pathol.* 13, 263–278. doi: 10.1111/j.1750-3639.2003.tb00027.x

Becerra-Calixto, A., and Cardona-Gómez, G. P. (2017). The role of astrocytes in neuroprotection after brain stroke: potential in cell therapy. *Front. Mol. Neurosci.* 10:88. doi: 10.3389/fnmol.2017.00088

Becerra-Calixto, A., Posada-Duque, R., and Cardona-Gómez, G. P. (2018). Recovery of neurovascular unit integrity by CDK5-KD astrocyte transplantation in a global cerebral ischemia model. *Mol. Neurobiol.* 55, 8563–8585. doi: 10.1007/s12035-018-0992-1

Beck, M., Brückner, M. K., Holzer, M., Kaap, S., Pannicke, T., Arendt, T., et al. (1999). Guinea-pig primary cell cultures provide a model to study expression and amyloidogenic processing of endogenous amyloid precursor protein. *Neuroscience* 95, 243–254. doi: 10.1016/S0306-4522(99)00390-5

Ben Halima, S., Mishra, S., Raja, K. M. P., Willem, M., Baici, A., Simons, K., et al. (2016). Specific inhibition of β-secretase processing of the Alzheimer disease amyloid precursor protein. *Cell Rep.* 14, 2127–2141. doi: 10.1016/j.celrep.2016.01.076

Bettegazzi, B., Mihailovich, M., Di Cesare, A., Consonni, A., Macco, R., Pelizzoni, I., et al. (2011). β-Secretase activity in rat astrocytes: translational block of BACE1 and modulation of BACE2 expression. *Eur. J. Neurosci.* 33, 236–243. doi: 10.1111/j.1460-9568.2010.07482.x

Bezvenyuk, Z., Miettinen, R., and Solovyan, V. (2003). Chromatin condensation during glutamate-induced excitotoxicity of celebellar granule neurons precedes disintegration of nuclear DNA into high molecular weight DNA fragments. *Mol. Brain Res.* 110, 140–146.

Blasko, I., Veerhuis, R., Stampfer-Kountchev, M., Saurwein-Teissl, M., Eikelenboom, P., and Grubeck-Loebenstein, B. (2000). Costimulatory effects

of interferon-β and interleukin-1β or tumor necrosis factor α on the synthesis of Aβ1-40 and Aβ1-42 by human astrocytes. *Neurobiol. Dis.* 7, 682–689. doi: 10.1006/nbdi.2000.0321

Botez, G., Probst, A., Ipsen, S., and Tolnay, M. (1999). Astrocytes expressing hyperphosphorylated tau protein without glial fibrillary tangles in argyrophilic grain disease. *Acta Neuropathol.* 98, 251–256.

Bulbarelli, A., Lonati, E., Brambilla, A., Orlando, A., Cazzaniga, E., Piazza, F., et al. (2012). Aβ42 production in brain capillary endothelial cells after oxygen and glucose deprivation. *Mol. Cell. Neurosci.* 49, 415–422. doi: 10.1016/j.mcn.2012.01.007

Cardona-Gómez, G. P., and Lopera, F. (2016). Dementia, preclinical studies in neurodegeneration and its potential for translational medicine in South America. *Front. Aging Neurosci.* 8:304. doi: 10.3389/fnagi.2016.00304

Costantino Iadecola, M. (2013). The pathobiology of vascular dementia. *Neuron* 80, 844–866. doi: 10.1016/j.neuron.2013.10.008

del Zoppo, G. J. (2010). The neurovascular unit in the setting of stroke. *J. Intern Med.* 267, 156–171. doi: 10.1111/j.1365-2796.2009.02199.x.The

Deng, X., Zhang, J., Liu, Y., Chen, L., and Yu, C. (2017). TNF-α regulates the proteolytic degradation of ST6Gal-1 and endothelial cell-cell junctions through upregulating expression of BACE1. *Sci. Rep.* 7:40256. doi: 10.1038/srep40256

Devraj, K., Poznanovic, S., Spahn, C., Schwall, G., Harter, P. N., Mittelbronn, M., et al. (2016). BACE-1 is expressed in the blood-brain barrier endothelium and is upregulated in a murine model of Alzheimer's disease. *J. Cereb. Blood Flow. Metab.* 36, 1281–1294. doi: 10.1177/0271678X15606463

Docagne, F., Gabriel, C., Lebeurrier, N., Lesné, S., Hommet, Y., Plawinski, L., et al. (2004). Sp1 and Smad transcription factors co-operate to mediate TGF-β-dependent activation of amyloid-β precursor protein gene transcription. *Biochem. J.* 383, 393–399. doi: 10.1042/BJ20040682

Durrant, C. S., Ruscher, K., Sheppard, O., Coleman, M. P., and Özen, I. (2020). Beta secretase 1-dependent amyloid precursor protein processing promotes excessive vascular sprouting through NOTCH3 signalling. *Cell Death Dis.* 11:98. doi: 10.1038/s41419-020-2288-4

ElAli, A. (2014). Neurovascular unit dysfunction in dementia: a brief summary. *Austin Alzheimers Park. Dis.* 1:5.

Elmore, S. (2007). Apoptosis: a review of programmed cell death. *Toxicol. Pathol.* 35, 495–516.

Escartin, C., Galea, E., Lakatos, A., O'Callaghan, J. P., Petzold, G. C., Serrano-Pozo, A., et al. (2021). Reactive astrocyte nomenclature, definitions, and future directions. *Nat. Neurosci.* 24, 312–325. doi: 10.1038/s41593-020-00783-4

Ferrer, I., López-González, I., Carmona, M., Arregui, L., Torrejón-Escribano, B., Diehl, R., et al. (2014). Glial and neuronal tau pathology in tauopathies: characterization of disease-specific phenotypes and tau pathology progression. *J. Neuropathol. Exp. Neurol.* 73, 81–97.

Fledrich, R., Abdelaal, T., Rasch, L., Bansal, V., Schütza, V., Brügger, B., et al. (2018). Targeting myelin lipid metabolism as a potential therapeutic strategy in a model of CMT1A neuropathy. *Nat. Commun.* 9:3025. doi: 10.1038/s41467-018-05420-0

Fogal, B., and Hewett, S. (2008). Interleukin-1B: a bridge between inflammation and excitotoxicity. *J. Neurochem.* 106, 1–23. doi: 10.1111/j.1471-4159.2008.05315.x

Gaillard, P. J., Cornelia, I., Sandt, J., Van Der Voorwinden, L. H., Vu, D., Nielsen, J. L., et al. (2000). Astrocytes increase the functional expression of P-glycoprotein in an in vitro model of the blood – brain barrier. *Pharm. Res.* 17, 1198–1205.

González-Molina, L. A., Villar-Vesga, J., Henao-Restrepo, J., Villegas, A., Lopera, F., Cardona-Gómez, G. P., et al. (2021). Extracellular vesicles from 3xTg-AD mouse and Alzheimer's disease patient astrocytes impair neuroglial and vascular components. *Front. Aging Neurosci.* 13:593927. doi: 10.3389/fnagi.2021.593927

Gosh, A. K., Brindisi, M., and Tang, J. (2012). Developing β-secretase inhibitors for treatment of Alzheimer's disease. *J. Neurochem.* 120, 71–83. doi: 10.1111/j.1471-4159.2011.07476.x.Developing

Gray, C. W., and Patel, A. J. (1993). Regulation of β-amyloid precursor protein isoform mRNAs by transforming growth factor-β1 and interleukin-1β in astrocytes. *Mol. Brain Res.* 19, 251–256.

Hartlage-Rübsamen, M., Zeitschel, U., Apelt, J., Gärtner, U., Franke, H., Stahl, T., et al. (2003). Astrocytic expression of the Alzheimer's disease β-secretase (BACE1) is stimulus-dependent. *Glia* 41, 169–179. doi: 10.1002/glia.10178

Hemming, M. L., Elias, J. E., Gygi, S. P., and Selkoe, D. J. (2009). Identification of β-secretase (BACE1) substrates using quantitative proteomics. *PLoS One* 4:8477. doi: 10.1371/journal.pone.0008477

Hirata, A., Baluk, P., Fujiwara, T., and McDonald, D. M. (1995). Location of focal silver staining at endothelial gaps in inflamed venules examined by scanning electron microscopy. *Am. J. Physiol. Cell. Mol. Physiol.* 269, L403–L418. doi: 10.1152/ajplung.1995.269.3.l403

Hishikawa, N., Hashizume, Y., Yoshida, M., Niwa, J., Tanaka, F., and Sobue, G. (2005). Tuft-shaped astrocytes in Lewy body disease. *Acta Neuropathol.* 109, 373–380. doi: 10.1007/s00401-004-0967-3

Huang, Z., Wong, L. W., Su, Y., Huang, X., Wang, N., Chen, H., et al. (2020). Blood-brain barrier integrity in the pathogenesis of Alzheimer's disease. *Front. Neuroendocrinol.* 59:100587. doi: 10.1016/j.yfrne.2020.100857

Iadecola, C. (2017). The neurovascular unit coming of age: a journey through neurovascular coupling in health and disease. *Neuron* 96, 17–42. doi: 10.1016/j.neuron.2017.07.030

Israelov, H., Ravid, O., Atrakchi, D., Rand, D., Elhaik, S., Bresler, Y., et al. (2020). Caspase-1 has a critical role in blood-brain barrier injury and its inhibition contributes to multifaceted repair. *J. Neuroinflam.* 17:267. doi: 10.1186/s12974-020-01927-w

Jean, V., Lecointre, M., Laudenbach, V., Ali, C., Macrez, R., Jullienne, A., et al. (2013). Neurobiology of Disease High t-PA release by neonate brain microvascular endothelial cells under glutamate exposure affects neuronal fate. *Neurobiol. Dis.* 50, 201–208. doi: 10.1016/j.nbd.2012.10.020

Jellinger, K. A., and Attems, J. (2007). Neurofibrillary tangle-predominant dementia: comparison with classical Alzheimer disease. *Acta Neuropathol.* 113, 107–117. doi: 10.1007/s00401-006-0156-7

Joy Yu, Y., Zhang, Y., Kenrick, M., Hoyte, K., Luk, W., Lu, Y., et al. (2011). Boosting brain uptake of a therapeutic antibody by reducing its affinity for a transcytosis target. *Sci. Transl. Med.* 3:84ra44. doi: 10.1126/scitranslmed.3002230

Koelsch, G. (2017). BACE1 Function and inhibition: implications of intervention in the amyloid pathway of Alzheimer's disease pathology. *Molecules* 22, 1–20. doi: 10.3390/molecules22101723

Kovacs, G. G., Milenkovic, I., Wöhrer, A., Höftberger, R., Gelpi, E., Haberler, C., et al. (2013). Non-Alzheimer neurodegenerative pathologies and their combinations are more frequent than commonly believed in the elderly brain: a community-based autopsy series. *Acta Neuropathol.* 126, 365–384. doi: 10.1007/s00401-013-1157-y

Lace, G., Ince, P., Brayne, C., Savva, G., Matthews, F., De Silva, R., et al. (2012). Mesial temporal astrocyte tau pathology in the MRC-CFAS ageing brain cohort. *Dement Geriatr. Cogn. Disord.* 34, 15–24. doi: 10.1159/000341581

Laird, F. M., Cai, H., Savonenko, A. V., Farah, M. H., He, K., Melnikova, T., et al. (2005). BACE1, a major determinant of selective vulnerability of the brain to amyloid-β amyloidogenesis, is essential for cognitive, emotional, and synaptic functions. *J. Neurosci.* 25, 11693–11709. doi: 10.1523/JNEUROSCI.2766-05.2005

Latacz, A., Russell, J. A., Ocloñ, E., Zubel-Lojek, J., and Pierzchala-Koziec, K. (2015). mTOR pathway - novel modulator of astrocyte activity. *Folia Biol.* 63, 95–105. doi: 10.3409/fb63_2.95

Lesné, S., Docagne, F., Gabriel, C., Liot, G., Lahiri, D. K., Buée, L., et al. (2003). Transforming growth factor-β1 potentiates amyloid-β generation in astrocytes and in transgenic mice. *J. Biol. Chem.* 278, 18408–18418. doi: 10.1074/jbc.M300819200

Liang, Y., Raven, F., Ward, J. F., Zhen, S., Zhang, S., Sun, H., et al. (2020). Upregulation of Alzheimer's disease amyloid-β protein precursor in astrocytes both in vitro and in vivo. *J. Alzheimers Dis.* 76, 1071–1082. doi: 10.3233/JAD-200128.Upregulation

Liu, C. C., Hu, J., Zhao, N., Wang, J., Wang, N., Cirrito, J. R., et al. (2017). Astrocytic LRP1 mediates brain Aβ clearance and impacts amyloid deposition. *J. Neurosci.* 37, 4023–4031. doi: 10.1523/JNEUROSCI.3442-16.2017

López-González, I., Carmona, M., Blanco, R., Luna-Muñoz, J., Martínez-Mandonado, A., Mena, R., et al. (2013). Characterization of thorn-shaped astrocytes in white matter of temporal lobe in Alzheimer' s disease brains. *Brain Pathol.* 23, 144–153. doi: 10.1111/j.1750-3639.2012.00627.x

Mao, H., Lockyer, P., Li, L., Ballantyne, C. M., Patterson, C., Xie, L., et al. (2017). Endothelial LRP1 regulates metabolic responses by acting as a co-activator of PPARγ. *Nat. Commun.* 8:14960. doi: 10.1038/ncomms14960

Martins, R. N., Taddei, K., Kendall, C., Evin, G., Bates, K. A., and Harvey, A. R. (2001). Altered expression of apolipoprotein E, amyloid precursor protein and presenilin-1 is associated with chronic reactive gliosis in rat cortical tissue. *Neuroscience* 106, 557–569. doi: 10.1016/S0306-4522(01)00289-5

Menon, D., Salloum, D., Bernfeld, E., Gorodetsky, E., Akselrod, A., Frias, M. A., et al. (2017). Lipid sensing by mTOR complexes via de novo synthesis of phosphatidic acid. *J. Biol. Chem.* 292, 6303–6311. doi: 10.1074/jbc.M116.772988

Michinaga, S., and Koyama, Y. (2019). Dual roles of astrocyte-derived factors in regulation of blood-brain barrier function after brain damage. *Int. J. Mol. Sci.* 20:571. doi: 10.3390/ijms20030571

Mishra, A., Reynolds, J. P., Chen, Y., Gourine, A. V., Rusakov, D. A., and Attwell, D. (2016). Astrocytes mediate neurovascular signaling to capillary pericytes but not to arterioles. *Nat. Neurosci.* 19, 1619–1627. doi: 10.1038/nn.4428

Miyazaki, H., Oyama, F., Wong, H., and Kaneko, K. (2007). BACE1 modulates filopodia-like protrusions induced by sodium channel b 4 subunit. *Biochem. Biophys. Res. Commun.* 361, 43–48. doi: 10.1016/j.bbrc.2007.06.170

Munoz, D. G., Woulfe, J., and Kertesz, A. (2007). Argyrophilic thorny astrocyte clusters in association with Alzheimer's disease pathology in possible primary progressive aphasia. *Acta Neuropathol.* 114, 347–357. doi: 10.1007/s00401-007-0266-x

Nation, D. A., Sweeney, M. D., Montagne, A., Sagare, A. P., D'Orazio, L. M., Pachicano, M., et al. (2019). Blood–brain barrier breakdown is an early biomarker of human cognitive dysfunction. *Nat. Med.* 25, 270–276. doi: 10.1038/s41591-018-0297-y

Ollion, J., Cochennec, J., Loll, F., Escudé, C., and Boudier, T. T. A. N. G. O. (2013). A generic tool for high-throughput 3D image analysis for studying nuclear organization. *Bioinformatics* 29, 1840–1841. doi: 10.1093/bioinformatics/btt276

Parfenova, H., Basuroy, S., Bhattacharya, S., Tcheranova, D., Qu, Y., Regan, R. F., et al. (2006). Glutamate induces oxidative stress and apoptosis in cerebral vascular endothelial cells: contributions of HO-1 and HO-2 to cytoprotection. *Am. J. Physiol.* 290, C1399–C1410. doi: 10.1152/ajpcell.00386.2005

Pekny, M., Wilhelmsson, U., Tatlisumak, T., and Pekna, M. (2018). Astrocyte activation and reactive gliosis—A new target in stroke? *Neurosci. Lett.* 689, 45–55. doi: 10.1016/j.neulet.2018.07.021

Piedrahita, D., Castro-Alvarez, J. F., Boudreau, R. L., Villegas-Lanau, A., Kosik, K. S., Gallego-Gomez, J. C., et al. (2016). β-Secretase 1's targeting reduces hyperphosphorylated tau, implying autophagy actors in 3xTg-AD mice. *Front. Cell. Neurosci.* 9:498. doi: 10.3389/fncel.2015.00498

Pigoni, M., Wanngren, J., Kuhn, P. H., Munro, K. M., Gunnersen, J. M., Takeshima, H., et al. (2016). Seizure protein 6 and its homolog seizure 6-like protein are physiological substrates of BACE1 in neurons. *Mol. Neurodegener.* 11:67. doi: 10.1186/s13024-016-0134-z

Posada-Duque, R. A., Barreto, G. E., and Cardona-Gomez, G. P. (2014). Protection after stroke: cellular effectors of neurovascular unit integrity. *Front. Cell. Neurosci.* 8:231. doi: 10.3389/fncel.2014.00231

Posada-Duque, R. A., Palacio-Castañeda, V., and Cardona-Gómez, G. P. (2015). CDK5 knockdown in astrocytes provide neuroprotection as a trophic source via Rac1. *Mol. Cell. Neurosci.* 68, 151–166. doi: 10.1016/j.mcn.2015.07.001

Posada-Duque, R. A., Ramirez, O., Härtel, S., Inestrosa, N. C., Bodaleo, F., González-Billault, C., et al. (2017). CDK5 downregulation enhances synaptic plasticity. *Cell. Mol. Life Sci.* 74, 153–172. doi: 10.1007/s00018-016-2333-8

R Core Team (2018). *R: A Language and Environment for Statistical Computing*. Vienna: R Foundation for Statistical Computing. Available online at: https://www.R-project.org

Roßner, S., Lange-Dohna, C., Zeitschel, U., and Perez-Polo, J. R. (2005). Alzheimer's disease β-secretase BACE1 is not a neuron-specific enzyme. *J. Neurochem.* 92, 226–234. doi: 10.1111/j.1471-4159.2004.02857.x

Sabogal-Guáqueta, A. M., Posada-Duque, R., Cortes, N. C., Arias-Londoño, J. D., and Cardona-Gómez, G. P. (2018). Changes in the hippocampal and peripheral phospholipid profiles are associated with neurodegeneration hallmarks in a long-term global cerebral ischemia model: attenuation by Linalool. *Neuropharmacology* 135, 555–571. doi: 10.1016/j.neuropharm.2018.04.015

Sayre, N. L., Sifuentes, M., Holstein, D., Cheng, S. Y., Zhu, X., and Lechleiter, J. D. (2017). Stimulation of astrocyte fatty acid oxidation by thyroid hormone is protective against ischemic stroke-induced damage. *J. Cereb. Blood Flow. Metab.* 37, 514–527. doi: 10.1177/0271678X16629153

Schultz, C., Ghebremedhin, E., Tredici, K., Del Rüb, U., and Braak, H. (2004). High prevalence of thorn-shaped astrocytes in the aged human medial temporal lobe. *Neurobiol. Aging* 25, 397–405. doi: 10.1016/S0197-4580(03)00113-1

Sil, S., Hu, G., Liao, K., Niu, F., Callen, S., Periyasamy, P., et al. (2020). HIV-1 tat-mediated astrocytic amyloidosis involves the HIF-1α/lncRNA BACE1-AS axis. *PLoS Biol.* 18:3000660. doi: 10.1371/journal.pbio.3000660

Simpson, I. A., Ponnuru, P., Klinger, M. E., Myers, R. L., Devraj, K., Coe, C. L., et al. (2014). A novel model for brain iron uptake: introducing the concept of regulation. *J. Cereb. Blood Flow. Metab.* 35, 48–57. doi: 10.1038/jcbfm.2014.168

Sofroniew, M. V., and Vinters, H. V. (2010). Astrocytes: biology and pathology. *Acta Neuropathol.* 10, 7–35. doi: 10.1007/s00401-009-0619-8

Stachel, S. J., Coburn, C. A., Steele, T. G., Jones, K. G., Loutzenhiser, E. F., Grego, A. R., et al. (2004). Structure-based design of a series of potent and selective CellPermeable inhibitors of human β-secretase (BACE-1). *J. Med. Chem.* 47, 6447–6450. doi: 10.1021/jm049379g

Vassar, R. (2014). BACE1 inhibitor drugs in clinical trials for Alzheimer's disease. *Alzheimers Res. Ther.* 6:89. doi: 10.1186/s13195-014-0089-7

Villabona-Rueda, A., Erice, C., Pardo, C. A., and Stins, M. F. (2019). The Evolving concept of the blood brain barrier (BBB): from a single static barrier to a heterogeneous and dynamic Relay center. *Front. Cell. Neurosci.* 13:405. doi: 10.3389/fncel.2019.00405

Villamil-Ortiz, J. G., Barrera-Ocampo, A., Piedrahita, D., Velásquez-Rodríguez, C. M., Arias-Londoño, J. D., and Cardona-Gómez, G. P. (2016). BACE1 RNAi restores the composition of phosphatidylethanolamine-derivates related to memory improvement in aged 3xTg-AD mice. *Front. Cell. Neurosci.* 10:260. doi: 10.3389/fncel.2016.00260

Villar-Vesga, J., Henao-Restrepo, J., Voshart, D. C., Aguillon, D., Villegas, A., Castaño, D., et al. (2020). Differential profile of systemic extracellular vesicles from sporadic and familial Alzheimer's disease leads to neuroglial and endothelial cell degeneration. *Front. Aging Neurosci.* 12:587989. doi: 10.3389/fnagi.2020.587989

Wang, P., Guan, P.-P., Wang, T., Yu, X., Guo, J.-J., and Wang, Z.-Y. (2014). Aggravation of Alzheimer's disease due to the COX-2- mediated reciprocal regulation of IL-1b and Ab between glial and neuron cells. *Aging Cell* 13, 605–615. doi: 10.1111/acel.12209

Xue, Z. Q., He, Z. W., Yu, J. J., Cai, Y., Qiu, W. Y., Pan, A., et al. (2015). Non-neuronal and neuronal BACE1 elevation in association with angiopathic and leptomeningeal β-amyloid deposition in the human brain. *BMC Neurol.* 15:71. doi: 10.1186/s12883-015-0327-z

Zamparo, I., Francia, S., Franchi, S. A., Redolfi, N., Costanzi, E., Kerstens, A., et al. (2019). Axonal odorant receptors mediate axon targeting. *Cell Rep.* 29, 4334–4348.e7. doi: 10.1016/j.celrep.2019.11.099

Zenaro, E., Piacentino, G., and Constantin, G. (2016). The blood-brain barrier in Alzheimer's disease. *Neurobiol. Dis.* 107, 41–56. doi: 10.1016/j.nbd.2016.07.007

Zhang, Y. K., Qu, Y. Y., Lin, Y., Wu, X. H., Chen, H. Z., Wang, X., et al. (2017). Enoyl-CoA hydratase-1 regulates mTOR signaling and apoptosis by sensing nutrients. *Nat. Commun.* 8:464. doi: 10.1038/s41467-017-00489-5

Zhao, J., O'Connor, T., and Vassar, R. (2011). The contribution of activated astrocytes to Aβ production: Implications for Alzheimer's disease pathogenesis. *J. Neuroinflam.* 8:150. doi: 10.1186/1742-2094-8-150

**Conflict of Interest:** The authors declare that the research was conducted in the absence of any commercial or financial relationships that could be construed as a potential conflict of interest.

frontiers in Cellular Neuroscience

ORIGINAL RESEARCH
published: 22 June 2021
doi: 10.3389/fncel.2021.679413

# IL-17 Inhibits Oligodendrocyte Progenitor Cell Proliferation and Differentiation by Increasing $K^+$ Channel Kv1.3

*Han Liu[1*†], Xueke Yang[1†], Jing Yang[1], Yanpeng Yuan[1], Yanlin Wang[1], Rui Zhang[1], Huangui Xiong[2*] and Yuming Xu[1*]*

[1] Department of Neurology, The First Affiliated Hospital of Zhengzhou University, Zhengzhou, China, [2] Neurophysiology Laboratory, Department of Pharmacology and Experimental Neuroscience, University of Nebraska Medical Center, Omaha, NE, United States

OPEN ACCESS

**Edited by:**
Xinchun Jin,
Capital Medical University, China

**Reviewed by:**
Peiying Li,
Shanghai Jiao Tong University School of Medicine, China
Xiaohuan Xia,
Tongji University, China

***Correspondence:**
Han Liu
fccliuh2@zzu.edu.cn
Huangui Xiong
hxiong@unmc.edu
Yuming Xu
xuyuming@zzu.edu.cn

[†] These authors have contributed equally to this work and share first authorship

**Specialty section:**
This article was submitted to Non-Neuronal Cells, a section of the journal Frontiers in Cellular Neuroscience

**Received:** 11 March 2021
**Accepted:** 20 May 2021
**Published:** 22 June 2021

**Citation:**
Liu H, Yang X, Yang J, Yuan Y, Wang Y, Zhang R, Xiong H and Xu Y (2021) IL-17 Inhibits Oligodendrocyte Progenitor Cell Proliferation and Differentiation by Increasing $K^+$ Channel Kv1.3. Front. Cell. Neurosci. 15:679413. doi: 10.3389/fncel.2021.679413

Interleukin 17 (IL-17) is a signature cytokine of Th17 cells. IL-17 level is significantly increased in inflammatory conditions of the CNS, including but not limited to post-stroke and multiple sclerosis. IL-17 has been detected direct toxicity on oligodendrocyte (Ol) lineage cells and inhibition on oligodendrocyte progenitor cell (OPC) differentiation, and thus promotes myelin damage. The cellular mechanism of IL-17 in CNS inflammatory diseases remains obscure. Voltage-gated $K^+$ (Kv) channel 1.3 is the predominant Kv channel in Ol and potentially involved in Ol function and cell cycle regulation. Kv1.3 of T cells involves in immunomodulation of inflammatory progression, but the role of Ol Kv1.3 in inflammation-related pathogenesis has not been fully investigated. We hypothesized that IL-17 induces myelin injury through Kv1.3 activation. To test the hypothesis, we studied the involvement of OPC/Ol Kv1.3 in IL-17-induced Ol/myelin injury in vitro and in vivo. Kv1.3 currents and channel expression gradually decreased during the OPC development. Application of IL-17 to OPC culture increased Kv1.3 expression, leading to a decrease of AKT activation, inhibition of proliferation and myelin basic protein reduction, which were prevented by a specific Kv1.3 blocker 5-(4-phenoxybutoxy) psoralen. IL-17-caused myelin injury was validated in LPC-induced demyelination mouse model, particularly in corpus callosum, which was also mitigated by aforementioned Kv1.3 antagonist. IL-17 altered Kv1.3 expression and resultant inhibitory effects on OPC proliferation and differentiation may by interrupting AKT phosphorylating activation. Taken together, our results suggested that IL-17 impairs remyelination and promotes myelin damage by Kv1.3-mediated Ol/myelin injury. Thus, blockade of Kv1.3 as a potential therapeutic strategy for inflammatory CNS disease may partially attribute to the direct protection on OPC proliferation and differentiation other than immunomodulation.

**Keywords: IL-17, myelin, oligodendrocyte, Kv1.3, inflammation**

## INTRODUCTION

In the central nervous system (CNS), neuronal axons are myelinated with oligodendrocytes (Ols), and damage of such a myelin sheath is a striking pathological feature of white matter damage in many inflammation-related diseases, including stroke (Oksala et al., 2009), Alzheimer disease (Nasrabady et al., 2018), and in particular multiple sclerosis (MS), which is a disseminated sclerosis in CNS affecting millions of people worldwide. While the mechanisms underlying MS pathogenesis are not fully understood, it is widely accepted that myelin sheath destruction induced by autoimmune response is most likely the cause. In MS, the immune system attacks myelin sheath leading to demyelination and impairs remyelination by retardation or inhibition of the myelin-producing cells to form myelin sheath after demyelination (Boulanger and Messier, 2014). Remyelination requires Ol progenitor cell (OPC) proliferation and migration to the lesion sites, where they differentiate, eventually to mature Ols and wrap neuronal axons to form myelin sheath. Remyelination readily occurs in MS, but it is incomplete and inefficient, and the reason is unfortunately unknown. It is believed that OPC differentiation is the key step for successful remyelination based on the fact revealed by pathological studies reported that approximately 60–70% of demyelinated lesions in MS contain immature OPCs. Those immature OPCs appeared to be in an arrested state, unable to fully differentiate (Lucchinetti et al., 1999; Chang et al., 2002; Boyd et al., 2013). Although current therapies targeting at suppression of overactive immune cells, such as lymphocytes, have some promising effects in retarding disease progression (Hauser et al., 2013), there is no effective way to stimulate and promote axonal remyelination once a demyelinated lesion has occurred.

The Voltage-gated K+ (Kv) channel is a largest and rapidly growing family of ion channels. In general, Kv channels are responsible for the driving force of $Ca^{2+}$ in non-excitable cells, thus mediating a variety of cellular activities. Previous studies have revealed an involvement of Kv channels in the regulation of Ol lineage cell proliferation and maturation (Pruss et al., 2011). It has also been shown that a decrease in Kv1.3 and Kv1.5 channel expression and outward $K^+$ currents in mature Ols is essential for synthesis of myelin structural proteins, and suppression of outward $K^+$ currents by increasing extracellular $K^+$ concentration (e.g., 25 mM KCl) promotes Ol maturation (Dai et al., 2001). These results indicate that Kv channels play an important role in the regulation of OPC/Ol differentiation and maturation (Chittajallu et al., 2002; Tegla et al., 2011). Kv1.3 is highly elevated in memory T cells in MS brain (Rus et al., 2005) and has been reported to be an immune-regulatory target in MS and inflammatory animal models (Wang et al., 2019). The inhibition of Kv1.3 activity may attenuate CNS inflammation and thus benefit remyelination according to its crucial role in regulation of T lymphocytes (Rus et al., 2005; Schmitz et al., 2005; Eil et al., 2016; Wang et al., 2019) and microglial physiological activity (Fordyce et al., 2005; Di Lucente et al., 2018) in inflammatory brains. Thus, blockade of Kv1.3 might benefit CNS remyelination by suppression of immune response. However, Kv1.3 colocalized with OPC marker NG2 in MS brain (Tegla et al., 2011), which suggests the beneficial effects of Kv1.3 blockade on MS may not be attributable solely to immune suppression; direct protection on OPCs may also contribute to the observed outcome. Nevertheless, the role of OPC/Ol Kv1.3 on axonal remyelination in brain white matter damage is unknown. In a previous study, we showed Kv1.3 was involved in HIV Tat protein-induced Ol injury in rat corpus callosum (Liu et al., 2017a). To further evaluate the role of OPC/Ol Kv1.3 on remyelination in white matter damage, we studied the effects of interleukin 17 (IL-17) on regulation of OPC/Ol proliferation and differentiation via Kv1.3.

IL-17 is a member of cytokine family of IL-17A–F (Waisman et al., 2015). As a signature cytokine of Th17 cells, IL-17A (referred to as IL-17 hereafter) is significantly elevated in MS patients' cerebrospinal fluid (CSF) (Kostic et al., 2014) and induces demyelination (Li et al., 2013; Waisman et al., 2015; Wang et al., 2017), due to its proinflammatory nature and direct toxicity on OPCs/Ols, as well as strong inhibitory effects on OPC maturation (Paintlia et al., 2011; Kang et al., 2013). Numerous immune-regulatory functions have been reported for IL-17 (Waisman et al., 2015; Kolbinger et al., 2016; Moser et al., 2020). It stimulates immune cell production of proinflammatory molecules leading to neurodegeneration, and its elevated levels in the CSF are associated with CNS inflammatory diseases. In addition, Kv1.3 expression has been found to correspond with an increase in IL-17 secretion in T cells (Gocke et al., 2012; Koch Hansen et al., 2014; Grishkan et al., 2015). To this end, we used IL-17 as a proinflammatory agent to investigate the inflammation-related mechanisms in OPC proliferation and differentiation through regulation of the levels of Kv1.3 expression.

## MATERIALS AND METHODS

### Animals

C57BL/6 male mice (21 days) were supplied by Charles River Laboratories, Beijing, China, and were housed in groups of five at the standard conditions of 22°C ± 1°C temperature and relative humidity conditions of 55–60% in an artificially lit animal room under a 12-h period of light and dark cycle and fed water and food *ad libitum*. Only male mice were used in the present research. This study was approved by the Life Science Ethics Review Committee of Zhengzhou University.

### Human Ol Precursor Cell Culture and Differentiation

Human Ol precursor cell was introduced from ScienCell Research Laboratories (San Diego, CA). Cells were cultured in complete medium containing 89% RPMI 1640 medium (HyClone, Logan, UT) and supplemented with 10% fetal bovine serum (Biological Industries, Beit-Haemek, Israel), 100 U/mL penicillin, and 100 μg/mL streptomycin (P/S; Solarbio, Beijing, China). Cells were kept in an incubator at 37°C under a humidified atmosphere of 5% $CO_2$ and 95% air. OPCs were maintained in complete medium for 24 h to adhere to the flask, after which the medium was replaced by

Ol precursor cell differentiation medium (OPCDM; ScienCell Research Laboratories, San Diego, CA) to differentiate into mature Ols. The experiments using Ols were performed with cells after 6 days or otherwise indicated cultured in OPCDM. OPCDM was replaced on a daily basis.

## Demyelination Mouse Model (Two-Point Injection)

Mice were anesthetized with isoflurane (induced at 3%, and maintained at 1.2–1.6%) and positioned in a stereotaxic frame. Corpus callosum demyelination was induced by stereotaxic injection of 2 μL (1 μL for each point) of 1% lysophosphatidylcholine (LPC; Sigma, St. Louis, MO), which was an endogenous lysophospholipid that disrupts myelin-associated lipids leading to focal demyelination, in 0.9% NaCl solution at the rate of 0.5 μL/min using 1 μL microsyringe at two points of corpus callosum. Mice of sham group were injected with equal volume of saline in double-point injection: (1) left: 1.0 mm lateral to the bregma, 1.1 mm anterior, and 2.4 mm deep; (2) right: 1.0 mm lateral to the bregma, 0.6 mm anterior, and 2.1 mm deep. After injection, the needle was kept in the place for an additional 5 min to prevent backflow. The day of injection was regarded as day 0 (0 dpi). For all groups, the mice were daily administered 5-bromo-2'-deoxyuridine (BrdU, 50 mg/kg; Solarbio, Beijing, China) at 2, 3, and 4 dpi by intraperitoneal (i.p.) injection. A specific Kv1.3 blocker 5-(4-phenoxybutoxy) psoralen (PAP, 6 mg/kg; Santa Cruz Biotechnology, Santa Cruz, CA) was applied by i.p. injection for the PAP and PAP + LPC groups at 2, 3, and 4 dpi. The brain tissues were taken at 5 dpi for cryostat section or Western blot analysis.

## Electrophysiology

Isolation of Kv1.3 currents was achieved as previously described (Liu et al., 2017a). Briefly, cells were seeded onto 3.5-cm culture dishes for whole-cell voltage clamp recording. Cells were perfused with oxygenated standard bath solution contained (in mM): 140 NaCl, 5.4 KCl, 2 CaCl2, 1 $MgCl_2$, 10 HEPES/NaOH, pH 7.3. The osmolarity was adjusted to 305 mOsm prior to recording by D-sucrose. The electrodes solution contained (in mM): 140 KCl, 2 CaCl2, 2 $MgCl_2$, 11 EGTA, 10 HEPES/KOH, pH 7.3, and had an osmolarity of 300 mOsm. Whole-cell $K^+$ currents were evoked by applying voltage steps from –150 to + 60 mV with a 15 mV increments, and current amplitudes were measured at the peak for each test potential. Current density (pA/pF) was calculated by dividing the digitized current values by whole-cell capacitance, which represents cell membrane surface area. Stock solution of Kv1.3-specific inhibitor PAP (Santa Cruz Biotechnology, Santa Cruz, CA) was prepared in deionized water. To access Kv1.3 current isolation, cells were recorded in standard bath and then superfused with PAP-contained bath solution at a concentration of 10 nM. Kv1.3-excluded currents were recorded at 20 min after perfusion. Isolated Kv1.3 currents were obtained by subtraction of Kv1.3-excluded current from total outward $K^+$ currents. All experiments were done at room temperature (22–23°C). Recordings were obtained with an Axopatch-200 B amplifier (Molecular Devices, Sunnyvale, CA). Current signals were filtered at 1 kHz and digitized at 5 kHz using a Digidata 1440A interface (Molecular Devices). The current and voltage traces were displayed and recorded on a computer using pCLAMP 10.0 data acquisition and analysis software (pClamp, RRID:SCR_011323). Data were analyzed by Clampfit 10.0 (Clampfit, RRID:SCR_011323). All final graphics in the present work were constructed by GraphPad Prism 9.0 (GraphPad Prism, RRID:SCR_002798).

## 3-(4,5-Dimethylthiazol-2-yl)-2,5-Diphenyl Tetrazolium Bromide Assay

Cell proliferation was measured by 3-(4,5-dimethylthiazol-2-yl)-2,5-diphenyl tetrazolium bromide (MTT) assay. The homogeneous stable solution of 5 mg/mL was prepared by dissolving MTT (Ameresco, Solon, OH) powder in phosphate-buffered saline (PBS). Cells were seeded in a 96-well plate with complete medium. IL-17 (Absin Bioscience Inc., Shanghai, China) and AKT activator SC79 (Selleck Chemicals, Houston, TX) were added to the cell cultures for 48 h in the absence or presence of prior (30 min) added Kv1.3 antagonist PAP. Cells were then incubated with a 1:10 dilution of the MTT solution to complete medium for 3 h at 37°C. The formazan crystals converted from MTT were completely dissolved in dimethyl sulfoxide (Solarbio) for cell lysis, and the optical density (OD) was measured at 570 nm using Multiskan Spectrum (Thermo Fisher Scientific, Waltham, MA). The ratio of OD between the treated cells and the control cells reflected cell viability.

## Immunocytochemistry

OPCs were seeded on coverslips at a density of $0.02 \times 10^6$/well in 24-well plates. Experimental treatments of PAP, IL-17, and SC79 were the same as described in MTT assay. After treatments as at indicated time, the prepared cells were fixed with 4% paraformaldehyde (PFA) in PBS for 20 min and punched holes in PBST supplemented with 0.1% Triton-X100 for 20 min. Cells were blocked in PBST containing 1% bovine serum albumin (BSA; Solarbio) for 30 min, and all the above experiments were performed at room temperature. Primary antibodies anti-Kv1.3 (Thermo Fisher Scientific cat. no. PA5-77618, RRID:AB_2736055) and anti-BrdU (ABclonal, cat. no.A20304, RRID:AB_2890022) were then applied to coverslips at 4°C overnight, and cells were incubated with the appropriate fluorescence-conjugated secondary antibody for 1 h at room temperature. For BrdU staining, cells on coverslips were pretreated with HCl. After washing, the coverslips were mounted in glass slides with mounting medium contained DAPI stain, and cells were visualized by a fluorescent microscope (Nikon Corporation, Tokyo, Japan). The ratio of $BrdU^+$ cells to DAPI was counted, and comparisons among groups were performed.

## Immunohistochemistry

The mice injected with LPC accepted BrdU by i.p. injection at 2, 3, and 4 dpi. The mice used for cryosectioning accepted cardiac perfusion before sacrifice. After anesthesia, the mice

were fixed on the operating table, and the thoracic cavity was cut to expose the heart. The left ventricle was punctured with a syringe filled with precooled saline. Then, the right auricula dextra of mice were snipped, and the syringe was pushed to allow the saline to rinse systemically through the vessels. After the effluent turned limpid, the mice were perfused with 4% PFA to systemic circulation for prefixation. Each mouse was given 200 mL saline and 200 mL PFA. The prepared brain tissue specimens were fixed in 4% PFA for 48 h, immersing in 15% and 30% sucrose for 24 h, respectively, and then embedded in optimal cutting temperature (OCT) media, freezing, and cryosectioning into 10-μm slices. The coronal brain slices were immunostained with primary antibody such as anti-myelin basic protein (MBP) antibody (Abcam cat. no. ab7349, RRID:AB_305869), anti-NG2 monoclonal antibody (Thermo Fisher Scientific cat. no. 37–2300, RRID:AB_2533306), and anti-BrdU antibody (ABclonal, cat. no.A20304, RRID:AB_2890022) to evaluate demyelination and proliferation, respectively. The sections were incubated with primary antibody followed by fluorescence-conjugated secondary antibodies for microscopic analysis. A minimum of five images were taken from each slide.

## Luxol Fast Blue Stain

Luxol fast blue (LFB) staining was used to measure the demyelination of myelin. The coronal brain slices were prepared as previously described. LFB staining was performed according to manufacturer's instructions for the Luxol fast blue stain kit (Solarbio). The slices were immerged in LFB dye at room temperature for 12 h. The slices were rinsed with distilled water after washing off the excess dye with 95% ethanol. The slices were differentiated successively in 0.05% lithium carbonate solution and 70% ethanol. Photographs were taken with an optical microscope after sealing the slices with neutral resin.

## Western Blot Analysis

The expression levels of proteins were quantified by Western blot. MBP has three isoforms, and we examined the predominant isoform of protein band at 18.5 kDa by Western blot analysis. Following experimental treatments, cells and brain tissue were washed thrice with prechilled PBS. The whole-cell lysates were prepared in RIPA lysis buffer (Absin Bioscience Inc.) followed by clarification with centrifugation. All protein concentrations were quantified using the BCA protein assay kit (Solarbio), and 25 μg of total protein was loaded onto 10% sodium dodecyl sulfate–polyacrylamide gels, separated by electrophoresis, and transferred to a polyvinylidene difluoride (PVDF; Millipore, Bedford, MA) membrane. The PVDF membrane was then blocked in 5% non-fat dry milk in Tris-buffered saline (TBS) at room temperature for 1.5 h, followed by overnight incubation of primary antibodies diluted in 5% BSA at 4°C on the shaker. Primary antibodies were rabbit anti-Kv1.3 (Thermo Fisher Scientific cat. no. PA5-77618, RRID:AB_2736055), rat anti-MBP (Abcam cat. no. ab7349, RRID:AB_305869), rabbit anti-phospho-AKT (p-AKT; Cell Signaling Technology cat. no. 4060, RRID:AB_2315049), rabbit anti-AKT (Cell Signaling Technology cat. no. 4691, RRID:AB_915783), rabbit anti-phospho-p38 mitogen-activated protein kinase (MAPK) (p-p38; Cell Signaling Technology cat. no. 4511, RRID:AB_2139682), rabbit anti-p38 MAPK (Cell Signaling Technology cat. no. 8690, RRID:AB_10999090), and mouse anti–β-actin (Proteintech cat. no. 66009-1-lg, RRID:AB_2782959). Afterward, membranes were washed in TBS with 0.1% Tween-20 (TBST) for 10 min × three times and then incubated in diluted secondary antibody for 1 h at room temperature on a shaker. The secondary antibodies were horseradish peroxidase (HRP)–conjugated anti-rabbit (Jackson ImmunoResearch Labs cat. no. 111–035–003, RRID:AB_2313567), HRP-conjugated anti-rat (Jackson ImmunoResearch Labs cat. no. 112–035–003, RRID:AB_2338128) and HRP-conjugated anti-mouse secondary antibodies (Proteintech cat. no. SA00001–1, RRID:AB_2722565). After washing, membranes were finally incubated with ECL Western blot substrate (Solarbio) to detect HRP-conjugated secondary antibodies and imaged using the Image Lab system (Image Lab Software, RRID:SCR_014210). Band densities were measured by ImageJ software (ImageJ, RRID:SCR_003070).

## Statistical Analysis

All data are expressed as mean ± SE unless otherwise indicated. Statistical analyses were performed by one-way analysis of variance followed by a Fisher least-significant difference test for multiple comparisons. The difference between groups was considered significant at $P < 0.05$.

# RESULTS

## Alteration of Kv1.3 Expression in Ol Lineage Cell Development

The expressions of MBP and Kv1.3 were first examined at different periods of development. Immunofluorescences showed the Kv1.3 protein decreased within the maturation. At the sixth day after cells were changed into OPCDM (DF 6d), the Kv1.3 immune density reduced approximately 30% of that in OPCs. At the eighth day in OPCDM (DF 8d), Kv1.3 immune density further decreased to 52.6% ± 2.8% of OPCs (**Figure 1A**). Similar result was observed in Western blot, the Ol Kv1.3 expression decreased approximately 28 and 58% when OPCs differentiated 6 and 8 days, respectively. In contrast to Kv1.3 expression, the MBP expression increased in the differentiating process. MBP started showing a significant increase after 6 days in OPCDM and further increased when the differentiating culture extended to 8 days (**Figure 1B**). MBP is a myelin structural protein that is widely used to illustrate the maturation and myelinating capability of Ols. Following the expression, we thought to test the function and activity of Kv1.3 in OPCs and Ols. Voltage clamp was performed to test the Kv1.3 currents in cultured cells. PAP 10 nM ($EC_{50}$ = 2 nM; Schmitz et al., 2005) was perfused into the extracellular solution immediately after total currents were recorded to particularly suppress Kv1.3 currents, and then the Kv1.3-excluded currents were recorded at the same cell. The isolated Kv1.3 currents were achieved by subtraction of Kv1.3-excluded currents from total currents. Kv1.3 contributed a major component in the OPC outward $K^+$ currents as shown

in the first line of **Figure 1C**, and the current density attenuated approximately 27.9, 47.7, and 65.1% after 4 days (DF 4d), 6 days, and 8 days in OPCDM (**Figure 1C**). As the changes of Kv1.3 and MBP expressions both reached significant enhancement after 6 days in differentiating culture, the time point of day 6 was chosen for the following studies regarding mature Ols.

## Involvement of Kv1.3 in IL-17–Induced Inhibition of OPC Proliferation and Differentiation

Cytokine IL-17 level is significantly elevated in MS patients CSF, and it is found to be associated with disease severity and progression in CNS demyelination model (Kostic et al., 2014). IL-17 is demonstrated to be enhancing oxidative stress–induced Ol apoptosis (Paintlia et al., 2011) and strongly inhibiting OPC differentiation (Kang et al., 2013). Here, we tested the consequence of IL-17 on OPCs and Ols. The dose of IL-17 was tittered by MTT assay performed in OPCs. IL-17 significantly decreased OPC viability to 83.40% ± 4.5% at the concentration of 200 ng/mL and (**Figure 2A**, $P = 0.0037$, IL-17 200 ng/mL vs. control) further decreased to 75.5% ± 5.9% at 400 ng/mL (**Figure 2A**, $P < 0.0001$, IL-17 400 ng/mL vs. control). Thus, the dose of 200 ng/mL was chosen for the following studies. Moreover, IL-17 up to 400 ng/mL did not affect the OPC apoptosis (data not shown) in our culture system. Previous studies reported that Kv1.3 on T lymphocytes and microglial cells play a key role in pathophysiological processes in inflammatory brains; we next explored whether OPC/Ol Kv1.3 was directly involved in inflammation-related myelin injury. Experiments were next performed to assess the expression of OPC Kv1.3 after exposure to IL-17. Exposure of IL-17 for 48 h enhanced the Kv1.3 protein expression in OPCs (**Figure 2E**, $P = 0.0114$, IL-17 vs. control). PAP was preadded to culture medium 30 min prior to following addition of BrdU with or without IL-17 for 48 h. PAP mitigated IL-17–induced OPC viability reduction (**Figure 2B**, $P = 0.0007$, PAP + IL-17 vs. IL-17), and counteracted IL-17–caused decrease in $BrdU^+$ cells percentage (**Figures 2C,D**; $P < 0.0001$, PAP + IL-17 vs. IL-17). These results together suggested IL-17 retarded the OPC proliferation at the concentration of 200 ng/mL, and blockade of Kv1.3 prevented IL-17–caused loss of cell viability and inhibition of proliferation. Consistent results were found in differentiated Ols. MBP is an essential myelin structural protein, which is believed to indicate the Ol myelinating ability *in vitro*. MBP classically has three isoforms due to the different transcription start sites. The analysis described below was based on the protein bands at 18.5 kDa, which is considered as the predominant isoform essential for CNS myelin stability (Smith et al., 2012; Vassall et al., 2013). IL-17 decreased the expression of MBP (**Figures 2F,G**; $P = 0.0015$, control vs. IL-17) and increased the Ol Kv1.3 protein expression (**Figures 2F,G**; $P = 0.0106$, control vs. IL-17). Pretreatment of PAP for 30 min counteracted MBP reduction (**Figures 2F,G**; $P = 0.0013$, PAP + IL-17 vs. IL-17) and Kv1.3 enhancement (**Figures 2F,G**; $P = 0.0082$, PAP + IL-17 vs. IL-17) caused by IL-17. These together suggested the involvement of Kv1.3 in IL-17–induced inhibition of OPC proliferation and differentiation.

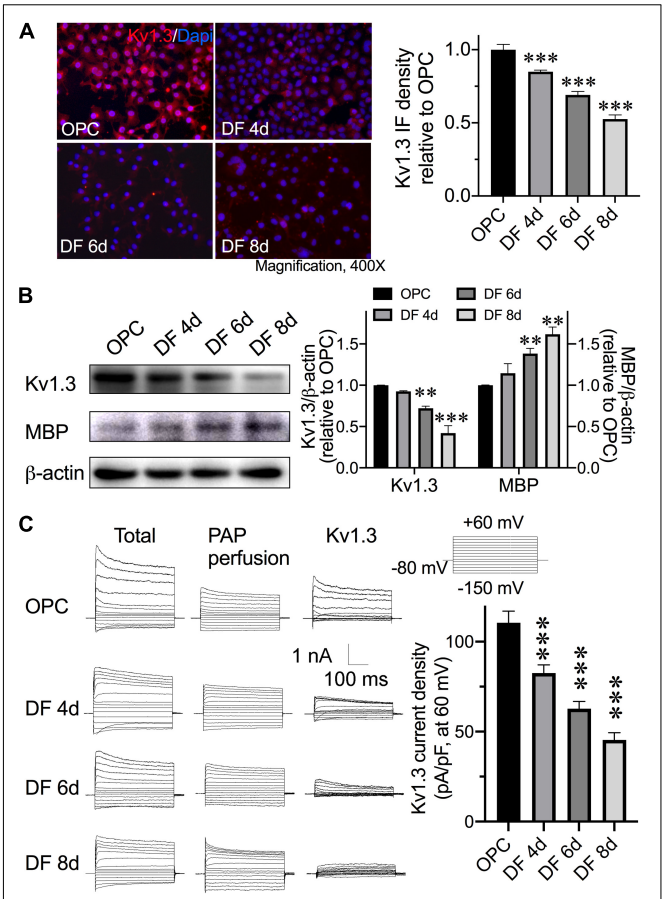


**FIGURE 1 |** Expression of Kv1.3 in OPCs/Ols during development. OPCs were cultured in OPCDM to differentiate into mature Ols. OPCs were transferred into OPCDM for 4 days (DF 4d), 6 days (DF 6d), and 8 days (DF 8d). **(A)** Representative images of Kv1.3 immunofluorescence staining (red) in cultures. Intact cell nuclei were visualized with DAPI (blue). The immunofluorescence density of Kv1.3 was summarized in a bar graph at the right. With the maturity of OPCs, Kv1.3 decreased in a development-dependent manner. **(B)** Western blot analysis of MBP expression in cells collected from different periods of OPCs/Ols. Band densitometry data are shown in the bar graph (right). Data are normalized to β-actin shown in each gel. In contrast to the Kv1.3 alterations, the expression of MBP increased with differentiation. **(C)** Representative current traces of outward $K^+$ currents recorded during depolarizing and hyperpolarizing pulses are shown in cells of OPCs, DF 4d, DF 6d, and DF 8d. The whole-cell outward $K^+$ currents recorded before (Total) and 15 min after superfusion of 10 nM PAP (PAP perfusion) to the bath. The Kv1.3 currents were then isolated by subtraction of outward $K^+$ currents recorded in the presence of PAP from the total currents (Kv1.3). The summary bar graph illustrating average Kv1.3 current density measured at +60 mV (pA/pF) obtained from OPCs and Ols ($n = 16$). With the maturation of Ols, the Kv1.3-conducted potassium currents decreased. All data expressed were obtained from three independent experiments unless otherwise indicated. $^{**}P < 0.01$ vs. control, $^{***}P < 0.001$ vs. control.

## Kv1.3 Involved in IL-17–Induced OPC Developmental Alterations by Diminishing AKT Signal

Thus far, we have demonstrated IL-17 up-regulated Kv1.3 protein expression in OPCs and Ols, and blockade of Kv1.3

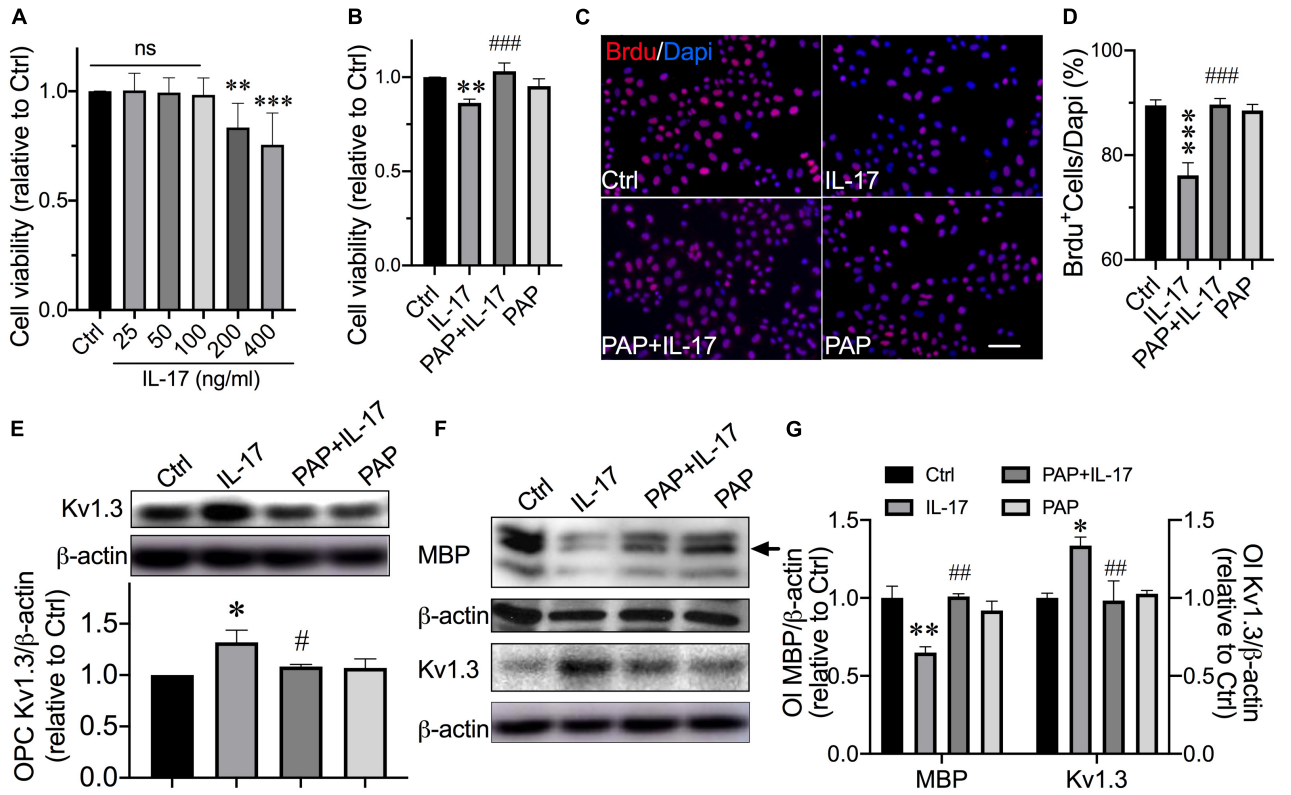


**FIGURE 2 |** Kv1.3 blockade prevented OPCs from IL-17–induced inhibition of proliferation and differentiation. OPCs were exposed to IL-17 (200 ng/mL) for 48 h with or without preaddition of PAP (10 nM) for 30 min. **(A)** The dose of IL-17 was tittered by MTT assay performed in OPCs ($n$ = 6). IL-17 significantly reduced cell viability at a concentration of 200 ng/mL and further reduced at the concentration of 400 ng/mL. **(B)** MTT assay was performed to detect OPC viability ($n$ = 7). PAP pretreatment counteracted the loss of cell viability induced by IL-17. **(C)** OPCs were treated with IL-17 with or without PAP in the presence of BrdU (10 μM) for 48 h. Representative images of merged BrdU immunofluorescence staining (red) and DAPI (blue) are shown. Scale bar = 20 μm. The average percentage of $BrdU^+$ cells from five independent experiments are summarized in **(D)** There were 10 randomly selected visual fields counted for each group from three independent experimental treatments. IL-17–induced reduction of $BrdU^+$ cells was attenuated by PAP. **(E)** Western blot analysis of Kv1.3 expression in OPCs. Band densitometry data are shown in the bar graph (below) ($n$ = 4). IL-17 treatment for 48 h elevated the Kv1.3 protein expression in OPCs, whereas the PAP attenuated this elevation. For experiments conducted with Ols in **(F,G)**, Ols were exposed to IL-17 (200 ng/mL) with or without prior addition of PAP (10 nM) for 30 min during the differentiation culture in OPCDM for 6 days. **(F**,**G)** Representative images and statistical analyses of MBP and Kv1.3 expression in mature Ols of Western blot ($n$ = 3). The band marked by the arrow is a protein band with a size of 18.5 kDa. Pretreatment with PAP for 30 min counteracted the decrease in MBP and increase in Kv1.3 protein expression in Ols induced by IL-17. $^*P < 0.05$ vs. control, $^{**}P < 0.01$ vs. control, $^{***}P < 0.001$ vs. control. $^{\#}P < 0.05$ vs. IL-17, $^{\#\#}P < 0.01$ vs. IL-17, $^{\#\#\#}P < 0.001$ vs. IL-17.

mitigated IL-17–induced OPC proliferation and differentiation retardation. The mechanisms of Kv1.3 involvement in IL-17–caused alterations of OPC proliferation and differentiation attracted our attention. It has been shown that OPC differentiation is controlled by a number of factors, many of which act to be inhibitory including leucine-rich repeat and immunoglobulin domain-containing 1 (Mi et al., 2004, 2005), Notch-1 (Bongarzone et al., 2000; Kim et al., 2008), Wnt (Shimizu et al., 2005) etc., whereas p38 MAPK (Bhat et al., 2007; Chew et al., 2010) and AKT (Flores et al., 2008) have been shown to be required for OPC differentiation and myelination. Previous studies reported that IL-17 increased total p38 levels and restricted neural stem cell differentiating to neurons, astrocytes, and OPCs (Li et al., 2013). AKT signal is reported to be protective for myelination under IL-17–enriched conditions (Tsiperson et al., 2013; Liu et al., 2017b). We next sought to clarify whether Kv1.3 regulated OPC proliferation and differentiation through AKT and/or p38 pathways. The phosphorylation forms of p38 (p-p38) and AKT (p-AKT) proteins were examined to illustrate the activation level of these signals. IL-17 decreased the expression of p-AKT in OPCs (**Figure 3A**; $P$ = 0.0074, IL-17 vs. control) and differentiated Ols (**Figure 3B**; $P$ = 0.0058, IL-17 vs. control) but did not alter the activation of p-p38 in OPCs (**Figure 3A**; $P$ = 0.94) and Ols (**Figure 3B**; $P$ = 0.54). In both OPCs and mature Ols, PAP prevented p-AKT from IL-17–caused reduction (PAP + IL-17 vs. IL-17, $P$ = 0.0297 in **Figure 3A** and $P$ = 0.0449 in **Figure 3B**). These results suggested Kv1.3 may be involved in IL-17–induced inhibition of OPC proliferation and differentiation by diminishing AKT signal pathways but not p38.

By knowing the contribution of AKT inactivation in Kv1.3 involvement of IL-17–induced OPC cell cycle alterations, a highly selective, efficient, and cell-permeable AKT activator SC79 (Jo et al., 2012) was employed to convince the contribution of AKT. We first confirmed the efficiency of SC79 on AKT activation

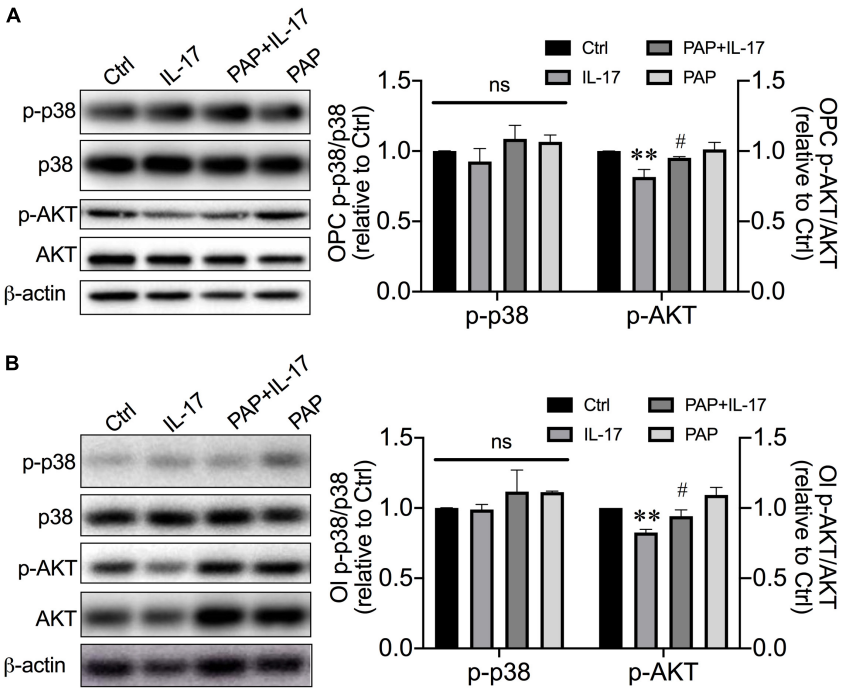


**FIGURE 3 |** Kv1.3 involved in IL-17–induced developmental alterations by diminishing AKT signal but not p38 MAPK. OPCs were treated as described in **Figure 2**. **(A)** Representative images and statistical analyses of p-p38 and p-AKT expression in OPCs of Western blot ($n$ = 3). IL-17 suppressed the p-AKT expression, which represented the activation level of AKT pathway in OPCs, but not p-38, whereas PAP relieved this suppression. **(B)** For experiments conducted with Ols, OPCs were transferred into OPCDM and treated the same as described in **Figure 2**. Representative images and band densitometry data (right) of p-p38 and p-AKT expression in Ols ($n$ = 4). The attenuation of p-AKT induced by IL-17 was mitigated by PAP, indicating the integral role of Kv1.3 in IL-17–caused decline of AKT activation. $^{**}P < 0.01$ vs. control, $^{\#}P < 0.05$ vs. IL-17.

in our culture system after a 6-day application (**Figure 4E**; $P$ = 0.018, SC79 vs. control). For cotreatment, SC79 was applied to culture medium at the same time with addition of IL-17. With the presence of IL-17, SC79 also performed effectively on AKT activation (**Figure 4E**; $P$ = 0.0094, IL-17 vs. SC79 + IL-17). SC79 showed the protective effects on OPC proliferation (**Figures 4A–C**) and Ol MBP expression (**Figure 4D**). Application of SC79 protected OPCs from IL-17–induced loss of viability (**Figure 4A**; $P$ = 0.0093, IL-17 vs. SC79 + IL-17) and mitigated IL-17–caused $BrdU^+$ cell number decrease (**Figures 4B,C**; $P$ = 0.0057, IL-17 vs. SC79 + IL-17). In differentiating culture, SC79 protected Ols from IL-17–induced attenuation of MBP expression (**Figure 4D**; $P$ = 0.0014, IL-17 vs. SC79 + IL-17) and mitigated IL-17–caused Kv1.3 elevation (**Figure 4F**; $P < 0.0001$, IL-17 vs. SC79 + IL-17). These results suggested that AKT activation promotes the OPC proliferation and differentiation in exposure of IL-17, and decreased AKT activation participated in Kv1.3 involvement of IL-17–induced inhibition of OPC proliferation and differentiation.

## Kv1.3 Blockade Prevented Ols From LPC-Induced Myelin Loss *in vivo*

Having observed the MBP expression altered in cell culture, the LPC-induced demyelination mice model was utilized to interrogate myelin repair in conditions more comparable with human disease to directly disclose the effects of Kv1.3 and its blockade on myelin sheath. The LPC-induced experimental demyelination is advantageous for characterizing the focal myelin morphology because the location of the damage is known. Because corpus callosum is a sensitive marker for damage of the cerebral white matter demyelination, the areas of corpus callosum were chosen to inject LPC and observe myelination. According to the previous publication, PAP distributes in parallel in plasma and brain following enteral administration and showed even higher concentration in most tested brain regions than in plasma (Maezawa et al., 2018). The plasma concentrations following 6 mg/kg i.p. injection achieved 300 nM after 8 h and still above 10 nM after 24 h (Azam et al., 2007). Considering the PAP $EC_{50}$ = 2 nM (Schmitz et al., 2005), a predicable concentration of greater than 10 nM is sufficient to achieve pharmacological Kv1.3 blockade in mice brains. We decided to administer PAP by i.p. injection at a dose of 6 mg/kg every 24 h. Demyelination lesions in the corpus callosum were revealed by the LFB method, which stains myelin in blue. Myelin showed intact appearance in the injection point of sham animals, while it appeared discontinuous and reduced significantly in overall density of staining in LPC-injected sites. PAP significantly improved the myelin integrity compared with that in LPC-injected corpus callosum (**Figure 5A**). Myelination was also evaluated by blotting reactivity of MBP. The tissue of injection areas was taken to examine MBP expression. In agreement

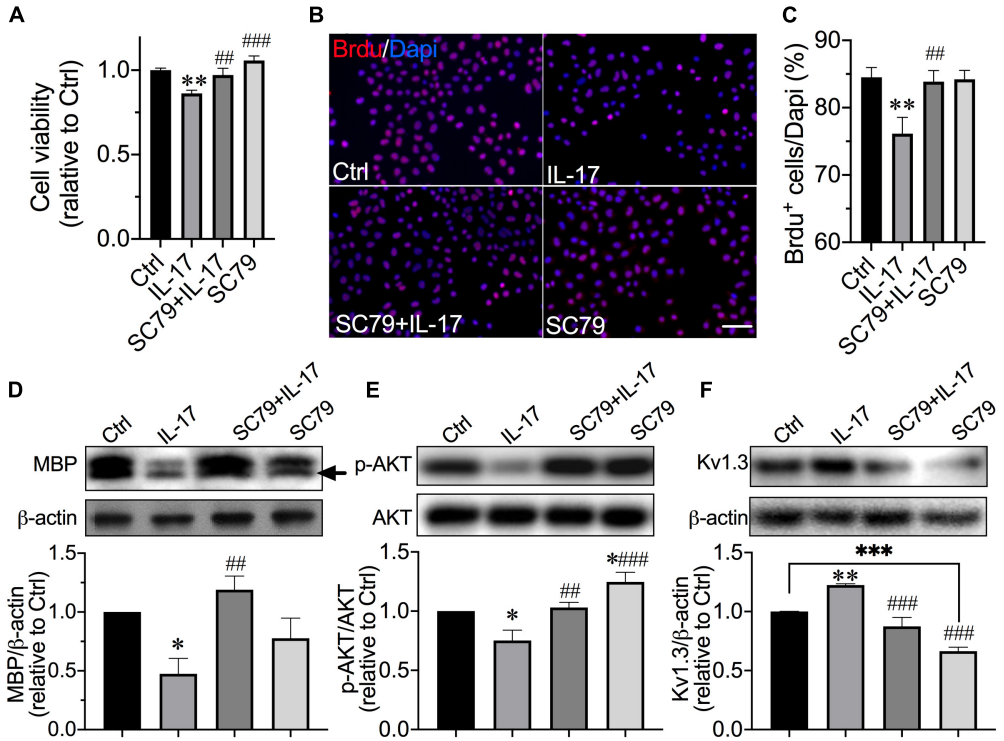


**FIGURE 4 |** Protection of AKT activator on IL-17–induced inhibition of OPC proliferation and differentiation. OPCs were exposed to IL-17 (200 ng/mL) for 48 h with or without AKT activator SC79 (10 μM). **(A)** MTT assay was performed to detect OPC viability ($n = 7$). SC79 counteracted the decrease in cell viability induced by IL-17. **(B)** OPCs were treated as described before in the presence of BrdU (10 μM) for 48 h. Representative images of merged BrdU immunofluorescence staining (red) and DAPI (blue) are shown. Scale bar = 20 μm. The average percentage of $BrdU^+$ cells from five independent experiments are summarized in **(C)** There were 10 randomly selected visual fields counted for each experimental group from three independent treatments. IL-17–induced reduction of $BrdU^+$ cell percentage was attenuated by SC79. For experiments conducted with OIs in **(D–F)**, OPCs were exposed to IL-17 (200 ng/mL) with or without SC79 (10 μM) in OPCDM for 6 days. **(D–F)** Representative images and statistical analyses of MBP ($n = 4$), p-AKT ($n = 4$), and Kv1.3 ($n = 5$) expressions in OIs of Western blot. Band densitometry data are shown in the bar graph (below). SC79 effectively activated AKT signal in our culture system. Similar to the PAP, SC79 counteracted the IL-17–induced decrease in MBP and increase in Kv1.3 expression and mitigated the decrease in p-AKT induced by IL-17. $^*P < 0.05$ vs. control, $^{**}P < 0.01$ vs. control, $^{***}P < 0.001$ vs. control. $^{\#\#}P < 0.01$ vs. IL-17, $^{\#\#\#}P < 0.001$ vs. IL-17.

with the morphological observation, LPC decreased the MBP expression to approximately 36% of sham (**Figure 5B**; $P < 0.0001$, LPC vs. sham), and this reduction was not observed in Kv1.3 inhibitor/LPC-cotreated mice (**Figure 5B**; $P < 0.0001$, LPC vs. PAP + LPC). By exploring the alterations of myelination, the OPC proliferation was next examined in mice. In LPC-treated mice, the number of $BrdU^+NG2^+$ cells were significantly lessened compared with sham mice (**Figure 5C**; $P = 0.0147$, LPC vs. sham), and administration of PAP prevented the decrease in number of $BrdU^+NG2^+$ cells (**Figure 5C**; $P = 0.0147$, LPC vs. PAP + LPC). These results together suggested that Kv1.3 blockade is protective for OPC proliferation and myelination *in vivo*.

## DISCUSSION

In the present study, we demonstrated that Kv1.3 blockade effectively promoted OPC proliferation and differentiation through activation of AKT signaling, leading to protection of myelin from IL-17– and LPC- induced myelin damage *in vitro* and *in vivo*, which is beneficial to remyelination in neurological disorders with demyelination.

IL-17–induced OI injury is closely relative to MS pathogenesis. MS is the most common cause of non-traumatic disability in young people, affecting approximately 2.5 million people worldwide (Pugliatti et al., 2002; Compston and Coles, 2008). Axonal remyelination has been a challenge in MS therapies. To date, there is no proven way to repair demyelinated lesions. Disease progression usually has two phases: relapsing–remitting phase and progressive phase. The different disease phases reflect different underlying neuropathology, with inflammation and demyelination in the relapsing–remitting phase and neurodegeneration in the progressive phase (Jolanda Munzel and Williams, 2013). Previous studies of Kv1.3 in MS and other neuroinflammatory diseases were mainly focused on the ionic immune regulating role of Kv1.3 in T cells (Rus et al., 2005; Schmitz et al., 2005; Eil et al., 2016; Wang et al., 2019) and microglia (Fordyce et al., 2005; Di Lucente et al., 2018), which were relative to the pathogenesis in relapsing–remitting phase. Here we demonstrated a direct toxic effect of IL-17–induced Kv1.3 overexpression on myelin-producing

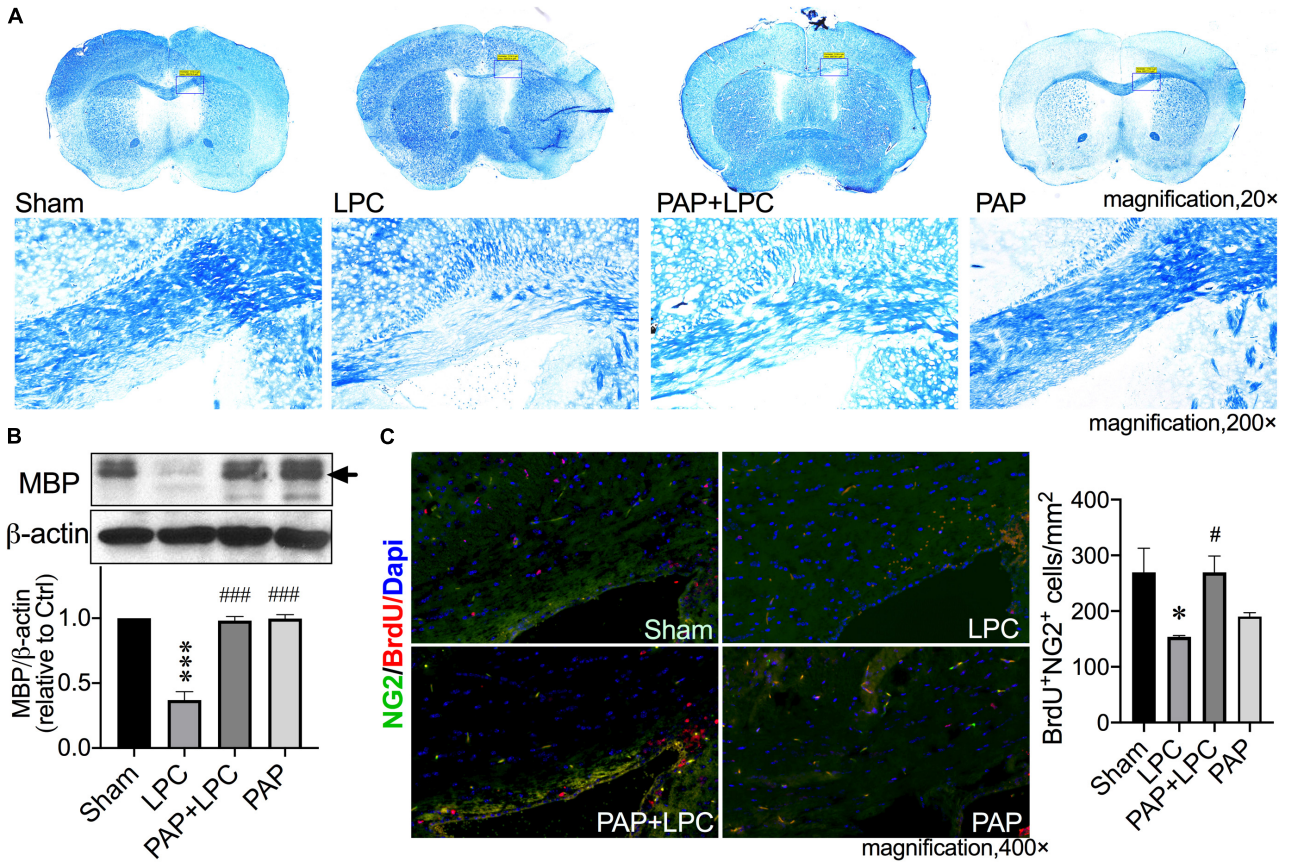


**FIGURE 5 |** Kv1.3 blockade protected corpus callosum from LPC-induced demyelination *in vivo*. The frozen sections were obtained from the demyelination model induced by stereotaxic injection of LPC (two points, 1%, 1 μL of each point) in corpus callosum. Mice were treated with or without PAP (6 mg/kg) and accepted BrdU (50 mg/kg) by i.p. injection. **(A)** Representative images of myelin sheath LFB staining (blue) in coronal sections of animal brain tissues. The low-magnification views (first line) show the complete coronal section, in which the framed parts are enlarged into the high-magnification views showing below. Compared with sham group, the injection site of LPC reduced significantly in overall density of staining for myelin. PAP significantly improved the LPC-induced myelin damage. **(B)** Western blot analysis of MBP expression in brain tissues around the injected points dissected out from the brain. The band marked by the arrow is a protein band with a size of 18.5 kDa. Blockade of Kv1.3 significantly prevented corpus callosum from LPC-induced MBP reduction ($n = 3$). **(C)** Representative images of merged BrdU immunofluorescence staining (red), NG2 (green), and DAPI (blue) in sections. There were 10 randomly selected visual fields counted for each experimental group from three independent treatments. Cell density of $BrdU^+NG2^+$ cells are shown in the bar graph (right). The LPC-induced decrease in $BrdU^+NG2^+$ cells density was mitigated by PAP. $^*P < 0.05$ vs. sham, $^{***}P < 0.001$ vs. sham. $^{\#}P < 0.05$ vs. LPC, $^{\#\#\#}P < 0.001$ vs. LPC.

cells OPCs and Ols. Such a direct toxicity was validated by using a relatively immune-independent mouse model that maximally eliminates the probable involvement of T-cell Kv1.3 in observed results. Myelin damage causes further axonal injury related to neurodegeneration in the progressive phase, because myelinated axons appear myelin dependency during development (Alizadeh et al., 2015). Additionally, an increased number of IL-17–expressing cells were observed in ischemic brain tissues of both human and rodent (Li et al., 2005; Gelderblom et al., 2012), suggesting that IL-17 participates in the CNS pathophysiology of secondary inflammation after ischemic stroke. The MS appears to be the disease mostly associated with IL-17, although IL-17 is relatively associated with different inflammatory conditions in the CNS.

IL-17–producing subset of $CD4^+$ T cells are identified as Th17 cells. The role of Th17 cells in the pathogenesis of relapsing–remitting MS has been demonstrated in several studies, showing the identification of Th17 cells in the MS lesions but not in normal-appearing white matter tissues or control brain specimens (Tzartos et al., 2008) and increased levels of Th17 cell gene expression as well as IL-17 protein in MS brain lesions (Lock et al., 2002; Komiyama et al., 2006; Tao et al., 2014). Although at certain conditions IL-17 may boost the differentiation of OPCs (Rodgers et al., 2015), most publications reported that IL-17 was harmful for OPC and Ol survival and function (Paintlia et al., 2011; Li et al., 2013; Waisman et al., 2015; Wang et al., 2017), thus promoting inflammatory injuries. Our results disclosed that IL-17 caused OPC loss of cell viability at the concentrations of 200 ng/mL or greater. Together with the results from BrdU experiments, we demonstrated that IL-17 inhibited OPC proliferation (**Figure 2**) without alteration of cell apoptosis (data not shown), which is consistent with previous results obtained with primary OPC culture (Rodgers et al., 2015). Similar results were also observed in neural stem cells that IL-17

stimulated neural stem cell way out of cell cycle despite no change of apoptosis (Li et al., 2013). Controversial results were reported in primary OPCs cultured with IL-17 for 4 days at the concentrations of 50 and 200 ng/mL (Kang et al., 2013). We next examined the effect of IL-17 on OPC differentiation. Application of IL-17 into OPCDM for 6 days at a concentration of 200 ng/mL inhibited the OPC differentiation (**Figure 2**). Kang et al. claimed an inhibitory effect on OPC maturation of 25 ng/mL IL-17 addition to culture medium with absence of proliferative signal platelet-derived growth factor (PDGF) (Kang et al., 2013). Rodgers et al. observed an enhancement of OPC differentiation in both absence and presence of PDGF, while culture treated with IL-17 at concentrations of 25 and 50 ng/mL within the first 2 h of plating (Rodgers et al., 2015). These contrast findings suggest the role of IL-17 on OPC differentiation is highly time- and dose-dependent. The discrepancies may also attribute to the culture system and stage of cells within the Ol lineage.

Kv1.3 is highly expressed in postmortem MS brain plaques, localized on inflammatory infiltrates (Rus et al., 2005) and OPCs (Tegla et al., 2011). These findings indicate the involvement of Kv1.3 in MS pathogenesis. Indeed, several groups reported the contribution of Kv1.3 in MS-related pathogenesis, and most data were from inflammatory cells in experimental autoimmune encephalomyelitis (EAE) model. Blockade of Kv1.3 revealed beneficial effects on alleviation of EAE (Huang et al., 2017; Fan et al., 2018; Yuan et al., 2018; Zhao et al., 2020). Preclinical trials targeting at Kv1.3 to treat autoimmune disease, including neuroinflammatory MS, were conducted and showed positive results (Perez-Verdaguer et al., 2016; Prentis et al., 2018). Although it is known that Kv1.3 is expressed on OPCs in MS lesion, the role of OPC/Ol Kv1.3 in MS pathogenesis is less appreciated. We showed that Kv1.3 currents and channel expression decreased during the OPC development in the cell culture (**Figure 1**), which is in agreement with previous observation on primary cultures (Chittajallu et al., 2002). IL-17–induced reduction of OPC proliferation and MBP expression in cultures were prevented by Kv1.3 antagonist, but antagonist alone did not alter proliferation and MBP expression (**Figure 2**), suggesting that Kv1.3 is involved in MS-related myelin damage, and Kv1.3 blockade affects OPC cell cycle particularly under pathological conditions. This may explain the controversial results from Vautier et al. (2004) that overexpression of Kv1.3 enhanced OPC proliferation but did not interfere differentiation when conducted under relatively physical conditions. Although we demonstrated an enhancement of Kv1.3 expression after IL-17 treatment, the molecular mechanisms remain obscure. In microglial cells, Kv1.3 expression is elevated by ERK1/2 activation (Liu et al., 2013), which is downstream molecular of IL-17. IL-17 may increase Kv1.3 expression potentially by activating ERK1/2 signal. AKT (Flores et al., 2008) and p38 MAPK (Bhat et al., 2007; Chew et al., 2010) are the main positive signals for OPC development. It is reported that AKT phosphorylation is dependent on Kv1.3 activation in Ol lineage cells and situated downstream of Kv1.3 (Tegla et al., 2011), and coexpression of PKB/AKT with Kv1.3 in oocytes enhanced the Kv1.3 channel abundance, suggesting AKT up-regulates Kv1.3 expression (Warsi et al., 2015). In both natural killer cells and T cells, Kv1.3 seems to activate AKT/mTOR signal cascade (Eil et al., 2016; Geng et al., 2020). Together, these findings suggest that Kv1.3 and AKT act synergistically. We examined the involvement of p38 MAPK and AKT in Kv1.3-mediated reduction of OPC proliferation and differentiation. The activation of AKT but not p38 MAPK was inhibited by IL-17–induced Kv1.3 enhancement, which was counteracted by AKT activator SC79 (**Figures 3**, **4**). This is a novel pattern different from previously demonstrated synergism of Kv1.3 and AKT. It is worth pointing out that downstream molecules of IL-17, including but not limited to ERK (Amatya et al., 2017; Xie et al., 2020; Allan et al., 2021), JNK (Amatya et al., 2017; Milovanovic et al., 2020), and nuclear factor κB (Jiang et al., 2017; Wu et al., 2018), may also contribute to the observed alterations of OPC cell cycle caused by IL-17, which were not examined in the present study. In addition, studying the role of the aforementioned negative signals in OPC development may be needed in the future, which will help us better understand the regulatory complex.

EAE is the most utilized animal model to explore MS-related pathogenesis and therapeutic strategy. The current immunosuppressive therapies are mainly based on the research done with EAE. Indeed, EAE is very heterogeneous regarding induction methods, clinical and pathological features, and amenability to treatments. The idea of EAE is based on the hypothesis that MS is mediated by autoreactive T-cell infiltration into CNS. But this hypothesis is challenged by studies that demonstrate occurrence of Ol death as the very early and perhaps the initial event in the pathology of the plaque, even before development of inflammation (Barnett and Prineas, 2004; Trapp, 2004). This brings EAE limitations when applied to human disease (Sriram and Steiner, 2005; Gold et al., 2006), particularly for remyelination. However, we focused on the OPC/Ol Kv1.3 function in inflammatory brains; LPC-induced demyelination was chosen to minimize the role of infiltrated T-cell Kv1.3 in the present study. Each model has its advantages and limitations. Other elements cannot be fully eliminated in LPC model, for example, the resident microglia around lesion site (Chen et al., 2020), which also expresses Kv1.3. Global administration of PAP may have the potential to inhibit Kv1.5 activity. However, the selectivity of PAP for Kv1.3 is approximately 23-fold higher than Kv1.5 (Schmitz et al., 2005; Vicente et al., 2006), making the possibility of Kv1.5 activation ignorable. In addition, systemic application of PAP to animals may also target on neuronal and microglial Kv1.3 channels; such a potential might be minimal as only small amounts of Kv1.3 are expressed on neurons in some brain regions.

In summary, our current data showed that IL-17 induced inhibition of OPC proliferation and differentiation through Kv1.3 channel, resulting in retardation in axonal remyelination and consequent brain white matter damage. We, for the first time, demonstrated that the integral role of Kv1.3 in IL-17 caused ATK signal decline, resulting in inhibitory effects of OPC proliferation and differentiation. Collectively, these findings serve to define the pathogenesis of CNS inflammation–induced myelin damage and support a potential therapeutic strategy of using

Kv1.3 blocker to treat MS and white matter damage in other neurological disorders.

## DATA AVAILABILITY STATEMENT

The raw data supporting the conclusions of this article will be made available by the authors, without undue reservation.

## ETHICS STATEMENT

The animal study was reviewed and approved by the Life Science Ethics Review Committee of Zhengzhou University.

## AUTHOR CONTRIBUTIONS

HL conceived and designed the project and carried out experiments together with XY. YW and YY participated in collating the experimental date and analysis. HL, XY, JY, and RZ edited the manuscript. HX and YX contributed to the revision of the manuscript and gave pertinent opinions. All authors contributed to the article and approved the submitted and final published version.

## FUNDING

This work was supported by the Chinese National Natural Science Foundation grant 81701247 awarded to HL. Furthermore, this study was also funded by the National Natural Science Foundation of China (Grant U190420029, 91849115 and 81530037 to YX) and the National Key R&D Program of China (Grant 2017YFA0105003 to YX).

## ACKNOWLEDGMENTS

We would like to express our heartfelt thanks to Yuzhen Liu of the First Affiliated Hospital of Xinxiang Medical University for her kindly help in the experiments.

## REFERENCES

Alizadeh, A., Dyck, S. M., and Karimi-Abdolrezaee, S. (2015). Myelin damage and repair in pathologic CNS: challenges and prospects. *Front. Mol. Neurosci.* 8:35. doi: 10.3389/fnmol.2015.00035

Allan, K. C., Hu, L. R., Scavuzzo, M. A., Morton, A. R., Gevorgyan, A. S., Cohn, E. F., et al. (2021). Non-canonical targets of HIF1a impair oligodendrocyte progenitor cell function. *Cell Stem Cell* 28:e211.

Amatya, N., Garg, A. V., and Gaffen, S. L. (2017). IL-17 Signaling: the Yin and the Yang. *Trends Immunol.* 38, 310–322. doi: 10.1016/j.it.2017.01.006

Azam, P., Sankaranarayanan, A., Homerick, D., Griffey, S., and Wulff, H. (2007). Targeting effector memory T cells with the small molecule Kv1.3 blocker PAP-1 suppresses allergic contact dermatitis. *J. Invest. Dermatol.* 127, 1419–1429. doi: 10.1038/sj.jid.5700717

Barnett, M. H., and Prineas, J. W. (2004). Relapsing and remitting multiple sclerosis: pathology of the newly forming lesion. *Ann. Neurol.* 55, 458–468. doi: 10.1002/ana.20016

Bhat, N. R., Zhang, P., and Mohanty, S. B. (2007). p38 MAP kinase regulation of oligodendrocyte differentiation with CREB as a potential target. *Neurochem. Res.* 32, 293–302. doi: 10.1007/s11064-006-9274-9

Bongarzone, E. R., Byravan, S., Givogri, M. I., Schonmann, V., and Campagnoni, A. T. (2000). Platelet-derived growth factor and basic fibroblast growth factor regulate cell proliferation and the expression of notch-1 receptor in a new oligodendrocyte cell line. *J. Neurosci. Res.* 62, 319–328. doi: 10.1002/1097-4547(20001101)62:3<319::aid-jnr1>3.0.co;2-g

Boulanger, J. J., and Messier, C. (2014). From precursors to myelinating oligodendrocytes: contribution of intrinsic and extrinsic factors to white matter plasticity in the adult brain. *Neuroscience* 269, 343–366. doi: 10.1016/j.neuroscience.2014.03.063

Boyd, A., Zhang, H., and Williams, A. (2013). Insufficient OPC migration into demyelinated lesions is a cause of poor remyelination in MS and mouse models. *Acta Neuropathol.* 125, 841–859. doi: 10.1007/s00401-013-1112-y

Chang, A., Tourtellotte, W. W., Rudick, R., and Trapp, B. D. (2002). Premyelinating oligodendrocytes in chronic lesions of multiple sclerosis. *N. Engl. J. Med.* 346, 165–173. doi: 10.1056/nejmoa010994

Chen, M., Yang, L. L., Hu, Z. W., Qin, C., Zhou, L. Q., Duan, Y. L., et al. (2020). Deficiency of microglial Hv1 channel is associated with activation of autophagic pathway and ROS production in LPC-induced demyelination mouse model. *J. Neuroinflamm.* 17:333.

Chew, L. J., Coley, W., Cheng, Y., and Gallo, V. (2010). Mechanisms of regulation of oligodendrocyte development by p38 mitogen-activated protein kinase. *J. Neurosci.* 30, 11011–11027. doi: 10.1523/jneurosci.2546-10.2010

Chittajallu, R., Chen, Y., Wang, H., Yuan, X., Ghiani, C. A., Heckman, T., et al. (2002). Regulation of Kv1 subunit expression in oligodendrocyte progenitor cells and their role in G1/S phase progression of the cell cycle. *Proc. Natl. Acad. Sci. U S A.* 99, 2350–2355. doi: 10.1073/pnas.042698399

Compston, A., and Coles, A. (2008). Multiple sclerosis. *Lancet* 372, 1502–1517.

Dai, X., Qu, P., and Dreyfus, C. F. (2001). Neuronal signals regulate neurotrophin expression in oligodendrocytes of the basal forebrain. *Glia* 34, 234–239. doi: 10.1002/glia.1057

Di Lucente, J., Nguyen, H. M., Wulff, H., Jin, L. W., and Maezawa, I. (2018). The voltage-gated potassium channel Kv1.3 is required for microglial pro-inflammatory activation in vivo. *Glia* 66, 1881–1895. doi: 10.1002/glia.23457

Eil, R., Vodnala, S. K., Clever, D., Klebanoff, C. A., Sukumar, M., Pan, J. H., et al. (2016). Ionic immune suppression within the tumour microenvironment limits T cell effector function. *Nature* 537, 539–543. doi: 10.1038/nature19364

Fan, C., Long, R., You, Y., Wang, J., Yang, X., Huang, S., et al. (2018). A novel PADRE-Kv1.3 vaccine effectively induces therapeutic antibodies and ameliorates experimental autoimmune encephalomyelitis in rats. *Clin. Immunol.* 193, 98–109. doi: 10.1016/j.clim.2018.02.012

Flores, A. I., Narayanan, S. P., Morse, E. N., Shick, H. E., Yin, X., Kidd, G., et al. (2008). Constitutively active Akt induces enhanced myelination in the CNS. *J. Neurosci.* 28, 7174–7183. doi: 10.1523/jneurosci.0150-08.2008

Fordyce, C. B., Jagasia, R., Zhu, X., and Schlichter, L. C. (2005). Microglia Kv1.3 channels contribute to their ability to kill neurons. *J. Neurosci.* 25, 7139–7149. doi: 10.1523/jneurosci.1251-05.2005

Gelderblom, M., Weymar, A., Bernreuther, C., Velden, J., Arunachalam, P., Steinbach, K., et al. (2012). Neutralization of the IL-17 axis diminishes neutrophil invasion and protects from ischemic stroke. *Blood* 120, 3793–3802. doi: 10.1182/blood-2012-02-412726

Geng, J., Wang, Y., Zhang, L., Wang, R., Li, C., Sheng, W., et al. (2020). The cajanine derivative LJ101019C regulates the proliferation and enhances the activity of NK cells via Kv1.3 channel-driven activation of the AKT/mTOR pathway. *Phytomedicine* 66:153113. doi: 10.1016/j.phymed.2019.153113

Gocke, A. R., Lebson, L. A., Grishkan, I. V., Hu, L., Nguyen, H. M., Whartenby, K. A., et al. (2012). Kv1.3 deletion biases T cells toward an immunoregulatory phenotype and renders mice resistant to autoimmune encephalomyelitis. *J. Immunol.* 188, 5877–5886. doi: 10.4049/jimmunol.1103095

Gold, R., Linington, C., and Lassmann, H. (2006). Understanding pathogenesis and therapy of multiple sclerosis via animal models: 70 years of merits and

culprits in experimental autoimmune encephalomyelitis research. *Brain* 129, 1953–1971. doi: 10.1093/brain/awl075

Grishkan, I. V., Tosi, D. M., Bowman, M. D., Harary, M., Calabresi, P. A., and Gocke, A. R. (2015). Antigenic stimulation of Kv1.3-Deficient th cells gives rise to a population of Foxp3-Independent T cells with suppressive properties. *J. Immunol.* 195, 1399–1407. doi: 10.4049/jimmunol.1403024

Hauser, S. L., Chan, J. R., and Oksenberg, J. R. (2013). Multiple sclerosis: prospects and promise. *Ann. Neurol.* 74, 317–327. doi: 10.1002/ana.24009

Huang, J., Han, S., Sun, Q., Zhao, Y., Liu, J., Yuan, X., et al. (2017). Kv1.3 channel blocker (ImKTx88) maintains blood-brain barrier in experimental autoimmune encephalomyelitis. *Cell Biosci.* 7:31.

Jiang, M., Wu, Y. L., Li, X., Zhang, Y., Xia, K. L., Cui, B. W., et al. (2017). Oligomeric proanthocyanidin derived from grape seeds inhibited NF-kappaB signaling in activated HSC: involvement of JNK/ERK MAPK and PI3K/Akt pathways. *Biomed. Pharmacother.* 93, 674–680. doi: 10.1016/j.biopha.2017.06.105

Jo, H., Mondal, S., Tan, D., Nagata, E., Takizawa, S., Sharma, A. K., et al. (2012). Small molecule-induced cytosolic activation of protein kinase Akt rescues ischemia-elicited neuronal death. *Proc. Natl. Acad. Sci. U S A.* 109, 10581–10586. doi: 10.1073/pnas.1202810109

Jolanda Munzel, E., and Williams, A. (2013). Promoting remyelination in multiple sclerosis-recent advances. *Drugs* 73, 2017–2029. doi: 10.1007/s40265-013-0146-8

Kang, Z., Wang, C., Zepp, J., Wu, L., Sun, K., Zhao, J., et al. (2013). Act1 mediates IL-17-induced EAE pathogenesis selectively in NG2+ glial cells. *Nat. Neurosci.* 16, 1401–1408. doi: 10.1038/nn.3505

Kim, H., Shin, J., Kim, S., Poling, J., Park, H. C., and Appel, B. (2008). Notch-regulated oligodendrocyte specification from radial glia in the spinal cord of zebrafish embryos. *Dev. Dyn.* 237, 2081–2089. doi: 10.1002/dvdy.21620

Koch Hansen, L., Sevelsted-Moller, L., Rabjerg, M., Larsen, D., Hansen, T. P., Klinge, L., et al. (2014). Expression of T-cell KV1.3 potassium channel correlates with pro-inflammatory cytokines and disease activity in ulcerative colitis. *J. Crohns Colitis* 8, 1378–1391. doi: 10.1016/j.crohns.2014.04.003

Kolbinger, F., Huppertz, C., Mir, A., and Padova, F. D. (2016). IL-17A and multiple sclerosis: signaling pathways, producing cells and target cells in the central nervous system. *Curr. Drug Targets* 17, 1882–1893. doi: 10.2174/1389450117666160307144027

Komiyama, Y., Nakae, S., Matsuki, T., Nambu, A., Ishigame, H., Kakuta, S., et al. (2006). IL-17 plays an important role in the development of experimental autoimmune encephalomyelitis. *J. Immunol.* 177, 566–573. doi: 10.4049/jimmunol.177.1.566

Kostic, M., Dzopalic, T., Zivanovic, S., Zivkovic, N., Cvetanovic, A., Stojanovic, I., et al. (2014). IL-17 and glutamate excitotoxicity in the pathogenesis of multiple sclerosis. *Scand. J. Immunol.* 79, 181–186. doi: 10.1111/sji.12147

Li, G. Z., Zhong, D., Yang, L. M., Sun, B., Zhong, Z. H., Yin, Y. H., et al. (2005). Expression of interleukin-17 in ischemic brain tissue. *Scand. J. Immunol.* 62, 481–486. doi: 10.1111/j.1365-3083.2005.01683.x

Li, Z., Li, K., Zhu, L., Kan, Q., Yan, Y., Kumar, P., et al. (2013). Inhibitory effect of IL-17 on neural stem cell proliferation and neural cell differentiation. *BMC Immunol.* 14:20. doi: 10.1186/1471-2172-14-20

Liu, H., Liu, J., Xu, E., Tu, G., Guo, M., Liang, S., et al. (2017a). Human immunodeficiency virus protein Tat induces oligodendrocyte injury by enhancing outward K(+) current conducted by KV1.3. *Neurobiol. Dis.* 97, 1–10. doi: 10.1016/j.nbd.2016.10.007

Liu, S. Q., Zhang, M. L., Zhang, H. J., Liu, F. Z., Chu, R. J., Zhang, G. X., et al. (2017b). Matrine promotes oligodendrocyte development in CNS autoimmunity through the PI3K/Akt signaling pathway. *Life Sci.* 180, 36–41. doi: 10.1016/j.lfs.2017.05.010

Liu, J., Xu, P., Collins, C., Liu, H., Zhang, J., Keblesh, J. P., et al. (2013). HIV-1 Tat protein increases microglial outward K(+) current and resultant neurotoxic activity. *PLoS One* 8:e64904. doi: 10.1371/journal.pone.0064904

Lock, C., Hermans, G., Pedotti, R., Brendolan, A., Schadt, E., Garren, H., et al. (2002). Gene-microarray analysis of multiple sclerosis lesions yields new targets validated in autoimmune encephalomyelitis. *Nat. Med.* 8, 500–508. doi: 10.1038/nm0502-500

Lucchinetti, C., Bruck, W., Parisi, J., Scheithauer, B., Rodriguez, M., and Lassmann, H. (1999). A quantitative analysis of oligodendrocytes in multiple sclerosis lesions. a study of 113 cases. *Brain* 122(Pt 12), 2279–2295. doi: 10.1093/brain/122.12.2279

Maezawa, I., Nguyen, H. M., Di Lucente, J., Jenkins, D. P., Singh, V., Hilt, S., et al. (2018). Kv1.3 inhibition as a potential microglia-targeted therapy for Alzheimer's disease: preclinical proof of concept. *Brain* 141, 596–612. doi: 10.1093/brain/awx346

Mi, S., Lee, X., Shao, Z., Thill, G., Ji, B., Relton, J., et al. (2004). LINGO-1 is a component of the Nogo-66 receptor/p75 signaling complex. *Nat. Neurosci.* 7, 221–228. doi: 10.1038/nn1188

Mi, S., Miller, R. H., Lee, X., Scott, M. L., Shulag-Morskaya, S., Shao, Z., et al. (2005). LINGO-1 negatively regulates myelination by oligodendrocytes. *Nat. Neurosci.* 8, 745–751. doi: 10.1038/nn1460

Milovanovic, J., Arsenijevic, A., Stojanovic, B., Kanjevac, T., Arsenijevic, D., Radosavljevic, G., et al. (2020). Interleukin-17 in chronic inflammatory neurological diseases. *Front. Immunol.* 11:947. doi: 10.3389/fimmu.2020.00947

Moser, T., Akgun, K., Proschmann, U., Sellner, J., and Ziemssen, T. (2020). The role of TH17 cells in multiple sclerosis: therapeutic implications. *Autoimmun Rev.* 19:102647. doi: 10.1016/j.autrev.2020.102647

Nasrabady, S. E., Rizvi, B., Goldman, J. E., and Brickman, A. M. (2018). White matter changes in Alzheimer's disease: a focus on myelin and oligodendrocytes. *Acta Neuropathol. Commun.* 6:22.

Oksala, N. K., Oksala, A., Pohjasvaara, T., Vataja, R., Kaste, M., Karhunen, P. J., et al. (2009). Age related white matter changes predict stroke death in long term follow-up. *J. Neurol. Neurosurg. Psychiatry* 80, 762–766. doi: 10.1136/jnnp.2008.154104

Paintlia, M. K., Paintlia, A. S., Singh, A. K., and Singh, I. (2011). Synergistic activity of interleukin-17 and tumor necrosis factor-alpha enhances oxidative stress-mediated oligodendrocyte apoptosis. *J. Neurochem.* 116, 508–521. doi: 10.1111/j.1471-4159.2010.07136.x

Perez-Verdaguer, M., Capera, J., Serrano-Novillo, C., Estadella, I., Sastre, D., and Felipe, A. (2016). The voltage-gated potassium channel Kv1.3 is a promising multitherapeutic target against human pathologies. *Expert Opin. Ther. Targets* 20, 577–591. doi: 10.1517/14728222.2016.1112792

Prentis, P. J., Pavasovic, A., and Norton, R. S. (2018). Sea anemones: quiet achievers in the field of peptide toxins. *Toxins (Basel)* 10:36. doi: 10.3390/toxins10010036

Pruss, H., Dewes, M., Derst, C., Fernandez-Klett, F., Veh, R. W., and Priller, J. (2011). Potassium channel expression in adult murine neural progenitor cells. *Neuroscience* 180, 19–29. doi: 10.1016/j.neuroscience.2011.02.021

Pugliatti, M., Sotgiu, S., and Rosati, G. (2002). The worldwide prevalence of multiple sclerosis. *Clin. Neurol. Neurosurg.* 104, 182–191. doi: 10.1016/s0303-8467(02)00036-7

Rodgers, J. M., Robinson, A. P., Rosler, E. S., Lariosa-Willingham, K., Persons, R. E., Dugas, J. C., et al. (2015). IL-17A activates ERK1/2 and enhances differentiation of oligodendrocyte progenitor cells. *Glia* 63, 768–779. doi: 10.1002/glia.22783

Rus, H., Pardo, C. A., Hu, L., Darrah, E., Cudrici, C., Niculescu, T., et al. (2005). The voltage-gated potassium channel Kv1.3 is highly expressed on inflammatory infiltrates in multiple sclerosis brain. *Proc. Natl. Acad. Sci. U S A.* 102, 11094–11099. doi: 10.1073/pnas.0501770102

Schmitz, A., Sankaranarayanan, A., Azam, P., Schmidt-Lassen, K., Homerick, D., Hansel, W., et al. (2005). Design of PAP-1, a selective small molecule Kv1.3 blocker, for the suppression of effector memory T cells in autoimmune diseases. *Mol. Pharmacol.* 68, 1254–1270. doi: 10.1124/mol.105.015669

Shimizu, T., Kagawa, T., Wada, T., Muroyama, Y., Takada, S., and Ikenaka, K. (2005). Wnt signaling controls the timing of oligodendrocyte development in the spinal cord. *Dev. Biol.* 282, 397–410. doi: 10.1016/j.ydbio.2005.03.020

Smith, G. S., Homchaudhuri, L., Boggs, J. M., and Harauz, G. (2012). Classic 18.5- and 21.5-kDa myelin basic protein isoforms associate with cytoskeletal and SH3-domain proteins in the immortalized N19-oligodendroglial cell line stimulated by phorbol ester and IGF-1. *Neurochem. Res.* 37, 1277–1295. doi: 10.1007/s11064-011-0700-2

Sriram, S., and Steiner, I. (2005). Experimental allergic encephalomyelitis: a misleading model of multiple sclerosis. *Ann. Neurol.* 58, 939–945. doi: 10.1002/ana.20743

Tao, Y., Zhang, X., Chopra, M., Kim, M. J., Buch, K. R., Kong, D., et al. (2014). The role of endogenous IFN-beta in the regulation of Th17 responses in patients with relapsing-remitting multiple sclerosis. *J. Immunol.* 192, 5610–5617. doi: 10.4049/jimmunol.1302580

Tegla, C. A., Cudrici, C., Rozycka, M., Soloviova, K., Ito, T., Singh, A. K., et al. (2011). C5b-9-activated, K(v)1.3 channels mediate oligodendrocyte cell cycle

activation and dedifferentiation. *Exp. Mol. Pathol.* 91, 335–345. doi: 10.1016/j.yexmp.2011.04.006

Trapp, B. D. (2004). Pathogenesis of multiple sclerosis: the eyes only see what the mind is prepared to comprehend. *Ann. Neurol.* 55, 455–457. doi: 10.1002/ana.20087

Tsiperson, V., Gruber, R. C., Goldberg, M. F., Jordan, A., Weinger, J. G., Macian, F., et al. (2013). Suppression of inflammatory responses during myelin oligodendrocyte glycoprotein-induced experimental autoimmune encephalomyelitis is regulated by AKT3 signaling. *J. Immunol.* 190, 1528–1539. doi: 10.4049/jimmunol.1201387

Tzartos, J. S., Friese, M. A., Craner, M. J., Palace, J., Newcombe, J., Esiri, M. M., et al. (2008). Interleukin-17 production in central nervous system-infiltrating T cells and glial cells is associated with active disease in multiple sclerosis. *Am. J. Pathol.* 172, 146–155. doi: 10.2353/ajpath.2008.070690

Vassall, K. A., Bessonov, K., De Avila, M., Polverini, E., and Harauz, G. (2013). The effects of threonine phosphorylation on the stability and dynamics of the central molecular switch region of 18.5-kDa myelin basic protein. *PLoS One* 8:e68175. doi: 10.1371/journal.pone.0068175

Vautier, F., Belachew, S., Chittajallu, R., and Gallo, V. (2004). Shaker-type potassium channel subunits differentially control oligodendrocyte progenitor proliferation. *Glia* 48, 337–345. doi: 10.1002/glia.20088

Vicente, R., Escalada, A., Villalonga, N., Texido, L., Roura-Ferrer, M., Martin-Satue, M., et al. (2006). Association of Kv1.5 and Kv1.3 contributes to the major voltage-dependent K+ channel in macrophages. *J. Biol. Chem.* 281, 37675–37685.

Waisman, A., Hauptmann, J., and Regen, T. (2015). The role of IL-17 in CNS diseases. *Acta Neuropathol.* 129, 625–637. doi: 10.1007/s00401-015-1402-7

Wang, C., Zhang, C. J., Martin, B. N., Bulek, K., Kang, Z., Zhao, J., et al. (2017). IL-17 induced NOTCH1 activation in oligodendrocyte progenitor cells enhances proliferation and inflammatory gene expression. *Nat. Commun.* 8:15508.

Wang, X., Li, G., Guo, J., Zhang, Z., Zhang, S., Zhu, Y., et al. (2019). Kv1.3 Channel as a key therapeutic target for neuroinflammatory diseases: state of the art and beyond. *Front. Neurosci.* 13:1393. doi: 10.3389/fnins.2019.01393

Warsi, J., Fezai, M., Fores, M., Elvira, B., and Lang, F. (2015). Up-Regulation of Voltage Gated K+ channels Kv1.3 and Kv1.5 by protein kinase PKB/Akt. *Cell Physiol. Biochem.* 37, 2454–2463. doi: 10.1159/000438598

Wu, M., Xu, L., Wang, Y., Zhou, N., Zhen, F., Zhang, Y., et al. (2018). S100A8/A9 induces microglia activation and promotes the apoptosis of oligodendrocyte precursor cells by activating the NF-kappaB signaling pathway. *Brain Res. Bull.* 143, 234–245. doi: 10.1016/j.brainresbull.2018.09.014

Xie, D., Ge, X., Ma, Y., Tang, J., Wang, Y., Zhu, Y., et al. (2020). Clemastine improves hypomyelination in rats with hypoxic–ischemic brain injury by reducing microglia-derived IL-1β via P38 signaling pathway. *J. Neuroinflamm.* 17:57.

Yuan, X. L., Zhao, Y. P., Huang, J., Liu, J. C., Mao, W. Q., Yin, J., et al. (2018). A Kv1.3 channel-specific blocker alleviates neurological impairment through inhibiting T-cell activation in experimental autoimmune encephalomyelitis. *CNS Neurosci. Ther.* 24, 967–977. doi: 10.1111/cns.12848

Zhao, Y., Qiu, W., Liu, J., Yuan, X., Mao, W., Yin, J., et al. (2020). Blockade of Kv1.3 potassium channel inhibits CD8(+) T cell-mediated neuroinflammation via PD-1/Blimp-1 signaling. *Faseb J.* 34, 15492–15503. doi: 10.1096/fj.202000861rr

**Conflict of Interest:** The authors declare that the research was conducted in the absence of any commercial or financial relationships that could be construed as a potential conflict of interest.

frontiers in Cellular Neuroscience

ORIGINAL RESEARCH
published: 08 July 2021
doi: 10.3389/fncel.2021.697449

# NLRP3 Inflammasome: A Potential Target in Isoflurane Pretreatment Alleviates Stroke-Induced Retinal Injury in Diabetes

*Hong-Bin Lin[1†], Ying-Hui Lin[1†], Jin-Yu Zhang[2], Wen-Jing Guo[1], Andrea Ovcjak[3], Zhi-Jian You[4], Zhong-Ping Feng[3], Hong-Shuo Sun[3,5,6,7], Feng-Xian Li[1]* and Hong-Fei Zhang[1]**

[1]Department of Anesthesiology, Zhujiang Hospital of Southern Medical University, Guangzhou, China, [2]State Key Laboratory of Ophthalmology, Zhongshan Ophthalmic Center, Sun Yat-Sen University, Guangzhou, China, [3]Department of Physiology, Temerty Faculty of Medicine, University of Toronto, Toronto, ON, Canada, [4]Department of Anesthesiology, Liuzhou People's Hospital, The Affiliated Liuzhou People's Hospital of Guangxi Medical University, Liuzhou, China, [5]Department of Surgery, Temerty Faculty of Medicine, University of Toronto, Toronto, ON, Canada, [6]Department of Pharmacology and Toxicology, Temerty Faculty of Medicine, University of Toronto, Toronto, ON, Canada, [7]Leslie Dan Faculty of Pharmacy, University of Toronto, Toronto, ON, Canada

Ischemic stroke remains a devastating disease which is the leading cause of death worldwide. Visual impairment after stroke is a common complication which may lead to vision loss, greatly impacting life quality of patients. While ischemic stroke is traditionally characterized by a blockage of blood flow to the brain, this may coincide with reduced blood flow to the eye, resulting in retinal ischemia and leading to visual impairment. Diabetes increases the risk of ischemic stroke and induces diabetic retinopathy; the latter may be more sensitive to the ischemic retinal injury. In diabetic status, the underlying mechanism in stroke-induced retinal injury has not been fully clarified. The NLR pyrin domain containing 3 (NLRP3) inflammasome is an important activator of inflammation, which may play a critical role in catalyzing and forming certain pro-inflammatory cytokines in both cerebral and retinal ischemia. Isoflurane has been demonstrated to inhibit the activation of the NLRP3 inflammasome and show neuroprotective effects. In this study, we established a diabetic mouse model and performed the middle cerebral artery occlusion procedure to induce ischemic stroke. Our results revealed that cerebral ischemia-induced retinal injury in the diabetic model. Isoflurane pretreatment alleviated the cerebral and retinal injury after ischemic stroke. Of note, isoflurane pretreatment inhibited the NLRP3 inflammasome activation in the retina, indicating that isoflurane pretreatment may provide substantial retinal protection in stroke-induced retinal injury in diabetes.

**Keywords: ischemic stroke (IS), retinal injury, diabetes, NLRP3 inflammasome, isoflurane**

**Abbreviations:** NLRP3, NLR pyrin domain containing 3; MCAO, middle cerebral artery occlusion; ISO, isoflurane; IL-1β, interleukin-1β; IL-18, interleukin-18; GCL, ganglion cell layer; OPA, ophthalmic artery.

OPEN ACCESS

***Edited by:***
*Junlei Chang,*
*Shenzhen Institutes of Advanced Technology, Chinese Academy of Sciences (CAS), China*

***Reviewed by:***
*Tao Tao,*
*Southern Medical University, China*
*Bin Cai,*
*Fujian Medical University, China*

****Correspondence:***
*Feng-Xian Li*
*lifengxian81@smu.edu.cn*
*Hong-Fei Zhang*
*zhanghongfei@smu.edu.cn*

*[†]These authors have contributed equally to this work and share first authorship*

***Specialty section:***
*This article was submitted to Cellular Neurophysiology, a section of the journal Frontiers in Cellular Neuroscience*

***Received:*** *19 April 2021*
***Accepted:*** *16 June 2021*
***Published:*** *08 July 2021*

***Citation:***
*Lin H-B, Lin Y-H, Zhang J-Y, Guo W-J, Ovcjak A, You Z-J, Feng Z-P, Sun H-S, Li F-X and Zhang H-F (2021) NLRP3 Inflammasome: A Potential Target in Isoflurane Pretreatment Alleviates Stroke-Induced Retinal Injury in Diabetes. Front. Cell. Neurosci. 15:697449. doi: 10.3389/fncel.2021.697449*

## INTRODUCTION

Stroke, the leading cause of death and disability, affects nearly 30 million people worldwide each year, with ischemic stroke accounting for upwards of 75% of all cases (Wang et al., 2017). Visual impairment is a common complication in stroke patients which affects functional recovery and quality of life (Sand et al., 2013). A previous study has reported that 92% of patients suffer from visual impairments after stroke, including eye movement disorders, visual acuity reduction, visual field impairment, and visual perceptual difficulty (Rowe, 2017). Visual impairments after stroke are also predictive of worse prognosis, stroke recurrence, and higher mortality (Deng et al., 2018; Sand et al., 2018). In rodent ischemic stroke models, visual impairments after stroke have also been widely reported which accompany neurological and retinal injury (Steele et al., 2008; Allen et al., 2014; Liu et al., 2015; Nguyen et al., 2019; Lee et al., 2020). The main pathogenesis of stroke-induced visual impairments includes higher visual center damage, retinal ischemia, and subsequent retinal damage (Steele et al., 2008; Rowe et al., 2013; Nguyen et al., 2019). Diabetes is a well-established independent risk factor related to cerebrovascular diseases and retinal ischemic injury (Ergul et al., 2014; Hendrick et al., 2015), which increases the incidence of ischemic stroke and visual impairments after stroke (Liu et al., 2016; Bragg et al., 2017; Sand et al., 2018). However, the underlying molecular mechanisms of stroke-induced retinal injury are still far from precisely dissected, especially in diabetic disease.

Inflammation plays an important role in the progression of a diabetic stroke, retinal ischemia, and diabetic retinopathy (Rivera et al., 2017; Hong et al., 2018; Forrester et al., 2020). The retina is an extension of the central nervous system and the pathological response to retinal ischemia is comparable in many ways to that of ischemic stroke. It is therefore reasonable to speculate that stroke-induced retinal injury shares similar inflammatory pathogenesis with cerebral ischemia and retinal ischemia. The NLR pyrin domain containing 3 (NLRP3) inflammasome is an important activator of inflammation which mediates the maturation and secretion of active pro-inflammatory cytokines such as interleukin 1β (IL-1β) and interleukin 18 (IL-18; Zhou et al., 2010a; Deng et al., 2019). Previous studies have shown that NLRP3 inflammasome activation participates in the underlying molecular pathway of ischemic stroke in diabetic mice (Hong et al., 2018) and retinal ischemic/reperfusion injury (Wan et al., 2020). However, it is unclear whether NLRP3 inflammasome is involved in stroke-induced retinal injury in diabetes.

Isoflurane (ISO) has been demonstrated to have anti-inflammatory and neuroprotective properties in ischemic stroke (Zhou et al., 2010b; Zhang et al., 2016; Jiang et al., 2017; Guo et al., 2020). Furthermore, a previous study has suggested that ISO can inhibit the activation of the NLRP3 inflammasome (Yin et al., 2016). To investigate whether ISO offers retinal protection against stroke-induced retinal injury in diabetes, we administered ISO prior to middle cerebral artery occlusion (MCAO) in diabetic mice and studied the role of NLRP3 inflammasome activation in the retina. Our results showed that ISO pretreatment ameliorates stroke-induced retinal injury in diabetes *via* inhibition of retinal NLRP3 inflammasome activation. Our results provide a causative pathway for stroke-induced retinal injury in diabetes and suggest a potential therapeutic target for retinal protection in ischemic stroke in diabetes.

## MATERIALS AND METHODS

### Animal

Male C57BL/6J mice (4–6 w, 14–18 g) were housed in 12 h light/dark cycle conditions and were supplied adequate food and water before the experiment ($n$ = 100). All experimental animals were purchased from the Zhujiang Hospital Animal Experimental Center of Southern Medical University. The study was approved by the Medical Faculty Ethics Committee of Southern Medical University. Firstly, we built the type 2 diabetic (DM) mouse model ($n$ = 65) and used non-DM mice as control ($n$ = 35). We excluded mice having fasting glucose less than 10.0 mmol/L ($n$ = 16). DM mice were randomly assigned to the sham group, MCAO ISO (−) group, and MCAO ISO (+) group ($n$ = 11–21). Mice which died after surgery were excluded in MCAO ISO (−) group and MCAO ISO (+) group ($n$ = 2 in each group). Mice were randomly chosen from sham group, MCAO ISO (−) group, and MCAO ISO (+) group ($n$ = 4–6) for retinal gene expression. The eyeballs were collected from sham group, MCAO ISO (−) group, and MCAO ISO (+) group ($n$ = 7–13) for tissue section and subsequent staining.

### Type 2 Diabetes Mellitus Mouse Model

The type 2 diabetic mouse model was generated as described previously (Lin et al., 2020). Briefly, we first fed each mouse on a high-fat diet (Guangdong Medical Laboratory Animal Center, Guangzhou, China) for 3 w. A dose of 100 mg/kg streptozotocin (STZ, Sigma, St. Louis, MO, USA) was then injected intraperitoneally. Mice were then fed with a high-fat diet for another 4 w. The blood glucose concentration was measured after fasting for 8 h on day 1, 22, 36, and 50. The criterion for a type 2 diabetes mellitus mouse was fasting glucose >10.0 mmol/L. Control (non-diabetic) mice were housed in the same environment, fed a normal diet, and given an equal-volume intraperitoneal injection of vehicle.

### Ischemic Stroke Mouse Model

The ischemic stroke mouse model was generated by MCAO following the protocol of our previous study (Lin et al., 2020). In brief, mice were anesthetized with 2% isoflurane (RWD Life Science Co., Ltd, Shenzhen, China). After a midline neck incision, a 4–0 nylon monofilament (3 cm) with a blunted tip (Sebiona Technology Co. Ltd., Guangzhou, China) was inserted into the origins of the right middle cerebral artery (MCA) through the right external carotid artery to block the blood flow to the MCA. The suture was left in place for 1 h and reperfusion was established after withdrawing the suture. The mice were sacrificed after maintaining reperfusion for 24 h for the subsequent experiments. Sham-operated

mice underwent the same procedure without insertion of the monofilament.

## Isoflurane (ISO) Pretreatment

The ISO pretreatment [ISO (+)] group inhaled 2% isoflurane for 1 h which was delivered by oxygen ($O_2$) at a rate of 0.2 L/min 24 h before MCAO procedure. The control group [ISO (−)] received the same procedure without ISO pretreatment. ISO pretreatment and control groups were randomly assigned to ischemic MCAO and sham groups.

## Brain 2,3,5-Triphenyltetrazolium Chloride (TTC) Staining

The whole brain was collected immediately after euthanasia. The brain was sectioned into 1 mm thick slices and stained with 2% TTC (BCCC4696, Sigma, St. Louis, MO, USA) for 15 min and then fixed in 4% paraformaldehyde (PFA).

## Hematoxylin and Eosin (H&E) Staining

The ipsilateral eyeball was isolated and fixed in 4% PFA before being embedded in paraffin. Eyeballs were sectioned in the same coronal sections (5 μm thick). H&E staining was employed to assess retinal ganglion cell layer (GCL) cells and inner retinal measurement. The slices were imaged using a bright-field microscope (DM2500 LED, Leica Microsystems, Germany) and analyzed in ImageJ (version 1.49, National Institutes of Health, Bethesda, MD, USA).

## Terminal Deoxynucleotidyl Transferase-Mediated Nick End Labeling (TUNEL) and Immunofluorescence Staining

Mice were perfused with 4% PFA. Eyeballs were removed and fixed with 4% PFA for 24 h. Frozen sections of 10 μm thickness were embedded in optimal cutting temperature compound (OCT, Tissue-Tek, Sakura Finetek, USA). TUNEL staining was performed using in situ Cell Death Detection Kit, Fluorescein (11684795910, Roche, USA). For immunofluorescence staining, the primary antibodies used were as follows: rabbit anti-NLRP3 (PA579740, 1:1,000, Thermo Fisher, USA), mouse anti-Caspase-1 (sc-56036, 1:100, Santa Cruz, USA), and Rabbit anti-IL-1β (12703, 1:100, Cell Signaling Technology, USA). The secondary antibodies used were goat anti-rabbit (A-11034, 1:1,000, Thermo Fisher, USA) and goat anti-mouse (A-11032, 1:1,000, Thermo Fisher, USA). After that, sections were imaged using a fluorescence microscope (TS100, Nikon, Japan) and analyzed using ImageJ.

## Quantitative RT-PCR (qPCR)

qPCR was performed to measure the expression of NLRP3 inflammasome mRNA in the retina. Primer sequences are as follow: NLRP3, ATT ACC CGC CCG AGA AAG G

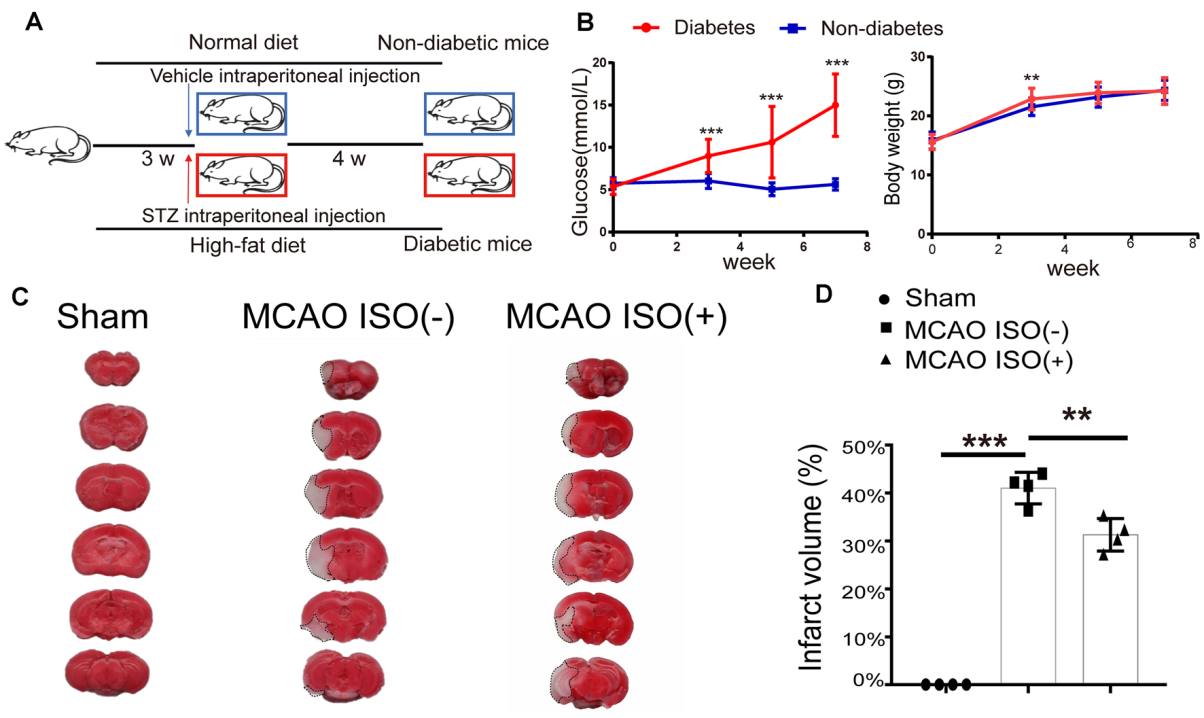


**FIGURE 1 |** Isoflurane (ISO) pretreatment protects the brain against ischemic damage in a diabetic mouse model. **(A)** Diagram of the protocol used to generate the type 2 diabetic mouse model. **(B)** Continuous monitoring of the blood glucose and body weight changes from the beginning of the high-fat diet (0 week) in diabetic mice and non-diabetic mice. $n = 24$ in each group. **(C)** Representative images of TTC-stained coronal brain slices of sham-operated (left), middle cerebral artery occlusion (MCAO) mice without ISO pretreatment (middle) and MCAO mice with ISO pretreatment (right). The infarct area is indicated *via* the dotted line. **(D)** The infarct volume in the sham-operated, MCAO mice without ISO pretreatment, and MCAO with ISO pretreatment. $n = 4$ in each group. $^{**}P < 0.01$, $^{***}P < 0.001$.

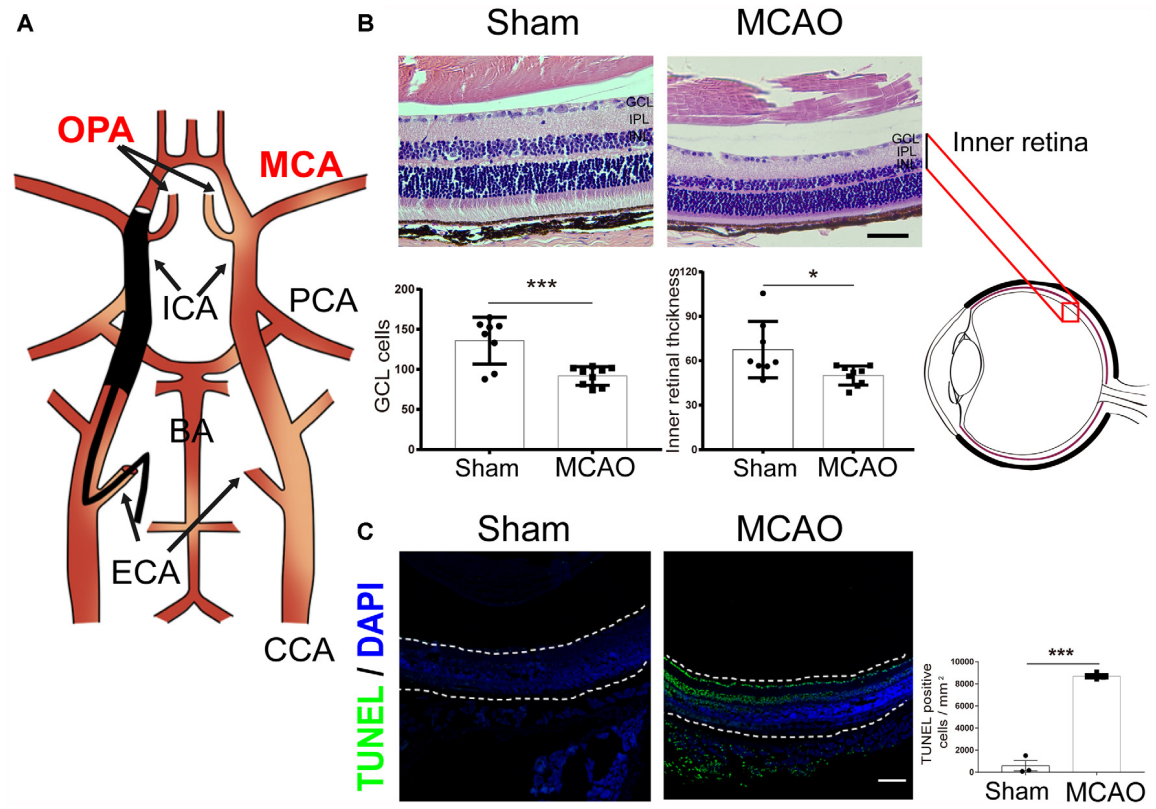


**FIGURE 2 |** Ischemic stroke induces retinal injury in diabetic mice. **(A)** Schematic diagram of MCAO model blocking the OPA. Monofilament is inserted into the right MCA to block blood flow, thereby blocking the OPA at the same time. **(B)** Top, representative H&E staining in retina post-MCAO. Scale bar, 50 μm. Bottom, bar graphs showing the GCL cell count and the inner retinal thickness in the sham ($n$ = 7) and MCAO group ($n$ = 9). **(C)** Left, representative images showing TUNEL staining in retina post-MCAO. The retina is indicated between the dotted lines. Green, TUNEL positive cell; Blue, DAPI (magnification, 100×; scale bar, 100 μm). Right, bar graphs showing the TUNEL positive cells density at GCL in the sham ($n$ = 3) and MCAO groups ($n$ = 4). Sham and MCAO mice were administered with vehicle pretreatment. OPA, ophthalmic artery; MCA, middle cerebral artery; PCA, posterior cerebral artery; ICA, internal carotid artery; BA, basilar artery; ECA, external carotid artery; CCA, common carotid artery; GCL, ganglion cell layer; IPL, inner plexiform layer; INL, inner nuclear layer. *$P < 0.05$, ***$P < 0.001$.

(forward primer); TCG CAG CAA AGA TCC ACA CAG (reverse primer). Caspase-1, AAT ACA ACC ACT CGT ACA CGTC (forward primer); AGC TCC AAC CCT CGG AGA AA (reverse primer). IL-1β, GAA ATG CCA CCT TTT GAC AGT G (forward primer); TGG ATG CTC TCA TCA GGA CAG (reverse primer). β-actin, GTG CTA TGT TGC TCT AGA CTT CG (forward primer); ATG CCA CAG GAT TCC ATA CC (reverse primer). Using RNAiso Plus kit (TaKaRa, 9109, Japan) to extract the total RNA from the right retina. qPCR was applied by the SYBR Green kit (Takara, RR820A, Japan) using 10 μl cDNA. β-actin was used as the housekeeping gene.

## Statistical Analysis

Data are shown as means ± SD and analyzed using Prism7 software (GraphPad7, San Diego, CA, USA). Statistical significances were determined using Student $t$-test (for two groups) or one-way ANOVA followed by a Tukey Kramer *post hoc* test (for three groups) or repeated measures ANOVA followed by a Bonferroni *post hoc* test (groups with repeated measurements). The difference between groups was considered statistically significant if $P < 0.05$.

# RESULTS

## Ischemic Stroke-Induced Retinal Injury in Diabetic Mice

To assess the retinal injury after ischemic stroke in diabetic mice, we first generated the type-2 diabetic mouse model by administering a high-fat diet and STZ intraperitoneal injection (**Figure 1A**). Compared to the control group, we found that the blood glucose level significantly increased in diabetic mice at all timepoints (**Figure 1B**). Although the diabetic mice gained significantly more body weight during the first 3 w, there was no significant difference in body weight compared to the non-diabetic mice after 4 w (**Figure 1B**).

In this MCAO model, the ophthalmic artery (OPA) was blocked while the monofilament was inserted into the right MCA (**Figure 2A**). A previous study has reported a 90% reduction in blood flow in the ipsilateral eye during MCAO (Lee et al., 2020). Correspondingly, when evaluating the histological changes in the retina by H&E staining, we found a significantly decreased ganglion cell layer (GCL) cell count and inner retinal thickness in the MCAO group (**Figure 2B**). Furthermore, compared to

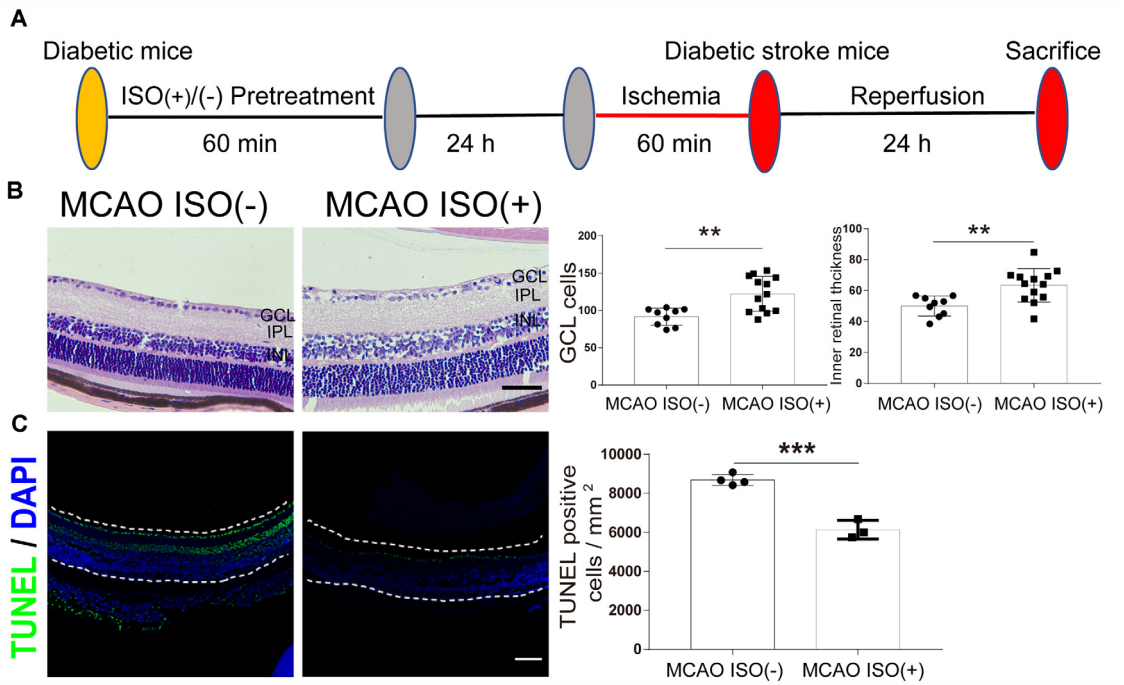


**FIGURE 3 |** ISO pretreatment reduces retinal injury after ischemic stroke in diabetic mice. **(A)** Diagram of ISO pretreatment protocol. **(B)** Left, representative H&E staining in the retina after MCAO with ISO pretreatment or without ISO pretreatment (magnification, 400×; scale bar, 50 μm). Right, bar graphs showing the GCL cell count and the inner retinal thickness in the MCAO ISO (–) group ($n$ = 9) and MCAO ISO (+) groups ($n$ = 13). **(C)** Left, representative images showing TUNEL staining in the retina after MCAO with ISO pretreatment or without ISO pretreatment. The retina is indicated between the dotted lines. Green, TUNEL positive cell; Blue, DAPI (magnification, 100×; scale bar, 100 μm). Scale bar, 100 μm. Right, bar graphs showing the TUNEL positive cells density at GCL in the MCAO ISO (–) group ($n$ = 4) and MCAO ISO (+) groups ($n$ = 3). GCL, ganglion cell layer; IPL, inner plexiform layer; INL, inner nuclear layer. $^{**}P < 0.01$, $^{***}P < 0.001$.

the sham group, MCAO mice exhibited significantly increased apoptotic cells in the GCL as assessed by TUNEL staining (**Figure 2C**). These results demonstrate that ischemic stroke induces a significant retinal injury in diabetic mice.

## ISO Pretreatment Reduced the Cerebral Damage and Retinal Injury Induced by an Ischemic Stroke in Diabetic Mice

To address whether ISO protects the brain and retinal injury after ischemic stroke in diabetes, 24 h before MCAO onset, we pretreated the diabetic mice with exposure to 2% ISO for 1 h. Mice were then subjected to MCAO, with the MCA occluded for 1 h, and 24 h post-reperfusion, mice were sacrificed (**Figure 3A**). We confirmed the distinct ischemic brain damage by TTC staining, a redox indicator that distinguishes between metabolically active and inactive tissue. Both diabetic MCAO mice with and without ISO pretreatment exhibited a significant brain ischemic infarct (**Figure 1C**). However, the infarct volume was significantly decreased in MCAO mice with ISO pretreatment when compared to the MCAO mice without ISO pretreatment (**Figure 1D**). These data demonstrate the neuroprotective effects of ISO pretreatment in diabetic mice after ischemic stroke.

In addition, the MCAO-induced reduction in GCL cell count and inner retinal thickness were attenuated by ISO pretreatment compared to diabetic MCAO mice pretreated without ISO (**Figure 3B**). Furthermore, MCAO mice with ISO pretreatment exhibited reduced apoptotic cells in the GCL compared to the MCAO mice without ISO pretreatment (**Figure 3C**). Our data thereby indicates that ISO pretreatment protects the retina against ischemic injury in diabetic stroke mice.

## ISO Pretreatment Inhibited NLRP3 Inflammasome Activation in Stroke-Induced Retinal Injury

Evidence suggests that cerebral and retinal ischemia share acute and chronic pathogenic mechanisms including NLRP3 inflammasome activation, which has been shown to be associated with injury severity (Hong et al., 2019; Wan et al., 2020). We therefore speculated that NLRP3 inflammasome activation may be associated with stroke-induced retinal injury in diabetes. First, we examined the mRNA expression of the NLRP3 inflammasome in the retina. As expected, the mRNA expression of NLRP3, caspase-1, and IL-1β showed more robust elevations in the retina of diabetic MCAO mice compared to sham-operated diabetic mice (**Figure 4A**). Next, we investigated the effects of ISO pretreatment and found reduced retinal NLRP3, caspase-1, and IL-1β mRNA expression in MCAO mice with ISO pretreatment compared to the MCAO group without ISO pretreatment (**Figure 4A**). NLRP3 inflammasome

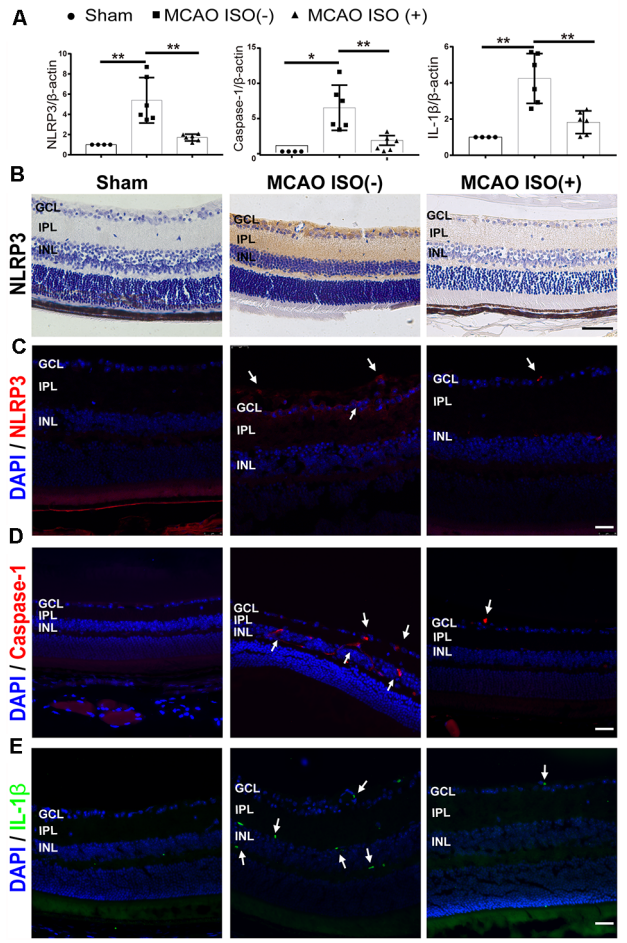


**FIGURE 4 |** ISO inhibits NLRP3 inflammasome activation in the retina after ischemic stroke in diabetic mice. **(A)** Relative gene expression of NLRP3, caspase-1, and IL-1β in the retina. β-Actin served as an endogenous reference gene ($n = 4$ in Sham group; $n = 6$ in MCAO ISO (–) group and MCAO ISO (+) group). **(B)** Representative immunohistochemical staining for the protein expression of NLRP3 in the retina (magnification, 400×; scale bar, 50 μm). **(C–E)** Representative immunofluorescence staining for the protein expression of NLRP3 **(C)**, Caspase-1 **(D)**, and IL-1β **(E)** in the retina. Arrow, NLRP3 (Red), Caspase-1 (Red), and IL-1β (Green) positive cells (magnification, 400×; scale bar, 25 μm). GCL, ganglion cell layer; IPL, inner plexiform layer; INL, inner nuclear layer. $^{*}P < 0.05$, $^{**}P < 0.01$.

protein expression also had a similar trend; compared to sham-operated mice, MCAO increased the NLRP3, caspase-1, and IL-1β protein expression in the retina, which was mitigated by ISO pretreatment (**Figures 4B–E**). Our results indicate that the suppression of NLRP3 inflammasome activation after ISO pretreatment plays an important role in protecting the retina from stroke–induced retinal injury in diabetic mice.

## DISCUSSION

In this study, we demonstrated that focal cerebral ischemia-induced retinal injury in diabetic mice and ISO pretreatment protected against brain damage and stroke-induced retinal injury. We first revealed that cerebral ischemia increased cell loss and induced apoptosis in the GCL in a diabetic mouse model. We next demonstrated that ISO pretreatment protected the brain indicated by reduced infarct volume and retinal injury as evidenced by preserved cell count and reduced apoptosis in the GCL in the MCAO mouse model. Finally, ISO pretreatment inhibited NLRP3 inflammasome activation in the retina after cerebral ischemia which may underlie its protective effects.

Visual impairment is a significant complication in stroke patients that may exacerbate other stroke-related impairments and impede rehabilitative efforts. The occipital lobe is the visual center and accordingly, posterior cerebral artery (PCA) occlusion-induced occipital infarction has been reported as the most common cause of visual impairment after stroke (Rowe et al., 2013). However, visual impairments have been reported in more than two-thirds of ischemic stroke patients with MCA occlusion (Sand et al., 2018). This suggests that ischemic stroke may induce retinal ischemia, thereby damaging the eyes and visual function directly, rather than impairing the visual center. The retinal blood supply is mainly from the central retinal artery, a branch of the ophthalmic artery (OPA), which is the first branch of the internal carotid artery in mice (Singh and Dass, 1960). Both OPA and MCA are the branches of the internal carotid artery. Due to the anatomical relationship between the OPA and MCA, the OPA is also prone to occlusion when MCA occlusion occurs. Approximately 25% of patients with ischemic stroke have complete occlusion of the OPA, leading to retinal ischemia and subsequent retinal damage (Helenius et al., 2012). Similar effects have been observed in rodent MCAO models, with the blood flow of the ipsilateral eye shown to be significantly reduced once the filament is inserted into the MCA (Steele et al., 2008; Nguyen et al., 2019; Lee et al., 2020). Furthermore, decreased blood flow leads to retinal ischemia with the severity of injury proportional to the cerebral ischemic area (Allen et al., 2014). In order to prevent as well as treat visual impairments after stroke, the underlying mechanism of stroke-induced retinal injury needs to be further investigated. A recent study has shown that mitochondrial dysfunction may be an important cause of stroke-induced retinal injury, and stem cell treatment may be a potential therapy (Nguyen et al., 2019). The present study aimed to identify conserved pathogenic mechanisms between stroke, retinal injury and associated risk factors, such as diabetes.

Diabetes is a prevalent disease and confers a greater risk of stroke and retinopathy occurrence. The risk of ischemic stroke with diabetes is 2.3-fold higher in comparison to non-diabetic patients (Liu et al., 2016; Bragg et al., 2017). Furthermore, diabetic retinopathy is a common complication of diabetes and the leading cause of blindness (Gross et al., 2018). In the diabetic population, approximately one-third have signs of diabetic retinopathy, and a third of these patients have more severe vision-threatening retinopathy (Saaddine et al., 2008). Complex pathophysiological mechanisms including increased production of free radicals, advanced glycosylation end-products, pro-inflammatory signaling, and vascular endothelial growth factor, trigger retinal injury in diabetic status. Diabetic retinopathy-induced

microvascular lesions can also cause retinal ischemic damage and contribute to visual impairments (Wong et al., 2016). Therefore, not only is the individual more susceptible to stroke, but the retina may also be more susceptible to stroke-induced retinal injury under diabetic status. Accordingly, in the present study, H&E and TUNEL staining revealed a remarkable retinal injury in the diabetic stroke-induced mouse model.

Cerebral blood flow is often temporarily blocked or reduced in surgical operations, such as cardiac and carotid artery extirpation surgeries, thereby inducing a temporary man-made cerebral ischemic event (Apostolakis and Akinosoglou, 2008). In such cases, it is crucial to use appropriate anesthetic drugs to induce clinical anesthesia and prevent the development of cerebral ischemic injury. The common and widely used clinical anesthetic drug, ISO, has been shown to have a dose-dependent protective effect on the incidence and severity of postoperative ischemic stroke (Raub et al., 2021). ISO preconditioning has furthermore been demonstrated to have significant neuroprotective potency in ischemic stroke in experimental studies. ISO preconditioning alleviated neurological deficits, reduced infarction volume, and attenuated apoptosis in rodent MCAO models *via* inhibiting neuroinflammation (Sun et al., 2015b), attenuating ubiquitin-conjugated protein aggregation (Zhang et al., 2010), and increasing lymphoma-2 expression (Li et al., 2008). Our results correspond well with the previous study, ISO pretreatment shows neuroprotective effects and reduced the infarct volume after ischemic stroke in diabetic mice. *In vitro*, ISO preconditioning provided neuroprotection by regulating the toll-like receptor 4 signaling pathway and inhibiting microglia activation in oxygen and glucose deprivation models (Xiang et al., 2014; Sun et al., 2015a,b). In our study, we provide evidence for the first time that ISO pretreatment exerts protection against retinal injury, specifically inhibiting ischemic-stroke induced retinal injury in diabetic mice.

The robust inflammatory response is an important contributor to the progression of cerebral ischemia, retinal ischemia, and diabetic retinopathy (Anrather and Iadecola, 2016; Capitao and Soares, 2016; Mathew et al., 2019; Yang et al., 2020). The NLRP3 inflammasome, a multimeric protein complex and critical component of the inflammatory response, has been linked to the pathogenesis of all three conditions (Hong et al., 2018; Raman and Matsubara, 2020; Yu et al., 2020). Upon recruitment to the inflammasome, caspase-1 is activated, leading to the release of proinflammatory IL-1β and IL-18, and triggering an infiltration of immune cells and intrinsic cell death mechanisms (Yu et al., 2020). The Nod-like receptor (NLR) signals pathway and NLRP3 inflammasome activation have been proven to play a predominant role in ischemic/reperfusion- induced retinal inflammation by RNA microarray profiling (Wan et al., 2020). Of note, previous studies have shown that inhibiting NLRP3 inflammasome activation is an effective means to alleviate the damage associated with ischemic stroke and retinal ischemia (Hong et al., 2018; Gong et al., 2019). Furthermore, ISO has been demonstrated to inhibit the activation of NLRP3 inflammasomes in acute lung injury (Yin et al., 2016). Our data shows that ISO pretreatment can downregulate NLRP3, caspase-1, and IL-1β mRNA and protein levels in the retina after ischemic stroke, suggesting that the protective mechanisms underlying ISO pretreatment may be related to the direct inhibition of retinal NLRP3 inflammasome activation.

In summary, our study provides important evidence attesting to the close associations between diabetes, stroke, and visual impairments, as well as retinal injury and cerebral ischemia. Our results furthermore suggest that ISO pretreatment can reduce ischemic stroke-induced retinal injury under diabetic conditions by inhibiting NLRP3 inflammasome activation. ISO may represent an important and clinically relevant agent to be used in patients who require general anesthesia and are vulnerable to postoperative ischemic stroke.

## DATA AVAILABILITY STATEMENT

The original contributions presented in the study are included in the article, further inquiries can be directed to the corresponding author/s.

## ETHICS STATEMENT

The animal study was reviewed and approved by Zhujiang Hospital Animal Experimental Center of Southern Medical University.

## AUTHOR CONTRIBUTIONS

F-XL and H-FZ contributed to the study plan and design. H-BL, Y-HL, J-YZ, and W-JG conducted the experiments. AO, Z-JY, Z-PF, and H-SS participated in experimental design and manuscript preparation. F-XL and H-FZ critically revised the work. All authors contributed to the article and approved the submitted version.

## FUNDING

This work was supported by the National Natural Science Foundation of China (82070526, 81771232 to H-FZ and 81974192 to F-XL); the Natural Science Foundation of Guangdong Province, China (2021A1515011652, 2019A1515010654 to H-FZ).

## REFERENCES

Allen, R. S., Sayeed, I., Cale, H. A., Morrison, K. C., Boatright, J. H., Pardue, M. T., et al. (2014). Severity of middle cerebral artery occlusion determines retinal deficits in rats. *Exp. Neurol.* 254, 206–215. doi: 10.1016/j.expneurol.2014.02.005

Anrather, J., and Iadecola, C. (2016). Inflammation and stroke: an overview. *Neurotherapeutics* 13, 661–670. doi: 10.1007/s13311-016-0483-x

Apostolakis, E., and Akinosoglou, K. (2008). The methodologies of hypothermic circulatory arrest and of antegrade and retrograde cerebral perfusion for aortic arch surgery. *Ann. Thorac. Cardiovasc. Surg.* 14, 138–148.

Bragg, F., Holmes, M. V., Iona, A., Guo, Y., Du, H., Chen, Y., et al. (2017). Association between diabetes and cause-specific mortality in rural and urban areas of china. *JAMA* 317, 280–289. doi: 10.1001/jama.2016.19720

Capitao, M., and Soares, R. (2016). Angiogenesis and inflammation crosstalk in diabetic retinopathy. *J. Cell. Biochem.* 117, 2443–2453. doi: 10.1002/jcb.25575

Deng, Q., Geng, Y., Zhao, L., Li, R., Zhang, Z., Li, K., et al. (2019). NLRP3 inflammasomes in macrophages drive colorectal cancer metastasis to the liver. *Cancer Lett.* 442, 21–30. doi: 10.1016/j.canlet.2018.10.030

Deng, Y. M., Chen, D. D., Wang, L. Y., Gao, F., Sun, X., Liu, L., et al. (2018). Visual field impairment predicts recurrent stroke after acute posterior circulation stroke and transient ischemic attack. *CNS Neurosci. Ther.* 24, 154–161. doi: 10.1111/cns.12787

Ergul, A., Abdelsaid, M., Fouda, A. Y., and Fagan, S. C. (2014). Cerebral neovascularization in diabetes: implications for stroke recovery and beyond. *J. Cereb. Blood Flow Metab.* 34, 553–563. doi: 10.1038/jcbfm.2014.18

Forrester, J. V., Kuffova, L., and Delibegovic, M. (2020). The role of inflammation in diabetic retinopathy. *Front. Immunol.* 11:583687. doi: 10.3389/fimmu.2020.583687

Gong, Y., Cao, X., Gong, L., and Li, W. (2019). Sulforaphane alleviates retinal ganglion cell death and inflammation by suppressing NLRP3 inflammasome activation in a rat model of retinal ischemia/reperfusion injury. *Int. J. Immunopathol. Pharmacol.* 33:2058738419861777. doi: 10.1177/2058738419861777

Gross, J. G., Glassman, A. R., Liu, D., Sun, J. K., Antoszyk, A. N., Baker, C. W., et al. (2018). Five-year outcomes of panretinal photocoagulation vs. intravitreous ranibizumab for proliferative diabetic retinopathy: a randomized clinical trial. *JAMA Ophthalmol.* 136, 1138–1148. doi: 10.1001/jamaophthalmol.2018.3255

Guo, X., Deng, J., Zheng, B., Liu, H., Zhang, Y., Ying, Y., et al. (2020). HDAC1 and HDAC2 regulate anti-inflammatory effects of anesthetic isoflurane in human monocytes. *Immunol. Cell. Biol.* 98, 318–331. doi: 10.1111/imcb.12318

Helenius, J., Arsava, E. M., Goldstein, J. N., Cestari, D. M., Buonanno, F. S., Rosen, B. R., et al. (2012). Concurrent acute brain infarcts in patients with monocular visual loss. *Ann. Neurol.* 72, 286–293. doi: 10.1002/ana.23597

Hendrick, A. M., Gibson, M. V., and Kulshreshtha, A. (2015). Diabetic retinopathy. *Prim Care* 42, 451–464. doi: 10.1016/j.pop.2015.05.005

Hong, P., Gu, R. N., Li, F. X., Xiong, X. X., Liang, W. B., You, Z. J., et al. (2019). NLRP3 inflammasome as a potential treatment in ischemic stroke concomitant with diabetes. *J. Neuroinflammation* 16:121. doi: 10.1186/s12974-019-1498-0

Hong, P., Li, F. X., Gu, R. N., Fang, Y. Y., Lai, L. Y., Wang, Y. W., et al. (2018). Inhibition of NLRP3 inflammasome ameliorates cerebral ischemia-reperfusion injury in diabetic mice. *Neural Plast.* 2018:9163521. doi: 10.1155/2018/9163521

Jiang, M., Sun, L., Feng, D. X., Yu, Z. Q., Gao, R., Sun, Y. Z., et al. (2017). Neuroprotection provided by isoflurane pre-conditioning and post-conditioning. *Med. Gas Res.* 7, 48–55. doi: 10.4103/2045-9912.202910

Lee, J. Y., Castelli, V., Bonsack, B., Garcia-Sanchez, J., Kingsbury, C., Nguyen, H., et al. (2020). Eyeballing stroke: blood flow alterations in the eye and visual impairments following transient middle cerebral artery occlusion in adult rats. *Cell Transplant* 29:963689720905805. doi: 10.1177/0963689720905805

Li, L., Peng, L., and Zuo, Z. (2008). Isoflurane preconditioning increases B-cell lymphoma-2 expression and reduces cytochrome c release from the mitochondria in the ischemic penumbra of rat brain. *Eur. J. Pharmacol.* 586, 106–113. doi: 10.1016/j.ejphar.2008.02.073

Lin, H. B., Wei, G. S., Li, F. X., Guo, W. J., Hong, P., Weng, Y. Q., et al. (2020). Macrophage-NLRP3 inflammasome activation exacerbates cardiac dysfunction after ischemic stroke in a mouse model of diabetes. *Neurosci. Bull.* 36, 1035–1045. doi: 10.1007/s12264-020-00544-0

Liu, J., Yeung, P. K., Cheng, L., Lo, A. C., Chung, S. S., and Chung, S. K. (2015). Epac2-deficiency leads to more severe retinal swelling, glial reactivity and oxidative stress in transient middle cerebral artery occlusion induced ischemic retinopathy. *Sci. China Life Sci.* 58, 521–530. doi: 10.1007/s11427-015-4860-1

Liu, R., Wang, H., Xu, B., Chen, W., Turlova, E., Dong, N., et al. (2016). Cerebrovascular safety of sulfonylureas: the role of KATP channels in neuroprotection and the risk of stroke in patients with type 2 diabetes. *Diabetes* 65, 2795–2809. doi: 10.2337/db15-1737

Mathew, B., Ravindran, S., Liu, X., Torres, L., Chennakesavalu, M., Huang, C. C., et al. (2019). Mesenchymal stem cell-derived extracellular vesicles and retinal ischemia-reperfusion. *Biomaterials* 197, 146–160. doi: 10.1016/j.biomaterials.2019.01.016

Nguyen, H., Lee, J. Y., Sanberg, P. R., Napoli, E., and Borlongan, C. V. (2019). Eye opener in stroke. *Stroke* 50, 2197–2206. doi: 10.1161/STROKEAHA.119.025249

Raman, K. S., and Matsubara, J. A. (2020). Dysregulation of the NLRP3 inflammasome in diabetic retinopathy and potential therapeutic targets. *Ocul. Immunol. Inflamm.* 1–9. doi: 10.1080/09273948.2020.1811350

Raub, D., Platzbecker, K., Grabitz, S. D., Xu, X., Wongtangman, K., Pham, S. B., et al. (2021). Effects of volatile anesthetics on postoperative ischemic stroke incidence. *J. Am. Heart Assoc.* 10:e018952. doi: 10.1161/JAHA.120.018952

Rivera, J. C., Dabouz, R., Noueihed, B., Omri, S., Tahiri, H., and Chemtob, S. (2017). Ischemic retinopathies: oxidative stress and inflammation. *Oxid. Med. Cell. Longev.* 2017:3940241. doi: 10.1155/2017/3940241

Rowe, F. J. (2017). Stroke survivors' views and experiences on impact of visual impairment. *Brain Behav.* 7:e00778. doi: 10.1002/brb3.778

Rowe, F. J., Wright, D., Brand, D., Jackson, C., Harrison, S., Maan, T., et al. (2013). A prospective profile of visual field loss following stroke: prevalence, type, rehabilitation and outcome. *Biomed. Res. Int.* 2013:719096. doi: 10.1155/2013/719096

Saaddine, J. B., Honeycutt, A. A., Narayan, K. M., Zhang, X., Klein, R., and Boyle, J. P. (2008). Projection of diabetic retinopathy and other major eye diseases among people with diabetes mellitus: united states, 2005–2050. *Arch. Ophthalmol.* 126, 1740–1747. doi: 10.1001/archopht.126.12.1740

Sand, K. M., Midelfart, A., Thomassen, L., Melms, A., Wilhelm, H., and Hoff, J. M. (2013). Visual impairment in stroke patients—a review. *Acta Neurol. Scand. Suppl.* 127, 52–56. doi: 10.1111/ane.12050

Sand, K. M., Naess, H., Thomassen, L., and Hoff, J. M. (2018). Visual field defect after ischemic stroke-impact on mortality. *Acta Neurol. Scand.* 137, 293–298. doi: 10.1111/ane.12870

Singh, S., and Dass, R. (1960). The central artery of the retina. I. Origin and course. *Br. J. Ophthalmol.* 44, 193–212. doi: 10.1136/bjo.44.4.193

Steele, E. C. Jr., Guo, Q., and Namura, S. (2008). Filamentous middle cerebral artery occlusion causes ischemic damage to the retina in mice. *Stroke* 39, 2099–2104. doi: 10.1161/STROKEAHA.107.504357

Sun, H. S., Xu, B., Chen, W., Xiao, A., Turlova, E., Alibraham, A., et al. (2015a). Neuronal K(ATP) channels mediate hypoxic preconditioning and reduce subsequent neonatal hypoxic-ischemic brain injury. *Exp. Neurol.* 263, 161–171. doi: 10.1016/j.expneurol.2014.10.003

Sun, M., Deng, B., Zhao, X., Gao, C., Yang, L., Zhao, H., et al. (2015b). Isoflurane preconditioning provides neuroprotection against stroke by regulating the expression of the TLR4 signalling pathway to alleviate microglial activation. *Sci. Rep.* 5:11445. doi: 10.1038/srep11445

Wan, P., Su, W., Zhang, Y., Li, Z., Deng, C., Li, J., et al. (2020). LncRNA H19 initiates microglial pyroptosis and neuronal death in retinal ischemia/reperfusion injury. *Cell Death Differ.* 27, 176–191. doi: 10.1038/s41418-019-0351-4

Wang, W., Jiang, B., Sun, H., Ru, X., Sun, D., Wang, L., et al. (2017). Prevalence, incidence and mortality of stroke in china: results from a nationwide population-based survey of 480 687 adults. *Circulation* 135, 759–771. doi: 10.1161/CIRCULATIONAHA.116.025250

Wong, T. Y., Cheung, C. M. G., Larsen, M., Sharma, S., and Simo, R. (2016). Diabetic retinopathy. *Nat. Rev. Dis. Primers* 2:16012. doi: 10.1016/S0140-6736(09)62124-3

Xiang, H. F., Cao, D. H., Yang, Y. Q., Wang, H. Q., Zhu, L. J., Ruan, B. H., et al. (2014). Isoflurane protects against injury caused by deprivation of oxygen and glucose in microglia through regulation of the toll-like receptor 4 pathway. *J. Mol. Neurosci.* 54, 664–670. doi: 10.1007/s12031-014-0373-9

Yang, L., Mao, K., Yu, H., and Chen, J. (2020). Neuroinflammatory responses and Parkinson' disease: pathogenic mechanisms and therapeutic targets. *J. Neuroimmune Pharmacol.* 15, 830–837. doi: 10.1007/s11481-020-09926-7

Yin, N., Peng, Z., Li, B., Xia, J., Wang, Z., Yuan, J., et al. (2016). Isoflurane attenuates lipopolysaccharide-induced acute lung injury by

inhibiting ROS-mediated NLRP3 inflammasome activation. *Am. J. Transl. Res.* 8, 2033–2046.

Yu, Z. W., Zhang, J., Li, X., Wang, Y., Fu, Y. H., and Gao, X. Y. (2020). A new research hot spot: the role of NLRP3 inflammasome activation, a key step in pyroptosis, in diabetes and diabetic complications. *Life Sci.* 240:117138. doi: 10.1016/j.lfs.2019.117138

Zhang, H., Xiong, X., Liu, J., Gu, L., Li, F., Wan, Y., et al. (2016). Emulsified isoflurane protects against transient focal cerebral ischemia injury in rats *via* the PI3K/Akt signaling pathway. *Anesth. Analg.* 122, 1377–1384. doi: 10.1213/ANE.0000000000001172

Zhang, H. P., Yuan, L. B., Zhao, R. N., Tong, L., Ma, R., Dong, H. L., et al. (2010). Isoflurane preconditioning induces neuroprotection by attenuating ubiquitin-conjugated protein aggregation in a mouse model of transient global cerebral ischemia. *Anesth. Analg.* 111, 506–514. doi: 10.1213/ANE.0b013e3181e45519

Zhou, R., Yazdi, A. S., Menu, P., Tschopp, J., Gao, L., Dong, Q., et al. (2010a). A role for mitochondria in NLRP3 inflammasome activation NLRP3 inflammasome: a promising target in ischemic stroke. *Nature* 469, 221–225. doi: 10.1038/nature09663

Zhou, Y., Lekic, T., Fathali, N., Ostrowski, R. P., Martin, R. D., Tang, J., et al. (2010b). Isoflurane posttreatment reduces neonatal hypoxic-ischemic brain injury in rats by the sphingosine-1-phosphate/phosphatidylinositol-3-kinase/Akt pathway. *Stroke* 41, 1521–1527. doi: 10.1161/STROKEAHA.110.583757

**Conflict of Interest**: The authors declare that the research was conducted in the absence of any commercial or financial relationships that could be construed as a potential conflict of interest.

frontiers in Cellular Neuroscience

ORIGINAL RESEARCH
published: 20 August 2021
doi: 10.3389/fncel.2021.731855

# Photobiomodulation Promotes Hippocampal CA1 NSC Differentiation Toward Neurons and Facilitates Cognitive Function Recovery Involving NLRP3 Inflammasome Mitigation Following Global Cerebral Ischemia

*Sihan Guo[1], Ruimin Wang[2]*, Jiewei Hu[2], Liping Sun[1], Xinru Zhao[1], Yufeng Zhao[1], Dong Han[1] and Shuqun Hu[1]**

[1] School of Life Sciences, Jiangsu Provincial Institute of Health Emergency, Xuzhou Medical University, Xuzhou, China, [2] Neurobiology Institute, School of Public Health, North China University of Science and Technology, Tangshan, China

OPEN ACCESS

**Edited by:**
Xinchun Jin,
Capital Medical University, China

**Reviewed by:**
Yong Li,
Shanghai Jiao Tong University, China
Luodan Yang,
Augusta University, United States

***Correspondence:**
Ruimin Wang
ruimin-wang@163.com
Shuqun Hu
hushuqun88@xzhmu.edu.cn

**Specialty section:**
This article was submitted to Cellular Neuropathology, a section of the journal Frontiers in Cellular Neuroscience

**Received:** 28 June 2021
**Accepted:** 27 July 2021
**Published:** 20 August 2021

**Citation:**
Guo S, Wang R, Hu J, Sun L, Zhao X, Zhao Y, Han D and Hu S (2021) Photobiomodulation Promotes Hippocampal CA1 NSC Differentiation Toward Neurons and Facilitates Cognitive Function Recovery Involving NLRP3 Inflammasome Mitigation Following Global Cerebral Ischemia. Front. Cell. Neurosci. 15:731855. doi: 10.3389/fncel.2021.731855

Our recent study revealed that photobiomodulation (PBM) inhibits delayed neuronal death by preserving mitochondrial dynamics and function following global cerebral ischemia (GCI). In the current study, we clarified whether PBM exerts effective roles in endogenous neurogenesis and long-lasting neurological recovery after GCI. Adult male rats were treated with 808 nm PBM at 20 mW/cm$^2$ irradiance for 2 min on cerebral cortex surface (irradiance ∼7.0 mW/cm$^2$, fluence ∼0.8 J/cm$^2$ on the hippocampus) beginning 3 days after GCI for five consecutive days. Cognitive function was evaluated using the Morris water maze. Neural stem cell (NSC) proliferation, immature neurons, and mature neurons were examined using bromodeoxyuridine (BrdU)-, doublecortin (DCX)-, and NeuN-staining, respectively. Protein expression, such as NLRP3, cleaved IL1β, GFAP, and Iba1 was detected using immunofluorescence staining, and ultrastructure of astrocyte and microglia was observed by transmission electron microscopy. The results revealed that PBM exerted a markedly neuroprotective role and improved spatial learning and memory ability at 58 days of ischemia/reperfusion (I/R) but not at 7 days of reperfusion. Mechanistic studies revealed that PBM suppressed reactive astrocytes and maintained astrocyte regeneration at 7 days of reperfusion, as well as elevated neurogenesis at 58 days of reperfusion, as evidenced by a significant decrease in the fluorescence intensity of GFAP (astrocyte marker) but unchanged the number of BrdU-GFAP colabeled cells at the early timepoint, and a robust elevation in the number of DCX-NeuN colabeled cells at the later timepoint in the PBM-treated group compared to the GCI group. Notably, PBM treatment protected the ultrastructure of astrocyte and microglia cells at 58 days but not 7 days of reperfusion in the hippocampal CA1 region. Furthermore, PBM treatment significantly attenuated the GCI-induced immunofluorescence intensity of NLRP3 (an inflammasome component),

cleaved IL1β (reflecting inflammasome activation) and Iba1, as well as the colocalization of NLRP3/GFAP or cleaved IL-1β/GFAP, especially in animals subjected to I/R at 58 days. Taken together, PBM treatment performed postischemia exerted a long-lasting protective effect on astrocytes and promoted endogenous neurogenesis in the hippocampal CA1 region, which might contribute to neurological recovery after GCI.

**Keywords: cognitive function, NLRP3 inflammasome, photobiomodulation, neurogenesis, global cerebral ischemia**

## INTRODUCTION

Pyramidal neuronal damage and subsequent cognitive defects are the major causes of disability in cardiac arrest patients (Moulaert et al., 2009). Global cerebral ischemia (GCI) induced by four-vessel occlusion perfectly mimics cardiac arrest, resulting in hippocampal CA1 neuronal death and delayed neurological deficits (Pulsinelli et al., 1982). Therefore, GCI animal models in rats or mice are widely used to determine molecular mechanisms and explore effective strategies. Unfortunately, except for therapeutic hypothermia, there are not yet effective therapies for preserving cognitive function after GCI. A recent meta-analysis failed to find a strong benefit of therapeutic hypothermia on survival or neurological outcome (Harukuni and Bhardwaj, 2006; Nielsen et al., 2011; Lindsay et al., 2018). Therefore, new therapeutic strategies for protecting the brain and promoting neurological recovery after cardiac arrest are urgently needed.

To our knowledge, brain injuries due to brain trauma, ischemic stroke, and transient GCI can induce prodeath signaling pathways due to oxidative stress, $Ca^{2+}$ overload, excitotoxicity, and neuroinflammation, leading to delayed neuronal death and neurological dysfunction. Meanwhile, these brain injuries also induce inherent prosurvival reactions for self-defense and self-repair. For example, brain injury increases NSC/neural progenitor cell (NPC) proliferation followed by production of new neurons in an attempt to replenish lost or damaged cells (Marques et al., 2019). Using a mouse model of nest-green fluorescent protein reporter, a previous study revealed that endogenous NSC proliferation was increased by 120% 2 days after a traumatic brain injury (Hong et al., 2016). In an ischemic stroke model, endogenous NSC proliferation in the ischemic cortex peaks on day 2 and returns to basal levels within 6 days after stroke (Luo et al., 2009). Furthermore, in the subventricular zone (SVZ), a well-known NSC niche, the number of bromodeoxyuridine (BrdU)-labeled cells is robustly increased as early as 2 days, sustained through 4 days, and then returning to basal levels (Luo et al., 2009). A succession of studies by Tonchev's group demonstrated that global cerebral ischemia in monkeys increases progenitor proliferation in the SVZ, subgranular zone (SGZ) of the dentate gyrus (DG), and even in the temporal neocortex at early postischemic time points during the first 15 days after ischemia (Tonchev et al., 2003a,b). Notably, newborn neurons are observed after ischemia in the hippocampal CA1 sector, the region most sensitive to ischemia (Rietze et al., 2000; Nakatomi et al., 2002), which is closely related to cognitive function. Unfortunately, several studies have revealed that almost all newborn hippocampal neurons die within days or weeks after induction of these processes (Tonchev and Yamashima, 2006; Jablonska and Lukomska, 2011; McAllister et al., 2020). Additionally, there is increasing evidence that chronic neurodegenerative diseases, such as Alzheimer's disease (AD) and Parkinson's disease (PD), cause significant decreases in inherent NSC proliferation and neurogenesis (Radad et al., 2017; Babcock et al., 2021). Therefore, targeting the survival of endogenous NSCs may extend the treatment window and have long-lasting beneficial effects for restoring neurobiological outcomes after brain injuries. Indeed, a recent review listed many endogenous neurogenesis-enhancing drugs, such as the P53 inhibitor pifithrin-α (PFT-α), trophic factors, and dietary supplementation, that can increase endogenous NSC proliferation, attenuate secondary cell death, and improve neurobiological functions after ischemic stroke and trauma brain injury (TBI) (Wu et al., 2017).

Recently, photobiomodulation (PBM), initially referred to as "low-level laser/light therapy (LLLT), has been attracting increasing interest in central nervous system disorders. Emerging evidence from our group and others demonstrated that PBM is promising for its many benefits, such as antioxidative, antiapoptotic, anti-inflammatory, and proneurogenic effects, mediating blood flow and the intracellular calcium response to brain injuries (Tucker et al., 2018; Wang et al., 2019; Bathini et al., 2020; Ravera et al., 2021). More importantly, PBM can activate signaling pathways and transcription factors that cause changes in protein expression, exerting long-lasting beneficial effects (Ando et al., 2011; de Freitas and Hamblin, 2016). In an ischemic stroke model, PBM is a promising treatment for inhibiting inflammasome activity (Lee et al., 2017), attenuating levels of the proinflammatory factors IL-1β and TNFα, and exerting long-lasting neuroprotective roles (Vogel et al., 2021). In traumatic brain injury animal model, transcranial low-level laser therapy not only enhances learning, memory, and neuroprogenitor cells in DG and SVZ regions of mice, but also increases brain derived neurotrophic factor (BDNF) and synaptogenesis (Xuan et al., 2014, 2015). Overall, regardless of whether the brain suffers from acute damage (stroke, traumatic brain injury, and global cerebral ischemia) or degenerative disease (dementia, Alzheimer's disease, and Parkinson's disease), all of these seemingly diverse conditions can be beneficially affected by applying low-level light intervention with the advantages of greater safety, lower cost, and better suitability for home use. Due to the growing interest in PBM use in the brain, we herein established a global cerebral ischemia model in adult male rats and, for the first time, investigated the roles and mechanisms of PBM treatment

performed postischemia on NSC proliferation, neurogenesis and functional recovery.

## MATERIALS AND METHODS

### Antibodies and Animals

The following primary antibodies were used, including NeuN (Millipore Biotechnology, MAB377, RRID: AB_2298772), BrdU (GeneTex, GTX28039, RRID: AB_385364), DCX (SCBT, sc271390, RRID: AB_10610966), GFAP (Abcam, ab53554, RRID: AB_880202), GFAP (SCBT, sc-33673, RRID: AB_627673), NLRP3 (Abcam, ab4207, RRID: AB_955792), cleaved IL1β (CST, #83186, RRID: AB_2800010), and Iba1 (Abcam, ab5076, RRID: AB_2224402).

All procedures performed in this study were approved by the Institutional Animal Care and Xu Zhou Medical University (Assurance No. 201505w001) and were conducted in accordance with the guidelines of the National Natural Science Foundation of China for animal research. Adult male Sprague-Dawley rats (3–4 months old) were housed in a temperature-controlled (22–24°C) room with freely available water and food, and ZT (zeitgeber time) was set on a 14/10 h cycle (ZT0-8:00, ZT12-22:00). The animal models including GCI model and PBM-treatment were performed in the morning in the animal model preparation room. Behavioral tests were carried out between 6:00–9:00 pm in the soundproof room of neurobehavioral laboratory. Experimental animals were sacrificed and all tissue samples were obtained in the morning.

### GCI and PBM Treatment

All surgeries were performed under isoflurane anesthesia (2–4%), and a dose of sustained release buprenorphine (Bup-SR) (0.3–1.2 mg/kg) was subcutaneously administered every 48–72 h to minimize postoperative pain. Rats were randomly assigned to the following groups: sham operation (Sham), ischemia reperfusion (I/R), photobiomodulation (PBM) treatment (I/R + PBM), and Sham with PBM treatment (Sham + PBM). The I/R group was further divided into I/R 3, 7, 28, and 58 days groups. Animals that exhibited no behavioral defects were used in this study. In order to reduce bias in the study, a double-blind procedure was carried out in which the experiments were performed by blinding investigators and statistical analysis was blindly worked out by the authors.

The global cerebral ischemia (GCI) animal model was induced by four-vessel occlusion as described in our previous study (Bai et al., 2020). In brief, rats were fixed on the stereotaxic instrument, and vertebral arteries were permanently occluded by electrocautery. Then, the bilateral common carotid arteries (CAAs) were exposed, and the incision was sutured. One day later, the bilateral common carotid arteries of the rats were re-exposed and clipped with an aneurysm for 12 min. Rats with an absence of the correctional reflex within 30 s that were unresponsive to light, resulting in dilated pupils during ischemia, were identified as successfully modeled. Rectal temperature was maintained at approximately 36.5–37.5°C during the procedure using an incubator. For sham-operated animals, all rats were treated exactly as for ischemic animals except that the CCA was not clamped. A total of 95 rats were utilized in this study. From all 95 animals, 8 rats died in ischemia reperfusion, and 11 rats were eliminated from further experiment due to not meeting the established criteria for evidence of successful GCI. The animal numbers for each experimental paradigm were indicated in the figure legends.

For PBM treatment, a diode laser (808 nm, model 808M100, Dragon Lasers) was used in the study, performed as our previously described (Wang et al., 2019). Briefly, laser penetration through tissues was measured with isolated rat samples of skin, skull, and brain tissues (cortex and hippocampus). A sample holder was made from black Plexiglas$^R$ with an 8 mm hole in its center. To evaluate the influence of the power in the penetration of light through different tissue samples, the laser source was located 15 cm away from the sample and two photodetectors let the simultaneous measurement of light power transmitted through the different tissues we placed on the holder, and a portion of the incident light. We measured the power without any sample between the light source and the detector (laser in mW/cm$^2$ across of air), and then detected the percentage of transmitted light when samples were placed on the system (laser in mW/cm$^2$ across of tissue). Based on the preliminary experiment of light penetration on cerebral tissues, we selected the laser power output at the tip of the fiberoptic probe (in contact with shaved skin) delivered a power density of 20 mW/cm$^2$ to the cerebral cortical surface. The laser irradiation was delivered for 2 min at this power density (20 mW/cm$^2$) so that the fluence at the cortical surface was 2.4 J/cm$^2$ and at the hippocampus was ∼0.8 J/cm$^2$. The dose of laser power (fluence) was calculated by total irradiated time (second) × power output (mW/cm$^2$)/1,000 and expressed as J/cm$^2$. A laser power meter (#FM33-056, Coherent Inc., United States) was applied to monitor the power output density.

Followed by slightly anesthetization using isoflurane, the rats were fixed in transparent bags, the laser beam transcranially focused on ∼8 mm diameter spot covering the shaved scalp (centered at 3 mm posterior to the eye and 2 mm anterior to the ear). The PBM treatment was begun at 3 days of reperfusion after GCI for 2 min, once daily for 5 consecutive days. Sham-operated controls underwent the same procedure as the laser-treated group but did not receive actual laser treatment.

### 5-Bromo-2′-Deoxyuridine (BrdU) Injection

BrdU (CAS# 19-160, Sigma-Aldrich) was diluted in 0.1 M PBS to make a sterile solution of 10 mg/mL. The rats received intraperitoneally BrdU injections (50 mg/kg body weight) twice daily over 7 consecutive days, starting reperfusion 1 day after GCI, and were, respectively, killed at I/R 7 days (2 h after the last BrdU injection), and I/R 58 days after GCI.

### Morris Water Maze (MWM) Test

The Morris water maze test was performed on days 7–9, and 56–58 as previously described (Wang et al., 2019). In brief, a circular pool filled with water (1.2 m in diameter, 35 cm in height)

containing a platform concealed below the surface (2.0 cm) was used. The pool was equally divided into four quadrants. During the adaptive training procedure, rats were randomly placed in one of the quadrants facing the wall of the pool and allowed to swim for a maximum time of 90 s until they discovered the fixed platform. If the rat was unable to find the platform within 90 s, it was gently guided to the platform and allowed to rest on the platform for 20 s. The test was repeated four times a day starting from different quadrants with a 2 min intertrial interval for 3 consecutive days. Six hours after the final experiment, the hidden platform was removed, and rats were placed in the pool in the same quadrant and allowed to explore for 60 s. The time spent in the quadrant that previously contained the platform was measured to evaluate the level of spatial reference memory for the given task. All behavioral tracks from the trials were recorded and analyzed using video tracking software, and the resultant data were statistically analyzed as described below.

## Immunofluorescence Staining and Confocal Microscopy

Immunofluorescence (IF) staining was performed as previously described (Bai et al., 2020). In brief, cardiac perfusion was performed in rats using 0.9% saline solution. The brains were rapidly isolated on an ice plate and subsequently fixed in 4% paraformaldehyde overnight at 4°C. The brain tissues were completely dehydrated with 30% sucrose, and make in continuous coronal frozen sections (25 μm) in the coronal plane of the dorsal hippocampus level at 2.5–4.5 mm posterior from bregma (∼100 sections per brain). To prevent double counting of cells, every fifth section was collected and used for staining. After washing in 0.1 M phosphate-buffered saline (PBS) for 30 min, sections were permeabilized with 0.4% Triton X-100-PBS for 2 h and incubated with 10% normal donkey serum for 1 h at room temperature before being incubated overnight at 4°C with primary antibodies. The following primary antibodies were used in the current study: NeuN (1:300), NLRP3 (1:200), cleaved IL-1β (1:500), and Iba1 (1:1,000). For double IF staining of BrdU with GFAP, a set of sections containing every sixth slice were denatured with 1 N HCl in a 37°C water bath for 20 min. Sections were then washed with 0.1% Triton X-100-PBS three times and blocked in 10% normal donkey serum at room temperature for 1 h. Sections were then incubated with anti-BrdU antibody (1:500) and GFAP (1:1000) overnight at 4°C. After washing, the sections were incubated with Highly Cross-Adsorbed Alexa Fluro IgG second antibodies (Thermo Fisher Scientific) for 1 h at room temperature. In detail, donkey anti-mouse 488 nm (A-21202, RRID: AB_141607, Excitation 488 nm and Emission 525 nm) was for NeuN or BrdU staining; donkey anti-goat 488 nm (A32814, RRID: AB_2762838) was for Iba1 staining; donkey anti-mouse 488 nm (A-21202, RRID: AB_141607) and donkey anti-goat 594 nm (A-11058, RRID: AB_2534105, Excitation 566 nm and Emission 610 nm) were for BrdU and GFAP double staining; donkey anti-goat 488 nm (A32814, RRID: AB_2762838) and donkey anti-mouse 594 nm (A-21203, RRID: AB_141633) were for DCX and NeuN double staining; donkey anti-mouse 488 nm (A-21202, RRID: AB_141607) and donkey anti-goat 594 nm (A-11058, RRID: AB_2534105) were for GFAP and NLRP3 double staining; donkey anti-rabbit 488 nm (A-21206, RRID: AB_2535792) and donkey anti-goat 594 nm (A-11058, RRID: AB_2534105) were for Cleaved-IL1β and GFAP double staining. Following three final washes for 10 min each, sections were mounted and cover slipped in Vectashield mounting medium with DAPI (H-1200; Vector Laboratories, Inc., CA, United States). All confocal images were captured on an FV1000 confocal laser microscope (Olympus) and digital imaging software (FV10-ASW 1.5 Viewer). For quantitative analysis, the number of surviving neurons per 250 μm length of medial CA1 pyramidal cell layer was counted bilaterally in five representative sections per animal. Furthermore, the fluorescence intensity of the targeting protein was normalized as the percent change compared to the control group as indicated in the figures. If necessary, colocalization was analyzed using Fiji software (version 1.52q).

## Ultrastructural Morphology of Astrocytes and Microglia Cells the Hippocampal CA1 Region by Transmission Electron Microscopy (TEM)

According to a previous description (Zhou et al., 2011), the hippocampal CA1 region was cut into small tissue blocks (1 $mm^3$) and fixed in 2.5% glutaraldehyde and 2.0% paraformaldehyde for 4 h in 0.1 mol/l phosphate buffer at 4°C. After fixation with 2% osmium tetroxide for 30 min, tissues were dehydrated in a series of graded ethanol solutions. Subsequently, ethanol was substituted with propylene oxide, and tissues were then embedded in Epon 812. Ultrathin sections (70 nm) were mounted on 200-mesh copper grids that were counterstained with uranyl acetate (30 min) followed by lead citrate for 10 min. Finally, the copper grids were washed with PBS and distilled water, and the ultrastructure was observed by transmission electron microscopy (H Hitachi-7650).

## Statistical Analysis

Data were analyzed by one- or two-way ANOVA followed by the Student–Newman–Keuls program using SigmaStat 3.5 software and are presented as the mean ± SEM. Differences were considered significant at *, **, and ***, which denote $P < 0.05$, $P < 0.01$, and $P < 0.001$, respectively. The statistical figures were generated using GraphPad Prism 8 software.

# RESULTS

## PBM Treatments Preserves CA1 Neurons After GCI

Transient global cerebral ischemia in gerbil for 15 min causes significant neuronal loss 2 days after reperfusion in the hippocampal CA1 region (Lee et al., 2019). On the other hand, cerebral ischemia can also activate endogenous programs of NSC proliferation, such as gliosis and neurogenesis, beginning 4 days after reperfusion in the hippocampal CA1 region, while newborn cells become gradually injured following reperfusion

after GCI (Wang et al., 2005; Tonchev and Yamashima, 2006). To determine whether PBM treatment protects newborn cells and favors recovery of cognitive outcome after GCI, we performed PBM treatment beginning 3 days after reperfusion for 5 consecutive days and evaluated neuronal survival in the hippocampal CA1 region following the time course after GCI (I/R 3, 7, 28, and 58 days). Immunofluorescence staining for NeuN was used to assess neuronal survival. Quantification of the results is provided in **Figure 1A,a**. As expected, the number of surviving neurons (NeuN-positive cells, green) was significantly decreased at all four timepoints (I/R 3, 7, 28, and 58 days) and reached a trough I/R 7 days after GCI compared to sham group animals. Intriguingly, at later timepoints (I/R 28 and 58 days), PBM-treated animals exhibited a greater number of NeuN+ cells than early timepoints (I/R 3 and 7 days), and PBM significantly increased NeuN+ cells compared to I/R animals at the same timepoints. These results indicate that PBM treatment for 5 consecutive days postischemia exerted long-lasting, effective protection against ischemic insult, likely involving attenuation of cell loss in the hippocampal CA1 region.

## PBM Treatment Only Improves Cognitive Function at Later Timepoints After GCI

We next examined whether PBM treatment preserved hippocampal-dependent working memory using the Morris water maze 7–9 and 56–58 days after GCI reperfusion. **Figures 2A,B** show the results of the latency trial (reflecting learning ability) and probe trial (reflecting memory ability) at early and later timepoints of reperfusion, respectively. We found that all non-ischemic animals spent less time (latency time) finding the target platform and increased the time (probe time) spent exploring the quadrant where the platform had been (**Figures 2Aa1,a2,Bb1,b2**). PBM treatment only improved cognitive function at the later timepoint but not at the early timepoint, as evidenced by PBM-treated animals exhibiting a significantly decreased latency time and significantly enhanced probe time at the later timepoint but no significant change at the early timepoint (**Figures 2Aa1,a2,Bb1,b2**). Representative tracings indicating sample swim paths of the rats from the latency trial and probe trial are shown in **Figures 2Aa3,a4,Bb3,b4**. The escape velocity of all animals showed no significant changes both in latency and probe trails (**Figures 2Aa5,Bb5**). Taken together, our findings suggest that short-term PBM treatment postischemia may provide a long-lasting beneficial effect for cognitive recovery after GCI, but mechanistic studies need to be performed.

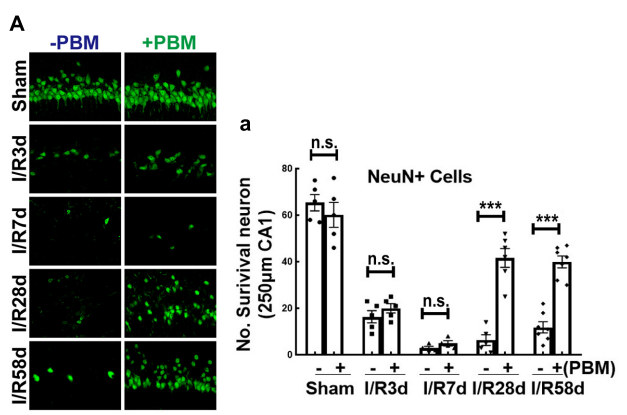


**FIGURE 1 |** The effect of photobiomodulation (PBM) treatment on neuronal survival in the hippocampal CA1 region following global cerebral ischemia (GCI). **(A)** Representative images of NeuN staining (green, reflecting surviving neurons) in the indicated groups and quantification of NeuN+ cells **(A-a)** in the 250 μm hippocampal CA1 region, showing the beneficial effects of PBM on the 28th and 58th days but not on the 3rd or 7th day after GCI ($n$ = 5–7 in each group). ***$P < 0.001$ between the two groups. n.s., no significant difference. Scale bar: 50 μm; magnification: 40×.

## PBM Treatment Elevates Endogenous NSC Proliferation Following GCI

It is well known that neurogenesis can replenish lost or damaged cells (Marques et al., 2019), which contributes to neurological repair after brain injury (Parpura et al., 2012). However, it is unknown whether PBM treatment improves neurogenesis following GCI. The traditional view is that neurogenesis occurs in two discrete regions, the subventricular zone (SVZ) of the olfactory bulb and the subgranular zone (SGZ) of the hippocampal dentate gyrus (DG). Herein, we examined the effects of PBM on the NSC proliferation program in the hippocampal CA1 region, which is the region most vulnerable to GCI. We first assessed the effect of PBM treatment on NSC proliferation following GCI by BrdU staining. As shown in **Figure 3A,a**, compared to the sham group, the number of BrdU+ cells (green, reflecting NSC proliferation) was dramatically enhanced at I/R 7 days and then markedly decreased over time (I/R 58 days) after GCI. PBM treatment did not significantly affect the number of BrdU+ cells in the hippocampal CA1 region of I/R 7 days or non-ischemic animals. Notably, PBM treatment markedly enhanced BrdU+ cells in the hippocampal CA1 region 58 days after reperfusion compared to those in the I/R 58 days group. These results indicate that PBM treatment may prevent cell loss by enhancing NSC proliferation at later time points after GCI in the hippocampal CA1 region.

## PBM Promotes Neurogenesis at the Later Timepoint After GCI Reperfusion

Neural stem cells possess multipotential to differentiate into both neuronal and glial subtypes, such as astrocytes, microglia and oligodendrocytes (Rolando et al., 2016). To further assess NSC fate induced by GCI with or without PBM, we next performed double IF staining for NeuN (reflecting mature neurons) and DCX (reflecting newborn/immature neurons). **Figure 4A-a1** shows that there was no significant change in the number of DCX+ cells (green) in the CA1 region in the sham or I/R 7 days groups with or without PBM treatment. Compared to sham controls, DCX+ cells significantly increased at I/R 7 days and decreased at I/R 58 days after reperfusion, but PBM treatment robustly enhanced DCX+ cells in the hippocampal CA1 region compared to I/R 58 days without PBM treatment. Only I/R 58 days PBM-treated animals displayed significantly enhanced

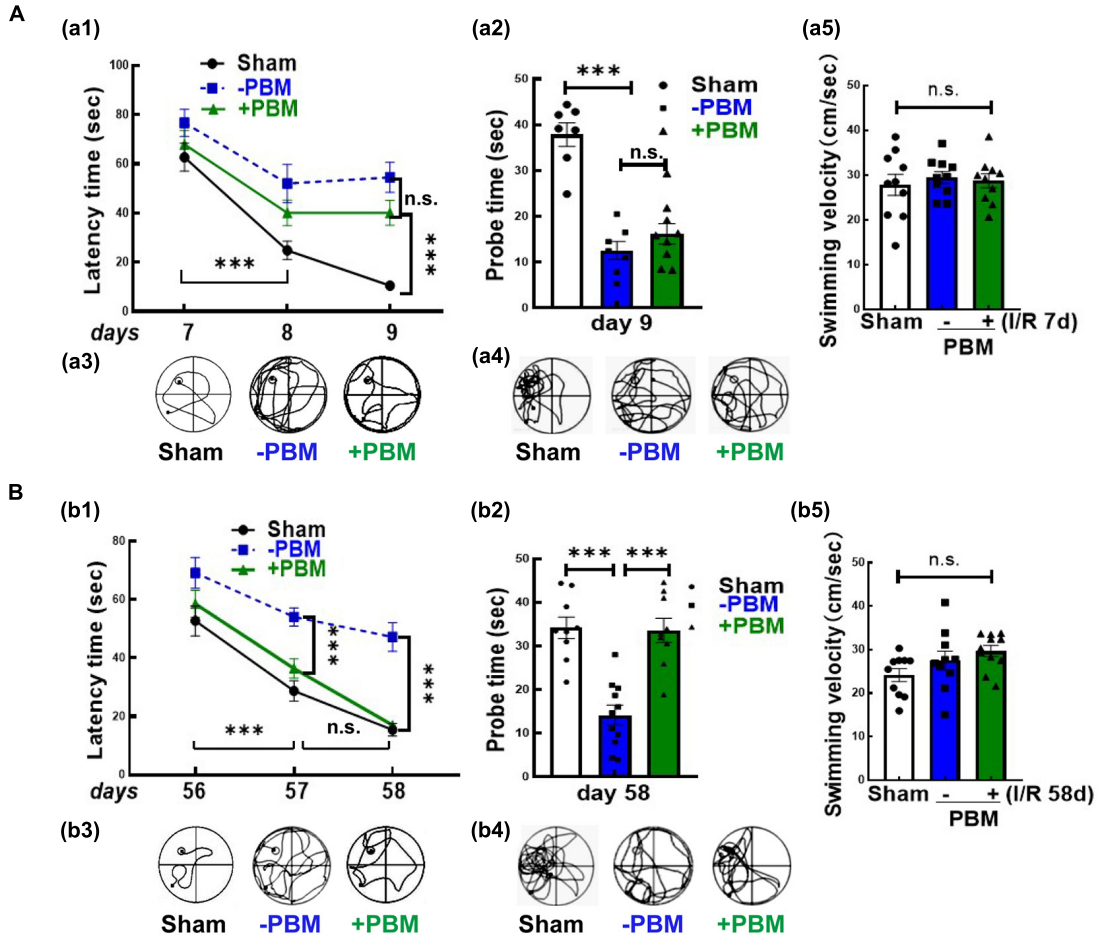


**FIGURE 2 |** Photobiomodulation treatment only improves functional outcome at the later time point (56–58 days) but not at the early time point (7–9 days) after GCI. Spatial learning/memory test in the Morris water maze 7–9 days **(A)** and 56–58 days **(B)** after GCI. **(a1,b1)** Latency trial and **(a2,b2)** probe trial; swimming paths of the rats from latency trials and probe trials on day 9 **(a3,a4)** and day 58 **(b3,b4)**; swimming velocity of probe trials on day 9 **(a5)** and day 58 **(b5)** after GCI ($n$ = 10–11 in each group). ***$P$ < 0.001 between the two groups. n.s., no significant difference. GCI, global cerebral ischemia; PBM, photobiomodulation.

numbers of DCX-NeuN colabeled cells, and there were no significant changes in the other groups (**Figure 4A-a2**). These results indicate that PBM treatment drives endogenous NSCs toward neuronal lineages in the hippocampal CA1 region only at later time points after GCI. Based on these results, we conclude that neurogenesis in the hippocampal CA1 region may contribute to neurological functional recovery caused by PBM treatment at I/R 58 days after GCI, while further studies will be necessary to elucidate its mechanism.

## PBM Suppresses Extensive Activation of Astrocytes in the Hippocampal CA1 Region Following GCI

Neural stem cells can also differentiate into glial cells, which mediate the microenvironment to determine the destiny of newborn neurons (Koehl, 2015). We therefore performed double IF staining for BrdU and GFAP (astrocyte marker) to examine astrocytic glial regeneration and activation. As shown in **Figure 5A-a1**, GCI significantly enhanced the fluorescence intensity of GFAP (reflecting astrocyte activation) in the hippocampal CA1 region compared to that of the sham group, and PBM treatment markedly suppressed this enhancement at both time points. The morphology of astrocytes in the GCI groups presented far fewer and shorter branches with hypertrophic bodies than that of PBM-treated animals. Furthermore, BrdU+/GFAP+ colabeled cells were quantified in the hippocampal CA1 region, which reflects NSC differentiation toward astrocytes (astrogliosis). PBM treatment did not exhibit a significant effect on the number of BrdU+/GFAP+ colabeled cells; however, I/R 7 days either with or without PBM treatment dramatically elevated the number of BrdU+/GFAP+ colabeled cells compared to the sham group, and I/R 58 days led to a significant reduction in colabeled BrdU+/GFAP+ cells compared to the I/R 7 days group (**Figure 5A-a2**). Taken together, our findings demonstrate that PBM treatment suppresses extensive activation of astrocytes, which is likely a major cause of locally enhanced neurogenesis in the hippocampal CA1 region at the later time point after GCI.

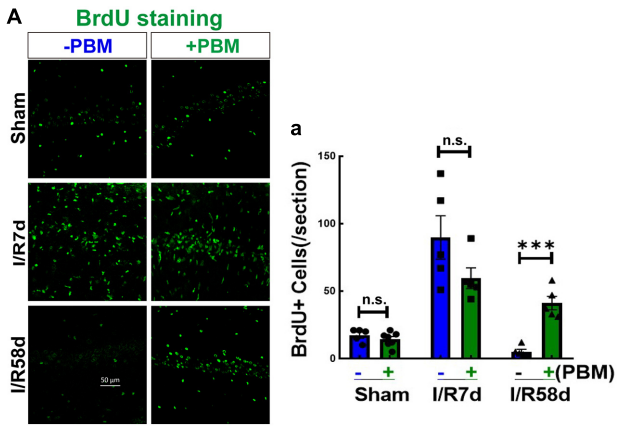


**FIGURE 3 |** Photobiomodulation elevates NSC proliferation at I/R 58 days reperfusion after GCI in the hippocampal CA1 region. Hippocampal coronal sections from sham and I/R 7 days and I/R 58 days rats treated with or without PBM were used to detect NSC proliferation (BrdU+).
**(A)** Representative images of IF staining for BrdU (green) in the hippocampal CA1 regions and **(a)** quantification of BrdU+ cells in the sections. n.s., no significant difference ($n$ = 5–7 in each group). ***$P$ < 0.001 between the two groups. Scale bar: 50 μm; magnification: 40×.

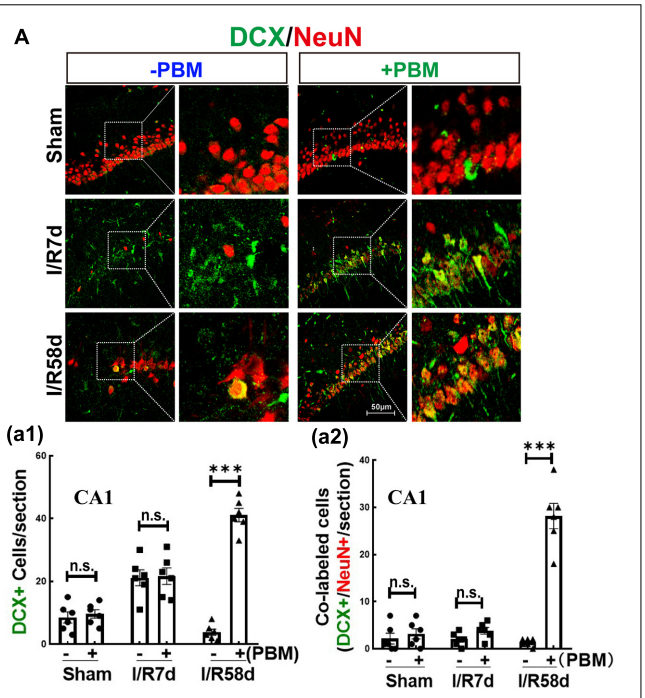


**FIGURE 4 |** Photobiomodulation promotes proliferating NSCs toward neurons 58 days after GCI reperfusion in the hippocampal CA1 region. Hippocampal coronal sections from sham, I/R 7 days and I/R 58 days rats treated with or without PBM were used to detect neurogenesis by IF staining. DCX is a marker of newborn immature migrating neurons, and NeuN is a marker for surviving neurons. Colabeled cells reflect proliferating neurons.
**(A)** Representative images of double IF staining for DCX (green) and NeuN (red) in the hippocampal CA1 region. Quantification of DCX+ cells **(a1)** and DCX+/NeuN+ colabeled cells (yellow) **(a2)** in the hippocampal CA1 region ($n$ = 5–7 in each group). ns, no significant difference. ***$P$ < 0.001 between the two groups. Scale bar: 50 μm; magnification: 40×.

## PBM Treatment Attenuates Astrocyte NLRP3 Inflammasome and Inflammatory Impairment in the Hippocampal CA1 Region After GCI

Upon inflammasome activation, NLRP3 assembles its adaptor ASC and produces a multiprotein complex with pro-caspase-1, which leads to caspase-1 activation and IL-1β maturation (cleaved IL-1β). Thus, we hypothesized that NLRP3 inflammasome activation, particularly in damaged astrocytes, may represent an important pathway in early-stage impairment after GCI; therefore, inhibition of the NLRP3 pathway by PBM treatment favors neurological recovery. To confirm our hypothesis, we examined protein expression of NLPR3 and cleaved IL-1β in the hippocampal CA1 region following GCI using IF staining analysis. Representative images of double IF staining for NLRP3 (red) and GFAP (green), cleaved IL-1β (Cle- IL1β, green) and GFAP (red) are shown in **Figure 6A**. These results indicate that the immunofluorescence intensity of NLRP3 (**Figure 6A-a1**) and Cle-IL1β (**Figure 6A-a2**) was robustly enhanced in both the I/R 7 days and I/R 58 days groups and strongly colocalized in the I/R 7 days group compared to the sham control (**Figures 6A-a3,a4**). We did not observe strong colocalization of NLPR3/GFAP or Cle-IL1β/GFAP in the I/R 58 days group, although the immunofluorescence intensity of NLPR3 or Cle-IL1β was still strong in these groups. PBM treatment significantly mitigated the I/R-induced enhancement of NLRP3 or Cle-IL1β and their colocalization with GFAP (**Figures 6A-a3,a4**). Finally, we performed IF staining for Iba1, a microglial marker, to detect inflammatory injury in the hippocampal CA1 region following GCI. Similarly, we found that the immunofluorescence intensity of Iba1 exhibited a similar pattern, with a robust elevation in Iba1 reactivity expression in the I/R groups compared to the sham group. In I/R 58 days animals, amoeboid Iba1+ cells nearly entirely occupied the hippocampal CA1 region, showing a similar pattern to NLRP3 and Cle-IL-1β. Importantly, PBM treatment attenuated I/R-induced enhancement in Iba1 protein levels (**Figure 6B-b**). Overall, our findings suggest that PBM treatment suppresses NLPR3 inflammasome activation in astrocytes at the early stage of reperfusion, which prevents later-phase inflammatory impairment following GCI.

## PBM Treatment Preserves the Ultrastructure of Astrocytes and Microglia Cells in the Hippocampal CA1 Region Following GCI

Recently, astrocyte-microglia communication has attracted increased attention because it directly mediates the surrounding microenvironment to determine the fate of resident precursor cells and impacts tissue repair and recovery after brain injury (Cope and Gould, 2019; Greenhalgh et al., 2020). Given that PBM significantly affects the morphology and activation of

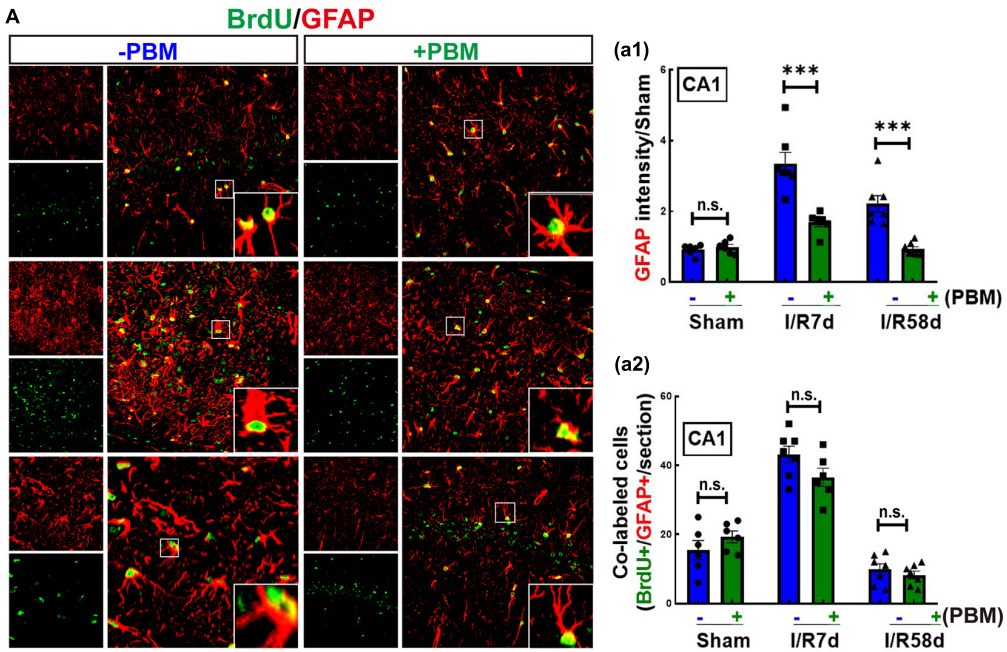


**FIGURE 5 |** Global cerebral ischemia enhances astrogliosis and reactive astrocytes 7 days after GCI reperfusion, and PBM suppresses astrocyte activation in both I/R 7 days and I/R 58 days animals. **(A)** Representative images of double IF staining for BrdU (green) and GFAP (red, an astrocyte marker). **(a1)** Quantification of GFAP fluorescence intensity (reflecting astrocyte activation), showing that PBM treatments attenuated reactive astrocytes compared to the I/R groups at the same timepoint in the hippocampal CA1 region. **(a2)** Quantification of the number of BrdU/GFAP colabeled cells (reflecting astrocytic regeneration/astrogliosis), showing that PBM had no significant effect on any of the indicated groups ($n$ = 6–7). $^{***}P < 0.001$. n.s., no significant difference. scale bar 50 μm; magnification 40×.

astrocytes and microglia cells following GCI, we performed transmission electron microscopy (TEM) to observe their ultrastructural changes in the hippocampal CA1 region in response to PBM treatment. Under physiological condition, astrocytes have pale nuclei that are usually regular in shape and their cytoplasm is also pale. A characteristic of astrocytes is that they are sometimes partially surrounding synapsing axons, spines and dendrites, and their processes are extending into the surrounding neuropil. However, response to ischemic injury or neurodegenerative diseases, astrocytic ultrastructure shows unhealthy features, such as astrocytic swelling, nuclear shrinkage, chromatin condensation, organelles (mitochondria and endoplasmic reticulum) damage/loss, and translucence of matrix (gliofilament disappearance) (Kwon et al., 2009). As shown in **Figure 7A**, a significant amount of chromatin condensation was observed on top of the nuclear membrane, and the nuclear membrane partly disappeared in the I/R 7 days group, indicating overactivation. In the I/R 58 days group, the cytoplasm of the astrocytes appeared completely empty, with disappeared organelles and gliofilaments. PBM treatment reduced the damage to I/R 58 days animals, showing distinct normalization in the ultrastructural picture with pale nuclei and plumpy cytoplasm (intact mitochondria, yellow arrow), as well as adhering to a relatively normal neuron (N) (**Figure 7A**). Meanwhile, **Figure 7B** shows that in the GCI groups (I/R 7 days and I/R 58 days), the microglia ultrastructure exhibited severe mitochondrial impairment, characterized by numerous vacuolated mitochondria with some partially broken cristae (green arrow) and even disaggregation (red arrow). In striking contrast, we found that sections from I/R 58 days in PBM-treated animals clearly showed nearly normal ultrastructure of microglia cells, in which the majority of mitochondrial structure was intact with round and very few broken cristae (yellow arrow), while I/R 7 days PBM-treated animals did not experience a beneficial effect and displayed obvious mitochondrial damage. These results suggest that PBM protects astrocyte and microglia at only the later timepoint but not the early timepoint after GCI, which might contribute to the long-lasting protective and repair roles observed for cognitive outcomes.

## DISCUSSION

The traditional view is that neurogenesis initiates in the SVZ and the SGZ, which are the major niches of NPCs and NSCs. Furthermore, brain injuries due to ischemic stroke and brain trauma promote NPCs and NSCs to migrate toward the lesion area and differentiate into neurons and glial cell (Marques et al., 2019). However, it has been reported that in a transient global ischemia animal model, selectively leading to hippocampal CA1 neuronal delayed death, ischemia-induced SGZ neurogenesis is not attributed to CA1 neuronal loss (Liu et al., 1998; Salazar-Colocho et al., 2008; Song et al., 2021). Notably, several studies have found that locally increased NSC proliferation and newborn neurons appear in the hippocampal CA1 region, although neurogenesis is very

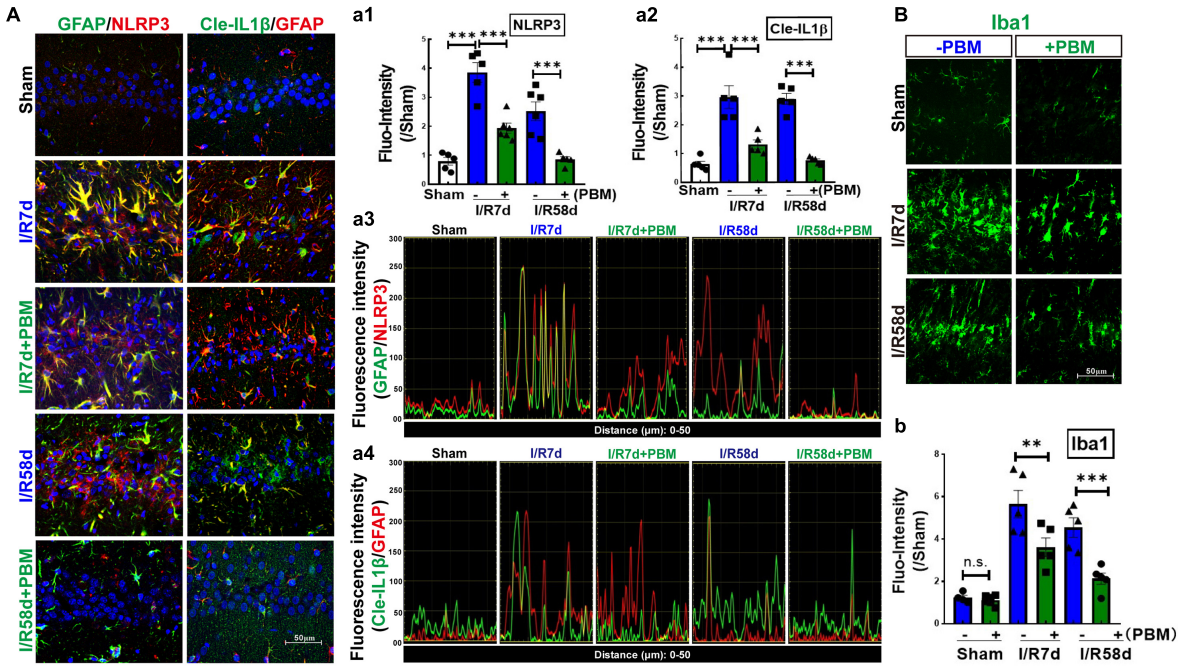


**FIGURE 6 |** Photobiomodulation treatment inhibits GCI-induced expression of NLRP3 and activates IL-1β in the hippocampal CA1 region following GCI. **(A)** Representative images of double IF staining of GFAP/NLRP3 and Cle-IL-1β/GFAP in the indicated groups. Fluorescence intensity quantification of NLRP3 **(a1)** or Cle-IL-1β **(a2)**. Data are expressed by the ratio of fluorescence intensity of the section compared to sham. Colocalization between the two stained proteins for GFAP/NLRP3 **(a3)** and Cle-IL-1β/GFAP **(a4)**. **(B)** Representative images of IF staining for Iba1 (a microglial marker) and fluorescence intensity quantification **(b)** ($n$ = 5–6 in each group). $^{**}P < 0.01$; $^{***}P < 0.001$; scale bar 50 μm; magnification 40×.

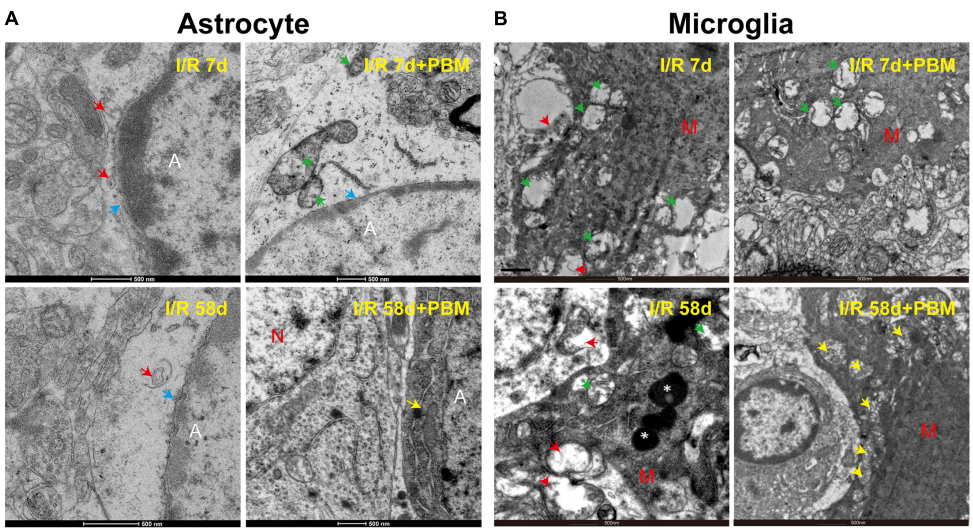


**FIGURE 7 |** The effects of PBM on astrocyte and microglia ultrastructure in the hippocampal CA1 region of I/R 7 days and I/R 58 days animals. Representative electron microscopy images show the ultrastructure of astrocytes **(A)** and microglia cells **(B)** in the indicated groups. Yellow arrows: integrity mitochondria; red arrows: disaggregated mitochondria; green arrows: mitochondria with broken cristae; white star: lysosome; blue arrows: nuclear membrane. A, astrocyte; M, microglia; N, neuron.

limited due to the extreme vulnerability of the CA1 region to ischemia insult (Schmidt and Reymann, 2002) and a very harsh environment, such as inflammation (Tobin et al., 2014), in which newly born hippocampal neurons die within days or weeks (Jablonska and Lukomska, 2011). Therefore, in the current study, we aimed to develop a potential strategy that promotes local NSC proliferation and direct differentiation toward neurons in the hippocampal CA1 region.

Photobiomodulation therapy has emerged as a potential novel non-invasive intervention for acute brain injuries caused by stroke, traumatic brain injury, and global ischemia (Wang et al., 2019; Dompe et al., 2020), as well as chronic neurodegenerative diseases, such as pain, Parkinson's disease, and Alzheimer's disease (Farfara et al., 2015; Berman and Nichols, 2019; Salehpour and Hamblin, 2020). The results of our current study demonstrate that (1) PBM treatment enhances endogenous NPC proliferation and local neurogenesis at I/R 58 days after GCI reperfusion in the hippocampal CA1 region; (2) PBM treatment not only attenuates the early inflammatory response but also maintains the NPC proliferation induced by GCI (I/R 7 days after GCI); (3) notably, PBM treatment improves neurological recovery only at the later time point (I/R 58 days) but not at the early time point (I/R 7 days) after GCI reperfusion.

In our current study, we used an 808 nm laser with a power dose of 20 mW/cm$^2$. Supporting our study, Tedford et al. (2015) confirmed that 808 nm light can reach a depth in the brain of 40–50 mm (Hamblin, 2016) and that a laser power dose of 20 mW/cm$^2$ significantly improves the neurological function of mice in a traumatic brain injury model (Oron et al., 2007; Oron et al., 2012). A novel discovery by our research group is the remarkable protection of hippocampal CA1 region neurons in male rats 1 week and 6 months after ischemia, along with prominent functional improvements in cognition induced by 808 nm 8 mW/cm$^2$ PBM-treatment at the hippocampus tissue (Wang et al., 2019). Herein, to explore whether laser treatment altered local neurogenesis in the hippocampal CA1 region, we treated animals with PBM 3 days after reperfusion onset for 5 successive days. The reason we chose this time window for PBM treatment was based on the survival curves of hippocampal CA1 neurons following GCI from other studies (Lee et al., 2019) and our current studies. We found that NeuN-positive cells (reflecting surviving neurons) were sharply decreased at I/R 3 days and were hardly detectable at I/R 7 days and I/R 28 days after GCI compared to the sham group in the CA1 region. However, there was a slight increase in the number of NeuN+ neurons at I/R 58 days compared to I/R 7 days animals, but there was no significant difference compared to I/R 28 days after GCI in the CA1 region. Importantly, PBM treatment did not increase neuron survival at I/R 3 days or I/R 7 days; however, PBM significantly enhanced neuron survival at I/R 58 days, as evidenced by increased NeuN+ cells in the hippocampal CA1 region compared to I/R animals at the same time-point. These results suggest that PBM might improve neurogenesis rather than protect impaired neurons in the hippocampal CA1 region. To confirm this hypothesis, we next performed BrdU staining, a marker to examine the proliferation of NSCs *in situ* (Nemirovich-Danchenko and Khodanovich, 2019). Our results revealed that BrdU+ cells were dramatically elevated at I/R 7 days and then significantly decreased at I/R 58 days compared to the sham group in the hippocampal CA1 region. Intriguingly, NSC proliferation was retained at I/R 7 days and at I/R 58 days in the PBM-treated group because increased BrdU+ cells primarily occupied the CA1 region of the hippocampus. Furthermore, we observed substantial neurogenesis in the hippocampal CA1 region of I/R 58 days animals treated with PBM, as evidenced by a significant increase in DCX+/NeuN+ colabeled cells. Additionally, astrogliosis was significantly enhanced at the early time point (I/R 7 days) with or without PBM treatment, as evidenced by a dramatic enhancement in BrdU+/GFAP+ colabeled cells. Notably, extensive activation of astrocytes in the I/R 7 days group was suppressed by PBM treatment as shown by a marked decrease in the fluorescence intensity of GFAP in the PBM-treated animals compared to the I/R 7 days animals. The Morris water maze test is used to determine the function of hippocampal-dependent learning and memory (Nakazawa, 2006). Further functional studies revealed that PBM treatment improved cognitive deficits induced by GCI at the later time point but not the earlier time point. A few studies have shown that in global cerebral ischemia animal models, increased NSC proliferation starts at 3–4 days, peaks at 7–10 days and then dramatically decreases in the hippocampal DG region (Liu et al., 1998; Song et al., 2021). In contrast to these reports, our current study, for the first time, elucidates that PBM preserves endogenous proliferative NSCs induced by GCI and promotes their differentiation toward neurons in the hippocampal CA1 region. Supporting our findings, Oron et al. (2006) reveal that low level PBM performed at 24 h post-stroke exerts a significant functional benefit with an underlying mechanism possibly being induction of neurogenesis. More importantly, an excessive number of laser-treatments can temporarily delay the process of brain repair stimulated by PBM by causing temporary induction of reactive gliosis (Xuan et al., 2016).

Overactivation of astrocytes leads to the accumulation of damaged ROS-generating mitochondria, and this triggers Nod-like receptor protein 3 (NLRP3) inflammasome activity, which in turn leads to a neuroinflammatory response and neuronal impairment (Schultz et al., 2004; Jones et al., 2018). The active NLRP3 inflammasome cleaves proinflammatory IL-1β to its active form, which is a key determinant of outcome after brain injuries (Mezzasoma et al., 2016; Bai et al., 2020). Several studies have revealed that astrocytes are the predominant source of IL-1β in traumatic brain and ischemic disorders (Jones et al., 2018). Consistent with these reports, our current study revealed that GCI triggers increased NLRP3 expression at both early and later time points, and cleaved IL1β was correlated with significant enhancement in overactivated astrocytes of the hippocampal CA1 region. Furthermore, protein expression of Iba1, a marker of inflammatory injury, was persistently elevated, which perfectly mirrored changes in NLRP3 activity. Importantly, the increased NLRP3 activity and inflammation caused by GCI were suppressed by PBM treatment. PBM exerts anti-inflammatory effects in a wide range of animal models, such as acute traumatic brain injury, experimental autoimmune encephalomyelitis, spinal cord injury and wound healing (Hamblin, 2017; Xu et al., 2017). *In vitro* studies also confirmed that PBM treatment has the ability to change the phenotype of activated microglia (Fernandes et al., 2015; Hwang et al., 2015; Lim et al., 2015; Saha et al., 2016), especially at lower power doses (von Leden et al., 2013). Recent work from Zhang's Lab. demonstrates that PBM-treatment from 2 to 8 post-stroke in rats can effectively switch an M1 microglial phenotype to an anti-inflammatory M2 phenotype, and promotes

neurogenesis (Arsac and Frileux, 1988). In addition, treatment with PBM has been shown to enhance cognitive capability in normal people (Barrett and Gonzalez-Lima, 2013) and healthy animals (Gonzalez-Lima and Barrett, 2014). In acute brain injuries in humans, such as ischemic stroke and traumatic brain injury (Lampl et al., 2007; Figueiro Longo et al., 2020), as well as chronic neurodegenerative diseases, such as AD and PD (Liu et al., 2020; Hong et al., 2021), PBM intervention has likewise been shown to elevate functional cognitive recovery in both humans and animals. Based on these findings, we propose that inhibition of NLRP3 inflammasome activation and IL-1β in astrocytes of the hippocampal CA1 region could contribute, in part, to pro-neurogenesis and cognitive recovery in response to PBM treatment after GCI.

Additionally, we demonstrated that although PBM treatment attenuated the early extensive inflammatory response at I/R 7 days after GCI in the hippocampal CA1 region, the number of surviving neurons was not significantly increased, and working memory was not improved at this time point. This may be due to the unhealthy ultrastructure of glial cells, which may be caused by other damage, such as oxidative stress and endoplasmic reticulum stress. Indeed, our EM data corroborate the hypothesis that mitochondria were damaged in microglia cells and degradative subcellular organelles in astrocytes at I/R 7 days with or without PBM treatment after GCI in the hippocampal CA1 region. On the other hand, in line with our findings, increasing evidence has demonstrates that glial cells such as astrocyte, microglia and oligodendrocyte cells, act directly on neurons to protect against ischemic insults (Carmen et al., 2007; Nutma et al., 2020). However, further studies will be necessary to elucidate the precise mechanism underlying the effects induced by PBM treatment.

## CONCLUSION

The current study is the first to demonstrate that PBM treatment protects endogenous NSCs and promotes local neurogenesis in the hippocampal CA1 region, which is partly due to mitigating the inflammatory impairment induced by NLPR3 inflammasome activation. The current study provides a potential strategy for repairing hippocampal CA1 neurons and improving cognitive function in cardiac arrest patients.

## DATA AVAILABILITY STATEMENT

The raw data supporting the conclusions of this article will be made available by the authors, without undue reservation, to any qualified researcher.

## ETHICS STATEMENT

The animal study was reviewed and approved by Institutional Animal Care and Xuzhou Medical University.

## AUTHOR CONTRIBUTIONS

SH designed the research. SG wrote the main manuscript text. RW and SH helped to polish the manuscript. SG, LS, and JH performed the experiments. SG and RW analyzed data and prepared figures. DH and XZ helped to perform the experiments. YZ participated in the manuscript modification. All authors reviewed the manuscript.

## FUNDING

This research was supported by Xuzhou National Clinical Key Specialty Cultivation Project (2018ZK004), Jiangsu Provincial Commission of Health and Family Planning (LGY2019085), the excellent young and middle-age talents project of The affiliated hospital of Xuzhou Medical University (2019128009), National Undergraduate Training Program for Innovation and Entrepreneurship (202010313035), and the National Natural Science Foundation of China (81671223).

## ACKNOWLEDGMENTS

We thank Elsevier Language Editing Services for editing the English text of a draft of this manuscript.

## REFERENCES

Ando, T., Xuan, W., Xu, T., Dai, T., Sharma, S. K., Kharkwal, G. B., et al. (2011). Comparison of therapeutic effects between pulsed and continuous wave 810-nm wavelength laser irradiation for traumatic brain injury in mice. *PLoS One* 6:e26212. doi: 10.1371/journal.pone.0026212

Arsac, M., and Frileux, C. (1988). Comparative analgesic efficacy and tolerability of ketorolac tromethamine and glafenine in patients with post-operative pain. *Curr. Med. Res. Opin.* 11, 214–220. doi: 10.1185/03007998809114238

Babcock, K. R., Page, J. S., Fallon, J. R., and Webb, A. E. (2021). Adult Hippocampal Neurogenesis in Aging and Alzheimer's Disease. *Stem Cell Reports* 16, 681–693. doi: 10.1016/j.stemcr.2021.01.019

Bai, N., Zhang, Q., Zhang, W., Liu, B., Yang, F., Brann, D., et al. (2020). G-protein-coupled estrogen receptor activation upregulates interleukin-1 receptor antagonist in the hippocampus after global cerebral ischemia: implications for neuronal self-defense. *J. Neuroinflammation* 17:45. doi: 10.1186/s12974-020-1715-x

Barrett, D. W., and Gonzalez-Lima, F. (2013). Transcranial infrared laser stimulation produces beneficial cognitive and emotional effects in humans. *Neuroscience* 230, 13–23. doi: 10.1016/j.neuroscience.2012.11.016

Bathini, M., Raghushaker, C. R., and Mahato, K. K. (2020). The Molecular Mechanisms of Action of Photobiomodulation Against Neurodegenerative Diseases: a Systematic Review. *Cell Mol. Neurobiol.* [Epub Online ahead of print]. doi: 10.1007/s10571-020-01016-9

Berman, M. H., and Nichols, T. W. (2019). Treatment of Neurodegeneration: integrating Photobiomodulation and Neurofeedback in Alzheimer's Dementia and Parkinson's: a Review. *Photobiomodul. Photomed. Laser Surg.* 37, 623–634. doi: 10.1089/photob.2019.4685

Carmen, J., Magnus, T., Cassiani-Ingoni, R., Sherman, L., Rao, M. S., and Mattson, M. P. (2007). Revisiting the astrocyte-oligodendrocyte relationship in the adult CNS. *Prog. Neurobiol.* 82, 151–162. doi: 10.1016/j.pneurobio.2007.03.001

Cope, E. C., and Gould, E. (2019). Adult Neurogenesis, Glia, and the Extracellular Matrix. *Cell Stem Cell* 24, 690–705. doi: 10.1016/j.stem.2019.03.023

de Freitas, L. F., and Hamblin, M. R. (2016). Proposed Mechanisms of Photobiomodulation or Low-Level Light Therapy. *IEEE J. Sel. Top. Quantum Electron.* 22:7000417. doi: 10.1109/JSTQE.2016.2561201

Dompe, C., Moncrieff, L., Matys, J., Grzech-Lesniak, K., Kocherova, I., Bryja, A., et al. (2020). Photobiomodulation-Underlying Mechanism and Clinical Applications. *J. Clin. Med.* 9:1724 doi: 10.3390/jcm9061724

Farfara, D., Tuby, H., Trudler, D., Doron-Mandel, E., Maltz, L., Vassar, R. J., et al. (2015). Low-level laser therapy ameliorates disease progression in a mouse model of Alzheimer's disease. *J. Mol. Neurosci.* 55, 430–436. doi: 10.1007/s12031-014-0354-z

Fernandes, K. P., Souza, N. H., Mesquita-Ferrari, R. A., Silva Dde, F., Rocha, L. A., Alves, A. N., et al. (2015). Photobiomodulation with 660-nm and 780-nm laser on activated J774 macrophage-like cells: effect on M1 inflammatory markers. *J. Photochem. Photobiol. B* 153, 344–351. doi: 10.1016/j.jphotobiol.2015.10.015

Figueiro Longo, M. G., Tan, C. O., Chan, S. T., Welt, J., Avesta, A., Ratai, E., et al. (2020). Effect of Transcranial Low-Level Light Therapy vs Sham Therapy Among Patients With Moderate Traumatic Brain Injury: a Randomized Clinical Trial. *JAMA Netw. Open* 3:e2017337. doi: 10.1001/jamanetworkopen.2020.17337

Gonzalez-Lima, F., and Barrett, D. W. (2014). Augmentation of cognitive brain functions with transcranial lasers. *Front. Syst. Neurosci.* 8:36. doi: 10.3389/fnsys.2014.00036

Greenhalgh, A. D., David, S., and Bennett, F. C. (2020). Immune cell regulation of glia during CNS injury and disease. *Nat. Rev. Neurosci.* 21, 139–152. doi: 10.1038/s41583-020-0263-9

Hamblin, M. R. (2016). Shining light on the head: photobiomodulation for brain disorders. *BBA Clin.* 6, 113–124. doi: 10.1016/j.bbacli.2016.09.002

Hamblin, M. R. (2017). Mechanisms and applications of the anti-inflammatory effects of photobiomodulation. *AIMS Biophys.* 4, 337–361. doi: 10.3934/biophy.2017.3.337

Harukuni, I., and Bhardwaj, A. (2006). Mechanisms of brain injury after global cerebral ischemia. *Neurol. Clin.* 24, 1–21. doi: 10.1016/j.ncl.2005.10.004

Hong, C. T., Hu, C. J., Lin, H. Y., and Wu, D. (2021). Effects of concomitant use of hydrogen water and photobiomodulation on Parkinson disease: a pilot study. *Medicine* 100:e24191. doi: 10.1097/MD.0000000000024191

Hong, S., Washington, P. M., Kim, A., Yang, C. P., Yu, T. S., and Kernie, S. G. (2016). Apolipoprotein E Regulates Injury-Induced Activation of Hippocampal Neural Stem and Progenitor Cells. *J. Neurotrauma* 33, 362–374. doi: 10.1089/neu.2014.3860

Hwang, M. H., Shin, J. H., Kim, K. S., Yoo, C. M., Jo, G. E., Kim, J. H., et al. (2015). Low level light therapy modulates inflammatory mediators secreted by human annulus fibrosus cells during intervertebral disc degeneration *in vitro*. *Photochem. Photobiol.* 91, 403–410. doi: 10.1111/php.12415

Jablonska, A., and Lukomska, B. (2011). Stroke induced brain changes: implications for stem cell transplantation. *Acta Neurobiol. Exp.* 71, 74–85.

Jones, M. E., Lebonville, C. L., Paniccia, J. E., Balentine, M. E., Reissner, K. J., and Lysle, D. T. (2018). Hippocampal interleukin-1 mediates stress-enhanced fear learning: a potential role for astrocyte-derived interleukin-1beta. *Brain Behav. Immun.* 67, 355–363. doi: 10.1016/j.bbi.2017.09.016

Koehl, M. (2015). Gene-environment interaction in programming hippocampal plasticity: focus on adult neurogenesis. *Front. Mol. Neurosci.* 8:41. doi: 10.3389/fnmol.2015.00041

Kwon, I., Kim, E. H., del Zoppo, G. J., and Heo, J. H. (2009). Ultrastructural and temporal changes of the microvascular basement membrane and astrocyte interface following focal cerebral ischemia. *J. Neurosci. Res.* 87, 668–676. doi: 10.1002/jnr.21877

Lampl, Y., Zivin, J. A., Fisher, M., Lew, R., Welin, L., Dahlof, B., et al. (2007). Infrared laser therapy for ischemic stroke: a new treatment strategy: results of the NeuroThera Effectiveness and Safety Trial-1 (NEST-1). *Stroke* 38, 1843–1849. doi: 10.1161/STROKEAHA.106.478230

Lee, H. I., Lee, S. W., Kim, N. G., Park, K. J., Choi, B. T., Shin, Y. I., et al. (2017). Low-level light emitting diode (LED) therapy suppresses inflammasome-mediated brain damage in experimental ischemic stroke. *J. Biophotonics* 10, 1502–1513. doi: 10.1002/jbio.201600244

Lee, T. K., Kim, H., Song, M., Lee, J. C., Park, J. H., Ahn, J. H., et al. (2019). Time-course pattern of neuronal loss and gliosis in gerbil hippocampi following mild, severe, or lethal transient global cerebral ischemia. *Neural Regen. Res.* 14, 1394–1403. doi: 10.4103/1673-5374.253524

Lim, W., Choi, H., Kim, J., Kim, S., Jeon, S., Zheng, H., et al. (2015). Anti-inflammatory effect of 635 nm irradiations on *in vitro* direct/indirect irradiation model. *J. Oral Pathol. Med.* 44, 94–102. doi: 10.1111/jop.12204

Lindsay, P. J., Buell, D., and Scales, D. C. (2018). The efficacy and safety of pre-hospital cooling after out-of-hospital cardiac arrest: a systematic review and meta-analysis. *Crit. Care* 22:66. doi: 10.1186/s13054-018-1984-2

Liu, J., Solway, K., Messing, R. O., and Sharp, F. R. (1998). Increased neurogenesis in the dentate gyrus after transient global ischemia in gerbils. *J. Neurosci.* 18, 7768–7778.

Liu, Y. L., Gong, S. Y., Xia, S. T., Wang, Y. L., Peng, H., Shen, Y., et al. (2020). Light therapy: a new option for neurodegenerative diseases. *Chin. Med. J.* 134, 634–645. doi: 10.1097/CM9.0000000000001301

Luo, Y., Kuo, C. C., Shen, H., Chou, J., Greig, N. H., Hoffer, B. J., et al. (2009). Delayed treatment with a p53 inhibitor enhances recovery in stroke brain. *Ann. Neurol.* 65, 520–530. doi: 10.1002/ana.21592

Marques, B. L., Carvalho, G. A., Freitas, E. M. M., Chiareli, R. A., Barbosa, T. G., Di Araujo, A. G. P., et al. (2019). The role of neurogenesis in neurorepair after ischemic stroke. *Semin. Cell Dev. Biol.* 95, 98–110. doi: 10.1016/j.semcdb.2018.12.003

McAllister, B. B., Pochakom, A., Fu, S., and Dyck, R. H. (2020). Effects of social defeat stress and fluoxetine treatment on neurogenesis and behavior in mice that lack zinc transporter 3 (ZnT3) and vesicular zinc. *Hippocampus* 30, 623–637. doi: 10.1002/hipo.23185

Mezzasoma, L., Antognelli, C., and Talesa, V. N. (2016). Atrial natriuretic peptide down-regulates LPS/ATP-mediated IL-1beta release by inhibiting NF-kB, NLRP3 inflammasome and caspase-1 activation in THP-1 cells. *Immunol. Res.* 64, 303–312. doi: 10.1007/s12026-015-8751-0

Moulaert, V. R., Verbunt, J. A., van Heugten, C. M., and Wade, D. T. (2009). Cognitive impairments in survivors of out-of-hospital cardiac arrest: a systematic review. *Resuscitation* 80, 297–305. doi: 10.1016/j.resuscitation.2008.10.034

Nakatomi, H., Kuriu, T., Okabe, S., Yamamoto, S., Hatano, O., Kawahara, N., et al. (2002). Regeneration of hippocampal pyramidal neurons after ischemic brain injury by recruitment of endogenous neural progenitors. *Cell* 110, 429–441. doi: 10.1016/s0092-8674(02)00862-0

Nakazawa, K. (2006). Inducible and cell-type restricted manipulation in the entorhinal cortex. *Neuron* 50, 183–185. doi: 10.1016/j.neuron.2006.04.007

Nemirovich-Danchenko, N. M., and Khodanovich, M. Y. (2019). New Neurons in the Post-ischemic and Injured Brain: migrating or Resident? *Front. Neurosci.* 13:588. doi: 10.3389/fnins.2019.00588

Nielsen, N., Friberg, H., Gluud, C., Herlitz, J., and Wetterslev, J. (2011). Hypothermia after cardiac arrest should be further evaluated–a systematic review of randomised trials with meta-analysis and trial sequential analysis. *Int. J. Cardiol.* 151, 333–341. doi: 10.1016/j.ijcard.2010.06.008

Nutma, E., van Gent, D., Amor, S., and Peferoen, L. A. N. (2020). Astrocyte and Oligodendrocyte Cross-Talk in the Central Nervous System. *Cells* 9:600. doi: 10.3390/cells9030600

Oron, A., Oron, U., Chen, J., Eilam, A., Zhang, C., Sadeh, M., et al. (2006). Low-level laser therapy applied transcranially to rats after induction of stroke significantly reduces long-term neurological deficits. *Stroke* 37, 2620–2624. doi: 10.1161/01.STR.0000242775.14642.b8

Oron, A., Oron, U., Streeter, J., de Taboada, L., Alexandrovich, A., Trembovler, V., et al. (2007). low-level laser therapy applied transcranially to mice following traumatic brain injury significantly reduces long-term neurological deficits. *J. Neurotrauma* 24, 651–656. doi: 10.1089/neu.2006.0198

Oron, A., Oron, U., Streeter, J., De Taboada, L., Alexandrovich, A., Trembovler, V., et al. (2012). Near infrared transcranial laser therapy applied at various modes to mice following traumatic brain injury significantly reduces long-term neurological deficits. *J. Neurotrauma* 29, 401–407. doi: 10.1089/neu.2011.2062

Parpura, V., Heneka, M. T., Montana, V., Oliet, S. H., Schousboe, A., Haydon, P. G., et al. (2012). Glial cells in (patho)physiology. *J. Neurochem.* 121, 4–27. doi: 10.1111/j.1471-4159.2012.07664.x

Pulsinelli, W. A., Brierley, J. B., and Plum, F. (1982). Temporal profile of neuronal damage in a model of transient forebrain ischemia. *Ann. Neurol.* 11, 491–498. doi: 10.1002/ana.410110509

Radad, K., Moldzio, R., Al-Shraim, M., Kranner, B., Krewenka, C., and Rausch, W. D. (2017). Recent Advances on the Role of Neurogenesis in the Adult Brain: therapeutic Potential in Parkinson's and Alzheimer's Diseases. *CNS Neurol. Disord. Drug Targets* 16, 740–748. doi: 10.2174/1871527316666170623094728

Ravera, S., Colombo, E., Pasquale, C., Benedicenti, S., Solimei, L., Signore, A., et al. (2021). Mitochondrial Bioenergetic, Photobiomodulation and Trigeminal Branches Nerve Damage, What's the Connection? A Review. *Int. J. Mol. Sci.* 22:4347. doi: 10.3390/ijms22094347

Rietze, R., Poulin, P., and Weiss, S. (2000). Mitotically active cells that generate neurons and astrocytes are present in multiple regions of the adult mouse hippocampus. *J. Comp. Neurol.* 424, 397–408.

Rolando, C., Erni, A., Grison, A., Beattie, R., Engler, A., Gokhale, P. J., et al. (2016). Multipotency of Adult Hippocampal NSCs *In Vivo* Is Restricted by Drosha/NFIB. *Cell Stem Cell* 19, 653–662. doi: 10.1016/j.stem.2016.07.003

Saha, B., Kodys, K., and Szabo, G. (2016). Hepatitis C Virus-Induced Monocyte Differentiation Into Polarized M2 Macrophages Promotes Stellate Cell Activation via TGF-beta. *Cell. Mol. Gastroenterol. Hepatol.* 2, 302–316.e8.doi: 10.1016/j.jcmgh.2015.12.005

Salazar-Colocho, P., Lanciego, J. L., Del Rio, J., and Frechilla, D. (2008). Ischemia induces cell proliferation and neurogenesis in the gerbil hippocampus in response to neuronal death. *Neurosci. Res.* 61, 27–37. doi: 10.1016/j.neures.2008.01.008

Salehpour, F., and Hamblin, M. R. (2020). Photobiomodulation for Parkinson's Disease in Animal Models: a Systematic Review. *Biomolecules* 10:610. doi: 10.3390/biom10040610

Schmidt, W., and Reymann, K. G. (2002). Proliferating cells differentiate into neurons in the hippocampal CA1 region of gerbils after global cerebral ischemia. *Neurosci. Lett.* 334, 153–156. doi: 10.1016/s0304-3940(02)01072-8

Schultz, J., Schwarz, A., Neidhold, S., Burwinkel, M., Riemer, C., Simon, D., et al. (2004). Role of interleukin-1 in prion disease-associated astrocyte activation. *Am. J. Pathol.* 165, 671–678. doi: 10.1016/S0002-9440(10)63331-7

Song, D., Chen, Y., Chen, C., Chen, L., and Cheng, O. (2021). GABAB receptor antagonist promotes hippocampal neurogenesis and facilitates cognitive function recovery following acute cerebral ischemia in mice. *Stem Cell Res. Ther.* 12:22. doi: 10.1186/s13287-020-02059-x

Tedford, C. E., DeLapp, S., Jacques, S., and Anders, J. (2015). Quantitative analysis of transcranial and intraparenchymal light penetration in human cadaver brain tissue. *Lasers Surg. Med* 47, 312–322. doi: 10.1002/lsm.22343

Tobin, M. K., Bonds, J. A., Minshall, R. D., Pelligrino, D. A., Testai, F. D., and Lazarov, O. (2014). Neurogenesis and inflammation after ischemic stroke: what is known and where we go from here. *J. Cereb. Blood Flow Metab.* 34, 1573–1584. doi: 10.1038/jcbfm.2014.130

Tonchev, A. B., and Yamashima, T. (2006). Differential neurogenic potential of progenitor cells in dentate gyrus and CA1 sector of the postischemic adult monkey hippocampus. *Exp. Neurol.* 198, 101–113. doi: 10.1016/j.expneurol.2005.11.022

Tonchev, A. B., Yamashima, T., Zhao, L., and Okano, H. (2003a). Differential proliferative response in the postischemic hippocampus, temporal cortex, and olfactory bulb of young adult macaque monkeys. *Glia* 42, 209–224. doi: 10.1002/glia.10209

Tonchev, A. B., Yamashima, T., Zhao, L., Okano, H. J., and Okano, H. (2003b). Proliferation of neural and neuronal progenitors after global brain ischemia in young adult macaque monkeys. *Mol. Cell. Neurosci.* 23, 292–301. doi: 10.1016/s1044-7431(03)00058-7

Tucker, L. D., Lu, Y., Dong, Y., Yang, L., Li, Y., Zhao, N., et al. (2018). Photobiomodulation Therapy Attenuates Hypoxic-Ischemic Injury in a Neonatal Rat Model. *J. Mol. Neurosci.* 65, 514–526. doi: 10.1007/s12031-018-1121-3

Vogel, D. D. S., Ortiz-Villatoro, N. N., Araujo, N. S., Marques, M. J. G., Aimbire, F., Scorza, F. A., et al. (2021). Transcranial low-level laser therapy in an *in vivo* model of stroke: relevance to the brain infarct, microglia activation and neuroinflammation. *J. Biophotonics* 14:e202000500. doi: 10.1002/jbio.202000500

von Leden, R. E., Cooney, S. J., Ferrara, T. M., Zhao, Y., Dalgard, C. L., Anders, J. J., et al. (2013). 808 nm wavelength light induces a dose-dependent alteration in microglial polarization and resultant microglial induced neurite growth. *Lasers Surg. Med.* 45, 253–263. doi: 10.1002/lsm.22133

Wang, Q., Sun, A. Y., Simonyi, A., Jensen, M. D., Shelat, P. B., Rottinghaus, G. E., et al. (2005). Neuroprotective mechanisms of curcumin against cerebral ischemia-induced neuronal apoptosis and behavioral deficits. *J. Neurosci. Res.* 82, 138–148. doi: 10.1002/jnr.20610

Wang, R., Dong, Y., Lu, Y., Zhang, W., Brann, D. W., and Zhang, Q. (2019). Photobiomodulation for Global Cerebral Ischemia: targeting Mitochondrial Dynamics and Functions. *Mol. Neurobiol.* 56, 1852–1869. doi: 10.1007/s12035-018-1191-9

Wu, K. J., Yu, S., Lee, J. Y., Hoffer, B., and Wang, Y. (2017). Improving Neurorepair in Stroke Brain Through Endogenous Neurogenesis-Enhancing Drugs. *Cell Transpl.* 26, 1596–1600. doi: 10.1177/0963689717721230

Xu, H., Wang, Z., Li, J., Wu, H., Peng, Y., Fan, L., et al. (2017). The Polarization States of Microglia in TBI: a New Paradigm for Pharmacological Intervention. *Neural Plast.* 2017:5405104. doi: 10.1155/2017/5405104

Xuan, W., Agrawal, T., Huang, L., Gupta, G. K., and Hamblin, M. R. (2015). Low-level laser therapy for traumatic brain injury in mice increases brain derived neurotrophic factor (BDNF) and synaptogenesis. *J. Biophotonics* 8, 502–511. doi: 10.1002/jbio.201400069

Xuan, W., Huang, L., and Hamblin, M. R. (2016). Repeated transcranial low-level laser therapy for traumatic brain injury in mice: biphasic dose response and long-term treatment outcome. *J. Biophotonics* 9, 1263–1272. doi: 10.1002/jbio.201500336

Xuan, W., Vatansever, F., Huang, L., and Hamblin, M. R. (2014). Transcranial low-level laser therapy enhances learning, memory, and neuroprogenitor cells after traumatic brain injury in mice. *J. Biomed. Opt.* 19:108003. doi: 10.1117/1.JBO.19.10.108003

Zhou, C., Tu, J., Zhang, Q., Lu, D., Zhu, Y., Zhang, W., et al. (2011). Delayed ischemic postconditioning protects hippocampal CA1 neurons by preserving mitochondrial integrity via Akt/GSK3beta signaling. *Neurochem. Int.* 59, 749–758. doi: 10.1016/j.neuint.2011.08.008

**Conflict of Interest:** The authors declare that the research was conducted in the absence of any commercial or financial relationships that could be construed as a potential conflict of interest.

**Publisher's Note:** All claims expressed in this article are solely those of the authors and do not necessarily represent those of their affiliated organizations, or those of the publisher, the editors and the reviewers. Any product that may be evaluated in this article, or claim that may be made by its manufacturer, is not guaranteed or endorsed by the publisher.

frontiers in Cellular Neuroscience

ORIGINAL RESEARCH
published: 26 August 2021
doi: 10.3389/fncel.2021.699736

# Profiling of Blood-Brain Barrier Disruption in Mouse Intracerebral Hemorrhage Models: Collagenase Injection vs. Autologous Arterial Whole Blood Infusion

*Peijun Jia[1,2], Jinxin He[1], Zefu Li[1], Junmin Wang[1], Lin Jia[1], Ruochen Hao[1], Jonathan Lai[3], Weidong Zang[1], Xuemei Chen[1]* and Jian Wang[1]*

[1] Department of Anatomy, College of Basic Medical Sciences, Zhengzhou University, Zhengzhou, China, [2] School of Life Sciences, Zhengzhou University, Zhengzhou, China, [3] Pre-med Track Majoring in Biology, Baylor University, Waco, TX, United States

OPEN ACCESS

**Edited by:**
Junlei Chang,
Shenzhen Institutes of Advanced Technology, Chinese Academy of Sciences (CAS), China

**Reviewed by:**
Yaohui Tang,
Shanghai Jiao Tong University, China
Guo-He Tan,
Guangxi Medical University, China

***Correspondence:**
Xuemei Chen
chenxm@zzu.edu.cn

**Specialty section:**
This article was submitted to Stem Cell Research, a section of the journal Frontiers in Cellular Neuroscience

**Received:** 24 April 2021
**Accepted:** 16 June 2021
**Published:** 26 August 2021

**Citation:**
Jia P, He J, Li Z, Wang J, Jia L, Hao R, Lai J, Zang W, Chen X and Wang J (2021) Profiling of Blood-Brain Barrier Disruption in Mouse Intracerebral Hemorrhage Models: Collagenase Injection vs. Autologous Arterial Whole Blood Infusion. Front. Cell. Neurosci. 15:699736. doi: 10.3389/fncel.2021.699736

Disruption of the blood-brain barrier (BBB) and the subsequent formation of brain edema is the most severe consequence of intracerebral hemorrhage (ICH), leading to drastic neuroinflammatory responses and neuronal cell death. A better understanding of ICH pathophysiology to develop effective therapy relies on selecting appropriate animal models. The collagenase injection ICH model and the autologous arterial whole blood infusion ICH model have been developed to investigate the pathophysiology of ICH. However, it remains unclear whether the temporal progression and the underlying mechanism of BBB breakdown are similar between these two ICH models. In this study, we aimed to determine the progression and the mechanism of BBB disruption via the two commonly used murine ICH models: the collagenase-induced ICH model (c-ICH) and the double autologous whole blood ICH model (b-ICH). Intrastriatal injection of 0.05 U collagenase or 20 μL autologous blood was used for a comparable hematoma volume in these two ICH models. Then we analyzed BBB permeability using Evan's blue and IgG extravasation, evaluated tight junction (TJ) damage by transmission electron microscope (TEM) and Western blotting, and assessed matrix metalloproteinase-9 (MMP-9) activity and aquaporin 4 (AQP4) mRNA expression by Gelatin gel zymography and RT-PCR, respectively. The results showed that the BBB leakage was associated with a decrease in TJ protein expression and an increase in MMP-9 activity and AQP4 expression on day 3 in the c-ICH model compared with that on day 5 in the b-ICH model. Additionally, using TEM, we found that the TJ was markedly damaged on day 3 in the c-ICH model compared with that on day 5 in the b-ICH model. In conclusion, the BBB was disrupted in the two ICH models; compared to the b-ICH model, the c-ICH model

presented with a more pronounced disruption of BBB at earlier time points, suggesting that the c-ICH model might be a more suitable model for studying early BBB damage and protection after ICH.

**Keywords: intracerebral hemorrhage, collagenase, autologous blood, blood-brain barrier, tight junction, aquaporin 4, matrix metalloproteinase-9, transmission electron microscope**

## INTRODUCTION

Intracerebral hemorrhage (ICH) is the second most common subtype of stroke, and it has a high mortality and disability rate (Wang, 2010; Lan et al., 2017). The pathophysiologic mechanism of ICH is complex, with excessive neuroinflammatory responses due to the activation of immune cells as well as the release of inflammatory cytokines (Hua et al., 2020; Ren et al., 2020; Boltze et al., 2021), which lead to the degradation of the blood-brain barrier (BBB) and neuron death (Yang et al., 2017). Subsequently, BBB disruption further aggravates vasogenic brain edema, facilitates the migration of leukocytes from blood to the brain (Jiang et al., 2020), and causes an influx of potential neurotoxic components from the blood (Madangarli et al., 2019). There has been great interest in maintaining BBB integrity and inhibiting brain inflammation after ICH.

As a dynamic structure, the BBB separates peripheral circulation from the brain. The BBB is composed of brain microvascular endothelial cells (BMECs) and their tight junctions (TJs), basement membranes, pericytes, and astrocyte terminals. Severe inflammation has been shown to have a deleterious effect on the BBB (Varatharaj and Galea, 2017). Additionally, there is evidence that secondary injury induces BMEC cell death and impairment of peri-cellular TJs which result in BBB dysfunction after stroke (Wu et al., 2019).

Many preclinical and clinical research evidence has further shown the progress of pathophysiology in ICH, but truly effective clinical treatments are limited (Ren et al., 2020). The substantial gap in applying preclinical research within clinical applications has not been solved. To study the potential therapeutic targets of BBB after ICH, it is vital to establish an appropriate animal model which directly relates to clinical therapy. Collagenase ICH model (c-ICH) and autologous blood ICH model (b-ICH) are reported to be widely used animal experiment models (Wang, 2010; Liesz et al., 2011; Li and Wang, 2017). However, there are currently no studies to comprehensively compare the cellular molecular markers of BBB disruption in these two animal models of ICH. Therefore, the dynamic changes of BBB components were compared including TJs, matrix metalloproteinases 9 (MMP), and aquaporin 4 (AQP4) after ICH between the two animal models. It is our goal to discover the model most representative of the pathophysiology of ICH patients in the clinic.

The insights gained from this study will enhance our understanding of the underlying mechanism and pathologic progress of ICH, and help determine the best animal model for preclinical ICH research targeting BBB damage and protection.

**Abbreviations:** AQP4, aquaporin 4; BBB, blood brain barrier; BCA, bicinchoninic acid; BMECs, micro-vascular endothelial cells; BWC, brain water content; CV-LFB, cresyl violet and Luxol fast blue; c-ICH, collagenase intracerebral hemorrhage model; b-ICH, autologous blood intracerebral hemorrhage model; EB, Evans blue; ECL, enhanced chemiluminescence; ECs, endothelial cells; ICH, intracerebral hemorrhage; MMP9, matrix metalloproteinases 9; NDS, neurological deficit scores; PB, phosphate buffer; PVDF, polyvinylidene fluoride; SDS-PAGE, sodium dodecyl sulfate polyacrylamide gel electrophoresis; SPF, specific pathogen-free; TEM, Transmission electron microscope; TJ, tight junction; WB, western blotting.

## MATERIALS AND METHODS

### Animals

All animal experiments followed the ARRIVE guidelines[1]. Male mice were used in this study due to the reported hormone levels of male mice, which are more stable than those of the female mice, as shown in a previous study (Hughes, 2007). Animals for each group were randomized with the website[2]. Mice that were 6 months of age are defined as adult mice according to our previous report (Wu et al., 2011). A total number of 213 C57BL/6 male mice (6-month-old, 30–35 g) were used in our study. Mice were purchased from the Beijing Vital River Laboratory Animal Technology Co., Ltd. The mice were housed in a specific pathogen-free environment with 24-h cycles of controlled temperature and relative humidity (45–55%) with normal access to standard food and water. Animals that passed away or were euthanized were excluded from the sample size. All animal experiments were approved by the Animal Ethics Committee of Zhengzhou University and performed according to national guidelines. All assessments were performed by investigators who were blinded to experimental group assignments.

### ICH Mouse Model

The procedure for the two ICH models has been described in previous publications (Wang et al., 2008; Li et al., 2017a; Zhu et al., 2018). In brief, the mice were anesthetized with isoflurane (70% $N_2O$ and 30% $O_2$; 4% induction, 2% maintenance). The mice were then fixed in a stereotaxic instrument with a 1 cm incision made along the sagittal suture. ICH was induced by injecting collagenase VII-S (0.05 U in 0.5 μL sterile saline, Sigma, St. Louis, MO) or 20 μL of blood was drawn from the mice's tail artery and was injected into the left striatum which coordinates were 0.5 mm anterior, 2.1 mm lateral, and 3.1 mm ventral to the bregma. For the sham operation, 0.5 μL of sterile saline was injected. The collagenase was infused with a micro-infusion pump (1 μL, HAMILTON, 80100, United States) at a constant rate of 0.1 μL/min and veinous blood was infused by a 50 μL micro-infusion pump in two-time blocks (7 μL

[1]http://www.nc3rs.org.uk/arrive-guidelines

[2]www.randomization.com

followed by a 10-min pause and then 13 μL followed by a 10-min pause) a rate of 1 μL/min. During the operation, internal body temperature was maintained at 37.0 ± 0.5°C by the body temperature maintenance instrument (Thermo Star, 69020). Mice that died within 24 h after surgery or with a neurological deficit score <4 were excluded from the experiment. The sham mice were treated the same way but were infused with saline. The mice were allowed to recover in separate cages with access to sufficient food and water.

## Neurologic Function

The functional outcome was evaluated using neurologic deficit score (NDS), forelimb and hind limb placing test, and the corner turn test at 6 h, 12 h, days 1, 3, and 5 after ICH. In the NDS system, mice were tested by body symmetry, gait, climbing, circling behavior, front limb symmetry, and compulsory circling. Each test was graded on a scale from 0 to 4, establishing a maximum deficit score of 24 (Li et al., 2017a). Forelimb placement was evaluated by the vibrissae-elicited forelimb placing test. The mice were placed at the edge of the table, and the vibrissae on one side were brushed. The placement was quantified as a percentage of successful responses (placed the contralateral forelimb quickly on the tabletop) in 10 trials (Chang et al., 2014). Hindlimb placing was assessed with the muscle strength of the hind limbs. The animals were placed on the edge of a table and the contralateral hind limb was pulled down. Straighten the hind limbs and given scores according to the retraction time. The test was scored as follows: immediate pullback of limb = 0; delayed pullback = 1; inability to pull back = 2. The placing was quantified in 10 successful trials, and scores were quantified as the total scores of 10 trials (Zhou et al., 2013; Li et al., 2017a). For the corner turn test, the mouse was allowed to proceed into a 30° corner and was allowed to freely turn either left or right when exiting the corner. The choice of direction during 10 repeats was recorded, and the percentage of left turns was calculated (Chang et al., 2014).

## Hemorrhagic Injury Analysis

Mice were euthanized with deep anesthesia using 3% isoflurane and perfused through the left ventricle with saline followed by 4% paraformaldehyde. Coronal brain sections were stained with cresyl violet (CV for neurons, Sigma-Aldrich) or with Luxol fast blue (LFB for myelin) at 20 μM that were spaced 180 μM apart. Sections were digitized and analyzed by Image J software. The injury volume in cubic millimeters was computed by summation of the damaged areas multiplied by the interslice distance (180 μM) (Han et al., 2016; Zhu et al., 2018).

## Brain Water Content Measurement

On day 3 or 5 after ICH, mice were euthanized under deep anesthesia with 3% isoflurane and the brain was harvested and dissected into the ipsilateral, the ipsilateral, and cerebellum, which served as an internal control. The wet weight of the brain was measured immediately and the brain tissue was heated to 100°C in a drying oven for 3 or 5 days before measuring the dry weight. We determined brain edema by calculating brain water content as follows: [(wet weight - dry weight)/wet weight] × 100% (Li et al., 2017c).

## Western Blotting

On 6 h, 12 h, days 1, 3, and 5 after ICH, occluding, cadherin-10 protein expression levels were evaluated by Western blotting (WB) according to our previous studies (Zhao et al., 2015; Wang et al., 2019). The brain tissues were sampled 2–3 mm away from the hematoma and homogenized on ice ice-cold lysis buffer (RIPA: PMSF = 100:1). The total protein count was quantified by bicinchoninic acid (BCA) protein assay (PC0020, Solarbio Science & Technology Co., Ltd., Beijing). Fifty micrograms of protein sample was separated by 10% sodium dodecyl sulfate-polyacrylamide gel electrophoresis (SDS-PAGE) and transferred to polyvinylidene fluoride (PVDF) membrane. After blocking the membrane with the skimmed milk powder, it was incubated with the primary antibodies: rabbit anti-mouse occludin (1:1,000, Abcam, Cambridge, MA), rabbit anti-mouse cadherin-10 (1:1,000, Abcam, Cambridge, MA) (1:1,000, Affinity Biosciences, OH, United States), rabbit anti-mouse GAPDH (1:1,000, Abcam, Cambridge, MA) at 4°C overnight. The membranes were then incubated with HRP-labeled anti-rabbit secondary antibodies (1:10,000, Santa Cruz, Dallas, TX) at room temperature for 2 h. The blots were detected with the Fluor Chem imaging system (San Jose, CA) after immersing in enhanced chemiluminescence (ECL) solution (Solarbio, catalog: PE0010). The relative intensity of protein signals was normalized to the corresponding loading control intensity and quantified by Image J software.

## Gelatin Gel Zymography

Gelatin gel zymography was utilized on 6 h, 12 h, days 1, 3, and 5 post-ICH to measure the MMP-9 (Gelatinase B, 98 kD) gelatinolytic activity in the hemorrhagic brain as previously described (Li et al., 2017b). Protein samples were extracted from the ipsilateral brain area containing the striatum after the c-ICH and b-ICH models. Samples were loaded onto 10% Tris-tricine gels with 0.1% gelatin as a substrate and separated by electrophoresis. Following electrophoresis, gels were washed twice with 2.5% Triton X-100 for 1 h to remove the SDS and incubated 40 h at 37°C in digestion buffer (50 mM Tris–HCl, 50 mM NaCl, 5 mM $CaCl_2$, 2 μM $ZnCl_2$, 0.02% Brij-35, pH = 7.6). Then, the gel was stained with 0.5% wt/vol Coomassie blue R-250 for 2 h and then destained appropriately to be photographed. Bands were visualized with a gel-imaging system (BIO-RAD, United States), and band intensity was quantified with Image J analysis software.

## Quantification of Evans Blue Leakage

A solution of 2% Evans blue (EB) dye (4 mL/kg, Sigma Aldrich, St. Louis, United States) was slowly administered through the tail vein on 6 h, 12 h, days 1, 3, and 5 after ICH as previous describe (Wang et al., 2017; Yang et al., 2017). The mice were euthanized after a 3 h infusion and were then perfused transcardially with PBS. The brain tissue was removed, divided into right and left hemispheres, and weighed. Each part of the brain was homogenized in 1 mL of PBS and then sonicated and centrifuged (30 min, 9,424 g/min, 4°C) and the supernatant was collected. EB stain was measured by spectrophotometry at 620 nm and quantified according to a standard curve (Diluted with different

concentrations of EB dye). The results are presented as the ratio of the left to right hemisphere.

## Measurement of Endogenous Immunoglobulin G (IgG) Extravasation

Immunohistochemical staining was performed according to previously reported methods (Mao et al., 2017). It was used to determine the area of extravasation of endogenous IgG molecules on days 3 and 5 in both ICH models. The mice were anesthetized and intracardially perfused with phosphate-buffered saline, followed by 4% paraformaldehyde. After dehydration, the brain was sliced into 20-mm-thick sections. Sections were blocked with 5% goat serum in phosphate-buffered saline with 0.1% Triton-X 100 for 1 h and were incubated in DyLight$^{TM}$ 488-conjugated goat anti-rat IgG antibody (1:1,000; Jackson Immuno-Research Laboratories, West Grove, United States) at room temperature. Finally, stained sections were examined with a fluorescence microscope (Eclipse TE2000-E; Nikon, Japan).

## Transmission Electron Microscope

The BBB ultrastructure was scanned by transmission electron microscopy (TEM) on 6 h, 12 h, days 1, 3, and 5 after ICH (Li et al., 2017a, 2018). The mice were anesthetized and transcardially perfused with 0.9% saline, followed by a 0.1 M phosphate buffer (PB) containing 2.5% paraformaldehyde and 2% glutaraldehyde. The brain was extracted and divided into 1 mm three pieces and immersed in the same fixative at 4°C overnight. After being washed thoroughly with 7.5% sucrose buffer, samples were post-fixed with 1% osmium tetroxide, at 4°C for 2 h. The tissue proceeded to be block-stained with a 2% aqueous solution of uranyl acetate for 1 h. The tissue was dehydrated with a graded series of ethanol and embedded in acrylic resin. Serial ultrathin sections were cut with an ultramicrotome, stained with lead citrate and uranyl acetate, and observed with an electron microscope (HITACHI, HT7700, Japan). The length and number of the TJ were analyzed by using Image J software.

## Real-Time Polymerase Chain Reaction Analysis

Total mRNA was extracted from the brain tissues around the hematoma by QIAzol Lysis Reagent (miRNeasy Mini Kit; QIAGEN, Gaithersburg, MD) (Li et al., 2017b; Su et al., 2017). One thousand nanograms of RNA from each sample was transcribed into cDNA with the SuperScript VILO cDNA Synthesis Kit (Invitrogen, Carlsbad, United States). Reverse-transcribed RNA was amplified by PCR under the following conditions: 95°C for 5 min, 40 cycles of the 30 s at 94°C, 30 s at 65°C, 20 s at 72°C, and a final extension step for 10 min at 72°C. The quantitative polymerase chain reaction was performed with the Opticon 2 Real-Time Polymerase Chain Reaction Detection System (Bio-Rad, Hercules, United States) using corresponding primers and the SYBR green Polymerase Chain Reaction Master Mix (Applied Biosystems, Waltham, United States). The primer sequences that were utilized are listed in following:

AQP4:
5'- CTTTCTGGAAGGCAGTCTCAG -3' (forward),
5'- CCACACCGAGCAAAACAAAGAT -3' (reverse).
GAPDH:
5'- CAGTGGCAAAGTGGAGATTGTTG -3' (forward),
5'- TCGCTCCTGGAAGATGGTGAT -3' (reverse).

## Statistical Analysis

All data are reported as mean ± SD, dot plots, or bar graphs. One-way or two-way ANOVA and the Bonferroni *post-hoc* test were used to compare differences among multiple groups. All analyses were carried out with GraphPad Prism 5.0 Software. The criterion for statistical significance was $P < 0.05$.

# RESULTS

## The Comparison of Injury Volume Between the c-ICH and the b-ICH Groups

Injecting 20 μL autologous blood or 0.05 U collagenase VII into the left striatum resulted in a similar bleeding volume. Images of fresh brain slices illustrated that the cerebral hemorrhage was located in the striatum at 24 h (**Figure 1A**). LFB/CV staining slides portrayed the injury volume of the c-ICH and b-ICH group and was shown to be identical at 24 h after ICH (**Figure 1B**). The injury volume results further verified that hemorrhage volume had no statistical significance between the two groups (7.570 ± 2.264 $mm^3$ in c-ICH groups vs. 7.493 ± 2.524 $mm^3$ in b-ICH groups; $F = 1.242$, $n = 8$ mice/group, $P > 0.05$; **Figure 1C**). The total mortality of mice throughout the experiment differed between the experimental models in this study. No mice died in the sham group, but the mortality rate of the b-ICH group was shown to be higher than that of the c-ICH [10.20% (10 of 98) group vs. 5.10% (5 of 98) in the b-ICH group; **Figure 1D**]. Both ICH models were associated with a pronounced weight loss compared with the sham mice on days 3 and 5. However, there was no significant difference in the body weight between the c-ICH and b-ICH groups on days 1, 3, and 5 ($P > 0.05$; **Figure 1E**).

## The Comparison of Motor Function Between the c-ICH and the b-ICH Groups

The NDS of the two model groups were significantly higher than those of the sham group which peaked on day 1 and proceeded to decrease gradually. The NDS of the b-ICH group was significantly higher than that of the c-ICH group only at 6 h after surgery (8.111 ± 0.261 in b-ICH groups vs. 6.833 ± 0.386 in c-ICH groups; $n = 12$ mice/group; $P < 0.05$). There was no significant difference at any other time points ($P > 0.05$, $n = 12$ mice/group; **Figure 2A**). Additionally, there were no significant differences in the results of the forelimb and hind limb placement and corner turn test between the two model groups at 6 h, 12 h, days 1, 3, and 5 ($n = 10$ mice/group; $P > 0.05$, **Figures 2B–D**).

## The Comparison of BBB Breakdown Between the c-ICH and the b-ICH Groups

The BBB breakdown was evaluated by EB staining and measurement of IgG extravasation. The EB dye can be combined with albumin (67 kD) in serum and therefore was utilized to

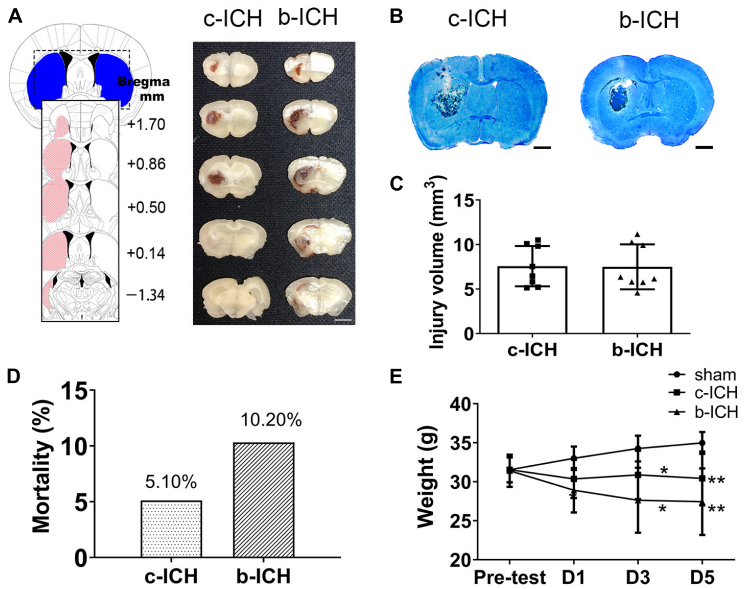


**FIGURE 1 |** The comparison of injury volume between c-ICH and b-ICH groups. **(A)** Left: Schematic illustration of the spatial extent of the striatum. Right: Representative fresh brain sections show hematomas (red areas) at 24 h after intrastriatal injection of 0.050 U collagenase ("Collagenase") or 20 μL autologous blood ("Blood"). **(B)** Representative Luxol fast blue/Cresyl violet-stained brain sections from c-ICH and b-ICH groups (scale bar = 1 mm). **(C)** Injury volume was detected at 24 h after ICH by integration of serial coronal sections stained with Luxol fast blue/Cresyl violet, no difference between the c-ICH and b-ICH model was detected. $n$ = 8 mice/group ($t$-test). **(D)** Overall mortality was determined for all animals used in this study. **(E)** Bodyweight was measured in all groups on days 1, 3, and 5 respectively. $n$ = 12 mice/group. $^{*}P < 0.05$, $^{**}P < 0.01$ vs. sham group (Repeated measures ANOVA followed by Bonferroni *post-hoc* test). Data are expressed as mean ± SD (the repeated measures ANOVA followed by the Bonferroni *post-hoc* test). Values are mean ± SD.

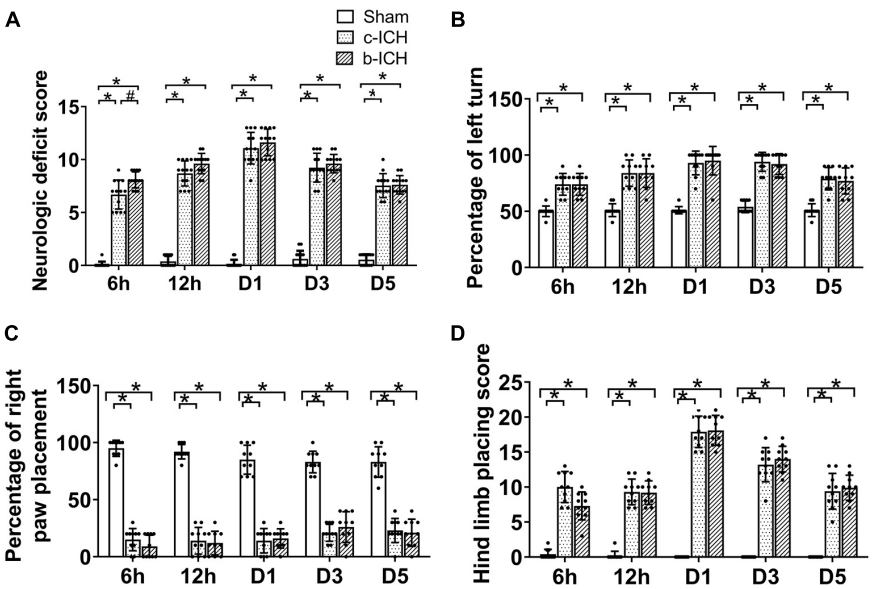


**FIGURE 2 |** Motor function of the two ICH models. **(A)** Mice in the b-ICH group had a more severe neurologic deficit score (NDS) than the c-ICH group at 6 h after ICH. $n$ = 10 mice/group. $^{*}P < 0.05$ vs. sham group; $^{\#}P < 0.05$ vs. ICH group (repeated measures ANOVA followed by Bonferroni *post-hoc* test). **(B–D)** The corner turn test and right front paw and hindlimb placement tests on 6 h, days 1, 3, and 5 after ICH. $n$ = 10 mice/group. $^{*}P < 0.05$ vs. sham group (the repeated measures ANOVA followed by the Bonferroni *post-hoc* test). Values are mean ± SD.

measure the integrity of the BBB at 6 h, 12 h, days 1, 3, and 5 post-ICH. EB leakage was prominent on day 3 in the c-ICH group compared with that on day 5 in the b-ICH group (**Figure 3A**). The quantitative analysis further revealed that the ratio of EB concentration (ipsilateral/contralateral hemisphere) peaked on day 3 in the c-ICH group compared to that on day 5 in the b-ICH

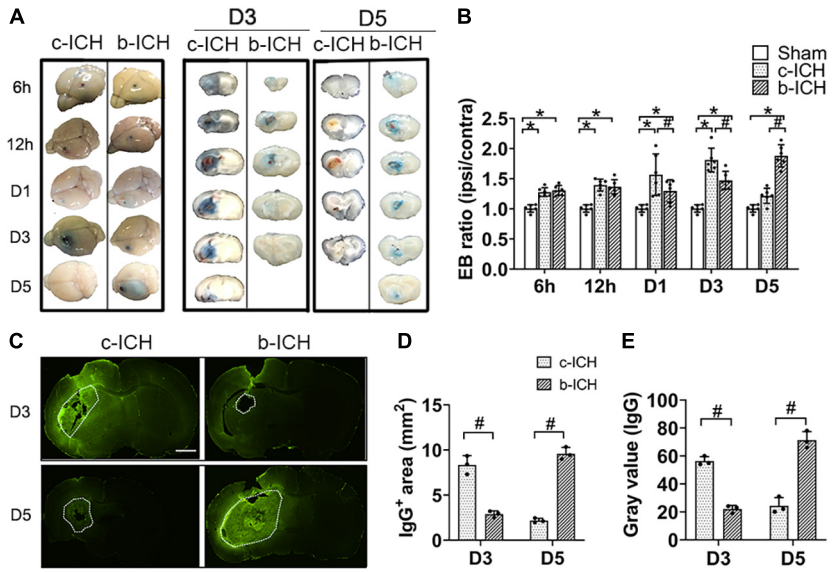


**FIGURE 3 |** The comparison of BBB breakdown between the c-ICH and the b-ICH groups. **(A)** The Evans blue staining showed that BBB leakage was present from 6 h to day 5 after ICH in two groups. **(B)** Quantitative analysis showed that the Evans blue (EB) concentration peaked at day 3 in the c-ICH group but on day 5 in the b-ICH group ($n$ = 6 mice/group for each time point; $^{*}P < 0.05$ vs. sham group, $^{\#}P < 0.05$ vs. the c-ICH group; repeated measures ANOVA followed by Bonferroni *post-hoc* test). **(C)** The IgG-positive area was determined by immunohistochemical staining on days 3 and 5, respectively (scale bar = 1 mm). **(D,E)** Quantification of endogenous IgG-positive area and gray values of IgG immunostaining; $n$ = 3 mice/group; $^{\#}P < 0.05$ vs. c-ICH group ($t$-test). Values are Mean ± SD.

group (D3: 1.783 ± 0.392% in the c-ICH group vs. 1.472 ± 0.149 in the b-ICH group; D5: 1.216 ± 0.216% in the c-ICH group vs. 1.879 ± 0.815 in the b-ICH group; $n$ = 6 mice/group; $P < 0.05$; **Figure 3B**). The EB staining data were further supported by the pronounced intrastriatal leakage of the plasma-derived IgG. The IgG leakage around the hematoma was more prominent in the c-ICH group than in the b-ICH group on day 3, whereas it was more prominent in the b-ICH group than in the c-ICH group on day 5 ($n$ = 3 mice/group; $P < 0.05$; **Figures 3C–E**).

## The Comparison of the Changes of Tight Junction Expression Between the c-ICH and the b-ICH Groups

Endothelial cells (ECs) and their TJs are the primary components of the structure of the BBB. WB was used to detect the protein expression changes of TJs proteins including occludin and cadherin-10 in both ICH groups at 6 h, 12 h, days 1, 3, and 5 after ICH. The results revealed that the expression of occludin and cadherin-10 protein were significantly lower on day 3 in the c-ICH group (occludin: 0.498 ± 0.133% in the c-ICH group vs. 0.764 ± 0.106% in the b-ICH group; cadherin-10: 0.411 ± 0.136% in c-ICH group vs. 0.753 ± 0.058% in b-ICH group; $P < 0.05$; $n$ = 6 mice/group) and on day 5 in the b-ICH group (occludin: 0.819 ± 0.178% in the c-ICH group vs. 0.647 ± 0.067% in the b-ICH group; cadherin-10: 0.738 ± 0.189% in the c-ICH group vs. 0.615 ± 0.133% in the b-ICH group; $P < 0.05$; $n$ = 6 mice/group; **Figure 4A**). Reduction and the breaking of TJs in ECs after ICH was further confirmed by TEM. The ultrastructural changes of BBB were observed at 6 h, 12 h, days 1, 3, and 5 after ICH. Mice in the sham group showed intact and normal capillary endothelial cells as well as basal lamina. A high density of undamaged TJs was observed in the sham group (**Figure 4B**). However, BBB ultrastructural was dramatically damaged at the beginning of the 6th hour after ICH. The ECs were swollen, and TJs were shorter and blurred. Moreover, the basement membrane was thinner compared to the sham control (**Figure 4B**). Among them, the shortest width of TJs appeared on day 3 in the c-ICH group but on day 5 in the b-ICH group (day 3: 0.390 ± 0.036 in the c-ICH group vs. 0.827 ± 0.159 in the b-ICH group; day 5: 0.767 ± 0.10 in the c-ICH group vs. 0.298 ± 0.057 in the b-ICH group; $P < 0.05$; $n$ = 3 mice/group; **Figure 4C**). There was no difference in the total numbers of TJs per vessel ($P > 0.05$; **Figure 4D**).

## The Comparison of the Expressions of Aquaporin 4 (AQP4) and MMP-9 Activity in Brain Tissue Between the c-ICH and the b-ICH Groups

Brain water content in the ipsilateral brain tissue in the c-ICH group was more severe than that in the b-ICH group on day 3 (82.012 ± 2.077% in the c-ICH group vs. 79.638 ± 0.803% in the b-ICH group; $P < 0.05$; $n$ = 6 mice/group; **Figure 5A**) whereas it was more severe in the b-ICH group than that in the c-ICH group on day 5 (78.646 ± 0.944% in the c-ICH group vs. 80.392 ± 1.058% in the b-ICH group; $P < 0.05$; $n$ = 6 mice/group; **Figure 5B**). The MMP-9 activity was detected by the gelatin zymography at 6 h, 12 h, days 1, 3, and 5 after ICH. The results showed that MMP-9 activity began to increase on day 1 after ICH in both models and it reached its peak on day 3 in the c-ICH group (4.575 ± 0.195% in the c-ICH group vs. 2.82 ± 0.39% in

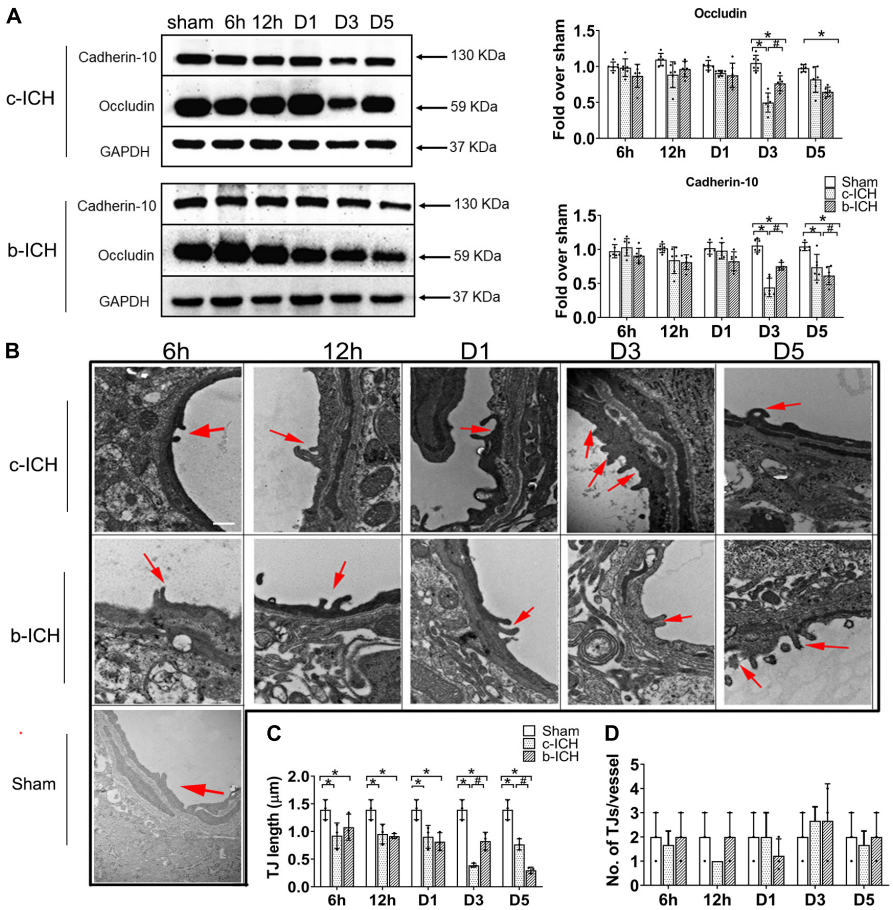


**FIGURE 4 |** The comparison of the expressions of tight junction proteins between c-ICH and b-ICH groups. **(A)** Western blots showed occludin expression and cadherin-10 expression at 6 h, 12 h, days 1, 3, and 5 after ICH. Quantification of occluding and cadherin-10 levels at 6 h, 12 h, day 1, day 3, and day 5 after ICH in both models ($n$ = 6 mice/group; $^{*}P < 0.05$ vs. sham group, $^{\#}P < 0.05$ vs. c-ICH group; repeated measures ANOVA followed by Bonferroni *post-hoc* test). Values are mean ± SD. **(B)** Representative electron microscopic images of TJ ultrastructure at 6 h, 12 h, day 1, day 3, and day 5 after ICH in both models and sham group. Arrowheads = tight junctions (TJ); Scale bar = 1 μM. **(C)** Quantification of tight junction length ($n$ = 3/group). **(D)** Quantification of the number of tight junctions per vessel ($n$ = 3 mice/group, four image fields quantified per mouse; $^{*}P < 0.05$ vs. sham group, $^{\#}P < 0.05$ vs. c-ICH group (the repeated measures ANOVA followed by the Bonferroni *post-hoc* test). Values are mean ± SD.

the b-ICH group; $P < 0.05$) and on day 5 in the b-ICH group (3.517 ± 0.337% vs. 1.668 ± 0.516%; $P < 0.05$; $n$ = 6 mice/group; **Figure 5B**). At 6 h, 12 h, days 1, 3, and 5 after ICH, compared to the sham group, the relative expression of AQP4 mRNA began to increase on day 3 in the c-ICH group, and the expression was significantly higher than that in the b-ICH group (2.349 ± 0.305% vs. 1.251 ± 0.453%; $P < 0.05$). However, the relative expression of AQP4 mRNA was significantly higher in the b-ICH group than that in the c-ICH group on day 5 (6.491 ± 0.678% vs. 2.974 ± 0.399%; $P < 0.05$; $n$ = 3 mice/group; **Figure 5C**).

## DISCUSSION

In this study, we found that the BBB leakage was associated with a decrease in TJ protein expression and an increase in MMP-9 activity and AQP4 mRNA expression on day 3 in the c-ICH model but on day 5 in the b-ICH model. Additionally, utilizing TEM, we demonstrated that the ECs were swollen, and TJs were shorter and blurred after ICH compared to sham controls. Moreover, the basement membrane was thinner in the c-ICH model on day 3 compared to that in the b-ICH model on day 5. Therefore, combined with the characteristics of clinical ICH patients with locally elevated perihematomal permeability-surface area product (PS) derived from computed tomographic perfusion (CTP) imaging within 24 to 72 h after ICH (Xu et al., 2017), we conclude that the c-ICH model might be a more suitable model for studying early BBB damage and protection comparing to the b-ICH model.

The high morbidity and mortality of ICH promote the development of various ICH animal models in preclinical studies (Strbian et al., 2008; Li and Wang, 2017). It is speculated that a better model is the one that closely simulates the pathophysiology and functional consequences of ICH in humans. Infusions of autologous blood or collagenase are the most widely used rodent models to investigate pathophysiologic mechanisms and test

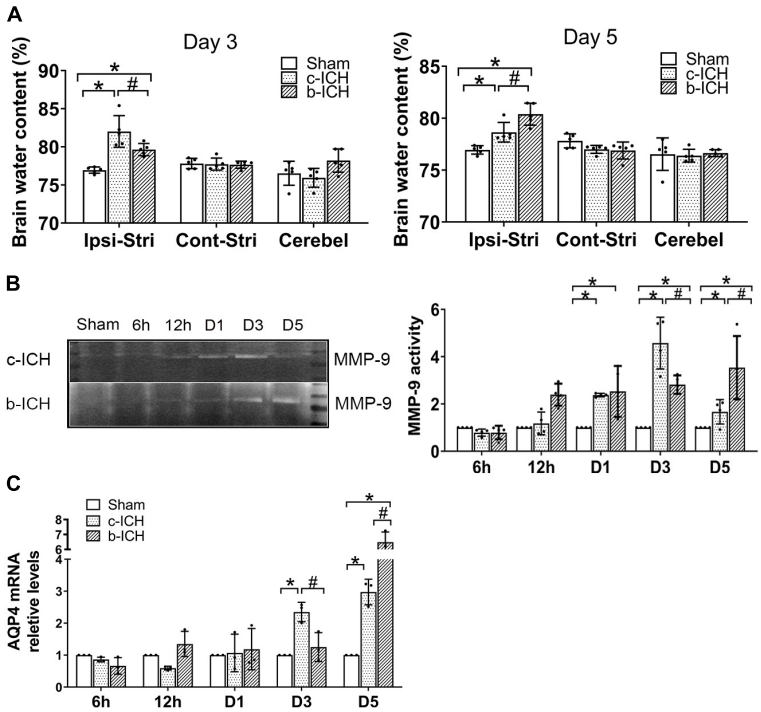


**FIGURE 5 |** The comparison of the expressions of aquaporin 4 (AQP4) and MMP-9 activity in brain tissue between c-ICH and b-ICH groups. **(A)** Measurement of brain water content on days 3 and 5 ($n$ = 6 mice/group; $^{*}P < 0.05$ vs. sham group, $^{\#}P < 0.05$ vs. the c-ICH group repeated measures ANOVA followed by Bonferroni *post-hoc* test). Cont-Stri, contralateral striatum; Ipsi-Stri, ipsilateral striatum. Values are mean ± SD. **(B)** Gelatin zymography shows MMP-9 activity in brain tissue at 6 h, 12 h, day 1, day 3, and day 5 after ICH in both models. Quantification of MMP-9 activity in the brain ($n$ = 4 mice/group, $^{*}P < 0.05$ vs. sham group, $^{\#}P < 0.05$ vs. the c-ICH group; the repeated measures ANOVA followed by the Bonferroni *post-hoc* test). **(C)** Quantification of AQP4 mRNA levels in the brain at 6 h, 12 h, day 1, day 3, and day 5 after ICH in the c-ICH and the b-ICH groups ($n$ = 3 mice/group, four fields quantified per mouse; $^{*}P < 0.05$ vs. sham group, $^{\#}P < 0.05$ vs. the c-ICH group; the repeated measures ANOVA followed by the Bonferroni *post-hoc* test). Values are mean ± SD.

experimental treatments after ICH (MacLellan et al., 2008). The b-ICH model that mimics a single intracerebral bleed can be applied to transgenic or knockout mice to study its specific signaling pathway or brain injury mechanism (Rynkowski et al., 2008). However, the model lacks underlying angiopathy and rupture (Wang et al., 2008). The c-ICH model utilizes enzymatic disruption of blood vessels to imitate spontaneous ICH. However, the induced bleeding is usually caused by the rupture of the large vessels, while the clinical ICH patients often have small deep penetrating artery rupture (Chu et al., 2004). During the operation of our experiment, we found that collecting enough blood quickly within 1 min is a key step to ensure the success of the b-ICH model.

In the early stage after ICH, the motor function of mice was slightly different between the c-ICH group and the b-ICH group. The mortality rate of b-ICH is higher than that of c-ICH (5.10 vs. 10.20%) in our study, which may be due to the direct space-occupying effect of brain tissue caused by the direct injection of hematoma pressure, increasing the death rate of animals. Based on our experience, the NSS is higher in the b-ICH group than that in the c-ICH group in the early time points (1–6 h) after ICH. A probable reason for this discrepancy may be that blood vessel damage by collagenase is a dynamic process, and consequently, blood accumulates and hematoma develops in the striatum gradually within 4–5 h (Liebner and Plate, 2010; Wang et al., 2015), which results in delayed neurologic deficits. The difference in early neurologic impairment cannot be detected by the other three behavioral tests, suggesting that the 24-point neurologic deficit scoring system is more sensitive for evaluating locomotor abnormalities, especially at early time points after ICH. The result is consistent with our previous research (Zhu et al., 2018). In the clinic, acutely increased intracranial pressure (ICP) after ICH is a life-threatening neurosurgical emergency (Leinonen et al., 2017). In addition, the dynamics of perihematomal edema (PHE) induced by BBB integrity occurs within hours after ICH, which has been implicated in secondary brain injury and could be a therapeutic target (Sprugel et al., 2019). In our research, we found that brain water content in the ipsilateral brain tissue in the c-ICH group was higher than that in the b-ICH group on day 3, whereas it was higher in the b-ICH group than that in the c-ICH group on day 5, indicating that both models can imitate the clinical PHE occurred after ICH. All inflammation, thrombin activation, and red blood cell lysis can lead to BBB destruction and edema formation, which has three stages: (1) clot retraction can force the serum into the surrounding space of hematoma and form angiogenic edema (1 h after ICH); (2) cytotoxic brain edema (peak D1-2) caused by inflammation and thrombin activation through coagulation cascade reaction; and (3) erythropoietin

cytolysis and Hb toxicity related injury (delay) appeared edema on D3 (Zheng et al., 2016).

BBB, consisting of endothelial cells, pericytes, astrocytes, basement membrane, and extracellular matrix (Lv et al., 2018), is an important component of NVU that plays a crucial role in maintaining the homeostasis of the CNS but limits the number of potential therapeutic drugs capable of gaining access to the brain. Thus, it is important to study the characteristics of BBB injury for the treatment of nervous system diseases. We compared the BBB damage at 6 h, 12 h, 24 h, day 3, and day 5 after ICH between the two most common murine ICH models based on the similar injury volume. In our study, EB extravasation assay showed that an increase in leakage at 6 h in both models and the ratio of EB concentration (ipsilateral/contralateral hemisphere) peaked on day 3 in the c-ICH model whereas on day 5 in the b-ICH model, which was consistent with our previous study using the c-ICH model (Yang et al., 2017). In contrast to EB, the IgG (∼140 kD) extravasation was prominent around the hematoma on day 3 in the c-ICH group and day 5 in the b-ICH group after ICH. However, the exact mechanism of the IgG leakage after hemorrhage is still unclear. Transcellular mechanisms may contribute to IgG (∼140 kD) extravasation after ICH. FcRnh (The neonatal Fc receptor for IgG) and low-density lipoprotein receptor-related protein 1 (LRP1) that both expressed on BBB mediates the efflux of IgG across the BBB and facilitate IVIg internalization (Halliday et al., 2016).

MMPs are a group of important extracellular matrix-degrading enzymes, with various biologic functions. Thrombin, hemoglobin, cytokines, oxidative stress, hypoxia, and other factors can lead to increased expression/activity of MMPs (Wang, 2010). MMPs are a family of proteases that participate in physiologic and pathophysiologic processes, including at the BBB interface. It is shown that MMP-9 expression/activity is increased in the human ICH brain (Wu et al., 2010a). Once activated, MMPs disrupt the BBB by degrading tight junctions and basal lamina proteins, leading to BBB leakage and brain edema. We have reported in an early study that post-ICH application of GM6001 (a broad-spectrum MMP inhibitor) protected BBB and reduced brain edema, thereby mitigating neurologic deficits (Wang and Tsirka, 2005). Furthermore, knockout of the MMP-9 gene significantly decreases IgG accumulation in the parenchyma 24 h after neonatal H/I, suggesting that MMP-9 contributes to the early BBB opening. In addition, it is reported that Hb-induced oxidative stress after ICH may contribute to early BBB dysfunction and subsequent cell death through MMP activation (Katsu et al., 2010). Aquaporin-4 (AQP4) is expressed in pericapillary astrocyte foot processes and contributes to edema formation after ICH (Wu et al., 2010b). Prior research suggests that AQP4 deletion increases ICH damage, including edema formation, BBB damage, and neuronal death (Chu et al., 2014). There also is a significant increase in AQP4 expression in ICH patients (Dardiotis et al., 2019). In our research, by comparing MMP-9 enzymatic activity and APQ4 mRNA levels between the c-ICH model and the b-ICH model after ICH, we found that the MMP9 activity reached the peak on day 3 in the c-ICH group and on day 5 in the b-ICH group. Furthermore, the relative expression of AQP4 mRNA began to increase on day 3 in the c-ICH group while on day 5 in the b-ICH group. In conclusion, we are the first study to report that the severe BBB injury occurred on day 5 in the b-ICH model which has guiding value for future b-ICH research.

In this study, we examined the ultrastructural features of the mouse brain after collagenase- and whole blood-induced ICH. Both models share pathologic similarities in terms of basement membrane damage and TJ fracture at 6 h after ICH. However, the collagenase injection model does have the most serious TJ damage on day 3 and the blood injection model does have on day 5. Using TEM, we observed that the ECs were swollen, and TJs were shorter and blurred; furthermore, the basement membrane was thinner on day 3 in the c-ICH group and on day 5 in the b-ICH group, respectively. We also observed axonal demyelination and degeneration after ICH in both models.

## CONCLUSION

In conclusion, the progression of the BBB damage differs in the c-ICH and the b-ICH model; the BBB damage occurs earlier in the c-ICH model than that in the b-ICH model. The underlying mechanism of BBB breakdown is similar between these two ICH models. Combined with the characteristics of clinical ICH with a prominent increase in BBB leakage in the perihematomal regions of the patients with spontaneous basal ganglia ICH within 24–72 h after symptom onset (Li et al., 2018), we can conclude that the c-ICH model might be a more suitable model for studying early BBB damage and protection than the b-ICH model.

## DATA AVAILABILITY STATEMENT

The original contributions presented in the study are included in the article/**Supplementary Material**, further inquiries can be directed to the corresponding author/s.

## ETHICS STATEMENT

The animal study was reviewed and approved by the Animal Ethics Committee of Zhengzhou University and followed the ARRIVE guidelines.

## AUTHOR CONTRIBUTIONS

PJ performed the experiments and wrote and revised the manuscript. XC and JiW supervised the research and wrote

and revised the manuscript. All the authors participated in commenting on and approving the final manuscript.

## FUNDING

XC was supported by the National Natural Science Foundation of China (U1704166) and the Key Project of Science and Technology of the Department of Science and Technology of Henan Province (Grant No. 212102310220).

## SUPPLEMENTARY MATERIAL

The Supplementary Material for this article can be found online at: https://www.frontiersin.org/articles/10.3389/fncel.2021.699736/full#supplementary-material

**Supplementary Figure 1 |** Experimental design route. NFE, Neurologic function evaluations; EB, Evans's blue; WB, Western blot; TEM, Transmission electron microscope; GEZ, Gelatin gel zymography; CV-LFB, cresyl violet and Luxol fast blue; HIA, Hemorrhagic injury analysis; IgG ET, IgG extravasation test.

## REFERENCES

Boltze, J., Aronowski, J. A., Badaut, J., Buckwalter, M. S., Caleo, M., Chopp, M., et al. (2021). New Mechanistic Insights, Novel Treatment Paradigms, and Clinical Progress in Cerebrovascular Diseases. *Front. Aging Neurosci.* 13:623751. doi: 10.3389/fnagi.2021.623751

Chang, C. F., Cho, S., and Wang, J. (2014). (-)-Epicatechin protects hemorrhagic brain via synergistic Nrf2 pathways. *Ann. Clin. Transl. Neurol.* 1, 258–271. doi: 10.1002/acn3.54

Chu, H., Xiang, J., Wu, P., Su, J., Ding, H., Tang, Y., et al. (2014). The role of aquaporin 4 in apoptosis after intracerebral hemorrhage. *J. Neuroinflam.* 11:184. doi: 10.1186/s12974-014-0184-5

Chu, K., Jeong, S. W., Jung, K. H., Han, S. Y., Lee, S. T., Kim, M., et al. (2004). Celecoxib induces functional recovery after intracerebral hemorrhage with reduction of brain edema and perihematomal cell death. *J. Cereb. Blood Flow Metab.* 24, 926–933. doi: 10.1097/01.wcb.0000130866.25040.7d

Dardiotis, E., Siokas, V., Marogianni, C., Aloizou, A. M., Sokratous, M., Paterakis, K., et al. (2019). AQP4 tag SNPs in patients with intracerebral hemorrhage in Greek and Polish population. *Neurosci. Lett.* 696, 156–161. doi: 10.1016/j.neulet.2018.12.025

Halliday, M. R., Rege, S. V., Ma, Q., Zhao, Z., Miller, C. A., Winkler, E. A., et al. (2016). Accelerated pericyte degeneration and blood-brain barrier breakdown in apolipoprotein E4 carriers with Alzheimer's disease. *J. Cereb. Blood Flow Metab.* 36, 216–227. doi: 10.1038/jcbfm.2015.44

Han, X., Lan, X., Li, Q., Gao, Y., Zhu, W., Cheng, T., et al. (2016). Inhibition of prostaglandin E2 receptor EP3 mitigates thrombin-induced brain injury. *J. Cereb. Blood Flow Metab.* 36, 1059–1074. doi: 10.1177/0271678x15606462

Hua, W., Chen, X., Wang, J., Zang, W., and Wang, J. (2020). Mechanisms and potential therapeutic targets for spontaneous intracerebral hemorrhage. *Brain Hemorrhages* 1, 99–104.

Hughes, R. N. (2007). Sex does matter: comments on the prevalence of male-only investigations of drug effects on rodent behaviour. *Behav. Pharmacol.* 18, 583–589. doi: 10.1097/FBP.0b013e3282eff0e8

Jiang, C., Wang, Y., Hu, Q., Shou, J., Zhu, L., Tian, N., et al. (2020). Immune changes in peripheral blood and hematoma of patients with intracerebral hemorrhage. *FASEB J.* 34, 2774–2791. doi: 10.1096/fj.201902478R

Katsu, M., Niizuma, K., Yoshioka, H., Okami, N., Sakata, H., and Chan, P. H. (2010). Hemoglobin-induced oxidative stress contributes to matrix metalloproteinase activation and blood-brain barrier dysfunction in vivo. *J. Cereb. Blood Flow Metab.* 30, 1939–1950. doi: 10.1038/jcbfm.2010.45

Lan, X., Han, X., Li, Q., Yang, Q. W., and Wang, J. (2017). Modulators of microglial activation and polarization after intracerebral haemorrhage. *Nat. Rev. Neurol.* 13, 420–433. doi: 10.1038/nrneurol.2017.69

Leinonen, V., Vanninen, R., and Rauramaa, T. (2017). Raised intracranial pressure and brain edema. *Handb. Clin. Neurol.* 145, 25–37. doi: 10.1016/B978-0-12-802395-2.00004-3

Li, Q., Han, X., Lan, X., Gao, Y., Wan, J., Durham, F., et al. (2017a). Inhibition of neuronal ferroptosis protects hemorrhagic brain. *JCI Insight* 2:e90777. doi: 10.1172/jci.insight.90777

Li, Q., Han, X., Lan, X., Hong, X., Li, Q., Gao, Y., et al. (2017b). Inhibition of tPA-induced hemorrhagic transformation involves adenosine A2b receptor activation after cerebral ischemia. *Neurobiol. Dis.* 108, 173–182. doi: 10.1016/j.nbd.2017.08.011

Li, Q., Wan, J., Lan, X., Han, X., Wang, Z., and Wang, J. (2017c). Neuroprotection of brain-permeable iron chelator VK-28 against intracerebral hemorrhage in mice. *J. Cereb. Blood Flow Metab.* 37, 3110–3123. doi: 10.1177/0271678x17709186

Li, Q., and Wang, J. (2017). Animal Models: Cerebral Hemorrhage. *Primer Cerebrovasc. Dis.* 2017, 306–311.

Li, Q., Weiland, A., Chen, X., Lan, X., Han, X., Durham, F., et al. (2018). Ultrastructural Characteristics of Neuronal Death and White Matter Injury in Mouse Brain Tissues After Intracerebral Hemorrhage: Coexistence of Ferroptosis, Autophagy, and Necrosis. *Front. Neurol.* 9:581. doi: 10.3389/fneur.2018.00581

Liebner, S., and Plate, K. H. (2010). Differentiation of the brain vasculature: the answer came blowing by the Wnt. *J. Angiogenes Res.* 2:1. doi: 10.1186/2040-2384-2-1

Liesz, A., Middelhoff, M., Zhou, W., Karcher, S., Illanes, S., and Veltkamp, R. (2011). Comparison of humoral neuroinflammation and adhesion molecule expression in two models of experimental intracerebral hemorrhage. *Exp. Transl. Stroke Med.* 3:11. doi: 10.1186/2040-7378-3-11

Lv, J., Hu, W., Yang, Z., Li, T., Jiang, S., Ma, Z., et al. (2018). Focusing on claudin-5: A promising candidate in the regulation of BBB to treat ischemic stroke. *Prog. Neurobiol.* 161, 79–96. doi: 10.1016/j.pneurobio.2017.12.001

MacLellan, C. L., Silasi, G., Poon, C. C., Edmundson, C. L., Buist, R., Peeling, J., et al. (2008). Intracerebral hemorrhage models in rat: comparing collagenase to blood infusion. *J. Cereb. Blood Flow Metab.* 28, 516–525. doi: 10.1038/sj.jcbfm.9600548

Madangarli, N., Bonsack, F., Dasari, R., and Sukumari-Ramesh, S. (2019). Intracerebral Hemorrhage: Blood Components and Neurotoxicity. *Brain Sci.* 9:11. doi: 10.3390/brainsci9110316

Mao, L., Li, P., Zhu, W., Cai, W., Liu, Z., Wang, Y., et al. (2017). Regulatory T cells ameliorate tissue plasminogen activator-induced brain haemorrhage after stroke. *Brain* 140, 1914–1931. doi: 10.1093/brain/awx111

Ren, H., Han, R., Chen, X., Liu, X., Wan, J., Wang, L., et al. (2020). Potential therapeutic targets for intracerebral hemorrhage-associated inflammation: An update. *J. Cereb. Blood Flow Metab.* 40, 1752–1768. doi: 10.1177/0271678x20923551

Rynkowski, M. A., Kim, G. H., Komotar, R. J., Otten, M. L., Ducruet, A. F., Zacharia, B. E., et al. (2008). A mouse model of intracerebral hemorrhage using autologous blood infusion. *Nat. Protoc.* 3, 122–128. doi: 10.1038/nprot.2007.513

Sprugel, M. I., Kuramatsu, J. B., Volbers, B., Gerner, S. T., Sembill, J. A., Madzar, D., et al. (2019). Perihemorrhagic edema: Revisiting hematoma volume, location, and surface. *Neurology* 93, e1159–e1170. doi: 10.1212/WNL.0000000000008129

Strbian, D., Durukan, A., and Tatlisumak, T. (2008). Rodent models of hemorrhagic stroke. *Curr. Pharm. Des.* 14, 352–358. doi: 10.2174/138161208783497723

Su, S., Shao, J., Zhao, Q., Ren, X., Cai, W., Li, L., et al. (2017). MiR-30b Attenuates Neuropathic Pain by Regulating Voltage-Gated Sodium Channel Nav1.3 in Rats. *Front. Mol. Neurosci.* 10:126. doi: 10.3389/fnmol.2017.00126

Varatharaj, A., and Galea, I. (2017). The blood-brain barrier in systemic inflammation. *Brain Behav. Immun.* 60, 1–12. doi: 10.1016/j.bbi.2016.03.010

Wang, J. (2010). Preclinical and clinical research on inflammation after intracerebral hemorrhage. *Prog. Neurobiol.* 92, 463–477. doi: 10.1016/j.pneurobio.2010.08.001

Wang, J., Fields, J., and Doré, S. (2008). The development of an improved preclinical mouse model of intracerebral hemorrhage using double infusion of autologous whole blood. *Brain Res.* 1222, 214–221. doi: 10.1016/j.brainres.2008.05.058

Wang, J., Jiang, C., Zhang, K., Lan, X., Chen, X., Zang, W., et al. (2019). Melatonin receptor activation provides cerebral protection after traumatic brain injury by mitigating oxidative stress and inflammation via the Nrf2 signaling pathway. *Free Radic. Biol. Med.* 131, 345–355. doi: 10.1016/j.freeradbiomed.2018.12.014

Wang, J., and Tsirka, S. E. (2005). Neuroprotection by inhibition of matrix metalloproteinases in a mouse model of intracerebral haemorrhage. *Brain* 128, 1622–1633. doi: 10.1093/brain/awh489

Wang, M., Hong, X., Chang, C. F., Li, Q., Ma, B., Zhang, H., et al. (2015). Simultaneous detection and separation of hyperacute intracerebral hemorrhage and cerebral ischemia using amide proton transfer MRI. *Magn. Reson Med.* 74, 42–50. doi: 10.1002/mrm.25690

Wang, W., Li, M., Wang, Y., Wang, Z., Zhang, W., Guan, F., et al. (2017). GSK-3β as a target for protection against transient cerebral ischemia. *Int. J. Med. Sci.* 14, 333–339. doi: 10.7150/ijms.17514

Wu, H., Wu, T., Xu, X., Wang, J., and Wang, J. (2011). Iron toxicity in mice with collagenase-induced intracerebral hemorrhage. *J. Cereb. Blood Flow Metab.* 31, 1243–1250. doi: 10.1038/jcbfm.2010.209

Wu, H., Zhang, Z., Hu, X., Zhao, R., Song, Y., Ban, X., et al. (2010a). Dynamic changes of inflammatory markers in brain after hemorrhagic stroke in humans: a postmortem study. *Brain Res.* 1342, 111–117. doi: 10.1016/j.brainres.2010.04.033

Wu, H., Zhang, Z., Li, Y., Zhao, R., Li, H., Song, Y., et al. (2010b). Time course of upregulation of inflammatory mediators in the hemorrhagic brain in rats: correlation with brain edema. *Neurochem. Int.* 57, 248–253. doi: 10.1016/j.neuint.2010.06.002

Wu, X., Fu, S., Liu, Y., Luo, H., Li, F., Wang, Y., et al. (2019). NDP-MSH binding melanocortin-1 receptor ameliorates neuroinflammation and BBB disruption through CREB/Nr4a1/NF-kappaB pathway after intracerebral hemorrhage in mice. *J. Neuroinflam.* 16:192. doi: 10.1186/s12974-019-1591-4

Xu, H., Li, R., Duan, Y., Wang, J., Liu, S., Zhang, Y., et al. (2017). Quantitative assessment on blood-brain barrier permeability of acute spontaneous intracerebral hemorrhage in basal ganglia: a CT perfusion study. *Neuroradiology* 59, 677–684. doi: 10.1007/s00234-017-1852-9

Yang, J., Li, Q., Wang, Z., Qi, C., Han, X., Lan, X., et al. (2017). Multimodality MRI assessment of grey and white matter injury and blood-brain barrier disruption after intracerebral haemorrhage in mice. *Sci. Rep.* 7:40358. doi: 10.1038/srep40358

Zhao, X., Wu, T., Chang, C. F., Wu, H., Han, X., Li, Q., et al. (2015). Toxic role of prostaglandin E2 receptor EP1 after intracerebral hemorrhage in mice. *Brain Behav. Immun.* 46, 293–310. doi: 10.1016/j.bbi.2015.02.011

Zheng, H., Chen, C., Zhang, J., and Hu, Z. (2016). Mechanism and Therapy of Brain Edema after Intracerebral Hemorrhage. *Cerebrovasc. Dis.* 42, 155–169. doi: 10.1159/000445170

Zhou, J., Zhuang, J., Li, J., Ooi, E., Bloom, J., Poon, C., et al. (2013). Long-term post-stroke changes include myelin loss, specific deficits in sensory and motor behaviors and complex cognitive impairment detected using active place avoidance. *PLoS One* 8:e57503. doi: 10.1371/journal.pone.0057503

Zhu, W., Gao, Y., Wan, J., Lan, X., Han, X., Zhu, S., et al. (2018). Changes in motor function, cognition, and emotion-related behavior after right hemispheric intracerebral hemorrhage in various brain regions of mouse. *Brain Behav. Immun.* 69, 568–581. doi: 10.1016/j.bbi.2018.02.004

**Conflict of Interest:** The authors declare that the research was conducted in the absence of any commercial or financial relationships that could be construed as a potential conflict of interest.

**Publisher's Note:** All claims expressed in this article are solely those of the authors and do not necessarily represent those of their affiliated organizations, or those of the publisher, the editors and the reviewers. Any product that may be evaluated in this article, or claim that may be made by its manufacturer, is not guaranteed or endorsed by the publisher.

frontiers in Cellular Neuroscience

REVIEW
published: 24 September 2021
doi: 10.3389/fncel.2021.739506

# Inflammation and Oxidative Stress: Potential Targets for Improving Prognosis After Subarachnoid Hemorrhage

*Fan Wu[1,2], Zongchi Liu[1,2], Ganglei Li[1,2], Lihui Zhou[1,2], Kaiyuan Huang[1,2], Zhanxiong Wu[3], Renya Zhan[1,2]* and Jian Shen[1,2]**

[1] First Affiliated Hospital, School of Medicine, Zhejiang University, Hangzhou, China, [2] Department of Neurosurgery, First Affiliated Hospital, College of Medicine, Zhejiang University, Hangzhou, China, [3] College of Electronics and Information, Hangzhou Dianzi University, Hangzhou, China

OPEN ACCESS

**Edited by:**
Junlei Chang,
Shenzhen Institutes of Advanced Technology, Chinese Academy of Sciences (CAS), China

**Reviewed by:**
Xiao-ming Meng,
Anhui Medical University, China
Yu-Feng Wang,
Harbin Medical University, China

***Correspondence:**
Renya Zhan
1196057@zju.edu.cn
Jian Shen
1314006@zju.edu.cn

**Specialty section:**
This article was submitted to Non-Neuronal Cells, a section of the journal Frontiers in Cellular Neuroscience

**Received:** 11 July 2021
**Accepted:** 20 August 2021
**Published:** 24 September 2021

**Citation:**
Wu F, Liu Z, Li G, Zhou L, Huang K, Wu Z, Zhan R and Shen J (2021) Inflammation and Oxidative Stress: Potential Targets for Improving Prognosis After Subarachnoid Hemorrhage. Front. Cell. Neurosci. 15:739506. doi: 10.3389/fncel.2021.739506

Subarachnoid hemorrhage (SAH) has a high mortality rate and causes long-term disability in many patients, often associated with cognitive impairment. However, the pathogenesis of delayed brain dysfunction after SAH is not fully understood. A growing body of evidence suggests that neuroinflammation and oxidative stress play a negative role in neurofunctional deficits. Red blood cells and hemoglobin, immune cells, proinflammatory cytokines, and peroxidases are directly or indirectly involved in the regulation of neuroinflammation and oxidative stress in the central nervous system after SAH. This review explores the role of various cellular and acellular components in secondary inflammation and oxidative stress after SAH, and aims to provide new ideas for clinical treatment to improve the prognosis of SAH.

**Keywords: subarachnoid hemorrhage, poor prognosis, delayed ischemic neurological deficit, inflammation, oxidative stress, anti-inflammatory, antioxidant**

## INTRODUCTION

Globally, six to nine in 100,000 people seek medical attention for subarachnoid hemorrhage (SAH) annually. More than 80% of SAHs are caused by ruptured intracranial aneurysms, with a mortality rate of 35% (Neifert et al., 2021). During aneurysmal SAH, increased intracranial pressure causes a sharp decrease in cerebral perfusion pressure that can lead to acute cerebral ischemia (CI) and loss of consciousness. Although SAH accounts for only 5% of all strokes, it imposes a significant health burden on society due to its young age of onset. Those who survive the initial bleeding often develop severe disability, with cognitive impairment, known as delayed ischemic neurological deficit (DIND) (Macdonald, 2014). Currently, poor long-term prognosis is attributed to delayed CI (DCI) in most cases. From day 5 to 14 after SAH, patients are at increased risk for DCI, which may be manifested as headache, confusion, focal neurological impairment, or decreased levels of consciousness (Østergaard et al., 2013).

Historically, spasm of the large arteries has been considered the only explanation for DCI. At present, angiography is still the gold standard for detecting vasospasm. However, even though

up to 70% of SAH patients develop angiographic vasoconstriction, only about 50% develop DCI (Francoeur and Mayer, 2016). Nimodipine may reduce the incidence of DCI and the risk of poor prognosis after SAH by preventing and reducing vasospasm through muscle wall relaxation. Even though angiographic vasospasm has been successfully alleviated, prognosis has not improved (Etminan et al., 2011).

In recent years, it has been shown that factors other than vasospasm are involved in the pathophysiology of DCI, including microcirculation contraction, microthrombosis, cortical diffusion ischemia, and delayed apoptosis (Macdonald, 2014). Neuroinflammation and oxidative damage after SAH link these factors together.

Similar to the biphasic course of SAH (early bleeding and late ischemia), the inflammatory response in the pathological course is also biphasic (Lucke-Wold et al., 2016). In the acute stage, the main manifestation is the local inflammatory response caused by blood components entering the subarachnoid space and triggering downstream inflammatory cascades. Subsequently, in the subacute and chronic stages, while central resident immune cells are activated, a large number of peripheral inflammatory cells enter the subarachnoid space under the chemotactic influence of inflammatory cytokines (**Figure 1**; Zhou et al., 2014). As the final effector of the inflammatory response, inflammatory cells secrete a variety of inflammatory cytokines. Inflammatory cells and cytokines play an important role in the process of neurodegenerative and neurobehavioral disorders (Healy et al., 2020). Thus, inflammation plays a central role in the development of post-SAH complications. The release of oxyhemoglobin, mitochondrial dysfunction, and overexpression of peroxidase lead to excess oxidative products that exceed the body's antioxidant capacity, leading to destruction of the blood–brain barrier (BBB), loss of neurons, glial hyperplasia, and permanent neurological impairment (Hu et al., 2016). While inflammation induces oxidative stress, oxidative stress can also induce an inflammatory response. The two complement each other and contribute to poor prognosis after SAH.

## ONSET OF INFLAMMATION AND OXIDATIVE STRESS

In the acute phase of SAH, the main manifestation is activation of local inflammation at the site of injury. Substances released from damaged cells and blood components enter the subarachnoid space as damage-associated molecular patterns (DAMPs) that act by initiating inflammation (Chaudhry et al., 2018). An increasing number of DAMPs has been identified, including high mobility group box (HMGB)1, heat shock protein (HSP), S100 protein, hemoglobin and its derivatives, mitochondrial DNA, IL-1α, IL-33, and extracellular matrix.

Damage-associated molecular patterns are primarily recognized by pattern recognition receptors (PRRs), such as Toll-like receptors (TLRs), cytoplasmic NOD-like receptors (NLRs) and non-PRRs (such as CD44, integrin, and CD91 receptor) (Zindel and Kubes, 2020). The TLR family is one of the most characteristic PRR families, and is widely expressed in the membranes of glial cells such as microglia, astrocytes and oligodendrocytes in the central nervous system (CNS) (Pascual et al., 2021; **Figure 2**). TLR-4 plays a major role in the inflammatory response after SAH (Okada and Suzuki, 2017). TLR4 is an important member of the TLR family in PRRs and can be activated by hemoglobin and its derivatives (Leitner et al., 2019).

TLR4-dependent proinflammatory cytokines trigger an inflammatory response similar to that induced by lipopolysaccharide (Grylls et al., 2021). With the help of myeloid differentiation factor (MD)-2 and CD14, TLR4 can interact with two different junction proteins: Myeloid differentiation primary-response protein 88 (MyD88) and Toll receptor associated activator of interferon (TRIF) (Okada and Suzuki, 2017).

In the MyD88-dependent nuclear factor (NF)-κB signaling pathway, TIR domain containing adaptor protein/MyD88 adaptor-like (TIRAP/MAL) is required to bridge TLR and MyD88 when DAMPs bind to TLR4. MyD88 then interacts with interleukin-1 receptor (IL-1R)-associated kinase (IRAK)-4, which activates other members of the IRAK family, including IRAK-1 and IRAK-2. Activated IRAKs interact with tumor necrosis factor receptor (TNFR)-associated factor (TRAF)6 (Leitner et al., 2019). TRAF6 is associated with transforming factor-β-activated kinase (TAK)1, which leads to activation of the NF-κB signaling pathway and increased transcription and expression of proinflammatory cytokines (Karimy et al., 2020). In the TRIF-dependent signaling pathway, TLR4 requires TRIF-related adaptor molecule (TRAM) to activate TRIF. Subsequently, activated TRIF induces activation of the NF-κB signaling pathway by recruiting and activating TRAF6 or receptor-interacting serine/threonine protein kinase (RIPK)1 (Ciesielska et al., 2021).

Although the two different connective proteins act in different ways, both ultimately activate the NF-κB signaling pathway and trigger further inflammatory cascades (Takeuchi and Akira, 2010).

## TOXICITY OF HEMOGLOBIN

Hemoglobin and its metabolites form a toxic cascade during early brain injury after SAH that is thought to play a key role in the development of delayed brain injury (Brathwaite and Macdonald, 2014). The neurotoxicity of hemoglobin is indisputable, and neurons seem to be more susceptible than glial cells (Li et al., 2012). The toxicity of hemoglobin is multifactorial, but is mediated mainly by four factors: inflammation, oxidation, nitric oxide (NO) depletion, and edema (Robicsek et al., 2020).

### Hemoglobin and Its Products Acting as DAMPs

Hemoglobin and hemoglobin-derived products are the most important DAMPs released by ruptured red blood cells (RBCs) in the subarachnoid space and are involved in the inflammatory activation of SAH (Bozza and Jeney, 2020). Hemoglobin and its products, such as methemoglobin, heme, heme chloride, and oxygenated hemoglobin, bind to the TLR-4 receptor as DAMPs.

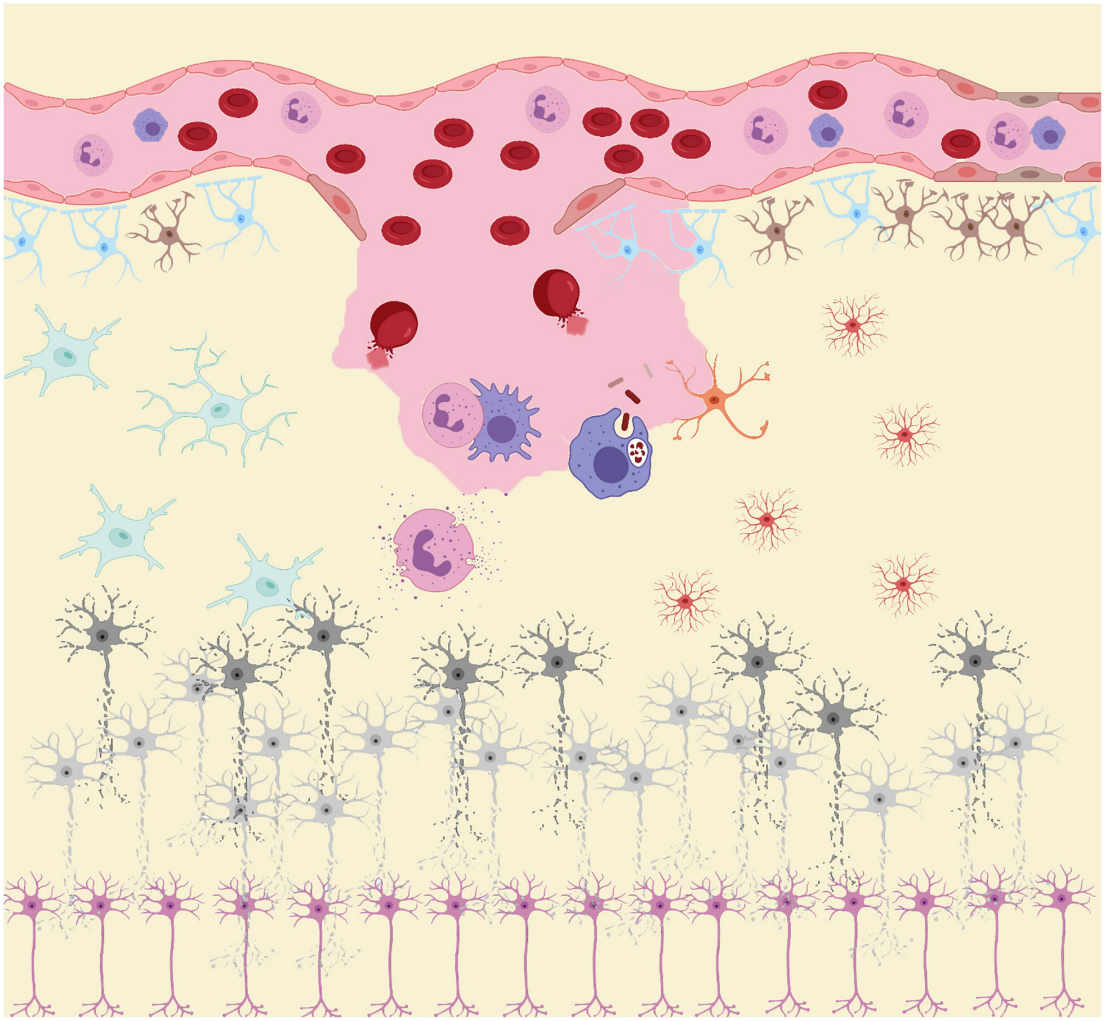

**FIGURE 1 |** After subarachnoid hemorrhage (SAH), blood components enter the subarachnoid space. RBC rupture hemoglobin and its metabolites, together with other damage-associated molecular patterns (DAMPs), act as inducers of the secondary inflammatory response after SAH to activate the innate immune cells (microglia and astrocytes) in central nervous system (CNS). Subsequently, immune cells such as neutrophils and macrophages in the peripheral circulation infiltrate into the injured site under the action of chemokine recruitment. These peripheral immune cells, together with innate immune cells in CNS, act as the carriers of secondary inflammation after SAH, releasing large amounts of pro-inflammatory cytokines and peroxides causing damage to neurons. Under the influence of these inflammatory products and peroxides, neurons gradually appear cell dysfunction and even apoptosis.

Methemoglobin is water soluble, which can lead to extensive TLR-4 activation with cerebrospinal fluid (CSF) circulation. In addition, heme stimulates the formation of more neutrophil extracellular traps (NETs) while activating TLR-4.

## Hemoglobin as a Source of Peroxide

Hemoglobin consists of four globin chains tightly bound to the heme group. Oxyhemoglobin and its metabolites are considered to be the main sources of reactive oxygen species (ROS) in the pathophysiological process of SAH (Hugelshofer et al., 2018). After hemolysis, tetrameric hemoglobin is released from RBCs and degrades gradually, producing toxic intermediates (Stokum et al., 2021). Among them, heme is considered more toxic than hemoglobin (Bulters et al., 2018). In the ferrous ($Fe^{2+}$) and trivalent ($Fe^{3+}$) states, heme can react with hydrogen peroxide to generate hydroxyl radicals through the Fenton reaction, which can damage lipid membranes and lead to the production of lipid ROS, cell dysfunction and even ferroptosis (Marnett et al., 2003; Yang and Stockwell, 2016).

These hemoglobin-derived products induce toxicity by producing ROS that can cause oxidation of cell lipids, proteins and DNA, leading to programmed cell death (Sinha et al., 2013). ROS can further activate TLR/NF-κB/MAPK, KEAP1–NRF2–ARE, eicosanoid and other signaling pathways as well as NLRP3 inflammasomes to mediate inflammatory responses (Reczek and Chandel, 2015). Oxyhemoglobin has been shown to induce cerebral artery contraction after SAH by inhibiting voltage-dependent $K^+$ channels in cerebral arteries and inducing R-type $Ca^{2+}$ channel expression in cerebral arteries (Ishiguro et al., 2006; Link et al., 2008).

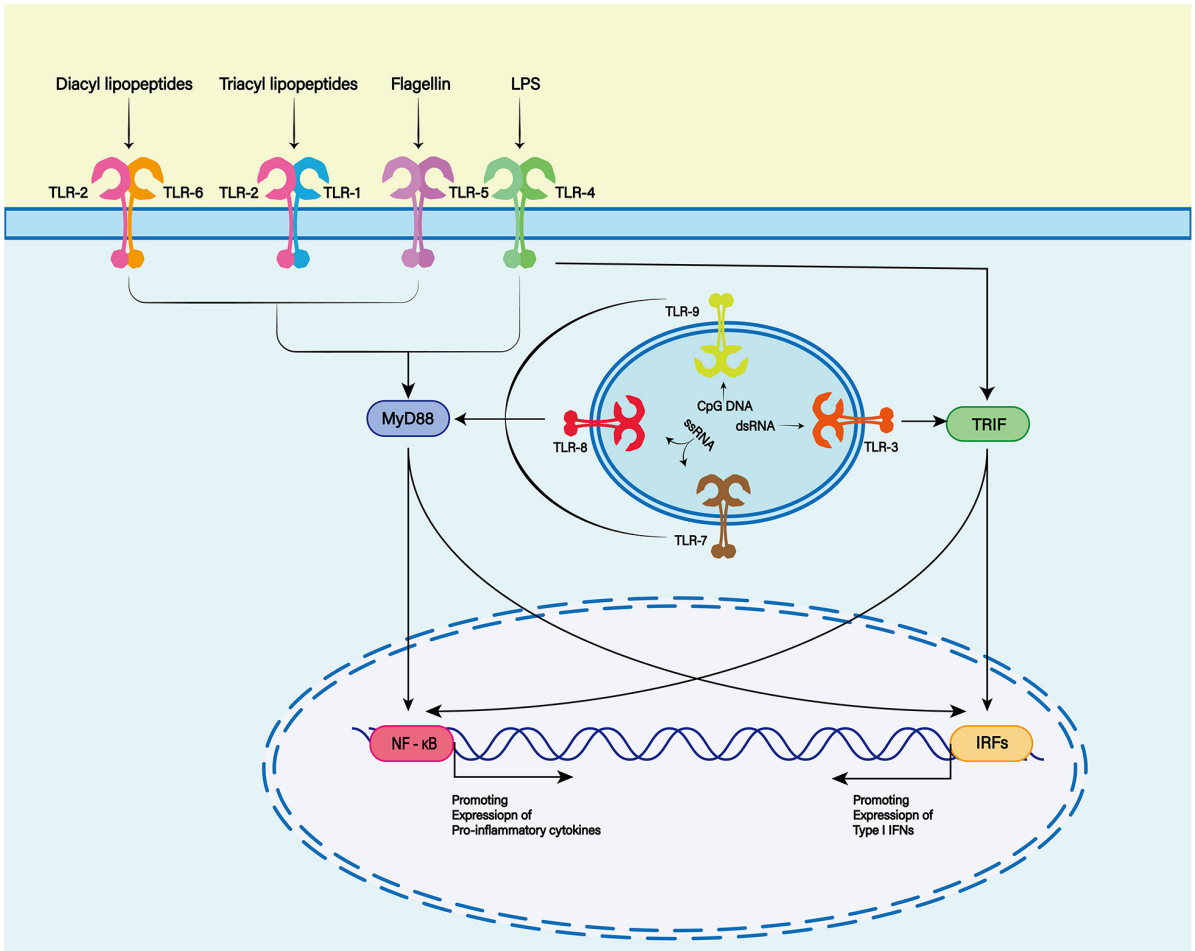


**FIGURE 2 |** The Toll-like receptor (TLR) family plays a key role in recognizing antigens produced by microorganisms. To date, 13 TLR family members have been discovered. TLR1, 2, 4, 5, and 6 were expressed on the cell surface, while TLR3, 7, 8, and 9 were expressed on the endosome membrane. Toll-like receptors are membrane receptors composed of extracellular domains, single transmembrane helical domains and intracellular signaling domains, which can bind to different ligands (TLR2 and TLR1 or TLR6 complexes recognize lipoproteins or lipopeptides, TLR3 recognizes double-stranded RNA, TLR4 recognizes lipopolysaccharides (LPS), TLR5 recognizes bacterial flagellins, TLR7 or TLR8 recognizes single-stranded RNA, and TLR9 recognizes CpG rich in hypomethylated DNA). When the TLR binds to the respective ligands, different downstream signals can be activated to produce different biological effects.

## NO Depletion

As an important endogenous vasodilator, NO can be produced by endothelial cells, neurons and microglia (Bulters et al., 2018). After SAH, peroxynitrite can be produced by the reaction of NO with superoxide radicals, a highly oxidative species. These peroxides damage the neurons that produce NO and reduce NO production. More importantly, hemoglobin released by subarachnoid blood inhibits the activity of endothelial NO synthase (eNOS), exacerbating the decrease in NO production (Sabri et al., 2011; Lenz et al., 2021). As a result, the availability of NO to vascular smooth muscle cells is reduced, leading to vasoconstriction (Li Q. et al., 2016, Li J. et al., 2016). In addition to regulating cerebrovascular tension, NO inhibits the formation of thrombocytopenic microthrombosis (Voetsch et al., 2004). As the result of the combination of these factors, cerebral perfusion is significantly reduced leading to neuronal dysfunction (Takeuchi et al., 2006). Reduced bioavailability of NO reduces the cortical diffusion depolarization threshold (Petzold et al., 2008). This leads to diffuse ischemia and neuronal death (Terpolilli et al., 2016).

## Hemoglobin Causing Encephaledema

Many studies have shown that cerebral edema in SAH is a biphasic phenomenon (Serrone et al., 2015). The formation of early cerebral edema is a direct result of early ischemic injury during initial bleeding, while subsequent delayed edema appears to be caused by BBB dysfunction (Hayman et al., 2017). There is evidence to show that hemoglobin and its metabolites can cause brain edema. In a model of intracranial hemorrhage (ICH), the iron deposition around the hematoma gradually increases after injection of autologous blood into the brain parenchyma of rats. Meanwhile, the water content in the brain tissue around the hematoma also gradually increases (Huang et al., 2002). However, the degree of cerebral edema in rats is significantly reduced

by chelating agents. Immunohistochemical analysis shows that aquaporin (AQP)4 is highly expressed in astrocytes. Therefore, iron overload and AQP4 may play a key role in the formation of hemoglobin-mediated brain edema after ICH (Qing et al., 2009). Hemoglobin-induced oxidative stress can increase expression of matrix metalloproteinase (MMP)-9 and lead to BBB dysfunction (Katsu et al., 2010; Ding et al., 2014). In view of this, delayed edema after SAH is thought to be caused at least in part by hemoglobin and its breakdown products (Urday et al., 2015).

## IMMUNOCYTE REACTION

Aside from hemoglobin activating SAH and producing ROS that damage the CNS, some inflammatory cell infiltrates cause further damage. Unlike other organs/tissues, the CNS hosts a variety of innate and peripheral immune cells. Analysis of blood, CSF and tissue sections from patients with SAH has revealed that peripheral neutrophils and monocytes/macrophages, as well as central resident microglia and astrocytes contribute most to post-SAH inflammation. However, as the course of the disease changes, so too does the immune cell spectrum involved in the inflammatory response. Recent studies have found that the accumulation and activation of neutrophils and microglia peak twice during the course of SAH, which corresponds to early and late neuronal apoptosis after SAH. However, monocytes and macrophages seem to increase from the subacute phase (Coulibaly et al., 2020). This suggests that different immune cells play different roles in the post-SAH inflammatory response. However, as the disease course changes, so too does the immune cell spectrum involved in the inflammatory response. Recent studies have found that the accumulation and activation of neutrophils and microglia peak twice during the course of SAH, which corresponds to early and late neuronal apoptosis after SAH. However, monocytes and macrophages seem to increase from the subacute phase (Coulibaly et al., 2020). This seems to suggest that different immune cells play different roles in the post-SAH inflammatory response.

### Microglia

Microglia act as the resident macrophages of the CNS and are an important component of innate and adaptive immune responses. TLR-mediated microglial activation leads to production of several inflammatory mediators that rapidly respond to different stimuli, such as DAMPs (Atangana et al., 2017). TLR4 is most abundantly expressed on microglial membranes (Lehnardt, 2010; Li et al., 2021). TLR4 and other PRRs lead to the activation of downstream inflammatory signaling cascades, including the NF-κB, MyD88/TRIF, and MAPK pathways (Geraghty et al., 2019). However, at different stages in SAH, microglia exhibit different phenotypes: the proinflammatory M1 phenotype predominates in the early stages and this is gradually replaced by the anti-inflammatory M2 phenotype as the disease progresses (Zheng et al., 2020). Between them, M1 has the ability to release proinflammatory cytokines, such as TNF-α and IL-6 (Hu et al., 2015). In animal models, increased expression of proinflammatory cytokines is associated with poor prognosis of SAH (Kooijman et al., 2014; Wang et al., 2021). Neuronal cell death and microglial cell accumulation follow similar time courses. Thus, microglial accumulation can cause secondary brain damage after SAH (Schneider et al., 2015). Therefore, early post-SAH promotion of activation of these microglia toward an anti-inflammatory phenotype may have a neuroprotective effect (Schneider et al., 2018).

### Astrocytes

Astrocytes are the most abundant glial cells in the CNS. They play an important role in maintaining the integrity of the BBB and supporting the activity of neurons (Cunningham et al., 2019). Astrocytes can differentiate into different phenotypes under different stimuli, namely proinflammatory type A1 and anti-inflammatory type A2 (Shinozaki et al., 2017; Hyvärinen et al., 2019). DAMP-mediated activation of TLR contributes to the acquisition of A1 phenotype in astrocytes (Xu et al., 2018). TLR expression is low in the astrocytes of healthy individuals. However, TLRs, especially TLR-4, are abundant on the surface of the astrocyte membrane in the event of injury or inflammation (Azam et al., 2019). After SAH, various DAMPs are released into the subarachnoid space, promoting the activation of proinflammatory phenotype through TLRs (Ghaemi et al., 2018). One study found that changes in astrocyte $Ca^{2+}$ signaling after SAH led to a neurovascular coupling response that shifts blood vessels from a diastolic to a constrictive state, and ultimately exacerbates brain tissue damage (MacVicar and Newman, 2015; Pappas et al., 2015). At the same time, the dysfunction of glutamate uptake mediated by astrocytes may be the possible mechanism of DCI after SAH (Tao C. et al., 2020, Tao K. et al., 2020). Additionally, A1 astrocytes cause depression-like behavior and cognitive dysfunction in mice (Zhang et al., 2020). Current interventions targeting type A1 astrocytes in animal models reduce neuronal death as well as neurogenesis decline and cognitive impairment (Lu et al., 2020; Zhang et al., 2021). Therefore, therapies targeting astrocytes may help improve outcomes in patients with SAH.

### Neutrophils

Neutrophils are the most abundant type of white blood cells in peripheral blood, and they are significantly increased after SAH (Gris et al., 2019; Morga et al., 2020). Activation of astrocytes challenges the integrity of the BBB and vascular permeability is increased. Many chemokines are produced in the local inflammatory response after SAH. Under the combined action of the two, numerous neutrophils enter the subarachnoid space from the peripheral circulation (Coulibaly et al., 2020; Osuka et al., 2021). Related observational studies have found that increased neutrophil-to-lymphocyte ratio is inversely associated with prognosis in patients with SAH (Giede-Jeppe et al., 2019). Neutrophils have also been found to mediate early cortical hypoperfusion in animal models (Neulen et al., 2019). On the one hand, neutrophils can release IL-6, transforming growth factor-β1 and other inflammatory cytokines to produce a cascade reaction, which plays an important role in post-SAH inflammation (Takizawa et al., 2001). On the other hand, these neutrophils can produce peroxide by

NADPH oxidase (NOX) and myeloperoxidase (MPO), causing damage to neurons and other support cells in the CNS and even apoptosis and cerebral cortex insufficiency (Chu et al., 2015; Neulen et al., 2019). Recent studies have shown that the presence of NETs released by neutrophils can transform microglia into a more proinflammatory phenotype, thereby aggravating neuroinflammation after SAH and leading to poor prognosis (Hanhai et al., 2021).

## Monocytes/Macrophages

Monocytes are innate immune cells produced mainly in the bone marrow. When they are released into the circulation, they quickly differentiate into macrophages and perform different functions. Within 24 h after SAH, there is a large number of monocytes infiltrating into the site of hemorrhage and gradually increasing (Jedrzejowska-Szypułka et al., 2010; Gris et al., 2019). Monocytes mediate cerebral vasospasm after SAH in animal models, which may be the mechanism related to DCI and DIND (Jackson et al., 2021). Once monocytes infiltrate brain tissue, they mature into macrophages and take on different morphological and biochemical characteristics (Coulibaly et al., 2020). Meanwhile, peripheral circulating macrophages are recruited by monocyte chemotactic protein-1 to enter the site of injury (Lu et al., 2009; Niwa et al., 2016). Similar to microglia, monocytes and macrophages are likely to be involved in the inflammatory response or oxidative damage after SAH and lead to poor prognosis (Kwan et al., 2019; Unda et al., 2020). Therefore, further research on its mechanism will help to develop more effective treatment regimens.

## Neurotoxicity of Immunocytes

The toxic effect of immune cells on the CNS may be the result of combined action of cytokine-mediated inflammatory response and ROS-mediated oxidative stress.

### Proinflammatory Cytokines

After SAH, proinflammatory cytokines are initially secreted by innate immune cells that reside in the CNS (Gris et al., 2019). Appropriate inflammatory response is thought to be beneficial. Then, circulating immune cells, aided by chemokines, enter the subarachnoid space and produce a storm of inflammatory cytokines that tip the balance in the wrong direction (Schneider et al., 2012; Coulibaly et al., 2020). Proinflammatory cytokines can induce brain injury by triggering apoptotic pathways, interfering with the balance of endogenous vasodilators and vasoconstrictors, and activating coagulation factors, leading to microthrombosis (Becher et al., 2017).

Currently, several factors have been identified to induce or aggravate cerebral vasoconstriction after SAH, including interleukins, TNF-α, lymphocyte function-associated antigen-1 (LFA-1), leukotrienes, arachidonic acid, von Willebrand factor, MMP-9 and vascular endothelial growth factor (Schneider et al., 2018). Typically, IL-1, IL-6, IL-8, and TNF-α reported to be correlated with the prognosis of patients with SAH (López-Cortés et al., 2000; Zeiler et al., 2017). IL-6, for example, is considered to be a biomarker for DCI-associated infarction after SAH (Ridwan et al., 2021). IL-6 regulates the expression of many genes related to inflammation, oxidative stress, and apoptosis. IL-6 mediates the endothelial barrier, resulting in dysregulation of cell connections and damage to the BBB (Blecharz-Lang et al., 2018). At the same time, vascular cell adhesion molecule-1 on vascular endothelial cells is upregulated to induce proliferation of circulating immune cells and infiltration into the CNS (Erta et al., 2012). IL-6 can induce the accumulation of abnormal proteins and molecules in neurons, leading to neurodegeneration (Kaur et al., 2019). IL-6 may also play a neuroprotective role. For example, against *N*-methyl-D-aspartic acid receptor-mediated brain excitatory toxicity (Ali et al., 2000).

The dual role of cytokines in secondary inflammation after SAH has been demonstrated. Moderate levels of cytokines contribute to injury repair; however, prolonged chronic stimulation can be harmful. Therefore, early anti-inflammatory treatment in patients with SAH will help improve prognosis.

### Oxidative Damage

When cell are in homeostasis, there is a balance between ROS produced by mitochondria and peroxidases [such as NOX, NOS, MPO, and cyclo-oxygenase (COX)] that produce ROS and antioxidant enzymes (such as catalase, superoxide dismutase (SOD), and glutathione reductase) and endogenous antioxidant molecules (such as glutathione, ascorbic acid, and tocopherol) (Eastman et al., 2020). However, after SAH, this balance is broken and oxidative stress occurs.

#### *Mitochondrial dysfunction*

Mitochondria are known to play a major role in tissue oxidative damage and dysfunction due to their ability to produce free radicals (Venditti and Di Meo, 2020). With the development of SAH, nerve cells in the responsible vascular supply region suffer ischemia injury, leading to mitochondrial dysfunction (Qu et al., 2016; Halcrow et al., 2021). Mitochondrial dysfunction can lead to a series of harmful consequences, including breakdown of transmembrane potential in mitochondria, disruption of mitochondrial biosynthesis, excessive production of ROS, outflow of matrix calcium, and release of apoptotic proteins (Chan, 2006). Respiratory chain complex I–IV and oxidants may be the main reasons for the enhanced mitochondrial ROS production after SAH (**Figure 3**; Dröse and Brandt, 2012). A growing body of evidence supports the role of mitochondrial oxidants in ROS production after intracerebral hemorrhage (Wu et al., 2019; Nolfi-Donegan et al., 2020). In addition, mitochondrial dysfunction produces ROS that contribute to CNS dysfunction (Marzatico et al., 1990). That has been proved in most neurodegenerative diseases, including Parkinson's disease, Alzheimer's disease, Huntington's disease, and amyotrophic lateral sclerosis (Wang et al., 2019; Johnson et al., 2021). For SAH patients, mitochondrial dysfunction is also thought to be a key mechanism for cognitive dysfunction and poor prognosis (Youn et al., 2020). Therefore, we can reduce the nerve damage after SAH by inhibiting mitochondrial ROS production.

#### *NADPH oxidase*

The NADPH oxidase (NOX) family (NOX1–5 and dual oxidase (DUOX1 and 2) is an important source of ROS (**Figure 4**; Mittal et al., 2014). Under physiological conditions, ROS produced

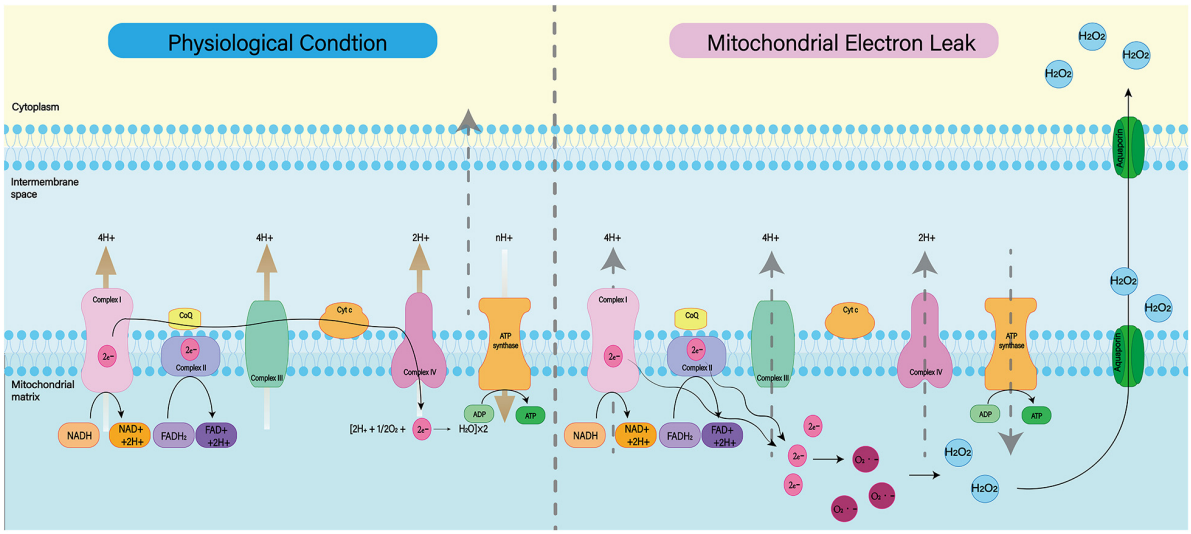


**FIGURE 3 |** Under normal physiological conditions, mitochondrial oxidative respiratory chain composed of complex I–IV can transfer electrons and $H^+$ and produce ATP together with ATP synthase. When complex I–IV is dysfunctional, electron leakage occurs. This leads to the production of ROS and $H_2O_2$.

by NOX function as a defense mechanism against pathogens and signaling molecules. In pathological conditions, ROS cause oxidative damage through oxidative stress (Sorce et al., 2012). NOX catalyzes the transfer of two electrons through the biofilm to produce superoxide anion $O2^{-}\bullet$ by using intracellular NADPH as electron donor and extracellular molecular oxygen as receptor. Then $O2^{-}\bullet$ is progressively metabolized to $H_2O_2$ and •OH (Nayernia et al., 2014). NOX is expressed widely in CNS cells, while oligodendrocytes may be the only CNS cells that do not express NOX (Cinelli et al., 2020). NOX2 and 4 appear to be the major subtypes expressed in the brain under physiological conditions, with NOX2 being the most abundant (Miller et al., 2006). A study found significantly increased levels of NOX2 and 4 proteins in perihematoma neurons and astrocytes in SAH patients (Zhang et al., 2017). In animal models, NOX can trigger delayed cerebral vasospasm after SAH (Kim et al., 2002). NOX is associated with neurodegenerative diseases such as Alzheimer's disease (Ganguly et al., 2021). This suggests that NOX is likely to be a risk factor for DIND after SAH. Therefore, NOX is a potential target for the treatment and prognosis improvement of SAH.

### *Myeloperoxidase*

Myeloperoxidase (MPO) is a heme-containing peroxidase. It was found in the primary azurophilic granules of neutrophils and a small amount in the primary lysosomes of monocytes (Guilpain et al., 2008; Aratani, 2018). Neutrophils, in the middle and late stages of SAH, are recruited by chemokines into the subarachnoid space. While producing ROS through NOX, they can also use MPO to produce ROS (Winterbourn et al., 2016). Hypochlorous acid is the main product of MPO (Kargapolova et al., 2021), which can damage lipids, proteins and DNA due to its high dispersibility and oxidative activity (**Figure 5**; Chen J. et al., 2020). MPO-mediated nerve damage has been shown to cause cognitive impairment and neurodegeneration (Ray and Katyal, 2016). In SAH patients, serum MPO levels are positively correlated with DCI (Lim et al., 2012), and this has been confirmed in animal models (Oruckaptan et al., 2000). These suggest a negative role of MPO in the course of SAH.

### *NOS*

The nitric oxide synthase (NOS) family consists of three subtypes: endothelial NOS (eNOS), neuronal NOS (nNOS), and inductive NOS (iNOS) (**Figure 6**). The first two are constitutively expressed, while the latter is usually induced during inflammation (Pluta, 2006). In most cell types, expression of iNOS requires stimulation by cytokines or other inflammatory products. As the resident innate immune cells in the CNS, microglial cells are among the earliest activated immune cells after SAH (Coulibaly and Provencio, 2020). After SAH, microglia can transform into M1 phenotype, which can express iNOS depending on transcription factors including hypoxia-inducible factor-1 and NF-κB responding to inflammatory factors and hypoxic environment (Robinson et al., 2011; Rawlinson et al., 2020). Subsequently iNOS can increases NO levels and lead to free-radical-mediated neuronal damage (Bai et al., 2020).

### *COX*

COX, also known as prostaglandin oxidase reductase, is a bifunctional enzyme with activities of cyclo-oxygenase and catalase. It has two isozymes, COX-1 and COX-2, and is the key enzyme to catalyze the conversion of arachidonic acid to prostaglandins (Rouzer and Marnett, 2020). Thromboxane A2 (TXA2) synthesized by COX-1 induces platelet aggregation, vasoconstriction, and smooth muscle proliferation, while prostacyclin synthesized by COX-2 in the vascular endothelium antagonizes TXA2 in the macrovascular endothelium through smooth muscle relaxation and vasodilation (Young et al., 2012). In animal models, COX-2 overexpression is found in arterial

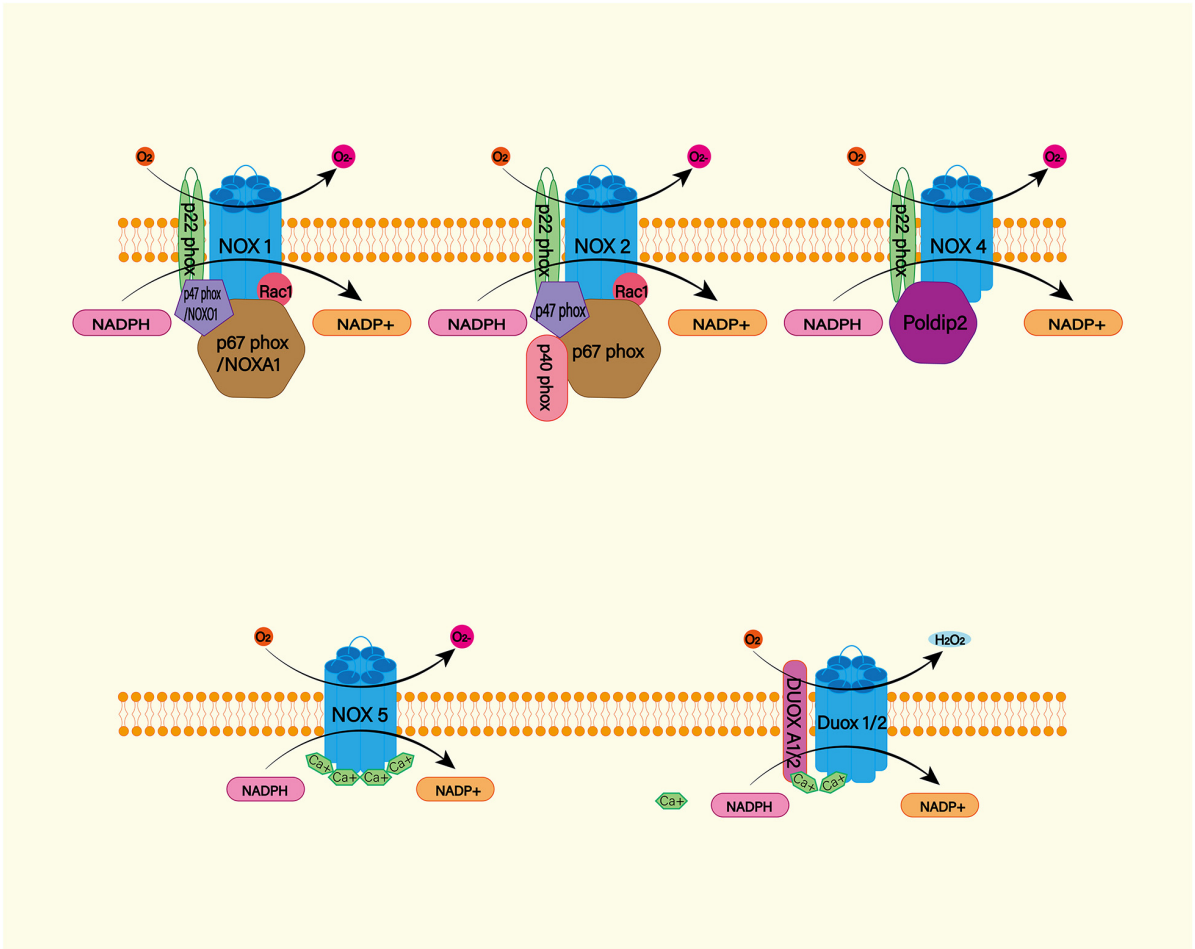


**FIGURE 4 |** The NADPH oxidase (NOX) family consists of seven catalytic subunits (NOX1-5 and DUOX1-2), regulatory subunits p22Phox, P47Phox or Noxo1, P67phox or Noxa1, and P40phox and Rac. They are widely expressed in endothelial cells (EC), vascular smooth muscle cells (VSMC), macrophages and other cells. Specifically, NOX1, 2, 4, and 5 are highly expressed in cardiovascular tissues. NOX – mediated ROS production mainly occurs on catalytic subunit Nox or Duox. For Nox1 and Nox2, ROS production requires complex interactions of regulatory subunits in the cytoplasm. Nox4, on the other hand, requires protein termed δ-interacting protein 2 (Poldip2). In addition, the increase in intracellular calcium was sufficient to promote the activation of NOX5 and DUOX1-2.

endothelial cells after SAH, while COX-1 expression level does not change significantly (Tran Dinh et al., 2001). Subsequent studies have shown that COX-2 inhibitors are effective in preventing brain edema and protecting neurological function (Ayer et al., 2011). However, nonsteroidal anti-inflammatory drugs (NSAIDs), such as aspirin, may also increase the risk of rebleeding while reducing SAH inflammation (Roumie et al., 2008; Parkhutik et al., 2012). Therefore, the use of COX inhibitors in the treatment of SAH should be carefully considered.

## ENDOTHELIAL CELL DYSFUNCTION

Blood-brain barrier is mainly composed of tightly connected vascular endothelial cells, astrocyte terminal, and extracellular matrix. Among them, normal endothelial cells play an important role in maintaining BBB, regulating thrombosis and regulating vascular tone. After SAH, the integrity of the BBB is destroyed (Peeyush Kumar et al., 2019). Therefore, vascular endothelial damage will damage the blood-brain barrier, exacerbating neurological dysfunction (Graves and Baker, 2020).

After SAH, the CNS experiences a transient systemic ischemia. Normally, vasoactive substances have a delicate balance between vasodilation and contraction. Early in the course of the disease, the balance becomes out of balance, with endothelial cells responding more to vasoconstrictors and less to vasodilators (Geraghty et al., 2019; Lenz et al., 2021). Therefore, the cerebrovascular contraction and even spasm are stimulated by a variety of vasoconstrictor substances such as endothelin. In quick succession, there will be lack of cerebral blood flow and cerebral perfusion (Jullienne et al., 2016). In the ischemic environment, in addition to impaired nerve cell function, vascular endothelial cells undergo morphological changes and become dysfunctional (Sehba and Friedrich, 2013; Østergaard et al., 2013).

As the disease progresses, secondary inflammation and oxidative stress further damage the endothelial cells.

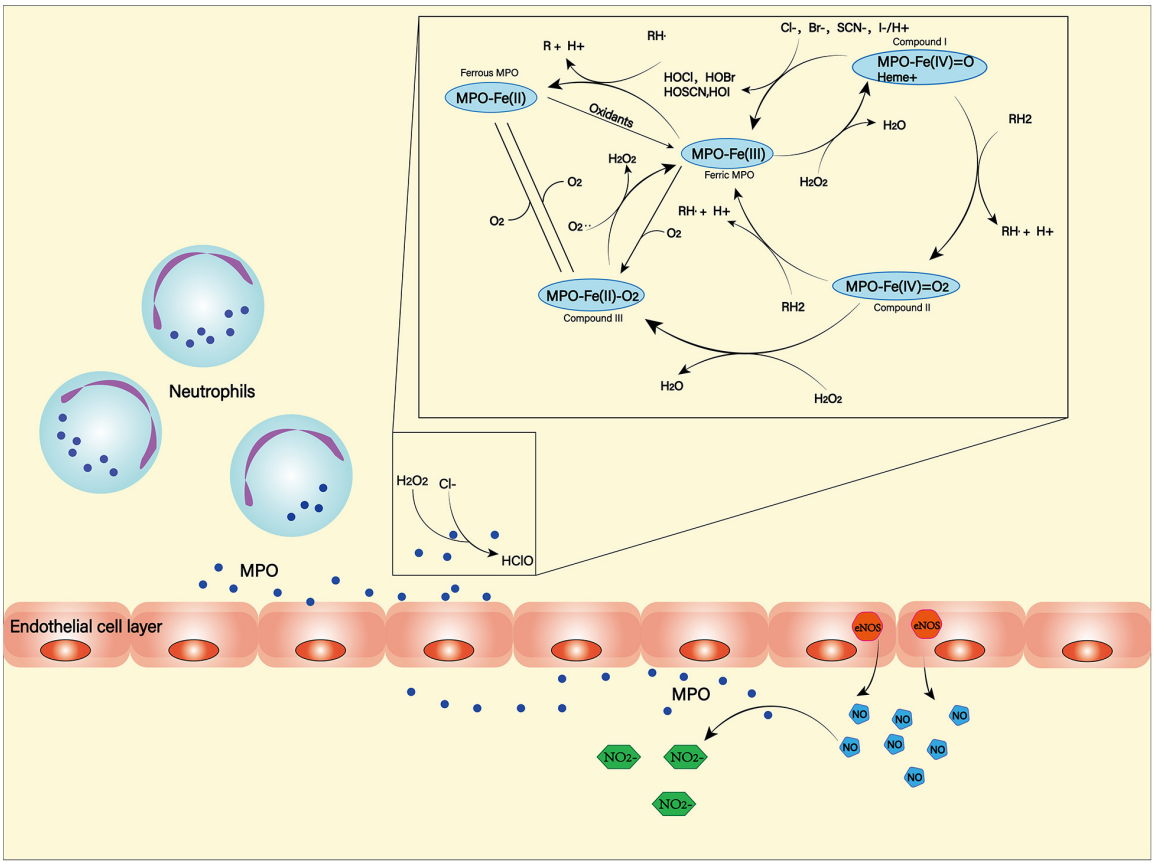


**FIGURE 5 |** Myeloperoxidase (MPO) is produced and secreted mainly by neutrophils. It can produce a variety of oxidation products through halogenation cycle and peroxidation cycle and then cause damage to tissues and cells. In halogen cycle, MPO catalyzes halogen to produce HOCl and other strong oxides. In the peroxidation cycle, MPO can react with oxidizable molecules (RH) to form free radical intermediates. In addition, MPO can react with NO generated by NOS to form $NO2^-$.

Under the joint action of many factors, endothelial cell dysfunction is aggravated and eventually apoptosis. In addition, damaged endothelial cells release substances such as matrix metalloproteinase 9 (MMP-9) (Wang et al., 2018). Mmp-9 can degrade the extracellular vascular matrix, including collagen IV, laminin, and fibronectin, etc. (Lu et al., 2011). Therefore, the integrity of the BBB is lost. This exposes nerve cells to a large amount of harmful substances and causes brain tissue edema and other central nervous dysfunction (Willis et al., 2008; Hayman et al., 2017; Swissa et al., 2019).

## HEMOGLOBIN AS A THERAPEUTIC TARGET

Hemoglobin causes direct and indirect neurotoxicity; therefore, therapies that targeting hemoglobin are important for patients with SAH.

### Physical Clearance

Surgery is the only way to completely remove the blood clot. Especially for SAH patients with large hematomas or ruptures in the cerebroventricular system, surgery can effectively remove the hematoma and reduce the occurrence of vasospasm (Zhang et al., 2001). However, due to the anatomical structure of SAH, blood can be widely distributed in various parts of the subarachnoid space. Therefore, for patients with small hematomas and mild symptoms, surgical treatment is no longer appropriate.

For patients in whom craniotomy for removal of hematoma is not recommended, continuous drainage of CSF by external ventricular drainage and lumbar cistern drainage can be performed to reduce the hemoglobin concentration in CSF (Wolf, 2015). Continuous CSF drainage can significantly reduce the incidence of vasospasm (Klimo et al., 2004; Alcalá-Cerra et al., 2016). However, CSF drainage is of limited use and it does not clear the blood clot that has formed. Blood clots can still release hemoglobin, which can damage brain tissue. Therefore, CSF drainage results in a small improvement in long-term outcomes after SAH (Al-Tamimi et al., 2012).

In recent years, CSF drainage combined with intrathecal drug therapy has received attention. A randomized controlled trial in Japan used magnesium sulfate solution for intrathecal irrigation. Although vasospasm was significantly improved, the incidence of DCI and functional outcomes in patients with SAH were not

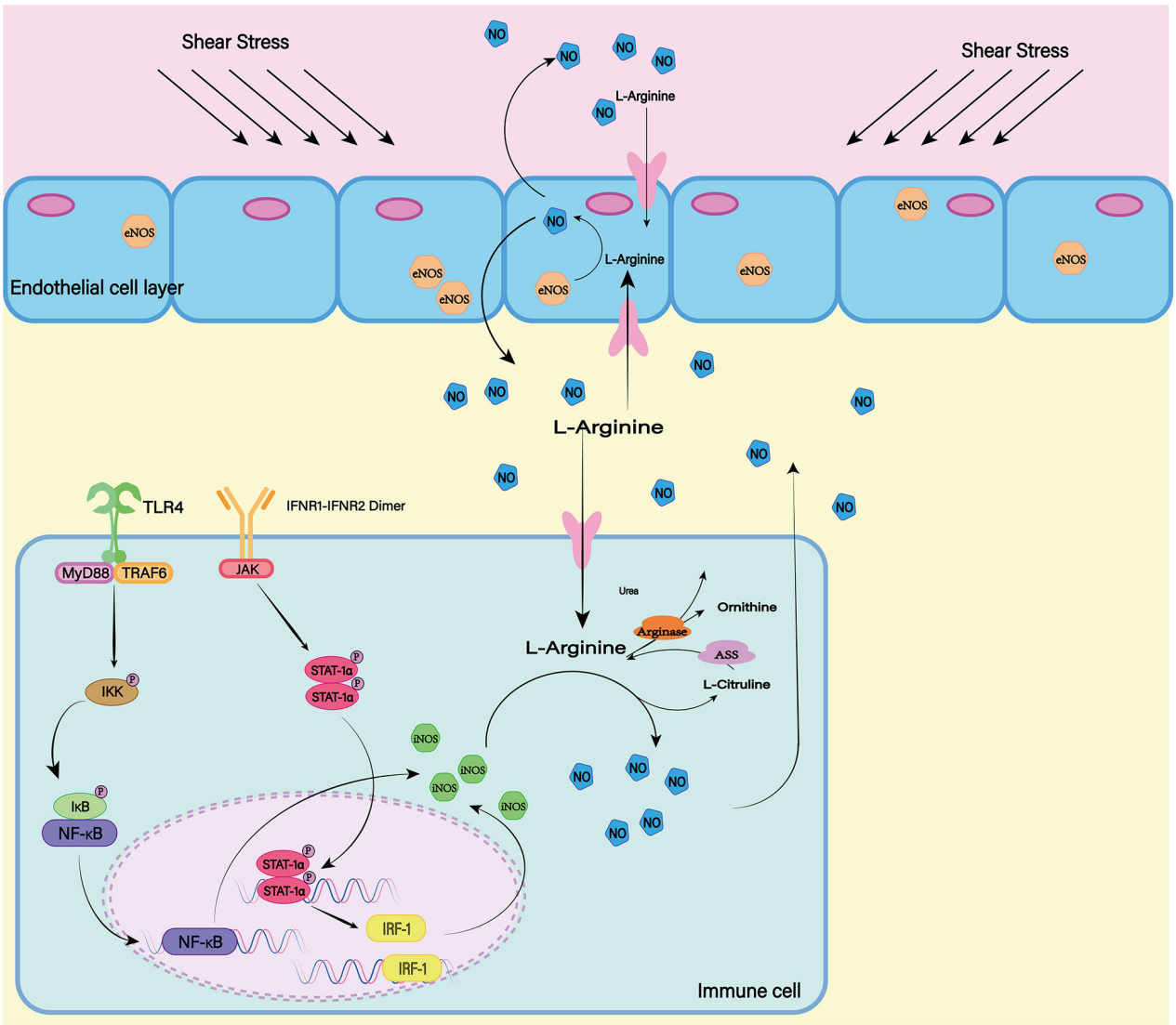


**FIGURE 6 |** In mammals, there are three isotypes of nitric oxide synthase (NOS) (eNOS, iNOS, and nNOS). ENOS is the most important source of NO in endothelial cells. The shear stress of blood flow on the vascular wall is the main mechanism by which eNOS produces NO. INOS can be induced in a variety of cell types. LPS as a proinflammatory medium can induce the expression of iNOS. At the same time, the transcription factors NF-κB and STAT-1α are believed to be necessary for iNOS transcription in most cells. nNOS is highly expressed mainly in peripheral nerve fibers and is thought to have a protective effect on atherosclerosis. The release of L-Glutamate (L-Glu) from baroreceptors activates nNOS and promotes the production of NO. Although the expression mechanisms of the three isotypes are different, all of them can generate NO and L-Citrulline (L-CCP) as the substrate.

significantly improved (Yamamoto et al., 2016). The combined intrathecal use of thrombolytic agents has not yielded satisfactory results (Etminan et al., 2013). It has also been found that intrathecal use of thrombolytic agents increases inflammation. However, this may be due to the release of hematoma breakdown products rather than thrombolytic drugs (Kramer et al., 2015).

## Enhancing Endogenous Hemoglobin Clearance

Hemoglobin can be engulfed by cells in three ways: erythrophagocytosis, endocytosis of erythrocytes mediated by haptoglobin, and endocytosis of heme mediated by hemopexin (**Figure 7**; Bulters et al., 2018; Pan et al., 2020). These mechanisms of endogenous hemoglobin clearance provide an entry point for therapeutic regimens that target hemoglobin.

### Erythrophagocytosis

Erythrophagocytosis is the removal of abnormal RBCs by monocytes/macrophages with type II scavenger receptors (CD36) expressed on their membranes. After SAH, macrophages/microglia recognize exposure to phosphatidylserine via CD36 and mediate erythrophagocytosis. In particular, transcription factor Nrf2 (nuclear factor- erythroid 2 p45-related factor 2) regulates the expression of CD36 on

microglia, thereby improving RBC clearance (Zhao et al., 2015). Recent studies have shown that CD47 can enhance RBC clearance (Tao K. et al., 2020). However, the exact role of CD47 in erythrocyte clearance remains to be further studied. Although erythrophagocytosis appears to be an effective scavenging mechanism, macrophages that ingest more than two erythrocytes undergo cell death and release heme and iron into the extracellular matrix (Knutson et al., 2005). This means that the use of erythrophagocytosis does not provide beneficial help to clear RBCs.

## Haptoglobin

Haptoglobin, an acute-phase reactant produced primarily by the liver, is the primary hemoglobin-binding protein in humans and most mammals (Buehler et al., 2020). The hemoglobin dimer produced after RBC rupture can immediately and irreversibly bind to binding haptoglobin, which is known as one of the strongest naturally occurring noncovalent interactions (Andersen et al., 2017). The binding of haptoglobin to hemoglobin reduces the redox potential of hemoglobin to reduce oxidative damage and prevent the release of heme

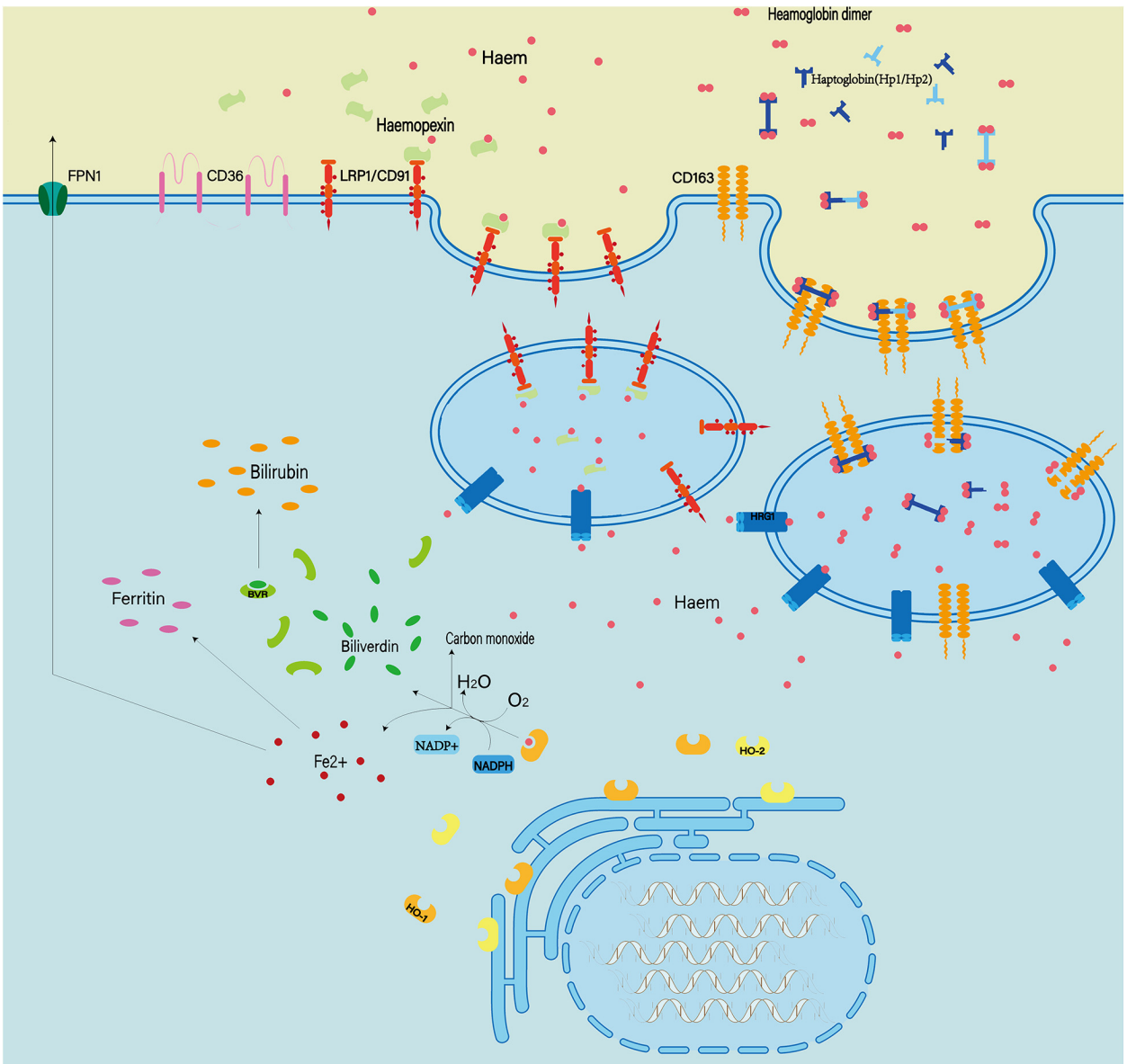


**FIGURE 7 |** Extracellular hemoglobin can be metabolized into hemoglobin dimer as well as heme. The hemoglobin dimer can bind to the haptoglobin and enter the cell mediated by CD163. Soon afterward, the hemoglobin dimer that enters the cell will be decomposed into heme. On the other hand, extracellular heme can bind to hemopexin and enter the cell mediated by CD91. In quick succession, heme and oxygen in the cell are catalyzed by heme oxygenased (HO1/2) to produce $Fe^{2+}$ ions, CO and bilirubin. In addition, abnormal red blood cells can also be cleared by phagocytosis mediated by the expression of type II scavenger receptor (CD36) on the phagocytic membrane.

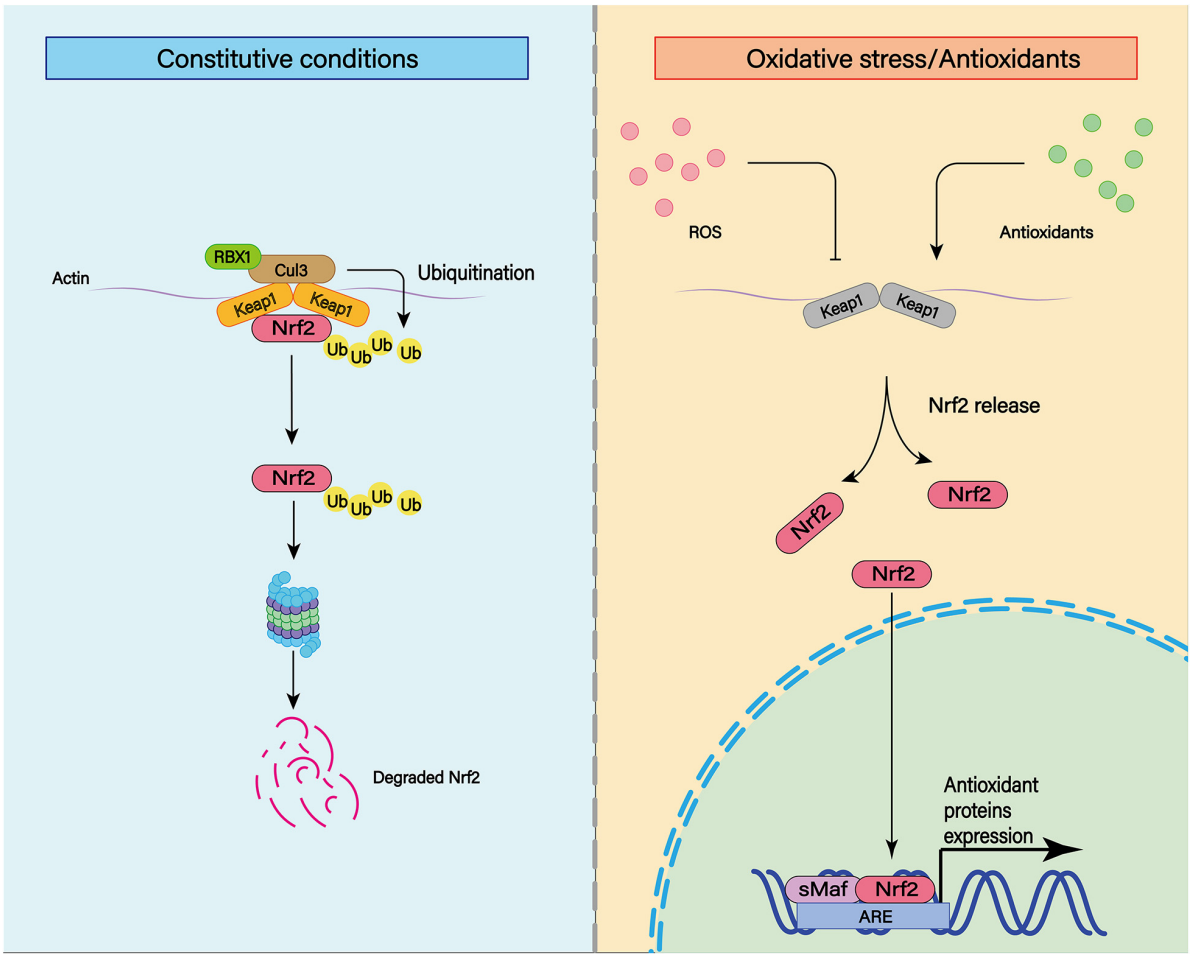


**FIGURE 8 |** The transcription factor nuclear factor erythroid-derived 2-like 2 (Nrf2) plays an important role in cellular antioxidant and other important physiological processes. Under physiological conditions, Nrf2 can be ubiquitinated and bind to Keap1. Subsequently, Nrf2 can be degraded by keAP1-dependent proteasome. In addition to ubiquitination, various post-translational modifications such as phosphorylation can affect the stability of Nrf2 structure. Under moderate oxidative stress and antioxidant stimulation, Nrf2 can enhance its stability through various post-translational modifications such as phosphorylation. At the same time, Nrf2 with enhanced stability can be translocated to the nucleus and combined with the cis-acting element ARE to activate the transcription of antioxidant genes.

and the generation of free iron during degradation of heme (Garland et al., 2020). Following the formation of haptoglobin–hemoglobin complex, CD163 (the scavenger membrane receptor) on macrophages and microglia can internalize the complex, leading to decomposition of hemoglobin in phagolysosomes (Jing et al., 2018).

The researchers found that haptoglobin has three distinct genotypes, homozygous HP1–HP1 and HP2–HP2, and heterozygous HP2–HP1, due to the two major alleles of the haptoglobin gene presented on chromosome 16 (Nielsen and Moestrup, 2009). HP1–HP1 has the best affinity with hemoglobin, and hemoglobin combined with HP1–HP1 is cleared fastest (Azarov et al., 2008; Morton et al., 2020). In the 1980s, Japanese scientists were using haptoglobin to treat hemolysis secondary to burns (Imaizumi et al., 1994). Since then, scientists have tried using haptoglobin in animal models with some success (Lipiski et al., 2013; Schaer et al., 2018). However, haptoglobin therapies have not been reported in clinical trials. In the future, many advances in recombinant protein design, truncated binding constructs, and fusion protein design will contribute to novel haptoglobin-based therapies.

## Hemopexin

Hemopexin is an acute phase plasma glycoprotein that is primarily produced by the liver and released into plasma, but it can also be expressed by neurons and glia (Morris et al., 1993; Tolosano et al., 2010). However, the level of hemopexin in the CSF is usually 10 times lower than the normal circulating level (Garland et al., 2016). Hemopexin can bind heme with high affinity to form complexes. Subsequently, the complex can bind to CD91 (low-density lipoprotein receptor-related protein-1). CD91 is a transmembrane protein that is expressed on membranes of various cells (such as macrophages, astrocytes, and oligodendrocytes) and mediates endocytosis of the complexes, leading to clearance of heme. However, one study found that approximately one-third of patients with SAH had elevated

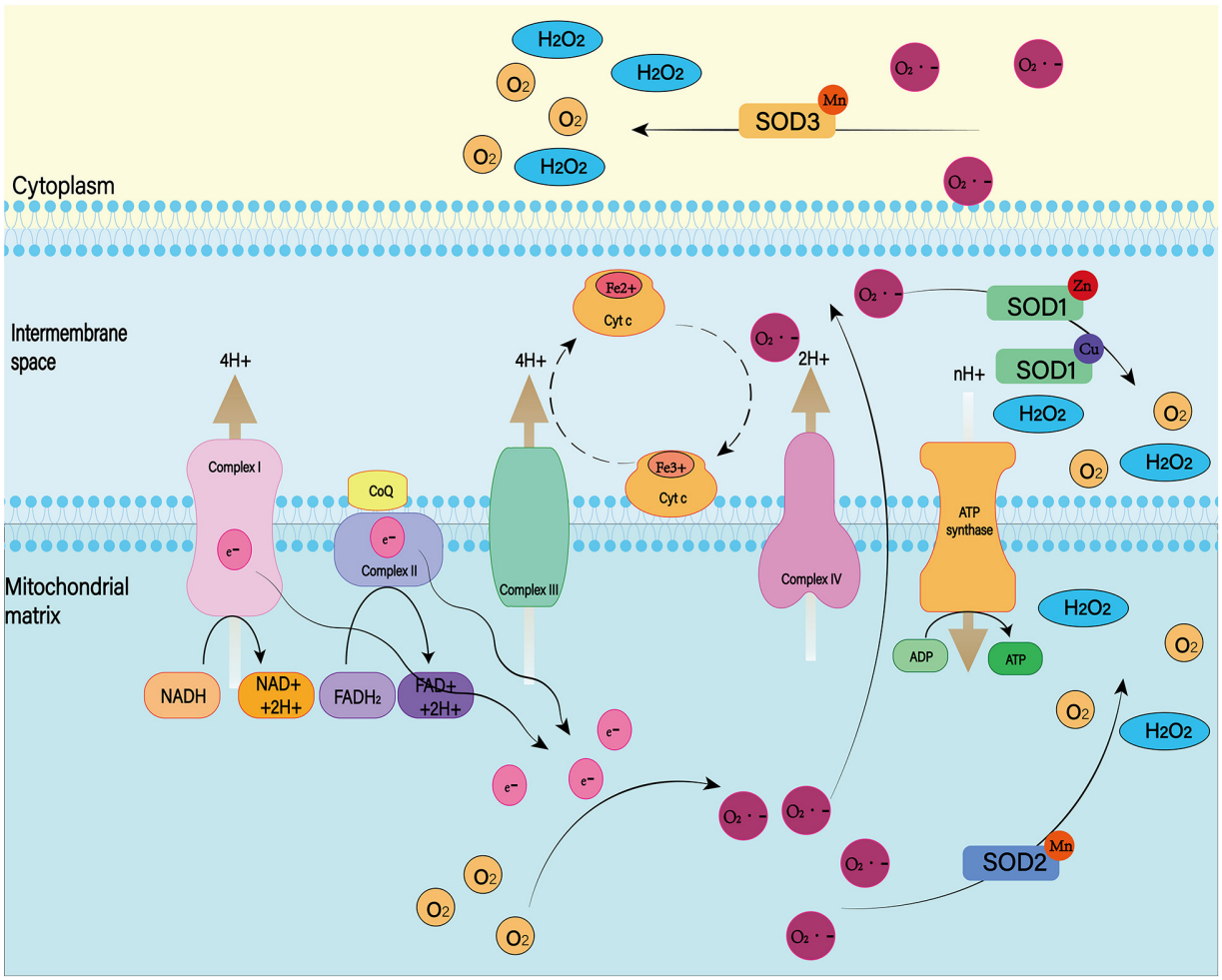


**FIGURE 9 |** There are many isotypes of SOD. Among them, SOD1, SOD2, and SOD3 play major roles in the cell. Both were able to reduce superoxide to produce $H_2O_2$ and $O_2$, but they worked in different places. SOD1 exists in the mitochondrial membrane space, SOD2 is distributed in the mitochondrial matrix, and SOD3 is distributed in the cell matrix.

heme-binding proteins in the CSF. Meanwhile, these patients were more likely to develop DCI and had poorer neurological outcomes (Garland et al., 2016). Animal studies have shown that hemopexin reduces early post-ICH damage, but does not reduce neurological deficits, inflammatory cell infiltration, or perihematoma cell viability and improve patients prognosis in the long term (Chen-Roetling et al., 2021). Nevertheless, hemopexin is recognized as protective after systemic hemolysis and may be helpful for patients with SAH (Smith and McCulloh, 2015). However, further study is still needed to confirm the neuroprotective effects of hemopexin after SAH (Griffiths et al., 2020). In the future, research should focus on more effective targeting of CNS delivery and the sustainability of efficacy.

## ANTI-INFLAMMATORY THERAPY

Clinical trials of anti-inflammatory drugs have only been studied in a small number of subjects. Therapies with steroids, statins and NSAIDs have yet to show significant clinical benefit (de Oliveira Manoel and Macdonald, 2018).

### Steroid Hormones

Steroid hormones are effective in combating inflammation and inhibiting the production of proinflammatory cytokines (Whitehouse, 2011). A retrospective study found that dexamethasone treatment appeared to reduce the risk of adverse outcomes after SAH (Czorlich et al., 2017). However, another study showed that dexamethasone use reduced poor outcomes, but not for DCI (Mohney et al., 2018). This may be because steroid hormones help maintain the water and electrolyte balance and reduce brain edema (Mistry et al., 2016).

### Statins

Statins, or 3-hydroxy-3-methylglutaryl-CoA inhibitors, can reduce total cholesterol and low-density lipoprotein (LDL), as well as triglyceride. They also increase high-density lipoprotein. Simvastatin has been shown to reduce the occurrence of

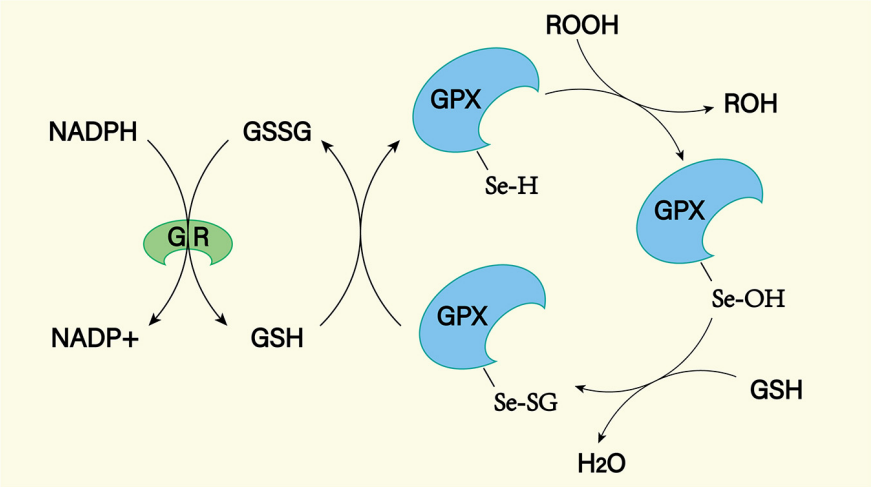


**FIGURE 10 |** The GPX mediated reduction of hydrogen peroxide and lipid hydroperoxides involves the formation of multiple intermediates with the assistance of glutathione (GSH). The selenol (–SeH) of GPX reacts with peroxides to form selenic acid (Se-OH). Then the selenic acid is reduced by GSH to form the Se-SG intermediate of GPX. GPX-Se-SG was reduced by the second GSH to form GSSG. GSSG can be reduced by glutathione reductase (GR) as reduced equivalent by NADPH.

DCI in animal models (Sugawara et al., 2008). This may be because statins exert a neuroprotective effect through a cholesterol-dependent mechanism (Tseng et al., 2007). However, a retrospective trial found that atorvastatin reduced cerebral vasospasm and infarction after SAH, but had little effect on long-term prognosis (Chen S. et al., 2020). Therefore, more evidence is needed to support the need for statins in patients with SAH (Bohara et al., 2021).

### COX Inhibitors

As mentioned above, COX is important in the pathophysiological process of SAH. Aspirin, as a nonselective COX inhibitor, inhibits the synthesis of TXA2 and prostacyclin simultaneously. Thus, aspirin inhibits the formation of microthrombosis and reduces the inflammatory response in SAH (Muroi et al., 2014; Darkwah Oppong et al., 2019). However, there are considerable differences of opinion regarding the use of NSAIDs. Although feasible in theory, they seem to have little effect in clinical practice (Young et al., 2012).

### Other Potentially Anti-inflammatory Drugs

Minocycline, a tetracycline antibiotic, has recently been found to prevent inflammation and p53-related apoptosis induced by NLRP3 inflammasomes (Li Q. et al., 2016, Li J. et al., 2016). In addition, fluoxetine, which has been shown to have anti-inflammatory effects in many diseases, attenuates NLRP3 inflammasome and caspase-1 activation through autophagy activation in animal models (Li et al., 2017). Melatonin has also been found to reduce the inflammatory response and be beneficial for early post-SAH brain injury (Dong et al., 2016).

## ANTIOXIDANT THERAPY

Excessive ROS can cause irreversible oxidative damage to cells, proteins, lipids, and DNA, leading to cell necrosis or apoptosis and subsequent cell or tissue damage. At present, there are two possible therapeutic approaches to reduce ROS: enhancing the activity of endogenous antioxidant enzymes, and preventing or reducing the production of peroxides.

### Enhance Antioxidant Capacity: Nrf2 Regulation

Nuclear factor-erythroid 2 p45-related factor 2 is a transcription factor that recognizes antioxidant response elements (AREs) to regulate the expression of a variety of genes (**Figure 8**; Shao et al., 2020). Nrf2 binds to the Kelch-like ECH-associated protein 1 (Keap1) in the cytoplasm through its binding domain. Therefore, the function of Nrf2 is regulated by Keap1 (Itoh et al., 1999). The Nrf2 system is widely expressed in CNS and is usually upregulated in response to inflammation and brain injury (Sandberg et al., 2014).

In animal experiments, Nrf2 expression is upregulated in cerebral arteries of rats after experimental SAH (Wang et al., 2010). It attenuates early brain injury such as cerebral edema, BBB injury and cortical cell apoptosis through the Nrf2–ARE pathway (Chen et al., 2011). Nrf2 can also reduce the occurrence of cerebral vasospasm (Zhao et al., 2016). After the Nrf2 gene is knocked out, brain injury of SAH rats is aggravated, including increased cerebral edema, BBB destruction, apoptosis of nerve cells, and severe neurological impairment (Li et al., 2014). Thus, existing studies have demonstrated that Nrf2 plays an important role in alleviating secondary complications induced by SAH.

Currently, sulforaphane, curcumin, astaxanthin, lycopene, melatonin, erythropoietin, and other Nrf2 system activators are

available. All of this works by binding to Keap1 to release Nrf2. Released Nrf2 translocation into the nucleus leads to increased transcription (Zolnourian et al., 2019). Currently, there is growing clinical interest in the use of Nrf2 activators in the treatment of SAH (Guo et al., 2018; Zolnourian et al., 2020). We may use this mechanism to treat patients with SAH in the future.

### Reducing Peroxides

Superoxide dismutase, glutathione peroxidase (GPX), and catalase are important peroxidase scavengers in the CNS (**Figures 9**, **10**; Lewén et al., 2000). However, the antioxidant capacity of these enzyme systems is reduced after SAH (Marzatico et al., 1993). This leads to a negative effect on the antioxidant stress after SAH. For example, decreased concentrations of SOD in plasma and CSF have been shown to be associated with long-term poor outcomes after SAH (Krenzlin et al., 2021). In addition, gene transfer of SOD was found to reduce cerebral vasospasm after experimental SAH (Watanabe et al., 2003). So far, no clinical treatment associated with exogenous antioxidant enzymes has been reported. In the future, exogenous supplementation of these enzymes will possibly reduce the level of oxidative stress in SAH patients, reduce the damage of peroxides to the CNS, and improve prognosis.

## CONCLUSION

Subarachnoid hemorrhage is a complex disease with multiple mechanisms involved in its pathophysiology. Many studies have shown that inflammatory response and oxidative stress play an important role in the progression and prognosis of SAH. It has been demonstrated that inflammatory response and oxidative stress have adverse effects on CNS function. They play a negative role in the pathophysiological processes of cognitive dysfunction, neurodegeneration and psychiatric diseases.

RBCs are the earliest cell component to enter the subarachnoid space after SAH and become the initiator of secondary SAH inflammation. Subsequently, microglia and immune cells such as neutrophils recruited from the peripheral circulation are the main bearers of SAH inflammatory response, producing and releasing a large number of proinflammatory cytokines and ROS. These, together with ROS formed during hemoglobin metabolism, which is released after rupture of RBCs, mediate damage to the CNS.

Treatment regimens (surgery and drugs) targeting secondary inflammation and oxidative stress after SAH have been shown to improve the outcomes of patients with SAH. However, there is not enough detailed basic research and sufficient, well-controlled clinical trials to draw definitive conclusions about safety and efficacy. In the future, more effective treatment regimens will be developed to help prevent complications and improve outcomes.

## AUTHOR CONTRIBUTIONS

FW: conceptualization, writing – original draft, and drawing-graph. ZL: conceptualization and drawing-graph. GL and LZ: writing – original draft. KH and ZW: drawing-graph. JS and RZ: writing – review and editing. All authors contributed to the article and approved the submitted version.

## FUNDING

This work was supported by the National Natural Science Foundation of China (82071285).

## REFERENCES

Alcalá-Cerra, G., Paternina-Caicedo, Á, Díaz-Becerra, C., Moscote-Salazar, L. R., Gutiérrez-Paternina, J. J., and Niño-Hernández, L. M. (2016). External lumbar cerebrospinal fluid drainage in patients with aneurysmal subarachnoid hemorrhage: a systematic review and meta-analysis of controlled trials. *Neurologia* 31, 431–444. doi: 10.1016/j.nrleng.2014.01.008

Ali, C., Nicole, O., Docagne, F., Lesne, S., MacKenzie, E. T., Nouvelot, A., et al. (2000). Ischemia-induced interleukin-6 as a potential endogenous neuroprotective cytokine against NMDA receptor-mediated excitotoxicity in the brain. *J. Cereb. Blood Flow Metab.* 20, 956–966. doi: 10.1097/00004647-200006000-00008

Al-Tamimi, Y. Z., Bhargava, D., Feltbower, R. G., Hall, G., Goddard, A. J., Quinn, A. C., et al. (2012). Lumbar drainage of cerebrospinal fluid after aneurysmal subarachnoid hemorrhage: a prospective, randomized, controlled trial (LUMAS). *Stroke* 43, 677–682. doi: 10.1161/strokeaha.111.625731

Andersen, C. B. F., Stødkilde, K., Sæderup, K. L., Kuhlee, A., Raunser, S., Graversen, J. H., et al. (2017). Haptoglobin. *Antioxid. Redox Signal.* 26, 814–831.

Aratani, Y. (2018). Myeloperoxidase: its role for host defense, inflammation, and neutrophil function. *Arch. Biochem. Biophys.* 640, 47–52. doi: 10.1016/j.abb.2018.01.004

Atangana, E., Schneider, U. C., Blecharz, K., Magrini, S., Wagner, J., Nieminen-Kelhä, M., et al. (2017). Intravascular inflammation triggers intracerebral activated microglia and contributes to secondary brain injury after experimental subarachnoid hemorrhage (eSAH). *Transl. Stroke Res.* 8, 144–156. doi: 10.1007/s12975-016-0485-3

Ayer, R., Jadhav, V., Sugawara, T., and Zhang, J. H. (2011). The neuroprotective effects of cyclooxygenase-2 inhibition in a mouse model of aneurysmal subarachnoid hemorrhage. *Acta Neurochir. Suppl.* 111, 145–149. doi: 10.1007/978-3-7091-0693-8_24

Azam, S., Jakaria, M., Kim, I. S., Kim, J., Haque, M. E., and Choi, D. K. (2019). Regulation of toll-like receptor (TLR) signaling pathway by polyphenols in the treatment of age-linked neurodegenerative diseases: focus on TLR4 signaling. *Front. Immunol.* 10:1000. doi: 10.3389/fimmu.2019.01000

Azarov, I., He, X., Jeffers, A., Basu, S., Ucer, B., Hantgan, R. R., et al. (2008). Rate of nitric oxide scavenging by hemoglobin bound to haptoglobin. *Nitric Oxide* 18, 296–302. doi: 10.1016/j.niox.2008.02.006

Bai, Q., Xue, M., and Yong, V. W. (2020). Microglia and macrophage phenotypes in intracerebral haemorrhage injury: therapeutic opportunities. *Brain* 143, 1297–1314. doi: 10.1093/brain/awz393

Becher, B., Spath, S., and Goverman, J. (2017). Cytokine networks in neuroinflammation. *Nat. Rev. Immunol.* 17, 49–59. doi: 10.1038/nri.2016.123

Blecharz-Lang, K. G., Wagner, J., Fries, A., Nieminen-Kelhä, M., Rösner, J., Schneider, U. C., et al. (2018). Interleukin 6-mediated endothelial barrier disturbances can be attenuated by blockade of the IL6 receptor expressed in brain microvascular endothelial cells. *Transl. Stroke Res.* 9, 631–642. doi: 10.1007/s12975-018-0614-2

Bohara, S., Gaonkar, V. B., Garg, K., Rajpal, P. M. S., Singh, P. K., Singh, M., et al. (2021). Effect of statins on functional outcome and mortality following aneurysmal subarachnoid hemorrhage–results of a meta-analysis, metaregression and trial sequential analysis. *Clin. Neurol. Neurosurg.* 207:106787. doi: 10.1016/j.clineuro.2021.106787

Bozza, M. T., and Jeney, V. (2020). Pro-inflammatory actions of heme and other hemoglobin-derived DAMPs. *Front. Immunol.* 11:1323. doi: 10.3389/fimmu.2020.01323

Brathwaite, S., and Macdonald, R. L. (2014). Current management of delayed cerebral ischemia: update from results of recent clinical trials. *Transl. Stroke Res.* 5, 207–226. doi: 10.1007/s12975-013-0316-8

Buehler, P. W., Humar, R., and Schaer, D. J. (2020). Haptoglobin therapeutics and compartmentalization of cell-free hemoglobin toxicity. *Trends Mol. Med.* 26, 683–697. doi: 10.1016/j.molmed.2020.02.004

Bulters, D., Gaastra, B., Zolnourian, A., Alexander, S., Ren, D., Blackburn, S. L., et al. (2018). Haemoglobin scavenging in intracranial bleeding: biology and clinical implications. *Nat. Rev. Neurol.* 14, 416–432. doi: 10.1038/s41582-018-0020-0

Chan, D. C. (2006). Mitochondria: dynamic organelles in disease, aging, and development. *Cell* 125, 1241–1252. doi: 10.1016/j.cell.2006.06.010

Chaudhry, S. R., Hafez, A., Rezai Jahromi, B., Kinfe, T. M., Lamprecht, A., Niemelä, M., et al. (2018). Role of damage associated molecular pattern molecules (DAMPs) in aneurysmal subarachnoid hemorrhage (aSAH). *Int. J. Mol. Sci.* 19:2035. doi: 10.3390/ijms19072035

Chen, G., Fang, Q., Zhang, J., Zhou, D., and Wang, Z. (2011). Role of the Nrf2-ARE pathway in early brain injury after experimental subarachnoid hemorrhage. *J. Neurosci. Res.* 89, 515–523. doi: 10.1002/jnr.22577

Chen, J., Li, M., Zhu, X., Chen, L., Yang, S., Zhang, C., et al. (2020). Atorvastatin reduces cerebral vasospasm and infarction after aneurysmal subarachnoid hemorrhage in elderly Chinese adults. *Aging (Albany N. Y.)* 12, 2939–2951. doi: 10.18632/aging.102788

Chen, S., Chen, H., Du, Q., and Shen, J. (2020). Targeting myeloperoxidase (MPO) mediated oxidative stress and inflammation for reducing brain ischemia injury: potential application of natural compounds. *Front. Physiol.* 11:433. doi: 10.3389/fphys.2020.00433

Chen-Roetling, J., Li, Y., Cao, Y., Yan, Z., Lu, X., and Regan, R. F. (2021). Effect of hemopexin treatment on outcome after intracerebral hemorrhage in mice. *Brain Res.* 1765, 147507. doi: 10.1016/j.brainres.2021.147507

Chu, Y., Wilson, K., Gu, H., Wegman-Points, L., Dooley, S. A., Pierce, G. L., et al. (2015). Myeloperoxidase is increased in human cerebral aneurysms and increases formation and rupture of cerebral aneurysms in mice. *Stroke* 46, 1651–1666. doi: 10.1161/strokeaha.114.008589

Ciesielska, A., Matyjek, M., and Kwiatkowska, K. (2021). TLR4 and CD14 trafficking and its influence on LPS-induced pro-inflammatory signaling. *Cell. Mol. Life Sci.* 78, 1233–1261. doi: 10.1007/s00018-020-03656-y

Cinelli, M. A., Do, H. T., Miley, G. P., and Silverman, R. B. (2020). Inducible nitric oxide synthase: regulation, structure, and inhibition. *Med. Res. Rev.* 40, 158–189. doi: 10.1002/med.21599

Coulibaly, A. P., Gartman, W. T., Swank, V., Gomes, J. A., Ruozhuo, L., DeBacker, J., et al. (2020). RAR-related orphan receptor gamma T (RoRγt)-related cytokines play a role in neutrophil infiltration of the central nervous system after subarachnoid hemorrhage. *Neurocrit. Care* 33, 140–151. doi: 10.1007/s12028-019-00871-9

Coulibaly, A. P., and Provencio, J. J. (2020). Aneurysmal subarachnoid hemorrhage: an overview of inflammation-induced cellular changes. *Neurotherapeutics* 17, 436–445. doi: 10.1007/s13311-019-00829-x

Cunningham, C., Dunne, A., and Lopez-Rodriguez, A. B. (2019). Astrocytes: heterogeneous and dynamic phenotypes in neurodegeneration and innate immunity. *Neuroscientist* 25, 455–474. doi: 10.1177/1073858418809941

Czorlich, P., Sauvigny, T., Ricklefs, F., Abboud, T., Nierhaus, A., Vettorazzi, E., et al. (2017). Impact of dexamethasone in patients with aneurysmal subarachnoid haemorrhage. *Eur. J. Neurol.* 24, 645–651.

Darkwah Oppong, M., Gembruch, O., Pierscianek, D., Köhrmann, M., Kleinschnitz, C., Deuschl, C., et al. (2019). Post-treatment antiplatelet therapy reduces risk for delayed cerebral ischemia due to aneurysmal subarachnoid hemorrhage. *Neurosurgery* 85, 827–833. doi: 10.1093/neuros/nyy550

de Oliveira Manoel, A. L., and Macdonald, R. L. (2018). Neuroinflammation as a target for intervention in subarachnoid hemorrhage. *Front. Neurol.* 9:292. doi: 10.3389/fneur.2018.00292

Ding, R., Chen, Y., Yang, S., Deng, X., Fu, Z., Feng, L., et al. (2014). Blood-brain barrier disruption induced by hemoglobin in vivo: involvement of up-regulation of nitric oxide synthase and peroxynitrite formation. *Brain Res.* 1571, 25–38. doi: 10.1016/j.brainres.2014.04.042

Dong, Y., Fan, C., Hu, W., Jiang, S., Ma, Z., Yan, X., et al. (2016). Melatonin attenuated early brain injury induced by subarachnoid hemorrhage via regulating NLRP3 inflammasome and apoptosis signaling. *J. Pineal. Res.* 60, 253–262. doi: 10.1111/jpi.12300

Dröse, S., and Brandt, U. (2012). Molecular mechanisms of superoxide production by the mitochondrial respiratory chain. *Adv. Exp. Med. Biol.* 748, 145–169. doi: 10.1007/978-1-4614-3573-0_6

Eastman, C. L., D'Ambrosio, R., and Ganesh, T. (2020). Modulating neuroinflammation and oxidative stress to prevent epilepsy and improve outcomes after traumatic brain injury. *Neuropharmacology* 172:107907. doi: 10.1016/j.neuropharm.2019.107907

Erta, M., Quintana, A., and Hidalgo, J. (2012). Interleukin-6, a major cytokine in the central nervous system. *Int. J. Biol. Sci.* 8, 1254–1266. doi: 10.7150/ijbs.4679

Etminan, N., Beseoglu, K., Eicker, S. O., Turowski, B., Steiger, H. J., and Hänggi, D. (2013). Prospective, randomized, open-label phase II trial on concomitant intraventricular fibrinolysis and low-frequency rotation after severe subarachnoid hemorrhage. *Stroke* 44, 2162–2168.

Etminan, N., Vergouwen, M. D., Ilodigwe, D., and Macdonald, R. L. (2011). Effect of pharmaceutical treatment on vasospasm, delayed cerebral ischemia, and clinical outcome in patients with aneurysmal subarachnoid hemorrhage: a systematic review and meta-analysis. *J. Cereb. Blood Flow Metab.* 31, 1443–1451. doi: 10.1038/jcbfm.2011.7

Francoeur, C. L., and Mayer, S. A. (2016). Management of delayed cerebral ischemia after subarachnoid hemorrhage. *Crit. Care* 20:277.

Ganguly, U., Kaur, U., Chakrabarti, S. S., Sharma, P., Agrawal, B. K., Saso, L., et al. (2021). Oxidative stress, neuroinflammation, and NADPH oxidase: implications in the pathogenesis and treatment of Alzheimer's disease. *Oxid. Med. Cell. Longev.* 2021:7086512.

Garland, P., Durnford, A. J., Okemefuna, A. I., Dunbar, J., Nicoll, J. A., Galea, J., et al. (2016). Heme-hemopexin scavenging is active in the brain and associates with outcome after subarachnoid hemorrhage. *Stroke* 47, 872–876. doi: 10.1161/strokeaha.115.011956

Garland, P., Morton, M. J., Haskins, W., Zolnourian, A., Durnford, A., Gaastra, B., et al. (2020). Haemoglobin causes neuronal damage in vivo which is preventable by haptoglobin. *Brain Commun.* 2:fcz053.

Geraghty, J. R., Davis, J. L., and Testai, F. D. (2019). Neuroinflammation and microvascular dysfunction after experimental subarachnoid hemorrhage: emerging components of early brain injury related to outcome. *Neurocrit. Care* 31, 373–389. doi: 10.1007/s12028-019-00710-x

Ghaemi, A., Alizadeh, L., Babaei, S., Jafarian, M., Khaleghi Ghadiri, M., Meuth, S. G., et al. (2018). Astrocyte-mediated inflammation in cortical spreading depression. *Cephalalgia* 38, 626–638. doi: 10.1177/0333102417702132

Giede-Jeppe, A., Reichl, J., Sprügel, M. I., Lücking, H., Hoelter, P., Eyüpoglu, I. Y., et al. (2019). Neutrophil-to-lymphocyte ratio as an independent predictor for unfavorable functional outcome in aneurysmal subarachnoid hemorrhage. *J. Neurosurg.* 132, 400–407. doi: 10.3171/2018.9.jns181975

Graves, S. I., and Baker, D. J. (2020). Implicating endothelial cell senescence to dysfunction in the ageing and diseased brain. *Basic Clin. Pharmacol. Toxicol.* 127, 102–110. doi: 10.1111/bcpt.13403

Griffiths, S., Clark, J., Adamides, A. A., and Ziogas, J. (2020). The role of haptoglobin and hemopexin in the prevention of delayed cerebral ischaemia after aneurysmal subarachnoid haemorrhage: a review of current literature. *Neurosurg. Rev.* 43, 1273–1288. doi: 10.1007/s10143-019-01169-2

Gris, T., Laplante, P., Thebault, P., Cayrol, R., Najjar, A., Joannette-Pilon, B., et al. (2019). Innate immunity activation in the early brain injury period following subarachnoid hemorrhage. *J. Neuroinflammation* 16:253.

Grylls, A., Seidler, K., and Neil, J. (2021). Link between microbiota and hypertension: focus on LPS/TLR4 pathway in endothelial dysfunction and vascular inflammation, and therapeutic implication of probiotics. *Biomed. Pharmacother.* 137:111334.

Guilpain, P., Servettaz, A., Batteux, F., Guillevin, L., and Mouthon, L. (2008). Natural and disease associated anti-myeloperoxidase (MPO) autoantibodies. *Autoimmun. Rev.* 7, 421–425. doi: 10.1016/j.autrev.2008.03.009

Guo, Z. N., Jin, H., Sun, H., Zhao, Y., Liu, J., Ma, H., et al. (2018). Antioxidant melatonin: potential functions in improving cerebral autoregulation after subarachnoid hemorrhage. *Front. Physiol.* 9:1146. doi: 10.3389/fphys.2018.01146

Halcrow, P. W., Lynch, M. L., Geiger, J. D., and Ohm, J. E. (2021). Role of endolysosome function in iron metabolism and brain carcinogenesis. *Semin. Cancer Biol.* (in press). doi: 10.1016/j.semcancer.2021.06.013

Hanhai, Z., Bin, Q., Shengjun, Z., Jingbo, L., Yinghan, G., Lingxin, C., et al. (2021). Neutrophil extracellular traps, released from neutrophil, promote microglia inflammation and contribute to poor outcome in subarachnoid hemorrhage. *Aging (Albany N. Y.)* 13, 13108–13123. doi: 10.18632/aging.202993

Hayman, E. G., Wessell, A., Gerzanich, V., Sheth, K. N., and Simard, J. M. (2017). Mechanisms of global cerebral edema formation in aneurysmal subarachnoid hemorrhage. *Neurocrit. Care* 26, 301–310. doi: 10.1007/s12028-016-0354-7

Healy, L. M., Yaqubi, M., Ludwin, S., and Antel, J. P. (2020). Species differences in immune-mediated CNS tissue injury and repair: a (neuro)inflammatory topic. *Glia* 68, 811–829. doi: 10.1002/glia.23746

Hu, X., Leak, R. K., Shi, Y., Suenaga, J., Gao, Y., Zheng, P., et al. (2015). Microglial and macrophage polarization—new prospects for brain repair. *Nat. Rev. Neurol.* 11, 56–64. doi: 10.1038/nrneurol.2014.207

Hu, X., Tao, C., Gan, Q., Zheng, J., Li, H., and You, C. (2016). Oxidative stress in intracerebral hemorrhage: sources, mechanisms, and therapeutic targets. *Oxid. Med. Cell Longev.* 2016:3215391.

Huang, F. P., Xi, G., Keep, R. F., Hua, Y., Nemoianu, A., and Hoff, J. T. (2002). Brain edema after experimental intracerebral hemorrhage: role of hemoglobin degradation products. *J. Neurosurg.* 96, 287–293. doi: 10.3171/jns.2002.96.2.0287

Hugelshofer, M., Sikorski, C. M., Seule, M., Deuel, J., Muroi, C. I., Seboek, M., et al. (2018). Cell-free oxyhemoglobin in cerebrospinal fluid after aneurysmal subarachnoid hemorrhage: biomarker and potential therapeutic target. *World Neurosurg.* 120, e660–e666.

Hyvärinen, T., Hagman, S., Ristola, M., Sukki, L., Veijula, K., Kreutzer, J., et al. (2019). Co-stimulation with IL-1β and TNF-α induces an inflammatory reactive astrocyte phenotype with neurosupportive characteristics in a human pluripotent stem cell model system. *Sci. Rep.* 9:16944.

Imaizumi, H., Tsunoda, K., Ichimiya, N., Okamoto, T., and Namiki, A. (1994). Repeated large-dose haptoglobin therapy in an extensively burned patient: case report. *J. Emerg. Med.* 12, 33–37. doi: 10.1016/0736-4679(94)90009-4

Ishiguro, M., Morielli, A. D., Zvarova, K., Tranmer, B. I., Penar, P. L., and Wellman, G. C. (2006). Oxyhemoglobin-induced suppression of voltage-dependent K+ channels in cerebral arteries by enhanced tyrosine kinase activity. *Circ. Res.* 99, 1252–1260. doi: 10.1161/01.res.0000250821.32324.e1

Itoh, K., Wakabayashi, N., Katoh, Y., Ishii, T., Igarashi, K., Engel, J. D., et al. (1999). Keap1 represses nuclear activation of antioxidant responsive elements by Nrf2 through binding to the amino-terminal Neh2 domain. *Genes Dev.* 13, 76–86. doi: 10.1101/gad.13.1.76

Jackson, C. M., Choi, J., Routkevitch, D., Pant, A., Saleh, L., Ye, X., et al. (2021). PD-1+ monocytes mediate cerebral vasospasm following subarachnoid hemorrhage. *Neurosurgery* 88, 855–863. doi: 10.1093/neuros/nyaa495

Jedrzejowska-Szypułka, H., Straszak, G., Larysz-Brysz, M., Karpe, J., Marcol, W., Olakowska, E., et al. (2010). Interleukin-1beta plays a role in the activation of peripheral leukocytes after blood-brain barrier rupture in the course of subarachnoid hemorrhage. *Curr. Neurovasc. Res.* 7, 39–48. doi: 10.2174/156720210790820226

Jing, C., Zhang, H., Shishido, H., Keep, R. F., and Hua, Y. (2018). Association of brain CD163 expression and brain injury/hydrocephalus development in a rat model of subarachnoid hemorrhage. *Front. Neurosci.* 12:313. doi: 10.3389/fnins.2018.00313

Johnson, J., Mercado-Ayon, E., Mercado-Ayon, Y., Dong, Y. N., Halawani, S., Ngaba, L., et al. (2021). Mitochondrial dysfunction in the development and progression of neurodegenerative diseases. *Arch. Biochem. Biophys.* 702:108698.

Jullienne, A., Obenaus, A., Ichkova, A., Savona-Baron, C., Pearce, W. J., and Badaut, J. (2016). Chronic cerebrovascular dysfunction after traumatic brain injury. *J. Neurosci. Res.* 94, 609–622. doi: 10.1002/jnr.23732

Kargapolova, Y., Geißen, S., Zheng, R., Baldus, S., Winkels, H., and Adam, M. (2021). The enzymatic and non-enzymatic function of myeloperoxidase (MPO) in inflammatory communication. *Antioxidants (Basel)* 10:562. doi: 10.3390/antiox10040562

Karimy, J. K., Reeves, B. C., and Kahle, K. T. (2020). Targeting TLR4-dependent inflammation in post-hemorrhagic brain injury. *Expert Opin. Ther. Targets* 24, 525–533. doi: 10.1080/14728222.2020.1752182

Katsu, M., Niizuma, K., Yoshioka, H., Okami, N., Sakata, H., and Chan, P. H. (2010). Hemoglobin-induced oxidative stress contributes to matrix metalloproteinase activation and blood-brain barrier dysfunction in vivo. *J. Cereb. Blood Flow Metab.* 30, 1939–1950. doi: 10.1038/jcbfm.2010.45

Kaur, D., Sharma, V., and Deshmukh, R. (2019). Activation of microglia and astrocytes: a roadway to neuroinflammation and Alzheimer's disease. *Inflammopharmacology* 27, 663–677. doi: 10.1007/s10787-019-00580-x

Kim, D. E., Suh, Y. S., Lee, M. S., Kim, K. Y., Lee, J. H., Lee, H. S., et al. (2002). Vascular NAD(P)H oxidase triggers delayed cerebral vasospasm after subarachnoid hemorrhage in rats. *Stroke* 33, 2687–2691. doi: 10.1161/01.str.0000033071.99143.9e

Klimo, P. Jr., Kestle, J. R., MacDonald, J. D., and Schmidt, R. H. (2004). Marked reduction of cerebral vasospasm with lumbar drainage of cerebrospinal fluid after subarachnoid hemorrhage. *J. Neurosurg.* 100, 215–224. doi: 10.3171/jns.2004.100.2.0215

Knutson, M. D., Oukka, M., Koss, L. M., Aydemir, F., and Wessling-Resnick, M. (2005). Iron release from macrophages after erythrophagocytosis is up-regulated by ferroportin 1 overexpression and down-regulated by hepcidin. *Proc. Natl. Acad. Sci. U.S.A.* 102, 1324–1328. doi: 10.1073/pnas.0409409102

Kooijman, E., Nijboer, C. H., van Velthoven, C. T., Mol, W., Dijkhuizen, R. M., Kesecioglu, J., et al. (2014). Long-term functional consequences and ongoing cerebral inflammation after subarachnoid hemorrhage in the rat. *PLoS One* 9:e90584. doi: 10.1371/journal.pone.0090584

Kramer, A. H., Jenne, C. N., Zygun, D. A., Roberts, D. J., Hill, M. D., Holodinsky, J. K., et al. (2015). Intraventricular fibrinolysis with tissue plasminogen activator is associated with transient cerebrospinal fluid inflammation: a randomized controlled trial. *J. Cereb. Blood Flow Metab.* 35, 1241–1248. doi: 10.1038/jcbfm.2015.47

Krenzlin, H., Wesp, D., Schmitt, J., Frenz, C., Kurz, E., Masomi-Bornwasser, J., et al. (2021). Decreased superoxide dismutase concentrations (SOD) in plasma and csf and increased circulating total antioxidant capacity (TAC) are associated with unfavorable neurological outcome after aneurysmal subarachnoid hemorrhage. *J. Clin. Med.* 10:1188. doi: 10.3390/jcm10061188

Kwan, K., Arapi, O., Wagner, K. E., Schneider, J., Sy, H. L., Ward, M. F., et al. (2019). Cerebrospinal fluid macrophage migration inhibitory factor: a potential predictor of cerebral vasospasm and clinical outcome after aneurysmal subarachnoid hemorrhage. *J. Neurosurg.* [E pub ahead of print],

Lehnardt, S. (2010). Innate immunity and neuroinflammation in the CNS: the role of microglia in Toll-like receptor-mediated neuronal injury. *Glia* 58, 253–263.

Leitner, G. R., Wenzel, T. J., Marshall, N., Gates, E. J., and Klegeris, A. (2019). Targeting toll-like receptor 4 to modulate neuroinflammation in central nervous system disorders. *Expert. Opin. Ther. Targets* 23, 865–882. doi: 10.1080/14728222.2019.1676416

Lenz, I. J., Plesnila, N., and Terpolilli, N. A. (2021). Role of endothelial nitric oxide synthase for early brain injury after subarachnoid hemorrhage in mice. *J. Cereb. Blood Flow Metab.* 41, 1669–1681. doi: 10.1177/0271678x20973787

Lewén, A., Matz, P., and Chan, P. H. (2000). Free radical pathways in CNS injury. *J. Neurotrauma* 17, 871–890. doi: 10.1089/neu.2000.17.871

Li, B., Luo, C., Tang, W., Chen, Z., Li, Q., Hu, B., et al. (2012). Role of HCN channels in neuronal hyperexcitability after subarachnoid hemorrhage in rats. *J. Neurosci.* 32, 3164–3175. doi: 10.1523/jneurosci.5143-11.2012

Li, J., Chen, J., Mo, H., Chen, J., Qian, C., Yan, F., et al. (2016). Minocycline protects against NLRP3 inflammasome-induced inflammation and P53-associated apoptosis in early brain injury after subarachnoid hemorrhage. *Mol. Neurobiol.* 53, 2668–2678. doi: 10.1007/s12035-015-9318-8

Li, J. R., Xu, H. Z., Nie, S., Peng, Y. C., Fan, L. F., Wang, Z. J., et al. (2017). Fluoxetine-enhanced autophagy ameliorates early brain injury via inhibition of NLRP3 inflammasome activation following subrachnoid hemorrhage in rats. *J. Neuroinflammation* 14:186.

Li, L., Acioglu, C., Heary, R. F., and Elkabes, S. (2021). Role of astroglial toll-like receptors (TLRs) in central nervous system infections, injury and neurodegenerative diseases. *Brain Behav. Immun.* 91, 740–755. doi: 10.1016/j.bbi.2020.10.007

Li, Q., Chen, Y., Li, B., Luo, C., Zuo, S., Liu, X., et al. (2016). Hemoglobin induced NO/cGMP suppression deteriorate microcirculation via pericyte phenotype transformation after subarachnoid hemorrhage in rats. *Sci. Rep.* 6:22070.

Li, T., Wang, H., Ding, Y., Zhou, M., Zhou, X., Zhang, X., et al. (2014). Genetic elimination of Nrf2 aggravates secondary complications except for vasospasm

after experimental subarachnoid hemorrhage in mice. *Brain Res.* 1558, 90–99. doi: 10.1016/j.brainres.2014.02.036

Lim, M., Bower, R. S., Wang, Y., Sims, L., Bower, M. R., Camara-Quintana, J., et al. (2012). The predictive value of serum myeloperoxidase for vasospasm in patients with aneurysmal subarachnoid hemorrhage. *Neurosurg. Rev.* 35, 413–419; discussion 149.

Link, T. E., Murakami, K., Beem-Miller, M., Tranmer, B. I., and Wellman, G. C. (2008). Oxyhemoglobin-induced expression of R-type Ca2+ channels in cerebral arteries. *Stroke* 39, 2122–2128. doi: 10.1161/strokeaha.107.508754

Lipiski, M., Deuel, J. W., Baek, J. H., Engelsberger, W. R., Buehler, P. W., and Schaer, D. J. (2013). Human Hp1-1 and Hp2-2 phenotype-specific haptoglobin therapeutics are both effective in vitro and in guinea pigs to attenuate hemoglobin toxicity. *Antioxid. Redox Signal.* 19, 1619–1633. doi: 10.1089/ars.2012.5089

López-Cortés, L. F., Marquez-Arbizu, R., Jimenez-Jimenez, L. M., Jimenez-Mejías, E., Caballero-Granado, F. J., Rey-Romero, C., et al. (2000). Cerebrospinal fluid tumor necrosis factor-alpha, interleukin-1beta, interleukin-6, and interleukin-8 as diagnostic markers of cerebrospinal fluid infection in neurosurgical patients. *Crit. Care Med.* 28, 215–219. doi: 10.1097/00003246-200001000-00035

Lu, H., Shi, J. X., Chen, H. L., Hang, C. H., Wang, H. D., and Yin, H. X. (2009). Expression of monocyte chemoattractant protein-1 in the cerebral artery after experimental subarachnoid hemorrhage. *Brain Res.* 1262, 73–80. doi: 10.1016/j.brainres.2009.01.017

Lu, P., Takai, K., Weaver, V. M., and Werb, Z. (2011). Extracellular matrix degradation and remodeling in development and disease. *Cold Spring Harb. Perspect. Biol.* 3:a005058. doi: 10.1101/cshperspect.a005058

Lu, Y., Yang, Y., Peng, Z., Xie, L., Zhong, X., Liang, F., et al. (2020). Silencing IFNγ inhibits A1 astrocytes and attenuates neurogenesis decline and cognitive impairment in endotoxemia. *Biochem. Biophys. Res. Commun.* 533, 1519–1526. doi: 10.1016/j.bbrc.2020.10.084

Lucke-Wold, B. P., Logsdon, A. F., Manoranjan, B., Turner, R. C., McConnell, E., Vates, G. E., et al. (2016). Aneurysmal subarachnoid hemorrhage and neuroinflammation: a comprehensive review. *Int. J. Mol. Sci.* 17:497. doi: 10.3390/ijms17040497

Macdonald, R. L. (2014). Delayed neurological deterioration after subarachnoid haemorrhage. *Nat. Rev. Neurol.* 10, 44–58. doi: 10.1038/nrneurol.2013.246

MacVicar, B. A., and Newman, E. A. (2015). Astrocyte regulation of blood flow in the brain. *Cold Spring Harb. Perspect. Biol.* 7:a020388. doi: 10.1101/cshperspect.a020388

Marnett, L. J., Riggins, J. N., and West, J. D. (2003). Endogenous generation of reactive oxidants and electrophiles and their reactions with DNA and protein. *J. Clin. Invest.* 111, 583–593. doi: 10.1172/jci200318022

Marzatico, F., Gaetani, P., Cafè, C., Spanu, G., and Rodriguez y Baena, R. (1993). Antioxidant enzymatic activities after experimental subarachnoid hemorrhage in rats. *Acta Neurol. Scand.* 87, 62–66. doi: 10.1111/j.1600-0404.1993.tb04077.x

Marzatico, F., Gaetani, P., Silvani, V., Lombardi, D., Sinforiani, E., and Rodriguez y Baena, R. (1990). Experimental isobaric subarachnoid hemorrhage: regional mitochondrial function during the acute and late phase. *Surg. Neurol.* 34, 294–300. doi: 10.1016/0090-3019(90)90004-9

Miller, A. A., Drummond, G. R., and Sobey, C. G. (2006). Novel isoforms of NADPH-oxidase in cerebral vascular control. *Pharmacol. Ther.* 111, 928–948. doi: 10.1016/j.pharmthera.2006.02.005

Mistry, A. M., Mistry, E. A., Ganesh Kumar, N., Froehler, M. T., Fusco, M. R., and Chitale, R. V. (2016). Corticosteroids in the management of hyponatremia, hypovolemia, and vasospasm in subarachnoid hemorrhage: a meta-analysis. *Cerebrovasc. Dis.* 42, 263–271. doi: 10.1159/000446251

Mittal, M., Siddiqui, M. R., Tran, K., Reddy, S. P., and Malik, A. B. (2014). Reactive oxygen species in inflammation and tissue injury. *Antioxid. Redox Signal.* 20, 1126–1167. doi: 10.1089/ars.2012.5149

Mohney, N., Williamson, C. A., Rothman, E., Ball, R., Sheehan, K. M., Pandey, A. S., et al. (2018). A propensity score analysis of the impact of dexamethasone use on delayed cerebral ischemia and poor functional outcomes after subarachnoid hemorrhage. *World Neurosurg.* 109, e655–e661.

Morga, R., Dziedzic, T., Moskala, M., Slowik, A., and Pera, J. (2020). Clinical relevance of changes in peripheral blood cells after intracranial aneurysm rupture. *J. Stroke Cerebrovasc. Dis.* 29:105293. doi: 10.1016/j.jstrokecerebrovasdis.2020.105293

Morris, C. M., Candy, J. M., Edwardson, J. A., Bloxham, C. A., and Smith, A. (1993). Evidence for the localization of haemopexin immunoreactivity in neurones in the human brain. *Neurosci. Lett.* 149, 141–144. doi: 10.1016/0304-3940(93)90756-b

Morton, M. J., Hostettler, I. C., Kazmi, N., Alg, V. S., Bonner, S., Brown, M. M., et al. (2020). Haptoglobin genotype and outcome after aneurysmal subarachnoid haemorrhage. *J. Neurol. Neurosurg. Psychiatry* 91, 305–313.

Muroi, C., Hugelshofer, M., Seule, M., and Keller, E. (2014). The impact of nonsteroidal anti-inflammatory drugs on inflammatory response after aneurysmal subarachnoid hemorrhage. *Neurocrit. Care* 20, 240–246. doi: 10.1007/s12028-013-9930-2

Nayernia, Z., Jaquet, V., and Krause, K. H. (2014). New insights on NOX enzymes in the central nervous system. *Antioxid. Redox Signal.* 20, 2815–2837. doi: 10.1089/ars.2013.5703

Neifert, S. N., Chapman, E. K., Martini, M. L., Shuman, W. H., Schupper, A. J., Oermann, E. K., et al. (2021). Aneurysmal subarachnoid hemorrhage: the last decade. *Transl. Stroke Res.* 12, 428–446.

Neulen, A., Pantel, T., Kosterhon, M., Kramer, A., Kunath, S., Petermeyer, M., et al. (2019). Neutrophils mediate early cerebral cortical hypoperfusion in a murine model of subarachnoid haemorrhage. *Sci. Rep.* 9:8460.

Nielsen, M. J., and Moestrup, S. K. (2009). Receptor targeting of hemoglobin mediated by the haptoglobins: roles beyond heme scavenging. *Blood* 114, 764–771. doi: 10.1182/blood-2009-01-198309

Niwa, A., Osuka, K., Nakura, T., Matsuo, N., Watabe, T., and Takayasu, M. (2016). Interleukin-6, MCP-1, IP-10, and MIG are sequentially expressed in cerebrospinal fluid after subarachnoid hemorrhage. *J. Neuroinflammation.* 13:217.

Nolfi-Donegan, D., Braganza, A., and Shiva, S. (2020). Mitochondrial electron transport chain: oxidative phosphorylation, oxidant production, and methods of measurement. *Redox Biol.* 37:101674. doi: 10.1016/j.redox.2020.101674

Okada, T., and Suzuki, H. (2017). Toll-like receptor 4 as a possible therapeutic target for delayed brain injuries after aneurysmal subarachnoid hemorrhage. *Neural. Regen. Res.* 12, 193–196. doi: 10.4103/1673-5374.200795

Oruckaptan, H. H., Caner, H. H., Kilinc, K., and Ozgen, T. (2000). No apparent role for neutrophils and neutrophil-derived myeloperoxidase in experimental subarachnoid haemorrhage and vasospasm: a preliminary study. *Acta Neurochir. (Wien.)* 142, 83–90. doi: 10.1007/s007010050011

Østergaard, L., Aamand, R., Karabegovic, S., Tietze, A., Blicher, J. U., Mikkelsen, I. K., et al. (2013). The role of the microcirculation in delayed cerebral ischemia and chronic degenerative changes after subarachnoid hemorrhage. *J. Cereb. Blood Flow Metab.* 33, 1825–1837. doi: 10.1038/jcbfm.2013.173

Osuka, K., Watanabe, Y., Suzuki, C., Iwami, K., and Miyachi, S. (2021). Sequential expression of neutrophil chemoattractants in cerebrospinal fluid after subarachnoid hemorrhage. *J. Neuroimmunol.* 357:577610. doi: 10.1016/j.jneuroim.2021.577610

Pan, P., Xu, L., Zhang, H., Liu, Y., Lu, X., Chen, G., et al. (2020). A review of hematoma components clearance mechanism after subarachnoid hemorrhage. *Front. Neurosci.* 14:685. doi: 10.3389/fnins.2020.00685

Pappas, A. C., Koide, M., and Wellman, G. C. (2015). Astrocyte Ca2+ signaling drives inversion of neurovascular coupling after subarachnoid hemorrhage. *J. Neurosci.* 35, 13375–13384. doi: 10.1523/jneurosci.1551-15.2015

Parkhutik, V., Lago, A., Tembl, J. I., Rubio, C., Fuset, M. P., Vallés, J., et al. (2012). Influence of COX-inhibiting analgesics on the platelet function of patients with subarachnoid hemorrhage. *J. Stroke Cerebrovasc. Dis.* 21, 755–759. doi: 10.1016/j.jstrokecerebrovasdis.2011.04.002

Pascual, M., Calvo-Rodriguez, M., Núñez, L., Villalobos, C., Ureña, J., and Guerri, C. (2021). Toll-like receptors in neuroinflammation, neurodegeneration, and alcohol-induced brain damage. *IUBMB Life* 73, 900–915. doi: 10.1002/iub.2510

Peeyush Kumar, T., McBride, D. W., Dash, P. K., Matsumura, K., Rubi, A., and Blackburn, S. L. (2019). Endothelial cell dysfunction and injury in subarachnoid hemorrhage. *Mol. Neurobiol.* 56, 1992–2006. doi: 10.1007/s12035-018-1213-7

Petzold, G. C., Haack, S., von Bohlen Und Halbach, O., Priller, J., Lehmann, T. N., Heinemann, U., et al. (2008). Nitric oxide modulates spreading depolarization threshold in the human and rodent cortex. *Stroke* 39, 1292–1299. doi: 10.1161/strokeaha.107.500710

Pluta, R. M. (2006). Dysfunction of nitric oxide synthases as a cause and therapeutic target in delayed cerebral vasospasm after SAH. *Neurol. Res.* 28, 730–737. doi: 10.1179/016164106x152052

Qing, W. G., Dong, Y. Q., Ping, T. Q., Lai, L. G., Fang, L. D., Min, H. W., et al. (2009). Brain edema after intracerebral hemorrhage in rats: the role of iron overload and aquaporin 4. *J. Neurosurg.* 110, 462–468. doi: 10.3171/2008.4.jns17512

Qu, J., Chen, W., Hu, R., and Feng, H. (2016). The injury and therapy of reactive oxygen species in intracerebral hemorrhage looking at mitochondria. *Oxid. Med. Cell. Longev.* 2016:2592935.

Rawlinson, C., Jenkins, S., Thei, L., Dallas, M. L., and Chen, R. (2020). Post-ischaemic immunological response in the brain: targeting microglia in ischaemic stroke therapy. *Brain Sci.* 10:159.

Ray, R. S., and Katyal, A. (2016). Myeloperoxidase: bridging the gap in neurodegeneration. *Neurosci. Biobehav. Rev.* 68, 611–620. doi: 10.1016/j.neubiorev.2016.06.031

Reczek, C. R., and Chandel, N. S. (2015). ROS-dependent signal transduction. *Curr. Opin. Cell Biol.* 33, 8–13. doi: 10.1016/j.ceb.2014.09.010

Ridwan, S., Grote, A., and Simon, M. (2021). Interleukin 6 in cerebrospinal fluid is a biomarker for delayed cerebral ischemia (DCI) related infarctions after aneurysmal subarachnoid hemorrhage. *Sci. Rep.* 11:12.

Robicsek, S. A., Bhattacharya, A., Rabai, F., Shukla, K., and Doré, S. (2020). Blood-related toxicity after traumatic brain injury: potential targets for neuroprotection. *Mol. Neurobiol.* 57, 159–178. doi: 10.1007/s12035-019-01766-8

Robinson, M. A., Baumgardner, J. E., and Otto, C. M. (2011). Oxygen-dependent regulation of nitric oxide production by inducible nitric oxide synthase. *Free Radic. Biol. Med.* 51, 1952–1965. doi: 10.1016/j.freeradbiomed.2011.08.034

Roumie, C. L., Mitchel, E. F. Jr., Kaltenbach, L., Arbogast, P. G., Gideon, P., and Griffin, M. R. (2008). Nonaspirin NSAIDs, cyclooxygenase 2 inhibitors, and the risk for stroke. *Stroke* 39, 2037–2045. doi: 10.1161/strokeaha.107.508549

Rouzer, C. A., and Marnett, L. J. (2020). Structural and chemical biology of the interaction of cyclooxygenase with substrates and non-steroidal anti-inflammatory drugs. *Chem. Rev.* 120, 7592–7641. doi: 10.1021/acs.chemrev.0c00215

Sabri, M., Ai, J., Knight, B., Tariq, A., Jeon, H., Shang, X., et al. (2011). Uncoupling of endothelial nitric oxide synthase after experimental subarachnoid hemorrhage. *J. Cereb. Blood Flow Metab.* 31, 190–199. doi: 10.1038/jcbfm.2010.76

Sandberg, M., Patil, J., D'Angelo, B., Weber, S. G., and Mallard, C. (2014). NRF2-regulation in brain health and disease: implication of cerebral inflammation. *Neuropharmacology* 79, 298–306. doi: 10.1016/j.neuropharm.2013.11.004

Schaer, C. A., Owczarek, C., Deuel, J. W., Schauer, S., Baek, J. H., Yalamanoglu, A., et al. (2018). Phenotype-specific recombinant haptoglobin polymers co-expressed with C1r-like protein as optimized hemoglobin-binding therapeutics. *BMC Biotechnol.* 18:15. doi: 10.1186/s12896-018-0424-3

Schneider, U. C., Davids, A. M., Brandenburg, S., Müller, A., Elke, A., Magrini, S., et al. (2015). Microglia inflict delayed brain injury after subarachnoid hemorrhage. *Acta Neuropathol.* 130, 215–231. doi: 10.1007/s00401-015-1440-1

Schneider, U. C., Schiffler, J., Hakiy, N., Horn, P., and Vajkoczy, P. (2012). Functional analysis of Pro-inflammatory properties within the cerebrospinal fluid after subarachnoid hemorrhage in vivo and in vitro. *J. Neuroinflammation* 9:28.

Schneider, U. C., Xu, R., and Vajkoczy, P. (2018). Inflammatory events following subarachnoid hemorrhage (SAH). *Curr. Neuropharmacol.* 16, 1385–1395. doi: 10.2174/1570159x16666180412110919

Sehba, F. A., and Friedrich, V. (2013). Cerebral microvasculature is an early target of subarachnoid hemorrhage. *Acta Neurochir. Suppl.* 115, 199–205. doi: 10.1007/978-3-7091-1192-5_37

Serrone, J. C., Maekawa, H., Tjahjadi, M., and Hernesniemi, J. (2015). Aneurysmal subarachnoid hemorrhage: pathobiology, current treatment and future directions. *Expert Rev. Neurother.* 15, 367–380. doi: 10.1586/14737175.2015.1018892

Shao, A., Lin, D., Wang, L., Tu, S., Lenahan, C., and Zhang, J. (2020). Oxidative stress at the crossroads of aging, stroke and depression. *Aging Dis.* 11, 1537–1566. doi: 10.14336/ad.2020.0225

Shinozaki, Y., Shibata, K., Yoshida, K., Shigetomi, E., Gachet, C., Ikenaka, K., et al. (2017). Transformation of astrocytes to a neuroprotective phenotype by microglia via P2Y(1) receptor downregulation. *Cell Rep.* 19, 1151–1164. doi: 10.1016/j.celrep.2017.04.047

Sinha, K., Das, J., Pal, P. B., and Sil, P. C. (2013). Oxidative stress: the mitochondria-dependent and mitochondria-independent pathways of apoptosis. *Arch. Toxicol.* 87, 1157–1180. doi: 10.1007/s00204-013-1034-4

Smith, A., and McCulloh, R. J. (2015). Hemopexin and haptoglobin: allies against heme toxicity from hemoglobin not contenders. *Front. Physiol.* 6:187. doi: 10.3389/fphys.2015.00187

Sorce, S., Krause, K. H., and Jaquet, V. (2012). Targeting NOX enzymes in the central nervous system: therapeutic opportunities. *Cell. Mol. Life Sci.* 69, 2387–2407. doi: 10.1007/s00018-012-1014-5

Stokum, J. A., Cannarsa, G. J., Wessell, A. P., Shea, P., Wenger, N., and Simard, J. M. (2021). When the blood hits your brain: the neurotoxicity of extravasated blood. *Int. J. Mol. Sci.* 22:5132. doi: 10.3390/ijms22105132

Sugawara, T., Ayer, R., Jadhav, V., Chen, W., Tsubokawa, T., and Zhang, J. H. (2008). Simvastatin attenuation of cerebral vasospasm after subarachnoid hemorrhage in rats via increased phosphorylation of Akt and endothelial nitric oxide synthase. *J. Neurosci. Res.* 86, 3635–3643. doi: 10.1002/jnr.21807

Swissa, E., Serlin, Y., Vazana, U., Prager, O., and Friedman, A. (2019). Blood-brain barrier dysfunction in status epileptics: mechanisms and role in epileptogenesis. *Epilepsy Behav.* 101(Pt B):106285. doi: 10.1016/j.yebeh.2019.04.038

Takeuchi, K., Miyata, N., Renic, M., Harder, D. R., and Roman, R. J. (2006). Hemoglobin, NO, and 20-HETE interactions in mediating cerebral vasoconstriction following SAH. *Am. J. Physiol. Regul. Integr. Comp. Physiol.* 290, R84–R89.

Takeuchi, O., and Akira, S. (2010). Pattern recognition receptors and inflammation. *Cell* 140, 805–820. doi: 10.1016/j.cell.2010.01.022

Takizawa, T., Tada, T., Kitazawa, K., Tanaka, Y., Hongo, K., Kameko, M., et al. (2001). Inflammatory cytokine cascade released by leukocytes in cerebrospinal fluid after subarachnoid hemorrhage. *Neurol. Res.* 23, 724–730. doi: 10.1179/016164101101199243

Tao, C., Keep, R. F., Xi, G., and Hua, Y. (2020). CD47 blocking antibody accelerates hematoma clearance after intracerebral hemorrhage in aged rats. *Transl. Stroke Res.* 11, 541–551. doi: 10.1007/s12975-019-00745-4

Tao, K., Cai, Q., Zhang, X., Zhu, L., Liu, Z., Li, F., et al. (2020). Astrocytic histone deacetylase 2 facilitates delayed depression and memory impairment after subarachnoid hemorrhage by negatively regulating glutamate transporter-1. *Ann. Transl. Med.* 8:691. doi: 10.21037/atm-20-4330

Terpolilli, N. A., Feiler, S., Dienel, A., Müller, F., Heumos, N., Friedrich, B., et al. (2016). Nitric oxide inhalation reduces brain damage, prevents mortality, and improves neurological outcome after subarachnoid hemorrhage by resolving early pial microvasospasms. *J. Cereb. Blood Flow Metab.* 36, 2096–2107. doi: 10.1177/0271678x15605848

Tolosano, E., Fagoonee, S., Morello, N., Vinchi, F., and Fiorito, V. (2010). Heme scavenging and the other facets of hemopexin. *Antioxid. Redox Signal.* 12, 305–320. doi: 10.1089/ars.2009.2787

Tran Dinh, Y. R., Jomaa, A., Callebert, J., Reynier-Rebuffel, A. M., Tedgui, A., Savarit, A., et al. (2001). Overexpression of cyclooxygenase-2 in rabbit basilar artery endothelial cells after subarachnoid hemorrhage. *Neurosurgery* 48, 626–633; discussion 633–635.

Tseng, M. Y., Hutchinson, P. J., Turner, C. L., Czosnyka, M., Richards, H., Pickard, J. D., et al. (2007). Biological effects of acute pravastatin treatment in patients after aneurysmal subarachnoid hemorrhage: a double-blind, placebo-controlled trial. *J. Neurosurg.* 107, 1092–1100. doi: 10.3171/jns-07/12/1092

Unda, S. R., Birnbaum, J., Labagnara, K., Wong, M., Vaishnav, D. P., and Altschul, D. J. (2020). Peripheral monocytosis at admission to predict cerebral infarct and poor functional outcomes in subarachnoid hemorrhage patients. *World Neurosurg.* 138, e523–e529.

Urday, S., Kimberly, W. T., Beslow, L. A., Vortmeyer, A. O., Selim, M. H., Rosand, J., et al. (2015). Targeting secondary injury in intracerebral haemorrhage–perihaematomal oedema. *Nat. Rev. Neurol.* 11, 111–122. doi: 10.1038/nrneurol.2014.264

Venditti, P., and Di Meo, S. (2020). The role of reactive oxygen species in the life cycle of the mitochondrion. *Int. J. Mol. Sci.* 21:2173. doi: 10.3390/ijms21062173

Voetsch, B., Jin, R. C., and Loscalzo, J. (2004). Nitric oxide insufficiency and atherothrombosis. *Histochem. Cell Biol.* 122, 353–367. doi: 10.1007/s00418-004-0675-z

Wang, J., Liang, J., Deng, J., Liang, X., Wang, K., Wang, H., et al. (2021). Emerging role of microglia-mediated neuroinflammation in epilepsy after subarachnoid hemorrhage. *Mol. Neurobiol.* 58, 2780–2791. doi: 10.1007/s12035-021-02288-y

Wang, T., Fu, W., Song, S., Han, Y., Yao, L., Lu, Y., et al. (2018). Matrix metalloproteinase-9 gene polymorphisms and their interaction with environment on subarachnoid hemorrhage risk. *Exp. Biol. Med. (Maywood)* 243, 749–753. doi: 10.1177/1535370218775042

Wang, Y., Xu, E., Musich, P. R., and Lin, F. (2019). Mitochondrial dysfunction in neurodegenerative diseases and the potential countermeasure. *CNS Neurosci. Ther.* 25, 816–824. doi: 10.1111/cns.13116

Wang, Z., Chen, G., Zhu, W. W., and Zhou, D. (2010). Activation of nuclear factor-erythroid 2-related factor 2 (Nrf2) in the basilar artery after subarachnoid hemorrhage in rats. *Ann. Clin. Lab. Sci.* 40, 233–239.

Watanabe, Y., Chu, Y., Andresen, J. J., Nakane, H., Faraci, F. M., and Heistad, D. D. (2003). Gene transfer of extracellular superoxide dismutase reduces cerebral vasospasm after subarachnoid hemorrhage. *Stroke* 34, 434–440. doi: 10.1161/01.str.0000051586.96022.37

Whitehouse, M. W. (2011). Anti-inflammatory glucocorticoid drugs: reflections after 60 years. *Inflammopharmacology* 19, 1–19. doi: 10.1007/s10787-010-0056-2

Willis, C. L., Brooks, T. A., and Davis, T. P. (2008). Chronic inflammatory pain and the neurovascular unit: a central role for glia in maintaining BBB integrity? *Curr. Pharm. Des.* 14, 1625–1643. doi: 10.2174/138161208784705414

Winterbourn, C. C., Kettle, A. J., and Hampton, M. B. (2016). Reactive oxygen species and neutrophil function. *Annu. Rev. Biochem.* 85, 765–792. doi: 10.1146/annurev-biochem-060815-014442

Wolf, S. (2015). Rationale for lumbar drains in aneurysmal subarachnoid hemorrhage. *Curr. Opin. Crit. Care.* 21, 120–126. doi: 10.1097/mcc.0000000000000183

Wu, Y., Chen, M., and Jiang, J. (2019). Mitochondrial dysfunction in neurodegenerative diseases and drug targets via apoptotic signaling. *Mitochondrion* 49, 35–45. doi: 10.1016/j.mito.2019.07.003

Xu, X., Zhang, A., Zhu, Y., He, W., Di, W., Fang, Y., et al. (2018). MFG-E8 reverses microglial-induced neurotoxic astrocyte (A1) via NF-κB and PI3K-Akt pathways. *J. Cell. Physiol.* 234, 904–914. doi: 10.1002/jcp.26918

Yamamoto, T., Mori, K., Esaki, T., Nakao, Y., Tokugawa, J., and Watanabe, M. (2016). Preventive effect of continuous cisternal irrigation with magnesium sulfate solution on angiographic cerebral vasospasms associated with aneurysmal subarachnoid hemorrhages: a randomized controlled trial. *J. Neurosurg.* 124, 18–26. doi: 10.3171/2015.1.jns142757

Yang, W. S., and Stockwell, B. R. (2016). Ferroptosis: death by lipid peroxidation. *Trends Cell Biol.* 26, 165–176. doi: 10.1016/j.tcb.2015.10.014

Youn, D. H., Kim, B. J., Kim, Y., and Jeon, J. P. (2020). Extracellular mitochondrial dysfunction in cerebrospinal fluid of patients with delayed cerebral ischemia after aneurysmal subarachnoid hemorrhage. *Neurocrit. Care* 33, 422–428. doi: 10.1007/s12028-019-00895-1

Young, A. M., Karri, S. K., and Ogilvy, C. S. (2012). Non-steroidal anti-inflammatory drugs used as a treatment modality in subarachnoid hemorrhage. *Curr. Drug Saf.* 7, 197–201. doi: 10.2174/157488612803251342

Zeiler, F. A., Thelin, E. P., Czosnyka, M., Hutchinson, P. J., Menon, D. K., and Helmy, A. (2017). Cerebrospinal fluid and microdialysis cytokines in aneurysmal subarachnoid hemorrhage: a scoping systematic review. *Front. Neurol.* 8:379. doi: 10.3389/fneur.2017.00379

Zhang, H. Y., Wang, Y., He, Y., Wang, T., Huang, X. H., Zhao, C. M., et al. (2020). A1 astrocytes contribute to murine depression-like behavior and cognitive dysfunction, which can be alleviated by IL-10 or fluorocitrate treatment. *J. Neuroinflammation* 17:200.

Zhang, L., Guo, K., Zhou, J., Zhang, X., Yin, S., Peng, J., et al. (2021). Ponesimod protects against neuronal death by suppressing the activation of A1 astrocytes in early brain injury after experimental subarachnoid hemorrhage. *J. Neurochem.* 158, 880–897. doi: 10.1111/jnc.15457

Zhang, L., Li, Z., Feng, D., Shen, H., Tian, X., Li, H., et al. (2017). Involvement of Nox2 and Nox4 NADPH oxidases in early brain injury after subarachnoid hemorrhage. *Free Radic. Res.* 51, 316–328. doi: 10.1080/10715762.2017.1311015

Zhang, Z. D., Yamini, B., Komuro, T., Ono, S., Johns, L., Marton, L. S., et al. (2001). Vasospasm in monkeys resolves because of loss of and encasement of subarachnoid blood clot. *Stroke* 32, 1868–1874. doi: 10.1161/01.str.32.8.1868

Zhao, X., Sun, G., Ting, S. M., Song, S., Zhang, J., Edwards, N. J., et al. (2015). Cleaning up after ICH: the role of Nrf2 in modulating microglia function and hematoma clearance. *J. Neurochem.* 133, 144–152. doi: 10.1111/jnc.12974

Zhao, X., Wen, L., Dong, M., and Lu, X. (2016). Sulforaphane activates the cerebral vascular Nrf2-ARE pathway and suppresses inflammation to attenuate cerebral vasospasm in rat with subarachnoid hemorrhage. *Brain Res.* 1653, 1–7. doi: 10.1016/j.brainres.2016.09.035

Zheng, Z. V., Lyu, H., Lam, S. Y. E., Lam, P. K., Poon, W. S., and Wong, G. K. C. (2020). The dynamics of microglial polarization reveal the resident neuroinflammatory responses after subarachnoid hemorrhage. *Transl. Stroke Res.* 11, 433–449. doi: 10.1007/s12975-019-00728-5

Zhou, Y., Wang, Y., Wang, J., Anne Stetler, R., and Yang, Q. W. (2014). Inflammation in intracerebral hemorrhage: from mechanisms to clinical translation. *Prog. Neurobiol.* 115, 25–44. doi: 10.1016/j.pneurobio.2013.11.003

Zindel, J., and Kubes, P. (2020). DAMPs, PAMPs, and LAMPs in immunity and sterile inflammation. *Annu. Rev. Pathol.* 15, 493–518. doi: 10.1146/annurev-pathmechdis-012419-032847

Zolnourian, A., Galea, I., and Bulters, D. (2019). Neuroprotective role of the Nrf2 pathway in subarachnoid haemorrhage and its therapeutic potential. *Oxid. Med. Cell. Longev.* 2019:6218239.

Zolnourian, A. H., Franklin, S., Galea, I., and Bulters, D. O. (2020). Study protocol for SFX-01 after subarachnoid haemorrhage (SAS): a multicentre randomised double-blinded, placebo controlled trial. *BMJ Open* 10:e028514. doi: 10.1136/bmjopen-2018-028514

**Conflict of Interest:** The authors declare that the research was conducted in the absence of any commercial or financial relationships that could be construed as a potential conflict of interest.

**Publisher's Note:** All claims expressed in this article are solely those of the authors and do not necessarily represent those of their affiliated organizations, or those of the publisher, the editors and the reviewers. Any product that may be evaluated in this article, or claim that may be made by its manufacturer, is not guaranteed or endorsed by the publisher.

frontiers in Cellular Neuroscience

REVIEW
published: 07 October 2021
doi: 10.3389/fncel.2021.739699

# The Structure and Function of the Glycocalyx and Its Connection With Blood-Brain Barrier

*Jing Jin[1†], Fuquan Fang[2†], Wei Gao[3], Hanjian Chen[2], Jiali Wen[2], Xuehua Wen[4*] and Junfa Chen[4*]*

[1] Zhejiang Center for Clinical Laboratory, Zhejiang Provincial People's Hospital, Affiliated People's Hospital, Hangzhou Medical College, Hangzhou, China, [2] Department of Anesthesiology, The First Affiliated Hospital, Zhejiang University School of Medicine, Hangzhou, China, [3] The First Affiliated Hospital of Wenzhou Medical University, Wenzhou, China, [4] Department of Radiology, Zhejiang Provincial People's Hospital, Affiliated People's Hospital, Hangzhou Medical College, Hangzhou, China

OPEN ACCESS

**Edited by:**
Xiaoxing Xiong,
Renmin Hospital of Wuhan University, China

**Reviewed by:**
Weihua Ding,
Massachusetts General Hospital and Harvard Medical School, United States
Steven Sloan,
Emory University, United States
Dong Dao Xian,
University Hospital of Macau, Macao, SAR China

***Correspondence:**
Junfa Chen
cjf2002@126.com
Xuehua Wen
xuehuasuqian@126.com

[†] These authors have contributed equally to this work

**Specialty section:**
This article was submitted to Non-Neuronal Cells, a section of the journal Frontiers in Cellular Neuroscience

**Received:** 11 July 2021
**Accepted:** 17 September 2021
**Published:** 07 October 2021

**Citation:**
Jin J, Fang F, Gao W, Chen H, Wen J, Wen X and Chen J (2021) The Structure and Function of the Glycocalyx and Its Connection With Blood-Brain Barrier. Front. Cell. Neurosci. 15:739699. doi: 10.3389/fncel.2021.739699

The vascular endothelial glycocalyx is a dense, bush-like structure that is synthesized and secreted by endothelial cells and evenly distributed on the surface of vascular endothelial cells. The blood-brain barrier (BBB) is mainly composed of pericytes endothelial cells, glycocalyx, basement membranes, and astrocytes. The glycocalyx in the BBB plays an indispensable role in many important physiological functions, including vascular permeability, inflammation, blood coagulation, and the synthesis of nitric oxide. Damage to the fragile glycocalyx can lead to increased permeability of the BBB, tissue edema, glial cell activation, up-regulation of inflammatory chemokines expression, and ultimately brain tissue damage, leading to increased mortality. This article reviews the important role that glycocalyx plays in the physiological function of the BBB. The review may provide some basis for the research direction of neurological diseases and a theoretical basis for the diagnosis and treatment of neurological diseases.

**Keywords: glycocalyx, blood-brain barrier, neurovascular unit, neurological function, neurological diseases**

## INTRODUCTION

The surface of the vascular endothelium is covered with a layer of villiform substance, which is called the glycocalyx. It is synthesized by vascular endothelial cells and extends to vascular lumen and surface. In 1966, Rambourg et al. (1966) used methylamphetamine labeled with Ag to observe a layer of proteoglycan (PG) protein polymers on the surface of endothelial cells of mice for the first time. With the development of modern methods of fixation and rapid-freeze techniques as well as a variety of confocal microscopy, there have been more in-depth studies on the structure and functions of the glycocalyx (Ebong et al., 2011). The glycocalyx on endothelial cells is a kind of PG polymer. It mainly includes PGs and glycosaminoglycan chains (GAGs). The core protein of PG mainly consists of members of syndecan and glypican families. GAGs, including heparan sulfate (HS), chondroitin sulfate (CS), and hyaluronan (HA), are the most abundant components of the glycocalyx (Salmon and Satchell, 2012; Alphonsus and Rodseth, 2014; Mende et al., 2016). Glycocalyx extends from the membrane of endothelial cells to vascular lumen, prevents leukocytes and platelets from contacting with endothelial cells, and plays a key role in maintaining the stability of the internal environment (Salmon and Satchell, 2012; Ushiyama et al., 2016). Research has proved that glycocalyx can maintain the stability of many physiological functions, such as maintaining the

permeable barrier of microcirculation, preventing trigger inflammation and coagulation response, and conducting the shear force of blood flow (Iba and Levy, 2019; Nikmanesh et al., 2019; Zuurbier, 2019). It can also protect the functions of vital organs including the brain, heart, lungs, and kidneys (Becker et al., 2010b; van Golen et al., 2014; Brettner et al., 2017; Rabelink et al., 2017; Zhu et al., 2017).

The BBB prevents sensitive neurons from being attacked by toxic metabolites and exogenous materials in the circulation. Therefore, stable and intact BBB is crucial for maintaining normal physiological functions of the brain. The cerebrovascular dysfunction, such as destruction of the BBB, endothelium dysfunction, or capillary degeneration, is also related to the pathogenesis and progression of many nervous system diseases, including neuroinflammation, cognitive decline related to aging, multiple sclerosis, brain tumor, and epilepsy (Zenaro et al., 2017; Abdullahi et al., 2018; Abrahamson and Ikonomovic, 2020). With the development of the confocal technique and photon fluorescence imaging technique, the microstructure of the BBB has gradually become clear to researchers. The unique system structure mainly consists of pericytes, endothelial cells, glycocalyx of endothelial cells, basement membrane, and astrocyte cells (Kutuzov et al., 2018; Santa-Maria et al., 2021).

After the glycocalyx in the endothelium of the BBB is impaired, a series of pathophysiological changes related to the microcirculation occurs. If the glycocalyx is degraded, the permeability of the BBB increases, leading to neuroedema. The number of leukocyte and platelets binding with the exposed surface receptors of endothelial cells increases, causing inflammation, a blood clotting response, cerebral microcirculation ischemia, and damage to the nervous tissue (Kutuzov et al., 2018; Zhao et al., 2021). Currently, there are few overviews of the glycocalyx and cerebrovascular microcirculation. In this review, we discuss the structure and physiological functions of endothelial glycocalyx and the progress of related research on endothelial glycocalyx and cerebral vessels in detail and provide some clues for subsequent research and disease treatment.

## The Structure of the Glycocalyx

The endothelial glycocalyx is a layer of dense and uneven grass-like substance covering the surface of vascular endothelial cells (Fang et al., 2021). The endothelial glycocalyx is a PG polymer synthesized and secreted by endothelial cells. Through the skeleton consisting of PG and glycoproteins (GLYs), it binds with endothelial cells. In this net structure, soluble factors from plasma and endothelial cells are bound and attached. This grass-like structure maintains the dynamic balance under physiological conditions. The main core PG proteins are members of the syndecan and glypican families. These core proteins firmly bind with the cell membrane and pass the membrane-spanning domain (syndecans) or a glycosylphosphatidylinositol anchor (glypicans) (Kabedev and Lobaskin, 2018; Purcell and Godula, 2019). The syndecan family comprises 5 members: syndecan-1, syndecan-2, syndecan-3, and syndecan-4. Among these members of the syndecan family, syndecan-1 expressed by vascular endothelial cells can bind HS, CS, and keratan sulfate. Syndecan is closely related to the shear force of blood flow (Koo et al., 2013). Members of the glypican family include glypican-1, glypican-2, glypican-3, glypican-4, glypican-5, and glypican-6. Glpyican-1 is the only member of the glypican family expressed on endothelial cells. The branch linkage includes HS (Tarbell, 2010).

The side chain of GAGs binds with the main part of core protein or CD44 receptors on the surface of endothelial cells. There are 5 types of GAGs, namely, HS, CS, dermatan sulfate, keratan sulfate, and HA (or hyaluronic acid). HS, CS, and dermatan sulfate with negative charges bind the core protein through covalent binding. HS is the most abundant components of GAG side chains, comprising 50–90% of these chains (Pries et al., 2000). The next most abundant components are CS and dermatan sulfate, whose content is approximately one-quarter of that of HS (Rapraeger et al., 1985). The details of keratan sulfate are currently unknown. In contrast to the four abovementioned GAGs, non-sulfated HA, which has no charge, does not bind the core protein, but covalently binds the cell membrane through CD44 receptors (Nandi et al., 2000). GAG chains with negative charges can bind plasma proteins and positively charged ions through the electric charge effect (Van den Berg et al., 2006; Reitsma et al., 2007).

Similar to PGs, GLYs are skeleton proteins of the glycocalyx that link the glycocalyx and endothelial cells. GLYs are adhesion molecules on the surface of endothelial cells. They mainly consist of members of the selectin family, the integrin family, and the immunoglobulin superfamily. The selectin family members that are expressed on the surface of endothelial cells mainly include E-selectin and P-selectin. They participate in the adhesion of leukocytes and endothelial cells (Sperandio, 2006). The main function of the integrin family on the surface of endothelial cells is mediating the adhesion of endothelial cells and platelets and the linkage of extracellular matrix, such as lantinin, fibronectin, and collagen (Bombeli et al., 1998; Ruegg and Mariotti, 2003). The immunoglobulin superfamily of glycocalyx includes the cytoplasmic domain, transmembrane domain, and intracellular domain. The main molecules include intercellular adhesion molecules 1 and 2 (ICAM-1 and –2), vascular cell adhesion molecule 1 (VCAM-1), and platelet/endothelial cell adhesion molecule 1 (PECAM-1) (Reitsma et al., 2007). It has been observed under an electron microscope that the thickness of the glycocalyx of the vascular endothelium is 0.1–11 μm (Becker et al., 2010a). A schematic diagram of cerebral vascular endothelial glycocalyx is shown in **Figure 1**.

## The Role of Glycocalyx in Permeability

The endothelial glycocalyx is an important gatekeeper of vascular permeability. Damage to the glycocalyx increases the transport of water, proteins, and other molecules from the plasma to outside of blood vessels (Butler et al., 2020). The endothelial glycocalyx can restrict certain molecules from passing through the endothelial cell membrane, as confirmed by injecting of fluorescently labeled dextran into rat mesenteric arteries (van Haaren et al., 2003). It was observed that the in rat myocardial capillaries, the glycocalyx is degraded by enzymes, and the subsequent hyperosmolarity leads to myocardial edema (Araibi et al., 2020). Degradation of 42% of the endothelial glycocalyx

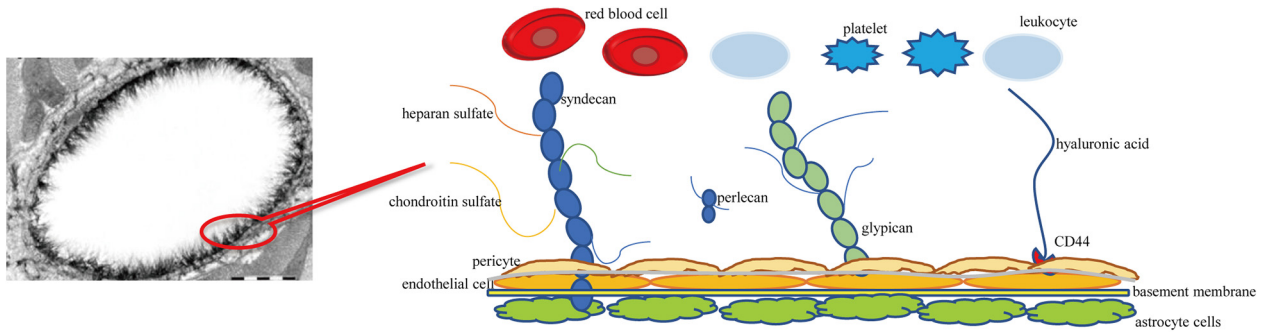


**FIGURE 1 |** Schematic diagram of cerebral vascular endothelial glycocalyx. Syndecan and glypican are membrane-bound proteoglycans-core skeletons, to which chondroitin sulfate and heparan sulfate are connected. Syndecans are transmembrane proteoglycans. Glypicans attach to the cell surface through glycosylphosphatidylinositol anchors. Hyaluronic acid is connected to the endothelial cell membrane through the CD44 receptor.

in the isolated rat abdominal aorta by hyaluronidase (HAase) facilitates water and low-density lipoprotein transport across the vessel wall, suggesting that the endothelial glycocalyx is a transport barrier (Kang et al., 2021). Not only does the molecular sieve effect of the glycocalyx structure determine the permeability of blood vessels, but the negatively charged nature of glycocalyx also makes blood vessels act as a charge barrier. Heparan sulfate and chondroitin sulfate in glycosaminoglycan side chain components are negatively charged, so the glycocalyx facing the plasma is also negatively charged. Studies have found that neutralizing the negative charge of the glycocalyx by myeloperoxidase can induce permeability and increase vascular permeability (Kolarova et al., 2021). According to the traditional Starling model, two opposite forces passing through the endothelial cell layer maintain fluid distribution balance, which is determined by four factors: capillary pressure, tissue fluid hydrostatic pressure, plasma colloid osmotic pressure, and tissue fluid colloid osmotic pressure (Starling, 1896). In recent years, the discovery of microvascular barrier functions has questioned this notion, suggesting that the structural net consisting of the endothelial glycocalyx binds with the endothelial cell membrane of blood vessels and forms the endothelial surface layer, which bears the blood vessel barrier. The resulting osmotic pressure of the transendothelial PG protein colloid is the main determining factor of the internal and external flow of fluid in capillaries (Michel, 1997). A schematic diagram of the physiological functions of glycocalyx is shown in **Figure 2**.

## The Role of Glycocalyx in Inflammation

The vascular response is the central part of the inflammatory response. Lipowsky et al. (2011) observed that, in a mouse model of inflammation, after the vascular endothelial glycocalyx structure is destroyed, vascular endothelial cell intercellular adhesion molecule-1 (ICAM-1) and vascular cell adhesion molecule-1 (VCAM-1) make it easier for leukocytes in the blood circulation to adhere to the vascular endothelial cells, which in turn cause a series of inflammation and pathological changes (Mulivor and Lipowsky, 2004; Devaraj et al., 2009; Mulivor and Lipowsky, 2009; Schmidt et al., 2012; Lipowsky and Lescanic, 2013). Therefore, glycocalyx shedding is the response of vascular endothelial cells to inflammatory mediators. In an inflammatory state, the glycocalyx of vascular endothelial cells falls off, but it also plays an important role in regulating the occurrence and development of inflammation. HS is the main component of the vascular endothelial glycocalyx and exists on the surface and matrix of cerebrovascular cells (Bernfield et al., 1999). A series of *in vitro* cell experiments confirmed that HS is a potential ligand of P and L-selectin, which binds to pro-inflammatory chemokines and promotes the transmembrane transport of chemokines (Hoogewerf et al., 1997; Koenig et al., 1998). Vascular endothelial HS participates in and regulates multiple stages of an inflammatory response, but its exact role in the process of inflammatory response is not fully understood.

## The Role of the Glycocalyx in the Anticoagulant Process

Glycocalyx's dense and bush-like structure can hide coagulation-related molecules. Under physiological conditions, direct contact between endothelial cells and blood cells can be avoided, thereby avoiding thrombosis. In addition, glycocalyx can also achieve anticoagulant effects by interacting with antithrombin III, thrombomodulin, and tissue factor pathway inhibitor (TFPI). The main mechanisms of actions include (Bell et al., 2017; Lupu et al., 2020): (1) PECAM is exposed by the shed glycocalyx; (2) Antithrombin III binds to HS in the glycocalyx to enhance its anticoagulant effect; (3) Thrombomodulin can bind to CS to convert thrombin into the protein C activator of the pathway, thereby forming the anticoagulation pathway; (4) TFPI is an effective inhibitor of FVIIa and FXa in the coagulation pathway, and the anticoagulation effect is achieved mainly through the interaction of TFPI and glycocalyx (Kozar and Pati, 2015).

## The Glycocalyx as a Signal Sensor

The glycocalyx can sense changes in blood flow shear force and transmit it to endothelial cells, which induces corresponding morphological and functional responses, such as the release of endogenous vasoactive substances and nitric oxide (NO) and cytoskeleton changes (Lyu et al., 2020). In the rat blood vessel model, the amount of NO produced by blood vessels was detected after HS enzymatically degraded under changes of blood flow

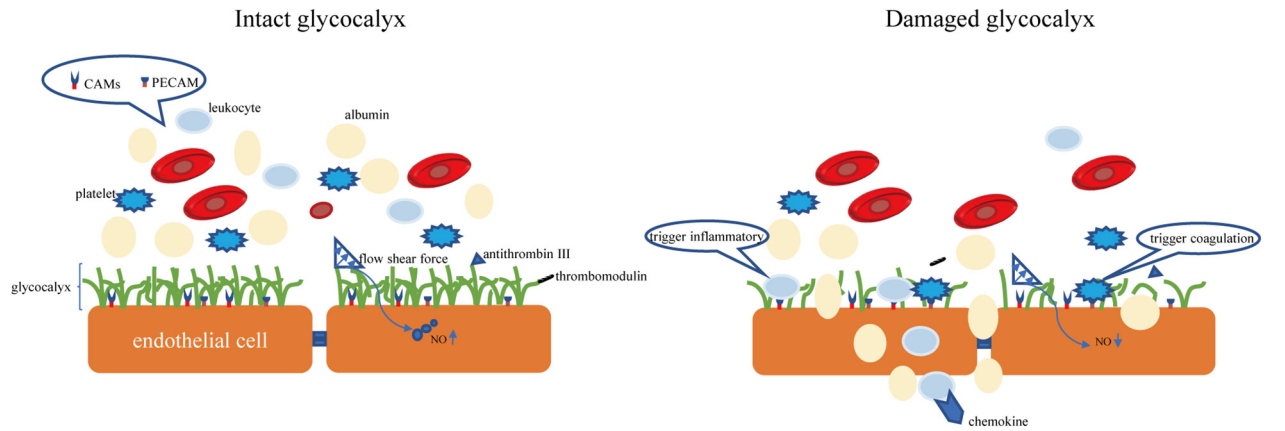


**FIGURE 2 |** The intact glycocalyx can maintain the permeability of the blood-brain barrier. Damage to the glycocalyx will increase the permeability of the blood-brain barrier (for example, albumin exudation). The CAMs and PECAM hidden in the glycocalyx are exposed due to the shedding of the glycocalyx, causing the aggregation of leukocytes and platelets. CAMs, endothelial cell adhesion molecules. PECAM, platelet/endothelial cell adhesion molecule.

shear force. Researchers have found that the production of nitric oxide is significantly reduced (Yen et al., 2015). However, not all components of the glycocalyx can mediate shear-induced NO release. Anne Marie W Bartosch et al. (2017) used atomic force microscopy (AFM) to selectively apply forces onto glycocalyx components, including PGs and GAGs, to observe how each component individually promotes force-induced NO production. They concluded that HS and the glypican-1, not syndecan-1, CD44, and HA, are the main mechanical sensors for shear-induced NO production (Bartosch et al., 2017). According to the report of Eno E Ebong, core protein syndecan-1 of HS mediates flow-induced endothelial cells elongation and alignment because SDC1 is linked to the cytoskeleton which impacts cell shape (Ebong et al., 2014). Kang et al. (2021) found that 24-h shear exposure increased the average maximum infiltration distance of low-density lipoprotein and enhanced endothelial cells apoptosis and that both of these effects were inhibited by HAase, indicating that the glycocalyx of endothelial cells can also serve as shearing mechanical sensors regulate endothelial cell apoptosis, thereby affecting leaky connections and regulating low-density lipoprotein transport.

## The Effect of the Endothelial Glycocalyx in Cerebrovascular Micro-Homeostasis

The BBB is a unique structure that is mainly composed of pericytes, endothelial cells, the glycocalyx, basement membranes, and astrocytes (Kutuzov et al., 2018). Glycocalyx plays an irreplaceable role in maintaining the barrier function of cerebral blood vessels. Through EB and IgG extravasation assays, Zhu et al. (2018) found that in the group with integral glycocalyx structure, EB and IgG did not leak into the hippocampus. However, upon treatment with heparanase (HPSE), leakage was obvious (Zhu et al., 2018). The glycocalyx can prevent some molecules from passing through the BBB. Kutuzov et al. (2018) used a two-photon microscopy to observe the transport of four different sizes of molecules, i.e., fluorescein sodium (376 Da), Alexa Fluor (643 Da), 40-kDa dextran, and 150-kDa dextran from blood to the brain tissue in the cortical capillaries of anesthetized mice. Fluorescein and Alexa penetrate almost the entire glycocalyx structure layer, while the penetration rate of dextran is less than 60% of the volume. This indicates that glycocalyx can block large molecules in the BBB very well, but the ability to prevent small molecules from infiltrating is limited (Kutuzov et al., 2018). In the rat cardiac arrest/cardiopulmonary resuscitation model, the degree of glycocalyx destruction caused by HAase treatment was related to the high BBB permeability and aggravation of cerebral edema after circulation recovery and perfusion, as well as the decrease in survival rate at day 7 and poor nervous system-related prognosis (Zhu et al., 2018). The mechanisms by which the glycocalyx maintains the permeability of the BBB mainly include the following. First, the dense bush-like structure can play a physical isolation effect (Kutuzov et al., 2018). Second, HS and CS in the side chain of GAGs carry negative charges. Therefore, glycocalyx can prevent negatively charged molecules such as albumin from passing through the BBB due to charge repulsion (Deen et al., 2001). And third, after damage to the endothelial glycocalyx, the levels of inflammatory molecules and matrix metalloproteinases (MMPs) increase, resulting in disruption of the close interactions that form the BBB and further increasing vascular permeability.

In addition to regulating the permeability of the blood-brain barrier (BBB), glycocalyx is also involved in cerebrovascular coagulation and neuroinflammatory processes (Lupu et al., 2020). Delayed cerebral ischemia is a common complication of aneurysmal subarachnoid hemorrhage, but the specific mechanism is not clear. Bell et al. (2017) study on patients with aneurysmal subarachnoid hemorrhage found that in patients with delayed cerebral ischemia, specific markers of glycocalyx damage, including SDC-1, were significantly elevated and that this elevation of syndecan-1 expression was related to vascular adhesion protein-1 in the plasma and endothelial cell adhesion molecules (CAMs) in the cerebrospinal fluid. This indicates

**TABLE 1 |** The function, shedding enzyme and protection strategies of glycocalyx in cerebrovascular.

| | | | |
|---|---|---|---|
| (A) Functions | Regulation of vascular permeability | Mechanical barrier and charge barrier | Deen et al., 2001; Kutuzov et al., 2018; Zhu et al., 2018 |
| | Regulation of vascular tone | Inducing and transmitting the shear stress change signal to the endothelial cells to synthesize and release nitric oxide | Ebong et al., 2014; Yen et al., 2015; Bartosch et al., 2017 |
| | Attenuation of leukocyte adhesion | Reducing leukocyte contact with ICAM-1,ICAM-2, and VCAM-1 | Van den Berg et al., 2006; Kim et al., 2013 |
| | Attenuation of platelet adhesion | Reducing platelet contact with PECAM-1 | Bell et al., 2017; Lupu et al., 2020 |
| (B) Major shedding enzyme | MMPs | Cleaving core protein backbone of glycocalyx, directly | Endo et al., 2003; Song et al., 2015; Reine et al., 2019; Ali et al., 2019 |
| | HPSE | Cutting HS | Shteper et al., 2003; Baraz et al., 2006; Qu et al., 2016; Zheng et al., 2016 |
| | HAase | Cutting HA | Nieuwdorp et al., 2007; Becker et al., 2015 |
| (C) Protection strategies of glycocalyx | Glucocorticoid | Stabilizing mast cells | Cui et al., 2015; Yu et al., 2019 |
| | Antithrombin agents | Stabilizing glycocalyx structure by combining with it | Chappell et al., 2009a,b |
| | Abumin | Similar to that of antithrombin | Becker et al., 2015; Aldecoa et al., 2020 |
| | Etanercept | TNF-α inhibitor | Nieuwdorp et al., 2009 |
| | Sulodexide | Inhibiting HPSE and MMPs activities | Mannello and Raffetto, 2011; van Haare et al., 2017 |
| | Doxycycline and batimastat | Inhibitors of MMPs | Lipowsky et al., 2011; Lipowsky and Lescanic, 2013 |
| | Sevoflurane | Reduce MMPs production | Annecke et al., 2010; Fang et al., 2021 |

*ICAM, intercellular adhesion molecules; VCAM, vascular cell adhesion molecule; PECAM, platelet/endothelial cell adhesion molecule; HPSE, heparinase; HAase, hyaluronidase; MMPs, matrix metalloproteinases; TIMPs tissue inhibitor of matrix metalloproteinases; HDAC, histone deacetylase; HA, hyaluronic acid; HS, heparan sulfate.*

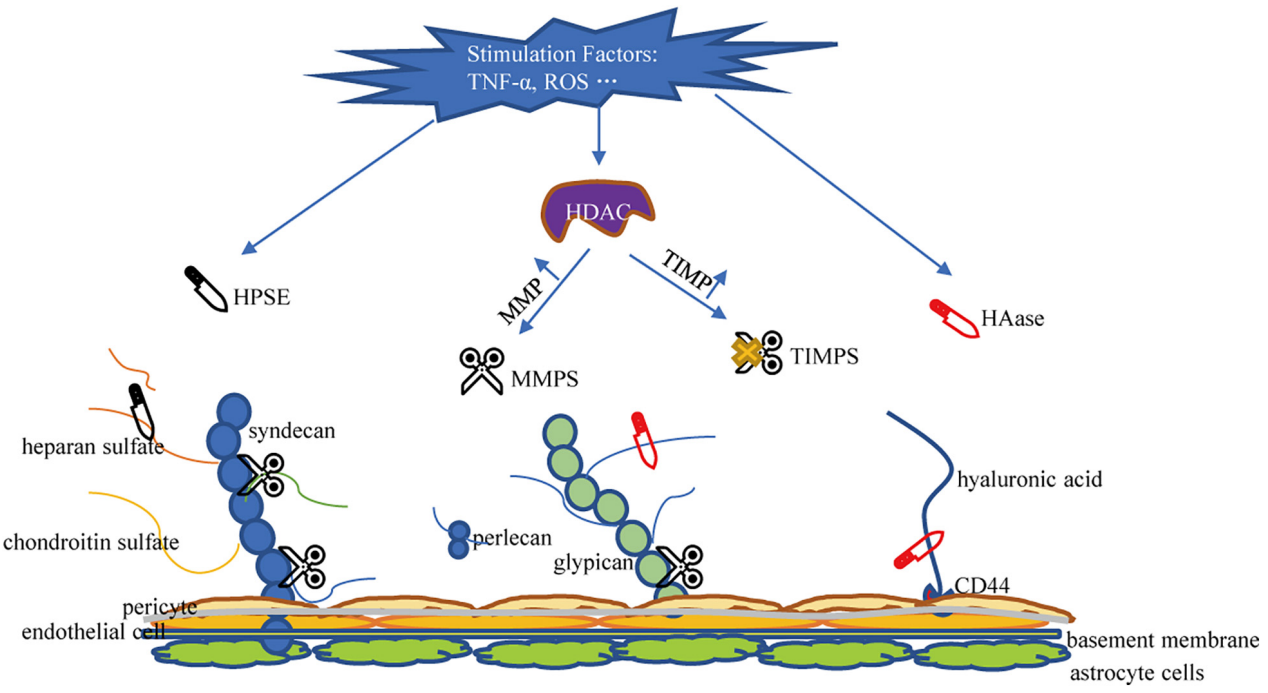


**FIGURE 3 |** Mechanisms of glycocalyx damage. HPSE, Heparanase; HAase, hyaluronidase; MMPS, matrix metalloproteinases; TIMPS, tissue inhibitor of matrix metalloproteinases; HDAC, histone deacetylase; HA, hyaluronic acid; HS, heparan sulfate; CS, chondroitin sulfate.

that the breakdown of cerebrovascular glycocalyx integrity may be related to ischemic brain diseases (Bell et al., 2017). Moreover, the endothelial adhesion molecules ICAM-1 and VCAM-1 within the glycocalyx are exposed after glycocalyx degradation (Simard et al., 2012). This adhesion molecules are known as the central mediators of leukocyte adhesion to and

transmigration across BBB (Schnoor et al., 2015). Upregulation of proinflammatory cytokines as a response to leakage of leucocytes further contributes to the subsequent increased neuronal excitability (Rana and Musto, 2018). Kim et al. found that after glycocalyx degradation, ICAM-1 and NF-kB not only increase leukocyte adhesion, but also up-regulate the expression of iNOS and COX-2 (Kim et al., 2013). Inflammatory factors such as TNF-α and oxygen free radicals increase the production of MMPs, which in turn damage brain tissue. The function, shedding enzyme and strategies of glycocalyx protection are summarized in **Table 1**.

## Major Shedding Enzyme Responsible for Glycocalyx Damage

The glycocalyx is degraded via inflammatory mechanisms such as MMPs, HPSE, and HAase. These sheddases are activated by reactive oxygen species and pro-inflammatory cytokines such as tumor necrosis factor alpha and interleukin-1beta (Iba and Levy, 2019; Uchimido et al., 2019). Several studies have determined that MMPs is the primary molecule responsible for glycocalyx degradation (Song et al., 2015). MMP-2, MMP-7, and MMP-9 directly cleave CS, MMP-1 cleaves syndecan-1, and MMP-9 is the main shedding enzyme of syndecan-4 (Endo et al., 2003; Reine et al., 2019). ADAM17 also participates in glycocalyx degradation by removing the extracellular domain of syndecan-4 (Piperigkou et al., 2016). In addition, studies have confirmed that ADAM15 causes vascular BBB dysfunction by inducing glycocalyx degradation. The underlying mechanism includes ADAM15-mediated CD44 cleavage and the release of the extracellular domain (HA) into the circulation, thereby promoting hyperpermeability of blood vessels and BBB destruction (Yang et al., 2018). Therefore, blocking ADAM15 may be a potential strategy to maintain the integrity of the glycocalyx. MMP is regulated by the activity of histone deacetylase (HDAC) inhibitors. When HDAC is up-regulated under stimulation, the expression of tissue inhibitors of matrix metalloproteinases (TIMPs) decreases and the expression of MMP increases, leading to accelerated glycocalyx degradation in endothelial cells (Ali et al., 2019). Ischemia and hypoxia can induce the activation of mast cells, so that the HPSE stored in the mast cells is released into the extracellular space, resulting in cleavage of HS from the endothelial glycocalyx (Becker et al., 2010b). HPSE is the only enzyme known to cleave HS and is another important factor that promotes the shedding of the glycocalyx (Becker et al., 2015). Research on HPSE has helped elucidate the catabolic processes involved in the decomposition of HS. Methylation of the HPSE promoter may regulate HPSE expression (Shteper et al., 2003). Recently, the transcription factor SMAD4, a key protein in the TGF-β signaling pathway, was found to inhibit HPSE by binding to the HPSE promoter region (Qu et al., 2016; Zheng et al., 2016). The inhibitory effect of p53 combined with the promoter on HPSE expression also resulted in the decrease of HPSE activity, indicating p53 is an effective regulator of HPSE expression (Baraz et al., 2006). Enzyme that promotes the shedding of HA is HAase. HAase cracks HA. Atherosclerosis and HAase activity is related (Nieuwdorp et al., 2007). Volume overload is encountered during neurosurgery. Volume overload will cause an increase in the release of natriuretic peptides. Experiments showed that A-, B-, and C-type natriuretic peptides have the ability to promote glycocalyx shedding (Jacob et al., 2013). A summary of the mechanism of damage to glycocalyx shedding is shown in **Figure 3**.

## Potential Strategies of Clinical Protection

The physiological function of the BBB is inseparable from the complete glycocalyx structure. The search for measures to protect the glycocalyx from degradation has always been a research hotspot. Glucocorticoid can stabilize mast cells, inhibit the activation of white blood cells, relieve the downstream inflammatory response, and protect glycocalyx, but its clinical application is limited by the adverse complications of immunosuppression caused by large doses (Cui et al., 2015; Yu et al., 2019). Antithrombin agents can stabilize its structure by combining with endothelial glycocalyx, thereby reducing the enzymatic decomposition of glycocalyx. However, the use of antithrombin during neurosurgery will affect the coagulation function of patients and cause adverse events of postoperative massive bleeding (Chappell et al., 2009a,b). The protective mechanism of albumin is similar to that of antithrombin, but excessive use of albumin will increase the cost of hospitalization for patients, and albumin is an allogeneic source, which will increase the risk of allergy in patients (Becker et al., 2015; Aldecoa et al., 2020). TNF-α inhibitor etanercept has been reported to have a protective effect, but the effect needs to be further studied (Nieuwdorp et al., 2009). Sulodexide has anti-inflammatory, anticoagulant and vascular protection effects, which may be achieved by inhibiting HPSE and MMP activities to reduce glycocalyx shedding (Mannello and Raffetto, 2011; van Haare et al., 2017). Doxycycline and batimastat, all rather non-selective inhibitors of MMPs, can attenuate syndecan and glycan shedding (Lipowsky et al., 2011; Lipowsky and Lescanic, 2013). In addition, sevoflurane has been shown to have a certain protective effect on the glycocalyx. The application of sevoflurane anesthesia in neurosurgery may be more beneficial to the protection of the BBB function (Annecke et al., 2010; Fang et al., 2021).

# CONCLUSION AND FUTURE DIRECTIONS OF RESEARCH

Vascular endothelial glycocalyx plays an indispensable role in BBB, such as inflammation, vascular permeability, blood coagulation, and vascular tone. However, it is not clear whether the glycocalyx in the BBB is different from the glycocalyx in the general vascular structure. Reviewing the relevant literature, details on the neuro-specific contributions of the glycocalyx are still lacking. In addition, the structural and functional relationships between glycocalyx and pericytes are also worth exploring. The therapeutic strategies for glycocalyx

also need further research because the drugs reported in the current research will inevitably have some adverse reactions or application limitations. Therefore, innovative strategies in this emerging field of experimental medicine are desperately needed.

## AUTHOR CONTRIBUTIONS

JC and XW were involved in the study design. WG, HC, and JW provided and prepared the samples. JJ and FF wrote the manuscript. All authors contributed to the article and approved the submitted version.

## FUNDING

This work was supported by the fund of the Public Welfare Technology Research Program/Analysis and Test of Zhejiang Provincial Natural Science Foundation Committee No. GC22H188083 and the fund of Zhejiang Medical and Health Science and Technology Project Nos. 2020KY406 and 2021KY508 to JC.

## REFERENCES

Abdullahi, W., Tripathi, D., and Ronaldson, P. T. (2018). Blood-brain barrier dysfunction in ischemic stroke: targeting tight junctions and transporters for vascular protection. *Am. J. Physiol. Cell Physiol.* 315, C343–C356. doi: 10.1152/ajpcell.00095.2018

Abrahamson, E. E., and Ikonomovic, M. D. (2020). Brain injury-induced dysfunction of the blood brain barrier as a risk for dementia. *Exp. Neurol.* 328:113257. doi: 10.1016/j.expneurol.2020.113257

Aldecoa, C., Llau, J. V., Nuvials, X., and Artigas, A. (2020). Role of albumin in the preservation of endothelial glycocalyx integrity and the microcirculation: a review. *Ann. Intensive Care* 10:85. doi: 10.1186/s13613-020-00697-1

Ali, M. M., Mahmoud, A. M., Le Master, E., Levitan, I., and Phillips, S. A. (2019). Role of matrix metalloproteinases and histone deacetylase in oxidative stress-induced degradation of the endothelial glycocalyx. *Am. J. Physiol. Heart Circ. Physiol.* 316, H647–H663. doi: 10.1152/ajpheart.00090.2018

Alphonsus, C. S., and Rodseth, R. N. (2014). The endothelial glycocalyx: a review of the vascular barrier. *Anaesthesia* 69, 777–784. doi: 10.1111/anae.12661

Annecke, T., Chappell, D., Chen, C., Jacob, M., Welsch, U., Sommerhoff, C. P., et al. (2010). Sevoflurane preserves the endothelial glycocalyx against ischaemia-reperfusion injury. *Br. J. Anaesth.* 104, 414–421. doi: 10.1093/bja/aeq019

Araibi, H., van der Merwe, E., Gwanyanya, A., and Kelly-Laubscher, R. (2020). The effect of sphingosine-1-phosphate on the endothelial glycocalyx during ischemia-reperfusion injury in the isolated rat heart. *Microcirculation* 27:e12612. doi: 10.1111/micc.12612

Baraz, L., Haupt, Y., Elkin, M., Peretz, T., and Vlodavsky, I. (2006). Tumor suppressor p53 regulates heparanase gene expression. *Oncogene* 25, 3939–3947. doi: 10.1038/sj.onc.1209425

Bartosch, A. M. W., Mathews, R., and Tarbell, J. M. (2017). Endothelial Glycocalyx-Mediated Nitric Oxide Production in Response to Selective AFM Pulling. *Biophys. J.* 113, 101–108. doi: 10.1016/j.bpj.2017.05.033

Becker, B. F., Chappell, D., and Jacob, M. (2010b). Endothelial glycocalyx and coronary vascular permeability: the fringe benefit. *Basic Res. Cardiol.* 105, 687–701. doi: 10.1007/s00395-010-0118-z

Becker, B. F., Chappell, D., Bruegger, D., Annecke, T., and Jacob, M. (2010a). Therapeutic strategies targeting the endothelial glycocalyx: acute deficits, but great potential. *Cardiovasc. Res.* 87, 300–310. doi: 10.1093/cvr/cvq137

Becker, B. F., Jacob, M., Leipert, S., Salmon, A. H., and Chappell, D. (2015). Degradation of the endothelial glycocalyx in clinical settings: searching for the sheddases. *Br. J. Clin. Pharmacol.* 80, 389–402. doi: 10.1111/bcp.12629

Bell, J. D., Rhind, S. G., Di Battista, A. P., Macdonald, R. L., and Baker, A. J. (2017). Biomarkers of Glycocalyx Injury are Associated with Delayed Cerebral Ischemia Following Aneurysmal Subarachnoid Hemorrhage: a Case Series Supporting a New Hypothesis. *Neurocrit. Care* 26, 339–347. doi: 10.1007/s12028-016-0357-4

Bernfield, M., Gotte, M., Park, P. W., Reizes, O., Fitzgerald, M. L., Lincecum, J., et al. (1999). Functions of cell surface heparan sulfate proteoglycans. *Annu. Rev. Biochem.* 68, 729–777. doi: 10.1146/annurev.biochem.68.1.729

Bombeli, T., Schwartz, B. R., and Harlan, J. M. (1998). Adhesion of activated platelets to endothelial cells: evidence for a GPIIbIIIa-dependent bridging mechanism and novel roles for endothelial intercellular adhesion molecule 1 (ICAM-1), alphavbeta3 integrin, and GPIbalpha. *J. Exp. Med.* 187, 329–339. doi: 10.1084/jem.187.3.329

Brettner, F., von Dossow, V., and Chappell, D. (2017). The endothelial glycocalyx and perioperative lung injury. *Curr. Opin. Anaesthesiol.* 30, 36–41. doi: 10.1097/ACO.0000000000000434

Butler, M. J., Down, C. J., Foster, R. R., and Satchell, S. C. (2020). The Pathological Relevance of Increased Endothelial Glycocalyx Permeability. *Am. J. Pathol.* 190, 742–751. doi: 10.1016/j.ajpath.2019.11.015

Chappell, D., Hofmann-Kiefer, K., Jacob, M., Rehm, M., Briegel, J., Welsch, U., et al. (2009a). TNF-alpha induced shedding of the endothelial glycocalyx is prevented by hydrocortisone and antithrombin. *Basic Res. Cardiol.* 104, 78–89. doi: 10.1007/s00395-008-0749-5

Chappell, D., Jacob, M., Hofmann-Kiefer, K., Rehm, M., Welsch, U., Conzen, P., et al. (2009b). Antithrombin reduces shedding of the endothelial glycocalyx following ischaemia/reperfusion. *Cardiovasc. Res.* 83, 388–396. doi: 10.1093/cvr/cvp097

Cui, N., Wang, H., Long, Y., Su, L., and Liu, D. (2015). Dexamethasone Suppressed LPS-Induced Matrix Metalloproteinase and Its Effect on Endothelial Glycocalyx Shedding. *Mediators Inflamm.* 2015:912726. doi: 10.1155/2015/912726

Deen, W. M., Lazzara, M. J., and Myers, B. D. (2001). Structural determinants of glomerular permeability. *Am. J. Physiol. Renal Physiol.* 281, F579–F596. doi: 10.1152/ajprenal.2001.281.4.F579

Devaraj, S., Yun, J. M., Adamson, G., Galvez, J., and Jialal, I. (2009). C-reactive protein impairs the endothelial glycocalyx resulting in endothelial dysfunction. *Cardiovasc. Res.* 84, 479–484. doi: 10.1093/cvr/cvp249

Ebong, E. E., Lopez-Quintero, S. V., Rizzo, V., Spray, D. C., and Tarbell, J. M. (2014). Shear-induced endothelial NOS activation and remodeling via heparan sulfate, glypican-1, and syndecan-1. *Integr. Biol.* 6, 338–347. doi: 10.1039/c3ib40199e

Ebong, E. E., Macaluso, F. P., Spray, D. C., and Tarbell, J. M. (2011). Imaging the endothelial glycocalyx in vitro by rapid freezing/freeze substitution transmission electron microscopy. *Arterioscler. Thromb. Vasc. Biol.* 31, 1908–1915. doi: 10.1161/ATVBAHA.111.225268

Endo, K., Takino, T., Miyamori, H., Kinsen, H., Yoshizaki, T., Furukawa, M., et al. (2003). Cleavage of syndecan-1 by membrane type matrix metalloproteinase-1 stimulates cell migration. *J. Biol. Chem.* 278, 40764–40770. doi: 10.1074/jbc.M306736200

Fang, F. Q., Sun, J. H., Wu, Q. L., Feng, L. Y., Fan, Y. X., Ye, J. X., et al. (2021). Protective effect of sevoflurane on vascular endothelial glycocalyx in patients undergoing heart valve surgery: a randomised controlled trial. *Eur. J. Anaesthesiol.* 38, 477–486. doi: 10.1097/EJA.0000000000001429

Hoogewerf, A. J., Kuschert, G. S., Proudfoot, A. E., Borlat, F., Clark-Lewis, I., Power, C. A., et al. (1997). Glycosaminoglycans mediate cell surface oligomerization of chemokines. *Biochemistry* 36, 13570–13578. doi: 10.1021/bi971125s

Iba, T., and Levy, J. H. (2019). Derangement of the endothelial glycocalyx in sepsis. *J. Thromb. Haemost.* 17, 283–294. doi: 10.1111/jth.14371

Jacob, M., Saller, T., Chappell, D., Rehm, M., Welsch, U., and Becker, B. F. (2013). Physiological levels of A-, B- and C-type natriuretic peptide shed the endothelial glycocalyx and enhance vascular permeability. *Basic Res. Cardiol.* 108:347. doi: 10.1007/s00395-013-0347-z

Kabedev, A., and Lobaskin, V. (2018). Structure and elasticity of bush and brush-like models of the endothelial glycocalyx. *Sci. Rep.* 8:240. doi: 10.1038/s41598-017-18577-3

Kang, H., Yang, J., Zhang, W., Lu, J., Ma, X., Sun, A., et al. (2021). Effect of endothelial glycocalyx on water and LDL transport through the rat abdominal aorta. *Am. J. Physiol. Heart Circ. Physiol.* 320, H1724–H1737. doi: 10.1152/ajpheart.00861.2020

Kim, D. H., Chung, J. H., Yoon, J. S., Ha, Y. M., Bae, S., Lee, E. K., et al. (2013). Ginsenoside Rd inhibits the expressions of iNOS and COX-2 by suppressing NF-kappaB in LPS-stimulated RAW264.7 cells and mouse liver. *J Ginseng Res.* 37, 54–63. doi: 10.5142/jgr.2013.37.54

Koenig, A., Norgard-Sumnicht, K., Linhardt, R., and Varki, A. (1998). Differential interactions of heparin and heparan sulfate glycosaminoglycans with the selectins. Implications for the use of unfractionated and low molecular weight heparins as therapeutic agents. *J. Clin. Invest.* 101, 877–889. doi: 10.1172/JCI1509

Kolarova, H., Vitecek, J., Cerna, A., Cernik, M., Pribyl, J., Skladal, P., et al. (2021). Myeloperoxidase mediated alteration of endothelial function is dependent on its cationic charge. *Free Radic. Biol. Med.* 162, 14–26. doi: 10.1016/j.freeradbiomed.2020.11.008

Koo, A., Dewey, C. F. Jr., and Garcia-Cardena, G. (2013). Hemodynamic shear stress characteristic of atherosclerosis-resistant regions promotes glycocalyx formation in cultured endothelial cells. *Am. J. Physiol. Cell Physiol.* 304, C137–46. doi: 10.1152/ajpcell.00187.2012

Kozar, R. A., and Pati, S. (2015). Syndecan-1 restitution by plasma after hemorrhagic shock. *J. Trauma Acute Care Surg.* 78, S83–S86. doi: 10.1097/TA.0000000000000631

Kutuzov, N., Flyvbjerg, H., and Lauritzen, M. (2018). Contributions of the glycocalyx, endothelium, and extravascular compartment to the blood-brain barrier. *Proc. Natl. Acad. Sci. U. S. A.* 115, E9429–E9438. doi: 10.1073/pnas.1802155115

Lipowsky, H. H., and Lescanic, A. (2013). The effect of doxycycline on shedding of the glycocalyx due to reactive oxygen species. *Microvasc. Res.* 90, 80–85. doi: 10.1016/j.mvr.2013.07.004

Lipowsky, H. H., Sah, R., and Lescanic, A. (2011). Relative roles of doxycycline and cation chelation in endothelial glycan shedding and adhesion of leukocytes. *Am. J. Physiol. Heart Circ. Physiol.* 300, H415–H422. doi: 10.1152/ajpheart.00923.2010

Lupu, F., Kinasewitz, G., and Dormer, K. (2020). The role of endothelial shear stress on haemodynamics, inflammation, coagulation and glycocalyx during sepsis. *J. Cell. Mol. Med.* 24, 12258–12271. doi: 10.1111/jcmm.15895

Lyu, N., Du, Z., Qiu, H., Gao, P., Yao, Q., Xiong, K., et al. (2020). Mimicking the Nitric Oxide-Releasing and Glycocalyx Functions of Endothelium on Vascular Stent Surfaces. *Adv Sci.* 7:2002330. doi: 10.1002/advs.202002330

Mannello, F., and Raffetto, J. D. (2011). Matrix metalloproteinase activity and glycosaminoglycans in chronic venous disease: the linkage among cell biology, pathology and translational research. *Am. J. Transl. Res.* 3, 149–158.

Mende, M., Bednarek, C., Wawryszyn, M., Sauter, P., Biskup, M. B., Schepers, U., et al. (2016). Chemical Synthesis of Glycosaminoglycans. *Chem. Rev.* 116, 8193–8255. doi: 10.1021/acs.chemrev.6b00010

Michel, C. C. (1997). Starling: the formulation of his hypothesis of microvascular fluid exchange and its significance after 100 years. *Exp. Physiol.* 82, 1–30. doi: 10.1113/expphysiol.1997.sp004000

Mulivor, A. W., and Lipowsky, H. H. (2004). Inflammation- and ischemia-induced shedding of venular glycocalyx. *Am. J. Physiol. Heart Circ. Physiol.* 286, H1672–H1680. doi: 10.1152/ajpheart.00832.2003

Mulivor, A. W., and Lipowsky, H. H. (2009). Inhibition of glycan shedding and leukocyte-endothelial adhesion in postcapillary venules by suppression of matrixmetalloprotease activity with doxycycline. *Microcirculation* 16, 657–666. doi: 10.3109/10739680903133714

Nandi, A., Estess, P., and Siegelman, M. H. (2000). Hyaluronan anchoring and regulation on the surface of vascular endothelial cells is mediated through the functionally active form of CD44. *J. Biol. Chem.* 275, 14939–14948. doi: 10.1074/jbc.275.20.14939

Nieuwdorp, M., Holleman, F., de Groot, E., Vink, H., Gort, J., Kontush, A., et al. (2007). Perturbation of hyaluronan metabolism predisposes patients with type 1 diabetes mellitus to atherosclerosis. *Diabetologia* 50, 1288–1293. doi: 10.1007/s00125-007-0666-4

Nieuwdorp, M., Meuwese, M. C., Mooij, H. L., van Lieshout, M. H., Hayden, A., Levi, M., et al. (2009). Tumor necrosis factor-alpha inhibition protects against endotoxin-induced endothelial glycocalyx perturbation. *Atherosclerosis* 202, 296–303. doi: 10.1016/j.atherosclerosis.2008.03.024

Nikmanesh, M., Cancel, L. M., Shi, Z. D., and Tarbell, J. M. (2019). Heparan sulfate proteoglycan, integrin, and syndecan-4 are mechanosensors mediating cyclic strain-modulated endothelial gene expression in mouse embryonic stem cell-derived endothelial cells. *Biotechnol. Bioeng.* 116, 2730–2741. doi: 10.1002/bit.27104

Piperigkou, Z., Mohr, B., Karamanos, N., and Gotte, M. (2016). Shed proteoglycans in tumor stroma. *Cell Tissue Res.* 365, 643–655. doi: 10.1007/s00441-016-2452-4

Pries, A. R., Secomb, T. W., and Gaehtgens, P. (2000). The endothelial surface layer. *Pflugers Arch.* 440, 653–666. doi: 10.1007/s004240000307

Purcell, S. C., and Godula, K. (2019). Synthetic glycoscapes: addressing the structural and functional complexity of the glycocalyx. *Interface Focus* 9:20180080. doi: 10.1098/rsfs.2018.0080

Qu, H., Zheng, L., Jiao, W., Mei, H., Li, D., Song, H., et al. (2016). Smad4 suppresses the tumorigenesis and aggressiveness of neuroblastoma through repressing the expression of heparanase. *Sci. Rep.* 6:32628. doi: 10.1038/srep32628

Rabelink, T. J., van den Berg, B. M., Garsen, M., Wang, G., Elkin, M., and van der Vlag, J. (2017). Heparanase: roles in cell survival, extracellular matrix remodelling and the development of kidney disease. *Nat. Rev. Nephrol.* 13, 201–212. doi: 10.1038/nrneph.2017.6

Rambourg, A., Neutra, M., and Leblond, C. P. (1966). Presence of a "cell coat" rich in carbohydrate at the surface of cells in the rat. *Anat. Rec.* 154, 41–71. doi: 10.1002/ar.1091540105

Rana, A., and Musto, A. E. (2018). The role of inflammation in the development of epilepsy. *J. Neuroinflammation* 15:144. doi: 10.1186/s12974-018-1192-7

Rapraeger, A., Jalkanen, M., Endo, E., Koda, J., and Bernfield, M. (1985). The cell surface proteoglycan from mouse mammary epithelial cells bears chondroitin sulfate and heparan sulfate glycosaminoglycans. *J. Biol. Chem.* 260, 11046–11052.

Reine, T. M., Lanzalaco, F., Kristiansen, O., Enget, A. R., Satchell, S., Jenssen, T. G., et al. (2019). Matrix metalloproteinase-9 mediated shedding of syndecan-4 in glomerular endothelial cells. *Microcirculation* e12534. doi: 10.1111/micc.12534 [Online ahead of print].

Reitsma, S., Slaaf, D. W., Vink, H., van Zandvoort, M. A., and Oude Egbrink, M. G. (2007). The endothelial glycocalyx: composition, functions, and visualization. *Pflugers Arch.* 454, 345–359. doi: 10.1007/s00424-007-0212-8

Ruegg, C., and Mariotti, A. (2003). Vascular integrins: pleiotropic adhesion and signaling molecules in vascular homeostasis and angiogenesis. *Cell. Mol. Life Sci.* 60, 1135–1157. doi: 10.1007/s00018-003-2297-3

Salmon, A. H., and Satchell, S. C. (2012). Endothelial glycocalyx dysfunction in disease: albuminuria and increased microvascular permeability. *J. Pathol.* 226, 562–574. doi: 10.1002/path.3964

Santa-Maria, A. R., Walter, F. R., Figueiredo, R., Kincses, A., Vigh, J. P., Heymans, M., et al. (2021). Flow induces barrier and glycocalyx-related genes and negative surface charge in a lab-on-a-chip human blood-brain barrier model. *J. Cereb. Blood Flow Metab.* 41, 2201–2215. doi: 10.1177/0271678X21992638

Schmidt, E. P., Yang, Y., Janssen, W. J., Gandjeva, A., Perez, M. J., Barthel, L., et al. (2012). The pulmonary endothelial glycocalyx regulates neutrophil adhesion and lung injury during experimental sepsis. *Nat. Med.* 18, 1217–1223. doi: 10.1038/nm.2843

Schnoor, M., Alcaide, P., Voisin, M. B., and van Buul, J. D. (2015). Crossing the Vascular Wall: common and Unique Mechanisms Exploited by Different Leukocyte Subsets during Extravasation. *Mediators Inflamm.* 2015:946509. doi: 10.1155/2015/946509

Shteper, P. J., Zcharia, E., Ashhab, Y., Peretz, T., Vlodavsky, I., and Ben-Yehuda, D. (2003). Role of promoter methylation in regulation of the mammalian heparanase gene. *Oncogene* 22, 7737–7749. doi: 10.1038/sj.onc.1207056

Simard, J. M., Tosun, C., Ivanova, S., Kurland, D. B., Hong, C., Radecki, L., et al. (2012). Heparin reduces neuroinflammation and transsynaptic neuronal apoptosis in a model of subarachnoid hemorrhage. *Transl. Stroke Res.* 3, 155–165. doi: 10.1007/s12975-012-0166-9

Song, J., Wu, C., Korpos, E., Zhang, X., Agrawal, S. M., Wang, Y., et al. (2015). Focal MMP-2 and MMP-9 activity at the blood-brain barrier promotes chemokine-induced leukocyte migration. *Cell Rep.* 10, 1040–1054. doi: 10.1016/j.celrep.2015.01.037

Sperandio, M. (2006). Selectins and glycosyltransferases in leukocyte rolling in vivo. *FEBS J.* 273, 4377–4389. doi: 10.1111/j.1742-4658.2006.05437.x

Starling, E. H. (1896). On the Absorption of Fluids from the Connective Tissue Spaces. *J. Physiol.* 19, 312–326. doi: 10.1113/jphysiol.1896.sp000596

Tarbell, J. M. (2010). Shear stress and the endothelial transport barrier. *Cardiovasc. Res.* 87, 320–330. doi: 10.1093/cvr/cvq146

Uchimido, R., Schmidt, E. P., and Shapiro, N. I. (2019). The glycocalyx: a novel diagnostic and therapeutic target in sepsis. *Crit. Care* 23:16. doi: 10.1186/s13054-018-2292-6

Ushiyama, A., Kataoka, H., and Iijima, T. (2016). Glycocalyx and its involvement in clinical pathophysiologies. *J. Intensive Care* 4:59. doi: 10.1186/s40560-016-0182-z

Van den Berg, B. M., Nieuwdorp, M., Stroes, E. S., and Vink, H. (2006). Glycocalyx and endothelial (dys) function: from mice to men. *Pharmacol. Rep.* 58, 75–80.

van Golen, R. F., Reiniers, M. J., Vrisekoop, N., Zuurbier, C. J., Olthof, P. B., van Rheenen, J., et al. (2014). The Mechanisms and Physiological Relevance of Glycocalyx Degradation in Hepatic Ischemia/Reperfusion Injury. *Antioxid. Redox Sign.* 21:1098. doi: 10.1089/ars.2013.5751

van Haare, J., Kooi, M. E., van Teeffelen, J. W., Vink, H., Slenter, J., Cobelens, H., et al. (2017). Metformin and sulodexide restore cardiac microvascular perfusion capacity in diet-induced obese rats. *Cardiovasc. Diabetol.* 16:47. doi: 10.1186/s12933-017-0525-7

van Haaren, P. M., VanBavel, E., Vink, H., and Spaan, J. A. (2003). Localization of the permeability barrier to solutes in isolated arteries by confocal microscopy. *Am. J. Physiol. Heart Circ. Physiol.* 285, H2848–56. doi: 10.1152/ajpheart.00117.2003

Yang, X., Meegan, J. E., Jannaway, M., Coleman, D. C., and Yuan, S. Y. (2018). A disintegrin and metalloproteinase 15-mediated glycocalyx shedding contributes to vascular leakage during inflammation. *Cardiovasc. Res.* 114, 1752–1763. doi: 10.1093/cvr/cvy167

Yen, W., Cai, B., Yang, J., Zhang, L., Zeng, M., Tarbell, J. M., et al. (2015). Endothelial surface glycocalyx can regulate flow-induced nitric oxide production in microvessels in vivo. *PLoS One* 10:e0117133. doi: 10.1371/journal.pone.0117133

Yu, W. Q., Zhang, S. Y., Fu, S. Q., Fu, Q. H., Lu, W. N., Zhang, J., et al. (2019). Dexamethasone protects the glycocalyx on the kidney microvascular endothelium during severe acute pancreatitis. *J. Zhejiang Univ. Sci. B* 20, 355–362. doi: 10.1631/jzus.B1900006

Zenaro, E., Piacentino, G., and Constantin, G. (2017). The blood-brain barrier in Alzheimer's disease. *Neurobiol. Dis.* 107, 41–56. doi: 10.1016/j.nbd.2016.07.007

Zhao, F., Zhong, L., and Luo, Y. (2021). Endothelial glycocalyx as an important factor in composition of blood-brain barrier. *CNS Neurosci. Ther.* 27, 26–35. doi: 10.1111/cns.13560

Zheng, L., Jiao, W., Song, H., Qu, H., Li, D., Mei, H., et al. (2016). miRNA-558 promotes gastric cancer progression through attenuating Smad4-mediated repression of heparanase expression. *Cell Death Dis.* 7:e2382. doi: 10.1038/cddis.2016.293

Zhu, J., Li, X., Yin, J., Hu, Y., Gu, Y., and Pan, S. (2017). Glycocalyx degradation leads to blood-brain barrier dysfunction and brain edema after asphyxia cardiac arrest in rats. *J. Cereb. Blood Flow Metab.* 38, 1979–1992. doi: 10.1177/0271678X17726062

Zhu, J., Li, X., Yin, J., Hu, Y., Gu, Y., and Pan, S. (2018). Glycocalyx degradation leads to blood-brain barrier dysfunction and brain edema after asphyxia cardiac arrest in rats. *J. Cereb. Blood Flow Metab.* 38, 1979–1992.

Zuurbier, C. J. (2019). Ketamine-(Dex)Medetomidine, Hyperglycemia, Glycocalyx, and Vascular Permeability. *Anesth. Analg.* 129:e102. doi: 10.1213/ANE.0000000000004181

**Conflict of Interest:** The authors declare that the research was conducted in the absence of any commercial or financial relationships that could be construed as a potential conflict of interest.

**Publisher's Note:** All claims expressed in this article are solely those of the authors and do not necessarily represent those of their affiliated organizations, or those of the publisher, the editors and the reviewers. Any product that may be evaluated in this article, or claim that may be made by its manufacturer, is not guaranteed or endorsed by the publisher.

frontiers in Cellular Neuroscience

REVIEW
published: 12 October 2021
doi: 10.3389/fncel.2021.706025

# Emerging Roles of Microglia in Neuro-vascular Unit: Implications of Microglia-Neurons Interactions

*Zhe Ding[1†], Shaohui Guo[1†], Lihui Luo[1], Yueying Zheng[1], Shuyuan Gan[1], Xianhui Kang[1], Xiaomin Wu[2]* and Shengmei Zhu[1]**

[1]*Department of Anesthesiology, The First Affiliated Hospital, Zhejiang University School of Medicine, Hangzhou, China,* [2]*Department of Anesthesiology, Zhejiang Provincial People's Hospital, People's Hospital of Hangzhou Medical College, Hangzhou, China*

Microglia, which serve as the defensive interface of the nervous system, are activated in many neurological diseases. Their role as immune responding cells has been extensively studied in the past few years. Recent studies have demonstrated that neuronal feedback can be shaped by the molecular signals received and sent by microglia. Altered neuronal activity or synaptic plasticity leads to the release of various communication messages from neurons, which in turn exert effects on microglia. Research on microglia-neuron communication has thus expanded from focusing only on neurons to the neurovascular unit (NVU). This approach can be used to explore the potential mechanism of neurovascular coupling across sophisticated receptor systems and signaling cascades in health and disease. However, it remains unclear how microglia-neuron communication happens in the brain. Here, we discuss the functional contribution of microglia to synapses, neuroimmune communication, and neuronal activity. Moreover, the current state of knowledge of bidirectional control mechanisms regarding interactions between neurons and microglia are reviewed, with a focus on purinergic regulatory systems including ATP-$P_2RY_{12}R$ signaling, ATP-adenosine-$A_1Rs/A_{2A}Rs$, and the ATP-pannexin 1 hemichannel. This review aims to organize recent studies to highlight the multifunctional roles of microglia within the neural communication network in health and disease.

**Keywords: microglia, microglia-neurons communication, synaptic plasticity, neuronal activity, NVU, ATP**

OPEN ACCESS

***Edited by:***
*Xinchun Jin,*
*Capital Medical University, China*

***Reviewed by:***
*Daqing Ma,*
*Imperial College London, United Kingdom*
*Hongfei Zhang,*
*Southern Medical University, China*

****Correspondence:***
*Xiaomin Wu*
*wuxiaomin@hmc.edu.cn*
*Shengmei Zhu*
*smzhu20088@zju.edu.cn*

*†These authors share first authorship*

***Specialty section:***
*This article was submitted to Cellular Neurophysiology, a section of the journal Frontiers in Cellular Neuroscience*

***Received:*** *06 May 2021*
***Accepted:*** *10 September 2021*
***Published:*** *12 October 2021*

***Citation:***
*Ding Z, Guo S, Luo L, Zheng Y, Gan S, Kang X, Wu X and Zhu S (2021) Emerging Roles of Microglia in Neuro-vascular Unit: Implications of Microglia-Neurons Interactions. Front. Cell. Neurosci. 15:706025. doi: 10.3389/fncel.2021.706025*

## INTRODUCTION

Research on central nervous system (CNS) disorders has largely concentrated on neurons; however, an increasing body of research suggests that a purely neurocentral focus is insufficient. All cell types in the brain—including neuronal, glial, and vascular components such as endothelia, pericytes, and vascular smooth muscular cells—should be examined in an integrated context (Muoio et al., 2014). Together, these components are termed the neurovascular unit (NVU; **Figure 1**), which plays an important role in brain function and disease through cell–cell signaling (Iadecola, 2017). The NVU is reported to control blood-brain barrier (BBB) permeability and cerebral blood flow (CBF) and to regulate the neuronal 'milieu' (Zlokovic, 2011). Signaling perturbations within the NVU comprise potential mechanisms for neuronal dysfunction and injury (Sweeney et al., 2016; Yu et al., 2020). Recent studies have shown that the NVU contributes to both stroke and neurodegenerative diseases (Cai et al., 2017; Giaume et al., 2021; Minhas et al., 2021). In light of such findings, increasing research efforts have focused on the NVU as a therapeutic target (Quaegebeur et al., 2011).

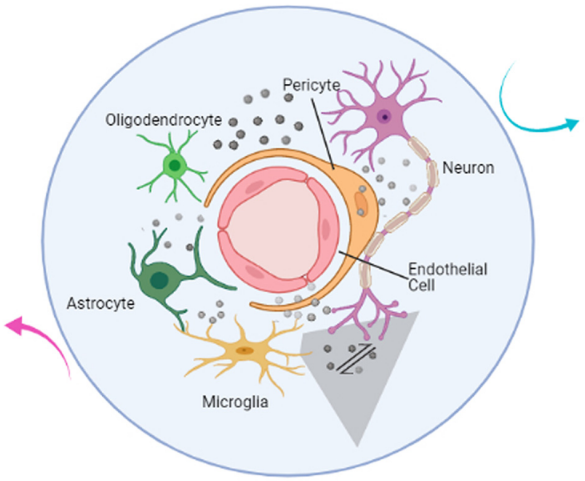


**FIGURE 1 |** Illustration of the components of the neurovascular unit. The neurovascular unit (NVU) is composed of neurons (purple), microglia (yellow), astrocytes (dark green), oligodendrocytes (light green), endothelial cells (red), and pericytes (orange). Based on intimate anatomical relationships and chemical signals (gray sphere) secreted by oneself or others, these components establish an anatomical and functional whole (blue circle) that participates in physiological and pathological processes in the brain. The communication network also includes the interactions between NVU and the outside world (cyan and magenta arrow). The mutual communication and cooperation between microglia and neurons (gray shaded trapezoid) in the brain is the focus of this article and will be discussed below.

Microglia perform an immune surveillance function through highly motile protrusions and ramified processes that sense their environment during their "resting" state or after activation *in vivo* (Nimmerjahn et al., 2005). Notably, microglia do not patrol in an aimless manner; rather, microglial surveillance is associated with neuronal activity and synaptic plasticity (Nayak et al., 2014). Emerging evidence suggests that microglia contribute to the development, maturation, and aging of the brain (Liu et al., 2020; Verkhratsky et al., 2021) and are recognized to express many risk genes for CNS disorders, including genes associated with Alzheimer's disease (AD), Parkinson's disease (PD), schizophrenia, autism, and multiple sclerosis (MS; Kékesi et al., 2019; Prinz et al., 2019). Neuron-microglia signaling can be detected under physiological and pathological conditions in the brain (Cserép et al., 2020, 2021). The interactions between microglia and neurons establish complex regulatory loops that involve either the establishment of neural networks and maintenance of neural circuits in health or the development of neurological disorders in disease (Cserép et al., 2021).

Microglia, as a component of the NVU, play significant roles in neuroinflammation and innate immunity (Lehnardt, 2010; Joost et al., 2019). Not only do microglia-derived mediators participate in inflammation and immune-related responses they also serve as important messengers in cell-cell signaling between neuronal and glial cells. In this review, we discuss the evidence of the contribution of microglia to synapses, neuroimmune communication, and neuronal activity. In particular, we focus on bidirectional interactions between microglia and neurons that depend on soluble factors and intercellular signaling pathways, with the ultimate aim of better understanding the recently recognized functional roles of microglial actions in synaptic function, neuroimmune responses, and regulation of neural activity.

## A SYNAPTIC ROLE FOR MICROGLIA

During postnatal development of the brain, microglia play major roles in the rapid elimination of dying neurons and synaptic structures (Tremblay et al., 2010; Ayata et al., 2018), synaptic pruning (Paolicelli et al., 2011; Schafer et al., 2012) and promoting the survival of cortical neurons (Ueno et al., 2013). Maternal immune activation (MIA), which is induced by injecting pregnant mice with polycytidylic acid (poly I:C), has been shown to have a significant impact on the pre-microglia (from embryonic day 14 to a few weeks after birth) of newborn offspring. As this impact on pre-microglia is influencing neurogenesis and synaptic pruning, it explains the later occurrence of behavioral disorders when the offspring are adults (Matcovitch-Natan et al., 2016). Emerging evidence suggests that microglia regulate activity-dependent structural plasticity and promote memory consolidation by locally clearing the extracellular matrix (ECM). Furthermore, cytokine interleukin-33 (IL-33), which is expressed by hippocampal neurons, significantly upregulates ECM protease genes (namely *Adamts4* and *Mmp14*), thereby promoting microglial phagocytosis and engulfment of aggrecan around parvalbumin+ interneurons in the CA1 hippocampal subregion (Nguyen et al., 2020). Moreover, this mechanism is demonstrated in both young mouse (3 months) and old mouse (18 months) under physiological conditions.

The release of immunological mediators from microglia has also been shown to influence synaptic function. Beattie et al. (2002) reported that tumor-necrosis factor-alpha (TNFα) significantly increases the mean miniature excitatory postsynaptic currents (mEPSCs) frequency and promotes the maintenance of synaptic strength, as indicated by mEPSCs at excitatory synapses that call for the continual presence of TNFα, which enhances synaptic efficacy by increasing surface expression of AMPA receptors. Since microglia are a source of TNFα, they potentiate glutamate-mediated neurotoxicity or participate in synaptic connectivity in an indirect way (Stellwagen and Malenka, 2006; Olmos and Lladó, 2014). Interleukin 1β (IL-1β) has been shown to impair long-term potentiation (LTP) directly at the synapse, which could explain why cognitive impairment is worse in aged hippocampal synapses (Prieto et al., 2015). Aberrant expression of IL-1β also results in damage to hippocampus-dependent memory (Patterson, 2015). It is interesting that either TNFα or IL-1β plays a role in sleep regulation by changing neuromodulator/neurotransmitter receptor expression, resulting in altering neuron sensitivity (Krueger et al., 2011). Brain-derived neurotrophic factor (BDNF), which is reported to influence synaptic plasticity, learning, and memory formation (Parkhurst et al., 2013; Leal et al., 2014), also appears to be a crucial signaling molecule in microglia-neuron communication.

Preventing BDNF release from microglia has been shown to reverse allodynia and anion shift, and may thus provide a new therapeutic strategy for treating neuropathic pain (Coull et al., 2005). Interleukin 10 (IL-10), which acts on IL-10 receptors expressed on hippocampal neurons, plays a role in the induction of synaptic formation, including dendritic spines and excitatory and inhibitory synapses (Lim et al., 2013). It has been shown that IL-10 can facilitate LTP in the CA1 region of the hippocampus and increase synaptic strength, based on observations that the presynaptic fiber volley field excitatory postsynaptic potential (FV-fEPSP) slope increases after IL-10 treatment, thereby promoting synaptic plasticity (Nenov et al., 2019).

These soluble factors, which have been extensively studied in the context of neuroinflammation (Perry and Holmes, 2014), exert their effects on synaptic function as discussed above. The released cytokines act on neurons in a flexible way and are not limited by distance. Studies conducted in recent years have shown that the administration of cytokines, including TNFα and IL-1β, results in significantly increased astrogliosis at the brain injury site in neonatal mouse (Balasingam et al., 1994). Liddelow et al. (2017) reported that the release of IL-1α, TNF, and C1q from microglia is necessary and sufficient to induce a subtype of reactive astrocytes (termed A1 astrocytes), leading to impairment of neuronal survival, outgrowth, synaptogenesis, and phagocytosis and the death of neurons and oligodendrocytes. In response to cytokines, astrocytes can produce IL-1, IL-4, IL-6, IL-10, IL-12, TNF-α, and interferon (IFN) to act on microglia (Benveniste, 1998). Taken together, these studies have shown that soluble factors contribute to the establishment of the interplay between different cell types within the NVU. The influence of microglia on neuronal networks appears to be sophisticated since interactions within the NVU cannot be ignored. Thus, the net effects must be taken into consideration. In light of this knowledge, the application should be carefully considered, since the ultimate effects of immunological mediators appear to depend on time, concentration, and environmental milieu.

## NEUROIMMUNE COMMUNICATION WITH MICROGLIA

Microglia are the resident myeloid cells of the brain (Nayak et al., 2014). Equipped with specialized pattern recognition receptors (PRRs) that identify pathogen-associated molecular patterns (PAMPs) and host-derived danger-associated molecular patterns (DAMPs) in microorganisms, microglia play a key role in the neuroimmune system by quickly inducing a fine-tuned inflammatory response (Scheiblich et al., 2020). Activation of microglia that play a role in innate immune function is pivotal in neuroinflammation. In addition to their influences on synaptic plasticity, the release of cytokines and chemokines further amplifies the inflammatory process, which has been well documented in previous studies (Nayak et al., 2014; Prinz et al., 2019).

The nervous system is involved in regulating immunity and inflammation, whereas immune dysregulation and inflammation also affect brain function in disease (Pavlov et al., 2018). For instance, neural circuits may promote immunosuppression after injury or stroke by altering microglia function (Pavlov and Tracey, 2017). Notably, MIA, which involves alterations in the number and state of activated microglia, is closely associated with early disruptions in neurodevelopment and may result in later neuropsychiatric disorders in offspring, including anxiety-like or depression-like behavior, sensorimotor deficits, social deficits, and repetitive behaviors. Gumusoglu and Stevens (2019) proposed that the most common outcomes of maternal immune perturbation are elevations in the proinflammatory cytokines IL-6 and IL-1β, resulting in alterations in synapse formation and function and driving neural progenitors from a neurogenic to gliogenic fate. Brown et al. (2017) revealed that exposure to intrauterine inflammation altered metabolic profiles, including amino acid metabolism, purine metabolism, and lipid metabolism, in the amniotic fluid and fetal and neonatal brain of exposed offspring. Interestingly, the changes were sex-specific and persisted at a later time point (48 h vs. 6 h after intrauterine inflammation; Brown et al., 2017). Furthermore, metabolic pathways disturbances, including mitochondrial function, arborization, and synapse formation, have been observed in the developmental interneurons of individuals with schizophrenia (SCZ) co-cultured with activated microglia. Intriguingly, SCZ cortical interneurons (cINs) show prolonged compromised metabolic pathways after removal of the activated microglia, which indicates an interaction between the genetic background of SCZ donors and the inflammatory environment provided by activated microglia (Park et al., 2020). It has been suggested that neuroinflammation mediated by microglia specifically acting on cINs has long–term effects during brain development. Notably, the microglial gene expression profiles of the offspring of mothers administered poly I:C were realigned with the normal microglial phenotype at adulthood, indicating that transient perturbation in the early stage of microglia development (such as the pre-microglia stage) may have far-reaching implications on the brain at adulthood (Matcovitch-Natan et al., 2016).

Recent studies suggest that any assessment of the impact of microglia-mediated immune responses on neurons should consider differences between short-term and long-term effects. It can be concluded that the activation of microglia following immune activation induces inflammation of the brain, which has a profound impact on neurodevelopment. Although microglia are primary initiators and effectors of neuroinflammation (Thurgur and Pinteaux, 2019), the pathological process includes the contributions of various cell types. It has been established that astrocytes along with microglia participate in the amplification of inflammation signals, which in turn may cause apoptosis of oligodendroglioma cancer cells (Liddelow et al., 2020). More precisely, microglia are essential for triggering the standard immune response of microglia with astrocytes, as confirmed by studies revealing that astrocytes show no response to pathogens/damage in the absence of microglia (Liu et al., 2021). At the same time, neuroimmune communication also occurs between microglia and endothelial cells, where microglia play a role in maintaining the integrity of the BBB and thus the influx of blood-derived molecules into the brain (Muoio et al., 2014).

In addition, recent studies have uncovered that neuroimmune interactions are also important regulators of physiology (Huh and Veiga-Fernandes, 2020). For example, microglia work to maintain homeostasis in the brain, not only to resolve infections (Norris and Kipnis, 2019). Pavlov and Tracey (2017) revealed neural reflex regulation of immunity, finding that neural circuits are triggered by and control inflammation. Sensory neurons are capable of monitoring the immune state in the periphery and interacting with immune cells, which are defined as neuroimmune cell units. The communicating immune signals, which then activate the CNS, can derive from any major body organ including skin, lung, and intestines (reviewed in Huh and Veiga-Fernandes, 2020). Ultimately, the brain integrates neuro-immune communication in order to maintain a steady-state.

## MICROGLIA-NEURONS COMMUNICATION

New evidence suggests that exacerbated activation of microglia can promote microglia-mediated neuronal degeneration (Zhao et al., 2018). It has been shown that loss of striatal microglia triggers seizures *via* activation of cortical and hippocampal neurons in mice (Badimon et al., 2020). Moreover, similar to inhibitory neurons, microglia can sense neuronal activation and then lower the activation of dopaminergic neurons to achieve negative feedback control of neuronal activity (Badimon et al., 2020). In addition, neuronal excitation affects the process extension and motility of microglia (Liu et al., 2019; Stowell et al., 2019). Overall, these studies support reciprocal connections between microglia and neurons. Understanding the molecular mechanisms that underlie these bidirectional interactions will be necessary to achieve an integrated view of microglia-neuron communication systems, thereby enabling real insight into the importance of these communication systems in the control of brain function.

### ATP-$P_2RY_{12}$ Signaling Is Essential for Microglia Neuron Communication

Purinergic signaling plays a central role in microglia-neuron interactions, of which ATP is recognized as an efferent neurotransmitter in the CNS (Burnstock, 2006; Burnstock et al., 2011). ATP, which is mediated by G-protein-coupled $P_2$ receptors, acts as an activity-dependent signal under physiological conditions or as a danger signal when dysfunction or damage occurs in the brain (Agostinho et al., 2020). There is evidence of the vesicular release of ATP from neurons (Pankratov et al., 2007; Larsson et al., 2012) and from astrocytes (Darby et al., 2003; Bowser and Khakh, 2007). ATP released by astrocytes regulates microglial branch dynamics in the intact brain and chemotactic responses of activated microglia toward the local injury site in the brain (Davalos et al., 2005). In neuron-microglia interactions, ATP supports communication from neurons to microglia *via* $P_2RY_{12}$ signaling activation (Badimon et al., 2020; **Figure 2**). In general, ATP results in a decrease in neuronal activity both in normal (Li et al., 2012) and in pathological conditions (Cserép et al., 2020). Microglial $P_2RY_{12}$ receptors are exclusively expressed by microglia and are viewed as an indispensable component of microglia-neuron junctions (Eyo et al., 2014; Cserép et al., 2020). 3D electron tomography showed that $P_2RY_{12}$ receptor density was negatively correlated with the distance between microglial and neuronal membranes within the junctions. Meanwhile, *in vivo* 2P imaging further confirmed that microglial process recruitment to somatic junctions is linked to the metabolic activity of neuronal mitochondria through a $P_2RY_{12}$ receptor–dependent mechanism (Cserép et al., 2020). Emerging evidence suggests that $P_2RY_{12}$Rs are involved in chemotaxis and the motility of microglia (Dissing-Olesen et al., 2014) as well as in microglia activation in the trigeminal nucleus caudalis (Jing et al., 2019), neuropathic pain (Tozaki-Saitoh et al., 2008; Gu et al., 2016), epilepticus (Avignone et al., 2008; Milior et al., 2020), and stroke (Kluge et al., 2017; Li et al., 2020). Thus, ATP-$P_2RY_{12}$R signaling responses between microglia and neurons appear to contribute to an important loop in neural crosstalk (**Figure 2**).

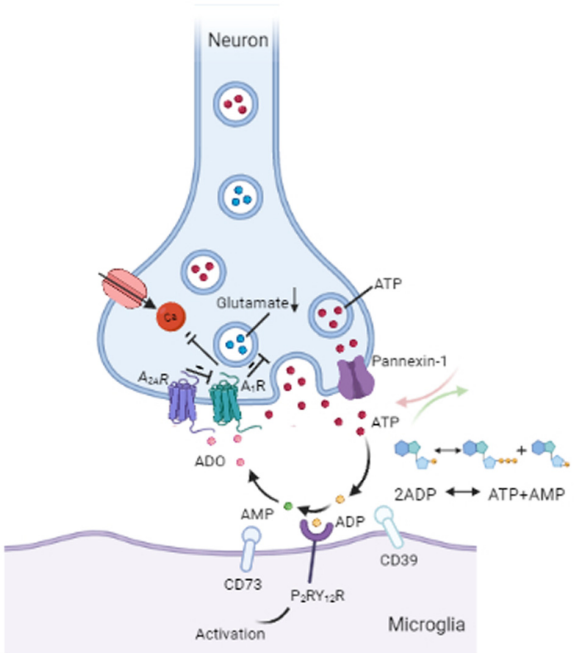


**FIGURE 2 |** Communication between microglia and neurons. ATP can be secreted from neurons through vesicles or the pannexin-1 channel. Released ATP (red) is converted into ADP (yellow) by the microglial enzyme CD39. ADP acts on $P_2RY_{12}$ receptors to induce activation of $P_2RY_{12}$ signaling, which attracts microglial processes to synaptic connections. CD39 also converts ADP into AMP (green). Next, AMP is converted into ADO (pink) by the enzyme CD73 on microglia. ADO suppresses neuronal activity by acting on $A_1$Rs by decreasing glutamate (blue) release and inhibiting calcium ($Ca^{2+}$) channels. In addition, $A_{2A}$Rs can weaken the inhibitory effect of A1Rs on glutamate release. ATP = adenosine triphosphate, ADP = adenosine diphosphate, AMP = adenosine monophosphate, ADO = adenosine, $A_1R$ = $A_1$ receptor, $A_{2A}R$ = $A_{2A}$ receptor.

### ATP-Adenosine-$A_1$Rs/$A_{2A}$Rs Are Essential for Microglia Neuron Communication

Following ectoenzymatic breakdown of extracellular ATP, adenosine is produced and binds to $A_1$ or $A_{2A}$ receptors in

the brain, thereby regulating nerve activity and transmitter release (Fredholm et al., 2005). It has been demonstrated that adenosine (ADO) lowers neuronal excitability by acting on $A_1$Rs and is a prominent physiological mediator of sleep homeostasis (Ribeiro et al., 2002). Recent studies have revealed that cholinergic and glutamatergic neurons show highly correlated activity with changes in adenosine concentration, with glutamatergic neurons contributing much more to adenosine increases in the mouse basal forebrain (BF; Peng et al., 2020). $A_1$Rs and $A_{2A}$Rs are widely abundant in the brain, particularly in glutamatergic synapses (Yoon and Rothman, 1991; Rosin et al., 1998; Rebola et al., 2005). As a synaptic neuromodulator curtailing excitatory synaptic transmission, $A_1$Rs-mediated inhibition can fully block glutamatergic transmission (Coelho et al., 2006; Rodrigues et al., 2008) by inhibiting adenylate cyclase (AC), increasing potassium ($K^+$) conductance, and inhibiting presynaptic calcium ($Ca^{2+}$) channels (Benarroch, 2008). $A_{2A}$Rs are activated by ATP-derived adenosine upon increased synaptic activity to act on synaptic plasticity (d'Alcantara et al., 2001; Augusto et al., 2013; Kerkhofs et al., 2018). In contrast, presynaptic $A_{2A}$Rs may form heteromeric receptor complexes with presynaptic $A_1$Rs (Benarroch, 2008), which antagonizes the inhibitory effect of presynaptic $A_1$Rs on glutamate release from axon terminals in the striatum, cerebral cortex, and brainstem (Ribeiro et al., 2002; Boison, 2006). In addition to ATP-$P_2RY_{12}$R signaling as described above, a recent study demonstrated that ATP-adenosine-$A_1$Rs signaling in mice suppresses D1 neuronal activity in the striatum, which could be regarded as a novel mechanism for communication between microglia and neurons (Badimon et al., 2020). Metabolic stress, such as ischemia, seizures, or trauma, may result in the upregulation of extracellular adenosine (Benarroch, 2008). The release of adenosine from parallel fibers has also been reported in the rat cerebellum. Moreover, activity-dependent adenosine release is known to regulate cerebellar circuit output through feedback inhibition of parallel fiber-Purkinje cell transmission (Wall and Dale, 2007). Much research consideration has surrounded adenosine as an endogenous neuromodulator in the CNS (Benarroch, 2008). Such studies have revealed roles for adenosine as well as adenosine receptors, greatly adding to our understanding while simultaneously expanding the complexity of the signaling system's mechanisms of action.

## ATP-Pannexin 1 Hemichannel Are Essential for Microglia Neuron Communication

Pannexin 1 forms intercellular hemichannels and plays multiple roles in channel-mediated ATP release (Dahl and Locovei, 2006; Bhat and Sajjad, 2021). As nonjunctional membrane channels, pannexin 1 is abundantly expressed in the brain, including the hippocampus, olfactory bulb, cortex, and cerebellum (Bruzzone et al., 2003; Ray et al., 2005). These hemichannels can be activated by extracellular $Ca^{2+}$ under physiological conditions (Barbe et al., 2006), and alterations in intracellular $Ca^{2+}$ levels also open pannexin 1 channels (Giaume et al., 2021). Pannexin 1 channel-mediated ATP release has been shown to contribute to cell communication *in vivo* (Giaume et al., 2021; **Figure 2**). Reciprocal regulation between microglia and neurons involves pannexin-1 hemichannels in neurons and ATP/$P_2$ receptors in microglia, and so intraneuronal calcium plays a functional role in neuronal activity-induced microglia-neuron contact (Li et al., 2012). When pannexin 1 hemichannels are inhibited by trovafloxacin, both ATP release and migration of microglia are significantly repressed, resulting in the reduction of pro-inflammatory cytokines (Garg et al., 2018). Probenecid, which is an inhibitor of the pannexin 1 hemichannel, has been demonstrated to attenuate cognitive impairment after cecal ligation and puncture (CLP)-induced sepsis in mice by inhibiting pannexin 1-dependent ATP release in the hippocampus (Zhang et al., 2019). In addition, recent findings have proposed a role for pannexin-1 hemichannels in the suppression of glutamate release from hippocampal CA1 pyramidal neurons in male rat or mouse brains (Bialecki et al., 2020). In mice with pannexin-1 channels blocked or genetically deleted, the onset of seizures is reduced in neocortical slices *in vitro* (seizure-like events) and the hippocampal CA3 region *in vivo*, indicating a pivotal role of pannexin-1 in maintaining neuronal hyperexcitability (Aquilino et al., 2020). Similarly, the activation of pannexin-1 hemichannels in postoperative tissue samples from patients with epilepsy promotes seizure generation and maintenance through ATP signaling *ex vivo* (Dossi et al., 2018). Importantly, the ATP, glutamate, and other metabolites released from stimulated pannexin-1 hemichannels can go on participating in cell-to-cell communication in the brain (Aquilino et al., 2019).

Collectively, microglia are tightly regulated by the brain microenvironment and controlled by a sophisticated system of receptors and signaling cascades (**Figure 2**). However, there are some open questions worth discussing. For instance, ATP itself can act presynaptically, rather than solely postsynaptically, in the CNS (Cunha and Ribeiro, 2000). Despite a series of articles on the mechanisms of purinergic regulatory systems during microglia-neuron communication (Phillis and Wu, 1981), the balance between the effects of different signaling is yet to be considered. Besides acting on microglia and neurons, both ATP and adenosine are recognized to play a role in astrocyte proliferation and the formation of reactive astrocytes (Fumagalli et al., 2003). Similar to microglia, astrocytes are capable of releasing ATP and adenosine, which are then involved in cell–cell communication (Stout et al., 2002; Agostinho et al., 2020). ATP can be released along with neurotransmitters from nerve terminals, acting either as a neurotransmitter in central synapses or as a neuromodulator (Agostinho et al., 2020). Hence, the proposal of the NVU was quite significant and has inspired researchers to explore the signaling mechanisms spatially and temporally.

# CONCLUSIONS AND PERSPECTIVES

In this review, we have brought together a series of articles exploring the roles of microglia, including their contributions to synapses, neuroimmune communication, and neuronal activity.

In recent years, the development of imaging, genetics, and sequencing has made it possible to understand the real story of the complex and fascinating roles of microglia in health and disease. As a result, microglia manipulation has been proposed as a novel therapeutic method for modulating activity in various neurological diseases (Klawonn et al., 2021; Minhas et al., 2021). In the context of the neuroimmune roles of microglia, targeting microglia for immunotherapy in neurological disorders is aimed to maintain homeostasis of the brain by controlling neuroinflammation. However, the appropriate way to use microglia in immunotherapy remains unclear since they display both beneficial and detrimental roles. To gain deeper insight into the microglial shift from being protective to pathogenic, the molecular mechanisms involved warrant extensive study.

The overlapping results across MIA studies (reviewed in Gumusoglu and Stevens, 2019) inspire us that we can evaluate the psychiatric risk and disease etiologies by clinically testing the immune milieu of offspring. However, as discussed above, the transient perturbation in microglia development could have a profound impact on neurodevelopment. It still requires more efforts to prevent the occurrence of neuropsychiatric disorders in offspring. Moreover, inhibiting specific molecular pathways that mediate neuronal microglial communication is also a promising therapeutic approach, such as the application of probenecid in cerebral dysfunction of sepsis (Zhang et al., 2019). Novel research has reported that neuron-derived IL-33 (Nguyen et al., 2020) and astrocyte-derived IL-3 (McAlpine et al., 2021) as a key mediator of neuron-microglia crosstalk and astrocyte-microglia crosstalk, respectively, are associated with memory consolidation. It provides a new strategy for the future treatments of age-related memory decline (IL-33) and Alzheimer's disease (IL-3). In addition, eliminating about 80% microglia in the 5xfAD mouse model of AD by blocking the CSF1 receptor is able to reverse deficits in contextual memory *via* preventing dendritic spine loss and neuronal loss, despite the disease being at a late stage (Spangenberg et al., 2016).

Another challenge is that bulk interventions using microglia could veil the true physical function of microglia since the overall outcome would be determined by microglia-mediated changes at different temporal and spatial scales (Cserép et al., 2021). The different effects could also be explained by the multifunctional roles of microglia and their communication within the NVU. Therefore, future studies should consider the molecular anatomy and functional heterogeneity of microglial processes and compartment-specific actions by microglia.

## AUTHOR CONTRIBUTIONS

ZD and SG wrote this manuscript. LL, YZ, SG, and XK revised the manuscript. SZ and XW designed the general idea. All authors contributed to the article and approved the submitted version.

## FUNDING

This study was supported by grants from the National Natural Science Foundation of China (Grant No. 81971008 and 81771194) to SZ and Zhejiang Basic Public Welfare Research Program (Grant No. LDG21H090006) to XW.

## REFERENCES

Agostinho, P., Madeira, D., Dias, L., Simões, A. P., Cunha, R. A., and Canas, P. M. (2020). Purinergic signaling orchestrating neuron-glia communication. *Pharmacol. Res.* 162:105253. doi: 10.1016/j.phrs.2020.105253

Aquilino, M. S., Whyte-Fagundes, P., Lukewich, M. K., Zhang, L., Bardakjian, B. L., Zoidl, G. R., et al. (2020). Pannexin-1 deficiency decreases epileptic activity in mice. *Int. J. Mol. Sci.* 21:7510. doi: 10.3390/ijms21207510

Aquilino, M. S., Whyte-Fagundes, P., Zoidl, G., and Carlen, P. L. (2019). Pannexin-1 channels in epilepsy. *Neurosci. Lett.* 695, 71–75. doi: 10.1016/j.neulet.2017.09.004

Augusto, E., Matos, M., Sévigny, J., El-Tayeb, A., Bynoe, M. S., Müller, C. E., et al. (2013). Ecto-5'-nucleotidase (CD73)-mediated formation of adenosine is critical for the striatal adenosine A2A receptor functions. *J. Neurosci.* 33, 11390–11399. doi: 10.1523/JNEUROSCI.5817-12.2013

Avignone, E., Ulmann, L., Levavasseur, F., Rassendren, F., and Audinat, E. (2008). Status epilepticus induces a particular microglial activation state characterized by enhanced purinergic signaling. *J. Neurosci.* 28, 9133–9144. doi: 10.1523/JNEUROSCI.1820-08.2008

Ayata, P., Badimon, A., Strasburger, H. J., Duff, M. K., Montgomery, S. E., Loh, Y. E., et al. (2018). Epigenetic regulation of brain region-specific microglia clearance activity. *Nat. Neurosci.* 21, 1049–1060. doi: 10.1038/s41593-018-0192-3

Badimon, A., Strasburger, H. J., Ayata, P., Chen, X., Nair, A., Ikegami, A., et al. (2020). Negative feedback control of neuronal activity by microglia. *Nature* 586, 417–423. doi: 10.1038/s41586-020-2777-8

Balasingam, V., Tejada-Berges, T., Wright, E., Bouckova, R., and Yong, V. W. (1994). Reactive astrogliosis in the neonatal mouse brain and its modulation by cytokines. *J. Neurosci.* 14, 846–856. doi: 10.1523/JNEUROSCI.14-02-00846.1994

Barbe, M. T., Monyer, H., and Bruzzone, R. (2006). Cell-cell communication beyond connexins: the pannexin channels. *Physiology* 21, 103–114. doi: 10.1152/physiol.00048.2005

Beattie, E. C., Stellwagen, D., Morishita, W., Bresnahan, J. C., Ha, B. K., Von Zastrow, M., et al. (2002). Control of synaptic strength by glial TNFα. *Science* 295, 2282–2285. doi: 10.1126/science.1067859

Benarroch, E. E. (2008). Adenosine and its receptors: multiple modulatory functions and potential therapeutic targets for neurologic disease. *Neurology* 70, 231–236. doi: 10.1212/01.wnl.0000297939.18236.ec

Benveniste, E. N. (1998). Cytokine actions in the central nervous system. *Cytokine Growth Factor Rev.* 9, 259–275. doi: 10.1016/s1359-6101(98)00015-x

Bhat, E. A., and Sajjad, N. (2021). Human Pannexin 1 channel: insight in structure-function mechanism and its potential physiological roles. *Mol. Cell. Biochem.* 476, 1529–1540. doi: 10.1007/s11010-020-04002-3

Bialecki, J., Werner, A., Weilinger, N. L., Tucker, C. M., Vecchiarelli, H. A., Egaña, J., et al. (2020). Suppression of presynaptic glutamate release by postsynaptic metabotropic NMDA receptor signalling to pannexin-1. *J. Neurosci.* 40, 729–742. doi: 10.1523/JNEUROSCI.0257-19.2019

Boison, D. (2006). Adenosine kinase, epilepsy and stroke: mechanisms and therapies. *Trends Pharmacol. Sci.* 27, 652–658. doi: 10.1016/j.tips.2006.10.008

Bowser, D. N., and Khakh, B. S. (2007). Vesicular ATP is the predominant cause of intercellular calcium waves in astrocytes. *J. Gen. Physiol.* 129, 485–491. doi: 10.1085/jgp.200709780

Brown, A. G., Tulina, N. M., Barila, G. O., Hester, M. S., and Elovitz, M. A. (2017). Exposure to intrauterine inflammation alters metabolomic profiles in the amniotic fluid, fetal and neonatal brain in the mouse. *PLoS One* 12:e0186656. doi: 10.1371/journal.pone.0186656

Bruzzone, R., Hormuzdi, S. G., Barbe, M. T., Herb, A., and Monyer, H. (2003). Pannexins, a family of gap junction proteins expressed in brain. *Proc. Natl. Acad. Sci. U S A* 100, 13644–13649. doi: 10.1073/pnas.2233464100

Burnstock, G. (2006). Purinergic signalling. *Br. J. Pharmacol.* 147, S172–S181. doi: 10.1038/sj.bjp.0706429

Burnstock, G., Krügel, U., Abbracchio, M. P., and Illes, P. (2011). Purinergic signalling: from normal behaviour to pathological brain function. *Prog. Neurobiol.* 95, 229–274. doi: 10.1016/j.pneurobio.2011.08.006

Cai, W., Zhang, K., Li, P., Zhu, L., Xu, J., Yang, B., et al. (2017). Dysfunction of the neurovascular unit in ischemic stroke and neurodegenerative diseases: an aging effect. *Ageing Res. Rev.* 34, 77–87. doi: 10.1016/j.arr.2016.09.006

Coelho, J. E., Rebola, N., Fragata, I., Ribeiro, J. A., de Mendonça, A., and Cunha, R. A. (2006). Hypoxia-induced desensitization and internalization of adenosine A1 receptors in the rat hippocampus. *Neuroscience* 138, 1195–1203. doi: 10.1016/j.neuroscience.2005.12.012

Coull, J. A., Beggs, S., Boudreau, D., Boivin, D., Tsuda, M., Inoue, K., et al. (2005). BDNF from microglia causes the shift in neuronal anion gradient underlying neuropathic pain. *Nature* 438, 1017–1021. doi: 10.1038/nature 04223

Cserép, C., Pósfai, B., and Dénes, Á. (2021). Shaping neuronal fate: functional heterogeneity of direct microglia-neuron interactions. *Neuron* 109, 222–240. doi: 10.1016/j.neuron.2020.11.007

Cserép, C., Pósfai, B., Lénárt, N., Fekete, R., László, Z. I., Lele, Z., et al. (2020). Microglia monitor and protect neuronal function through specialized somatic purinergic junctions. *Science* 367, 528–537. doi: 10.1126/science.aax6752

Cunha, R. A., and Ribeiro, J. A. (2000). ATP as a presynaptic modulator. *Life Sci.* 68, 119–137. doi: 10.1016/s0024-3205(00)00923-1

Dahl, G., and Locovei, S. (2006). Pannexin: to gap or not to gap, is that a question? *IUBMB Life* 58, 409–419. doi: 10.1080/15216540600794526

d'Alcantara, P., Ledent, C., Swillens, S., and Schiffmann, S. N. (2001). Inactivation of adenosine A2A receptor impairs long term potentiation in the accumbens nucleus without altering basal synaptic transmission. *Neuroscience* 107, 455–464. doi: 10.1016/s0306-4522(01)00372-4

Darby, M., Kuzmiski, J. B., Panenka, W., Feighan, D., and MacVicar, B. A. (2003). ATP released from astrocytes during swelling activates chloride channels. *J. Neurophysiol.* 89, 1870–1877. doi: 10.1152/jn.00510.2002

Davalos, D., Grutzendler, J., Yang, G., Kim, J. V., Zuo, Y., Jung, S., et al. (2005). ATP mediates rapid microglial response to local brain injury *in vivo*. *Nat. Neurosci.* 8, 752–758. doi: 10.1038/nn1472

Dissing-Olesen, L., LeDue, J. M., Rungta, R. L., Hefendehl, J. K., Choi, H. B., and MacVicar, B. A. (2014). Activation of neuronal NMDA receptors triggers transient ATP-mediated microglial process outgrowth. *J. Neurosci.* 34, 10511–10527. doi: 10.1523/JNEUROSCI.0405-14.2014

Dossi, E., Blauwblomme, T., Moulard, J., Chever, O., Vasile, F., Guinard, E., et al. (2018). Pannexin-1 channels contribute to seizure generation in human epileptic brain tissue and in a mouse model of epilepsy. *Sci. Transl. Med.* 10:eaar3796. doi: 10.1126/scitranslmed.aar3796

Eyo, U. B., Peng, J., Swiatkowski, P., Mukherjee, A., Bispo, A., and Wu, L. J. (2014). Neuronal hyperactivity recruits microglial processes *via* neuronal NMDA receptors and microglial P2Y12 receptors after status epilepticus. *J. Neurosci.* 34, 10528–10540. doi: 10.1523/JNEUROSCI.0416-14.2014

Fredholm, B. B., Chen, J. F., Cunha, R. A., Svenningsson, P., and Vaugeois, J. M. (2005). Adenosine and brain function. *Int. Rev. Neurobiol.* 63, 191–270. doi: 10.1016/S0074-7742(05)63007-3

Fumagalli, M., Brambilla, R., D'Ambrosi, N., Volonté, C., Matteoli, M., Verderio, C., et al. (2003). Nucleotide-mediated calcium signaling in rat cortical astrocytes: role of P2X and P2Y receptors. *Glia* 43, 218–230. doi: 10.1002/glia. 10248

Garg, C., Seo, J. H., Ramachandran, J., Loh, J. M., Calderon, F., and Contreras, J. E. (2018). Trovafloxacin attenuates neuroinflammation and improves outcome after traumatic brain injury in mice. *J. Neuroinflammation* 15:42. doi: 10.1186/s12974-018-1069-9

Giaume, C., Naus, C. C., Sáez, J. C., and Leybaert, L. (2021). Glial connexins and pannexins in the healthy and diseased brain. *Physiol. Rev.* 101, 93–145. doi: 10.1152/physrev.00043.2018

Gu, N., Eyo, U. B., Murugan, M., Peng, J., Matta, S., Dong, H., et al. (2016). Microglial P2Y12 receptors regulate microglial activation and surveillance during neuropathic pain. *Brain Behav. Immun.* 55, 82–92. doi: 10.1016/j.bbi. 2015.11.007

Gumusoglu, S. B., and Stevens, H. E. (2019). Maternal inflammation and neurodevelopmental programming: a review of preclinical outcomes and implications for translational psychiatry. *Biol. Psychiatry* 85, 107–121. doi: 10.1016/j.biopsych.2018.08.008

Huh, J. R., and Veiga-Fernandes, H. (2020). Neuroimmune circuits in inter-organ communication. *Nat. Rev. Immunol.* 20, 217–228. doi: 10.1038/s41577-019-0247-z

Iadecola, C. (2017). The neurovascular unit coming of age: a journey through neurovascular coupling in health and disease. *Neuron* 96, 17–42. doi: 10.1016/j. neuron.2017.07.030

Jing, F., Zhang, Y., Long, T., He, W., Qin, G., Zhang, D., et al. (2019). P2Y12 receptor mediates microglial activation *via* RhoA/ROCK pathway in the trigeminal nucleus caudalis in a mouse model of chronic migraine. *J. Neuroinflammation* 16:217. doi: 10.1186/s12974-019-1603-4

Joost, E., Jordão, M. J. C., Mages, B., Prinz, M., Bechmann, I., and Krueger, M. (2019). Microglia contribute to the glia limitans around arteries, capillaries and veins under physiological conditions, in a model of neuroinflammation and in human brain tissue. *Brain Struct. Funct.* 224, 1301–1314. doi: 10.1007/s00429-019-01834-8

Kékesi, O., Liang, H., Münch, G., Morley, J. W., Gyengesi, E., and Buskila, Y. (2019). The differential impact of acute microglia activation on the excitability of cholinergic neurons in the mouse medial septum. *Brain Struct. Funct.* 224, 2297–2309. doi: 10.1007/s00429-019-01905-w

Kerkhofs, A., Canas, P. M., Timmerman, A. J., Heistek, T. S., Real, J. I., Xavier, C., et al. (2018). Adenosine $A_{2A}$ receptors control glutamatergic synaptic plasticity in fast spiking interneurons of the prefrontal cortex. *Front. Pharmacol.* 9:133. doi: 10.3389/fphar.2018.00133

Klawonn, A. M., Fritz, M., Castany, S., Pignatelli, M., Canal, C., Similä, F., et al. (2021). Microglial activation elicits a negative affective state through prostaglandin-mediated modulation of striatal neurons. *Immunity* 54, 225–234.e6. doi: 10.1016/j.immuni.2020.12.016

Kluge, M. G., Kracht, L., Abdolhoseini, M., Ong, L. K., Johnson, S. J., Nilsson, M., et al. (2017). Impaired microglia process dynamics post-stroke are specific to sites of secondary neurodegeneration. *Glia* 65, 1885–1899. doi: 10.1002/glia. 23201

Krueger, J. M., Clinton, J. M., Winters, B. D., Zielinski, M. R., Taishi, P., Jewett, K. A., et al. (2011). Involvement of cytokines in slow wave sleep. *Prog. Brain Res.* 193, 39–47. doi: 10.1016/B978-0-444-53839-0.00003-X

Larsson, M., Sawada, K., Morland, C., Hiasa, M., Ormel, L., Moriyama, Y., et al. (2012). Functional and anatomical identification of a vesicular transporter mediating neuronal ATP release. *Cereb. Cortex* 22, 1203–1214. doi: 10.1093/cercor/bhr203

Leal, G., Comprido, D., and Duarte, C. B. (2014). BDNF-induced local protein synthesis and synaptic plasticity. *Neuropharmacology* 76, 639–656. doi: 10.1016/j.neuropharm.2013.04.005

Lehnardt, S. (2010). Innate immunity and neuroinflammation in the CNS: the role of microglia in Toll-like receptor-mediated neuronal injury. *Glia* 58, 253–263. doi: 10.1002/glia.20928

Li, Y., Du, X.-F., Liu, C.-S., Wen, Z.-L., and Du, J.-L. (2012). Reciprocal regulation between resting microglial dynamics and neuronal activity *in vivo*. *Dev. Cell* 23, 1189–1202. doi: 10.1016/j.devcel.2012.10.027

Li, F., Xu, D., Hou, K., Gou, X., and Li, Y. (2020). The role of P2Y12 receptor inhibition in ischemic stroke on microglia, platelets and vascular smooth muscle cells. *J. Thromb. Thrombolysis* 50, 874–885. doi: 10.1007/s11239-020-02098-4

Liddelow, S. A., Guttenplan, K. A., Clarke, L. E., Bennett, F. C., Bohlen, C. J., Schirmer, L., et al. (2017). Neurotoxic reactive astrocytes are induced by activated microglia. *Nature* 541, 481–487. doi: 10.1038/nature 21029

Liddelow, S. A., Marsh, S. E., and Stevens, B. (2020). Microglia and astrocytes in disease: dynamic duo or partners in crime? *Trends Immunol.* 41, 820–835. doi: 10.1016/j.it.2020.07.006

Lim, S.-H., Park, E., You, B., Jung, Y., Park, A.-R., Park, S. G., et al. (2013). Neuronal synapse formation induced by microglia and interleukin 10. *PLoS One* 8:e81218. doi: 10.1371/journal.pone.0081218

Liu, L.-R., Liu, J.-C., Bao, J.-S., Bai, Q.-Q., and Wang, G.-Q. (2020). Interaction of microglia and astrocytes in the neurovascular unit. *Front. Immunol.* 11:1024. doi: 10.3389/fimmu.2020.01024

Liu, Y. J., Spangenberg, E., Tang, B., Holmes, T. C., Green, K. N., and Xu, X. (2021). Microglia elimination increases neural circuit connectivity and activity in adult

mouse cortex. *J. Neurosci.* 41, 1274–1287. doi: 10.1523/JNEUROSCI.2140-20.2020

Liu, Y. U., Ying, Y., Li, Y., Eyo, U. B., Chen, T., Zheng, J., et al. (2019). Neuronal network activity controls microglial process surveillance in awake mice *via* norepinephrine signaling. *Nat. Neurosci.* 22, 1771–1781. doi: 10.1038/s41593-019-0511-3

Matcovitch-Natan, O., Winter, D. R., Giladi, A., Vargas Aguilar, S., Spinrad, A., Sarrazin, S., et al. (2016). Microglia development follows a stepwise program to regulate brain homeostasis. *Science* 353:aad8670. doi: 10.1126/science.aad8670

McAlpine, C. S., Park, J., Griciuc, A., Kim, E., Choi, S. H., Iwamoto, Y., et al. (2021). Astrocytic interleukin-3 programs microglia and limits Alzheimer's disease. *Nature* 595, 701–706. doi: 10.1038/s41586-021-03734-6

Milior, G., Morin-Brureau, M., Chali, F., Le Duigou, C., Savary, E., Huberfeld, G., et al. (2020). Distinct P2Y receptors mediate extension and retraction of microglial processes in epileptic and peritumoral human tissue. *J. Neurosci.* 40, 1373–1388. doi: 10.1523/JNEUROSCI.0218-19.2019

Minhas, P. S., Latif-Hernandez, A., McReynolds, M. R., Durairaj, A. S., Wang, Q., Rubin, A., et al. (2021). Restoring metabolism of myeloid cells reverses cognitive decline in ageing. *Nature* 590, 122–128. doi: 10.1038/s41586-020-03160-0

Muoio, V., Persson, P. B., and Sendeski, M. M. (2014). The neurovascular unit—concept review. *Acta Physiol.* 210, 790–798. doi: 10.1111/apha.12250

Nayak, D., Roth, T. L., and McGavern, D. B. (2014). Microglia development and function. *Annu. Rev. Immunol.* 32, 367–402. doi: 10.1146/annurev-immunol-032713-120240

Nenov, M. N., Malkov, A. E., Konakov, M. V., and Levin, S. G. (2019). Interleukin-10 and transforming growth factor-β1 facilitate long-term potentiation in CA1 region of hippocampus. *Biochem. Biophys. Res. Commun.* 518, 486–491. doi: 10.1016/j.bbrc.2019.08.072

Nguyen, P. T., Dorman, L. C., Pan, S., Vainchtein, I. D., Han, R. T., Nakao-Inoue, H., et al. (2020). Microglial remodeling of the extracellular matrix promotes synapse plasticity. *Cell* 182, 388–403.e15. doi: 10.1016/j.cell.2020.05.050

Nimmerjahn, A., Kirchhoff, F., and Helmchen, F. (2005). Resting microglial cells are highly dynamic surveillants of brain parenchyma *in vivo*. *Science* 308, 1314–1318. doi: 10.1126/science.1110647

Norris, G. T., and Kipnis, J. (2019). Immune cells and CNS physiology: microglia and beyond. *J. Exp. Med.* 216, 60–70. doi: 10.1084/jem.20180199

Olmos, G., and Lladó, J. (2014). Tumor necrosis factor α: a link between neuroinflammation and excitotoxicity. *Mediators Inflamm.* 2014:861231. doi: 10.1155/2014/861231

Pankratov, Y., Lalo, U., Verkhratsky, A., and North, R. A. (2007). Quantal release of ATP in mouse cortex. *J. Gen. Physiol.* 129, 257–265. doi: 10.1085/jgp.200609693

Paolicelli, R. C., Bolasco, G., Pagani, F., Maggi, L., Scianni, M., Panzanelli, P., et al. (2011). Synaptic pruning by microglia is necessary for normal brain development. *Science* 333, 1456–1458. doi: 10.1126/science.1202529

Park, G.-H., Noh, H., Shao, Z., Ni, P., Qin, Y., Liu, D., et al. (2020). Activated microglia cause metabolic disruptions in developmental cortical interneurons that persist in interneurons from individuals with schizophrenia. *Nat. Neurosci.* 23, 1352–1364. doi: 10.1038/s41593-020-00724-1

Parkhurst, C. N., Yang, G., Ninan, I., Savas, J. N., Yates, J. R. III., Lafaille, J. J., et al. (2013). Microglia promote learning-dependent synapse formation through brain-derived neurotrophic factor. *Cell* 155, 1596–1609. doi: 10.1016/j.cell.2013.11.030

Patterson, S. L. (2015). Immune dysregulation and cognitive vulnerability in the aging brain: interactions of microglia, IL-1β, BDNF and synaptic plasticity. *Neuropharmacology* 96, 11–18. doi: 10.1016/j.neuropharm.2014.12.020

Pavlov, V. A., Chavan, S. S., and Tracey, K. J. (2018). Molecular and functional neuroscience in immunity. *Annu. Rev. Immunol.* 36, 783–812. doi: 10.1146/annurev-immunol-042617-053158

Pavlov, V. A., and Tracey, K. J. (2017). Neural regulation of immunity: molecular mechanisms and clinical translation. *Nat. Neurosci.* 20, 156–166. doi: 10.1038/nn.4477

Peng, W., Wu, Z., Song, K., Zhang, S., Li, Y., and Xu, M. (2020). Regulation of sleep homeostasis mediator adenosine by basal forebrain glutamatergic neurons. *Science* 369:eabb0556. doi: 10.1126/science.abb0556

Perry, V. H., and Holmes, C. (2014). Microglial priming in neurodegenerative disease. *Nat. Rev. Neurol.* 10, 217–224. doi: 10.1038/nrneurol.2014.38

Phillis, J. W., and Wu, P. H. (1981). The role of adenosine and its nucleotides in central synaptic transmission. *Prog. Neurobiol.* 16, 187–239. doi: 10.1016/0301-0082(81)90014-9

Prieto, G. A., Snigdha, S., Baglietto-Vargas, D., Smith, E. D., Berchtold, N. C., Tong, L., et al. (2015). Synapse-specific IL-1 receptor subunit reconfiguration augments vulnerability to IL-1β in the aged hippocampus. *Proc. Natl. Acad. Sci. U S A* 112, E5078–E5087. doi: 10.1073/pnas.1514486112

Prinz, M., Jung, S., and Priller, J. (2019). Microglia biology: one century of evolving concepts. *Cell* 179, 292–311. doi: 10.1016/j.cell.2019.08.053

Quaegebeur, A., Lange, C., and Carmeliet, P. (2011). The neurovascular link in health and disease: molecular mechanisms and therapeutic implications. *Neuron* 71, 406–424. doi: 10.1016/j.neuron.2011.07.013

Ray, A., Zoidl, G., Weickert, S., Wahle, P., and Dermietzel, R. (2005). Site-specific and developmental expression of pannexin1 in the mouse nervous system. *Eur. J. Neurosci.* 21, 3277–3290. doi: 10.1111/j.1460-9568.2005.04139.x

Rebola, N., Rodrigues, R. J., Lopes, L. V., Richardson, P. J., Oliveira, C. R., and Cunha, R. A. (2005). Adenosine A1 and A2A receptors are co-expressed in pyramidal neurons and co-localized in glutamatergic nerve terminals of the rat hippocampus. *Neuroscience* 133, 79–83. doi: 10.1016/j.neuroscience.2005.01.054

Ribeiro, J. A., Sebastião, A. M., and de Mendonça, A. (2002). Adenosine receptors in the nervous system: pathophysiological implications. *Prog. Neurobiol.* 68, 377–392. doi: 10.1016/s0301-0082(02)00155-7

Rodrigues, R. J., Canas, P. M., Lopes, L. V., Oliveira, C. R., and Cunha, R. A. (2008). Modification of adenosine modulation of acetylcholine release in the hippocampus of aged rats. *Neurobiol. Aging* 29, 1597–1601. doi: 10.1016/j.neurobiolaging.2007.03.025

Rosin, D. L., Robeva, A., Woodard, R. L., Guyenet, P. G., and Linden, J. (1998). Immunohistochemical localization of adenosine A2A receptors in the rat central nervous system. *J. Comp. Neurol.* 401, 163–186. doi: 10.1002/(SICI)1096-9861(19981116)401:2<163::AID-CNE2>3.0.CO;2-D

Schafer, D. P., Lehrman, E. K., Kautzman, A. G., Koyama, R., Mardinly, A. R., Yamasaki, R., et al. (2012). Microglia sculpt postnatal neural circuits in an activity and complement-dependent manner. *Neuron* 74, 691–705. doi: 10.1016/j.neuron.2012.03.026

Scheiblich, H., Trombly, M., Ramirez, A., and Heneka, M. T. (2020). Neuroimmune connections in aging and neurodegenerative diseases. *Trends Immunol.* 41, 300–312. doi: 10.1016/j.it.2020.02.002

Spangenberg, E. E., Lee, R. J., Najafi, A. R., Rice, R. A., Elmore, M. R., Blurton-Jones, M., et al. (2016). Eliminating microglia in Alzheimer's mice prevents neuronal loss without modulating amyloid-β pathology. *Brain* 139, 1265–1281. doi: 10.1093/brain/aww016

Stellwagen, D., and Malenka, R. C. (2006). Synaptic scaling mediated by glial TNF-α. *Nature* 440, 1054–1059. doi: 10.1038/nature04671

Stout, C. E., Costantin, J. L., Naus, C. C., and Charles, A. C. (2002). Intercellular calcium signaling in astrocytes *via* ATP release through connexin hemichannels. *J. Biol. Chem.* 277, 10482–10488. doi: 10.1074/jbc.M109902200

Stowell, R. D., Sipe, G. O., Dawes, R. P., Batchelor, H. N., Lordy, K. A., Whitelaw, B. S., et al. (2019). Noradrenergic signaling in the wakeful state inhibits microglial surveillance and synaptic plasticity in the mouse visual cortex. *Nat. Neurosci.* 22, 1782–1792. doi: 10.1038/s41593-019-0514-0

Sweeney, M. D., Ayyadurai, S., and Zlokovic, B. V. (2016). Pericytes of the neurovascular unit: key functions and signaling pathways. *Nat. Neurosci.* 19, 771–783. doi: 10.1038/nn.4288

Thurgur, H., and Pinteaux, E. (2019). Microglia in the neurovascular unit: blood-brain barrier-microglia interactions after central nervous system disorders. *Neuroscience* 405, 55–67. doi: 10.1016/j.neuroscience.2018.06.046

Tozaki-Saitoh, H., Tsuda, M., Miyata, H., Ueda, K., Kohsaka, S., and Inoue, K. (2008). P2Y12 receptors in spinal microglia are required for neuropathic pain after peripheral nerve injury. *J. Neurosci.* 28, 4949–4956. doi: 10.1523/JNEUROSCI.0323-08.2008

Tremblay, M. È., Lowery, R. L., and Majewska, A. K. (2010). Microglial interactions with synapses are modulated by visual experience. *PLoS Biol.* 8:e1000527. doi: 10.1371/journal.pbio.1000527

Ueno, M., Fujita, Y., Tanaka, T., Nakamura, Y., Kikuta, J., Ishii, M., et al. (2013). Layer V cortical neurons require microglial support for survival

during postnatal development. *Nat. Neurosci.* 16, 543–551. doi: 10.1038/nn.3358

Verkhratsky, A., Sun, D., and Tanaka, J. (2021). Snapshot of microglial physiological functions. *Neurochem. Int.* 144:104960. doi: 10.1016/j.neuint.2021.104960

Wall, M. J., and Dale, N. (2007). Auto-inhibition of rat parallel fibre-Purkinje cell synapses by activity-dependent adenosine release. *J. Physiol.* 581, 553–565. doi: 10.1113/jphysiol.2006.126417

Yoon, K. W., and Rothman, S. M. (1991). Adenosine inhibits excitatory but not inhibitory synaptic transmission in the hippocampus. *J. Neurosci.* 11, 1375–1380. doi: 10.1523/JNEUROSCI.11-05-01375.1991

Yu, X., Ji, C., and Shao, A. (2020). Neurovascular unit dysfunction and neurodegenerative disorders. *Front. Neurosci.* 14:334. doi: 10.3389/fnins.2020.00334

Zhang, Z., Lei, Y., Yan, C., Mei, X., Jiang, T., Ma, Z., et al. (2019). Probenecid relieves cerebral dysfunction of sepsis by inhibiting pannexin 1-dependent ATP release. *Inflammation* 42, 1082–1092. doi: 10.1007/s10753-019-00969-4

Zhao, X., Liao, Y., Morgan, S., Mathur, R., Feustel, P., Mazurkiewicz, J., et al. (2018). Noninflammatory changes of microglia are sufficient to cause epilepsy. *Cell Rep.* 22, 2080–2093. doi: 10.1016/j.celrep.2018.02.004

Zlokovic, B. V. (2011). Neurovascular pathways to neurodegeneration in Alzheimer's disease and other disorders. *Nat. Rev. Neurosci.* 12, 723–738. doi: 10.1038/nrn3114

**Conflict of Interest:** The authors declare that the research was conducted in the absence of any commercial or financial relationships that could be construed as a potential conflict of interest.

**Publisher's Note:** All claims expressed in this article are solely those of the authors and do not necessarily represent those of their affiliated organizations, or those of the publisher, the editors and the reviewers. Any product that may be evaluated in this article, or claim that may be made by its manufacturer, is not guaranteed or endorsed by the publisher.

frontiers | Frontiers in Cellular Neuroscience

ORIGINAL RESEARCH
published: 11 May 2022
doi: 10.3389/fncel.2022.835649

# The Effects of Propofol on a Human *in vitro* Blood-Brain Barrier Model

*Jason M. Hughes[1†], Olivia R. Neese[1,2†], Dylan D. Bieber[1], Kirsten A. Lewis[1], Layla M. Ahmadi[1], Dustin W. Parsons[1] and Scott G. Canfield[1*]*

[1] Department of Anatomy, Cell Biology and Physiology, Indiana University School of Medicine, Terre Haute, IN, United States, [2] Department of Biology, Indiana State University, Terre Haute, IN, United States

**Background:** Recently, the safety of repeated and lengthy anesthesia administration has been called into question, a subset of these animal studies demonstrated that anesthetics induced blood-brain barrier (BBB) dysfunction. The BBB is critical in protecting the brain parenchyma from the surrounding micro-vasculature. BBB breakdown and dysfunction has been observed in several neurodegenerative diseases and may contribute to both the initiation and the progression of the disease. In this study we utilize a human induced pluripotent stem cell (iPSC) derived-BBB model, exhibiting near *in vivo* properties, to evaluate the effects of anesthetics on critical barrier properties.

**Methods:** iPSC-derived brain microvascular endothelial cells (BMECs) expressed near *in vivo* barrier tightness assessed by *trans*-endothelial electrical resistance and para-cellular permeability. Efflux transporter activity was determined by substrate transport in the presence of specific inhibitors. *Trans*-cellular transport was measured utilizing large fluorescently tagged dextran. Tight junction localization in BMECs was evaluated with fluorescent microscopy. The anesthetic, propofol was exposed to BMECs at varying durations and concentrations and BBB properties were monitored post-exposure.

**Results:** Following propofol exposure, BMECs displayed reduced resistance and increased permeability indicative of a leaky barrier. Reduced barrier tightness and the dysregulation of occludin, a tight junction protein, were partly the result of an elevation in matrix metalloproteinase (MMP) levels. Efflux transporter activity and *trans*-cellular transport were unaffected by propofol exposure. Propofol induced barrier dysfunction was partially restored following matrix metalloproteinase inhibition.

**Conclusion:** For the first time, we have demonstrated that propofol alters BBB integrity utilizing a human *in vitro* BBB model that displays key *in vivo* characteristics. A leaky BBB enables otherwise impermeable molecules such as pathogens and toxins the ability to reach vulnerable cell types of the brain parenchyma. A robust human *in vitro* BBB model will allow for the evaluation of several anesthetics at fluctuating clinical scenarios and to elucidate mechanisms with the goal of ultimately improving anesthesia safety.

**Keywords: blood-brain barrier, anesthesia toxicity, tight junction dysfunction, propofol, brain microvascular-like endothelial cells**

OPEN ACCESS

***Edited by:***
*Xinchun Jin,*
*Capital Medical University, China*

***Reviewed by:***
*Yongchao Mou,*
*University of Illinois at Rockford, United States*
*Yukari Shigemoto-mogami,*
*National Institute of Health Sciences, Japan*

****Correspondence:***
*Scott G. Canfield*
*sccanfie@iu.edu*

*† These authors have contributed equally to this work*

***Specialty section:***
*This article was submitted to Non-Neuronal Cells, a section of the journal Frontiers in Cellular Neuroscience*

***Received:*** *14 December 2021*
***Accepted:*** *14 March 2022*
***Published:*** *11 May 2022*

***Citation:***
*Hughes JM, Neese OR, Bieber DD, Lewis KA, Ahmadi LM, Parsons DW and Canfield SG (2022) The Effects of Propofol on a Human in vitro Blood-Brain Barrier Model. Front. Cell. Neurosci. 16:835649. doi: 10.3389/fncel.2022.835649*

## INTRODUCTION

The American Society of Anesthesiology estimates that millions of people undergo anesthesia each year in the United States. A substantial body of work has demonstrated that anesthesia, specifically at sustained or multiple exposures has cognitive and neurologic effects, primarily through neuron toxicity (Mason et al., 2010; Seubert et al., 2013; Acharya et al., 2015; Jiang et al., 2018). More recently, preclinical animal studies and a number of large population-based human studies presented limited associations between anesthesia exposure and negative outcomes in children (Ing and Brambrink, 2019). A subset of rodent studies have demonstrated that several anesthetics have detrimental effects on the blood-brain barrier (BBB) (Sharma et al., 2014; Zhao et al., 2014; Acharya et al., 2015; Cao et al., 2015). BBB breakdown and dysfunction are often associated with a variety of disease, including stroke, Alzheimer's disease, HIV infection and brain tumors (Hirano and Matsui, 1975; Jellinger and Attems, 2006; Sweeney et al., 2018). Interestingly, the effects of anesthetics on the human BBB have not been previously studied.

The BBB is critical in maintaining homeostasis between the brain parenchyma and the microvasculature (Weiss et al., 2009). The BBB is comprised of the barrier forming brain microvascular endothelial cells (BMECs) supported by neurovascular unit (NVU) cell types: astrocytes, neurons, and pericytes. NVU cell types are critical in the development, maintenance and support of the barrier forming BMECs (Obermeier et al., 2013). BMECs provide a physical, transport and metabolic barrier due to the expression of tight junction proteins and active nutrient and efflux transporters. These properties allow BMECs to tightly regulate the movement of ions, molecules and cells between the blood and the brain.

Anesthetics, specifically, isoflurane, sevoflurane, and propofol have been demonstrated to alter tight junction expression in rodent BBB models (Sharma et al., 2014; Zhao et al., 2014; Acharya et al., 2015; Cao et al., 2015). The dysregulation of tight junction proteins can induce barrier leakiness and enable otherwise impermeable pathogens, toxins, molecules and cells to reach the brain parenchyma, potentially contributing to anesthesia-induced damage (Acharya et al., 2015). Several cellular mechanisms have been proposed in animal models including: vascular endothelial growth factor (VEGF), heat shock protein (HSP), matrix metalloproteinase (MMPs) and heat inducible factor-1α (HIF-1α) (Hu et al., 2014; Sharma et al., 2014; Zhao et al., 2014), however, their role in human BBB degradation following anesthesia are unknown. A dysfunctional BBB may further exacerbate the actions of anesthetics or even increase the probability of developing a detrimental BBB-induced injury.

For the first time we investigated the detrimental effects of anesthesia on the human BBB. We hypothesize that clinically relevant anesthetics will diminish critical barrier properties of iPSC-derived BMECs. To evaluate and elucidate the cellular mechanisms of anesthesia on the human BBB we utilized BMECs derived from human induced pluripotent stem cells (iPSCs) (Stebbins et al., 2015; Canfield et al., 2017). iPSC-derived BMECs display several near *in vivo* like BBB properties including: elevated barrier integrity, expression of localized tight junction proteins, active efflux transporters and reduced transcellular transport. The enhanced BBB properties of iPSC-derived BMECs compared to other *in vitro* models in addition to their human origin enable them to screen the efficacy and safety of a number of anesthetics (Crone and Olesen, 1982).

**Abbreviations:** BBB, blood-brain barrier; BMECs, brain microvascular endothelial cells; NVU, neurovascular unit; HSP, heat shock protein; MMPs, matrix metalloproteinase; HIF-1α, heat inducible factor-1α; iPSCs, Human induced pluripotent stem cells; hESFM, human endothelial serum-free medium; bFGF, basic fibroblast growth factor; PDS, platelet-poor plasma derived bovine serum; RA, retinoic acid; TEER, *Trans*-endothelial electrical resistance; ZO-1, zonula occludens; PBS, phosphate-buffered saline; TBST, Tris-buffered saline containing 0.1% Tween 20; HRP, horseradish peroxidase; Pgp, P-glycoprotein; MRP-1, multi-drug resistance protein; BCRP, breast cancer resistance protein; CsA, Cyclosporin A; DCFDA, dichlorodihydrofluorescein diacetate; MTT, 3-(4,5-dimethylthiazol-2-Yl)-2,5-diphenyltetrazolium bromide; DMSO, dimethyl sulfoxide; ANOVA, analysis of variance.

## MATERIALS AND METHODS

### Differentiation of Brain Microvascular Endothelial Cells

Brain microvascular endothelial cells (BMECs) were differentiated from human induced pluripotent stem cells (iPSCs) as previously described (Canfield et al., 2017). Briefly, iPSCs (IMR90, WiCell, Madison, WI, United States) between passage 30–55 were singularized using Accutase (Life Technologies, Carlsbad, CA, United States) and plated ($1 \times 10^5$) onto Matrigel (Corning Life Sciences, Corning, NY, United States) coated 6-well plates (Thermo Fisher Scientific, Waltham, MA, United States) and maintained in mTESR nutrient medium (STEMCELL Technologies, Vancouver, BC, Canada) at 37°C for 3 days. Following stem cell expansion, cells were treated with unconditioned medium (UM) consisting of Dulbecco's Modified Eagle's Medium/Ham's F12 (DMEM-F12, Thermo Fisher Scientific, Waltham, MA, United States) supplemented with 20% Knockout Serum Replacement (Thermo Fisher Scientific, Waltham, MA, United States), 1 × minimum essential medium non-essential amino acids (Life Technologies, Carlsbad CA, United States), 1 mM L-glutamine (Life Technologies, Carlsbad, CA, United States), and 0.1 mM β-mercaptoethanol (Sigma-Aldrich, St. Louis, MO, United States) to initiate the differentiation. Cells were maintained in UM for 6 days at 37°C with daily media changes. Following UM treatment, the medium was switched to EC + / + consisting of human Endothelial Serum-Free Medium (hESFM, Life Technologies, Carlsbad, CA, United States) containing 20 ng/mL bFGF (STEMCELL), 1% platelet-poor plasma derived bovine serum (PDS, Thermo Fisher Scientific, Waltham, MA, United States) and 10 μM retinoic acid (RA, Sigma Aldrich, St. Louis, MO, United States) for 48 h. BMECs were plated onto their respective experimental platform and maintained in EC + / + with RA for 24 h at 37°C. Medium was then switched to EC ± media comprised of hESFM with 1% PDS for the duration of the experiment and BMECs comprised >99% of the cell types. Peak barrier properties are maintained for 4–7 days post sub-culture onto their respective

experimental platforms. All barrier phenotyping is conducted within 4 days of sub-culture. To evaluate barrier integrity we utilized *Trans*-endothelial electrical resistance (TEER) and sodium fluorescein permeability. Tight junction localization and expression were verified with immunocytochemistry and western blot, respectively. Efflux transporter expression and activity were assessed with flow cytometry and the transport and accumulation of specific efflux substrates, respectively. Transcellular transport was monitored with dextran transport.

## Propofol Exposure

Following differentiation, IMR90-derived BMECs were seeded ($10^6$ cells/cm$^2$) onto Transwell filter inserts (Thermo Fisher Scientific, Waltham, MA, United States) coated with a collagen IV (Sigma Aldrich, St. Louis, MO, United States) fibronectin (Sigma Aldrich, St. Louis, MO, United States) matrix for *trans*-endothelial electrical resistance (TEER), efflux transporter activity, *trans*-cellular transport/accumulation and/or sodium fluorescein permeability assays. For efflux transporter accumulation 125,000 cells/cm$^2$ were seeded onto matrigel coated 24 well plates (Thermo Fisher Scientific, Waltham, MA, United States). For immunostaining $10^6$ cells/cm$^2$ were seeded onto matrigel coated 18 mm round cover slips (Thermo Fisher Scientific, Waltham, MA, United States). For western blot lysates, BMECs were seeded ($10^4$ cells/cm$^2$) onto matrigel coated 6 well plates. Following 24 h, media was transitioned to EC ± medium. BMECs were treated with either 0 (Control; DMSO), intralipid (Sigma) alone, or 10, 30, 50, or 100 μM propofol (Sigma Aldrich, St. Louis, MO, United States) in fresh EC ± medium (0.5 mL top, 1.5 mL bottom) on a rotational platform at 37°C for 3 h. Following propofol exposure media was replaced with EC ± medium and the respective experiments commenced.

## *Trans*-Endothelial Electrical Resistance

*Trans*-endothelial electrical resistance (TEER) was measured immediately prior to propofol exposure and 30 min, 1 h, 2 h, 3 h, and every 24 h following propofol exposure. TEER was monitored up to 96 h post-exposure. Electrical resistance was measured using an EVOM ohmmeter with STX2 electrodes (World Precision Instruments, Sarasota, FL, United States). TEER values are presented as Ω × cm$^2$ following the subtraction of an unseeded Transwell insert and multiplication by 1.12 cm$^2$ to account for surface area. Measurements were recorded immediately following removal of the samples from the incubator. Resistance was measured at least three independent times on each sample and from a minimum of three triplicate filter inserts for each experimental condition.

## Sodium Fluorescein Permeability

Sodium fluorescein (10 μM, 376 Daltons; Sigma Aldrich, St. Louis, MO, United States) was utilized to determine the permeability of the iPSC-derived BMEC barrier. Following 3 h of exposure to propofol, fresh EC medium ± was added to the Transwell system (0.5 mL top, 1.5 mL bottom) with EC medium ± containing 10 μM sodium fluorescein added to the top chamber and EC medium ± without sodium fluorescein added to the bottom chamber. The Transwell filter inserts were then placed back on the rotational platform at 37°C for 1 h. 150 μL aliquots were sampled from the bottom chamber at 15, 30, and 45 min and immediately replaced with pre-warmed EC ± medium. At 60 min, 150 μL aliquots were sampled from both the top and bottom chambers and fluorescence was recorded using a Synergy HTX Multi-Mode reader (BioTek, Winooski, VT, United States). Permeability coefficients were calculated based on the cleared volume of sodium fluorescein from the top chamber to the bottom chamber.

## Immunocytochemistry and Analysis of Tight Junction Localization

Immunocytochemistry was performed on 50 μM propofol treatment and non-treatment control groups. Primary antibody sources, dilutions and corresponding fixing agents are presented in **Supplementary Table 1** After 3 h treatment with propofol, iPSC-BMECs were fixed in either cold 4% paraformaldehyde (diluted in PBS; Sigma Aldrich, St. Louis, MO, United States) or ice cold methanol (100%; Sigma Aldrich, St. Louis, MO, United States) for 15 min on a rocking platform at room temperature. Cells were blocked with 10% goat serum (diluted in PBS; Sigma Aldrich, St. Louis, MO, United States) for 1 h at room temperature on a rocking platform. Following blocking, cells were incubated in primary antibody (diluted in blocking solution) overnight at 4°C on a rocking platform. All secondary antibodies were diluted 1:200 in blocking solution. Cells were incubated for 1 h in secondary antibody solution on a rocking platform at room temperature, protected from light. Invitrogen ProLong™ Gold antifade reagent (Life Technologies, Carlsbad, NY, United States) was used in the preparation of slides. Images were taken on an Olympus PROVIS AX70 motorized fluorescent microscope (Olympus, Center Valley, PA, United States) fitted with a SPOT Pursuit USB camera (SPOT Imaging, Sterling Heights, MI, United States). Following immunostaining with claudin-5, occludin, and zonula occludens (ZO-1), discontinuous tight junctions were quantified and processed in Image J with a minimum of 10 fields containing approximately 30 cells/field from three separate differentiations. Area fraction index was calculated using the same images to determine the area of each image that displayed claudin-5, occludin, or ZO-1 immunoreactivity (Canfield et al., 2017).

## Western Blot

Following 50 μM propofol exposure, BMECs were washed three times with cold phosphate-buffered saline (PBS) and lysed using ice cold Pierce™ RIPA buffer (Thermo Fisher Scientific, Waltham, MA, United States) with Halt™ Protease and Phosphatase Inhibitor Cocktail (Thermo Fisher Scientific, Waltham, MA, United States). Cell lysates were quantified for total protein concentration using a Pierce™ Rapid Gold BCA Protein assay kit (Thermo Fisher Scientific, Waltham, MA, United States). Gels were run at 120 V for 1 h (12% precast gel; Claudin-5, Occludin, β-actin) or for 70 min (4–15% gels; ZO-1) in Tris/Glycine sodium dodecyl sulfate buffer using a Bio-Rad Mini-Protean® Tetra Vertical Electrophoresis Cell (Bio-Rad, Hercules, CA, United States). After samples were separated, the protein was

transferred to Bio-Rad Immun-Blot® PVDF membranes (Bio-Rad,Hercules, CA, United States) at 100 V for 1 h in transfer buffer (Tris/Glycine with 20% methanol). The membranes were washed one time with Tris-buffered saline containing 0.1% Tween 20 (TBST) and blocked for 1 h in blocking solution (5% non-fat dry milk dissolved in TBST) at room temperature on a rocking platform. Membranes were then probed with primary antibodies (**Supplementary Table 2**) in 10 mL of blocking solution at 4°C overnight on a rocking platform. Membranes were washed three times with TBST at room temperature on a rocking platform for 10 min. Membranes were probed with horseradish peroxidase (HRP) conjugated secondary antibodies (**Supplementary Table 2**) in blocking solution for 1 h at room temperature on a rocking platform and then washed three additional times in TBST at room temperature on a rocking platform. Membranes were imaged using a LI-COR C-DiGit® Blot Scanner (LI-COR, Lincoln, NE, United States) and images were quantified using ImageJ software version 1.52a.

## Efflux Transporter Activity

### Accumulation Assay

Three common efflux transporters were investigated: p-glycoprotein (Pgp), multi-drug resistance protein (MRP-1) and breast cancer resistance protein (BCRP). BMECs were treated with 50 μM propofol (Sigma Aldrich, St. Louis, MO, United States) in EC ± buffer at 37°C on a rotational platform for 3 h. Following propofol exposure, media was exchanged with EC ± buffer ± inhibitor. KO143 (10 μM, Sigma Aldrich, St. Louis, MO, United States) served as a BCRP inhibitor, MK157 (10 μM, Sigma Aldrich, St. Louis, MO, United States) served as a MRP-1 inhibitor, and Cyclosporin A (10 μM, Sigma Aldrich, St. Louis, MO, United States) served as a Pgp inhibitor. The plate was placed on a rotational platform in a 37°C incubator for 30 min. Media was exchanged with EC ± buffer ± inhibitor and substrate and the plate was placed on a rotational platform in a 37°C incubator for 1 h. Hoechst (5 μM, Sigma Aldrich, St. Louis, MO, United States) served as the BCRP substrate, DCFDA (20 μM, Thermo Fisher Scientific, Waltham, MA, United States) served as a MRP-1 substrate, and Rhodamine 123 (10 μM, Sigma Aldrich, St. Louis, MO, United States) served as the Pgp substrate. Following substrate exposure, each well was rinsed twice with cold Dulbecco's Phosphate Buffered Saline (Sigma Aldrich, St. Louis, MO, United States). Subsequently, 300 μl of RIPA assay buffer was added to each well. The plate was protected from light and placed on a rotational platform at 23°C for 10 min. The fluorescent intensity of the plate was measured using a Synergy HTX Multi-Mode reader.

### Transporter Assay

Brain microvascular endothelial cells were exposed to propofol (50 μM; Sigma Aldrich, St. Louis, MO, United States) for 3 h at 37°C. Subsequently, media was exchanged with EC ± buffer ± inhibitor (0.5 mL top, 1.5 mL bottom) and the plate was incubated at 37°C on a rotational platform for 30 min. The media on the top of the Transwell insert was replaced with a substrate ± inhibitor in EC ± buffer. The plate was incubated at 37°C for 1 h on a rotational platform. Following incubation, 150 μL was sampled from the bottom of each well and transferred to a 96-well plate (Thermo Fisher Scientific, Waltham, MA, United States). The fluorescent intensity of the plate was measured using a Synergy HTX Multi-Mode reader.

## Flow Cytometry

Following propofol (50 μM) exposure, cells were treated with Accutase at 37°C on a rotational platform for 30 min. Cells were fixed with 100% methanol and triturated briefly. Following fixation, BMECs were washed in $PBS^{-/-}$ twice. BMECs were blocked in 10% donkey serum (Sigma Aldrich, St. Louis, MO, United States) in $PBS^{-/-}$ for 1 h. Primary antibodies (**Supplementary Table 1**) were added to the suspension at appropriate dilutions. The microcentrifuge tubes were then vortexed before incubating overnight on a rotational platform at 4°C. Following two washes, BMECs were exposed to secondary antibodies (**Supplementary Table 1**) at the appropriate dilution in blocking solution for 30 min at 25°C on a rotational platform. Samples were vortexed once during the incubation period. Two washes were completed and after the final wash, the sample was resuspended in 400 μL of wash buffer. Samples were transferred to a 96-well round bottom plate (Thermo Fisher Scientific, Waltham, MA, United States) and read on the flow cytometer (Guava EasyCyte 8HT, Millipore Corporation, Burlington, MA, United States).

## Transcytosis

To determine the effects of propofol on transcellular movement in BMECs we utilized the transcytosis and accumulation of a 10 kDa dextran (Alexa Fluor 488, 10 μM; Sigma). BMECs displaying elevated and depressed barriers were utilized. To obtain BMECs with depressed barriers (200–400$\Omega \times cm^2$) the same differentiation was utilized as above but without RA. Three hours following propofol treatment (50 μM) on transwell-seeded BMECs, dextran was diluted in EC ± and added to the apical side of the transwell. Following 4 h on a rotating platform at 37°C, media was collected from the basolateral side of the transwell and read on a Synergy HTX Multi-Mode reader (BioTek, Winooski, VT, United States), revealing the rate of transcytosis. BMECs were then rinsed three times in PBS and lysed with RIPA. Following trituration, the lysate was collected and quantified using a fluorescent plate reader, indicating the level of dextran accumulation. Data was presented following subtraction of transcytosis and accumulation of dextran at 4°C to account for para-cellular movement of dextran.

## Matrix Metalloproteinase Activity

Brain microvascular endothelial cells were treated with 50 μM propofol in EC ± buffer at 37°C on a rotational platform for 3 h. The supernate of cell culture media was collected and centrifuged for 10 min at 1,000 *g*, 4°C. The MMP-2/MMP-9 activities were determined by a fluorescence kit (SensoLyte® Plus 520 MMP-2 and MMP-9 Assay Kit, Cat No. AS-72224, AS-72017; AnaSpec, Fremont, CA, United States) following the manufacturer's instructions. Briefly, MMP-2 and MMP-9 were isolated using antibody-coated 96 well plates, which were provided in the assay kit. MMP-2/9 substrates were added to antibody-coated plates and incubated at room temperature for 24 and 16 h, respectively. Fluorescent intensity was measured using a Synergy

HTX Multi-Mode reader (BioTek, Winooski, VT, United States) and data is presented as a percent change from control.

## Matrix Metalloproteinase Inhibition

Forty eight hours following seeding onto *trans*-wells, BMECs were treated with 25 μM GM-6001 MMP inhibitor (Thermo Fisher Scientific, Waltham, MA, United States) dissolved in EC medium (±) for 30 min at 37°C on a rotational platform. After 30 min of pre-treatment with GM-6001 inhibitor, media was aspirated and replaced with fresh EC medium (+PDS/-bFGF) containing 25 μM GM-6001 inhibitor (with or without 50 μM propofol) and incubated at 37°C for 3 h on a rotational platform. Propofol treatment was removed after 3 h of exposure and fluorescein permeability and tight junction analysis was conducted as previously described.

## Cell Viability

To determine cell viability, BMECs were treated with 10, 50, 100, or 1,000 μM propofol in EC ± media at 37°C on a rotational platform. Following 3 h of treatment, propofol was aspirated and replaced with 100 μL of EC ± media. A MTT Cell Viability Assay Kit (Biotium, Fremont, CA, United States) was utilized to determine cell viability following propofol exposure. Following manufacturer's instructions, 10 μL of MTT solution was added to each well and the plate was incubated at 37°C for 2 h on a rotational platform. After 2 h of incubation, 200 μL of DMSO (Sigma Aldrich, St. Louis, MO, United States) was added to each well, triturating several times to dissolve the formazan salt. Absorbance was measured at 570 nm using a Synergy HTX Multi-Mode reader and normalized by subtracting background absorbance measured at 630 nm.

## Statistical Analysis

Data are presented as mean ± SD. Each experimental group consisted of iPSC-derived BMECs from at least three separate differentiations. For the statistical analyses, SigmaStat software (Systat Software, Inc., San Jose, CA, United States) was used. Statistical comparisons were performed using one-way analysis of variance (ANOVA) from the pooled data. Equal Variance and Shapiro-Wilk Normality Assumptions were satisfied for the residuals of each ANOVA model with a $p$ value of 0.05 to reject. Within each condition, all pairwise comparisons were conducted within the ANOVA context using *post hoc* tests with the pooled variance estimate, followed by Holm-Sidak step down correction for multiple testing. Adjusted $p$-values displayed in the text. $P < 0.05$ was considered significant. The manuscript adheres to the applicable STROBE and ARRIVE guidelines.

# RESULTS

## Effects of Propofol on Barrier Tightness and Passive Permeability in Human Stem Cell-Derived Brain Microvascular Endothelial Cells

Forty eight hours after seeding, BMECs were treated with varying concentrations of propofol and barrier properties were evaluated

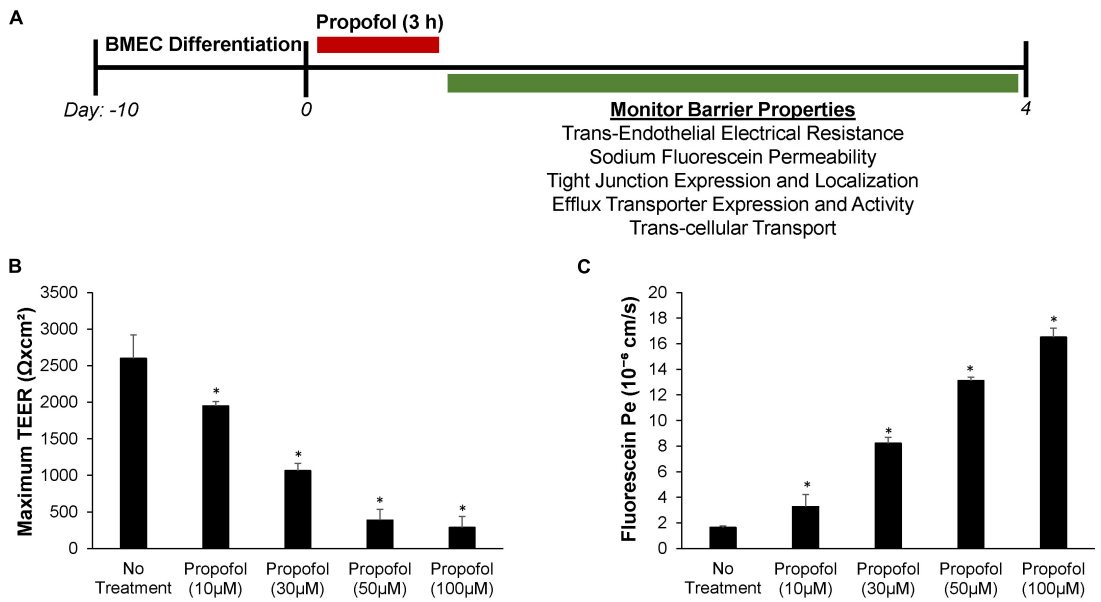


**FIGURE 1 |** Effects of propofol on barrier tightness and passive permeability in human stem cell-derived brain microvascular endothelial cells (BMECs). **(A)** Following 3 h of propofol exposure several barrier properties were monitored in the BMEC population. **(B)** Maximum transendothelial electrical resistance (TEER) values were measured following treatment with propofol (0, 10, 30, 50, and 100 μM). **(C)** Sodium fluorescein permeability was measured 3 h following application of propofol (0, 10, 30, 50, and 100 μM). Permeability coefficients were calculated based on the cleared volume of sodium fluorescein from top chamber to bottom chamber. Statistical significance was calculated using ANOVA. *$P < 0.05$ verses no treatment. Values are presented as mean ± SD of three replicates from a single differentiation and experiments were repeated on three independent differentiations to verify statistical trends reported.

(**Figure 1A**). To evaluate the effect of propofol on barrier tightness, TEER was measured immediately following propofol treatment and monitored every 24 h with maximum TEER values reported following treatment (**Figure 1B**). All concentrations of propofol evaluated significantly reduced TEER when compared to non-treatment control group ($2{,}600 \pm 321\ \Omega \times cm^2$). A 10 μM propofol reduced the TEER of BMECs to $1{,}950 \pm 61\ \Omega \times cm^2$ ($p < 0.05$) and 30 μM lowered TEER to $1{,}065 \pm 99\ \Omega \times cm^2$ ($p < 0.05$), while 50 μM and 100 μM propofol had an even greater influence on reducing barrier tightness, with 50 μM reducing TEER to $388 \pm 147\ \Omega \times cm^2$ ($p < 0.05$) and 100 μM to $288 \pm 148\ \Omega \times cm^2$ ($p < 0.05$), respectively. To confirm propofol-induced decrease in TEER levels was not a result of decreased cell viability we measured cell viability following propofol treatments (10, 50, 100, 1,000 μM). Only a propofol concentration of 1 mM significantly reduced cell viability (**Supplementary Figure 1**). Additionally, to confirm that the propofol-induced decrease in barrier integrity was not due to an intralipid vehicle we measured TEER following control, intralipid alone, and intralipid with propofol (50 μM). Intralipid alone was indistinguishable from control (**Supplementary Figure 2**).

Sodium fluorescein assays were used to evaluate the effect propofol has on barrier permeability (**Figure 1C**). Immediately following propofol exposure, sodium fluorescein permeability significantly increased in iPSC derived BMECs with all concentrations surveyed when compared to non-treatment control group ($P_e = 1.65 \pm 0.11 \times 10^{-6}$ cm/s). A 10 μM propofol elevated sodium fluorescein permeability to $P_e = 3.28 \pm 0.95 \times 10^{-6}$ cm/s ($p < 0.05$) and 30 μM increased the permeability to fluorescein even further to $P_e = 8.23 \pm 0.45 \times 10^{-6}$ cm/s ($p < 0.05$). While 50 μM propofol had a greater influence on fluorescein permeability than the latter with $P_e = 13.11 \pm 0.27 \times 10^{-6}$ cm/s ($p < 0.05$), additionally 100 μM propofol had a significant effect on permeability with $P_e = 16.52 \pm 0.69 \times 10^{-6}$ cm/s ($p < 0.05$).

Sodium fluorescein permeability was also used to evaluate the long term effects of propofol exposure on barrier integrity. Propofol treatments of 50 and 100 μM had significant effects on barrier permeability immediately following propofol treatment (6 h) and up to 4 days post-treatment (**Table 1**). Non-treatment BMECs exhibited a sodium fluorescein permeability of $P_e = 1.62 \pm 0.22 \times 10^{-6}$ cm/s. BMECs treated with 50 μM propofol resulted in an elevated $P_e$ of $6.44 \pm 0.92 \times 10^{-6}$ cm/s ($p < 0.05$) while treatment with 100 μM propofol further increased sodium fluorescein permeability to $P_e = 13.84 \pm 2.19 \times 10^{-6}$ cm/s ($p < 0.05$). Treatment of BMECs with 10 μM propofol ($P_e$ of $2.25 \pm 0.53 \times 10^{-6}$ cm/s) had no significant effect on sodium fluorescein permeability when compared to non-treatment BMECs. BMECs treated with propofol (50, 100 μM) exhibited an increased sodium fluorescein at 48 h [$4.17 \pm 0.04 \times 10^{-6}$ cm/s, $7.16 \pm 0.90 \times 10^{-6}$ cm/s vs. no treatment ($1.57 \pm 0.22 \times 10^{-6}$ cm/s)]. At 96 h post-propofol (50 and 100 μM) continued to display a weakened barrier [$2.03 \pm 0.31 \times 10^{-6}$ cm/s and $7.15 \pm 1.34 \times 10^{-6}$ cm/s vs. no treatment ($0.89 \pm 0.14 \times 10^{-6}$ cm/s)].

**TABLE 1 |** Barrier integrity was evaluated 3, 48, and 96 h following propofol exposure.

| Time (Post-treatment) | No treatment | Propofol (10 μM) | Propofol (50 μM) | Propofol (100 pM) |
|---|---|---|---|---|
| 3 h | 1.62 ± 0.22 | 2.25 ± 0.53 | 6.44 ± 0.92* | 13.84 ± 2.19* |
| 48 h | 1.57 ± 0.22 | 0.95 ± 0.04 | 4.17 ± 0.04* | 7.16 ± 0.90* |
| 96 h | 0.89 ± 0.14 | 0.98 ± 0.33 | 2.03 ± 0.31* | 7.15 ± 1.34* |

*Fluorescein permeability coefficients ($10^{-}6$ cm/s) were calculated in BMECs following propofol exposure (0 h/No treatment, 10, 50, 100 μM). Statistical significance was calculated using ANOVA at each time point. *P < 0.05 verses no treatment. Values are presented as mean ± SD of three differentiations.*

## Propofol Dysregulates Occludin Protein Localization in Induced Pluripotent Stem Cell Derived Brain Microvascular Endothelial Cells

Tight junction protein expression and localization were evaluated in the diminished barrier properties in BMECs following exposure to propofol. Utilizing immunocytochemistry, tight junction localization was observed in BMECs 48 h following propofol treatment. Following immunochemistry of occludin, several discontinuous junctions (white arrows) were observed in propofol treated BMECs (**Figure 2A**). Area fraction index, an indicator of tight junction immunoreactivity, revealed that occludin levels decreased by 34 ± 16%compared to no-treatment ($p < 0.05$) (**Figure 2B**). Western blot analysis of tight junction proteins expression validated the diminished occludin immunoreactivity observed in propofol treated BMECs (**Figure 2C**). Cells treated with 50 μM propofol showed a 37% reduction in relative intensity of occludin expression when compared to non-treatment ($p < 0.05$) (**Figure 2D**). No significant changes were observed in expression or localization of claudin-5 and ZO-1.

## Brain Microvascular Endothelial Cell Efflux Transporters Activity Is Unaffected by Propofol Exposure

The effects of 50 μM propofol on PgP, MRP-1, and BCRP expression and activity was investigated. Efflux transporter expression in BMECs was visualized by immunocytochemistry (**Figure 3A**) and quantified by flow cytometry (**Figure 3B**). Expression of PgP, MRP-1 and BCRP was unaffected by propofol exposure (**Figure 3B**). Efflux transporter activity was determined by measuring transport and accumulation of efflux transporter substrates (**Figure 3C**). There was no significant difference in Rhodamine 123 transport between control and propofol treatment conditions for PgP following inhibition with CsA (157.43 ± 33.39 and 145.99 ± 16.88). MRP-1 also showed an increased transport of DCFDA after inhibition with MK571 (137.11 ± 3.37 and 137.19 ± 6.28), but no significant difference between control and propofol groups. Likewise BCRP expressed in BMECs exhibited increased transport of Hoechst after exposure to the inhibitor KO143 (131.68 ± 3.49 and 133.33 ± 6.34) and no significant change between control

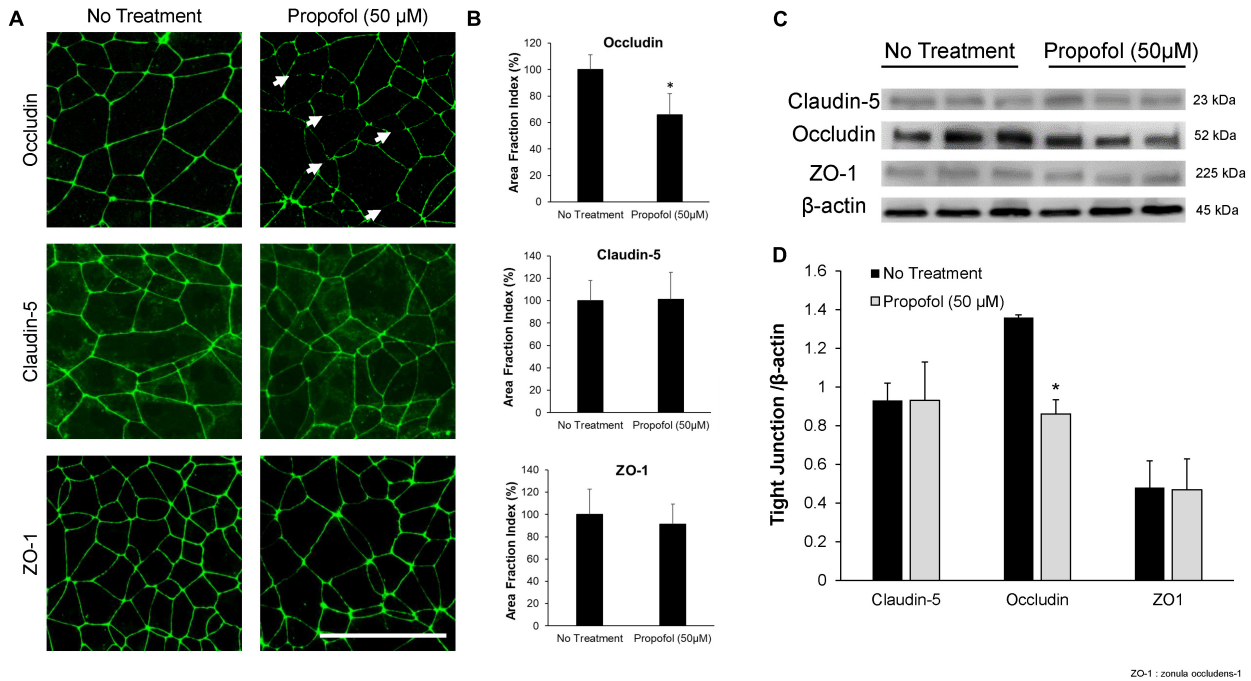


**FIGURE 2 |** Analysis of tight junction continuity and expression in iPSCs derived BMECs following treatment with propofol. Tight junction protein localization and expression levels were examined 48 h following treatment with propofol (50 μM) for 3 h. **(A)** BMECs were immunocytochemically labeled for tight junction proteins: claudin-5, occludin, and ZO-1. Discontinuous tight junctions are indicated by white arrows. Scale bar = 50 μm. **(B)** Quantification of discontinuous tight junctions was performed by calculating the area of each image that displays claudin-5, occludin, or ZO-1 immunoreactivity, respectively (area fraction index). Values are presented as mean ± SD of three replicates from a single differentiation, and experiments were repeated on three independent differentiations to verify statistical trends reported. **(C)** Western blot of tight junction proteins following propofol treatment with β-actin loading control. Each lane represents a separate BMEC differentiation. **(D)** Quantification of western blots to compare tight junction protein expression levels. Propofol samples were independently normalized to each respective no-treatment sample. Statistical significance was calculated using Student's *t*-test. $^*P < 0.05$ versus no treatment. Values are presented as mean ± SD of three differentiations.

and treatment groups. Accumulation of substrate was also investigated for PgP, MRP-1 and BCRP. There was no significant difference between control and treatment group accumulation for Pgp, MRP-1 or BCRP following inhibition.

## Propofol Does Not Affect Cellular Transcytosis in Brain Microvascular Endothelial Cells

To determine the effects of propofol on uptake and transcytosis of a large molecule, a 10 kDa Alexa-Fluor tagged dextran was utilized. Following propofol treatment BMECs were treated with a fluorescently tagged dextran. The tagged dextran was quantified both within the cell (accumulation) and in the chamber below the BMEC-seeded transwell (transcytosis) and compared to non-treated BMECs. Following propofol treatment, BMECs had similar levels of accumulation and transcytosed dextran (94 ± 5%, 97 ± 5%; respectively; n.s.) compared to no treatment (100 ± 8, 100 ± 8%; respectively) (**Figure 4A**). When 10 kDa dextran transcytosis was conducted at 4°C, vesicular transport was significantly reduced (**Figure 4B**). Additionally, BMECs with TEER values of 200–400 $\Omega \times cm^2$ had a similar level of dextran transcytosis compared to BMECs with TEER values ranging from 1,500 to 2,300 $\Omega \times cm^2$ (**Figure 4C**) indicating that 10 kDa dextran transcytosis is occurring via a transcellular route and not a para-cellular route.

## Propofol-Induced Blood-Brain Barrier Damage Is Restored Following Matrix Metalloproteinase Inhibition

The role of MMPs in propofol-induced BBB damage was investigated by utilizing a sodium fluorescein tracer in the presence of MMP inhibitor, GM6001. MMP2 and 9 activity were assessed after exposure to 50 μM propofol. Following propofol, BMECs had a 247 ± 88% increase in MMP2 activity compared to non-treatment (**Figure 5A**). Interestingly, propofol did not affect MMP 9 activity (increase of 4 ± 16% from control) (**Supplementary Figure 3**). To determine the role of MMP-2 induced barrier leakiness, BMECs were pretreated with an MMP inhibitor, GM 6001 (25 μM) for 30 min prior to and during propofol treatment (**Figure 5B**). Propofol (50 μM) increased sodium fluorescein permeability (11 ± 2.6 × $10^{-6}$ cm/s) compared to no-treatment control (0.9 ± 0.13 × $10^{-6}$ cm/s). GM6001 inhibition significantly attenuated the propofol-induced sodium fluorescein permeability increase observed following propofol treatment (4.5 ± 0.6 × $10^{-6}$ cm/s; $p < 0.05$ versus propofol). Additionally, GM6001 inhibition

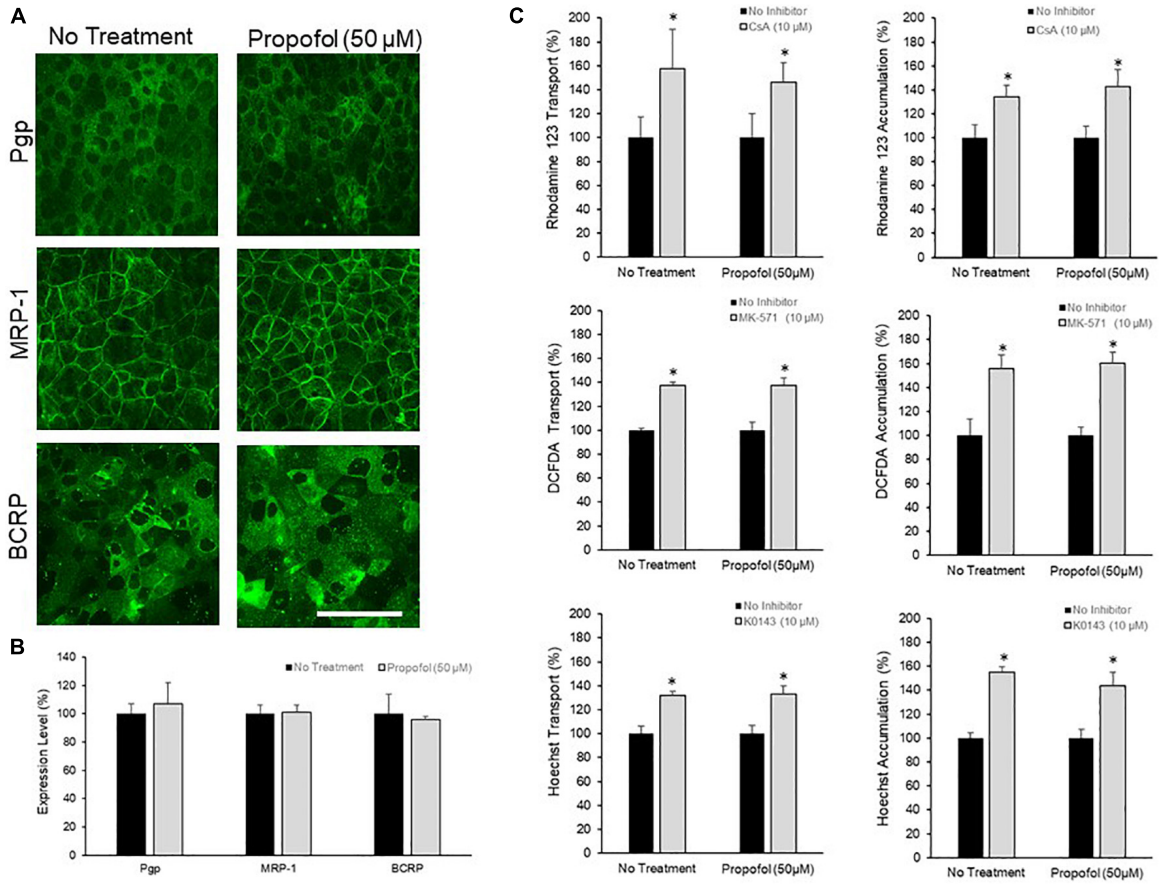


**FIGURE 3 |** The effects of propofol on efflux transporters in BMECs. **(A)** iPSC-derived BMECs were immunolabeled for efflux transporters: Pgp, MRP-1, and BCRP following 3 h of propofol (50 μM) treatment. Scale bar = 100 μm. **(B)** Transporter expression levels were determined using flow cytometry. Geometric means of positively immunolabeled cell populations were analyzed to compare expression levels with and without propofol exposure. The data are normalized to no treatment expression levels. Statistical significant was determined using a Student's *t*-test. Values are mean ± SD of three independent differentiations. **(C)** Efflux transporter activity was assessed by the transport of fluorescent substrates and optimized inhibitors (Pgp: Rhodamine/Cyclosporin A; MRP-1: DCFDA/MK571; BCRP: Hoechst/KO143) from the apical to the basolateral chamber in the two-compartment transwell model and the accumulation of substrate within the cells. Data is reported as a percentage change from no-inhibitor within each respective condition. Statistical significance was calculated using Student's *t*-test. $^*P < 0.05$ versus no inhibition. Values are presented as mean ± SD of three replicates from a single differentiation, and experiments were repeated on three independent differentiations to verify statistical trends reported.

attenuated a propofol-induced decrease in TEER [decrease of 54 ± 8% vs. a decrease of 87 ± 2% compared to no-treatment ($p < 0.05$)] (**Supplementary Figure 4**). Additionally, the effects of GM6001 on tight junction localization was visualized with immunohistochemistry (**Figure 5C**). Several discontinuous occludin junctions (white arrows) were observed in propofol treated BMECs, however, they were not observed when GM6001 was administered with propofol (**Figure 5C**). Area fraction index revealed that propofol-induced occludin levels decreased by 33 ± 15% compared to no-treatment ($p < 0.05$) but the co-administration of GM6001 and propofol restored occludin levels back to no-treatment levels (decrease 3 ± 15%; n.s.) (**Figure 5D**). Following visualization of tight junction localization we evaluated the effects of GM6001 on tight junction expression during propofol treatment. Similar to our previous results, occludin expression was significantly depressed following propofol treatment (decrease 0.313 ± 0.016). GM6001 administered during propofol exposure restored occludin expression back to no treatment levels (1.88 ± 0.09 vs. 1.83 ± 0.03; **Figure 5E**).

## DISCUSSION

This study demonstrates that an anesthetic, propofol, can induce blood-brain barrier defects in a human stem cell-derived blood-brain barrier model. The unique advantage of the study presented here is that the barrier model utilized is of human origin with several near *in vivo* barrier phenotypes. Our major findings are summarized as follows: (1) Propofol significantly diminished BBB integrity as observed as a decrease in TEER and an increase in sodium fluorescein permeability. (2) Propofol diminished occludin expression and localization. (3) Propofol does not affect cell viability, efflux transporter expression or activity, or

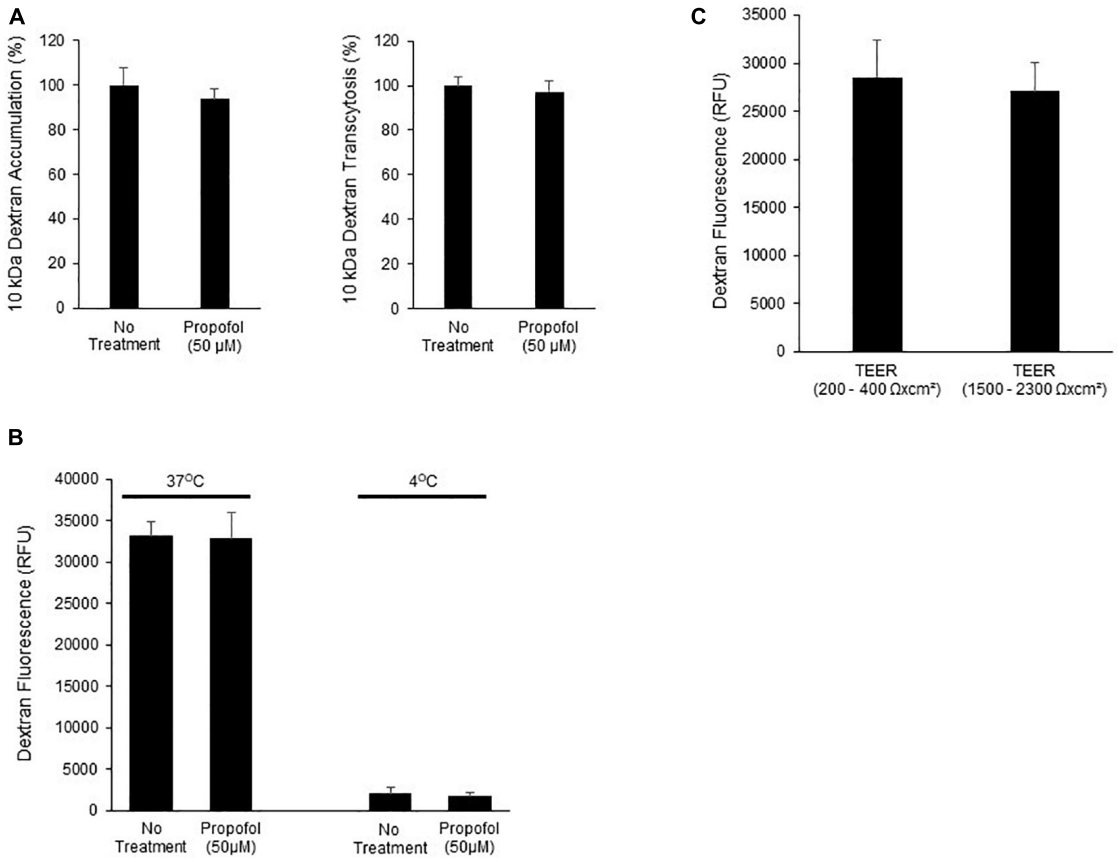


**FIGURE 4 |** Determination of the effects of propofol on the ability of a fluorescently labeled dextran to cross BMECs. **(A)** BMECs were treated with propofol (50 μM) for 3 h prior to being presented with a fluorescently tagged dextran for 2 h. Fluorescently tagged dextran was measured from the bottom chamber (transcytosis) and within the BMEC population (accumulation). Raw fluorescence units are normalized to control BMECs. **(B)** To account for membrane fluidity in the ability of dextran to cross BMECs we conducted the assays at both 37° and 4°C. **(C)** To validate that dextran transcytosis was not related to changes in barrier tightness we evaluated the ability of dextran to cross BMECs with low TEER values (200–400 $\Omega$xcm$^2$) and high TEER values (1,500–2,300 $\Omega$xcm$^2$). Statistical significance was calculated using Student's *t*-test. All experimental comparisons displayed no significance. Values are presented as mean ± SD of three replicates from a single differentiation, and experiments were repeated on three independent differentiations to verify statistical trends reported.

*trans*-cellular transport. (4) Propofol enhanced MMP-2 activity and inhibition of MMP activity in part reduced the propofol-induced barrier damage. In summary, propofol was detrimental to the integrity of the barrier but did not affect the active components (i.e., efflux transporters, *trans*-cellular transport). The damaging effects of propofol were in part mitigated by treating BMECs with a global MMP inhibitor prior to and during propofol exposure implicating that additional cellular mechanisms are responsible for barrier breakdown following propofol exposure.

Anesthetic agents are regularly used in a variety of medical procedures for individuals of all ages with very little known about the long-term effects on the brain (Dyer et al., 1995; Acharya et al., 2015; Disma et al., 2018; Olutoye et al., 2018). Rodent models have demonstrated that several anesthetics, both volatile and lipophilic, have detrimental effects on NVU populations and ultimately functional discrepancies later in life (Stratmann et al., 2009; Shen et al., 2013). Importantly, the anesthetic-induced neurotoxicity was specific to a limited brain development window often associated with a period of brain growth when neuronal populations are vulnerable (Jevtovic-Todorovic et al., 2003).

More recently, several human studies have demonstrated the negative effects observed in animal studies may not be as robust in the human population and illustrate a need for effective and competent *in vitro* human models to further evaluate the safety of anesthetics in the human population (O'Leary and Warner, 2017; Disma et al., 2018). A limited number of reports have investigated the effects of anesthetics on the structure and function of the BBB in a variety of models. The clinical significance of these studies must be carefully measured as interspecies differences in the BBB exist (Syvänen et al., 2009; Warren et al., 2009). The utilization of human primary or immortalized BBB models alleviate some of these concerns, however, suboptimal barrier phenotypes often limit the extent of their efficacy (Calabria and Shusta, 2008). The validity of iPSC-derived BBB models have been questioned due to a mixed endothelial: epithelial transcriptional profile (Lu et al., 2021); yet, these iPSC-derived like BMECs exhibit

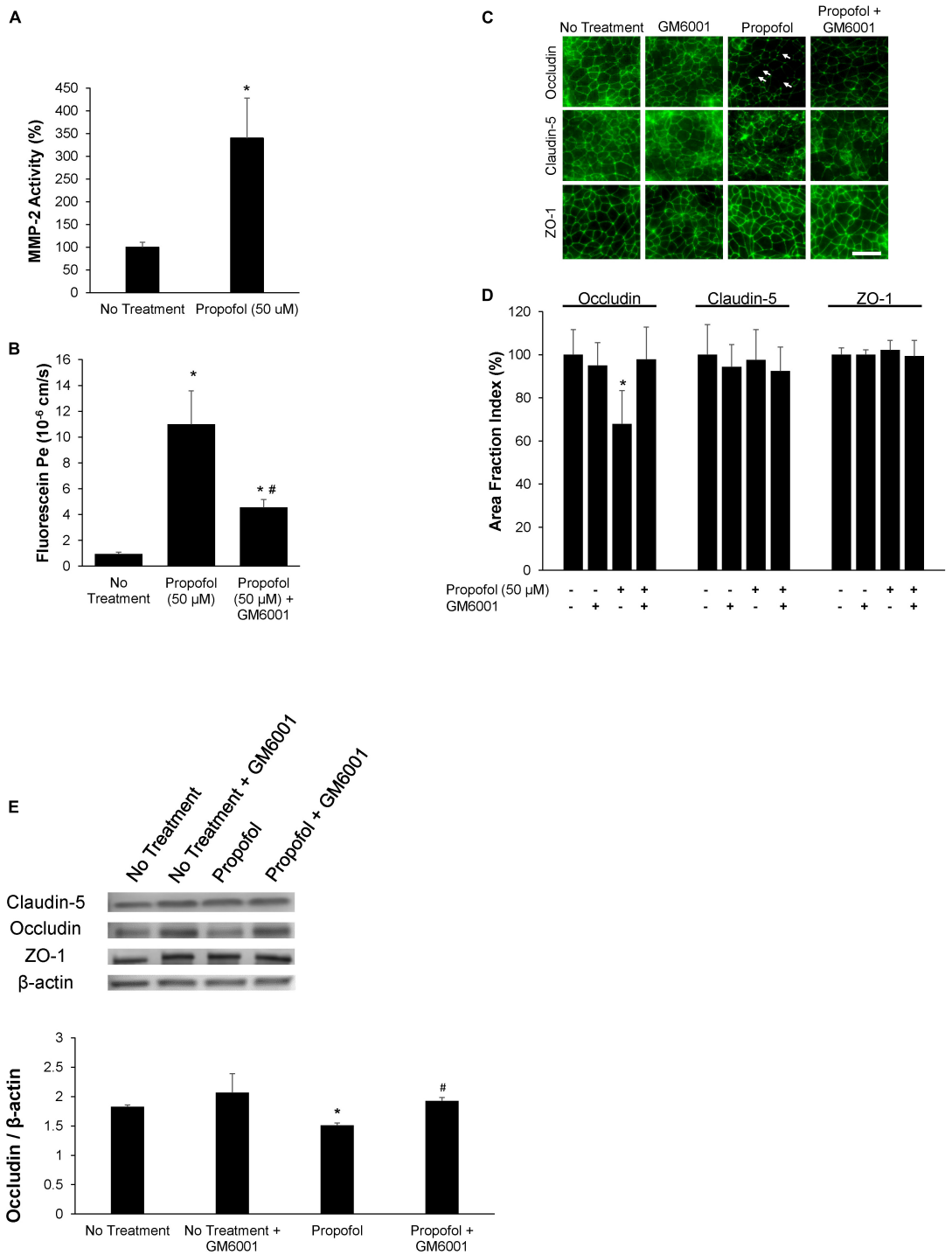


**FIGURE 5 |** Propofol-induced matrix metalloproteinase-2 (MMP-2) partially diminishes barrier integrity. **(A)** Following 3 h of propofol exposure in BMECs, culture medium was collected and MMP-2 activity was analyzed. Data is reported as a percentage change from no treatment. Statistical significance was calculated using Student's *t*-test. **(B)** An MMP-inhibitor, GM6001, was administered during propofol exposure. Following MMP-inhibition barrier integrity was assessed with fluorescein permeability. Permeability coefficients were calculated based on the cleared volume of sodium fluorescein from top chamber to bottom chamber. **(C)** Tight junction protein localization and expression levels were examined 48 h following treatment with either propofol, GM6001, or propofol and GM6001. BMECs were immunocytochemically labeled for tight junction proteins: claudin-5, occludin, and ZO-1. Discontinuous tight junctions are indicated by white arrows. Scale bar = 50 μm. **(D)** Quantification of discontinuous tight junctions was performed by calculating the area of each image that displays claudin-5, occludin, or ZO-1 immunoreactivity, respectively (area fraction index). **(E)** Western blot of tight junction proteins following propofol treatment with or without GM6001. Quantification of tight junction protein, occludin following normalization to β-actin. Statistical significance was calculated using ANOVA. $^*P < 0.05$ verses no treatment; $\#p < 0.05$ verses Propofol. Values are presented as mean ± SD of six differentiations.

near *in vivo* barrier function, an essential component of a BBB model (Workman and Svendsen, 2020). More recently, iPSC-derived BMECs have been utilized to enhance tissue engineering models, replicate pathological conditions, and unveil novel therapeutic approaches in the BBB (Li et al., 2021; Neal et al., 2021; Noorani et al., 2021; Raut et al., 2021; Wellens et al., 2021; Wu et al., 2021). Three common anesthetics, propofol, isoflurane, and sevoflurane, have independently demonstrated a degree of BBB damage (Sharma et al., 2014; Zhao et al., 2014; Acharya et al., 2015). Interestingly, propofol induces apoptosis in neuronal populations by potentially effecting astrocyte-derived brain derived neurotrophic factor (Liu et al., 2017). However, propofol does not appear to induce apoptosis in astrocytes and very little is known about the effects of propofol on pericytes, another critical cell type of the NVU (Yan et al., 2017). Due to the role of NVU cell types in the support, maintenance and the development of barrier forming BMECs any propofol-induced injuries could have a direct effect on barrier properties.

Propofol is an anesthetic agent commonly used for both the induction and maintenance of anesthesia in both short-term procedures and long-term sedation. Propofol similarly to the volatile anesthetics, isoflurane and sevoflurane, enhance GABA transmission but is administered intravenously compared to inhalation (Kim et al., 2018). Exposure of iPSC-derived BMECs to isoflurane and sevoflurane did not alter barrier integrity (data not shown). Determining an *in vivo* like concentration is challenging as propofol readily binds red-blood cells and circulating plasma proteins (Altmayer et al., 1995). However, propofol is lipophilic and the brain concentration is believed to be much higher compared to peripheral tissues (Riu et al., 2000). Representative *in vitro* concentrations have been reported to be as low as 3 μM and as high as 50 μM (Sall et al., 2012; Long et al., 2017). We observed a small reduction in barrier tightness (decreased TEER and increased fluorescein permeability) following 10 μM propofol administration, however, within 3 h barrier integrity (**Table 1**) was indistinguishable from no treatment implicating that barrier effects of propofol was not sustained. Additionally, tight junction localization was unchanged following 10 μM propofol. A robust barrier loss was observed following exposure to 50 μM propofol and was within clinical limits thus all subsequent experiments were conducted at this concentration. Without barrier supporting NVU cell types, iPSC-derived BMEC barrier properties begin to diminish four to 7 days post sub-culture; limiting the extent of propofol-induced barrier dysfunction we are able to observe. However, these results implicate at least in part that the safety of propofol anesthesia should be further studied, specifically in terms of its action on the blood-brain barrier.

Several studies have demonstrated a strong correlation between junctional continuity and barrier phenotype (Persidsky et al., 2006). Isoflurane was previously demonstrated to decrease occludin expression in primary human brain microvascular endothelial cells (Zhao et al., 2014). Similarly, we observed a significant decrease in expression and localization of occludin along with a loss in barrier tightness following propofol exposure. Loss of occludin localization and expression are likely responsible for the observed barrier loss following propofol exposure. Additionally, we investigated the effects of propofol on the expression and activity of efflux transporters. Regev et al. demonstrated that the anesthetics: benzyl alcohol, non-aromatic chloroform, and diethyl ether abolished Pgp activity; however, these studies were conducted in non-brain-microvascular endothelial cells (Regev et al., 1999). We previously demonstrated that iPSC-derived BMECs express functional efflux transporters including: Pgp, MRP-1 and BCRP (Canfield et al., 2017). Propofol exposure did not have an effect on efflux transporter activity in iPSC-derived BMECs. It is difficult to benchmark these results to the literature as there are no previous studies that have investigated the effects of propofol on efflux transporter activity or expression. Finally, we investigated non-specific transcytosis following propofol. Brain endothelium has a significantly reduced rate of transcytosis compared to peripheral endothelial cells (Daneman et al., 2010). Isoflurane has been demonstrated to increase caveolar-dependent transcytosis, however, propofol exposure did not alter non-specific transcytosis in iPSC-derived BMECs (Spieth et al., 2021).

Anesthetic-induced barrier damage mediators have been previously investigated, including the roles of reactive oxygen species, vascular endothelial growth factor, heat-inducible factor-1α, and matrix metalloproteinase (Sharma et al., 2014; Zhao et al., 2014). Previously, MMPs have been demonstrated to de-localize tight junctions and digest basement membrane proteins contributing to an increase in barrier leakiness (Feng et al., 2011). Specifically, MMP-2 and MMP-9 have been implicated in anesthetic-induced blood-brain barrier breakdown (Hu et al., 2014). MMP-9 activity is often associated with an increase in VEGF-induced BBB permeability (Valable et al., 2005). Human iPSC-derived BMECs had elevated MMP-2 activity following propofol exposure; however, MMP-9 activity and VEGF expression (data not shown) remained unchanged. The addition of a global MMP inhibitor during propofol exposure partially protected barrier tightness in iPSC-derived BMECs. These data indicate that other non-MMP signaling mechanisms either independently or in unison with MMP-2 contribute to propofol-induced barrier breakdown.

Finally, to our knowledge, we are the first to investigate the toxic effects of propofol on a relevant human BBB model. Similarly to models of different sources, we observed propofol diminishing barrier integrity by decreasing tight junction expression and localization. These actions were in part mitigated with the addition of a global MMP inhibitor. The utilization of a human iPSC-derived BBB model with robust *in vivo* like properties demonstrates that further studies are warranted in understanding the effects of anesthetics on the blood-brain barrier both acutely and long-term. Specifically, a better understanding of cellular mechanisms involved in anesthetic-induced BBB breakdown would unveil novel therapeutic interventions to further enhance anesthesia safety.

## DATA AVAILABILITY STATEMENT

The raw data supporting the conclusions of this article will be made available by the authors, without undue reservation.

## AUTHOR CONTRIBUTIONS

JH, ON, and SC designed and conducted the experiments, analysis, interpretation, and wrote the manuscript. DB, KL, LA, and DP conducted the experiments, data analysis, and interpretation. All authors contributed to the article and approved the submitted version.

## FUNDING

This work was supported by the Indiana University School of Medicine start-up funds and an award from the Indiana University School of Medicine. The content is solely the responsibility of the authors and does not necessarily represent the official views of the Indiana University School of Medicine (Canfield). Additional support was provided by Indiana Medical Student Program for Research and Scholarship (IMPRS) funded by the Indiana University School of Medicine and Indiana CTSI Collaboration in Translational Research Grants (UL1TR001108) (DB, KL, and DP).

## SUPPLEMENTARY MATERIAL

The Supplementary Material for this article can be found online at: https://www.frontiersin.org/articles/10.3389/fncel.2022.835649/full#supplementary-material

**Supplementary Figure 1 |** Cell viability was assessed in BMECs following propofol exposure. Following propofol exposure cell viability was determined utilizing a MTT cell viability assay kit. Data is reported as a percentage change from control (no Propofol). Statistical significance was calculated using ANOVA. $^{*}P < 0.05$ versus control. Values are presented as mean ± SD of three differentiations.

**Supplementary Figure 2 |** Barrier integrity was evaluated following intralipid exposure. BMECs were exposed to DMSO (control solvent), intralipid alone, and propofol with intralipid. Data is reported as a percentage change from control. Statistical significance was calculated using ANOVA. Values are presented as mean ± SD of three differentiations.

**Supplementary Figure 3 |** MMP-9 activity was assessed in BMECs following propofol exposure. Following 3 h of propofol exposure in BMECs, culture medium was collected and MMP-9 activity was analyzed. Data is reported as a percentage change from no treatment. Statistical significance was calculated using Student's *t*-test. Values are presented as mean ± SD of three replicates from a single differentiation, and experiments were repeated on three independent differentiations to verify statistical trends reported.

**Supplementary Figure 4 |** Propofol-induced matrix metalloproteinase-2 (MMP-2) partially diminishes *trans*-endothelial electrical resistance. An MMP-inhibitor, GM6001, was administered during propofol exposure. Following MMP-inhibition barrier integrity was assessed with *trans*-endothelial electrical resistance (TEER). TEER was normalized to a percentage change from no-treatment. Statistical significance was calculated using ANOVA. $^{*}P < 0.05$ verses no treatment; $\#p < 0.05$ verses Propofol. Values are presented as mean ± SD of three differentiations.

**Supplementary Table 1 |** Antibody information for immunocytochemistry assays.

**Supplementary Table 2 |** Antibody information for western blot assays.

## REFERENCES

Acharya, N. K., Goldwaser, E. L., Forsberg, M. M., Godsey, G. A., Johnson, C. A., and Sarkar, A. (2015). Sevoflurane and Isoflurane induce structural changes in brain vascular endothelial cells and increase blood-brain barrier permeability: Possible link to postoperative delirium and cognitive decline. *Brain Res.* 1620, 29–41. doi: 10.1016/j.brainres.2015.04.054

Altmayer, P., Büch, U., and Büch, H. P. (1995). Propofol binding to human blood proteins. *Arzneimittelforschung* 45, 1053–1056.

Calabria, A. R., and Shusta, E. V. (2008). A genomic comparison of in vivo and in vitro brain microvascular endothelial cells. *J. Cereb. Blood Flow Metab.* 28, 135–148. doi: 10.1038/sj.jcbfm.9600518

Canfield, S. G., Stebbins, M. J., Morales, B. S., Asai, S. W., Vatine, G. D., Svendsen, C. N., et al. (2017). An isogenic blood-brain barrier model comprising brain endothelial cells, astrocytes, and neurons derived from human induced pluripotent stem cells. *J. Neurochem.* 140, 874–888. doi: 10.1111/jnc.13923

Cao, Y., Ni, C., Li, Z., Li, L., Liu, Y., Wang, C., et al. (2015). Isoflurane anesthesia results in reversible ultrastructure and occludin tight junction protein expression changes in hippocampal blood-brain barrier in aged rats. *Neurosci. Lett.* 587, 51–56. doi: 10.1016/j.neulet.2014.12.018

Crone, C., and Olesen, S. P. (1982). Electrical resistance of brain microvascular endothelium. *Brain Res.* 241, 49–55. doi: 10.1016/0006-8993(82)91227-6

Daneman, R., Zhou, L., Kebede, A. A., and Barres, B. A. (2010). Pericytes are required for blood-brain barrier integrity during embryogenesis. *Nature* 468, 562–566. doi: 10.1038/nature09513

Disma, N., O'Leary, J. D., Loepke, A. W., Brambrink, A. M., Becke, K., Clausen, N. G., et al. (2018). Anesthesia and the developing brain: A way forward for laboratory and clinical research. *Paediatr. Anaesth.* 28, 758–763. doi: 10.1111/pan.13455

Dyer, C. B., Ashton, C. M., and Teasdale, T. A. (1995). Postoperative delirium. A review of 80 primary data-collection studies. *Arch. Intern. Med.* 155, 461–465. doi: 10.1001/archinte.155.5.461

Feng, S., Cen, J., Huang, Y., Shen, H., Yao, L., Wang, Y., et al. (2011). Matrix metalloproteinase-2 and −9 secreted by leukemic cells increase the permeability of blood-brain barrier by disrupting tight junction proteins. *PLoS One* 6:e20599. doi: 10.1371/journal.pone.0020599

Hirano, A., and Matsui, T. (1975). Vascular structures in brain tumors. *Hum. Pathol.* 6, 611–621. doi: 10.1016/s0046-8177(75)80045-1

Hu, N., Guo, D., Wang, H., Xie, K., Wang, C., Li, Y., et al. (2014). Involvement of the blood-brain barrier opening in cognitive decline in aged rats following orthopedic surgery and high concentration of sevoflurane inhalation. *Brain Res.* 1551, 13–24. doi: 10.1016/j.brainres.2014.01.015

Ing, C., and Brambrink, A. M. (2019). Mayo Anesthesia Safety in Kids continued: two new studies and a potential redirection of the field. *Br. J. Anaesth.* 122, 716–719. doi: 10.1016/j.bja.2019.03.011

Jellinger, K. A., and Attems, J. (2006). Prevalence and impact of cerebrovascular pathology in Alzheimer's disease and parkinsonism. *Acta Neurol. Scand.* 114, 38–46. doi: 10.1111/j.1600-0404.2006.00665.x

Jevtovic-Todorovic, V., Hartman, R. E., Izumi, Y., Benshoff, N. D., Dikranian, K., Zorumski, C. F., et al. (2003). Early exposure to common anesthetic agents causes widespread neurodegeneration in the developing rat brain and persistent learning deficits. *J. Neurosci.* 23, 876–882. doi: 10.1523/JNEUROSCI.23-03-00876.2003

Jiang, J., Tang, C., Ren, J., Zhang, C., Dong, L., and Zhu, Z. (2018). Effect of multiple neonatal sevoflurane exposures on hippocampal apolipoprotein E levels and learning and memory abilities. *Pediatr. Neonatol.* 59, 154–160. doi: 10.1016/j.pedneo.2017.08.007

Kim, D., Kim, H. J., and Ahn, S. (2018). Anesthetics Mechanisms: A Review of Putative Target Proteins at the Cellular and Molecular Level. *Curr. Drug Targets* 19, 1333–1343. doi: 10.2174/1389450119666180502112029

Li, Y., Xia, Y., Zhu, H., Luu, E., Huang, G., Sun, Y., et al. (2021). Investigation of Neurodevelopmental Deficits of 22 q11.2 Deletion Syndrome with a Patient-iPSC-Derived Blood-Brain Barrier Model. *Cells* 10:2576 doi: 10.3390/cells10102576

Liu, Y., Yan, Y., Inagaki, Y., Logan, S., Bosnjak, Z. J., and Bai, X. (2017). Insufficient Astrocyte-Derived Brain-Derived Neurotrophic Factor Contributes to Propofol-Induced Neuron Death Through Akt/Glycogen Synthase Kinase 3β/Mitochondrial Fission Pathway. *Anesth. Analg.* 125, 241–254. doi: 10.1213/ANE.0000000000002137

Long, B., Li, S., Xue, H., Sun, L., Kim, D. H., and Liu, Y. (2017). Effects of Propofol Treatment in Neural Progenitors Derived from Human-Induced Pluripotent Stem Cells. *Neural. Plast.* 2017:9182748. doi: 10.1155/2017/9182748

Lu, T. M., Houghton, S., Magdeldin, T., Durán, J. G. B., Minotti, A. P., and Snead, A. (2021). Pluripotent stem cell-derived epithelium misidentified as brain microvascular endothelium requires ETS factors to acquire vascular fate. *Proc. Natl. Acad. Sci.U.S.A.* 118:e2016950118 doi: 10.1073/pnas.2016950118

Mason, S. E., Noel-Storr, A., and Ritchie, C. W. (2010). The impact of general and regional anesthesia on the incidence of post-operative cognitive dysfunction and post-operative delirium: a systematic review with meta-analysis. *J. Alzheimers Dis.* 22, 67–79. doi: 10.3233/JAD-2010-101086

Neal, E. H., Katdare, K. A., Shi, Y., Marinelli, N. A., Hagerla, K. A., and Lippmann, E. S. (2021). Influence of basal media composition on barrier fidelity within human pluripotent stem cell-derived blood-brain barrier models. *J. Neurochem.*59, 980–991 doi: 10.1111/jnc.15532

Noorani, B., Bhalerao, A., Raut, S., Nozohouri, E., Bickel, U., and Cucullo, L. (2021). A Quasi-Physiological Microfluidic Blood-Brain Barrier Model for Brain Permeability Studies. *Pharmaceutics* 13:1474 doi: 10.3390/pharmaceutics13091474

Obermeier, B., Daneman, R., and Ransohoff, R. M. (2013). Development, maintenance and disruption of the blood-brain barrier. *Nat. Med.* 19, 1584–1596. doi: 10.1038/nm.3407

O'Leary, J. D., and Warner, D. O. (2017). What do recent human studies tell us about the association between anaesthesia in young children and neurodevelopmental outcomes? *Br. J. Anaesth.* 119, 458–464. doi: 10.1093/bja/aex141

Olutoye, O. A., Baker, B. W., Belfort, M. A., and Olutoye, O. O. (2018). Food and Drug Administration warning on anesthesia and brain development: implications for obstetric and fetal surgery. *Am. J. Obstet. Gynecol.* 218, 98–102. doi: 10.1016/j.ajog.2017.08.107

Persidsky, Y., Ramirez, S. H., Haorah, J., and Kanmogne, G. D. (2006). Blood-brain barrier: structural components and function under physiologic and pathologic conditions. *J. Neuroimmune. Pharmacol.* 1, 223–236. doi: 10.1007/s11481-006-9025-3

Raut, S., Patel, R., and Al-Ahmad, A. J. (2021). Presence of a mutation in PSEN1 or PSEN2 gene is associated with an impaired brain endothelial cell phenotype in vitro. *Fluids Barriers CNS* 18:3. doi: 10.1186/s12987-020-00235-y

Regev, R., Assaraf, Y. G., and Eytan, G. D. (1999). Membrane fluidization by ether, other anesthetics, and certain agents abolishes P-glycoprotein ATPase activity and modulates efflux from multidrug-resistant cells. *Eur. J. Biochem.* 259, 18–24. doi: 10.1046/j.1432-1327.1999.00037.x

Riu, P. L., Riu, G., Testa, C., Mulas, M., Caria, M. A., Mameli, S., et al. (2000). Disposition of propofol between red blood cells, plasma, brain and cerebrospinal fluid in rabbits. *Eur. J. Anaesthesiol.* 17, 18–22. doi: 10.1046/j.1365-2346.2000.00573.x

Sall, J. W., Stratmann, G., Leong, J., Woodward, E., and Bickler, P. E. (2012). Propofol at clinically relevant concentrations increases neuronal differentiation but is not toxic to hippocampal neural precursor cells in vitro. *Anesthesiology* 117, 1080–1090. doi: 10.1097/ALN.0b013e31826f8d86

Seubert, C. N., Zhu, W. T., Pavlinec, C., Gravenstein, N., and Martynyuk, A. E. (2013). Developmental Effects of Neonatal Isoflurane and Sevoflurane Exposure in Rats. *Anesthesiology* 119, 358–364. doi: 10.1097/ALN.0b013e318291c04e

Sharma, H. S., Pontén, E., Gordh, T., Eriksson, P., Fredriksson, A., and Sharma, A. (2014). Propofol promotes blood-brain barrier breakdown and heat shock protein (HSP 72 kd) activation in the developing mouse brain. *CNS Neurol. Disord. Drug Targets* 13, 1595–1603. doi: 10.2174/1871527313666140806122906

Shen, X., Liu, Y., Xu, S., Zhao, Q., Guo, X., Shen, R., et al. (2013). Early life exposure to sevoflurane impairs adulthood spatial memory in the rat. *Neurotoxicology* 39, 45–56. doi: 10.1016/j.neuro.2013.08.007

Spieth, L., Berghoff, S. A., Stumpf, S. K., Winchenbach, J., Michaelis, T., and Watanabe, T. (2021). Anesthesia triggers drug delivery to experimental glioma in mice by hijacking caveolar transport. *Neurooncol. Adv.* 3:vdab140. doi: 10.1093/noajnl/vdab140

Stebbins, M. J., Wilson, H. K., Canfield, S. G., Qian, T., Palecek, S. P., and Shusta, E. V. (2015). Differentiation and characterization of human pluripotent stem cell-derived brain microvascular endothelial cells. *Methods* 101, 93–102 doi: 10.1016/j.ymeth.2015.10.016

Stratmann, G., Sall, J. W., May, L. D., Bell, J. S., Magnusson, K. R., Rau, V., et al. (2009). Isoflurane differentially affects neurogenesis and long-term neurocognitive function in 60-day-old and 7-day-old rats. *Anesthesiology* 110, 834–848. doi: 10.1097/ALN.0b013e31819c463d

Sweeney, M. D., Sagare, A. P., and Zlokovic, B. V. (2018). Blood-brain barrier breakdown in Alzheimer disease and other neurodegenerative disorders. *Nat. Rev. Neurol.* 14, 133–150. doi: 10.1038/nrneurol.2017.188

Syvänen, S., Lindhe, O., Palner, M., Kornum, B. R., Rahman, O., Långström, B., et al. (2009). Species differences in blood-brain barrier transport of three positron emission tomography radioligands with emphasis on P-glycoprotein transport. *Drug Metab. Dispos.* 37, 635–643. doi: 10.1124/dmd.108.024745

Valable, S., Montaner, J., Bellail, A., Berezowski, V., Brillault, J., Cecchelli, R., et al. (2005). VEGF-induced BBB permeability is associated with an MMP-9 activity increase in cerebral ischemia: both effects decreased by Ang-1. *J. Cereb. Blood Flow Metab.* 25, 1491–1504. doi: 10.1038/sj.jcbfm.9600148

Warren, M. S., Zerangue, N., Woodford, K., Roberts, L. M., Tate, E. H., Feng, B., et al. (2009). Comparative gene expression profiles of ABC transporters in brain microvessel endothelial cells and brain in five species including human. *Pharmacol. Res.* 59, 404–413. doi: 10.1016/j.phrs.2009.02.007

Weiss, N., Miller, F., Cazaubon, S., and Couraud, P. O. (2009). The blood-brain barrier in brain homeostasis and neurological diseases. *Biochim. Biophys. Acta* 1788, 842–857. doi: 10.1016/j.bbamem.2008.10.022

Wellens, S., Dehouck, L., Chandrasekaran, V., Singh, P., Loiola, R. A., Sevin, E., et al. (2021). Evaluation of a human iPSC-derived BBB model for repeated dose toxicity testing with cyclosporine A as model compound. *Toxicol. In Vitro* 73:105112. doi: 10.1016/j.tiv.2021.105112

Workman, M. J., and Svendsen, C. N. (2020). Recent advances in human iPSC-derived models of the blood-brain barrier. *Fluids Barriers CNS* 17:30. doi: 10.1186/s12987-020-00191-7

Wu, Y. C., Sonninen, T. M., Peltonen, S., Koistinaho, J., and Lehtonen, Š (2021). Blood-Brain Barrier and Neurodegenerative Diseases-Modeling with iPSC-Derived Brain Cells. *Int. J. Mol. Sci.* 22:7710 doi: 10.3390/ijms22147710

Yan, Y., Qiao, S., Kikuchi, C., Zaja, I., Logan, S., Jiang, C., et al. (2017). Propofol Induces Apoptosis of Neurons but Not Astrocytes, Oligodendrocytes, or Neural Stem Cells in the Neonatal Mouse Hippocampus. *Brain Sci.* 7:130 doi: 10.3390/brainsci7100130

Zhao, J., Hao, J., Fei, X., Wang, X., Hou, Y., and Deng, C. (2014). Isoflurane inhibits occludin expression via up-regulation of hypoxia-inducible factor 1α. *Brain Res.* 1562, 1–10. doi: 10.1016/j.brainres.2014.03.025

**Conflict of Interest:** The authors declare that the research was conducted in the absence of any commercial or financial relationships that could be construed as a potential conflict of interest.

# Advantages of publishing in Frontiers

**OPEN ACCESS**
Articles are free to read for greatest visibility and readership

**FAST PUBLICATION**
Around 90 days from submission to decision

**HIGH QUALITY PEER-REVIEW**
Rigorous, collaborative, and constructive peer-review

**TRANSPARENT PEER-REVIEW**
Editors and reviewers acknowledged by name on published articles

**Frontiers**
Avenue du Tribunal-Fédéral 34
1005 Lausanne | Switzerland

**Visit us:** www.frontiersin.org
**Contact us:** frontiersin.org/about/contact

**REPRODUCIBILITY OF RESEARCH**
Support open data and methods to enhance research reproducibility

**DIGITAL PUBLISHING**
Articles designed for optimal readership across devices

**FOLLOW US**
@frontiersin

**IMPACT METRICS**
Advanced article metrics track visibility across digital media

**EXTENSIVE PROMOTION**
Marketing and promotion of impactful research

**LOOP RESEARCH NETWORK**
Our network increases your article's readership